

**Benchmarking against
Experimental Data of
Neutronics and Thermohydraulic
Computational Methods and
Tools for Operation and Safety
Analysis of Research Reactors**

Results of a Coordinated Research Project



IAEA

International Atomic Energy Agency

IAEA SAFETY STANDARDS AND RELATED PUBLICATIONS

IAEA SAFETY STANDARDS

Under the terms of Article III of its Statute, the IAEA is authorized to establish or adopt standards of safety for protection of health and minimization of danger to life and property, and to provide for the application of these standards.

The publications by means of which the IAEA establishes standards are issued in the **IAEA Safety Standards Series**. This series covers nuclear safety, radiation safety, transport safety and waste safety. The publication categories in the series are **Safety Fundamentals**, **Safety Requirements** and **Safety Guides**.

Information on the IAEA's safety standards programme is available on the IAEA Internet site

<http://www-ns.iaea.org/standards/>

The site provides the texts in English of published and draft safety standards. The texts of safety standards issued in Arabic, Chinese, French, Russian and Spanish, the IAEA Safety Glossary and a status report for safety standards under development are also available. For further information, please contact the IAEA at: Vienna International Centre, PO Box 100, 1400 Vienna, Austria.

All users of IAEA safety standards are invited to inform the IAEA of experience in their use (e.g. as a basis for national regulations, for safety reviews and for training courses) for the purpose of ensuring that they continue to meet users' needs. Information may be provided via the IAEA Internet site or by post, as above, or by email to Official.Mail@iaea.org.

RELATED PUBLICATIONS

The IAEA provides for the application of the standards and, under the terms of Articles III and VIII.C of its Statute, makes available and fosters the exchange of information relating to peaceful nuclear activities and serves as an intermediary among its Member States for this purpose.

Reports on safety in nuclear activities are issued as **Safety Reports**, which provide practical examples and detailed methods that can be used in support of the safety standards.

Other safety related IAEA publications are issued as **Emergency Preparedness and Response** publications, **Radiological Assessment Reports**, the International Nuclear Safety Group's **INSAG Reports**, **Technical Reports** and **TECDOCs**. The IAEA also issues reports on radiological accidents, training manuals and practical manuals, and other special safety related publications.

Security related publications are issued in the **IAEA Nuclear Security Series**.

The **IAEA Nuclear Energy Series** comprises informational publications to encourage and assist research on, and the development and practical application of, nuclear energy for peaceful purposes. It includes reports and guides on the status of and advances in technology, and on experience, good practices and practical examples in the areas of nuclear power, the nuclear fuel cycle, radioactive waste management and decommissioning.

BENCHMARKING AGAINST
EXPERIMENTAL DATA OF NEUTRONICS
AND THERMOHYDRAULIC
COMPUTATIONAL METHODS AND
TOOLS FOR OPERATION AND SAFETY
ANALYSIS OF RESEARCH REACTORS

The following States are Members of the International Atomic Energy Agency:

AFGHANISTAN	GERMANY	PAKISTAN
ALBANIA	GHANA	PALAU
ALGERIA	GREECE	PANAMA
ANGOLA	GRENADA	PAPUA NEW GUINEA
ANTIGUA AND BARBUDA	GUATEMALA	PARAGUAY
ARGENTINA	GUYANA	PERU
ARMENIA	HAITI	PHILIPPINES
AUSTRALIA	HOLY SEE	POLAND
AUSTRIA	HONDURAS	PORTUGAL
AZERBAIJAN	HUNGARY	QATAR
BAHAMAS	ICELAND	REPUBLIC OF MOLDOVA
BAHRAIN	INDIA	ROMANIA
BANGLADESH	INDONESIA	RUSSIAN FEDERATION
BARBADOS	IRAN, ISLAMIC REPUBLIC OF	RWANDA
BELARUS	IRAQ	SAINT LUCIA
BELGIUM	IRELAND	SAINT VINCENT AND THE GRENADINES
BELIZE	ISRAEL	SAN MARINO
BENIN	ITALY	SAUDI ARABIA
BOLIVIA, PLURINATIONAL STATE OF	JAMAICA	SENEGAL
BOSNIA AND HERZEGOVINA	JAPAN	SERBIA
BOTSWANA	JORDAN	SEYCHELLES
BRAZIL	KAZAKHSTAN	SIERRA LEONE
BRUNEI DARUSSALAM	KENYA	SINGAPORE
BULGARIA	KOREA, REPUBLIC OF	SLOVAKIA
BURKINA FASO	KUWAIT	SLOVENIA
BURUNDI	KYRGYZSTAN	SOUTH AFRICA
CAMBODIA	LAO PEOPLE'S DEMOCRATIC REPUBLIC	SPAIN
CAMEROON	LATVIA	SRI LANKA
CANADA	LEBANON	SUDAN
CENTRAL AFRICAN REPUBLIC	LESOTHO	SWEDEN
CHAD	LIBERIA	SWITZERLAND
CHILE	LIBYA	SYRIAN ARAB REPUBLIC
CHINA	LIECHTENSTEIN	TAJIKISTAN
COLOMBIA	LITHUANIA	THAILAND
CONGO	LUXEMBOURG	TOGO
COSTA RICA	MADAGASCAR	TRINIDAD AND TOBAGO
CÔTE D'IVOIRE	MALAWI	TUNISIA
CROATIA	MALAYSIA	TURKEY
CUBA	MALI	TURKMENISTAN
CYPRUS	MALTA	UGANDA
CZECH REPUBLIC	MARSHALL ISLANDS	UKRAINE
DEMOCRATIC REPUBLIC OF THE CONGO	MAURITANIA	UNITED ARAB EMIRATES
DENMARK	MAURITIUS	UNITED KINGDOM OF GREAT BRITAIN AND NORTHERN IRELAND
DJIBOUTI	MEXICO	UNITED REPUBLIC OF TANZANIA
DOMINICA	MONACO	UNITED STATES OF AMERICA
DOMINICAN REPUBLIC	MONGOLIA	URUGUAY
ECUADOR	MONTENEGRO	UZBEKISTAN
EGYPT	MOROCCO	VANUATU
EL SALVADOR	MOZAMBIQUE	VENEZUELA, BOLIVARIAN REPUBLIC OF
ERITREA	MYANMAR	VIET NAM
ESTONIA	NAMIBIA	YEMEN
ESWATINI	NEPAL	ZAMBIA
ETHIOPIA	NETHERLANDS	ZIMBABWE
FIJI	NEW ZEALAND	
FINLAND	NICARAGUA	
FRANCE	NIGER	
GABON	NIGERIA	
GEORGIA	NORTH MACEDONIA	
	NORWAY	
	OMAN	

The Agency's Statute was approved on 23 October 1956 by the Conference on the Statute of the IAEA held at United Nations Headquarters, New York; it entered into force on 29 July 1957. The Headquarters of the Agency are situated in Vienna. Its principal objective is "to accelerate and enlarge the contribution of atomic energy to peace, health and prosperity throughout the world".

IAEA-TECDOC-1879

BENCHMARKING AGAINST
EXPERIMENTAL DATA OF NEUTRONICS
AND THERMOHYDRAULIC
COMPUTATIONAL METHODS AND
TOOLS FOR OPERATION AND SAFETY
ANALYSIS OF RESEARCH REACTORS
RESULTS OF A COORDINATED RESEARCH PROJECT

INTERNATIONAL ATOMIC ENERGY AGENCY
VIENNA, 2019

COPYRIGHT NOTICE

All IAEA scientific and technical publications are protected by the terms of the Universal Copyright Convention as adopted in 1952 (Berne) and as revised in 1972 (Paris). The copyright has since been extended by the World Intellectual Property Organization (Geneva) to include electronic and virtual intellectual property. Permission to use whole or parts of texts contained in IAEA publications in printed or electronic form must be obtained and is usually subject to royalty agreements. Proposals for non-commercial reproductions and translations are welcomed and considered on a case-by-case basis. Enquiries should be addressed to the IAEA Publishing Section at:

Marketing and Sales Unit, Publishing Section
International Atomic Energy Agency
Vienna International Centre
PO Box 100
1400 Vienna, Austria
fax: +43 1 26007 22529
tel.: +43 1 2600 22417
email: sales.publications@iaea.org
www.iaea.org/publications

For further information on this publication, please contact:

Research Reactor Safety Section
International Atomic Energy Agency
Vienna International Centre
PO Box 100
1400 Vienna, Austria
Email: Official.Mail@iaea.org

© IAEA, 2019
Printed by the IAEA in Austria
August 2019

IAEA Library Cataloguing in Publication Data

Names: International Atomic Energy Agency.
Title: Benchmarking against experimental data of neutronics and thermohydraulic computational methods and tools for operation and safety analysis of research reactors / International Atomic Energy Agency.
Description: Vienna : International Atomic Energy Agency, 2019. | Series: IAEA TECDOC series, ISSN 1011-4289 ; no. 1879 | Includes bibliographical references.
Identifiers: IAEAL 19-01256 | ISBN 978-92-0-109619-7 (paperback : alk. paper)
Subjects: LCSH: Nuclear reactors — Computer programs. | Nuclear reactors — Thermodynamics. | Computer simulation.

FOREWORD

Research reactors are fundamental to progress in nuclear research and nuclear technology, and therefore the improvement of their design, performance and safety is of great importance. To deal with these challenges, computer codes allowing for better simulation of the complex processes of and conditions in research reactors have been developed. However, before these codes and methods can be used, it is necessary to validate their model predictions against experimental data in a process known as benchmarking. The computational methods and codes need to be validated against experimental data for phenomena expected to occur during transients of interest in the specific reactor where the methods and codes will be applied. A number of codes used for research reactor analysis were originally developed for nuclear power plants. While the principles at the basis of the development and use of these codes are the same or similar in both nuclear power plants and research reactors, the range of parameters for validation and the complexity of the systems to be modelled may be different for research reactors and among various types of research reactor.

In this regard, the IAEA organized a coordinated research project (CRP) entitled Innovative Methods in Research Reactor Analysis: Benchmark against Experimental Data on Neutronics and Thermohydraulic Computational Methods and Tools for Operation and Safety Analysis of Research Reactors, carried out from 2008 to 2013. The overall objective of the CRP was to encourage cooperation and foster exchange of information in the areas of neutronic and thermohydraulic numerical analyses for improving research reactor design, operation and safety. The CRP included chief scientific investigators from 20 Member States and focused on developing benchmark specifications (reactor descriptions and experimental data) for eight research reactors with different designs, power levels and utilization activities. The IAEA published the benchmark specifications in 2015 in Technical Reports Series No. 480, Research Reactor Benchmarking Database: Facility Specification and Experimental Data.

The objective of the present publication is to provide information on the benchmark analysis performed during the CRP as a resource for research reactor designers, analysts, operators and regulators performing benchmarking of their codes and methods for research reactor analysis. This publication compiles the results of the benchmark analysis performed by the CRP participants for all benchmark specifications developed during the CRP as well as specific conclusions on the benchmark specifications, modelling approaches and user effects, computer codes used and results.

The IAEA is grateful to the experts who contributed with their input and expertise, provided data, shared the results of their calculations and agreed to make it available to the research reactor community through this publication. The IAEA officers responsible for this publication were A.M. Shokr and W.B. Kennedy of the Division of Nuclear Installation Safety, A. Borio di Tigliole of the Division of Nuclear Fuel Cycle and Waste Technology and D. Ridikas of the Division of Physical and Chemical Sciences.

EDITORIAL NOTE

This publication has been prepared from the original material as submitted by the contributors and has not been edited by the editorial staff of the IAEA. The views expressed remain the responsibility of the contributors and do not necessarily represent the views of the IAEA or its Member States.

Neither the IAEA nor its Member States assume any responsibility for consequences which may arise from the use of this publication. This publication does not address questions of responsibility, legal or otherwise, for acts or omissions on the part of any person.

The use of particular designations of countries or territories does not imply any judgement by the publisher, the IAEA, as to the legal status of such countries or territories, of their authorities and institutions or of the delimitation of their boundaries.

The mention of names of specific companies or products (whether or not indicated as registered) does not imply any intention to infringe proprietary rights, nor should it be construed as an endorsement or recommendation on the part of the IAEA.

The authors are responsible for having obtained the necessary permission for the IAEA to reproduce, translate or use material from sources already protected by copyrights.

The IAEA has no responsibility for the persistence or accuracy of URLs for external or third party Internet web sites referred to in this publication and does not guarantee that any content on such web sites is, or will remain, accurate or appropriate.

CONTENTS

1. INTRODUCTION.....	1
1.1. BACKGROUND.....	1
1.2. OBJECTIVES.....	2
1.3. SCOPE.....	2
1.4. STRUCTURE.....	2
2. COORDINATED RESEARCH PROJECT DESCRIPTION AND WORK DONE	3
2.1 COORDINATED RESEARCH PROJECT DESCRIPTION.....	3
2.2. WORK DONE.....	3
2.2.1. First Research Coordination Meeting: 1–5 December 2008	3
2.2.2. Second Research Coordination Meeting: 14–18 June 2010.....	4
2.2.3. Third Research Coordination Meeting: 5–9 December 2011.....	5
2.2.4. Fourth Research Coordination Meeting: 17–21 December 2012.....	6
2.3. COORDINATED RESEARCH PROJECT ACTION MATRIX	7
3. RESULTS OF THE COORDINATED RESEARCH PROJECT.....	10
3.1 RESEARCH REACTOR FACILITIES AND AVAILABLE EXPERIMENTS.....	10
3.1.1. ETRR-2.....	10
3.1.2. IEA-R1	11
3.1.3. MNR.....	11
3.1.4. OPAL.....	12
3.1.5. RSG-GAS.....	12
3.1.6. SPERT III.....	13
3.1.7. SPERT IV.....	13
3.2. DESCRIPTIONS OF THE CODES USED IN THE COORDINATED RESEARCH PROJECT.....	14
3.2.1. ASTEC	14
3.2.2. CATHARE	14
3.2.3. COOLOD-N	15
3.2.4. CUCGP.....	15
3.2.5. EUREKA-2/RR	16
3.2.6. McCARD.....	16
3.2.7. MCNP(X).....	17
3.2.8. MERSAT	17
3.2.9. MTRCR	17
3.2.10. MTR-PC	18
3.2.11. MVP	18
3.2.12. OSCAR-4	18
3.2.13. PARET-ANL.....	19
3.2.14. REBUS	19
3.2.15. RELAP	19
3.2.16. SCALE-6.....	20
3.2.17. TRIPOLI4.....	20

3.2.18. WIMS-ANL.....	20
3.2.19. Summary of the computer codes used in the Coordinated Research Project.....	20
3.3. CONSOLIDATED RESULTS OF THE BENCHMARK ANALYSIS	22
3.3.1. ETRR-2.....	22
3.3.2. IEA-R1	22
3.3.3. MNR.....	23
3.3.4. OPAL.....	23
3.3.5. RSG-GAS	24
3.3.6. SPERT III.....	24
3.3.7. SPERT IV Static.....	25
3.3.8. SPERT IV Transient.....	25
4. CONCLUSIONS OF THE COORDINATED RESEARCH PROJECT	26
4.1. THE BENCHMARK SPECIFICATIONS	26
4.2. MODELLING APPROACH AND USER EFFECTS.....	27
4.3. COMPUTER CODES USED AND RESULTS	28
5. REFERENCES.....	29
ANNEX I BENCHMARK CONSOLIDATED RESULTS AGAINST EXPERIMENTAL DATA FROM ETRR-2.....	31
ANNEX II BENCHMARK CONSOLIDATED RESULTS AGAINST EXPERIMENTAL DATA FROM IEA-R1.....	51
ANNEX III BENCHMARK CONSOLIDATED RESULTS AGAINST EXPERIMENTAL DATA FROM MNR.....	85
ANNEX IV BENCHMARK CONSOLIDATED RESULTS AGAINST EXPERIMENTAL DATA FROM OPAL.....	131
ANNEX V BENCHMARK CONSOLIDATED RESULTS AGAINST EXPERIMENTAL DATA FROM RSG-GAS.....	149
ANNEX VI BENCHMARK CONSOLIDATED RESULTS AGAINST EXPERIMENTAL DATA FROM SPERT III	169
ANNEX VII BENCHMARK CONSOLIDATED RESULTS AGAINST EXPERIMENTAL DATA FROM SPERT IV TRANSIENTS.....	177
ANNEX VIII BENCHMARK CONSOLIDATED RESULTS AGAINST EXPERIMENTAL DATA FROM SPERT IV STATICS.....	223
ANNEX IX REPORTS OF THE PARTICIPANTS OF THE COORDINATED RESEARCH PROJECT ..	275
LIST OF ABBREVIATIONS.....	277
CONTRIBUTERS TO DRAFTING AND REVIEW	279

1. INTRODUCTION

1.1. BACKGROUND

Research reactors are fundamental to nuclear research and technology. The availability of computer codes and models that simulate the complex processes and conditions that occurs in research reactors are of key importance to enhancing the safety, operational effectiveness and utilization capabilities of these facilities world-wide. To this effect, computer codes have been developed to simulate neutronic and thermal-hydraulic processes for normal operation and transient conditions in research reactors. However, these codes and models need to be verified and validated, i.e. benchmarked by comparing their predictions with experimental data, the prediction of already validated codes, or through inter-comparison of different code results using benchmark specifications, before they are used by designers, operating organizations, researchers and regulatory bodies. The computational methods and codes need to be validated against experimental data for phenomena expected to occur during transients of interest in the specific reactor for which these methods and codes are to be applied. A number of codes used for research reactor analysis were originally developed for nuclear power plants. While the principles at the basis of the development and use of the codes are the same or similar, the range of parameters for validation and complexity of the systems to be modelled may be different for research reactors and among various types of research reactors.

In 2013, the International Atomic Energy Agency (IAEA) completed the implementation of a coordinated research project (CRP) on “Innovative Methods in Research Reactor Analysis: Benchmarking, against Experimental Data, of Neutronics and Thermal-hydraulic Computational Methods and Tools for Operation and Safety Analysis of Research Reactors.” The overall objective of the CRP was to encourage cooperation and foster exchange of information in the areas of neutronic and thermal-hydraulic numerical analyses for improving research reactor design, operation and safety. The CRP included two main activities: 1) develop and publish detailed benchmark specifications (database) on neutronics and thermal-hydraulics, including experimental data and measurements, for eight research reactors; and 2) benchmark computer codes and numerical analysis methods against the benchmark specifications and analyse the results.

Chief Scientific Investigators (CSIs) participated in the activities of the CRP by providing benchmark specifications, performing calculations with different computer codes, or both. The CRP participants collected and provided experimental neutronic and thermal-hydraulic data for various operating conditions in research reactors, simulating those operating conditions using different computer codes, and compared the outputs of the simulations with the measured data.

The participants in this CRP were CSIs from Algeria (ALG), Argentina (ARG), Australia (AUS), Bangladesh (BGD), Canada (CAN), Egypt (EGY), France (FRA), Ghana (GHA), Greece (GRE), Indonesia (IDN), Pakistan (PAK), Romania (ROM), South Africa (SAF), Syrian Arab Republic (SYR) and United States of America (USA). CSIs from Italy (ITL), Nigeria (NGA) and Uzbekistan (UZB) participated in some activities of the CRP. In addition, CSIs from Brazil (BRA) and Republic of Korea (ROK) participated as observers in some CRP activities. Herein after, country code will be used in this publication to represent CSI from that respective Member State, for example ARG is used for CSI from Argentina.

The CRP generated a large volume of experimental data and results from computer simulations of various neutronic and thermal-hydraulic conditions in eight research reactors representing a range of designs, power levels and experimental configurations. The benchmark specifications

developed by the participants were compiled into a database published in 2015 as IAEA Technical Report Series No. 480, “Research Reactor Benchmarking Database: Facility Specification and Experimental Data”. The database and each individual data set for the eight research reactors serve as resources that interested institutions world-wide can use to perform independent benchmarks using their commonly used computational tools and codes.

1.2. OBJECTIVE

The objective of this publication is to present the results of a completed CRP as an information resource for research reactor designers, operating organizations and regulators interested in benchmarking the computer codes and models they use for research reactor safety analysis, operation and utilization. From the results of various codes applied to a range of research reactor experimental data, it is possible to gauge the applicability and relevance of the codes and methodologies to consider benchmarks, to identify user effects on the results predicted by the computer codes, to note the sensitivity of results to modelling choices and to establish a database in support of training and in-house code validation and verification.

1.3. SCOPE

The scope of this publication is the benchmark analysis performed by the CRP participants for all benchmark specifications in Ref. [1]. These include the results of benchmarks performed by individual participants in the CRP. The results obtained by the individual CRP participants are consolidated for each benchmark specification in order to draw specific conclusions on the benchmark specifications, modelling approaches, user effects and computer codes used.

This publication also describes the conduct of the CRP, in the form of the work done during each research coordination meeting and the conclusions and recommendations of those meetings and provides information on the computer codes used.

This publication covers neutronic and thermal-hydraulic analysis of steady-state and transient conditions for research reactors with a range of designs, power levels, operating regimes and experimental facilities. This publication is intended for use by operating organizations, researchers, regulatory bodies, designers and other interested parties involved in the safety, operation and utilization of research reactors.

In the context of this publication, the term ‘benchmark specification’ means the well-defined reactor configurations with their standard parameters that describe facilities and associated facility evolutions contained with corresponding measured data as described in Ref. [1]. The term ‘code’ refers to a computer programme or suite of programmes for calculating and analysing the neutronic and thermal-hydraulic characteristics and behaviour of research reactors. The term ‘model’ refers to a specific set of input parameters and code instructions used by a code with the intent to predict reactor characteristics or behaviour or duplicate via calculation a benchmark specification.

1.4. STRUCTURE

Following this introductory section, Section 2 provides an overview of the CRP and summarizes the work done during the CRP related to modelling research reactors using computer codes. Section 3 contains three chapters that cover summary descriptions of the facilities and benchmark specifications, brief descriptions of the codes used by the CRP participants and consolidated results obtained by the participants for each benchmark specification. Section 4 presents the conclusions of the CRP, which cover the benchmark specifications, modelling

approaches and user effects, computer codes used and results. This publication also includes 8 Annexes (Annex I through VIII), which provide the consolidated results of the benchmarks performed by the CRP participants of each benchmark specification. The detailed individual reports of each CRP participant on the codes and models used and results obtained for their benchmark analysis are attached with this publication (CD-ROM attached).

2. COORDINATED RESEARCH PROJECT DESCRIPTION AND WORK DONE

2.1. COORDINATED RESEARCH PROJECT DESCRIPTION

The IAEA CRP on ‘Innovative Methods in Research Reactor Analysis: Benchmarking, against Experimental Data, of Neutronics and Thermalhydraulic Computational Methods and Tools for Operation and Safety Analysis of Research Reactors’ was designed and initiated in October 2008, as a cross-cutting activity jointly organized by the Division of Nuclear Installation Safety, Division of Department of Nuclear Safety and Security NSNI, Division of Nuclear Fuel Cycle and Waste Technology and the Division of Physical and Chemical Sciences of IAEA.

During the CRP, a great volume of experimental data was obtained from CRP participants, covering a wide range of research reactor types, neutronic and thermal-hydraulic parameters, power levels and experimental configurations. This data was compiled into the benchmark specifications that consist of the facility specifications, experiment descriptions and corresponding experimental data for eight research reactors. Each benchmark specification was prepared in a way to serve as a stand-alone resource to perform independent benchmarks by interested institutions world-wide.

Overall, the specific research outcomes of the CRP were:

- Transferred know-how in the area of research reactor numerical analysis, including design, safety analysis, operation and utilization;
- Collected sets of experimental data for benchmarking of neutronic and thermal-hydraulic computer codes;
- Benchmarked neutronic and thermal-hydraulic computer codes against experimental results;
- Identified user effects on the results predicted by the computer codes;
- Enhanced the capabilities of the CRP participants in performing numerical analysis and safety assessment of research reactors;
- Compiled a comprehensive database of research reactor characteristics, experiments and data useful for performing benchmarks;
- Provided recommendations for future research and development activities involving research reactors and the codes used in modelling them;
- Increased cooperation among research reactor analysts related to experiments and modelling.

2.2. WORK DONE

2.2.1. First Research Coordination Meeting: 1–5 December 2008

The participants offered experimental data for comparison and made brief presentations of the available experimental data and respective facilities. Discussions were held on the need to develop templates for the facility specification, for the experiment description and for the data submission for comparison of results.

Discussions continued during the meeting and culminated in the participants defining the final proposal for the template documents. The last sessions of the meeting were dedicated to finalizing the summary of conclusions and recommendations.

The research coordination meeting (RCM) resulted in the following conclusions and recommendations:

- The CSIs agreed to focus on the improvement of safety, operation and utilization of research reactors while selecting the relevant data sets. The meeting aimed to classify the available data from participants and identified areas where experimental data was lacking. In some cases, the available experimental data was very broad and therefore an appropriate subset was selected and prepared by the providers;
- The various presentations described the available data for experimental comparison in order to allow judgement by participants on the applicability and potential quality of the submissions. That information was used to finalize the action matrix with regard to the list of benchmarks available for calculations. Participants indicated in the action matrix the data sets they found applicable and in which they had interest in performing specific calculations;
- The participants agreed to provide, when possible, the available uncertainty data, along with the benchmark specifications, whether the uncertainties were obtained from experimental conditions, calculations, judgment or from published literature.
- The participants agreed that submissions, irrespective of the availability of uncertainty data, would be initially accepted and used;
- The completeness and clarity of benchmark specification was critical for successful implementation of the CRP. Neutronic and thermal-hydraulic working groups within the meeting produced template documents to facilitate both benchmark specification and the submission of results. Those templates were integrated, finalized and submitted to the IAEA for further distribution to participants. Participants from South African Nuclear Energy Corporation (Necsa) and Investigaciones Aplicadas (INVAP) agreed to coordinate the inputs from participants to finalize the template documents and distribute them through the dedicated website for the CRP;
- The benchmark specifications were subject to an internal review process, in which participants who intended to calculate the specific benchmark analysis reviewed and commented on the specification prior to its final submission to the IAEA. The quality and applicability of the experimental sets was also evaluated;
- The data supplied to this CRP was restricted for use only within the activities of the CRP, unless otherwise agreed by the data provider;
- The available experimental data was sufficient to conduct this CRP. However, it was recognised that the data does not contemplate areas like fuel management, depletion, hydraulic data (core input data), heat transfer data (steady state and transient), gamma flux, neutron beam line characterization, shielding, etc. Therefore, it was recommended that the IAEA consider an extension of the CRP, envisaging the possibility to find such data and/or to promote experiments to obtain it.

2.2.2. Second Research Coordination Meeting: 14–18 June 2010

The meeting included review by the IAEA representatives of the CRP objectives and the expected results, the status of the relevant research contracts and agreements, and assessment of the results obtained to date in comparison with the CRP objectives.

The participants discussed the validity of the available computer codes for the prediction of specific phenomena and parameters, modelling approaches for various cases, and assumptions and approximations used in the calculations, as well as a preliminary comparison of the results. The meeting also included presentations on the new experimental data provided to the CRP and were followed by the discussions to define the additional data needed for modelling and to revise the templates for results submission. It was agreed that the results of the CRP would be published in two separate IAEA documents. The first one dedicated to the description of the available experimental data, while the second dedicated to the detailed benchmarking results and the conclusions.

The individual participants progress reports, presentations and the associated discussions made by the participants during the second RCM on the status of their research contracts agreements showed that most of the tasks included in the individual work plans had been completed. The available sets of data covered different physical phenomena that was of concern for research reactor safety analysis, operation and utilization. The lack of uncertainty data associated with the experiment and measurement conditions was raised again as that data was vital for benchmarking analysis.

The thermal-hydraulic models and codes, including selection of appropriate correlations for prediction of different critical phenomena, involve larger uncertainties when compared to the codes used for neutronics modelling. In this regard, the CRP participants were encouraged to continue investigating the limitations of the thermal-hydraulic codes being benchmarked in this CRP for checking their validity for research reactor analysis.

The meeting recommended that in cases where multiple participants used the same codes for the same benchmarks, the most appropriate model parameters were to be distributed to all interested participants. These models could be run on a specific version of common codes to remove additional ambiguities. These benchmarks are also useful to evaluate the user effect influence which was one of the identified outputs of this CRP. In addition, a review process was incorporated into the CRP to assess the results obtained from all benchmark calculations, including identification of the discrepancies, their sources, and to suggest ways for further improvements.

The meeting recommended that since the work within this CRP involved application and analysis of methods and approaches (established and/or under development), the obtained results would be communicated to the code developers for further evaluation of the limitation of the codes.

2.2.3. Third Research Coordination Meeting: 5–9 December 2011

In addition to the CRP participants, this meeting was also attended by the Nuclear Energy Agency (NEA)/ Organization for Economic Cooperation and Development (OECD). A technical visit was also organized to the construction sites of Jules Horowitz research Reactor and International Thermonuclear Experimental Reactor at Commissariat à l'Énergie Atomique (CEA) Cadarache centre, France.

The meeting included several presentations from invited experts and observers. Topics included an overview of a set of tools developed by the NEA/OECD for describing, searching and analysing reactor neutronics benchmarks, an overview of the analysis performed following the Fukushima accident and various code systems and approaches used by the participants. The following was a summary of discussion:

- The participants were requested to formulate preliminary technical conclusions based on analyses performed;
- The possibility to identify certain benchmarks as high quality reference benchmarks and as such include more extensive calculation data for future comparison was discussed;
- The need for establishing a database of thermal-hydraulic benchmark analysis, similar to that which existed at the NEA/OECD for criticality and reactor physics benchmark analysis, was highlighted.

Further activities during the meeting focussed on the review and finalization of important draft documents such as the two IAEA publications, as well as results templates needed for submission of benchmark results.

The status of facility and experiment descriptions (benchmark specifications) were reviewed and final comments and clarifications were gathered prior to drafting the first IAEA publication.

In addition, the following conclusions were drawn by participants:

- The CRP was helpful to the research reactor community and had provided a set of data and results which were clearly missing from literature;
- The various benchmark analysis had been challenging and had provided opportunity for good practice and lessons learned. Although the CRP had achieved a great deal in gathering relevant benchmarks and perform preliminary analysis on all of these, it was noted that interaction between neutronics and thermal-hydraulics components of benchmarks was still not optimal. In most cases these disciplines were treated rather independently and suggestions for improvement included either coupled calculations, or at least coupled approaches by neutronic and thermal-hydraulic analysts;
- The comparison planned within this CRP between individual submissions by the participants and joint benchmarking efforts was an added value of this CRP in terms of evaluating both user effects and models used in the codes employed;
- It was strongly recommended to include input models, i.e. input files, in the final publication (at least electronically) so that the intended users could build upon the lessons learned;
- The benchmarks performed in the CRP showed that static multi-dimensional neutronics, with point kinetics and multi-channel thermal-hydraulics was a commonly used approach for the reactor problems in benchmark analysis. 3D time-dependent solutions could be evaluated for selected transients to define the added value of such detailed modelling;
- The benchmarks performed also showed that neutronics modelling had proven to be reasonably accurate; obtaining good agreement for thermal-hydraulics analysis was more challenging as similar problems were experienced by many of the users.

2.2.4. Fourth Research Coordination Meeting: 17–21 December 2012

The meeting participants were informed by the IAEA representatives about the status of the first publication of the CRP. The participants discussed the consolidated results and made observations and comments regarding the capabilities of the various codes to provide reliable predictions of the experimental data. During the discussions there were possible explanations on the causes for the observed discrepancies. This assisted the participants to elaborate on follow-up activities necessary to optimize the outcome of the results consolidation for the

benefit of the research reactor community and prepare inputs for the second publication of the CRP (i.e. the present publication).

Further activities were focussed on the review and finalization of the consolidated results. The following were highlighted:

- The distribution of ‘best’ input models for various benchmarks would be shared amongst participants at the end of the CRP;
- The user effect was identified as a major origin among code-to-code discrepancies. It was concluded that certain input parameters and nodalization methods affect significantly the results provided by the codes;
- The coupling between neutronics and thermal-hydraulics via the kinetic parameters and feedback coefficients seemed to be the major contributor to discrepancies between experimental measurements and codes estimates. It was recommended that harmonization efforts were to be made to improve the results of the models;
- The potential ways to reduce user effects were suggested by the participants. Among others, sensitivity analysis and adequate training through code benchmarking were the most prevalent.

The participants were informed that the second phase of this CRP was initiated by IAEA focusing on fuel burn-up and material activation.

Meeting participants suggested that the database and the benchmarking effort during the CRP would be made widely known throughout the research reactor community. Continuation of the benchmarking effort will be encouraged, and if there exist enough interested participants the IAEA was committed to organize and host a technical meeting to discuss the updated results.

Given the scope of this CRP, which includes eight benchmark analysis (with at least three experiments each) covering broad subjects related to research reactor safety, operation and utilization, the participants were informed of the status of the first publication of the CRP results (i.e. Ref. [1]).

2.3. COORDINATED RESEARCH PROJECT ACTION MATRIX

The action matrix presented in Table 1 was developed during the CRP to ensure that each benchmark specification would be modelled by at least two CRP participants. The leftmost column provides the name of the facility that is the subject of the benchmark specification. The remaining columns indicate the type of data available (i.e. neutronics, depletion/activation and thermal-hydraulics) and the type of benchmark that the data can be used for (e.g. flux spectrum, kinetics parameters, steady-state temperature and reactivity insertion transients). The rows of Table 1 show the CRP participants who performed the benchmark analysis.

TABLE 1. COORDINATED RESEARCH PROJECT ACTION MATRIX

Available Experimental Data from:	Neutronics					Depletion/Activation		Thermal-Hydraulics				
	Criticality (k_{eff} , k_{inf})	Flux Shape/Flux Profile	Flux Spectrum	Control Rod Worth	Reactivity Effects	Reactivity Coefficients	Kinetic Parameters	Depletion (Fuel, Burnable Poisons)	Activation Outside the Core	Steady-State Temperature	Loss of Flow Transient	Reactivity Insertion Transient
ETRR-2	ARG, SAF	ARG, SAF	ARG, SAF	ARG, SAF	ARG, SAF	ARG, SAF	ARG, SAF		ARG, EGY, GRE, SAF, SYR	ARG, EGY, GRE, SAF, SYR	ARG, EGY, GRE, SAF, SYR	ARG, EGY, GRE, SAF, SYR
IEA-R1									ALG, ARG, BGD, BRA, GRE, ROK, SYR	ALG, ARG, BGD, BRA, GRE, ROK, SYR	ALG, ARG, BGD, BRA, GRE, ROK, SYR	ARG, EGY, GRE, SAF, SYR
MNR	ARG, CAN, SAF, SYR	ARG, CAN, SAF, SYR		ARG, CAN, SAF, SYR	ARG, CAN, SAF, SYR	ARG, CAN, SAF, SYR	ARG, CAN, SAF, SYR					
MNSR-Y			GHA, PAK, SYR, USA	GHA, PAK, SYR, USA								
OPAL	ARG, AUS, ROK, SAF	ARG, AUS, ROK, SAF	ARG, AUS, ROK, SAF	ARG, AUS, ROK, SAF	ARG, AUS, ROK, SAF	ARG, AUS, ROK, SAF	ARG, AUS, SAF					ARG, AUS, SAF

TABLE 1. COORDINATED RESEARCH PROJECT ACTION MATRIX (cont.)

Available Experimental Data from:	Neutronics				Depletion/Activation		Thermal-Hydraulics					
	Criticality (k_{eff} , k_{inf})	Flux Shape/ Flux Profile	Flux Spectrum	Control Rod Worth	Reactivity Effects	Reactivity Coefficients	Kinetic Parameters	Depletion (Fuel, Burnable Poisons)	Activation Outside the Core	Steady-State Temperature	Loss of Flow Transient	Reactivity Insertion Transient
RSG-GAS												
SPERT III	GHA, ROM, USA	GHA, ROM, USA	GHA, ROM, USA	GHA, ROM, USA	GHA, ROM, USA	GHA, ROM, USA	GHA, ROM, USA			ARG, EGY, GRE, SYR	ARG, EGY, GRE, SYR	GHA, ROM, USA
SPERT IV	ALG, AUS, BGD, FRA, PAK, SYR	ALG, AUS, BGD, FRA, PAK, SYR	ALG, AUS, BGD, FRA, PAK, SYR	ALG, AUS, BGD, FRA, PAK, SYR	ALG, AUS, BGD, FRA, PAK, SYR	ALG, AUS, BGD, FRA, PAK, SYR	ALG, AUS, BGD, FRA, PAK, SYR					ALG, AUS, BGD, FRA, GRE, PAK, SYR

Experimental Training Research Reactor-2 (ETRR-2) Instituto de Energia Atômica (IEA-R1)
 McMaster Nuclear Reactor (MNR) Miniature Neutron Source Reactor (MNSR)
 Open Pool Australian Lightwater reactor (OPAL) Reactor Serba Guna GA Siwabessy (RSG-GAS)
 Special Power Excursion Reactor Test III (SPERT III) Special Power Excursion Reactor Test IV (SPERT IV)

3. RESULTS OF THE COORDINATED RESEARCH PROJECT

3.1. RESEARCH REACTOR FACILITIES AND AVAILABLE EXPERIMENTS

The first publication of the CRP, Ref. [1], compiled detailed facility descriptions and experiments from the following eight research reactors (and Member State contributors):

- ETRR-2 (Egypt);
- IEA-R1 (Brazil);
- McMaster (Canada);
- MNSR (Syrian Arab Republic);
- OPAL (Australia);
- RSG-GAS (Indonesia);
- SPERT III (United States of America);
- SPERT IV (Canada).

The following table presents the research reactors covered by the benchmark specifications and the type of experimental data available for each of them.

TABLE 2. RESEARCH REACTOR COVERED BY BENCHMARK SPECIFICATIONS AND AVAILABLE DATA

Reactor Name, Power Level	Type of Data Available	
	Neutronics	Thermal-hydraulics
ETRR-2, 22 MW	+	+
IEA-R1, 5 MW		+
McMaster, 3 MW	+	
MNSR, 30 kW	+	+
OPAL, 20 MW	+	
RSG-GAS, 30 MW		+
SPERT III, 40 MW	+	+
SPERT IV, variable power	+	+

In most of the cases, neutronics data include the reactor parameters such as core criticality (k_{eff}), neutron flux level/shape/profile, neutron flux energy distributions, control rod worth, reactivity effects, reactivity coefficient and some kinetics parameters. Similarly, thermal-hydraulics data include steady state temperatures, loss of flow transients, reactivity insertion transients and other parameters. The reader is referred to individual sections regarding the data available for different research reactors.

The following sections provide an overview of the individual research reactor and the experimental data provided for this CRP. The full details of the benchmark specifications are found in Ref. [1].

3.1.1. ETRR-2

The ETRR-2 reactor is located at Inshas, 60 km northwest from Cairo, Egypt. It is a multipurpose reactor, intended for radioisotope production, and is used for research and irradiation activities in the fields of neutron physics, neutron activation analysis, radioisotope production and research and development in boron neutron capture therapy. The ETRR-2, with

its varied installations, laboratories, and peripheral systems is a key tool for the continuous education and training of scientists and engineers. Furthermore, it allows Egypt to supply its domestic market with medical and industrial radioisotopes.

The reactor has a nominal power of 22 MW and is of open pool type. The core is cooled and moderated by light water and reflected by beryllium. The fuel is Material Testing Reactor (MTR) plate type with U_3O_8 fuel and aluminium cladding. In this benchmark specification the following experiments were provided.

Neutronics:

- Criticality parameters;
- Flux profile;
- Control rod worth;
- Reactivity coefficients.

Thermal-hydraulics:

- Steady state temperature;
- Loss of flow transient;
- Reactivity insertion transient.

3.1.2. IEA-R1

The Instituto de Pesquisas Energéticas e Nucleares (IPEN) IEA-R1 has a nominal power of 5 MW and is an open pool type. The reactor is cooled and moderated by light water and reflected by Beryllium. The fuel is MTR plate type with U_3O_8 and U_3Si_2 fuel and aluminium cladding. Application areas of the IEA-R1 include:

- Production of radioisotopes such as ^{153}Sm , ^{131}I and ^{192}Ir for use in nuclear medicine;
- Production of radioactive sources for industrial radiography;
- Irradiation of samples for multi-element analyses, using neutron activation analysis;
- Research in Nuclear Physics.

In this benchmark specification the following thermal-hydraulics experiments were made available for benchmarking:

Thermal-hydraulics:

- Steady state temperature;
- Loss of flow transient.

3.1.3. MNR

The McMaster Nuclear Reactor (MNR) is located on the main campus of McMaster University in Hamilton, Ontario, Canada. The MNR started its operation in 1959 as the first university-based research reactor in the British Commonwealth. MNR is one of the world's largest suppliers of the medical radioisotope ^{125}I , which is used for the treatment of prostate cancer.

The reactor has a nominal power of 3 MW and is of open pool type. The reactor is cooled and moderated by light water and reflected by graphite, lead and light water. The fuel is MTR plate type with U_3Si_2 fuel and aluminium cladding. In this benchmark specification the following neutronics experiments were provided for benchmarking purposes:

Neutronics:

- Criticality parameters;
- Flux profile;
- Control rod worth;
- Reactivity coefficients.

3.1.4. OPAL

Open Pool Australian Lightwater reactor (OPAL) is a 20 MW pool-type nuclear research reactor that was officially opened on April 2007 at the Australia's Nuclear Science and Technology Organization (ANSTO) Research Establishment at Lucas Heights, located in South Sydney, Australia. OPAL's main uses are:

- Irradiation of target materials to produce radioisotopes for medical and industrial applications;
- Research in the field of materials science using neutron beams and associated instruments;
- Analysis of minerals and samples using neutron activation techniques and delayed neutron activation techniques;
- Irradiation of silicon ingots for use in the manufacture of electronic semiconductor devices.

The reactor is cooled and moderated by light water and reflected by heavy water. The fuel is MTR plate type with U_3Si_2 fuel and aluminium cladding. In this benchmark specification the following neutronics experiments were provided for benchmarking purposes:

Neutronics:

- Criticality parameters;
- Flux profile;
- Control rod worth;
- Kinetic parameters.

3.1.5. RSG-GAS

Reactor Serba Guna GA Siwabessy (RSG-GAS) is a multipurpose nuclear reactor with a nominal power of 30 MW owned by Indonesia. The reactor, which was inaugurated in 1987, is operated by the National Nuclear Energy Agency of Indonesia, BATAN. It achieved full power operation, at 30 MW, in March 1992.

The reactor is of open pool type, is cooled and moderated by light water and reflected by Beryllium. The fuel is MTR plate type with U_3Si_2 fuel and aluminium cladding. In this benchmark specification the following thermal-hydraulics experiments were made available:

Thermal-hydraulics:

- Steady state temperature;
- Loss of flow transient.

3.1.6. SPERT III

The Special Power Excursion Reactor Test III (SPERT III) reactor located in the United States of America was a pressurized-water, nuclear research reactor which was constructed to provide a facility for conducting reactor kinetic behaviour and safety investigations. The experiments were designed to provide information for the advancement of pressurized-water and boiling-water reactor technology and safety.

The reactor had a nominal power of 40 MW, housed in a pressure vessel. The reactor is cooled, moderated, and reflected by light water. The fuel is pin type with UO₂ with stainless steel cladding. In this benchmark specification the following experiments were made available:

Neutronics:

- Criticality parameters;
- Flux profile;
- Control rod worth;
- Reactivity coefficients;
- Kinetic parameter.

Thermal-hydraulics:

- Reactivity insertion transient.

3.1.7. SPERT IV

The Special Power Excursion Reactor Test IV (SPERT IV) reactor located in the United States of America was a ‘zero power’ open pool type nuclear research reactor which was constructed to provide a facility for conducting reactor kinetic behaviour and safety investigations especially in the field of reactor stability. The facility was designed to incorporate a wide range of flexibility in flow rates and direction of flow.

The reactor was cooled, moderated and reflected by light water. The fuel was MTR plate type with UAl fuel and Aluminium cladding. In this benchmark analysis the following experiments were provided:

Neutronics:

- Criticality parameters;
- Flux profile;
- Control rod worth;
- Reactivity coefficients;
- Kinetic parameter.

Thermal-hydraulics:

- Reactivity insertion transient.

3.2. DESCRIPTIONS OF THE CODES USED IN THE COORDINATED RESEARCH PROJECT

The following sections provides brief descriptions of these codes. Additional information can be found in Annexes I-VIII.

3.2.1. ASTEC

Accident Source Term Evaluation Code (ASTEC) has been developed over a number of years by the Institut de Radioprotection et de Sûreté Nucléaire (IRSN), France and its German counterpart, the Gesellschaft für Anlagen und Reaktorsicherheit mbH (GRS) [2]. The purpose of the ASTEC software package is to simulate all the phenomena that occur during a severe accident in a water-cooled nuclear reactor, from the initiating event to the possible release of radioactive products (the 'source term') outside the containment. Its modular structure simplifies qualification by comparing the simulated results with those obtained experimentally. Each module simulates the phenomena occurring in one part of the reactor or at one stage of the accident. These include:

- Two-phase thermal-hydraulics of coolant flows in the reactor coolant primary and secondary systems using a numerical approach based on five equations;
- Core degradation processes driven by temperature rise due to as residual heat as chemical reactions followed by fuel and structures melting, up to 'corium' formation;
- Release of fission products, particularly iodine, from fuel in the core, together with their transport and chemical behaviour in the reactor coolant system and subsequently within the containment.

ASTEC also simulates other phenomena, associated with the accident, including direct containment heating by the transfer of hot gases and corium droplets from the reactor cavity, following the rupture of the vessel; the combustion of hydrogen accumulated within the containment and the associated risk of explosion; and the radioactivity production and aerosols transport and the associated residual heat in all parts of the reactor.

The ASTEC package has been validated by over 160 tests. Validation of ASTEC benefits from research and development programmes carried out under the auspices of the OECD Nuclear Energy Agency, together with other international and in-house IRSN programmes.

3.2.2. CATHARE

Code for Analysis of Thermal-Hydraulics during an Accident of Reactor and Safety Evaluation (CATHARE) [3] was developed initially for Pressurized Water Reactor (PWR) accidents best-estimate calculations: Loss of Coolant Accidents (LOCAs) small or large break in primary or secondary systems and reactivity insertion. The code is developed in France by CEA-Grenoble and is owned by four partners: CEA, IRSN, Électricité de France and AREVA. CATHARE is based on conservation equations for the two-phase flow of water with six equations for mass, energy and momentum. Additional optional equations for non-condensable gases and radio-

chemical components are also available. It is able to simulate thermal non-equilibrium (critical flow, re-flooding, etc.) and mechanical non-equilibrium (thermal stratification, counter current flow). All two-phase flow and heat transfer regimes are modelled, either with fuel assembly or with general wall heat structure. The domain of parameters is from 0.1 to 25 MPa for pressure, from 20°C to 2000°C for gas temperature, and up to sonic condition for fluid flow. The discretization of all terms of the equations is fully implicit in 1-D and 0-D modules and semi implicit in 3-D assemblies (which are dedicated to pressure vessels) including inter-phase exchange, pressure and convection terms, and the resulting non-linear equations are solved using an iterative Newton solver. The code enables also the calculation with several parallel processors.

The space discretization uses the staggered mesh and the donor cell principle. A specific treatment of the residual phases exists in order to manage their appearance and disappearance while minimizing convergence problems and with a quasi-perfect mass and energy conservation. The extensive experimental programme carried out for developing constitutive relations and for assessment includes separate effect tests, component tests and integral tests.

A Graphical User Interface (GUI) for CATHARE called GUITHARE has been developed over the last few years. It is available for both WINDOWS and LINUX platforms. When it is used for pre-processing, GUITHARE is a helpful interface to create an input deck and visualize the circuit. Existing input deck can also be imported and modified. All these functionalities are interactive. Calculations can be launched from the GUI. For post-processing, GUITHARE provides helpful interactive tool for results analysis.

3.2.3. COOLOD-N

COOLOD-N code is a modification of COOLOD code which was originally developed by Japan Atomic Energy Agency (JAEA) for steady state thermal hydraulic analysis under natural convection cooling of research reactors with plate-type fuels. Later, the code became COOLOD-N2 by including a heat transfer package based on heat transfer correlations obtained during heat transfer experiments of the upgraded JRR-3 core. COOLOD-N2 is capable of analysing the steady-state thermal-hydraulics of research reactors when plate-type or rod-type fuel is employed. The physical models can calculate fuel and clad temperatures under both forced and natural convection cooling modes in addition to Onset Nucleate Boiling (ONB) temperature, heat flux at onset of flow instability as well as Departure from Nucleate Boiling (DNB) heat flux Ref. [4]. Fuel plate temperatures are calculated assuming constant heat generation in fuel along the radial direction and one-dimensional heat conduction.

An axial fuel plate temperature distribution can be calculated from local bulk temperatures of the coolant and axial peaking factors. In case of fuel plates with different heat generation, the code can calculate the temperature distribution for each fuel plate. Given the fuel material and the uranium density, the code calculates the fuel thermal conductivities that can also be provided by the user from available data tables. The properties of light water, heavy water and aluminium alloy are included in the code, and no inputs are required in this case. A detailed code description is available in the code manual.

3.2.4. CUCGP

CUCGP (CUDA Course Grained Particles) is a Monte Carlo based three-dimensional transport code. It has full geometric flexibility and no restriction on the treatment of the energy variable. However, unlike traditional Monte Carlo simulations which transport point particles, the code

transports ‘coarse’ particles, that is, particles that cover a small volume in space. Reaction rates are then locally homogenized over the extent of the particle and a single particle history covers more of the overall phase space. This introduces an additional (deterministic) error, which is proportional to the particle size.

The code is designed and optimized to run on modern streaming processor architectures. In particular, the code has a very fine grained level of parallelism, running on thousands of concurrent threads and efficiently utilizes the vector-like architecture of streaming processors. It is written in a mixture of C++ and CUDA.

Currently, the geometry is represented using an unstructured tetrahedral mesh. Thus, tracking is performed through identical geometric primitives, as opposed to generic cells that may contain different numbers and kinds of boundary faces. Using an unstructured mesh retains a lot of geometric flexibility, but all the curved surfaces are triangulated (that is, approximated using first order surfaces). Each mesh element is restricted to a single material region; thus, no homogenization is performed.

CUCGP has the capability to estimate higher order spatial moments (e.g. Legendre and Fourier moments) directly, without resorting to small mesh tallies to obtain spatial distributions.

The code design makes heavy use of meta-programming techniques in order to save resources of the streaming processor. Thus, many user defined options and branches are resolved at compile time. This means that a dedicated executable is built from the underlying (in-lined and pre-compiled) libraries for each problem and there is no ‘master’ executable.

3.2.5. EUREKA-2/RR

EUREKA-2/RR is a coupled neutronics, thermal-hydraulics and point kinetics code [5]. It is a revised version of EUREKA-2 which was originally developed by JAEA for reactivity accident analysis in the case of nuclear power plants. A heat transfer package is added to EUREKA-2 to modify it to EUREKA-2/RR where the heat transfer correlations considered in the heat transfer package were obtained or estimated from heat transfer experiments.

3.2.6. McCARD

Monte Carlo Code for Advanced Reactor Design and analysis (McCARD) Refs. [6] and [7] has been developed exclusively for neutronics analysis of multiplying media (fuel pins, fuel assemblies, reactors). The code uses continuous energy nuclear data library generated by the ACER module of the NJOY [8] code. The code can handle systems of arbitrary geometrical shapes by dividing it into three-dimensional composition cells defined by combinations of surfaces such as planes, cylinders and spheres. It is capable of depletion calculations of nuclear systems. It has a built-in depletion subroutine which provides solutions to the nuclear transmutation equations. To improve accuracy of depletion analyses, the predictor-corrector method is incorporated. The general nuclear transmutation equations are solved with the matrix exponential method and it is possible to treat about 1,400 isotopes.

McCARD can perform kinetic parameter calculations and thermal-hydraulic feedback calculations for nuclear core analysis. In the code, kinetic parameters are effectively estimated using the expected number of fission neutrons in the next generation for the adjoint flux. It has parallel computing capabilities on clustered computers. Its functionality is augmented with the anterior stopping criteria for the inactive cycle run, the real variance estimation, the diffusion

theory group constant generation, sensitivity and uncertainty analysis, and the error propagation analysis of burnup calculations.

3.2.7. MCNP(X)

Monte Carlo N-Particle (MCNP) is a widely-used general-purpose transport-theory code that can be used for neutron, photon, electron or coupled neutron/photon/electron transport problems, with arbitrary 3-D geometry capability [9]. Pointwise energy dependent cross-sections are available for a large selection of isotopes for energies up to 20 MeV and for a smaller subset up to 150 MeV. The code has been developed at Los Alamos National Laboratory and is distributed by the Radiation Safety Information Computational Center at Oak Ridge National Laboratory (ORNL). MCNPX stands for Monte-Carlo N-Particle eXtended, it extends the capabilities of MCNP to nearly all particles, nearly all energies, and to nearly all applications without major computational time penalty. The combination of available data libraries as well as reaction models is used in this case.

The code can be used to calculate particle fluxes, reaction rates, and eigenvalues for critical assemblies and pulse heights for energy deposited in selected regions of space. To assist the users to obtain statistically significant results in reasonable time, several variance reduction techniques are available including phase space truncation (energy and time cut off), geometry splitting and modified sampling techniques. The code is highly parallelised to take advantage of modern multicore, multiprocessors computers to further speedup calculations.

3.2.8. MERSAT

Model for Evaluation of Reactor Safety and Analysis of Thermal-hydraulic (MERSAT) was developed and validated at the Atomic Energy Commission of Syrian Arab Republic [10]. It is a one-dimensional, two-phase fluid dynamic code used primarily for the thermal hydraulic and safety analysis of light-water reactors during transients and loss of flow accidents. The computational model is based on the conservation equations for the steam and water mass, mixture energy and the mixture momentum (four equations). Mechanical non-equilibrium of the two phases is described in the momentum equation using the drift-flux model of Zuber & Findlay. Thermodynamic non-equilibrium of the two phases in the sub-cooled boiling regime is described with a model. MERSAT includes models for various thermohydraulic phenomena covering the wide range of two-phase fluid dynamics. The heat conduction and heat transfer package describes a wide range of two phase flow conditions that enable flexible simulation of fuel rods and other solid structures. The nuclear heat generation is calculated by point-kinetics. The code includes basic control components for modelling special hydrodynamic components like fill, leak, time-dependent volume etc.

3.2.9. MTRCR

MTRCR is a simplified calculation model based on the commercial code Engineering Equation Solver (EES). MTRCR permits only steady-state thermal-hydraulics analysis. It allows also the analysis of fuel assembly parallel channels with different cooling flow and/or geometry. MTRCR is based on a set of balance equations of heat flux combined with correlations to calculate heat transfer coefficients. In the single-phase turbulent forced convection, the Dittus-Boelter correlation is applied (Umbehaun et al., 2012).

3.2.10. MTR-PC

MTR-PC is a system of computer codes based on deterministic methods developed to perform neutronic, thermal-hydraulic and shielding calculations of MTR-type reactors on personal computers. The MTR-PC code system has a complete set of programmes to perform calculations, manage data and plot results Ref. [11]. The system offers the following capabilities: steady-state neutronic and thermal-hydraulic calculations; time-dependent and burnup-dependent calculations; perturbation calculations (kinetic parameters); fuel management; control rod plate position calculations; transient calculations and calculation of shielding against gamma radiation. The capabilities benchmarked as part of this study were restricted to steady-state neutronic, time and burnup dependent calculations, kinetic parameters, control plate position and fuel management.

The two main codes utilized within MTR-PC were CONDOR and CITVAP. CONDOR is used in the preparation of multigroup cross-sections from cell calculations for fuel and other regions of interest. It solves the transport equation in two-dimensions, using collision probability method for regular slab or fuel rod cluster geometry and heterogeneous response method for general geometry. It incorporates its own nuclear data library (P0 and P1 cross sections, resonance parameters and burn-up information). Among other things it is used to obtain microscopic and macroscopic cross sections by collapsing and homogenising the cross-sections into typically a 3 to 10 group library which are used as input data for the core calculation code CITVAP. In addition, it allows calculation of the isotopic concentration as a function of the burnup.

CITVAP is a modified version of the CITATION-II [12] code for reactor calculations. It solves 1, 2 and 3 dimensional multigroup diffusion problems in rectangular, cylindrical, triangular or hexagonal geometries. Nuclear data can be provided as microscopic or macroscopic cross-section libraries and burnup dependent calculations can be performed. The code provides a simple user interface to allow for easy simulation of fuel replacement, control rod movement and changes in core state to address various operational requirements. Searches can be made for critical control rod configurations or eigenvalues.

3.2.11. MVP

MVP is a general purpose continuous-energy Monte Carlo code for neutron and photon transport calculations, developed at JAEA. Amongst the features of MVP are: i) flexible geometry description capability, ii) vectorization and parallelization, iii) multiple lattice capability, iv) periodic boundary conditions, and v) continuous energy calculations.

3.2.12. OSCAR-4

Overall System for Calculation of Reactors-4 (OSCAR-4) is the latest version of the OSCAR code system [13]. OSCAR-4 employs the traditional deterministic calculation path, hence utilizing transport solvers for spatial homogenization and spectral condensation and then full core nodal diffusion solutions for the global problem.

Collision probability based transport methods are utilized to generate few-group assembly homogenized equivalence parameters for each assembly type within the reactor core. Few-group equivalence parameters include node-averaged cross-sections, discontinuity factors at the assembly boundaries and flux/power form functions to allow the reconstruction of heterogeneous detail during the full core global diffusion calculation. Generated equivalence parameters are then parameterized against selected state parameters, in this case using burn-up,

fuel temperature, moderator temperature, and moderator density. Few-group parameters are then represented using a second order polynomial basis.

The actual reactor and cycle simulations are performed using a 3D multi-group nodal diffusion solver utilizing the multi-group analytic nodal method. The core solver further includes a microscopic depletion module utilizing a predictor-corrector scheme for quasi-static cycle depletion.

3.2.13. PARET-ANL

Programme for the Analysis of REactor Transients (PARET-ANL) was originally developed at Idaho National Engineering Laboratory (INEL) and later improved at Argonne National Laboratory (ANL). It is a widely used calculation tool for coupled neutronic, thermal-hydraulic simulations in research reactors. The code employs one-dimensional hydrodynamics, one-dimensional heat transfer and point kinetics with continuous reactivity feedback. A simplified void fraction model is included to estimate the void produced by sub-cooled boiling. The heat transfer coefficient required for predicting the wall temperature along the fuel plate is calculated using a set of constitutive equations for two phase flow. In the single-phase forced coolant convection turbulent regime, the Dittus-Boelter correlation is used. The Rosenthal-Miller correlation is used for both forced and natural convection cooling if this value is larger than the original heat transfer coefficient for laminar flow (i.e., $Re < 2000$) and if this coefficient is larger than that computed for the chosen forced convection correlation (i.e., $Re > 2000$). The Jens-Lottes or McAdams correlations are used to predict the onset of nucleate boiling. Since the single-phase heat transfer coefficient is not valid in two-phase flow regimes, PARET-ANL includes the Bergles-Rohsenow transition boiling model for predicting the wall temperature. The Bergles-Rohsenow correlation computes the wall temperature during the fully developed nucleate boiling regime. The code has been validated against experimental results from power transient tests in small power reactors (the SPERT experimental programme). Comparison with the experimental data showed that the code was generally conservative. The obtained agreement was in the range between 10 to 40% in terms of power, released energy and clad temperature, over a wide range of initial reactor conditions [14].

3.2.14. REBUS

REBUS-PC is a 3D deterministic diffusion-theory code currently supported by ANL as part of the Reduced Enrichment for Research and Test Reactor (RERTR) programme. REBUS-PC is a fuel management code which provides k_{eff} estimates, flux and reaction rate solutions, and tracks fuel depletion Ref. [15]. REBUS-PC version 1.4 (2002) was used for the analysis reported herein.

3.2.15. RELAP

The Reactor Excursion and Leak Analysis Programme (RELAP) is an advanced thermal-hydraulics system code used for the simulation of a wide range of power reactor transients and accidents such as LOCA, loss of flow incidents and reactivity transients. It is based on coupled equations that represent the thermal hydraulic reactor coolant system and neutron kinetics of the reactor core. This computer programme continued the development which began in 1966 with the RELAPSE code, followed by RELAP2, RELAP3, RELAP4 and RELAP5 (Ransom et al., 1982). The principal new feature of the RELAP5 series is the use of a two-fluid, non-equilibrium, non-homogeneous, hydrodynamic model for transient simulation of two-phase system behaviour. The hydrodynamic model is a one-dimensional, transient, two-fluid model

for flow of a two-phase liquid-vapour mixture which can contain non-condensable components in the vapour phase and/or a soluble component in the liquid phase. Eight field equations are solved for eight primary independent variables: pressure, two phases (i.e., one for liquid and one for vapour) specific internal energies, vapour volume (i.e., void) fraction, two phase velocities, non-condensable quality, and soluble component (e.g., boron) density Ref. [16].

The nuclear heat generation is simulated using point kinetics based on separating the power function into space and time functions where the first is assumed to remain constant over time. This approximation is adequate for cases in which the space distribution remains nearly constant. The point reactor kinetics model computes both the prompt fission power and the decay power from fission products. The user can select the decay power model based on either the American Nuclear Society Proposed Standard ANS 5.1, Decay Energy Release Rates Following Shutdown of Uranium-Fuelled Thermal Reactors, revised October 1973, or the American National Standard for Decay Heat Power in Light Water Reactors, ANSI/ANS-5.1-979.

3.2.16. SCALE-6

The ORNL SCALE 6.0 package is well known and frequently used tool, used to perform reactor physics, criticality safety, radiation shielding, and spent fuel characterization for nuclear facilities and transportation/storage package designs. It contains a large number of sub-codes and in particular provides 3D detailed geometry Monte-Carlo transport calculations via the SCALE/KENO module and can also perform perturbation theory calculations [17].

3.2.17. TRIPOLI4

The TRIPOLI4 code is a three-dimensional, continuous energy computer code for particle transport based on the Monte-Carlo method. The code can currently treat separately or simultaneously neutrons, photons, electrons, and positrons. TRIPOLI4 is designed for two major classes of problems, those relating to radiation shielding and those relating to core neutronics. Radiation shielding problems deal with particle propagation over long distances with many orders of magnitude of flux attenuation. These arise with sources in non-multiplying media, in steady-state and time-dependent conditions. Neutronics problems relate to the behaviour of particles in multiplying media. The system can be either critical or sub-critical, with or without fixed sources, in steady-state conditions. More information on the code and its capabilities can be found in the code manual [18].

3.2.18. WIMS-ANL

Winfrith Improved Multigroup Scheme (WIMS) is the ANL version of the widely used WIMS deterministic transport-theory code for lattice cell physics analysis Ref. [19]. WIMS-ANL, based on the WIMS-D4 version of the code, is supported by the RERTR programme at ANL and is a standard code for research reactors. The code has capability for writing burnup-dependent ISOTXS cross sections and 1-D slab, annular and super-cell geometry options, and now includes both the traditional 69-group as well as a 172-group ENDFB-VI based data library. WIMS-ANL Version 5.07 (Apr 2004) was used for the analysis reported herein.

3.2.19. Summary of the Computer Codes used in the Coordinated Research Project

Table 3 summarizes the codes used by the participants in the CRP for each benchmark specification including related references.

TABLE 3. CODES USED FOR THE BENCHMARK ANALYSIS DURING THE COORDINATED RESEARCH PROJECT

Benchmark	Participants and Codes Used						
ETRR-2	ARG	EGY	GRE	SAF	SYR		
Steady-State	RELAP5	RELAP5	RELAP5	RELAP5	RELAP5	MERSAT	
Transient	RELAP5	RELAP5	RELAP5	RELAP5	RELAP5	MERSAT	
IEA-R1	ARG	BGD	BRZ	GRE	ROK	ROM	SYR
Steady-State	RELAP5	COOLOD-N2	PARET-ANL MTRCR	RELAP	RELAP	CATHARE	RELAP MERSAT
Loss of Flow Accident	RELAP5	N/A	N/A	RELAP	RELAP	CATHARE	RELAP MERSAT
MNR	ARG	CAN	SAF				
	CONDOR	WIMS-ANL	OSCAR-4				
	CITVAP	REBUS-PC MCNP5					
OPAL	ARG	AUL	ROK	SAF			
	CITVAP	CITVAP	McCARD	OSCAR-4			
	MCNP			CUCGP MCNP			
RSG-GAS	ARG	EGY	GRE	SYR			
Steady-State	RELAP5	RELAP5	RELAP5	RELAP5	RELAP5	MERSAT	
Transient	RELAP5	RELAP5	RELAP5	RELAP5	RELAP5	MERSAT	
SPERT III	ROM	USA					
	MCNP5	MCNP5					
	WIMSD5B	PARET-ANL					
	CATHARE-2						
SPERT IV	AUL	BGD	FRA-CEA	FRA-IRSN	GRE	PAK	SYR
Steady-State	MCNP5	MVP	TRIPOLI-4	SCALE-6.0	N/A	MTR-PC	MCNP-4C
Transient	PARET-ANL	EUREKA-2	CATHARE-2	ASTEC	PARET-ANL	PARET-ANL	RELAP5 MERSAT

3.3. CONSOLIDATED RESULTS OF THE BENCHMARK ANALYSIS

The following sections highlight the most relevant issues related to the benchmark specifications, code applicability, modelling considerations and major results, including user effects, for eight benchmark specifications. Further details are available in the corresponding Annexes.

3.3.1. ETRR-2

Five sets of results were provided for the ETRR-2 benchmark specifications using the RELAP5 and MERSAT codes.

The ETRR-2 experiment data is generally well-documented. For the scope of this CRP, only the thermal-hydraulic data has been analysed.

The model estimations for the temperature and the transient behaviour throughout the transient course showed that the 1-D codes used can provide satisfactory predictions in cases when forced flow prevails. During natural circulation conditions, the 1-D codes give results that tend to deviate significantly from the experimental values. It may be inferred that in regions where significant 3-D effects exist, the 1-D models are of limited applicability and accuracy. However, in this case the calculated parameters were always conservative, i.e., on the ‘safe side’, as far as safety analysis is concerned.

This benchmark had noticeable user effects. Differences were noted in the flapper valve treatment, nodalization schemes used, fuel and cladding thermal properties and pump coast-down flow characteristics. Substantial user effects were also noted in the assessment of the natural convection regime for the same experimental data.

3.3.2. IEA-R1

The benchmark specifications are of a good quality, but a number of reasons exist that some of the input parameters lack of precise definition such as the thermocouple mounting technique or placement and response time to changes in the clad temperature. Specifically, the mounting of the thermocouples to the cladding provided data that was not representative of the clad temperature; they were not welded to the clad, and therefore most probably gave a temperature somewhere between the coolant and clad temperatures.

For the temperature range in the benchmark data, the codes give satisfactory results. The predicted evolution of coolant and cladding temperatures follow in general the overall trend of the measurements. However, the predicted clad temperature peaks are higher than measured, which may be a result of the issue regarding mounting of the thermocouples to the cladding, described above. Also, the time occurrences of the peak temperatures are generally earlier than the experimental results, but this could again be due to the mounting of the thermocouples. Temperature predictions (coolant and cladding) have much faster gradients than the measurement during a Loss of Flow Accident (LOFA). It is clear that there is room for improvement in all the models used in the benchmark. At the same time, in order to validate any such changes, the uncertainties in the experimental data mentioned above need to be carefully considered and re-examined.

It was found that it is possible to evaluate the user effect on this benchmark due to overlapping code usage. There was a clear user effect found in the case of RELAP usage as several models predicted significantly different times for flow reversal and peak transient temperature. The

differences in the model output can be attributed to several sources, including different input data, modelling assumptions and user choices about how to use the code (e.g., forcing operations within the code instead of allowing the code to operate without interruption).

From this exercise, it was concluded that benchmarking studies need to use standardized/unique initial conditions and assumptions in order to eliminate discrepancies in various models of the same benchmark data other than those caused by differences in the models themselves. Limited efforts were made to standardize the input parameters in this benchmark, the result of which is visible in the spread of the results obtained.

3.3.3. MNR

The experiments that comprise the MNR benchmark specification are based on standard operational measurements for an open-pool MTR-type research reactor and represent typical or routine neutronic simulation problems.

It is noteworthy that significant amount of interpretation is needed in the processing of some of the provided experimental data. Corresponding comparisons presented in this report are of qualitative value and may not be appropriate for code validation. For example, the calculated initial core number densities were supplied by the data provider as this is a benchmark on a burned core, so the experimental data for the control rod worth experiments had to be processed to some extent before being used for benchmarking. The data for the control rod worth experiment remains suitable for individual benchmark analysis.

The results showed that nodal diffusion theory, finite-difference diffusion theory, and explicit-geometry continuous-energy Monte Carlo models can all be used to accurately model such irradiation experiments.

The quality and extent of the experimental data and the limited participation in this benchmark analysis are not sufficient to evaluate the different modelling approaches apart from having identified a user effect due to modelling details of structural and reflector zones, and in the geometrical details of experimental equipment.

3.3.4. OPAL

The benchmark data describes a commissioning core with relatively low uncertainties in material distribution. The reactor was commissioned in 2006 and hence advanced methods were used to collect the experimental data. Furthermore, the described facility represents a multipurpose research reactor design with challenging modelling issues such as burnable absorbers, heavy water reflector and numerous ex-core facilities (e.g., cold neutron source, beam tubes and irradiation channels).

Research reactors with similar design are already planned. The OPAL benchmark specifications provide a relevant benchmark for designing the facility and to support its commissioning. In this context, the OPAL team was encouraged to collect and disseminate additional data in the future.

This benchmark included a variety of codes and methods spanning deterministic (full core transport and diffusion) and stochastic (Monte Carlo) approaches. Most of the calculated and measured results agreed well with no significant unresolved discrepancies. Those observed are

probably at the level of code convergence and cross-section library effects and resolution of these would require further sensitivity analyses.

No significant user effects were observed when different CRP participants used the same code.

3.3.5. RSG-GAS

In general, the experimental data is suitable for benchmarking codes for a loss of flow transient with flow reversal. Participants identified a need for clarification of the positions of the thermocouples and all models used a common interpretation of the positions. This interpretation was added to the benchmark specification as an addendum. Other uncertainties in the input parameters (for example, flow scram set point, fuel thermal conductivity and cladding thermal conductivity) had a minimal effect on model benchmarks for this particular transient. Similar uncertainties could be significant for more rapid or severe transients.

In general, the transient model predictions exhibit similar behaviour despite the differences among the codes, choice of input parameters and models. The small discrepancies observed between the model predictions and experimental measurements can be attributed to different interpretations and assumptions made by the modelling groups about issues such as transient sequence and flapper valve opening time, among others).

There were small user effects caused by different input parameters and model assumptions. In particular, the effects were magnified in the natural convection regime, where the models used different assumptions for operation of the flapper valve.

3.3.6. SPERT III

The SPERT III experiment data is well-documented and extensive. There is enough design information in text, photographs, and diagrams to enable a reasonably complete reconstruction of this 1965 SPERT III E-Core test series. Details of transient rod and control rod configuration at the junction between absorber and follower are not clear. This uncertainty affects predicted axial power shapes and reactivity.

The benchmark analysis was intended to provide fundamental experimental data to support licensing of PWRs and does not represent typical research reactor configurations. The benchmark analysis describes reactivity transients that range from mild to severe.

The results typically show that the codes and models give conservative predictions of peak power. Trends in peak power, energy release and peak clad temperature vs. reactivity insertion succeed in capturing the physical phenomena.

There are significant uncertainties in measured reactivity insertion that have a very large effect on computed results. It is recommended that future analysts fit reactivity to measured period rather than use quoted inferred reactivity in dollars.

Space-dependent feedback coefficients were not used in this work and could be included in the modelling methods to better predict the peak power measured in the benchmark analysis.

Given that only two CRP participants provided models of the SPERT III experiment, no conclusion was made regarding user effects.

3.3.7. SPERT IV Static

The SPERT IV experiment data is well-documented and extensive. Experimental data includes flux measurements, control rod calibrations, feedback coefficients and kinetic parameters. There is enough design information in the text, photographs, and diagrams to enable a reasonably complete reconstruction of the SPERT IV static tests. Details of control rod junction design and placement of void plates are not well specified.

The comprehensive data covers a variety of core configurations and therefore can be very useful to support the validation of neutronic codes and models.

In general, both stochastic and deterministic codes were well suited to the range of experiments and provided good agreement with the benchmark data. In particular, agreement was observed for core flux distribution with most values within 10%. Relative values and features such as peaks and troughs were generally well predicted. However, prediction of cadmium ratios proves to be a difficult problem.

Some limitations were noted for Monte Carlo simulations of small reactivity changes, such as the temperature coefficient of the system over small temperature ranges, where the statistical uncertainty and convergence of the Monte Carlo calculations requires many histories.

The modelling difference of most relevance to the comparison of the simulation results are the approximations/assumptions adopted by each participating group with respect to the absorber rod tapering.

No systematic user effects were notable among the various Monte Carlo codes utilized.

3.3.8. SPERT IV Transient

The SPERT IV transient experiment data is well-documented and extensive. Experimental data includes power, reactivity and temperature measurements. There is enough design information in the text, photographs, and diagrams to enable a reasonably complete reconstruction of the SPERT IV transient tests. However, the reactivity insertion times were not well specified.

The comprehensive benchmark data covers a variety of reactivity insertions for a range of flow conditions and regimes, and therefore can be very useful to support the validation of thermal hydraulic codes and models.

The codes reasonably predict the behaviour of reactivity transients for all but the most severe events (large reactivity insertion over a short time period), where the predictions vary widely in the peak power and clad temperatures. Extreme temperature predictions result from codes predicting film boiling while the benchmark data does not indicate that this phenomenon occurred in any of the experiments.

User effects are particularly noticeable in this benchmark and are prevalent in the choice of heat transfer correlations used in the models. This can be qualitatively seen in the spread of the results from the models using the same code.

4. CONCLUSIONS OF THE COORDINATED RESEARCH PROJECT

Performing calculations of coupled neutronics and thermal-hydraulics transients is one of the most challenging tasks. Based on the experience from this CRP, the following have been confirmed to influence the results of the modelling process:

- Identifying the purpose of the analysis, for example whether it is for safety analysis or reproducing experimental data, i.e. benchmarking;
- Determining of the scope of the analysis, in particular when modelling important physical phenomena;
- Selecting an appropriate set of tools (i.e. codes) for the analysis;
- Obtaining high quality benchmark data;
- Building appropriate models within the chosen codes;
- Understanding the limitation of the code to represent the physical phenomenon under consideration;
- Identifying issues with the models and codes that require further development.

During this CRP, there were successes and failures in predicting specific measured reactor performance data which showed ‘user effects’, where the same class of models or the same class of codes, was used by participating CSIs.

The work done during the CRP showed that tracking thermal-hydraulic phenomena adequately through a research reactor operating in transient mode is not a simple task. For example, selection of the most applicable thermal-hydraulic correlations for heat transfer, for onset of nucleate boiling, and for critical heat flux has a large effect on the quality of the predicted results.

It has been also shown that modelling complexity and computational efforts are to be commensurated to the expected outcome and observed effects. The choice of a complete set of codes and models is to be done carefully and need to be detailed enough to represent the phenomena that emerge from the modelled experimental configuration.

4.1. THE BENCHMARK SPECIFICATIONS

The set of benchmarks provided a wide range in quality and complexity and address the relevant steady state and transient phenomena prevalent in modelling both the operating regimes and safety cases of research reactors. Benchmarks such as SPERT III and SPERT IV represent custom designed experimental installations, while benchmarks such as OPAL, MNR and ETRR-2 describe measurements representative of what is available from typical operating research reactors today. In some cases, experimental data was not complete and interpretation by participants was needed.

For benchmark analysis standardized initial conditions and assumptions and complete data is used in order to eliminate or minimize discrepancies in various models of the same benchmark data other than those caused by differences in the models themselves. Challenges that were identified during the CRP included a lack of uncertainty data for some measurements, incomplete design information and inconsistency in specified data.

The judgment on the quality of a benchmark is only possible after code users have attempted to model the data. The modelling process highlighted gaps or deficiencies in the specificity of the data that can have significant effect on the results.

Based on analysis of the benchmark specifications within this CRP, Table 4 provides potential code users with an indication of the usefulness of the benchmark analysis for different purposes. The heading ‘Introductory Modelling Experience’ means that the benchmark specification has simpler aspects that can be modeled to provide initial familiarity with the general features of codes and models for research reactor analysis. The heading ‘Advanced Modelling Experience’ means that the benchmark specification includes some aspects that may require more advanced approaches or reveal more detailed features of the codes and, therefore, may require more experience in interpretation of the benchmark data. This heading also applies to benchmark specifications that could assist users in developing their own models and tools of research reactors. The heading ‘Validation Support’ means that the benchmark specifications are of sufficient quality that they can be used to support code validation.

TABLE 4. BENCHMARK SPECIFICATIONS AND THEIR USEFULNESS FOR VARIOUS APPLICATIONS

Facility	Introductory Modelling Experience	Advanced Modelling Experience	Validation Support
ETRR-2	Yes	Yes	
IEA-R1		Yes	
MNR		Yes	
OPAL	Yes	Yes	Yes
RSG-GAS	Yes	Yes	
SPERT III		Yes	Yes
SPERT IV Static		Yes	Yes
SPERT IV Transient		Yes	Yes

4.2. MODELLING APPROACH AND USER EFFECTS

The Annex I through VIII describe the models and tools used by the participants of this CRP. The individual phases of modelling that were highlighted by the participants include:

- Conversion from an engineering model to a computational model;
- Selection of the physics models and numerical techniques to be utilized by the codes;
- Interpretation of the benchmark data and adoption of plausible inputs where data is not available or incompletely specified.

In some cases, different assumptions were made in each of these phases, as described in the Annexes, which led to discrepancies of the obtained results. In particular, in cases where the same code was utilized for the same experiment, some discrepancies in results could be easily linked to differences in input parameters – ‘user effects.’

In many cases a clear user effect indicates that modelling choices may have a significant impact on the results. Efforts were made during this CRP to identify the source of discrepancies, as described in Annexes I through VIII. In these cases, sensitivity analyses are required to fully characterize the user effects and make informed choices for poorly defined parameters.

Specific physical phenomena have been identified as primary contributors to such discrepancies. Noticeable examples of this can be seen when analysing results of IEA-R1 and SPERT IV, where user effects were large and for RSG-GAS where user effects had minor significance. For example, some thermal-hydraulic codes require the user to select appropriate parameters, such as heat transfer correlations for the transient regime that were shown to have

a significant effect on the results. In this case, the user needs to be aware of the various physical models available and their relevance to the problem under consideration.

4.3. COMPUTER CODES USED AND RESULTS

The work within this CRP covered a wide range of codes and models, ranging from various levels of detail and innovation. The results of benchmarks allow quantification of accuracy and capability of this spectrum of approaches to be evaluated by future users.

Research reactor analysis are typically performed first by using simple models and then by adopting more complex models. Based on the experience from this CRP, the typical approach to modelling research reactor transients is to employ point kinetics to couple the neutronics and thermal-hydraulics portions of the model. In several cases, prediction of various transients with desirable accuracy remains challenging both in terms of physics models and modelling methodology. In this context, an attempt has to be made to apply fully-coupled 3-D neutronics and thermal-hydraulic codes to determine if they would provide significant improvement to the benchmarks (e.g. SPERT III and SPERT IV).

Based on the experience from this CRP, available neutronics codes can predict steady-state reactor characteristic with satisfactory accuracy. This is evident in the benchmarks that nodal diffusion theory, finite-difference diffusion theory, explicit-geometry continuous-energy Monte Carlo and full-core transport models can accurately model most of the irradiation experiments. On the other hand, different codes might be useful or necessary to check for consistency between methods and models.

In this CRP, advanced approaches (both with respect to code capability and modelling) were covered and documented. In this regard, see Annexes describing ETRR-2, OPAL and SPERT IV benchmarks.

In conclusion, the research reactor community has a wide selection of potential analysis tools which have the capability of representing relevant physical phenomena to a required accuracy. Many of these tools are evolutionary, having been developed over decades for nuclear power plants and not specifically targeting research reactors. Therefore, significant room for development exists when considering state-of-the-art capabilities. In this context, the CRP has provided a unique experimental database that is useful to support validation of existing and development of new codes for research reactor analysis. Documentation of this experience provides invaluable information to research reactor designers, operators, regulators and experimenters.

REFERENCES

- [1] INTERNATIONAL ATOMIC ENERGY AGENCY, Research Reactor Benchmarking Database: Facility Specification and Experimental Data, Technical Reports Series No. 480, IAEA, Vienna (2015).
- [2] VAN DORSSELAERE, J., P., SERPIAN, C., CHATELARD, P., JACQ, F., FLEUROT, J., GIORDANO, P., REINKE, N., LUTHER, W., The ASTEC integral code for severe accident simulation, *Nuclear Technology* **165** (2009) 293-307.
- [3] EYMARD, C., CATHARE2 V2. 5 User Manual, SSTH/LDAS/EM/2004-040, CEA, Grenoble, France (2005).
- [4] KAMINAGA, M., COOLOD-N2: A Computer Code for the analyses of Steady State Thermal Hydraulics in Research Reactors, JAERI-M-94-052, Japan (1994).
- [5] MASANORI, K., EUREKA-2/RR: A Computer Code for the Reactivity Accident Analyses in Research Reactors, Japan Atomic Energy Agency (1996).
- [6] SHIM, H.J., KIM, C.H., McCARD, Monte Carlo Code for Advanced Reactor Design and Analysis, User's Manual, Version 1.1, McCARD manual, Monte Carlo Laboratory, Seoul National University (2011).
- [7] SHIM, H.J., McCARD Criticality Benchmark Calculations, SNUMCL/TR001/2011(01), Monte Carlo Laboratory, Seoul National University (2011).
- [8] MACFARLANE R. E., MUIR D. W., The NJOY Data Processing System version 91, LA-12740-M, Los Alamos National Laboratory (1994).
- [9] BRIESMEISTER, J.F., MCNP—A General Monte Carlo N-Particle Transport Code 276 (Version C). Oak Ridge National Lab, (1997).
- [10] HAINOUN, A., GHAZI, N., ALHABIT, F., Simulation of LOFA and RIA for the IEA-R1 Research Reactor using the code MERSAT, *Ann. of Nuclear Energy* **35** (2008) 2093–2104.
- [11] MOCHI, I., INVAP's Nuclear Calculation System, Science and Technology of Nuclear Installations, (2011).
- [12] FOWLER, T. B., VONDY, D. R., CUNNINGHAM, G. W., Nuclear Reactor Core Analyses Code CITATION, ORNL – TM – 2496 Rev. 2 (1971).
- [13] STANDER, G., ET AL., OSCAR-4 Code System Application to SAFARI-1 Reactor, International Conference on Reactor Physics, Nuclear Power: A Sustainable Resource, (2008).
- [14] CHATZIDAKIS, S., IKONOMOPOULOS, A., DAY, S.E., PARENT-ANL modelling of a SPERT IV experiment under different departure from nucleate boiling correlations, *Nuclear Technology* **177** (2012) 119.
- [15] OLSON, A.P., A User's Guide for the REBUS-PC Code, Version 1.4, Argonne National Laboratory, December (2001).
- [16] NUCLEAR REGULATORY COMMISSION, RELAP5/MOD3.3 Code Manuals, Idaho National Engineering Laboratory, NUREG/CR-5535 (1995).
- [17] SCALE: A Modular Code System for Performing Standardized Computer Analyses for Licensing Evaluation, ORNL/TM-2005/39, Version 6, Vols. I–III, Oak Ridge National Laboratory, Oak Ridge (2009).
- [18] TRIPOLI-4 Version 7 USER GUIDE –SERMA/LTSD/RT/10-4941/A - Rapport DM2S – Notice d'utilisation du code TRIPOLI4
- [19] DEEN, J.R., WOODRUFF, W.L., COSTESCU, C.I., LEOPANDO L.S., WIMS-ANL User Manual, Rev. 6, Argonne National Laboratory, ANL/TD/TM99-07, February (2004).

ANNEX I

BENCHMARK CONSOLIDATED RESULTS AGAINST EXPERIMENTAL DATA FROM ETRR-2

A. HAINOUN*, N. GHAZI*, F. ALHABIT*, A. DOVAL**, F. FRANCONI**, S. CHATZIDAKIS***, A. IKONOMOPOULOS***, R. PRINSLOO+, B. ERASMUS+, F. VAN HEERDEN+, M. BELAL+, K. ELSAKHAWY+, I.D. ABDELRAZEK++, E.H. AMIN++, M. GAHEEN++, A. GAMAL++

*Atomic Energy Commission of Syria (AECS), Nuclear Engineering Department, P.O. Box 6091, Damascus, Syrian Arab Republic

**Nuclear Engineering Department, Av. Cmdt. Luis Piedrabuena 4950, C.P. 8400, S.C de Bariloche, Rio Negro, Argentina

***Institute of Nuclear Technology and Radiation Protection, National Center for Scientific Research ‘Demokritos’, 15130, Athens, Greece

+Necsa, Pelindaba, Church Street Extension West, Pretoria-West, Pretoria, South Africa, 0001

++ETRR-2, Egyptian Atomic Energy Authority

Annex Consolidator: S. Chatzidakis

Abstract

The IAEA CRP No. 1496 on ‘Benchmarking, against Experimental Data, of the Neutronic and Thermal-hydraulic Computational Methods and Tools for Operation and Safety Analysis for Research Reactors’ provides a novel opportunity to benchmark and compare the accuracy and efficiency of both off-the-shelf and locally developed computational tools to a wide set of experimental research reactor benchmark analysis. In the scope of this project, various analysis groups have evaluated the ETRR-2 benchmark analysis – consisting of steady state, loss of flow and negative reactivity insertion transient measurements. This report summarizes and compares the analysis methodologies adopted, the code systems employed, and the simulation results generated by the different analysis groups. A comparison of the computational results to supplied experimental results is also provided in this report.

I-1. FOREWORD

The ETRR-2 benchmark analysis is documented in Ref. [I-1] and is divided into two sections: (i) steady state measurements, and (ii) transient measurements (loss of flow and negative reactivity insertion). The participation for this benchmark is summarized in the following table.

TABLE I-1. ETRR-2 BENCHMARK ANALYSIS PARTICIPANTS

Group	Steady state	Transient
ARG	Yes	Yes
EGY	Yes	Yes
GRE	Yes	Yes
SAF	Yes	Yes
SYR	Yes	Yes

The consolidation report includes results related to the benchmark analysis associated with more than one submission. As such, the negative reactivity insertion transient is not described herein. Details on the individual results for the ETRR-2 benchmark analysis can be found in the individual participant reports.

I-2. DESCRIPTION OF TOOLS, CODES AND METHODS

A short description of the code combinations and tools used by each group is given in Table I-2 and in the following sections.

TABLE I-2. CODES USED BY PARTICIPATING GROUPS

Group	Steady State	Transient
ARG	RELAP5/MOD3.2	RELAP5/MOD3.2
EGY	RELAP5/MOD3.4	RELAP5/MOD3.4
GRE	RELAP5/MOD3.3	RELAP5/MOD3.3
SAF	RELAP5/MOD3.3	RELAP5/MOD3.3
SYR	MERSAT RELAP5/MOD3.3	MERSAT RELAP5/MOD3.3

I-2.1. Argentina: Codes, Tools and Methods

Argentina (ARG) employed the RELAP5/MOD3.2 code [I-2] to model the ETRR-2. The core and secondary cooling systems were modelled including the special features required for the transient analysis, such as the flap valves and the inertia flywheels for the pumps of the core cooling system. The two loops of the core cooling system were considered including the corresponding pipes, pumps and heat exchangers while the secondary cooling system was specified in terms of an inlet/outlet flow rate and a heat exchanger to allow the power removal generated in the core. The core was modelled as two different components, one representing the hot channel geometrically equal to a single fuel assembly, and the other one representing the rest of the core, characteristic of an average fuel assembly. The guide boxes, the control plates and the irradiation in-core position were not included in the model.

Both average and hot fuel assemblies were divided axially in five volumes, with a cosine power distribution in the axial direction. The power fractions for this cosine distribution were calculated considering an extrapolated length of 8 cm on each end of the active length. The total core pressure drop was obtained through the use of appropriate inlet and outlet junction loss coefficients.

The junction loss coefficients for the average and hot fuel assemblies were also chosen to obtain a flow rate in the hot fuel assembly equal to one twenty-ninth of the total core flow (i.e., the hot fuel assembly was assigned a flow arising from a uniform distribution in twenty-nine equal fuel assemblies). The chimney above the core was modelled as a pipe component, with a flow area and a hydraulic diameter corresponding to its actual rectangular cross-section. Three segments were used to divide the chimney axially. The lower and middle ones are of equal height and extend from the end of the fuel plates up to the connection of the outlet pipe. The upper segment extends from this connection up to the top of the chimney. The influence in the flow of the upper section of the fuel assemblies is included in the appropriate junction loss coefficient, as above mentioned. The three chimney segments are attached to a heat structure, to model the heat loss to the reactor pool.

of the pool (defined as level 0.0 in the model). In general, the geometrical data (i.e., area and hydraulic diameter) are taken directly from the corresponding connected volumes. Where changes in size take place and data from the smaller components are taken. For the flap valves, the area, the hydraulic diameter and loss coefficients were calculated taking into account the geometry from similar valves. Fig. I-1 shows the diagram of the nodalization used for ETRR-2.

I-2.2. Egypt: Codes, Tools and Methods

Egypt (EGY) employed RELAP5/MOD3.4 code [I-2] to model the ETRR-2. The coolant system nodalization is shown in Fig. I-2. The core was modelled as two different components, one representing the hot channel and geometrically equal to a single fuel assembly, and the other one representing the rest of the core having the characteristics of an average fuel assembly. The guide boxes, the control plates and the in-core irradiation position were not included in the model. The hot channel and the average core channel are divided axially into 21 intervals of equal fuel plate lengths (0.8 m the active zone of the fuel elements) and 6 radial intervals (2 for cladding and 4 for fuel). The axial power is a cosine shape distribution and the fraction of power allotted to the hot fuel assembly was selected to produce a maximum heat flux at the centre volume equal to the maximum allowable heat flux. For a core power of 22 MW, the maximum heat flux is 117 W/cm². The pool and its cooling system are not included in this model.

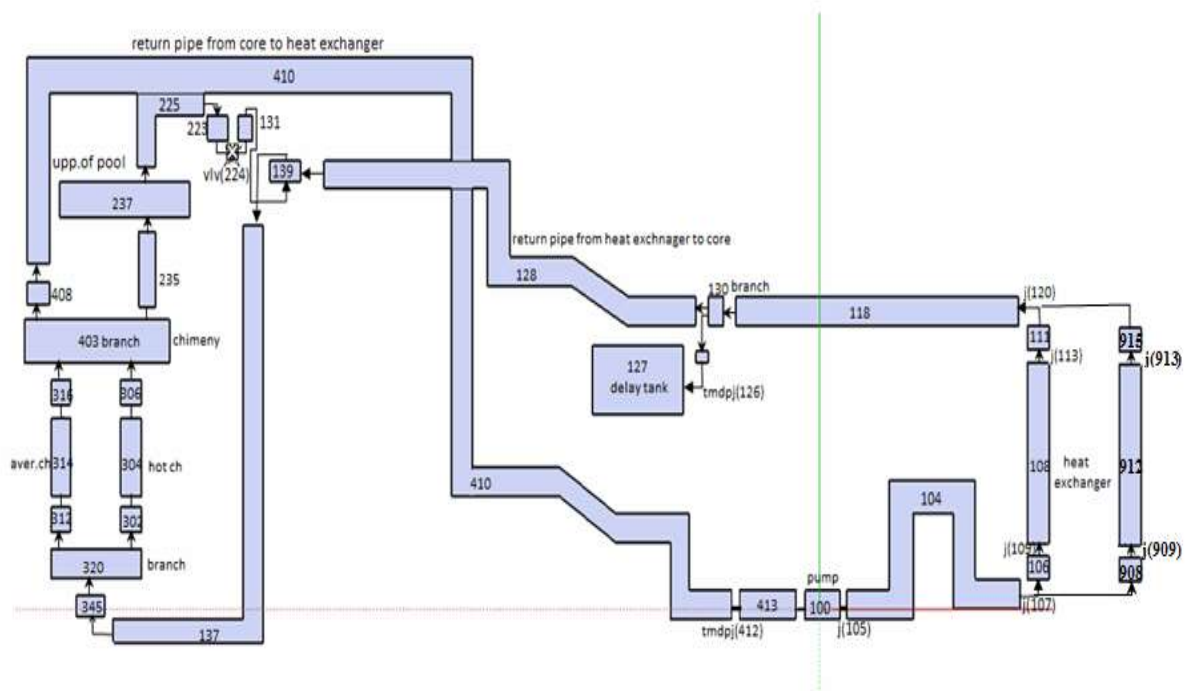


FIG. I-2. EGY nodalization of ETRR-2.

I-2.3. Greece: Codes, Tools and Methods

Greece (GRE) employed the RELAP5/MOD3.3 code [I-2] to model the ETRR-2. The nodalization used for ETRR-2 appears in Fig. I-3. The model includes the core with the associated heat structure, the primary cooling circuit with heat exchangers and piping, and the secondary cooling circuit. In the ETRR-2 case, a uniform discretization of the fuel and clad regions having uniform power profile was considered adequate since the thermocouples are located outside of the core. The core was modeled as a single channel with axial peaking factor

1.0. The reactor power after shutdown (decay heat power) was represented based on ANSI/ANS-5.1-1979. The model parameters (including neutron lifetime and delayed neutron fraction), were set in accordance to the provided reactor specifications, [I-1] while additional details can be found in [I-3].

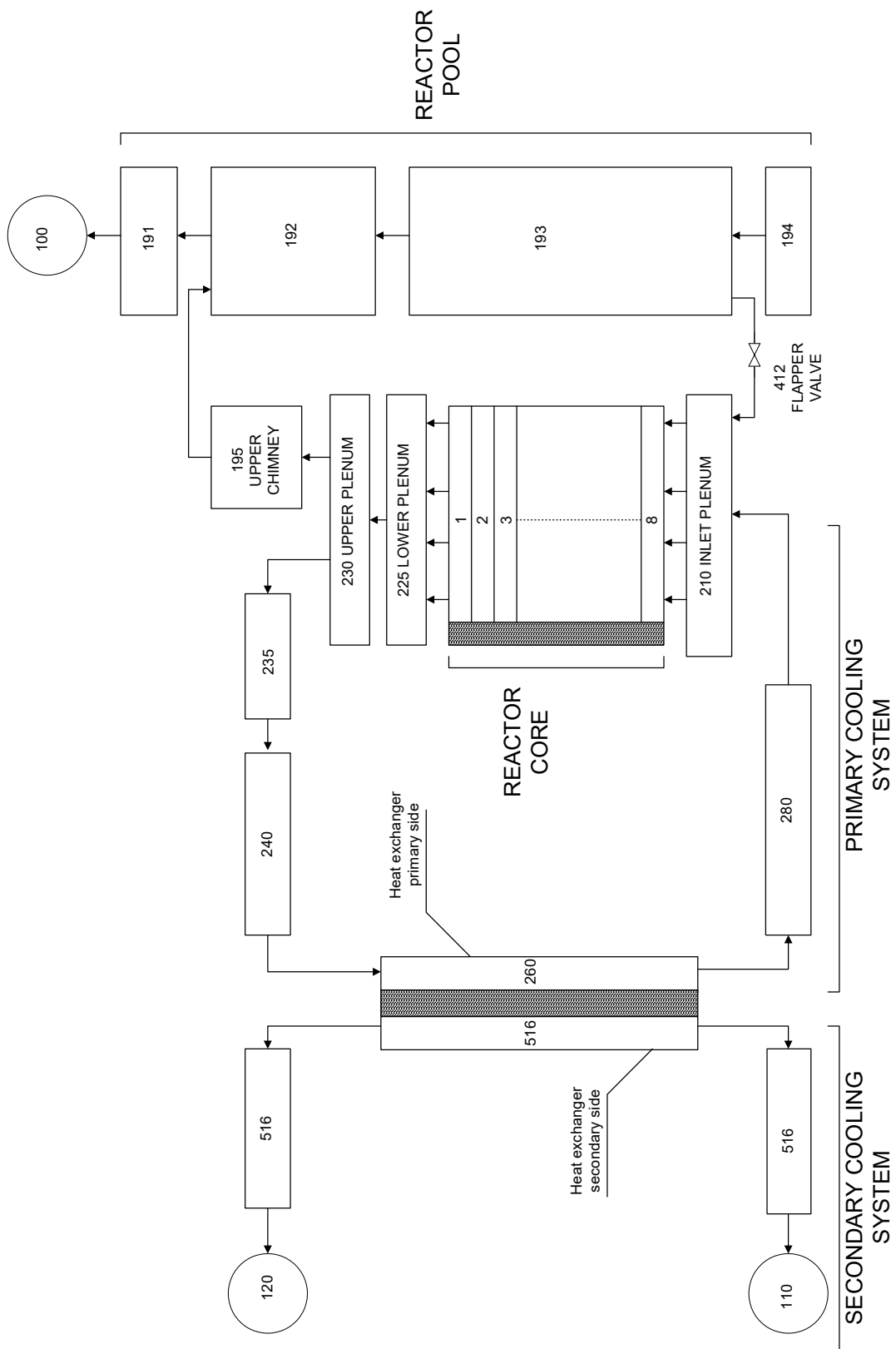


FIG. I-3. GRE nodalization of ETRR-2.

I-2.4. South Africa: Codes, Tools and Methods

South Africa (SAF) employed the RELAP5/MOD3.3 code [I-2] to model ETRR-2. The model includes: the reactor pool, the reactor core, the chimney and the primary and secondary cooling systems. All dimensions and reactor data used was based on the specifications given in [I-1]. In this model, the point kinetics was not included and therefore the negative reactivity insertion experiment was not performed in this work. The reactor power after shutdown (decay heat power) was represented based on ANSI/ANS-5.1-1979. Moreover, assumptions were made due to the lack of data in the benchmark specifications; these assumptions include the flapper valve dimensions and the fuel power profiles. The nodalization of ETRR-2 is shown in Fig. I-4.

The core hydrodynamic model is arranged in four parallel channels, two hot plate channels to separately represent the coolant gaps on either side of the hottest fuel plate in the core. A hot element channel consisting of 18 inter-plate channels (one fuel element excluding the above two hot channels). A balance of core channels comprised of the internal flow paths of 28 fuel elements and all heated flow paths between the elements. All the channels were divided into 10 axial sections. The reactor pool was modeled as annulus around the inlet and outlet plenum and the chimney. It was divided into 20 axial sections (4 volumes above the Chimney, 4 volumes around the chimney, 1 volume around the outlet plenum, 1 volume around the inlet plenum, and 10 volumes around the reactor core). Only nine meters of the pool height was modelled where the rest of the water level was modelled as a boundary condition (time dependent volume) connected to the reactor pool top (modelled).

The reactor chimney was modelled as three branches corresponding to the thermo-couples location in the experiment. Two cooling loops were modelled consisting of the primary pump, the heat exchanger, and the interconnection system and a flapper valve. The flapper valve was modelled as trip valve and the pumps were modelled as time dependent junctions. The secondary cooling circuits were modelled as boundary conditions, with four-time dependent volumes that represent the two cooling loops including each loop inlet and outlet lines.

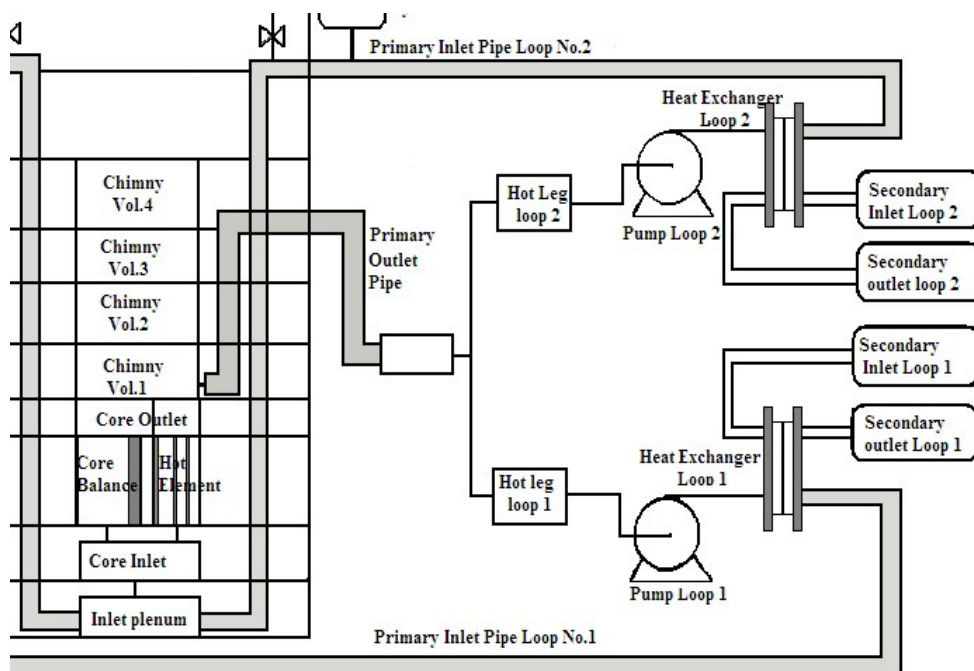


FIG. I-4. SAF nodalization of ETRR-2.

I-2.5. Syrian Arab Republic: Codes, Tools and Methods

Syrian Arab Republic (SYR) employed the MERSAT [I-4] and RELAP5/MOD3.3 [I-2] codes to model ETRR-2. For the benchmark analysis of ETRR2 a complete model for reactor core and cooling system was prepared using the code MERSAT. Fig. I-5 represents the MERSAT nodalization model of ETRR-2. The developed model consists of a full scale primary loop representation and a simplified version of secondary cooling loops. The primary cooling loop consists of reactor core, primary cooling pump, heat exchanger and other auxiliary components. For the secondary cooling loop, the special modelling components ‘fill and leak’ are used to model the flow condition around the secondary side of the heat exchanger. This approach is adequate as the envisaged transients are initiated in the primary loop and have no impact on the cooling behaviour of secondary loop. The core representation consists of three fuel element types of different fuel densities; absorber control plates and bypass channel. In the schematic of Figs. I-3 to 5 each fuel element is denoted by one channel and one fuel plate.

Similar to MERSAT a full-scale mode for ETRR-2 has been developed using the code RELAP5/MOD3.3 as shown in Fig. I-6. The modelling approach and the employed assumptions and simplifications are similar to those applied for MERSAT.

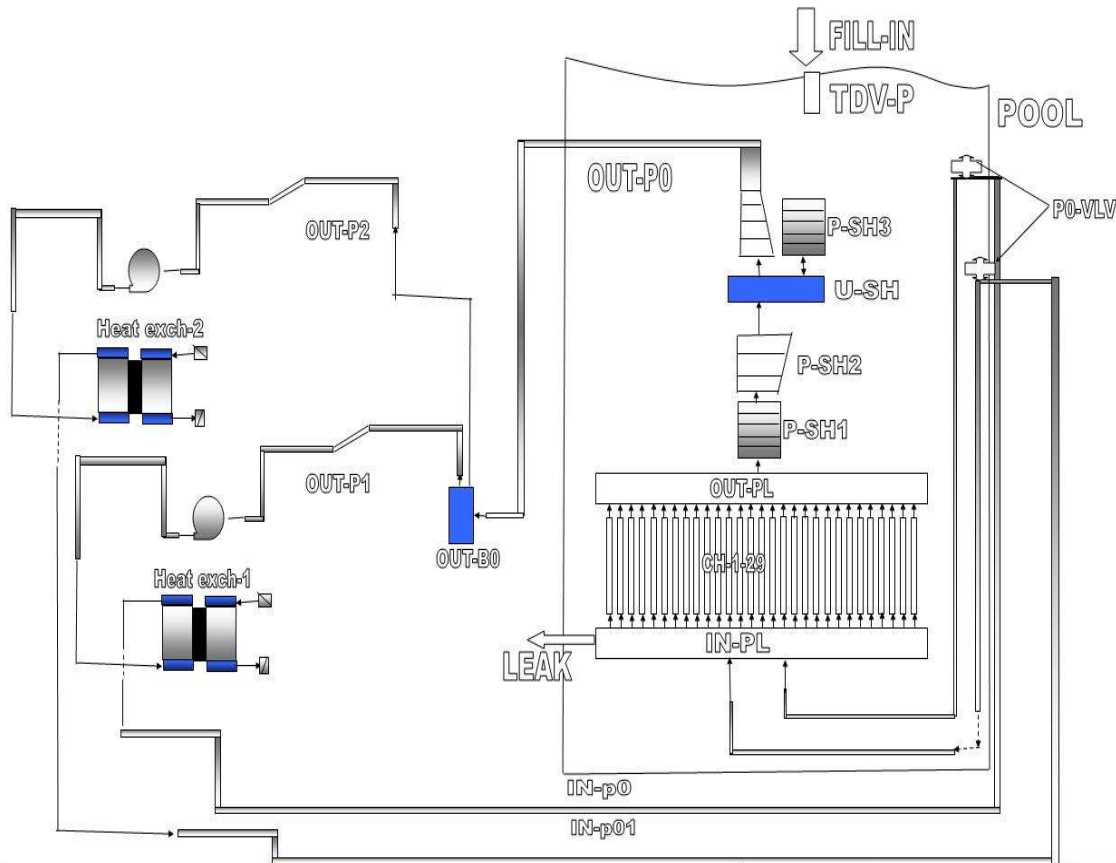


FIG. I-5. SYR nodalization for ETRR-2 using MERSAT.

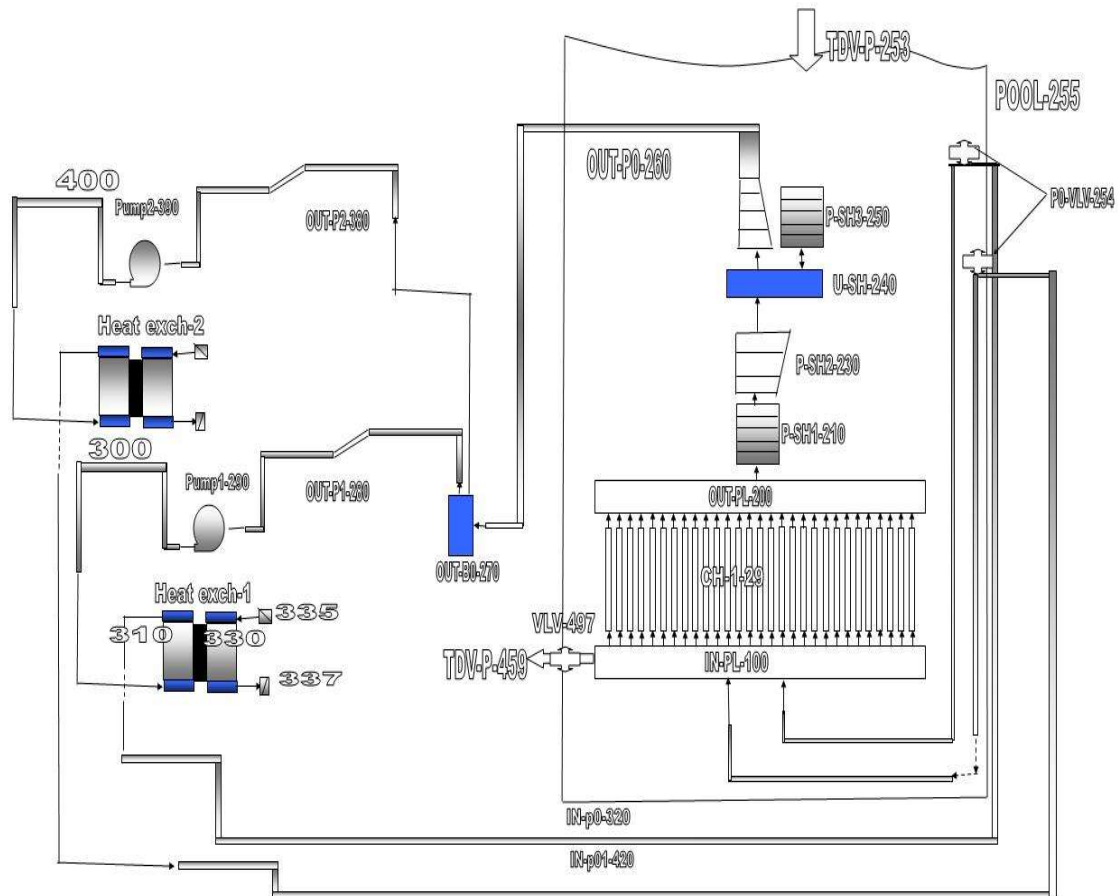


FIG. I-6. SYR nodalization for ETRR-2 using RELAP5.

I-3. DESCRIPTION OF FACILITY AND EXPERIMENTS

The ETRR-2 core is an array of fuel elements, reflectors, absorber rods, gadolinium injection boxes, and irradiation devices. Coolant circulation is accommodated via thirty (30) square-shaped holes housing fuel elements while a chimney installed above the core allows conducting the coolant to the primary system outlet pipe and enables water down-flow from the pool to the circuit. The chimney is open at its upper section to allow core access as well as natural circulation of the coolant in case of reactor shutdown.

The core cooling system consists of two closed loops. The coolant flows through the core in an upward direction removing the heat produced and continues via a plate-type heat exchanger where the heat is transferred to the secondary cooling system. A fraction of the flow rate is diverted to the pool cooling system, via an interconnection system, to establish a downward flow in the upper chimney preventing the activated water from reaching the pool top. During natural circulation all primary pumps are turned off while the two flapper valves are open. The water flow is driven by the density difference among the inlet piping and upper chimney above the core.

Because of the experiment the reactor is equipped with thermocouples installed at different positions inside the chimney and at different heights above the core. Three (3) thermocouples were used during the loss of flow experiment and their locations were at 0.0, 0.5, and 1.5 m above the core top, respectively. More information on the benchmark facility can be found in Ref. [I-1].

I-3.1. Benchmark Experiment

I-3.1.1. Short description of benchmark experiment

The reactor was operated at a range of steady state conditions with different power levels, flow rates, cooling tower outlet temperature (i.e. inlet to the heat exchanger secondary side), and average pool temperature. A loss of flow experiment was performed to measure the temperature profile inside the core upper chimney. The reactor was at a 9.4 MW steady state when a manual scram was triggered. Simultaneously, the core cooling pump and secondary pump were manually tripped. According to the experiment sequence the flapper valve opened 46 seconds later and natural circulation was established. More information on the benchmark experiment can be found in Ref. [I-1].

I-3.1.2. Summary and comparison of benchmark results

The steady state results for a number of locations are shown in Tables I-3 to I-12 and schematically in Figs. I-7 to I-10. The ETRR-2 thermocouple measurements for the loss of flow conditions at different heights above the reactor core along with their estimated temperature values are plotted in Figs. I-11 to I-14. Steady state conditions are followed by pump coast down and an immediate reactor shutdown that caused sudden temperature decrease. As pump coast down continued the temperature above the core increased at a slower rate. However, following the flapper opening the temperature rose faster and as soon as temperature reached roughly 35°C it dropped until it returned to steady state conditions. On the other hand, the numerical simulations calculated that the temperature above the core continued to rise to more than 50°C, contrary to the experimental results illustrating that some of the important physical phenomena occurring during these transients are not properly captured.

It may be stated that the present ETRR-2 models do not take into consideration that the thermocouples are located outside the core but rather treat them as if they were installed inside a fuel channel. This is attributed to the implementation of 1-D models resulting in significant overestimation of the clad temperature rise during the natural convection stage. As long as the 1-D phenomena prevail, such as in the forced convection region, the models yield good agreement with the experimental results. However, when the 3-D phenomena become more important, as in the case of natural convection outside the core, the calculations significantly deviate from the measurements. In all ETRR-2 cases, the model temperature estimations during natural convection are higher and hence from a safety analysis perspective more conservative than the actual measurements.

TABLE I-3. STEADY STATE RESULTS: CORE INLET TEMPERATURE

Case No.	Measured Core inlet (°C)	ARG ¹ Core inlet (°C)	GRE ¹ Core inlet (°C)	EGY ¹ Core inlet (°C)	SYR ¹ Core inlet (°C)	SYR ² Core inlet (°C)	SAF ¹ Core inlet (°C)
1	28.1	28.2	28.1	31.1	28.5	28.6	27.9
2	35.8	35.7	35.7	35.7	36.0	35.9	35.2
3	33.4	34.1	34.1	34.1	33.8	33.5	33.6
4	26.7	27.2	27.0	29.5	27.4	26.7	27.0
5	33.5	34.3	34.3	33.8	34.2	33.7	33.7
6	31.7	32.0	31.9	32.6	32.4	31.8	31.6
7	40.0	40.3	40.1	42.2	40.4	40.2	39.3
8	22.4	22.3	22.2	22.0	-	-	22.5
9	40.7	41.6	41.9	-	40.7	40.7	38.7
10	35.5	36.0	35.7	34.4	35.9	35.4	34.3

1: RELAP5, 2: MERSAT

TABLE I-4. STEADY STATE RESULTS: CORE OUTLET TEMPERATURE

Case No.	Measured Core outlet (°C)	ARG ¹ Core outlet (°C)	GRE ¹ Core outlet (°C)	EGY ¹ Core outlet (°C)	SYR ¹ Core outlet (°C)	SYR ² Core outlet (°C)	SAF ¹ Core outlet (°C)
1	33.2	32.3	32.1	37.1	32.9	32.7	32.0
2	41.3	40.9	40.7	40.1	41.5	41.2	40.3
3	41.8	41.9	41.8	40.8	42.2	41.4	41.5
4	28.6	28.9	28.6	33.0	29.2	28.4	28.7
5	42.3	42.5	42.3	41.2	42.9	42.0	41.9
6	35.8	35.5	35.3	36.1	36.0	35.3	35.0
7	49.3	49.3	49.0	51.9	50.0	49.3	48.4
8	25.1	24.2	24.2	23.6	-	-	24.5
9	47.6	47.4	47.9	-	46.9	46.9	45.0
10	44.8	45.3	44.7	43.7	45.8	44.8	43.2

1: RELAP5, 2: MERSAT

TABLE I-5. STEADY STATE RESULTS: HX1 PRIMARY SIDE INLET

Case No.	Measured	ARG ¹	GRE ¹	EGY ¹	SYR ¹	SYR ²	SAF ¹
	HX1 inlet (°C)	HX1 inlet (°C)	HX1 inlet (°C)	HX1 inlet (°C)	HX1 inlet (°C)	HX1 inlet (°C)	HX1 inlet (°C)
1	32.4	32.2	32.1	37.1	32.8	32.7	31.9
2	41.8	40.7	40.7	40.1	41.3	41.3	39.9
3	41.5	41.7	41.8	40.8	42.0	41.2	40.9
4	28.8	28.9	28.6	33.0	29.3	28.5	28.6
5	41.8	42.3	42.3	41.2	42.7	41.7	41.3
6	35.8	35.4	35.2	36.1	36.0	35.3	34.7
7	49.1	49.1	49.0	51.9	49.9	49.2	47.7
8	24.6	24.2	24.2	23.6	-	-	24.7
9	47.3	47.1	47.9	-	46.9	46.6	43.8
10	45.0	45.0	44.7	43.7	45.5	44.6	42.6

1: RELAP5, 2: MERSAT

TABLE I-6. STEADY STATE RESULTS: HX1 PRIMARY SIDE OUTLET

Case No.	Measured	ARG ¹	GRE ¹	EGY ¹	SYR ¹	SYR ²	SAF ¹
	HX1 outlet (°C)	HX1 outlet (°C)	HX1 outlet (°C)	HX1 outlet (°C)	HX1 outlet (°C)	HX1 outlet (°C)	HX1 outlet (°C)
1	28.4	28.2	28.1	31.1	28.3	28.6	27.9
2	36.9	35.7	35.7	35.7	35.8	35.9	35.2
3	34.0	34.2	34.2	34.1	33.8	33.6	38.3
4	27.3	27.2	27.0	29.5	27.3	26.7	28.0
5	33.9	34.4	34.4	33.8	34.2	33.7	33.7
6	32.6	32.0	31.9	32.6	33.4	31.8	33.6
7	40.7	40.2	40.1	42.2	40.5	40.3	39.3
8	22.6	22.3	22.2	22.1	-	-	21.7
9	41.3	41.6	41.9	-	40.6	40.7	39.1
10	36.5	36.0	35.7	33.0	36.0	35.5	34.6

1: RELAP5, 2: MERSAT

TABLE I-7. STEADY STATE RESULTS: HX1 SECONDARY SIDE INLET

Case No.	Measured HX1 inlet (°C)	ARG ¹ HX1 inlet (°C)	GRE ¹ HX1 inlet (°C)	EGY ¹ HX1 inlet (°C)	SYR ¹ HX1 inlet (°C)	SYR ² HX1 inlet (°C)	SAF ¹ HX1 inlet (°C)
1	23.7	23.6	23.6	24.0	23.2	24.0	23.6
2	30.7	30.7	30.7	31.0	30.3	30.7	31.8
3	26.0	26.4	26.4	26.8	25.8	26.4	28.2
4	25.2	25.2	25.2	25.4	24.8	25.2	25.6
5	25.7	26.1	26.1	25.6	25.6	26.0	27.9
6	28.4	28.4	28.4	28.6	28.3	28.4	29.1
7	31.5	31.7	31.7	32.3	31.5	31.6	33.6
8	20.2	20.0	20.0	20.1	-	-	20.5
9	29.6	29.7	29.7	-	30.1	29.7	32.9
10	26.4	26.4	26.0	20.7	26.3	26.4	27.4

1: RELAP5, 2: MERSAT

TABLE I-8. STEADY STATE RESULTS: HX1 SECONDARY SIDE OUTLET

Case No.	Measured HX1 outlet (°C)	ARG ¹ HX1 outlet (°C)	GRE ¹ HX1 outlet (°C)	EGY ¹ HX1 outlet (°C)	SYR ¹ HX1 outlet (°C)	SYR ² HX1 outlet (°C)	SAF ¹ HX1 outlet (°C)
1	27.4	26.9	26.8	28.5	27.1	27.3	26.9
2	34.6	34.5	34.5	34.0	34.7	34.5	34.2
3	32.3	32.2	32.2	31.4	32.1	32.3	32.1
4	26.4	26.6	26.4	27.9	26.7	26.6	26.5
5	32.1	32.3	32.3	30.8	32.3	32.3	32.1
6	31.0	31.0	31.0	31.1	31.5	31.0	30.8
7	38.3	38.3	38.3	38.6	38.6	38.4	37.9
8	22.0	21.5	21.4	21.2	-	-	21.7
9	40.7	34.9	40.6	-	39.6	40.2	38.1
10	34.3	33.7	33.5	27.8	34.0	33.9	32.3

1: RELAP5, 2: MERSAT

TABLE I-9. STEADY STATE RESULTS: HX2 PRIMARY SIDE INLET

Case No.	Measured HX2 inlet (°C)	ARG ¹ HX2 inlet (°C)	GRE ¹ HX2 inlet (°C)	EGY ¹ HX2 inlet (°C)	SAF ¹ HX2 inlet (°C)
1	32.3	32.2	32.1	37.1	31.9
2	41.9	40.7	40.7	40.1	39.9
3	41.6	41.7	41.8	40.8	40.9
4	29.0	28.9	28.6	33.0	28.6
5	41.9	42.3	42.3	41.2	41.3
6	36.0	35.4	35.3	36.1	34.7
7	49.4	49.1	49.0	51.9	47.7
8	24.5	24.2	24.2	23.6	24.7
9	-	-	-	-	-
10	45.2	45.0	44.7	43.7	42.5

1: RELAP5

TABLE I-10. STEADY STATE RESULTS: HX2 PRIMARY SIDE OUTLET

Case No.	Measured	ARG ¹	GRE ¹	EGY ¹	SAF ¹
	HX2 outlet (°C)	HX2 outlet (°C)	HX2 outlet (°C)	HX2 outlet (°C)	HX2 outlet (°C)
1	28.3	28.2	28.1	31.1	27.9
2	36.8	35.7	35.7	35.7	35.2
3	34.0	34.1	34.1	34.1	38.3
4	27.3	27.2	27.0	29.5	28.1
5	34.1	34.3	34.3	33.8	33.7
6	32.6	32.0	31.9	32.6	32.6
7	40.3	40.2	40.1	42.3	39.4
8	22.6	22.3	22.2	22.0	21.7
9	-	-	-	-	-
10	35.7	36.0	35.6	35.8	34.5

1: RELAP5

TABLE I-11. STEADY STATE RESULTS: HX2 SECONDARY SIDE INLET

Case No.	Measured	ARG ¹	GRE ¹	EGY ¹	SAF ¹
	HX2 inlet (°C)	HX2 inlet (°C)	HX2 inlet (°C)	HX2 inlet (°C)	HX2 inlet (°C)
1	23.9	23.6	23.6	24.0	23.6
2	30.9	30.7	30.7	31.0	31.8
3	26.5	26.4	26.4	26.8	28.2
4	25.3	25.2	25.2	25.4	25.6
5	26.2	26.1	26.1	25.6	27.9
6	28.5	28.4	28.4	28.6	29.2
7	31.8	31.7	31.7	32.3	33.6
8	20.4	20.0	20.0	20.1	20.5
9	-	-	-	-	-
10	26.4	26.4	26.0	26.9	27.4

1: RELAP5

TABLE I-12. STEADY STATE RESULTS: HX2 SECONDARY SIDE OUTLET

Case No.	Measured	ARG ¹	GRE ¹	EGY ¹	SAF ¹
	HX2 outlet (°C)	HX2 outlet (°C)	HX2 outlet (°C)	HX2 outlet (°C)	HX2 outlet (°C)
1	27.1	26.9	26.8	28.5	26.9
2	34.4	34.5	34.5	34.0	34.2
3	32.1	32.2	32.2	31.4	32.0
4	26.2	26.6	26.4	27.9	26.5
5	32.1	32.3	32.3	30.8	32.1
6	30.8	31.0	31.0	31.1	30.8
7	38.3	38.3	38.3	39.0	37.9
8	21.9	21.5	21.5	21.1	21.5
9	-	-	-	-	-
10	33.1	33.7	33.4	32.7	32.9

1: RELAP5

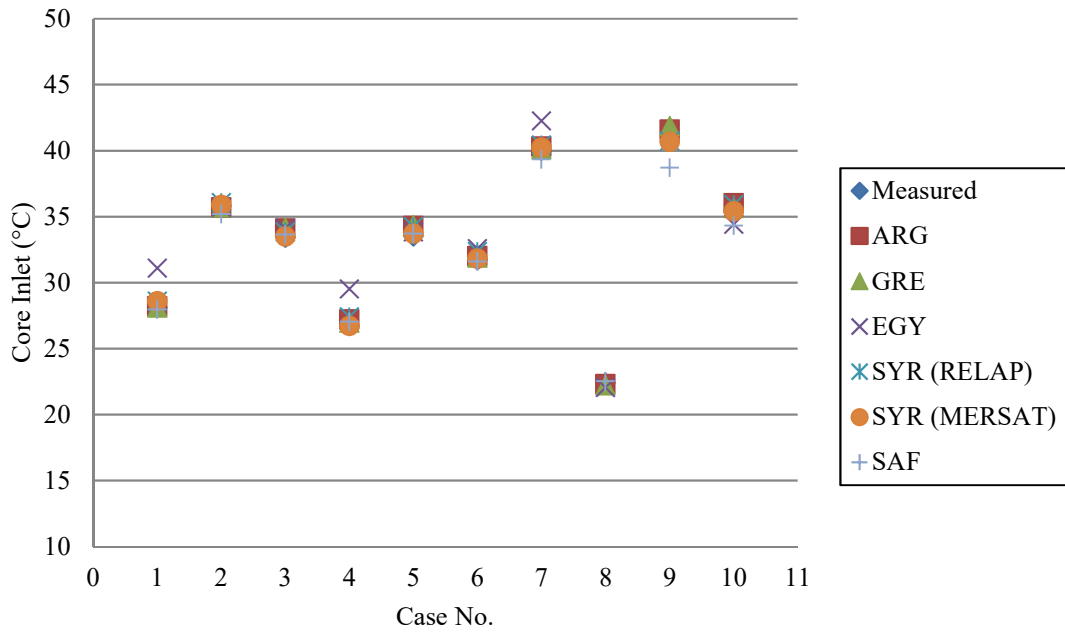


FIG. I-7. Steady state results: Core inlet.

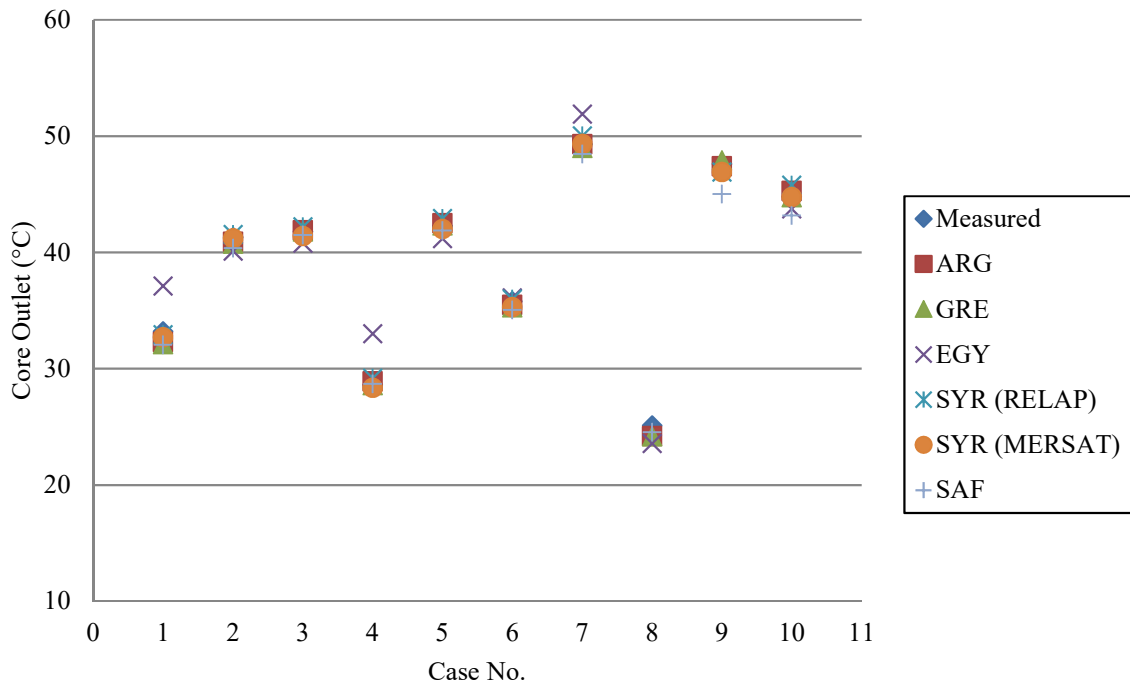


FIG. I-8. Steady state results: Core outlet.

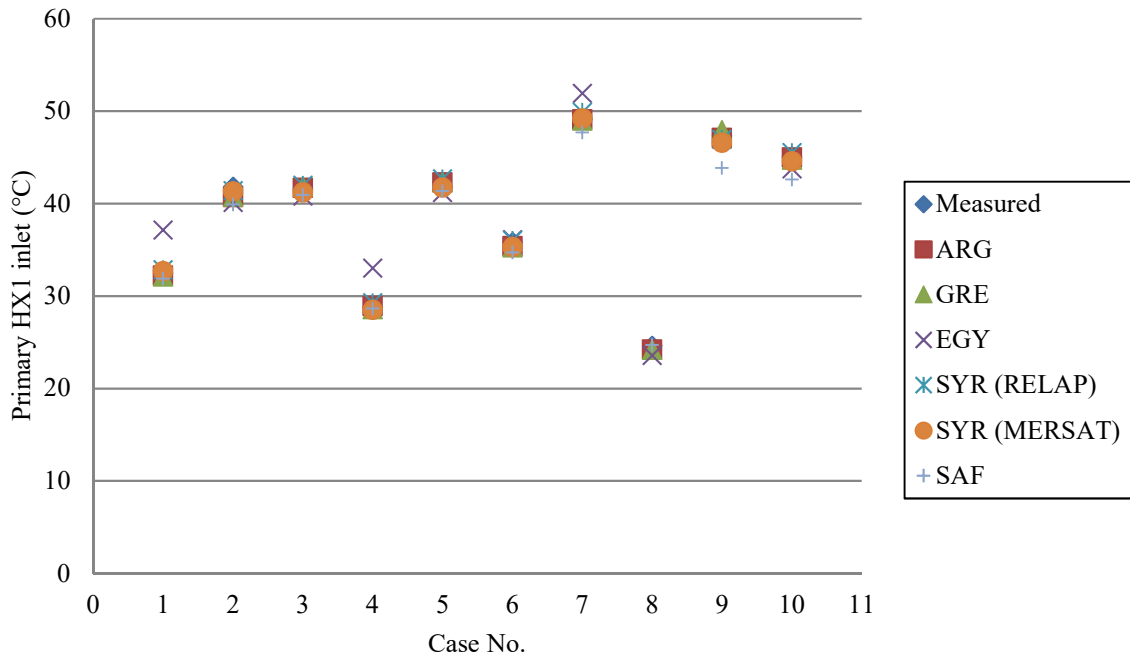


FIG. I-9. Steady state results: HX1 primary side inlet.

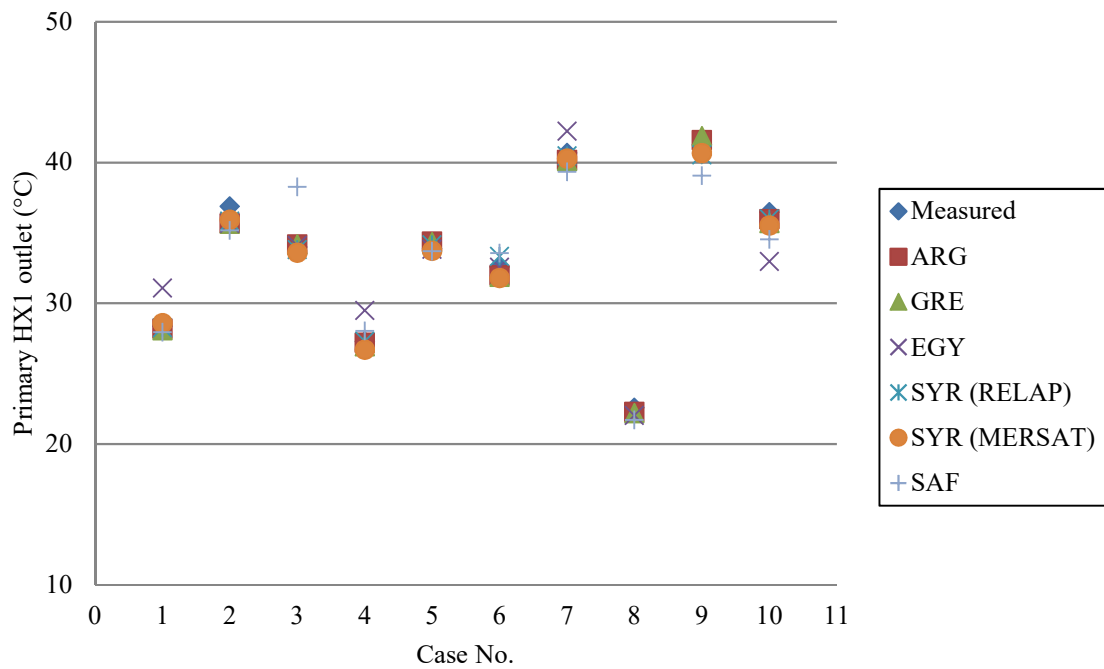


FIG. I-10. Steady state results: HX1 primary side outlet.

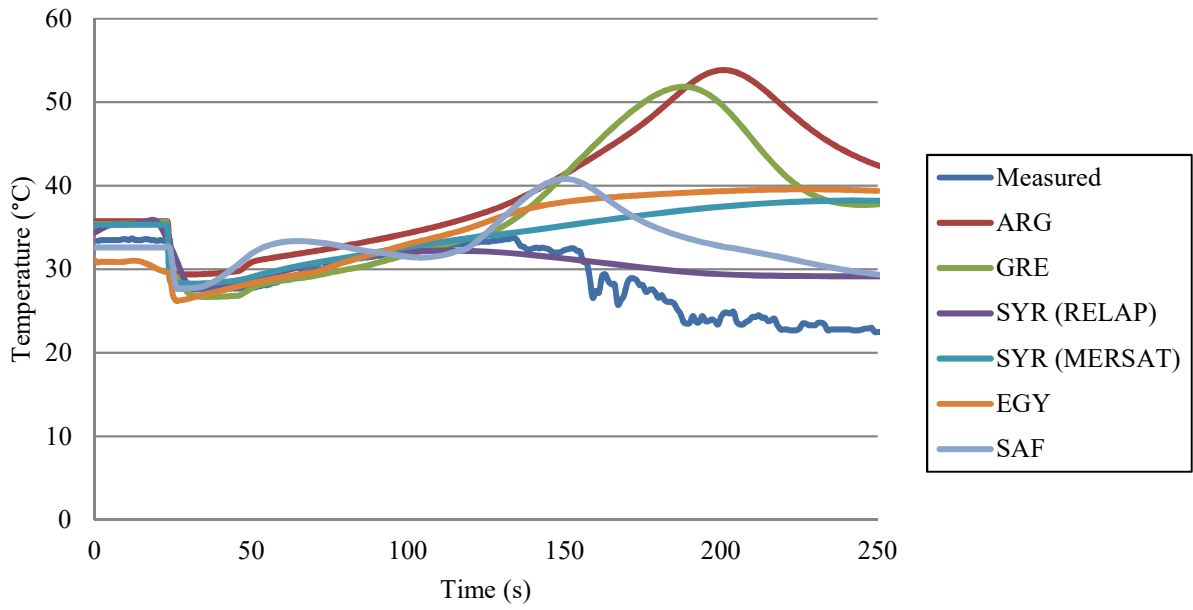


FIG. I-11. Thermocouple T0 (above core) vs. time.

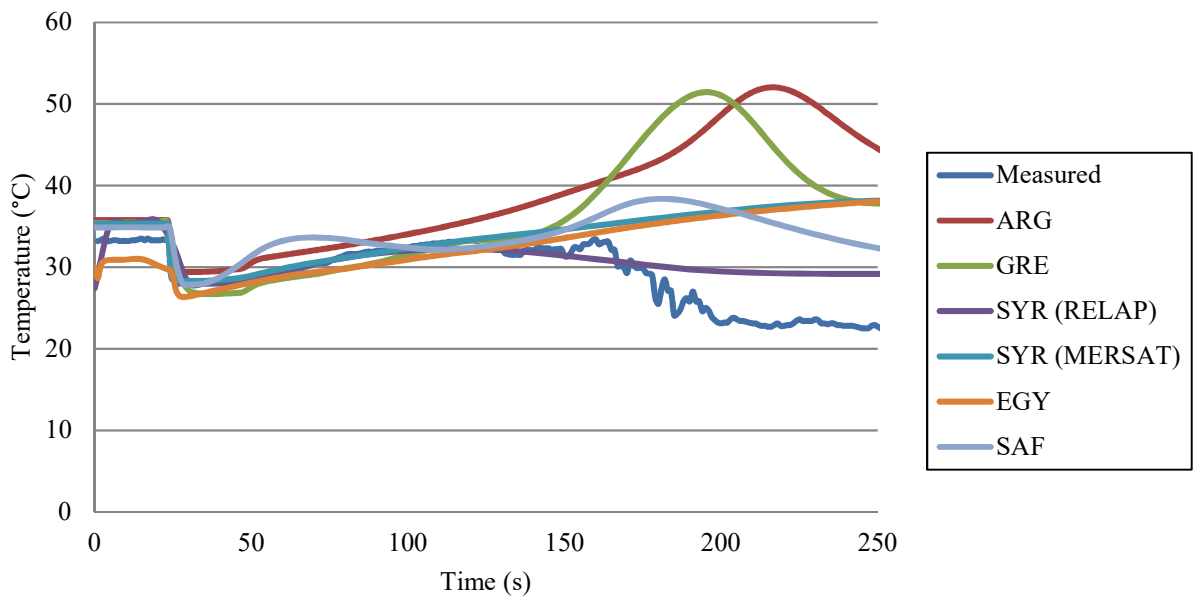


FIG. I-12. Thermocouple T1 (0.5 m above core) vs. time.

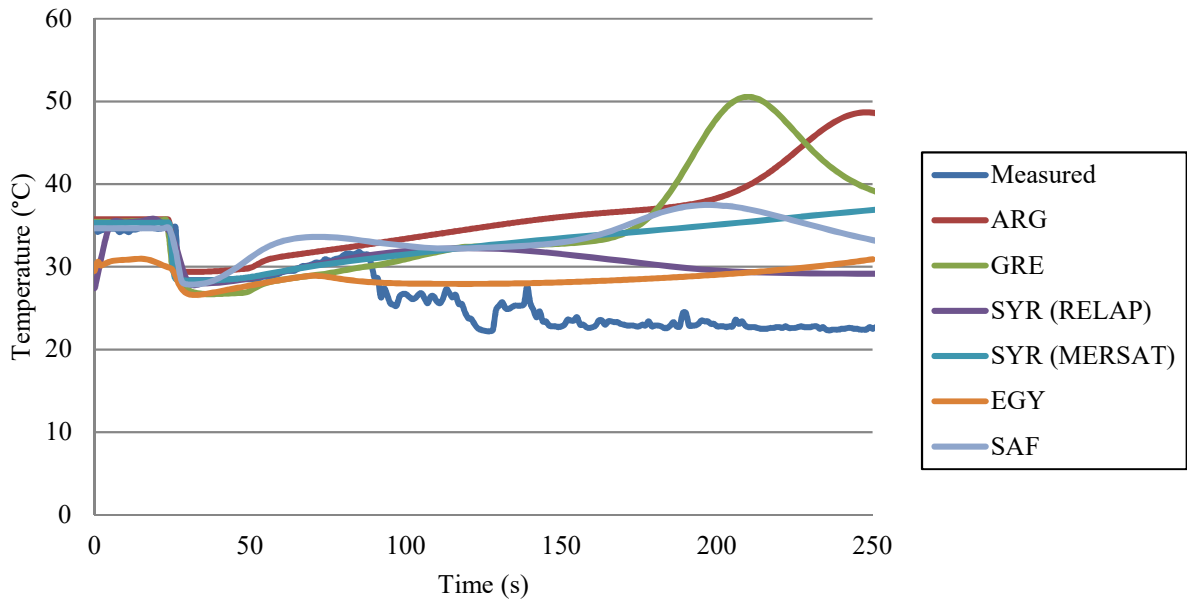


FIG. I-13. Thermocouple T2 (1.5 m above core) vs. time.

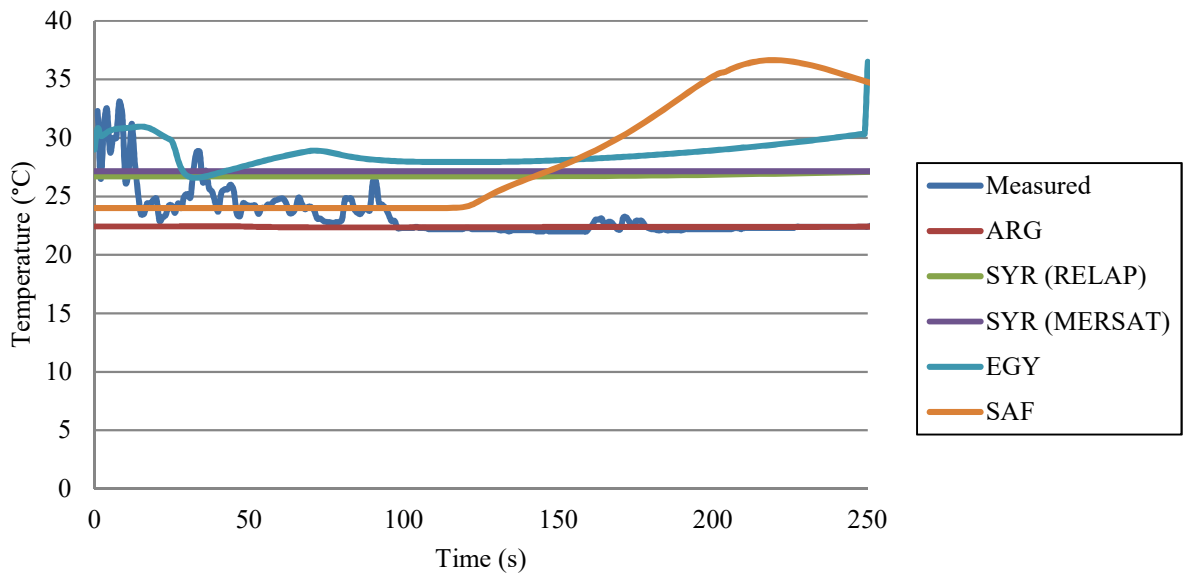


FIG. I-14. Thermocouple T3 (chimney top) vs. time.

I-4. CONCLUSIONS

The results of a modelling effort to evaluate the different codes and models under a series of loss of flow experiments have been presented and discussed. The analyses were performed for the ETRR-2 and the model predictions were compared with sets of experimental measurements. The main objective of this study was to demonstrate the model accuracy both qualitatively in terms of the general phenomena and quantitatively in terms of the numerical predictions.

The model estimations for the temperature and the behaviour throughout the transient evolution show that RELAP5/MOD3 and MERSAT can provide very good predictions when forced flow prevails but during natural circulation conditions, results tend to deviate significantly from the experimental values. Insufficient flapper valve geometrical details and decay heat models may have contributed to the discrepancies. It may be inferred that in regions where significant 3-D effects take presence, the models are of limited applicability and have to be used with caution. It may be appropriate to make a recommendation for the use of 3-D codes to capture the 3-D natural circulation phenomena present in this benchmark series although the required experimental setup details may not be available for a 3-D model. However, the calculated parameters, for the cases studied, were always conservative, i.e. on the 'safe side', as far as safety analysis is concerned. It could be claimed that this is a good benchmark to test code/model capability for 3-D phenomena in the natural convection regime.

REFERENCES TO ANNEX I

- [I-1] INTERNATIONAL ATOMIC ENERGY AGENCY, Research Reactor Benchmarking Database: facility specification and experimental data, Proceedings Series, IAEA, Vienna (2013).
- [I-2] NUCLEAR REGULATORY COMMISSION, RELAP5/MOD3.3 Code Manuals, Idaho National Engineering Laboratory, NUREG/CR-5535 (1995).
- [I-3] CHATZIDAKIS, S., IKONOMOPOULOS, A., RIDIKAS, D., Evaluation of RELAP5/MOD3 behavior against loss of flow experimental results from two research reactor facilities, Nuclear Engineering Desisng 255 (2013) 321-329.
- [I-4] HAINOUN, A., GHAZI, N., ALHABIT, F., Simulation of LOFA and RIA for the IEA-R1 Research Reactor using the code MERSAT, Ann. of Nuclear Energy 35 (2008) 2093–2104.

ANNEX II

BENCHMARK CONSOLIDATED RESULTS AGAINST EXPERIMENTAL DATA FROM IEA-R1

A. HAINOUN*, P. UMBEHAUN**, A. DOVAL***, M. J.H. KHAN+, S. CHATZIDAKIS++, S. PARK+++ , M. MLADIN§

*Atomic Energy Commission of Syria, Nuclear Engineering Department, P.O. Box 6091, Damascus, Syrian Arab Republic

**CEN, IPEN-CNEN/SP. São Paulo, SP, Brazil

***Nuclear Engineering Department, INVAP S.E., Av. Cmdt. Luis Piedrabuena 4950, S.C. de Boriloché, Rio Negro, Argentina

+ Reactor Physics and Engineering Division, Institute of Nuclear Science and Technology, Atomic Energy Research Establishment, Savar, Dhaka-1349, Bangladesh

++ Institute of Nuclear Technology and Radiation Protection, National Center for Scientific Research ‘Demokritos’, 15130, Athens, Greece

+++Korea Atomic Energy Research Institute, 1045 Daedeok-Daero, Republic of Korea

§Reactor Physics and Nuclear Safety Division, Institute for Nuclear Research, P.O. Box 78 Pitesti, Arges, Romania

Annex Consolidator: A. Hainoun

Abstract

In the framework of IAEA’s coordination research project on ‘Innovative methods in research reactor analysis: Benchmark against experimental data on neutronics and thermal-hydraulic computational methods and tools for operation and safety analysis of research reactors’ the Brazilian research reactor IEA-R1 has been selected as reference facility -that was equipped with an instrumented fuel assembly (IFA)- to perform benchmark calculations for a set of thermal-hydraulic codes being widely used by international teams in the field of research reactors deterministic safety analysis. The goals of the conducted benchmark aim at demonstrating the application of innovative reactor analysis tools in the research reactor community, validation of the applied codes and application of the validated codes to perform comprehensive safety analysis of research reactors. The measurements of the IFA cover data for SS operation and LOFA transients and comprise measurement for coolant and clad temperatures, reactor power and flow rate during SS and transient conditions. Temperatures are measured at three different radial and axial positions of IFA making together 12 measuring points in addition to coolant inlet and outlet temperatures.

The benchmark calculations were prepared independently by the participating teams using different thermal-hydraulic and safety analysis codes that comprise CATHARE, RELAP, MERSAT, PARET and COOLOD-N2. Since the code RELAP has been used by four of the participating teams the possibility is available to appraise the user effect and its impact on the code results.

The benchmark results show that most of the codes have the capability to predict the SS case. However, for the LOFA case the codes simulation results show discrepancies with the measurement although the majority of the applied codes predict correctly the time evolution of the considered transients for the coolant and clad temperatures, in particular the peak temperatures and the gradients around them are predicted conservatively. The quantitative assessments of benchmark results indicate different magnitude of discrepancy between predictions and measurement that vary between 7% and 20% for the important results of clad temperatures during LOFA.

II-1. FOREWORD

The qualification of an integrated set of thermal-hydraulic-neutronics codes is essential for performing comprehensive research reactor safety analysis that considers the interaction of thermal-hydraulic and neutronics phenomena. Thus, the ultimate task of the performed research

activities in this part of CRP aimed at assessing the capabilities and determining the suitability of various thermal-hydraulic codes for the application in design, operation and safety analysis of research reactors.

During the last two decades intensive effort has been undertaken to develop, modify and validate advanced computational tools for the application in the safety analysis of research reactors. Many of such tools have been adopted from the area of nuclear power reactors and were further extended to account for special design and operation features of research reactors. Prominent for this class of tools are the system codes like RELAP and CATHARE, ATHLET and MERSAT that are able to model the whole reactor system and have meanwhile special versions for the application on research reactors. Besides, other relatively simpler tools like PARET and PLTEMP-ANL were originally developed for the application on research reactors. They are limited to model part of the reactor core or selected fuel assemblies and remain useful for application on simple transients where special phenomena are investigated. However, for complex transients or accidents -like reactivity initiated accident (RIA), loss of flow transient/accident (LOFA), loss of coolant accident (LOCA)- where integrated neutronic-thermal-hydraulic phenomena are expected and various parts of reactor facility are involved, only advanced system codes are adequate to address the expected physical phenomena.

In the framework of qualification of the above mentioned computational tools for the design and safety analysis of research reactors instrumented fuel assemblies (IFA) prove to be an important source to provide realistic data both for understanding the reactor behaviour and validating the computer codes in a passable benchmark process. In line with this approach an IFA has been constructed and operated in the Brazilian IEA-R1 MTR reactor. This IFA was designed for the purpose of performing thermal-hydraulic measurements under steady state (SS) operation and during LOFA. The IFA was positioned in two different locations of the reactor core in order to account for the influence of radial power factors on the achieved measurements. Each of the two measurement sets comprises 14 points for coolant and clad temperatures distributed in radial and axial direction of IFA. The achieved experimental data serve as reference to benchmark the thermal-hydraulic codes CATHARE, MERSAT, PARET and RELAP in addition to the simple SS code COOLOD-N2. The computational tools have been used by seven teams from various countries participating in this international benchmark analysis and comprising Argentina, Bangladesh, Brazil, Greece, Republic of Korea, Romania and Syrian Arab Republic (Syria). The goals of the conducted benchmark analysis can be summarized as follow:

- Demonstrating the application of innovative reactor analysis tools in the research reactor community with the ultimate purpose of supporting the transfer of such tools to the larger research reactor community;
- Validation of the applied codes against experimental data, and application of the validated codes to simulate steady state and transients covering a variety of neutronic and thermal-hydraulic conditions for various selected research reactors;
- Application of the validated analysis tools in the safety analysis of research reactors;
- Completing the benchmark analysis by the code-to-code comparison for the same experimental sets in order to classify the confidence of the involved codes and identifying any user effects amongst the involved teams;
- Supporting the further development of innovative reactor analysis tools in the research reactor community with the ultimate purpose of facilitating the transfer of such tools to the larger research reactor community.

In addition to benchmarking the codes against the experimental data of the IFA, the broad-spectrum of the employed codes enables also the consideration of code-to-code comparison to evaluate the codes capabilities to simulate the relevant thermal-hydraulic phenomena and assess them regarding appropriateness for the application in the safety analysis of research reactors.

The structure of this contribution comprises a short description of the employed computer codes and the adopted approach to model the IEA-R1 reactor. The second step presents the benchmark results by comparing the code prediction with the experimental data and commenting on the observation. The comparison allowed for evaluating the prediction capability of the employed codes and indicate possible further development.

The last part is devoted to Code-to-Code comparison, where the results of various codes are compared for the purpose of comparative assessment to account for possible improvement of selected physical models in the employed codes. In addition, for the case of the RELAP code which is being used by various teams, the comparison of calculated results of all teams could also serve to evaluate the user effect. At this stage the impact of user experience and the applied modelling approach on the final code results can be evaluated and possible recommendation for future code application can be given.

II-2. DESCRIPTION OF TOOLS, CODES AND METHODS

For the benchmark analysis of IEA-R1 the thermal-hydraulic codes CATHARE, MERSAT, RELAP, PARET and COOLOD-N2 have been applied. The codes have been used by seven teams from different countries that participate in this international benchmark analysis and comprise Argentina (RELAP), Bangladesh (COOLOD-N2), Brazil (PARET-ANL and MTRCR), Greece (RELAP), Republic of Korea (RELAP), Romania (CATHARE) and Syria (MERSAT, RELAP) (Table II-1). The first three codes CATHARE, MERSAT and RELAP belong to the advanced thermal-hydraulic codes being able to model the main important thermal-hydraulic phenomena related to the safety analysis of light water cooled reactors up to the level of design basis accident. They are based on a one dimensional (1-D) fluid dynamics approach with a comprehensive heat transfer package in the two phase flow regime.

TABLE II-1. PARTICIPATING TEAMS AND CODES USED FOR IEA-R1 BENCHMARK ANALYSIS

Working Team	Applied Code	Type of Calculation
ARG	RELAP-5 mod 3.2	SS and LOFA
BGD	COOLOD-N2	SS
BRA	PARET-ANL, MTRCR	SS
GRE	RELAP	SS and LOFA
ROK	RELAP	SS and LOFA
ROM	CATHARE	SS and LOFA
SYR	MERSAT, RELAP	SS and LOFA

II-3. DESCRIPTION OF FACILITY AND EXPERIMENTS

This section presents a short description of the IEA-R1 reactor facility with special focus on the specification of the IFA. More detailed description of IEA-R1 facility is given in [II-1].

II-3.1. Description of IEA-R1 Reactor

The IEA-R1 is a 5 MW pool type research reactor using MTR fuel assemblies with low enrichment. Fig. II-1 shows a simplified scheme of the primary and secondary loop.

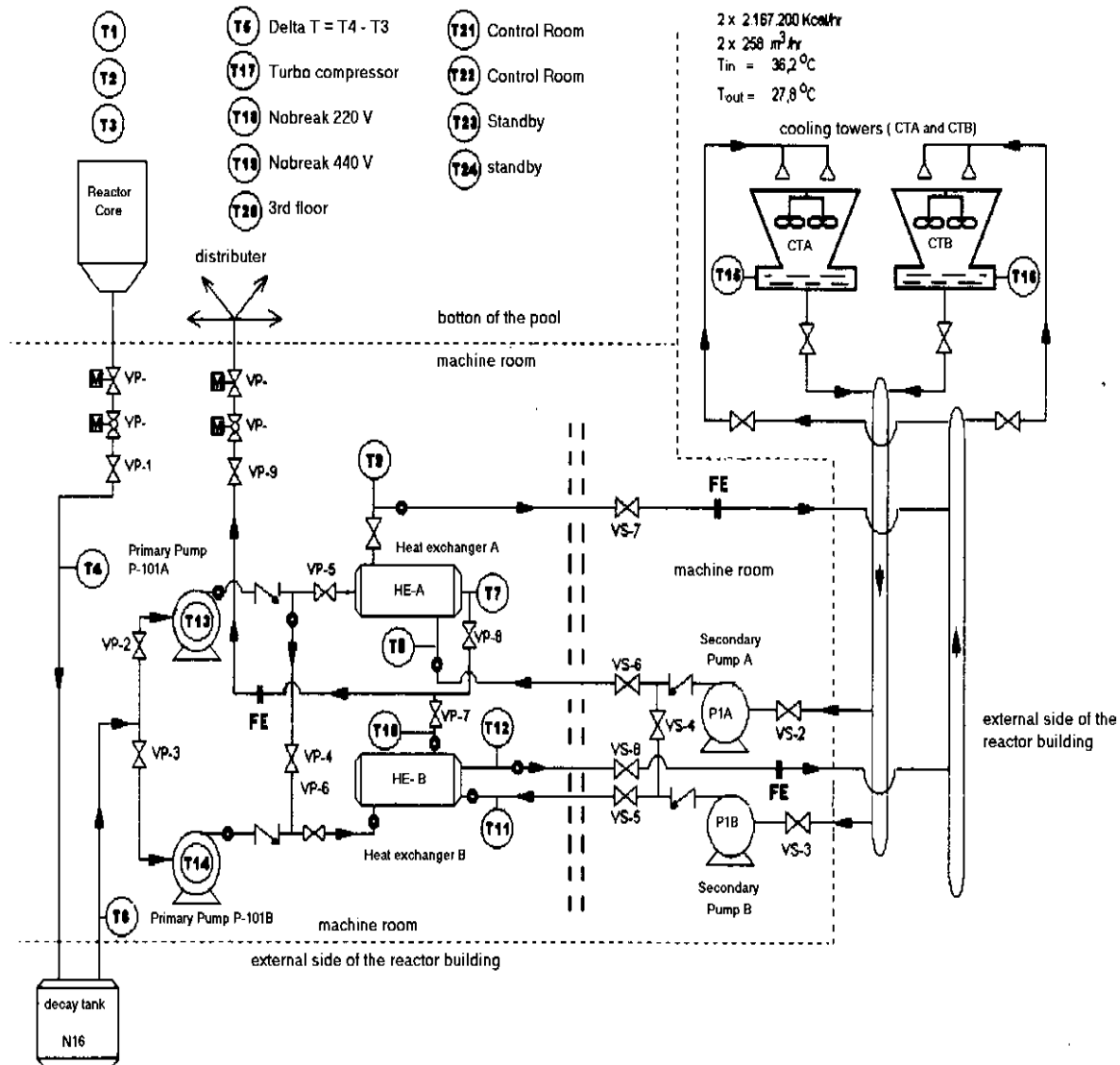


FIG. II-1. Schematic process diagram of the IEA-R1 reactor [II-2].

The reactor core is cooled by downward flow. Reactor heat removal is based on primary and secondary cooling systems. The pool water of the primary system is pumped downward through the fuel assemblies to remove the fission heat from the reactor core. A water to water heat exchanger transfers the generated heat to a secondary water cooling system. The secondary system carries heated water to the cooling tower which dissipates the heat to the atmosphere. The primary water is returned to the reactor pool. Water from the cooling tower is re-circulated through the secondary system.

By operating the reactor at 5 MW loop A is involved (Pump P-101A or P-101B, the Heat Exchanger HE-B, the Pump P1A or P1B and the Cooling Tower CTB). The other heat exchanger and cooling tower are used only for low power operation (< 3 MW).

The primary cooling system of the IEA-R1 consists of a pool, piping, decay tank, pumps, heat exchangers, flow meter system, distributor, valves and structures, as schematically shown in Fig. II-2. The primary pump circulates water through the core to remove the heat generated during the reactor operation. Then, the water flows through the decay tank to decrease the N16 activity before entering the heat exchanger, which transfers the heat to the secondary cooling system.

A manually actuated pneumatic system lifts a device, named header, to coupling the outlet nozzle to the core matrix plate. Then, the pump is turned on and the primary operating flow rate is adjusted. The pneumatic system is turned off and the device is kept coupled by hydrodynamic force resulting from the pressure difference. The reactor power operation is adjusted. If the primary flow rate decreases below the set-point value (90%), the reactor is shut down and the coupling device falls by action of gravity, and then the residual heat is removed by natural circulation in the reactor pool, Refs. [II-2] and [II-3].

Figure II-2 shows the location of reactor core inside the reactor pool. The total volume of water in the pool is $\sim 272 \text{ m}^3$.

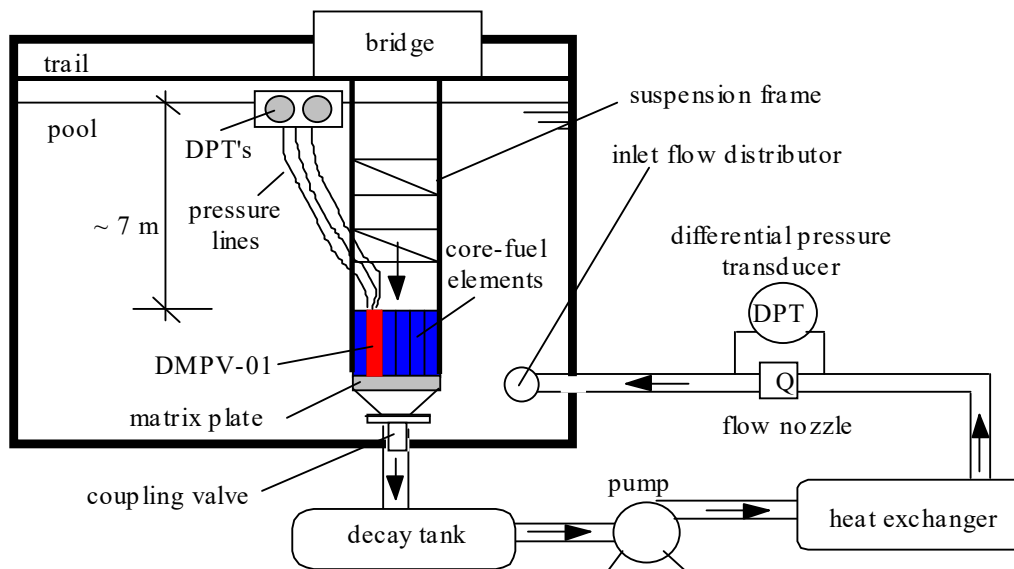


FIG. II-2. Simplified illustration of primary system of IEA-R1.

The reactor arrangement consists of fuel assemblies, beryllium reflector, control rods and irradiation positions inside the reactor core. The core comprises 20 fuel assemblies, 4 control fuel assemblies and a central irradiator, assembled in a square matrix 5x5. Each fuel element has 18 fuel plates assembled on two lateral support plates, forming 17 independent flow channels. The control fuel element includes only 12 plates as there are two dummy lateral plates and two guide channels for the control plates. More detailed description of IEA-R1 is given in Ref. [II-1]. Table II-2 summarizes the main reactor design parameters.

TABLE II-2. DESCRIPTION OF DESIGN PARAMETERS OF IEA-R1 RESEARCH REACTOR [II-2].

Reactor Parameter	Data	Notes
Steady State Power Level (MW)	2 to 5	Depends on irradiation necessity
Fuel		
Fuel Enrichment	< 19.75%	
Number of Fuel Assembly in the Core	24	
a) Standard Fuel Assembly	20	
b) Control Fuel Assembly	4	
Fuel Types		
U ₃ O ₈ -Al	Density 2.3 g/cm ³	Mass U-235 per fuel assembly 196.9 g
U ₃ Si ₂ -Al	Density 3.0 g/cm ³	Mass U-235 per fuel assembly 275.5 g
Maximum Inlet Temperature (°C)	40 °C	
ΔT _{CORE} at 5 MW	5.8 °C	Between inlet and outlet
Number of Fuel Plates in:		
a) Standard Fuel Assembly	18	
b) Control Fuel Assembly	12	
Fuel Thickness (mm)	0.76	
Clad Thickness (mm)	0.38	
Total Width of the plates (mm)	67.1	
Fuel Dimensions (mm)	0.76 × 62.6 × 600	
Thickness of water channel (mm)	2.89	
Water pool volume (m ³)	272	
	Total: 772	
Coolant Flow Rate (m ³ /h)	Core Flow: 547.2 Bypass: 224.8	
Pressure Drop – Normal Condition	7.835 kPa	Measured
Pressure drop of primary system	400 kPa	Approximately
Uncertainties		
Deviation in fuel loading per plate	12%	
Fluctuation in uranium density	2%	
Error in fuel thickness	10%	
Power measurement	5%	
Power density variation	10%	
Flow rate measurement	3,0%	

II-3.2. Experiment Description

To explore the detailed thermal-hydraulic behaviour of the fuel assembly under normal and transient behaviour, an IFA was manufactured and placed in a certain location in the reactor core. The impact of radial peaking factors on the thermal-hydraulic behaviour of the fuel assembly is assessed by positioning the IFA at two different locations inside the core resulting in two sets of experimental configurations (Fig. II-3). In the configuration 243 the IFA was located at the outermost core corner (lower right). For the configuration 246 the IFA was located

on the midline left to the core centre. The impact of these configurations on the thermal-hydraulic analysis of the IFA is reflected in the radial and axial power factors.

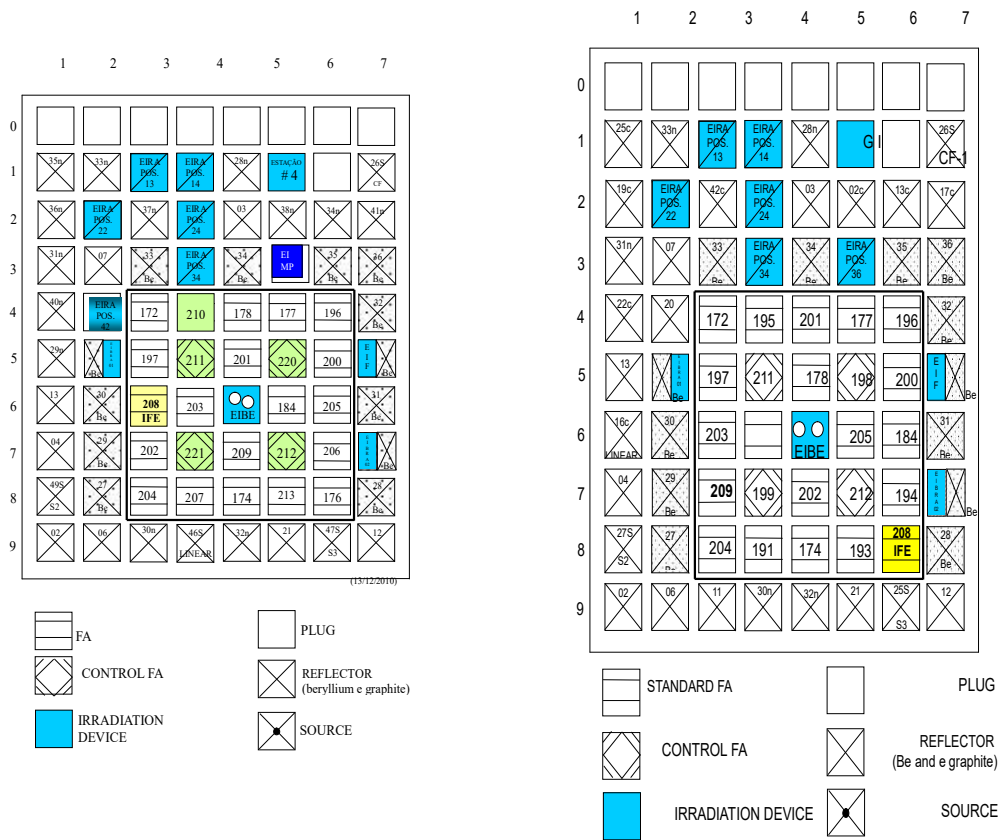


FIG. II-3. Position of IFA for the 243 (R) and 246 (L) core configurations.

Figure II-3 presents the IFA with the assigned measurements positions and Table II-3 summarizes the assigned temperatures at the considered positions. The IFA has fourteen thermocouples distributed as follows:

- Coolant inlet and outlet temperature;
- Three channels, one central and two lateral channels, each is equipped with 3 thermocouples for the clad and 1 for the fluid temperatures. Table II-3 summarizes the symbols and locations of temperatures.

The internal flow rate distribution inside the fuel assembly was measured in a previous work using a Dummy FE [II-4]. The measurement indicated almost parabolic distribution across the cooling channel. Based on this experiment the distribution parameters (local relative to average) for the central channel, reflector side and FA side are 1.041, 0.91 and 0.885 respectively.

TABLE II-3. LOCATIONS AND SYMBOLS OF TEMPERATURE MEASUREMENTS IN IFA

Position from channel entrance (mm)	Reflector side	Central	FA Side
Clad Temperatures			
252.5	TC2	TC3	TC4
432.5	TC5	TC6	TC7
552.5	TC8	TC10	TC12
Fluid Temperatures			
552.5	TF9	TF11	TF13

TF1: Fluid Inlet Temperature, TF14: Fluid Outlet Temperature

The distribution of fuel assembly flow rate of 22.8 m³/h on the 18 flow channels (17 internal and 2 half outer channels) of IFA gives an average channel velocity of 1.92 m/s (total flow area in channel region is 0.0033m²).

Merging the channels in 3 groups, gives the resulting channels velocities of IFA as follows:

- Central channel: 2 m/s;
- Reflector side channel: 1.8 m/s;
- FA side: 1.65 m/s.

The axial power distributions along the 3 groups of channels have been provided by the reactor operator and presented in Fig. II-4. Neutron kinetic data required to simulate reactor dynamic behaviour including nuclear heat generation are specified according to the supplied operator data in Ref. [II-1].

The steady state boundary conditions are specified as follows:

- Inlet pressure: 170 kPa;
- Nominal Power: 3.5 MW - 5 MW;
- Total Flow Rate (core and Bypass): 211 kg/s;
- Core inlet temperature: 32.7 °C – 40 °C;
- Pool Temperature: 32.7 °C.

The radial power peaking factor of the IFA was estimated from the experimental data of the steady state operation based on the underneath proposed approach. Another approach can be adopted subject to experimental data availability.

The local power of the IFA (P_{IFA}) has been calculated using the available experimental data of coolant flow rate (G_{IFA}), inlet (T_{in}) and outlet (T_{out}) temperatures as follows:

$$P_{IFA} = G_{IFA} c_p (T_{out} - T_{in}) \quad (II-1)$$

The resulting local power of the IFA and the corresponding radial peaking factors for the different reactor power levels are presented in Table II-4.

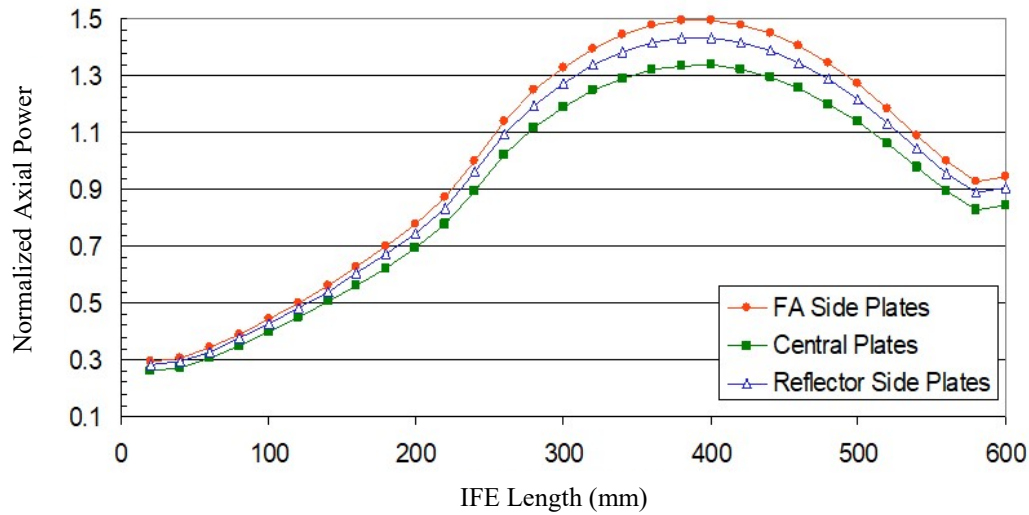


FIG. II-4. Normalized axial power distribution for the IFA (Configuration 243).

TABLE II-4. DERIVED LOCAL POWER OF THE IFA BASED ON MEASUREMENTS OF FLOW RATE, INLET AND OUTLET TEMPERATURES OF COOLANT.

Reactor Power (MW)	Experimental Data			Derived Parameters	
	Inlet (°C)	Outlet (°C)	Flow Rate (kg/s)	IFA Power (kW)	Radial Power Factor
3.5	32.69	37.57	6.27	128.0	0.829
4.0	31.61	37.23	6.27	147.4	0.835
4.5	32.53	38.69	6.27	161.6	0.814
5.0	33.43	40.21	6.27	177.68	0.805

For 3.5 MW:

Average power per plate: $3.5 / (20 \times 18 + 4 \times 12) = 3.5 / 408 = 8.578 \text{ kW}$

Average FA power, $P_{av} = 18 \times 8.578 = 154.4 \text{ kW}$

$P_{\bar{r}} = P_{IFA} / P_{av} = 0.829$

II-3.3. Input Models of IEA-R1

Different input models of IEA-R1 have been developed using the employed computational codes depending on the description scheme of each code. The code users adopted different levels of detailed description of primary and secondary loops and reactor core. However, all codes imply a detailed full-scale modelling of the IFA that is essential for the benchmark analysis.

The IFA was modelled as separate fuel assembly group that is in parallel arrangement linked with further fuel assemblies of reactor core. The model consists of inlet zone linked to the reactor inlet plenum, active fuel zone with flow channel and output zones linked to the reactor outlet plenum. To reflect radial and axial temperature distribution various sub-channels with adequate vertical discretization are applied. Figures II-5 to II-10 represents the various developed nodalization schemes of the IEA-R1 reactor using the applied codes. Detailed descriptions of the developed input models are provided in the Annex of the individual country reports.

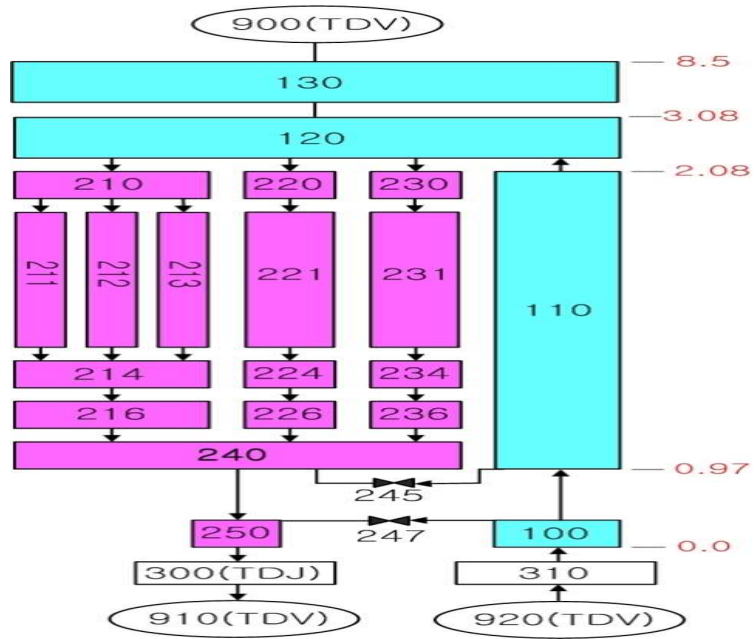


FIG. II-5. ROK nodalization scheme using RELAP.

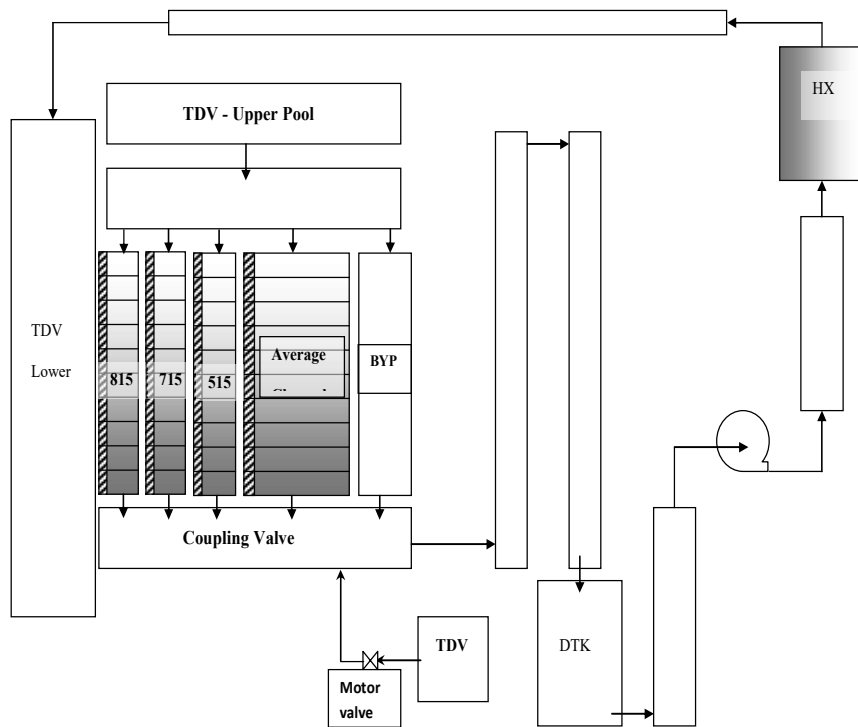


FIG. II-6. ARG nodalization scheme using RELAP.

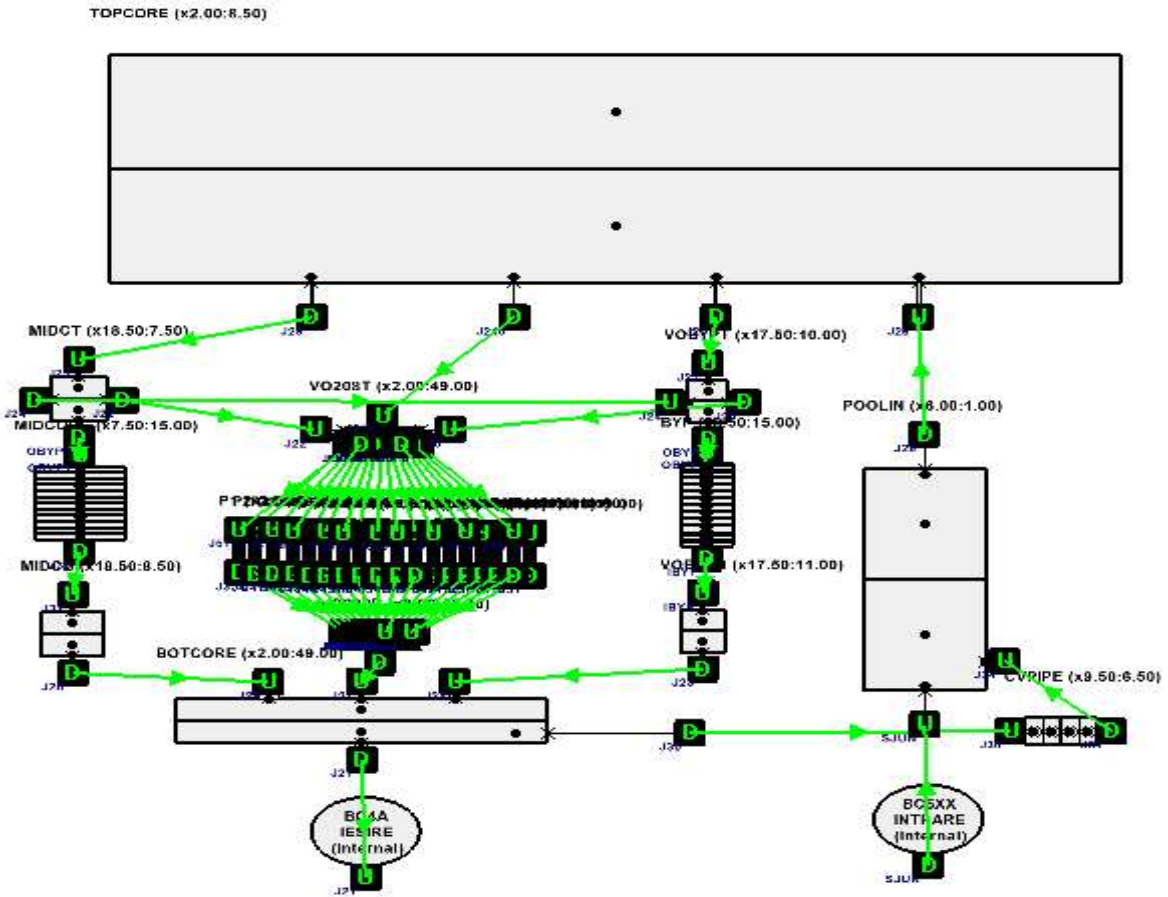


FIG. II-7. ROM nodalization scheme using CATHARE.

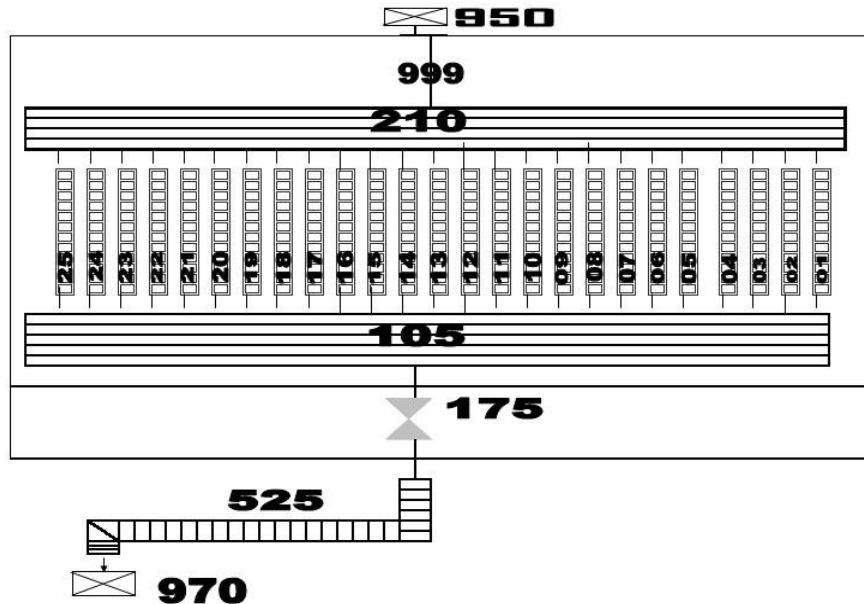


FIG. II-8. SYR nodalization scheme using RELAP.

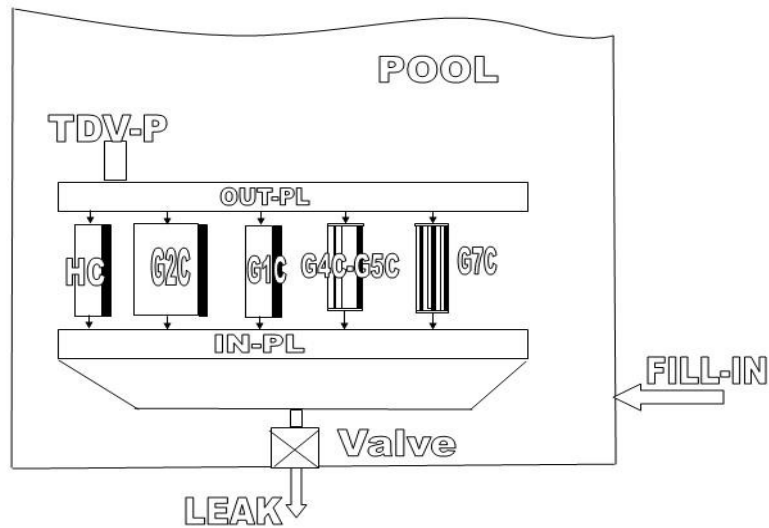


FIG. II-9. SYR nodalization scheme using MERSAT.

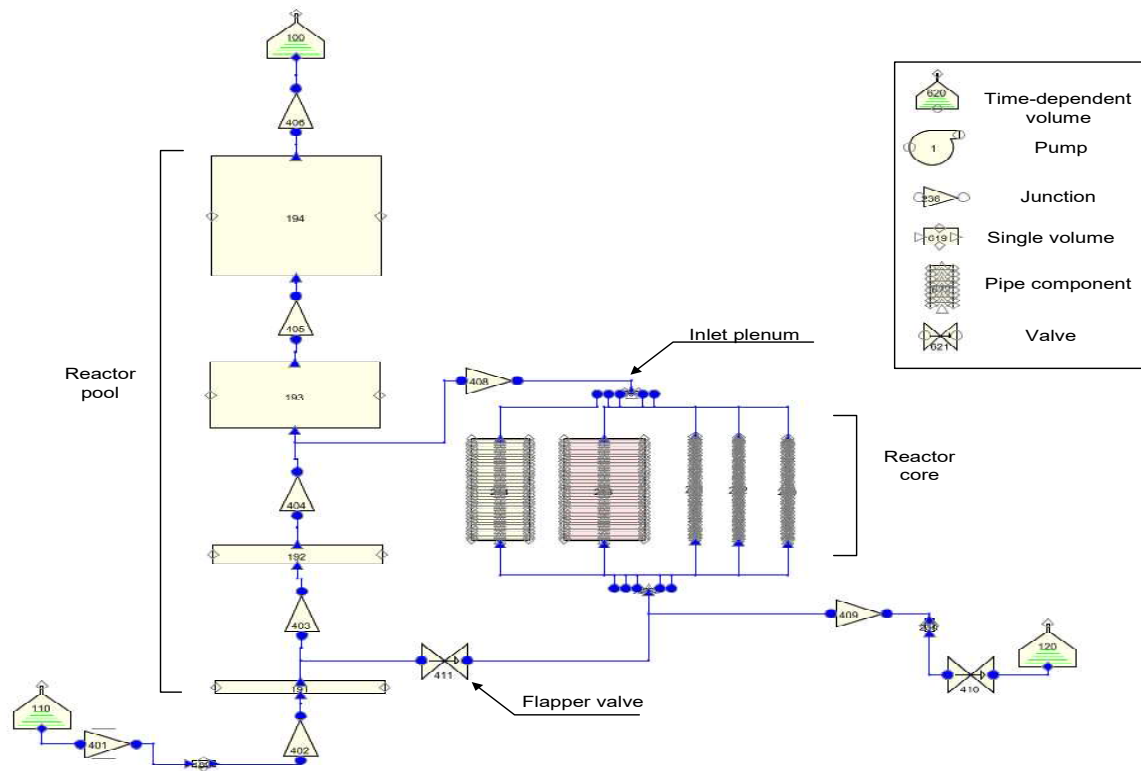


FIG. II-10. GRE nodalization scheme using RELAP.

II-3.4. Benchmark Results of IEA-R1 for Configuration 243

II-3.4.1. Steady state benchmark results of IEA-R1

The steady state (SS) data for the measured temperatures refer to the values averaged over the time interval immediately before starting the LOFA. For example, for the power level of 3.5 MW the temperatures are averaged over 70 seconds of measuring time. Table II-5 summarizes the SS benchmark results for all codes for the reactor power of 3.5 MW. The agreement between calculation and measurement is better for the lateral than for the central positions. The absolute

local difference of prediction to experiment varies between -5 °C and +8 °C corresponding to a maximum relative deviation of -12% and +21% respectively. This maximum discrepancy is observed at the central position of IFA (TC3). The trend of high deviation is observed by all teams which points to a possible source of uncertainty in the experimental data. For the quantitative assessment of the discrepancy between measurement and code prediction the average relative deviation has been applied as follow:

$$AVD = \frac{1}{n} \sqrt{\sum_{i=1}^n \left(\frac{T_{exp} - T_{cal}}{T_{exp}} \right)^2} \quad (II-2)$$

T_{exp} donates the experimental temperature and T_{cal} is its related calculation with one of the applied codes. n refers to the number of measurement points along the IFA which amounts to 14 temperature measurements of clad and coolant.

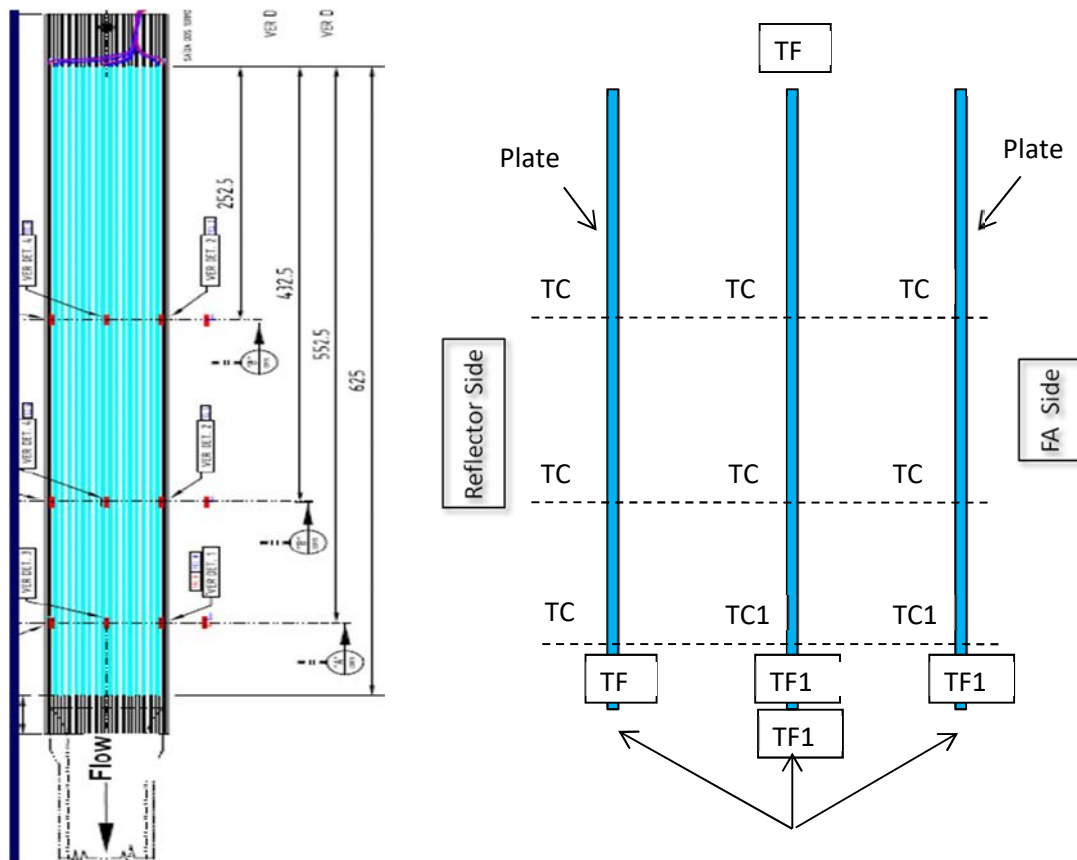


FIG. II-11. Vertical Section of Instrumented Fuel Assembly.

The resulting AVD shows best agreement for MTRCR from BRA with 3.3% followed by 4.8% for ROK, 4.9% for MERSAT from SYR, 5.2% for RELAP from SYR, 8.4% for PARET from BRA, 8.8% for ROM, 9.2% for ARG and GRE and finally 13.0% for BGD shown on Table II-5. The general trend of the achieved benchmark results of the SS condition indicates that the code predictions for clad temperatures tend to overestimate the measurements, whereas the calculated coolant temperatures underestimate the measurements.

Taking into account the uncertainty of parameter measurement that amounts to 5% of reactor power, 3% for flow rate –in addition to 12% deviation in fuel loading per plate- [II-1, II-2] the observed discrepancy can be considered as reasonable. In view of the fact that the expected thermal-hydraulic phenomena under SS conditions that are dominated by single phase flow, the

observed discrepancy arises mainly from the experimental arrangement used to measure clad temperatures in narrow channels. The weak contact between the thermocouple and the cladding can be the main source for the uncertainty. Furthermore, the cladding temperature was measured with a disk inserted between adjacent fuel plates with thermocouple welded at the disk centre (see Fig. II-11). This arrangement causes contact resistance between the disk and fuel cladding resulting in measuring lower temperatures than they are in reality. The highest discrepancy is observed in case of central fuel plates. The measured coolant temperatures could be higher than the considered channel mean temperature as the location of thermocouple in the inserted disk in the narrow channel was measured nearby the wall where the coolant thermal layer has higher temperature than the assumed average value. Since no measurements for axial power density distribution of IFA are available, the IEA-R1 operator supplied calculated values based on the neutronic code CITATION [II-2] (see also Fig. II-4). This approach could add additional source of uncertainty in view of the significant impact of this parameter on the axial temperature distribution.

TABLE II-5. BENCHMARK RESULTS OF THE APPLIED CODES FOR THE SS OPERATION AT 3.5 MW OF IEA-RI(CONFIGURATION 243)

T (°C)	ARG		BGD		BRA		GRE		ROK		ROM		SYR						
	Exp	RELAP	Diff.	COOLOD-N2	Diff.	PARET	Diff.	MTRCR	Diff.	MTRCR	Diff.	PARET	Diff.	MTRCR	Diff.	MERSAT	Diff.	RELAP	Diff.
TC2	43.8	44.2	0.8%	48.2	9.9%	46.0	4.9%	43.2	-1.5%	45.3	3.4%	42.6	-2.9%	46.8	6.8%	42.9	-2.1%	43.7	-0.4%
TC3	37.5	44.2	17.8%	49.1	30.9%	42.7	13.9%	38.2	1.7%	44.4	18.2%	42.1	12.2%	45.5	21.2%	42.1	12.2%	44.3	18.2%
TC4	44.5	44.2	-0.7%	51.3	15.3%	45.5	2.2%	42.2	-5.1%	46.0	3.3%	43.0	-3.4%	47.6	7.0%	43.1	-3.1%	43.7	-1.8%
TC5	48.0	52.6	9.6%	50.1	4.3%	54.0	12.4%	49.5	3.0%	50.9	6.0%	48.5	0.9%	46.8	-2.5%	48.8	1.6%	48.1	0.1%
TC6	42.5	51.0	19.9%	50.4	18.4%	48.8	14.7%	42.0	-1.3%	49.6	16.5%	47.8	12.2%	51.0	19.9%	47.4	11.4%	49.0	15.2%
TC7	49.2	53.5	8.8%	53.0	7.8%	53.1	8.0%	47.8	-2.8%	51.7	5.2%	49.1	-0.1%	53.7	9.2%	49.1	-0.2%	48.5	-1.4%
TC8	45.2	50.4	11.5%	48.4	7.1%	51.0	12.9%	47.4	4.8%	48.8	7.9%	46.3	2.5%	48.9	8.2%	47.1	4.2%	45.3	0.3%
TC10	41.7	49.0	17.5%	48.2	15.5%	46.5	11.6%	41.5	-0.5%	47.6	14.2%	45.8	9.8%	48.5	16.2%	45.8	9.9%	46.1	10.6%
TC12	46.6	51.4	10.3%	50.3	7.9%	50.3	7.9%	46.1	-1.1%	49.5	6.3%	46.9	0.6%	50.8	9.0%	47.4	1.7%	45.7	-1.9%
TF1	32.7	33.1	1.3%	NA	0.0%	32.7	0.0%	32.7	0.0%	30.8	-5.9%	32.7	0.0%	32.7	0.1%	32.7	0.0%	32.7	0.0%
TF9	40.9	NA	0.0%	NA	0.0%	36.4	-11.0%	36.4	-11.0%	35.8	-12.4%	37.1	-9.4%	36.8	-10.1%	37.5	-8.4%	37.1	-9.4%
TF11	38.8	NA	0.0%	NA	0.0%	36.4	-6.2%	36.4	-6.2%	35.5	-8.6%	37.1	-4.5%	37.9	-2.5%	37.0	-4.7%	37.4	-3.7%
TF13	41.0	NA	0.0%	NA	0.0%	36.4	-11.2%	36.3	-11.4%	36.0	-12.1%	37.2	-9.1%	37.2	-9.3%	37.6	-8.3%	37.5	-8.5%
TF14	37.6	38.7	3.0%	NA	0.0%	37.7	0.3%	37.7	0.3%	34.3	-8.8%	37.6	0.0%	38.3	1.8%	37.8	0.7%	37.9	0.7%
		AVD	9.2%	AVD	13.0%	AVD	8.4%	AVD	3.6%	AVD	9.2%	AVD	4.8%	AVD	8.8%	AVD	4.9%	AVD	5.2%

II-3.4.2. LOFA benchmark results of IEA-R1 for Configuration 243

LOFA or the loss of flow transient (LOFT) refers to the postulated initiated events of loss of pump energy supply. The resulting decrease of core flow rate triggers the reactor scram once the flow rate reaches 93% of its nominal value (due to the protection criteria ‘Low Flow Rate’). Figure II-12 shows the experimental pump coast down curve where the flow rate varies after the pump trip from its nominal value to about 20% of it in 27 seconds. After that time, the header (coupling valve) is decoupled and the reactor pool including the reactor core are no longer connected to the primary pump.

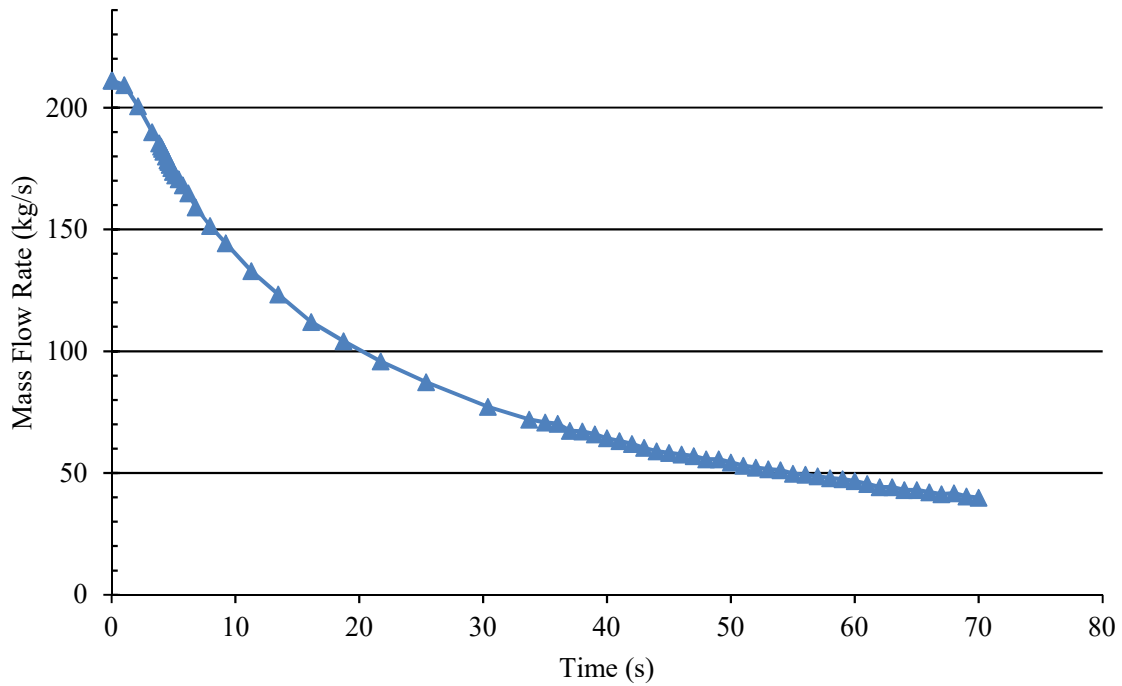


FIG. II-12. Measured pump coast down curve during LOFA for IEA-R1.

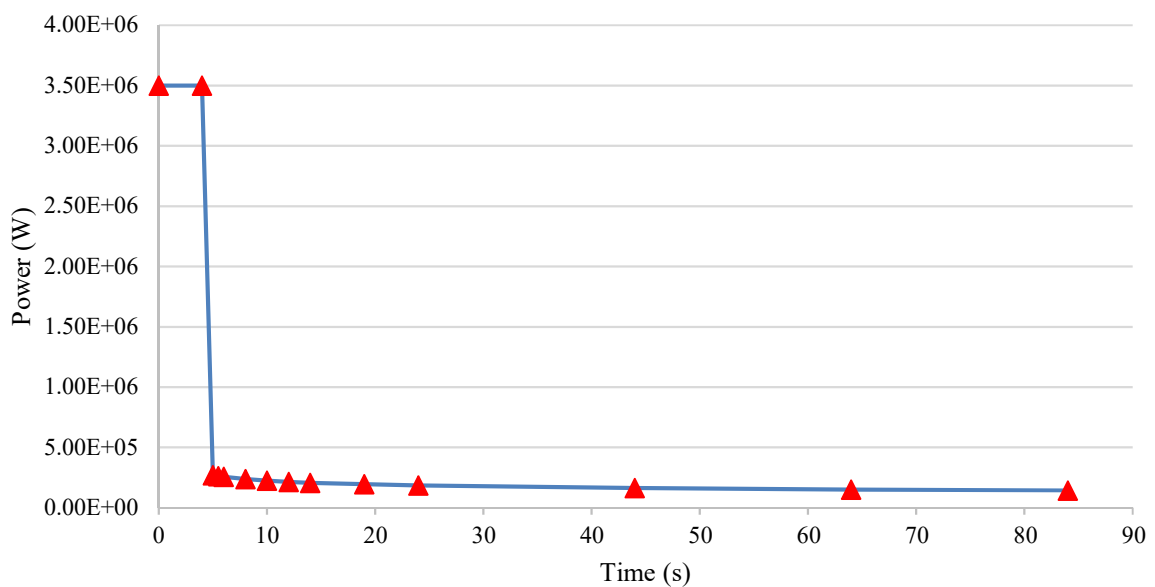


FIG. II-13. Evolution of reactor power after reactor scram (decay heat curve).

As already mentioned two core configurations have been used for evaluating the LOFA of IEA-R1 based on measurements in the IFA that have been located in two different positions inside the core associated to configuration 243 and 246. The results of both are presented and discussed below successively.

The LOFA experiment was started from an initial power level of 3.5 MW. The power distribution after reactor scram follows the time evolution of decay heat power that has been calculated by operator for the time up to 80 seconds after reactor scram (Fig. II-13). For the remaining time (80-800 seconds) the employed codes use either built in heat decay tables or the international standard ANS94 [II-5].

The transient is initiated from the nominal steady state conditions of 3.5 MW reactor power, 1.7 bar inlet pressure, 32.7 °C core inlet temperature and 211 kg/s total mass flow rate (corresponding to 6.27 kg/s for the IFA). The progression of the transient is summarized in the following event sequence:

- $t = 0$ sec.: pumps trip, and mass flow rate decreases according to Fig. II-12;
- $t = 3$ sec.: reactor scram due to low flow (flow rate 93% of nominal);
- $t = 46$ sec.: opening the coupling valve after decoupling the pump header (flow rate 27% of nominal);
- $t \sim 100$ sec: onset of flow reversal.

To demonstrate the typical evolution of predicted normalized core mass flow rate during LOFA, the results of the codes from SYR, both MERSAT and RELAP, and ROK's RELAP are presented in Fig. II-14. Following the reactor operation at nominal condition the transient begins with the pump trip that occurs at $t=0$. Once the flow rate reaches 93% of its nominal value (almost 3 seconds after the transient begins) the reactor scram is initiated. After reaching about 27% of nominal flow rate the pump header is decoupled and the coupling valve is opened (46 seconds after transient begin) so that the core outlet is directly linked to the reactor pool and the reactor core is no longer connected to the primary pump. In the following short time the forced downward flow through the core diminishes rapidly whereas at the same time the upward natural flow increases gradually and dominates finally inducing flow reversal from the downward forced circulation to the upward natural circulation (about 100 seconds after the transient begins). After a period of small oscillation, the core mass flow of the prevailing natural circulation stabilizes at a certain small value. Up to the time point of opening the coupling valve the three codes predict the same behaviour. However, the flow reversal is initiated earlier by RELAP at almost 75 seconds from transient initiation compared to 100 seconds by MERSAT. In addition, after 250 seconds from transient initiation the natural circulation flow rate of MERSAT reaches about 2.7% of the nominal value (-5.5 kg/s) compared to 1.9% (-4 kg/s) for RELAP from SYR and 1.26% (-2.7 kg/s) ROK.

The predicted different flow rates of both RELAP models demonstrate the sensitivity of flow reversal to the opening time of coupling valve. The predicted higher flow rate of MERSAT compared to RELAP refers to the possible impact of the employed heat transfer models in the natural circulation regime in both codes. Thus, comprehensive sensitivity analysis to the NC valve opening time is recommended to explaining the first evidence whereas additional validation –against single effect test- of the employed heat transfer models in both codes is advisable.

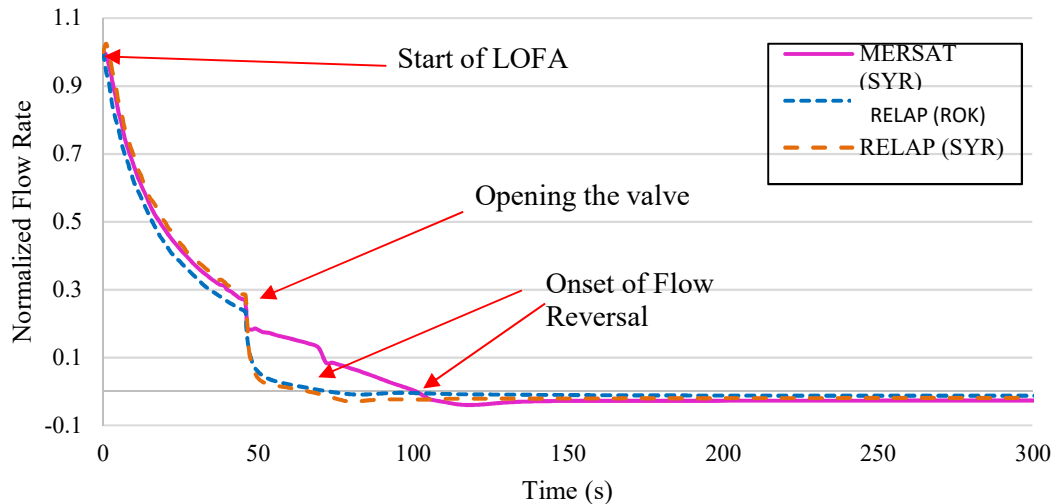


FIG. II-14. MERSAT result for the evolution of relative mass flow of IEA-R1 core during LOFA.

The behaviour of flow reversal can be taken from Fig. II-15 and Fig. II-16 representing comparatively the predicted and measured time evolution of coolant inlet and outlet temperatures of IFA during the considered LOFA.

The outlet temperature evolution shows two peaks. The first small peak is observed shortly after the transient begins (pump trip) as a consequence of mass flow decrease whereas the reactor power remains at its initial value (during the first 3 sec). Once the reactor scram is initiated the reactor power decreases faster than the mass flow and the coolant outlet temperature decreases abruptly from the first maximum to its minimum value. The measured outlet temperature reaches its first maximum of 37.8 °C at 6 seconds and decreases hereafter to a minimum of 33.3 °C at 12 seconds. After completing this phase and as a consequence of the continuing mass flow reduction (where at the same time the decay heat of medium and long lived fission products are decreasing slowly) the measured outlet temperature increases again and reaches its maximum of 38.65 °C (at 88 seconds). During the first 90 seconds of the transient, the inlet temperature remains constant at its initial value of 32.7 °C and prevails until the onset of flow reversal, where both temperatures interchange their positions. The outlet temperature (new inlet temperature) drops to the level of pool temperature (initial inlet temperature) whereas the inlet temperature (new outlet temperature) starts to increase and reaches a maximum of 44.4 °C after 123 seconds after transient initiation.

The observed spike of new outlet temperature is a direct consequence of flow stagnation at the outlet zone of fuel assembly immediately at the flow reversal. During this phase the transferred decay heat heats up the coolant along the fuel assemblies before establishing a fully developed natural circulation that assures the removal of remaining decay heat.

The qualitative comparison illustrates that all codes are able to simulate the trend of transient behaviour of coolant temperatures with different degrees of accuracy. The less accurate results are observed for the cases of GRE and ROM where the spikes of inlet and outlet temperatures are clearly underestimated. ROK and RELAP from SYR show similar trend with conservative estimation of inlet and outlet temperature spikes. ARG predicts the spike of outlet temperature correctly whenever the time interval around the peak is very sharp. For the inlet temperature the spike is underestimated, and its time occurrence is too early. MERSAT from SYR shows the best agreement for both temperature spikes.

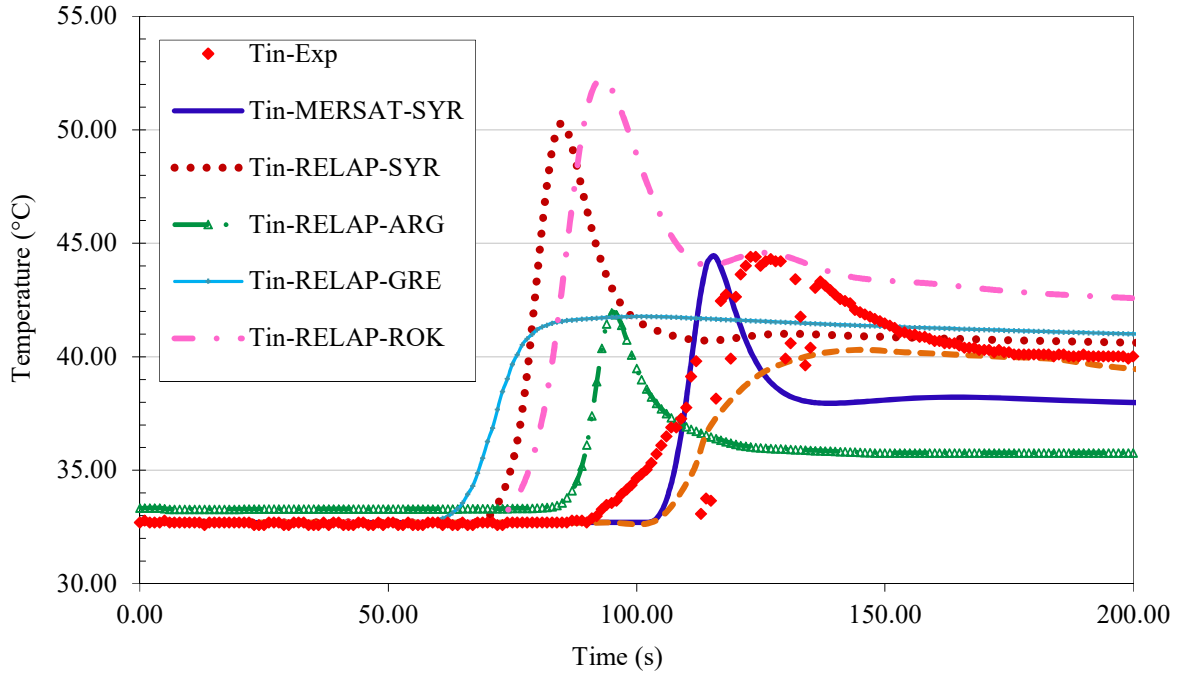


FIG. II-15. Evolution of coolant inlet temperatures of IFA during LOFA (Configuration 243).

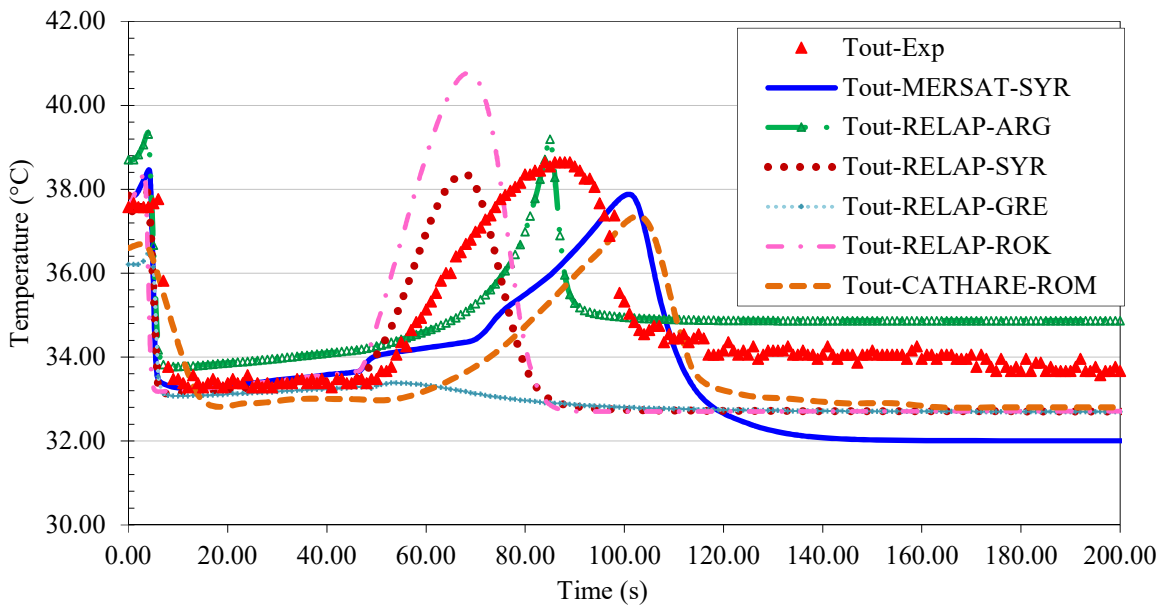


FIG. II-16. Evolution of coolant outlet temperatures of IFA during LOFA (Configuration 243).

The quantitative comparison of measured and predicted inlet and outlet temperature peaks is presented in Table II-6. The table shows the deviation of code predictions from experiment for both temperature peak values and its occurrence. The deviation varies between -5.4% and 17.6% for the inlet temperature peak and -31% and +17% for its onset time. For the outlet condition the deviation varies between -13.5% and +5.6% for outlet temperature peak and -38.6% and +18.2% for its onset time. The biggest discrepancy is observed for GRE for both coolant inlet and outlet temperatures. For this case the expected peaks is less apparent. The best agreement is by MERSAT from SYR followed by ARG. For ROM the one time of temperature peaks is delayed.

TABLE II-6. COMPARISON OF MEASURED AND PREDICTED COOLANT INLET AND OUTLET TEMPERATURE PEAKS AND THEIR TIME OCCURRENCES DURING LOFA OF IEA-R1 (CONFIGURATION 243)

	T_{in}^{max}	t_{in-max}	Deviation		T_{Out}^{max}	t_{out}^{max}	Deviation	
	(°C)	(s)	T	t	(°C)	(s)	T	t
Experiment	44.4	123	0.0%	0.0%	38.6	88	0.0%	0.0%
ARG	42.0	95	-5.4%	-22.8%	39.1	85	1.3%	-3.4%
GRE	41.8	102	-5.9%	-17.1%	33.4	54	-13.5%	-38.6%
ROK	52.2	93	17.6%	-24.4%	40.8	68	5.6%	-22.7%
ROM	40.3	144	-9.2%	17.1%	37.3	104	-3.4%	18.2%
SYR (RELAP)	50.3	85	13.3%	-30.9%	38.4	68	-0.6%	-22.7%
SYR (MERSAT)	44.4	115.8	0.0%	-5.9%	37.9	101	-1.8%	14.8%

Deviation: relative difference to experiment for temperature (T) and related time (t)

Figure II-17 presents the resulting evolution of temperature difference between inlet and outlet. It depicts the flow reversal time –where the temperature difference vanishes – and gives indication about the prevailed natural circulation during the following time. One can see that after establishing the fully developed natural circulation, i.e. 150 to 200 seconds after transient initiation, both inlet and outlet temperatures decrease to a quasi-constant level. The evolution trend of coolant temperature difference has direct impact on the clad temperature development demonstrated below. As presented in Table II-7 the observed temperature differences between inlet and outlet temperature are 6.35 °C for experiment, 1 °C for ARG, 8.3 °C for GRE, 9.9 °C for ROK, 9.3 for ROM, 6.65 °C for RELAP from SYR and 5.9 °C for MERSAT from SYR. MERSAT and CATHARE show the best agreement. RELAP predictions are relatively close to each other except in case of ARG that shows remarkable low value of about 1 °C. This result indicates the important impact of user effect since RELAP results vary between the involved teams.

TABLE II-7. MEASURED AND PREDICTED COOLANT TEMPERATURE DIFFERENCE AFTER ESTABLISHING THE FULLY DEVELOPED NATURAL CIRCULATION DURING LOFA OF IEA-R1 (CONFIGURATION 243)

	Experiment	ARG	GRE	ROK	ROM	SYR (RELAP)	SYR (MERSAT)
$\Delta T_{coolant}$ (°C)	6.35	1	8.3	9.9	6.65	7.9	5.97
Deviation (%)	0%	-84%	31%	56%	5%	24%	-6%

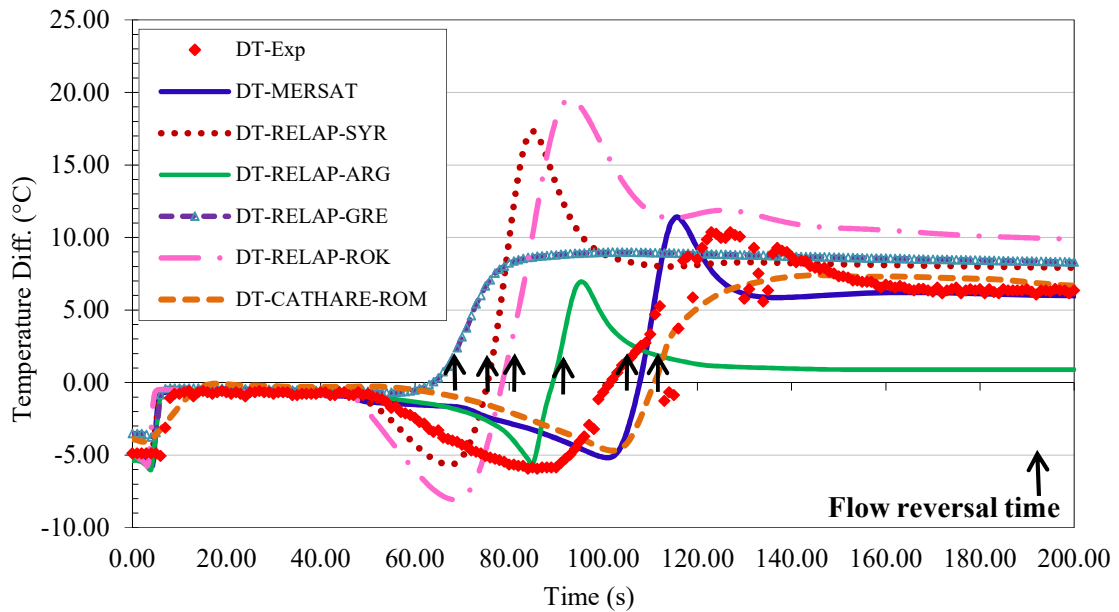


FIG. II-17. Evolution of coolant temperature difference of IFA during LOFA (Configuration 243).

Figure II-18, Fig. II-19 and Fig. II-20 present selected results of the benchmark calculation for the clad temperatures at 252.5 mm, 432.5 mm and 552.5 mm along the IFA for central and lateral fuel plates (compare with Fig. II-2). The predicted codes results show quantitatively clear differences regarding second peak and its time occurrences. However, the qualitative trend of the time evolution is relatively similar characterized by first and second peaks followed by stable final range. All predicted results of clad temperatures are conservative as the calculated peaks are higher than the experiment and their time occurrences are earlier. Remarkable is the time occurrence of clad temperature spike in case of GRE that appears about 50 seconds ahead of the experiment. The best qualitative agreement is observed by MERSAT from SYR followed by ARG and ROM.

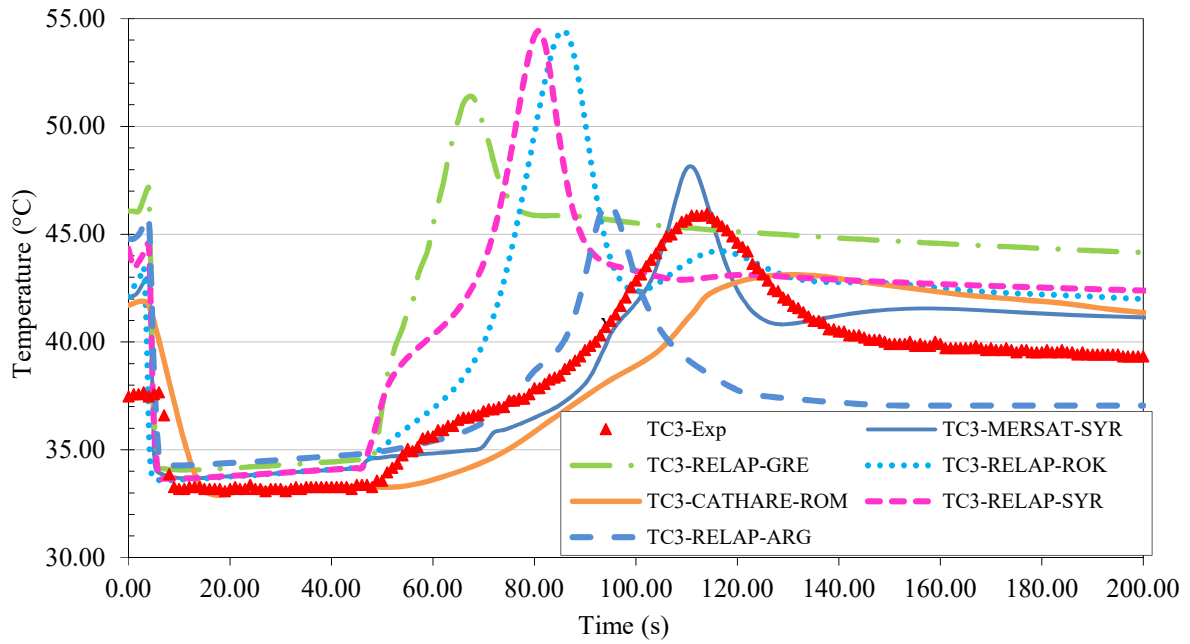


FIG. II-18. Evolution of clad temperatures at 252.5 mm from the inlet of IFA (Configuration 243).

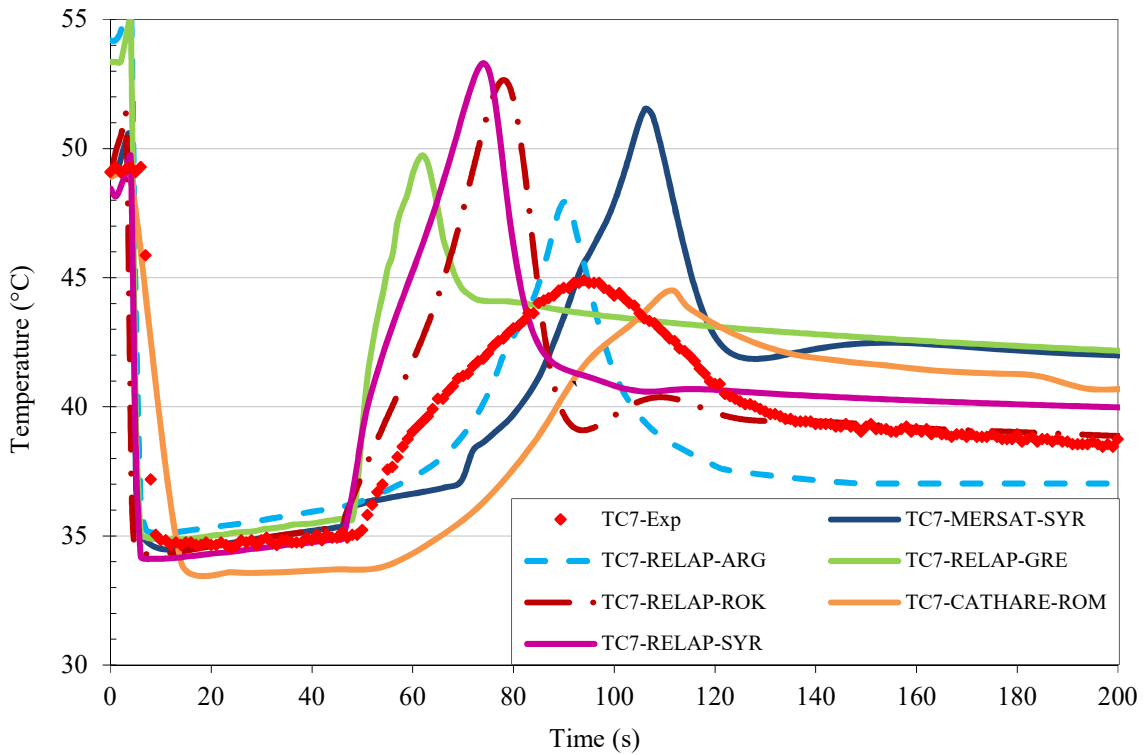


FIG. II-19. Evolution of clad temperatures at 432.5 mm from the inlet of IFA (Configuration 243).

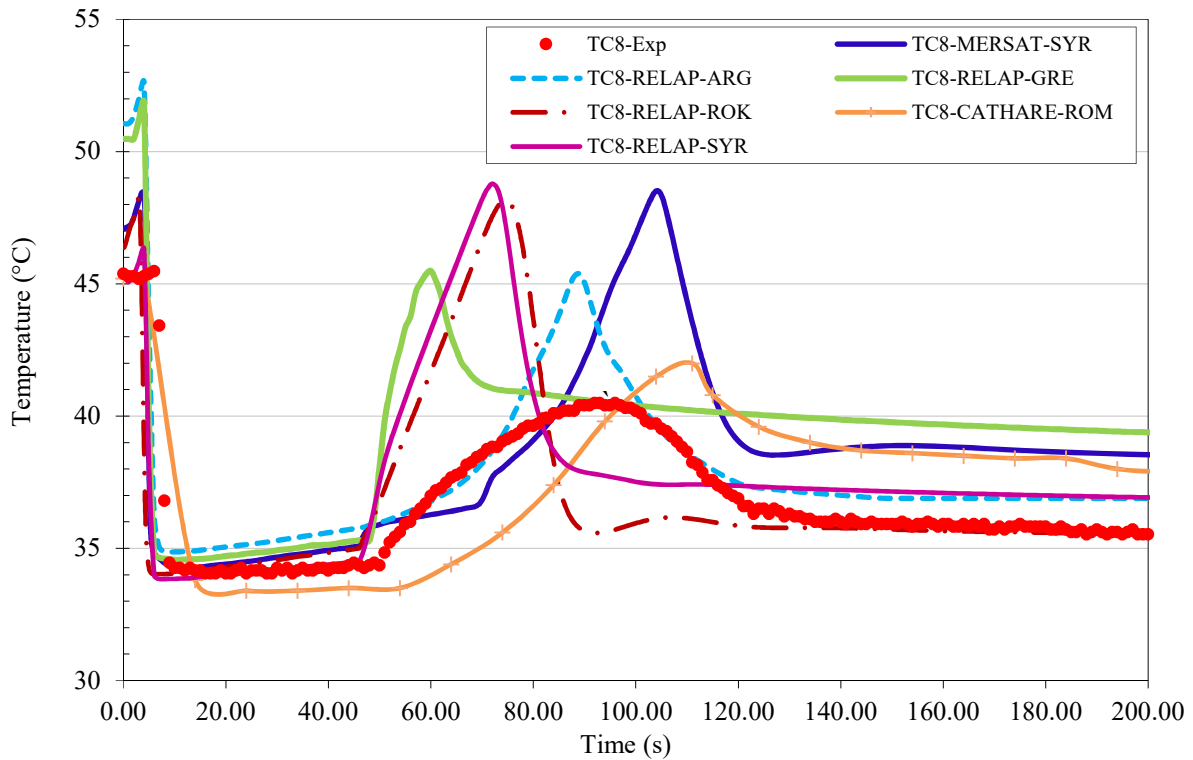


FIG. II-20. Evolution of clad temperatures at 552.5 mm from the inlet of IFA (Configuration 243).

Table II-8 summarizes the calculated peak clad temperatures in comparison with the experiment for all considered positions. The average relative deviation varies between +3% for ROM and +20% for RELAP from SYR. As depicted in Fig. II-21 the majority of codes predictions are scattered above the full agreement line within a deviation of +20%. Thus, they overestimate the measurements and are therefore conservative from the view point of safety analysis. One exception is observed for ROM where the predicted peaks underestimate slightly the measurements.

TABLE II-8. DEVIATION OF CALCULATED CLAD PEAK TEMPERATURES (°C) FROM THE MEASUREMENTS DURING LOFA OF IEA-R1 (CONFIGURATION 243)

	TC2	TC3	TC4	TC5	TC6	TC7	TC8	TC10	TC12	AVD
Experiment	44.2	46.0	45.7	42.7	45.1	44.9	40.5	42.5	41.9	
ARG	47.0	46.4	46.6	47.8	47.2	47.9	45.4	44.8	45.7	
Deviation	6%	1%	2%	12%	5%	7%	12%	6%	9%	7%
GRE	52.2	51.4	52.7	49.2	48.5	49.7	45.5	44.9	45.9	
Deviation	18%	12%	15%	15%	7%	11%	12%	6%	9%	12%
ROK	44.0	43.5	44.5	50.7	49.9	51.5	48.3	47.7	48.9	
Deviation	0%	-5%	-3%	19%	11%	15%	19%	12%	17%	11%
ROM	42.4	43.1	42.8	43.4	44.1	44.5	42.0	42.5	42.9	
Deviation	-4%	-6%	-6%	2%	-2%	-1%	4%	0%	2%	3%
SYR (RELAP)	54.4	54.4	55.6	53.3	53.3	53.3	48.8	48.8	48.6	
Deviation	23%	18%	22%	25%	18%	19%	20%	15%	16%	20%
SYR (MERSAT)	49.0	48.1	49.2	51.3	50.6	51.5	48.5	48	48.7	
Deviation	11%	5%	8%	20%	12%	15%	20%	13%	16%	13%

AVD: average relative deviation

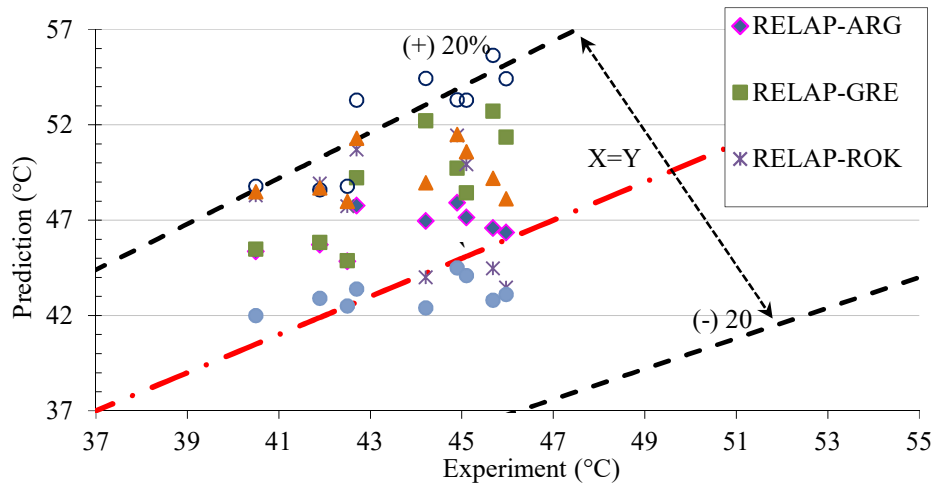


FIG. II-21. Comparison of measured and predicted maximum clad temperatures during LOFA of IEA-R1 (Configuration 243).

II-3.5. Benchmark Results of IEA-R1 for Configuration 246

This configuration is similar to the previous one (243) except the following differences related to geometrical and initial conditions of performed LOFA experiment [II-1], [II-3]:

- The IFA is located in a different radial position inside the core (see Fig. II-3). The consequence is different radial and axial power distributions.
- The configuration considers –for one part- a box around the IFA with the purpose of eliminating the cross flow between the bordering fuel assemblies in the outer zones of fuel assemblies and reflector. With this box the coolant flow in both zones is only downstream.
- The reactor was operated at nominal power of 4 MW before LOFA began, compared to 3.5 MW for configuration 243.

II-3.5.1. Estimation of inlet temperature

Due to an instrumentation failure during the experiment the thermocouple at inlet of the IFA failed. Thus, the coolant inlet temperature at the entrance of the IFA was not measured. Two approximations were applied to estimate the inlet temperature before the initiation of the transient.

- Assuming that the inlet temperature just before the transient is equal to the outlet coolant temperature measured after the core flow reversal and establishing the quasi-stationary upward flow of natural circulation. Since in both cases the water is flowing to the core directly from the pool. This assumption is valid by assuming a homogeneous pool water temperature that doesn't remain constant during the short time of LOFA (about 200 sec). In fact, the new inlet temperature (after flow reversal) has to be slightly lower than the inlet temperature before the LOFA, as the water after the flow reversal- is taken from the bottom of the pool where the water stagnates by slightly higher density compared to the water layers above the core. Thus, the Coolant Inlet Temperature is estimated to about 22.38 °C (averaged over the time interval (140 seconds to 300 seconds after establishing the natural circulation following the LOFA));

- Assuming a linear axial distribution of coolant temperature between the core inlet and outlet. The linear equation is established based on the coolant temperatures at the positions 252.5 mm and 552.5 mm from the inlet. The coolant temperature at 552.5 mm is known from the experiment whereas the coolant temperature at 252.5 mm is calculated using the measured clad temperatures TC2 and the temperature difference of clad and coolant at the position 552.5 mm (the calculation based on the average values for the lateral plates only as the central plate show odd values). All temperatures are averaged over the time before LOFA begin (measurement time is about 27 sec).

Average temperature difference between clad and coolant at position 552.5 mm:

$$\Delta\bar{T}_{CF} = [(TC8 - TF9) + (TC12 - TF13)] / 2 = 8.836 \text{ } ^\circ\text{C} \quad (\text{II-3})$$

Average clad temperature at position 255.2 mm:

$$\bar{TC} = (TC2 + TC4) / 2 = 34783 \text{ } ^\circ\text{C} \quad (\text{II-4})$$

The coolant temperature at position 252.5 mm is estimated as follow:

$$TF2 = \bar{TC} - \Delta\bar{T}_{CF} = 25.945 \text{ } ^\circ\text{C} \quad (\text{II-5})$$

Thus, the measured coolant temperature at position 552.5 mm (TF9) and the estimated coolant temperature at position 252.5 mm (TF2) gives the following linear fitting for coolant temperature along the IFA length (z) (only inside the lateral plates):

$$TFz = 0.1557 z + 22.014 \quad (\text{II-6})$$

For the unknown coolant inlet temperature one finds:

$$T_{Inlet} = TFz(0) = 22.014 \text{ } ^\circ\text{C} \quad (\text{II-7})$$

Based on both approaches the coolant inlet temperature is assumed to be 22.2°C.

The simulation and calculation procedure for configuration 246 is exactly similar to that of configuration 243.

All participants used the same code models for the facility as in configuration 243. As all the employed codes use the one dimensional approach for modelling the fluid dynamic no cross flow is simulated in the external zones. Hence, the adopted modelling approach for the reactor core including IFA is not capable to model the existence of a box surrounding the core. However, it is expected that the differences in the flow rate of the IFA will have a second order impact on the results. More important is the differences in the initial conditions of pool temperature. Thus, the discussion of calculation results below is limited to the case with box. The resulting temperatures behaviour for the case without box seems to be similar.

The transient is initiated from the nominal steady state conditions of 4 MW reactor power, 1.7 bar inlet pressure, 22.2 °C core inlet temperature and 211 kg/s total mass flow rate (corresponding to 6.27 kg/s for the IFA). The progression of the transient is summarized in the following event sequence:

- t= 0 seconds: pumps trip, and mass flow rate decreases according to Fig. II-12;

- t=4 seconds: reactor scram due to low flow (flow rate 93% of nominal);
- t=46 seconds: opening the coupling valve after decoupling the pump header (flow rate 27% of nominal).

The initial pool temperature, during reactor shutdown, was 18.3 °C and 20.9 °C for the case with box (WB) and without box (WOB) respectively.

II-3.5.2. Steady state benchmark results of IEA-R1

The SS data for the measured temperatures refer to the values averaged over the time interval immediately before starting the LOFA. Table II-9 summarizes the SS benchmark results at the reactor power of 4 MW for the employed codes that are -for configuration 246- limited to RELAP and MERSAT users.

The quantitative evaluation is similar to the configuration 243. The agreement between calculation and measurement is better for the lateral than for the central positions. The absolute local difference of prediction to experiment varies between -9.6 °C and +9.8 °C corresponding to a maximum relative deviation of -30% and +33% respectively. The discrepancy for configuration 246 is higher than for configuration 243. However, like by configuration 243 the maximum discrepancy is observed at the central position of IFA (TC3). The trend of high deviation is observed by all teams which points to a possible source of uncertainty in the experimental data.

The resulting AVD shows best agreement for MERSAT from SYR with 7.8% followed by RELAP from SYR with 9.5%, 9.9% for GRE, 10.7% for ROK and 12.6% for ARG.

TABLE II-9. BENCHMARK RESULTS OF THE APPLIED CODES FOR THE SS OPERATION AT 4 MW OF IEA-R1 (CONFIGURATION 246).

T (°C)	Exp	ARG		GRE		ROK		SYR		SYR	
		RELAP	Rel. Diff	RELAP	Rel. Diff	RELAP	Rel. Diff	MERSAT	Rel. Diff	RELAP	Rel. Diff
TC2	35.0	38.4	9.87%	38.97	11.5%	36.4	4.1%	36.6	4.6%	39.2	12.0%
TC3	29.3	37.6	28.2%	38.52	31.5%	35.4	20.9%	36.6	24.8%	39.1	33.5%
TC4	34.5	38.5	11.5%	38.85	12.6%	36.3	5.2%	36.5	5.8%	39.0	13.1%
TC5	46.0	46.7	1.6%	45.01	-2.1%	42.1	-8.4%	43.6	-5.0%	46.0	0.0%
TC6	36.9	45.6	23.5%	44.48	20.6%	40.8	10.6%	43.7	18.5%	45.6	23.5%
TC7	42.7	46.8	9.7%	45	5.5%	42.1	-1.4%	43.7	2.4%	45.6	6.8%
TC8	41.0	43.9	7.1%	42.66	4.0%	37.2	-9.2%	41.4	1.0%	41.7	1.6%
TC10	35.7	43.0	20.5%	42.21	18.3%	36.3	1.7%	41.5	16.4%	41.3	15.8%
TC12	39.4	44.0	11.9%	38.97	-1.0%	37.3	-5.3%	41.5	5.5%	41.3	5.0%
TF1	22.2	-	-	22.7	0.0%	22.4	0.0%	22.2	0.0%	22.2	0.0%
TF9	32.0	-	-	28	-12.5%	22.4	30.0%	28.2	11.8%	28.4	11.2%
TF11	29.8	-	-	27.87	-6.6%	22.4	24.9%	28.2	-5.3%	28.4	-4.7%
TF13	30.6	-	-	28	-8.5%	22.4	26.8%	28.2	-7.7%	28.9	-5.5%
TF14	28.8	28.2	-2.1%	27.56	-4.4%	29.1	0.9%	28.9	0.2%	29.0	0.6%
		AVD	12.6%	AVD	9.9%	AVD	10.7%	AVD	7.8%	AVD	9.5%

The general trend of the achieved benchmark results of the SS condition indicates that the code predictions for clad temperatures tend to overestimate the measurements, whereas the calculated coolant temperatures underestimate the measurements.

II-3.5.3. LOFA benchmark results of IEA-RI for Configuration 246

The transient behaviour can be taken from Fig. II-22 representing comparatively the predicted and measured time evolution of coolant outlet temperatures of IFA during the considered LOFA wit box around the IFA.

The general trend is similar to the case of configuration 243. The expected first peak after the pump trip isn't identifiable for this experiment due to the dominating fluctuation. Following the reactor shutdown, the measured outlet temperature decreases from about 28.6 °C to an average minimum of about 22.33 °C during the period 6-46 seconds from transient begin. It increases again and reaches its maximum of 30.55 °C (at 77 seconds). It drops thereafter to the level of pool temperature (initial inlet temperature) of about 22.5 °C. As the inlet temperature thermocouple failed during the experiment not time evolution can be tracked.

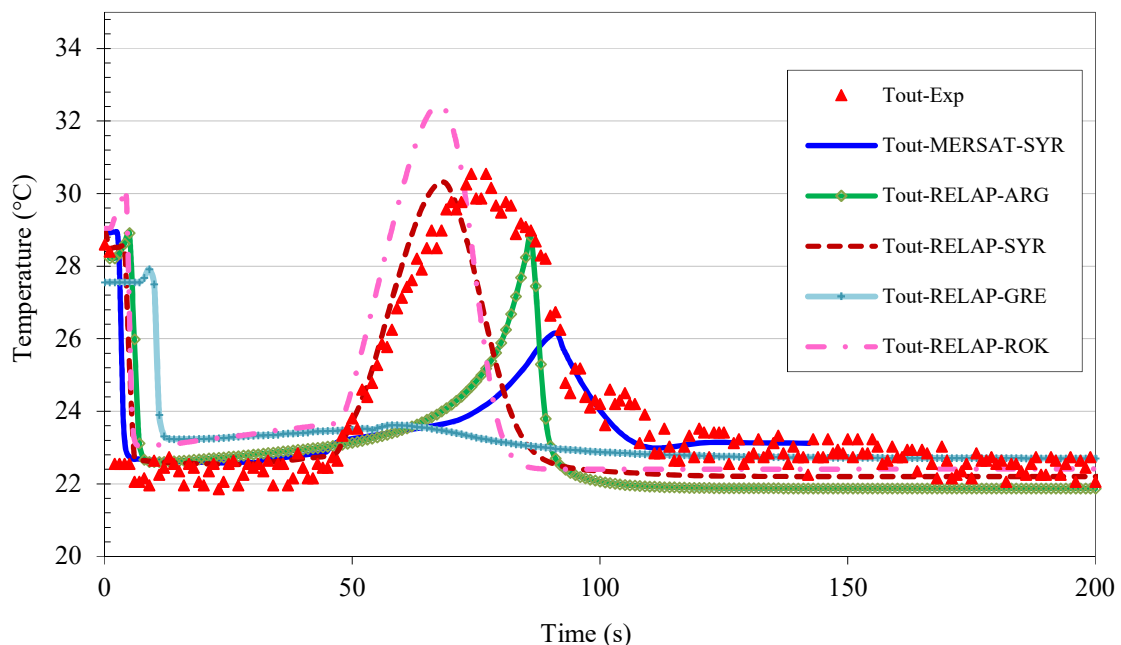


FIG. II-22. Evolution of coolant outlet temperatures of IFA during LOFA (Conf. 246).

The qualitative comparison illustrates that all codes are able to simulate the trend of transient behaviour of coolant temperatures with different degrees of accuracy. The poorer agreement is observed for the cases of GRE and MERSAT from SYR and ARG where the spikes of outlet temperatures are clearly underestimated and delayed in their time occurrences. ROK and RELAP from SYR show similar trend of outlet temperature spike. RELAP from SYR shows the best with slight underestimation of out let temperature peak.

The quantitative comparison of measured and predicted outlet temperature peaks are presented in Table II-10. The deviation varies between -22.7% and 6.2% for the outlet temperature peak and -24.7% and +10.4% for its onset time. The agreement is lower than for configuration 243. Again, the biggest discrepancy is observed for GRE where the expected peak mismatches by

fare the measurement. The best agreement is observed for RALAP from SYR followed by ARG.

TABLE II-10. COMPARISON OF MEASURED AND PREDICTED COOLANT OUTLET TEMPERATURE PEAKS AND THEIR TIME OCCURRENCES DURING LOFA OF IEA-R1 (CONFIGURATION 246)

	T_{Out}^{max} (°C)	t_{out}^{max} (s)	Deviation	
			T	t
Experiment	30.55	77	0.0%	0.0%
ARG	28.82	85	-5.7%	10.4%
GRE	23.62	58	-22.7%	-24.7%
ROK	32.45	67.6	6.2%	-12.2%
SYR (RELAP)	30.32	68	-0.7%	-11.7%
SYR (MERSAT)	26.15	91	-14.4%	18.2%

Deviation: relative difference to experiment for temperature (T) and related time (t)

Figure II-23, Fig. II-24 and Fig. II-25 present selected results of the benchmark results for the clad temperatures at 252.5 mm, 432.5 mm and 552.5 mm along the IFA for central and lateral fuel plates (compare with Fig. II-2). The predicted codes results show quantitatively clear differences regarding second peak and its time occurrences. However, the qualitative trend of the time evolution is relatively similar characterized by first and second peaks followed by stable final range.

All predicted results of clad temperatures are conservative as the calculated peaks are higher than the experiment –except for ARG- and their time occurrences are earlier. Remarkable is the time occurrence of clad temperature spike in case of GRE that appears about 50 seconds ahead of the experiment. The best qualitative agreement is observed by MERSAT from SYR followed by ARG.

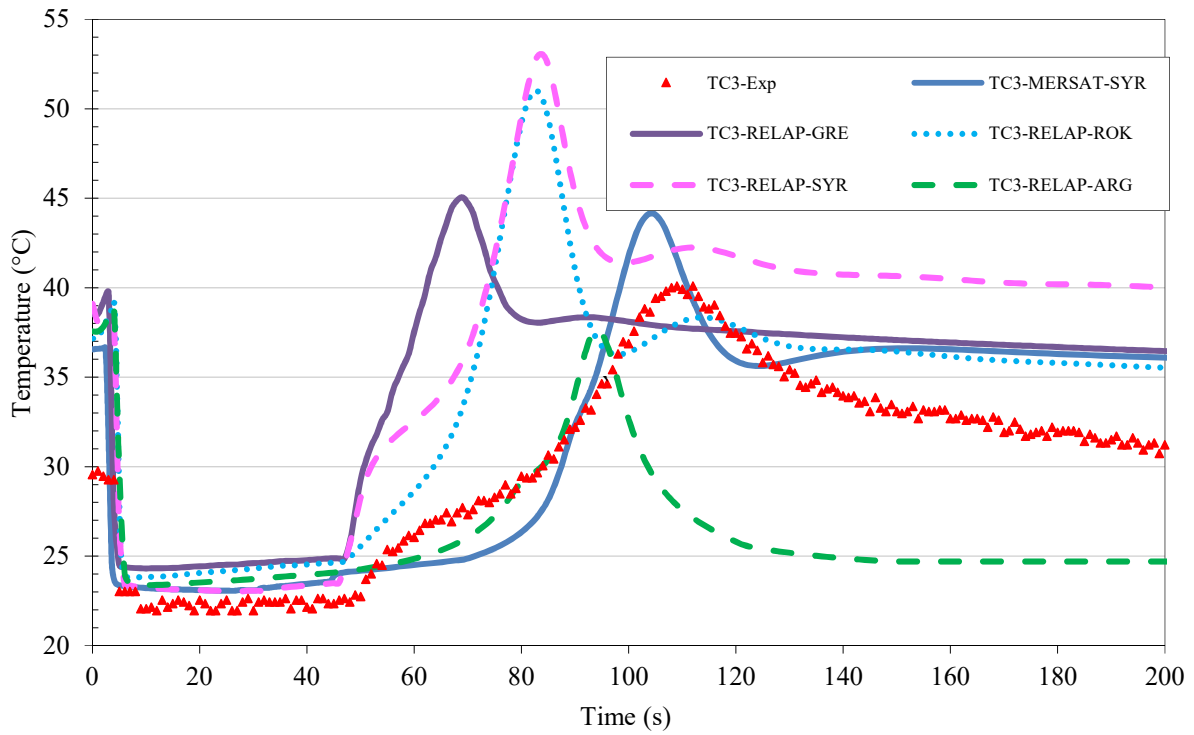


FIG. II-23. Evolution of clad temperatures at 252.5 mm from the inlet of IFA (Configuration 246)

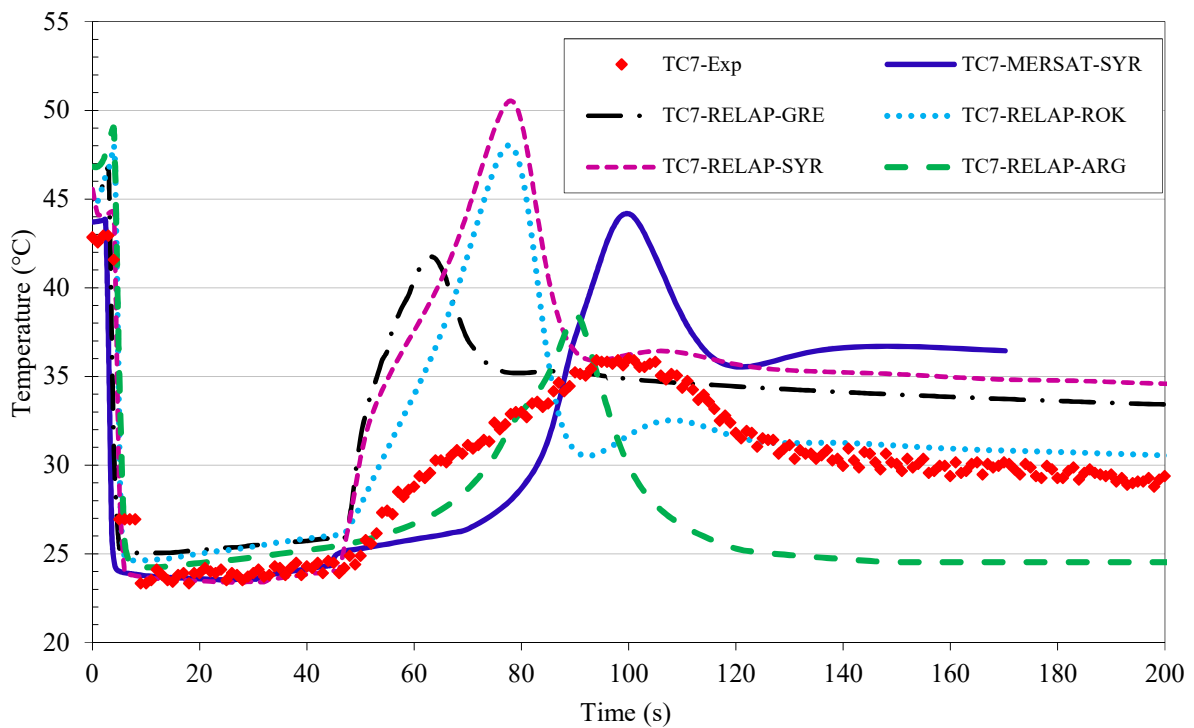


FIG. II-24. Evolution of clad temperatures at 432.5 mm from the inlet of IFA (Configuration 246).

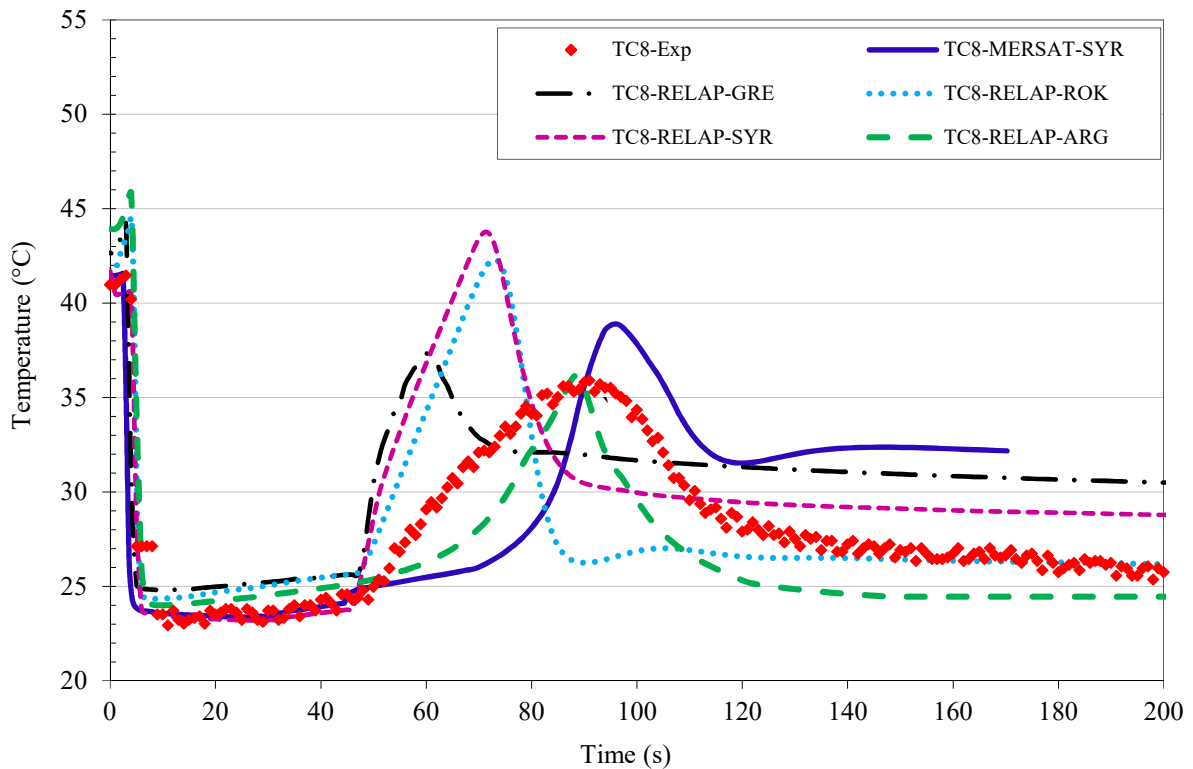


FIG. II-25. Evolution of clad temperatures at 552.5 mm from the inlet of IFA (Configuration 246).

Table II-11 summarizes the calculated peak clad temperatures in comparison with the experiment for all considered positions. The average relative deviation varies between +4% for ARG and +19% for ROK. As depicted in Fig. II-26 the majority of codes predictions are scattered above the full agreement line within a deviation of +20%. Thus, they overestimate the measurements and are therefore conservative from the view point of safety analysis. One exception is observed by ARG where the predicted peaks underestimate the measurements.

TABLE II-11. BENCHMARK RESULTS OF CLAD PEAK TEMPERATURES DURING LOFA OF IEA-R1 (CONFIGURATION 246)

	TC2	TC3	TC4	TC5	TC6	TC7	TC8	TC10	TC12	AVD
Experiment	40.2	40.1	37.5	39.2	39.2	36.0	35.9	36.1	32.7	
ARG	37.7	37.7	36.9	38.7	38.7	38.4	36.1	36.1	36.1	
Deviation	-6%	-6%	-2%	-1%	-1%	7%	1%	0%	10%	4%
GRE	45.4	45.1	45.3	41.7	41.4	41.7	37.3	37.1	37.4	
Deviation	13%	12%	21%	6%	6%	16%	4%	3%	14%	11%
ROK	39.4	39.2	39.3	48.0	48.0	48.0	44.6	44.7	44.6	
Deviation	-2%	-2%	5%	22%	22%	33%	24%	24%	36%	19%
SYR (RELAP)	53.7	53.0	53.0	50.1	50.5	50.5	43.7	43.9	43.9	
Deviation	34%	32%	41%	28%	29%	40%	22%	22%	34%	31%
SYR (MERSAT)	44.1	44.2	44.1	44.1	44.2	44.1	38.9	38.9	38.9	
Deviation	10%	10%	18%	12%	13%	23%	8%	8%	19%	13%

AVD: average relative deviation

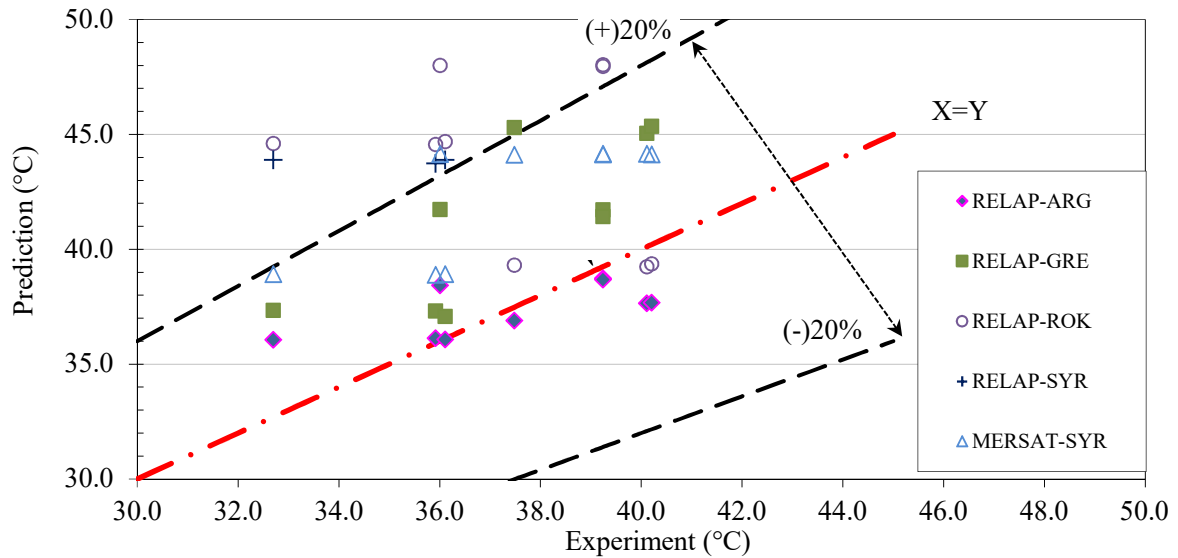


FIG. II-26. Comparison of measured and predicted maximum clad temperatures during LOFA of IEA-R1 (Configuration 246).

II-4. CONCLUSIONS

Special thermal-hydraulic measurements have been performed in the Brazilian research reactor IEA-R1 using an IFA that was placed in two different core positions. The achieved measurements cover coolant and clad temperatures as well flow rate during LOFT. The measurements have been used by 5 country teams to benchmark the thermal-hydraulic codes RELAP, MERSAT, CATHARE and PARET. The benchmark results indicate that the predicted evolution of coolant and cladding temperatures follow in general the overall trend of the measurements. However, the predicted clad temperature peaks overestimate the measurements by a maximum of about 20%. Furthermore, the time occurrences of the peak temperatures are generally earlier than the experimental results. The results are, from the safety assessment point of view, conservative and may be regarded as acceptable. Temperatures predictions (coolant and cladding) have much faster gradients than the measurement.

The comparison of RELAP results of 4 of the participating teams show remarkable differences which indicate the importance of user effect. Furthermore, the observed discrepancies to the experimental data and between the codes point to the need for possible improvement in selected physical models of the employed codes, in particular for the natural circulation regime. However, the final decision to rely upon such measurements to validate the envisaged code modifications requires considering following recommendations concerning the quality of experimental data.

- Special attention is required when measuring coolant and clad temperatures. Specifically, validation that the thermocouples are indeed measuring the required quantity i.e. clad temperature or coolant temperature at a well specified location. In the case of the coolant temperature there is a temperature gradient near the surface of the fuel plate and to be considered when locating the thermocouple;
- The impact of the process of instrumenting the FA on the thermal-hydraulic conditions and hence the parameters being measured have to be carefully considered and quantified

if possible. Hence, uncertainties analysis of experimental data could improve the data quality and allow sensitivity analyses to be performed;

- Verification of the flow rate distribution between the IFA channels is important, and has to be performed for the experiment or shown to be independent of core position;
- The time response of the thermocouples needs to be verified and stated in the benchmark;
- The installation of the box around the core of IEA-R1 is a good solution to reduce the temperature of the external plates. However, since the employed codes can only capture one dimensional thermal-hydraulic behaviour, the impact of such box on the cross flow cannot be covered;
- Due to the prevailed natural circulation (NC) during the second phase of the LOFA, detailed evaluation of heat transfer coefficient and flow rate evolution for NC is of importance for possible codes improvement.

REFERENCES TO ANNEX II

- [II-1] INTERNATIONAL ATOMIC ENERGY AGENCY, Research Reactor Benchmarking Database: facility specification and experimental data, Technical Report Series 480, IAEA, Vienna (2013).
- [II-2] UMBEHAUN, P.E., Description of IEA-R1 reactor, Technical Report Series 480, IAEA, Vienna, (2012).
- [II-3] UMBEHAUN, P.E., DELVONEI, D., TORRES, W., FILHO, W., Final report for the coordinated research project 1496. IPEN-CNEN, Brazil (2012).
- [II-4] W. M. TORRES, P. E. UMBEHAUN, D. A. ANDRADE AND J. A. B. SOUZA, A MTR fuel element flow distribution measurement, preliminary results. International Meeting on Reduced Enrichment for Research and Test Reactors, (2003).
- [II-5] HAINOUN, A., GHAZI, N., ALHABIT, F., Simulation of LOFA and RIA for the IEA-R1 Research Reactor using the Code MERSAT, ANE 35 **11** (2008) 2093-2104.

This Annex was reprinted from Nuclear Engineering and Design, Volume number 280, A. Hainoun, A. Doval, P. Umbehaun, S. Chatzidakis, N. Ghazi, S. Park, M. Mladin, A. Shokr, International benchmark study of advanced thermal-hydraulic safety analysis codes against measurements on IEA-R1 research reactor, Pages No. 233-250, Copyright 2014, with permission from Elsevier.

ANNEX III

BENCHMARK CONSOLIDATED RESULTS AGAINST EXPERIMENTAL DATA FROM MNR

S. E. DAY*, B. ERASMUS**, R. PRINSLOO**, J. TUÑÓN***, E. VILLARINO***

* McMaster Nuclear Reactor, McMaster University, 1280 Main St. W., Hamilton, Ontario, Canada, L8S 4K1

** Necsa, Pelindaba, Church Street extension west, Pretoria-West, Pretoria, South Africa, 0001

*** Nuclear Engineering Department, INVAP S.E., Av. Cmte. Luis Piedrabuena 4950 (R8403CPV) S.C. de Bariloche, Río Negro – Argentina

Annex Consolidator: S. E. Day

Abstract

The IAEA CRP (CRP 1496) on ‘Benchmarking, against Experimental Data, of the Neutronic and Thermal-hydraulic Computational Methods and Tools for Operation and Safety Analysis for Research Reactors’ provides a novel opportunity to benchmark and compare the accuracy and efficiency of both off-the-shelf and locally developed computational tools to a wide set of experimental research reactor benchmark analysis. In the scope of this project, various analysis groups have evaluated the McMaster Nuclear Reactor benchmark analysis – consisting of a variety of operational measurements. This report summarizes and compares the analysis methodologies adopted, the code systems employed, and the simulation results generated by the different analysis groups. A comparison of the computational results to supplied experimental results is provided in this report.

III-1. FOREWORD

The McMaster Nuclear Reactor (MNR) MNR Facility Specification has been documented in [III-1] and the associated benchmark specification is given in [III-2]. The participation for the MNR benchmark analysis is summarized in the following table.

TABLE III-1. MNR BENCHMARK ANALYSIS - PARTICIPANT SUBMISSION MATRIX

Group/Section	RR Worth	SSR Worth	Misc ρ Tests	Radial Wires	Axial Wires	Void Expt	Pool Temp
ARG	✓	✓	-	-	✓	✓	✓
CAN	-	-	-	✓	✓	-	-
SAF	✓	✓	-	✓	✓	-	-

Consolidation activities were limited to the sections of the benchmark analysis associated with more than one submission. The Miscellaneous Reactivity Tests section of the MNR benchmark analysis does present challenges to both discrete ordinate and Monte Carlo methods in terms of material discontinuities and magnitude of reactivity changes, respectively. However, due to time constraints, this section was not completed by any participants and is not included herein. Neither are the Void Experiment and Pool Temperature Experiment sections of the benchmark analysis associated with the single submission from the Argentina group.

III-2. DESCRIPTION OF THE FACILITY

MNR is an open pool facility, licenced to operate up to a thermal power of 5 MW. The core is comprised of MTR-type fuel assemblies in a nine-by-six grid plate (Fig. III-1). The core is light-water cooled and moderated. One side of the core is reflected by a row of graphite assemblies while the other sides are flanked by of a large lead block and six radial beam-tubes. Cooling is

either via natural circulation for low power operation or via forced down-flow driven by the hydrostatic head of the pool and returned by a pump. The primary water system includes a hold-up tank and is coupled to a secondary system via a tube-and-shell heat exchanger. The secondary system is open to the atmosphere and includes a pair of cooling towers.

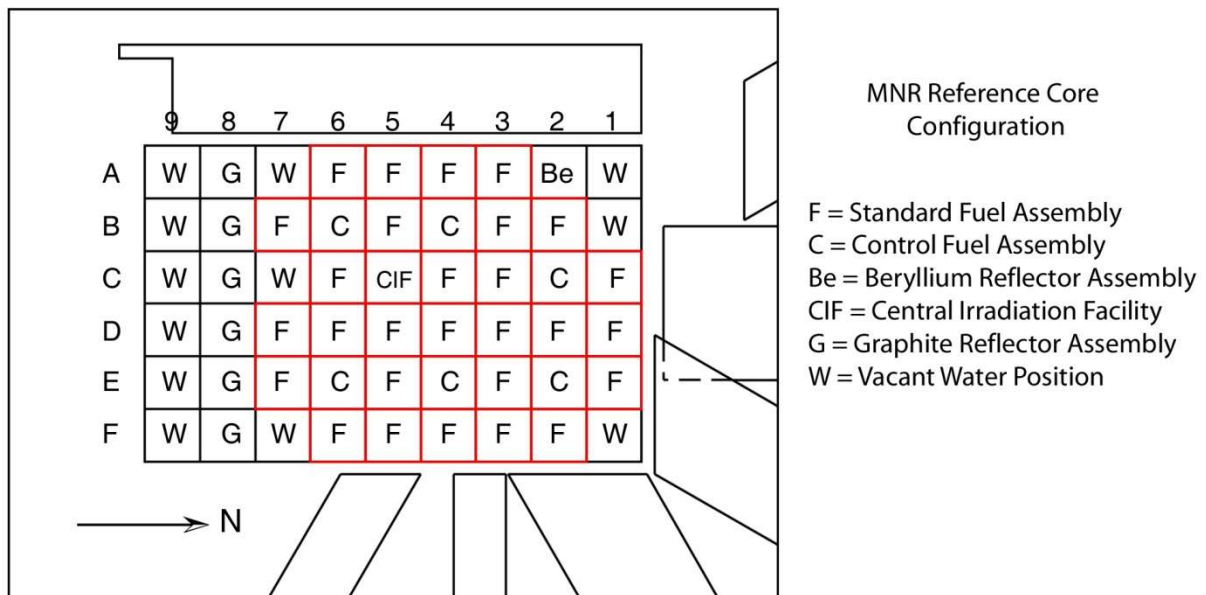


FIG. III-1. MNR reference core loading pattern.

The MNR core consists of a grid plate, fuel assemblies, reflector irradiation assemblies, a flux trap, a neutron source, and a fission chamber. Other devices which may be inserted in the grid plate are not considered part of the core but are treated as experimental facilities. Peripheral structures are six radial beam tubes (on the north and east sides of the grid plate) and a large lead block (on the west side of the grid plate). The MNR core is suspended from the operations bridge by the core support structure in the 10 m deep pool. The centreline of the active region of the core sits 1.67 m (5 ft 6 in) above the floor of the pool. The core is well removed from the pool walls, at the closest proximity there is on the order of 90 cm separation.

The MNR core is composed of standard-fuel, control-fuel, and reflector assemblies while also incorporating a series of irradiation positions. General core specifications are given in Table III-2. Typically, the fuelled region of the core is defined by Rows 1 to 7 on the grid plate (see Fig. III-1). A reflector row of graphite assemblies is situated in Row 8. The core also includes a central flux trap, which houses the cage of a graphite reflector assembly (geometrically the same as a graphite assembly but with the graphite block removed). A typical core contains on the order of 30 standard fuel assemblies and six control fuel assemblies. Presently the core is composed of LEU (19.75% enriched) fuel only. Past cores have also included HEU (93% enriched) fuel in both standard-style and 10-plate geometries as well as prototype LEU assemblies with slightly higher loading than standard. Refuelling is performed on a burn-up basis, i.e., fuel is replaced one assembly at a time once it reaches the nominal exit burn-up.

TABLE III-2. GENERAL CORE SPECIFICATIONS

Parameter	Value and Tolerance
Core shape	Varies within a 7 × 6 section of the 9 x 6 grid plate
Core lattice size (x)	8.100 cm
Core lattice size (y)	7.709 cm
Active core height	60 cm
Fuel Type	U ₃ Si ₂ -Al dispersion Al-clad curved plate fuel
Enrichment	Currently LEU (19.75%), and HEU (93%) prior to 2008
Coolant	Light water
Moderator	Light water
Reflector	Graphite
Recirculation	Natural circulation or forced downward flow
Nominal pool temperature	Room Temperature (approximately 20 °C)
Hydrostatic Head	Minimum 6.7 metres above core
Control system	5 gang operated shim-safety rods, 1 stainless steel regulating rod, all oval shell design

The MNR standard fuel assembly is comprised of 18 curved plates. The inner 16 plates contain fuel while the two outer plates are solid aluminium and are referred to as dummy plates. The plates are supported by two aluminium side-plates. An aluminium bottom end-fitting (or ‘snout’) is welded to the bottoms of the outer plates and side plates and fits into the MNR grid plate. This bottom end fitting provides a circular flow path for the coolant. The top extension of the outer plates and side plates constitutes a ‘top end fitting’ and includes a handle for latching with the MNR fuel tool.

The MNR core contains six control fuel assemblies which house the single regulating absorber rod and the five gang-operated shim-safety absorber rods. These assemblies have the same outer dimensions and bottom end fittings (snouts) as do the standard fuel assemblies. The MNR control fuel contains nine plates, all of which are fuelled (i.e., no dummy plates) and a central aluminium guide to house the absorber rod.

Further details and specifications of the MNR facility, core, and core components can be found in Ref. [III-1]. Specific core loading patterns and assembly burn-up estimates associated with the specific operational and experimental measurements are provided in Ref. [III-2].

III-3. DESCRIPTION OF TOOLS, CODES AND METHODS

A short description of the code combinations and tools used by each group is given in the following sections. Table III-3 summarizes the codes used by each group.

TABLE III-3. CODES USED BY PARTICIPATING GROUPS

Group	Codes
ARG	CONDOR/CITVAP
CAN	WIMS-ANL/REBUS-PC/MCNP5
SAF	OSCAR-4

III-3.1. Argentina: Codes, Tools, Models and Methods

The Argentina (ARG) group used CITVAP, a standard deterministic transport-theory cell code / diffusion-theory core code combination, for the simulation of the MNR benchmark analysis. CITVAP has the capability to perform neutronic calculations including a thermal-hydraulic feedback in the cross sections.

A high degree of detail was included in the spatial discretization of the cell calculations and a mesh spacing of less than 1 cm was adopted in the cell models. These models were used to provide three-group homogenized cross sections for the companion CITVAP core model of MNR, using the following energy group structure:

- Group 1: 10 MeV \rightarrow 0.825 MeV;
- Group 2: 0.821 MeV \rightarrow 0.625 eV;
- Group 3: 0.625 eV \rightarrow 0.0 eV.

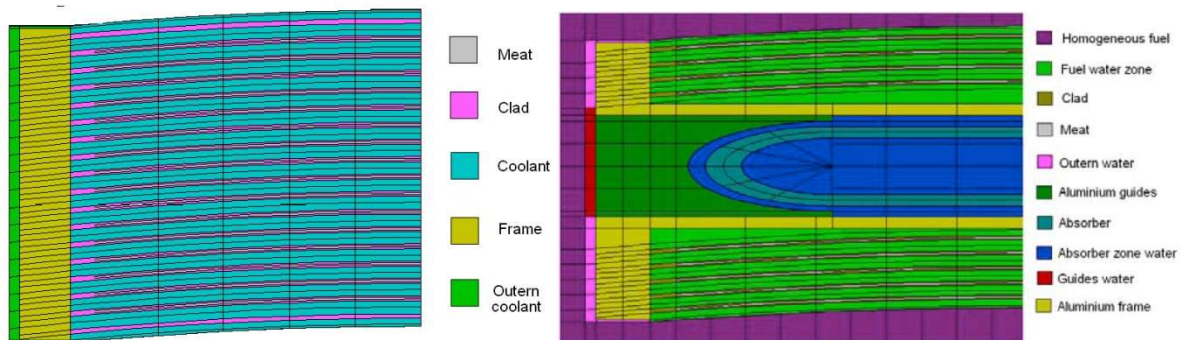


FIG. III-2. ARG standard fuel (left) and control-fuel (right) cell models.

At the cell level, a single cell model was constructed for each fuel type to model the active height of the assembly. For these cell models, half of the given assembly was modelled explicitly taking advantage of symmetry while fuel plate curvature was included, as shown in Fig. III-2.

For each control fuel assembly and absorber combination, a series of four cell models were constructed, with and without the absorber rod and guide insert. These cell models provide homogenized and condensed cross sections for the core model for all axial placements of the absorber rods within the control fuel.

Non-fuel assemblies (graphite, beryllium, irradiation positions) and other structures (lead block, beam tubes) were modeled at the cell level in 1-D infinite slab geometry using a homogeneous fuel material as a neutron source driver and including some extent of the specific assembly environment (e.g., some of the pool water for row 8 graphite assemblies). In the diffusion code, the core is modelled as follows, with its main constituents being:

axial burn-up distribution is for seven axial zones over the height of the fuel. This was retained in the CITVAP models and translated to 23 axial mesh zones. Specific model details related to individual sections of the MNR benchmark analysis are included in the experiment sections.

III-3.2. Canada: Codes, Tools, Models and Methods

The Canadian (McMaster University) (CAN) group performed analysis for this project based on the following codes:

- WIMS-ANL v.5.07;
- REBUS-PC v.1.4;
- MCNP5 v.1.60.

III-3.2.1. WIMS-ANL lattice cell models

The lattice/cell code WIMS-ANL (version 5.07, April 2004) is used to provide homogenized and collapsed cross section data, as a function of burn-up for fuel materials, for use in a full-core diffusion theory model. This code replaces the previously-used WIMS-AECL at MNR as the associated cross section libraries are more oriented towards research reactors as opposed to the CANDU power reactor system. The code is used in association with the WIMS-ANL 69-group library (based on ENDF/B-6, 2004/03/24) supplied with the code Version 5.07.

All models used the 69-group ENDF/B-VI based library supplied with the WIMS-ANL v. 5.07 code release. The PERSEUS (collision probability) transport solution method was used for the main transport routine with condensation to the 8-group energy structure summarized in Table III-4.

TABLE III-4. MNR CONDENSATION OF WIMS-ANL 69-GROUP LIBRARY

Broad Group Number	Main Transport Groups	Lower Energy Bound (eV)	Upper Energy Bound (eV)	Range
1	1-3	2.231×10^6	1.000×10^7	Fast
2	4-7	3.025×10^5	2.231×10^6	Fast
3	8-15	5.53×10^3	3.025×10^5	Fast
4	16-28	3.300	5.530×10^3	Resonance
5	29-33	1.150	3.30	Thermal
6	34-46	5.000×10^{-1}	1.150	Thermal
7	47-55	1.400×10^{-1}	5.00×10^{-1}	Thermal
8	56-69	1.000×10^{-5}	1.400×10^{-1}	Thermal

The MNR fuel is modeled using a 1-D slab unit cell 3-region geometry. These models incorporate fuel depletion via burn-up at average power ratings. For a standard fuel assembly, the side regions and dummy plate regions are modeled using a similar 1-D slab unit cell approach but with an additional ‘extra region’ slab representing the non-fuel region of interest.

For control fuel assemblies the same approach is taken for the fuel zones as for the standard fuel. Super-cell models in 1-D slab geometry are used to model the guide and control slot regions of the control fuel, with and without the absorber guide tube. The super-cell approach uses a fresh-fuel standard 1-D slab unit cell model to define a driver fuel region in the second geometry which includes the non-fuel regions. For the absorber rods multi-plate 1-D slab models were created to represent the entire control fuel assembly with absorber present. For the Ag-In-Cd shim-safety rods and the stainless-steel regulating rod, the thickness of the rod was

conserved as was the volume of the water both surrounding and inside the rod annulus. Burn-out of the absorber materials was not considered.

Due to geometric limitations of the WIMS-ANL code the curved plates of the SF and CF assemblies were modeled as straight. Material volumes were conserved, with nominal water gaps defined beyond the outer plates of the assemblies and between the fuel plates and guide plates in the CF assembly model.

A similar super-cell approach is adopted for the reflector block and sample hole regions of the sample irradiation assemblies (graphite, beryllium, and the central irradiation cage), with annular regions representing the reflector block and sample hole details, all surrounded by an annular driver fuel zone, the latter separately defined based on the standard 1-D slab unit cell fuel model.

A series of homogeneous Al and H₂O models are used to create cross sections for the top and bottom end fittings for the various assembly types, based on conservation of volume for the metal and water. A similar approach is adopted for the sample irradiation assemblies, where the sample section and end fitting sections are modeled separately. Separate models are used for the lead block, and beam-tubes. The reactor pool is modeled as a homogeneous light water region with a dilute fission source.

III-3.2.2. REBUS-PC full core models

Using REBUS-PC, the MNR core is modeled in three dimensions. Microscopic cross section data is provided by the WIMS-ANL cell models. The spatial discretization used in the REBUS MNR core model is consistent with the WIMS-ANL cell model homogenization. The regional homogenization of the active fuel region and the geometry of the ex-core structures included in the model are shown in Fig. III-4.

The only ex-core structures included in the model are the six beam tubes and the lead block, where the former were approximated on the Cartesian mesh. Approximately 40 cm of light water are modeled laterally beyond the 9x6 grid plate. Axially the model extends from 0 cm to 140 cm with the axial active zone of the fuel located between 30 cm and 90 cm. The active zone is divided into seven uniform zones for burn-up tracking. In the core model the surface area of the absorber rods is conserved and uses flux-to-current internal boundary conditions derived from an MCNP5 model of the MNR Reference Core configuration.

The REBUS-PC MNR model is used to produce fuel material compositions for the companion MCNP5 MNR model. Approximations associated with the fuel depletion calculation are:

- Average rod positions;
- Continuous burn times.

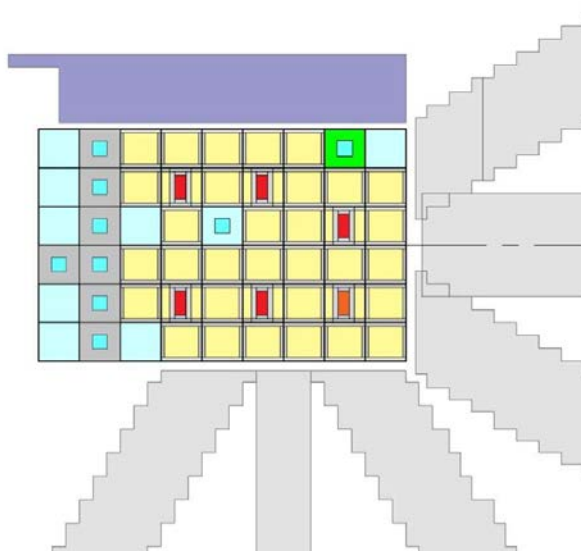


FIG. III-4. CAN REBUS model geometry.

Given that no simulation-based fuel management programme is currently in place at MNR, fuel material compositions were extracted from existing REBUS-PC models of specific core configurations, or in cases where these models were not available, from interpolation of generic fuel composition tables derived from a set of REBUS-PC equilibrium cases. The former specific core models approximated absorber rod positions as fixed ‘average’ positions of 80% withdrawn for the shim-safety rods and 50% withdrawn for the regulating rod. These average positions are representative of typical weekly operation. The generic fuel composition tables used in this study were created from a series of cases with the absorber rods fully withdrawn.

Some effort was made to approximate the ^{135}Xe composition for the specific operational core states being modeled.

III-3.2.3. MCNP full core models

MCNP5 provides a full core Monte Carlo transport theory modelling capability to Canada’s code collection. It is used for detailed static flux/activation/reactivity calculations. Fuel material input data for the MCNP5 models are provided by output from the REBUS-PC fuel management models.

The MCNP5 code allows a more complex geometry and continuous energy model of the MNR core. The MNR MCNP5 model incorporates a much finer degree of geometric detail compared to the MNR REBUS-PC model, with the discrete seven-axial-zone fuel composition as the only limitation associated with the REBUS-PC model. Homogenization is not used in the MNR MCNP5 model, i.e., structural detail is included explicitly, including individual fuel plates and structure of the grid plate and assembly end fittings.

To facilitate the use of the lattice capability of the MCNP5 code the curved fuel and dummy plates were modelled as straight. This approximation is purely geometrical as material volumes and coolant channel thicknesses were conserved.

Apart from the flat plate approximation, great detail was included in the MNR MCNP5 full core model including absorber shape, and end fitting details. Ex-core Beam Tubes were approximated as air-filled regions, ignoring the aluminium structure of the tubes and any internal components contained within the tubes. The lead block was modelled explicitly, but all other Ex-core structures were ignored. More than 200 cm of light water is included beyond the lateral extent of the MNR grid plate geometry and above and below the active zone of the fuel. Horizontal and vertical slices through the MCNP5 model are shown in Fig. III-5.

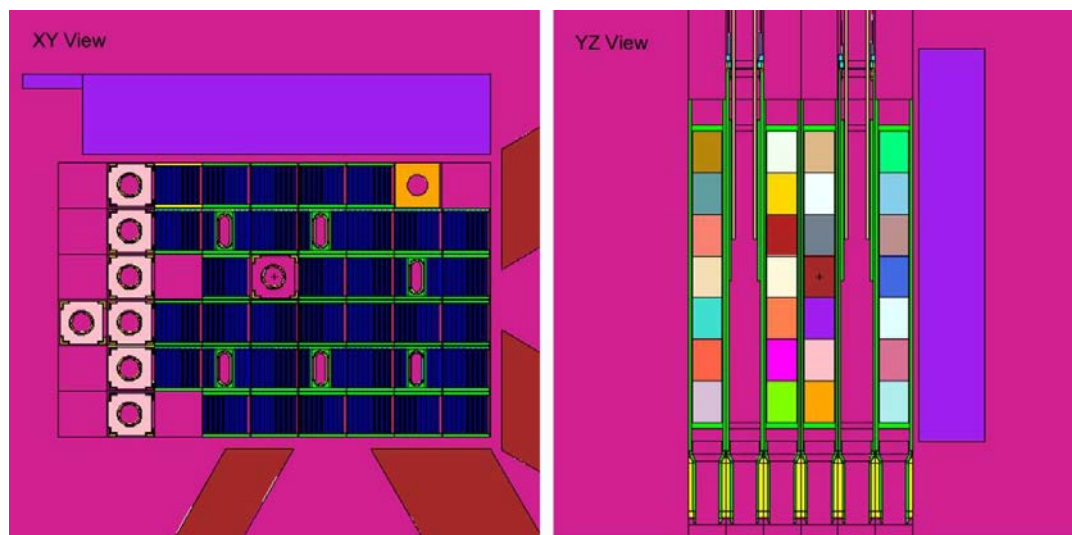


FIG. III-5. CAN MCNP5 model geometry.

Nuclear data based on ENDF/B-VI evaluations was selected from the libraries supplied with the MCNP5 distribution. Typically, these were the endf66a (ZAID = .66c) or actia (ZAID = .62c) libraries at room temperature (293.6 K). Notable exceptions are indicated in the specific experimental sections.

The MCNP5 model was executed as a critically (kcode) problem with 100,000 source histories per cycle. A crude starting source distribution was used but 80 cycles (8 million histories) were skipped before active histories were started. The total number of active cycles/histories was varied to achieve recommended statistical uncertainty on the quantities of interest. For all cases, in addition to checking standard diagnostic messages in the output text file, the MCNP plotting utility was used to examine plots of source (Shannon) entropy (kcode 6) and combined k_{eff} estimates per cycle (kcode 16) as part of convergence checking.

Various experiment-specific modifications were made to the model and are described in the following sections.

III-3.3. South Africa: Codes, Tools, Models and Methods

The South Africa (SAF) group used the OSCAR-4 code package for the simulation of the MNR benchmark analysis. The OSCAR nuclear reactor calculational software package has been incrementally developed over 20 years. The package is the primary calculational tool for the SAFARI-1 research reactor [III-3].

Homogenized few-group cross sections were generated for each of the MNR core components using the transport code HEADE. The cross sections were created from a 172-group WIMS-E library and condensed to 6 energy groups for use in the global diffusion calculation.

Cross sections for the fuel and control assemblies were created in an infinite lattice, through the use of white (i.e., reflective) boundary conditions. For all non-fuel components color-set environments were used, with a fuel assembly as a driver for the flux in each component.

As a result of geometric limitations in the transport code used to generate the few-group cross sections, some model approximations had to be made. These approximations pertain to the modelling of the curved fuel plates, the shape of the absorber rods and the central channels in the graphite and beryllium reflector assemblies. The approximations used for each of the components are outlined below. All component diagrams were taken from Ref. [III-1].

MNR standard fuel assemblies are made up of 16 curved fuel plates and 2 dummy plates. Curved plate geometry cannot be modelled with the transport code currently used in the OSCAR-4 system and is approximated by flat plates instead. This approximation is purely geometrical as fuel and cladding volumes are maintained as well as coolant channel widths. Figure III-6 shows the fuel assembly model used for few-group cross section generation with flat plates, compared to an MNR standard fuel assembly.

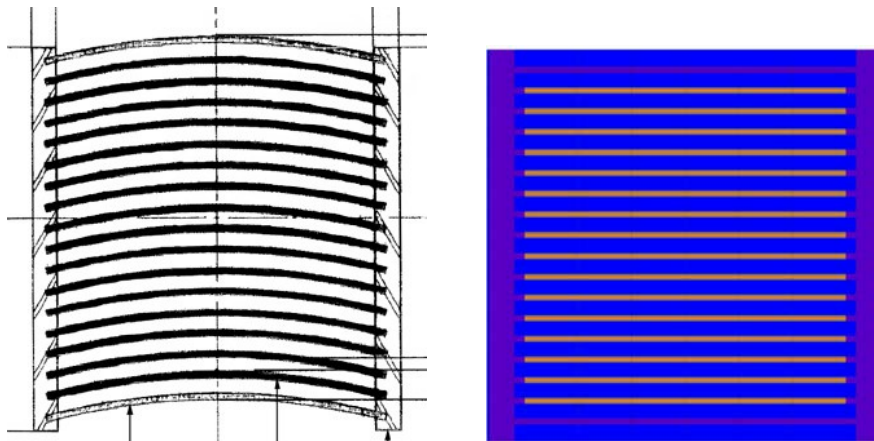


FIG. III-6. Fuel assembly model used to generate few-group cross sections compared to MNR standard fuel assembly.

Apart from the curved fuel plates an approximate model was used for the control assemblies. In Fig. III-7 the curved ends of the absorber rods were replaced with rectangles in the model, while preserving the overall absorber volume. As before the curved plates were replaced with flat plates in the control fuel assembly. Fig. III-7 shows the model of the control assembly with and without the absorber rod.

Furthermore, the cylindrical channels in both the graphite and beryllium reflector assemblies were replaced with square channels, conserving the volume of water contained in the central channel. The curved block of beryllium was also approximated with a square model.

Lastly, the ex-core structures were modelled in an approximate way so that the reactivity effects on the core could be considered. A horizontal cut of the full core model is shown in Fig. III-8.

For both the fuel and control elements 7 axial material zones with a total active height of 60 cm were used. This is the mesh on which the burn-up data for the fuel and control elements were provided. The top and bottom axial reflector zones were modeled with 15 cm of water, broken up into two zones of 6 cm and 9 cm respectively. All nodes depicted in Fig. III-8 are 8.1 cm by

7.709 cm, with a total model height of 90 cm. Vacuum (non-reentrant) boundary conditions were used on the periphery of the core model.

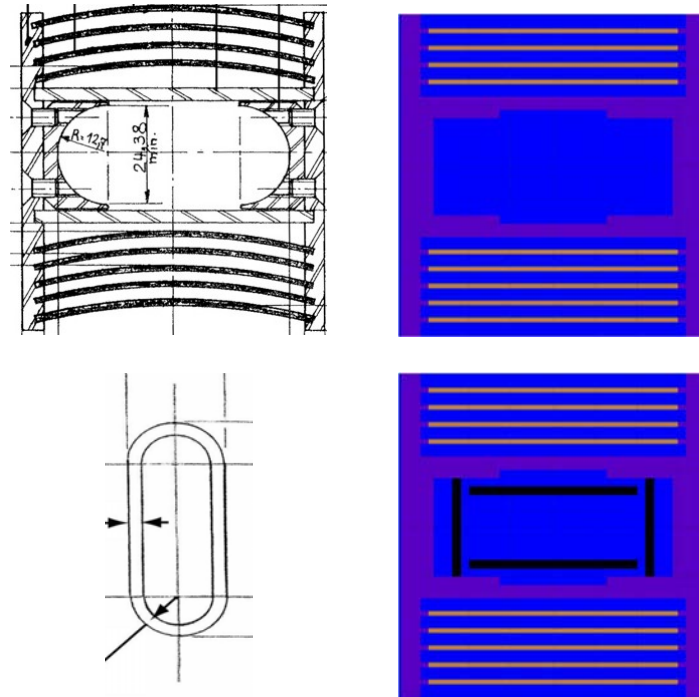


FIG. III-7. Model used for the control rod assemblies compared to the MNR control assembly.

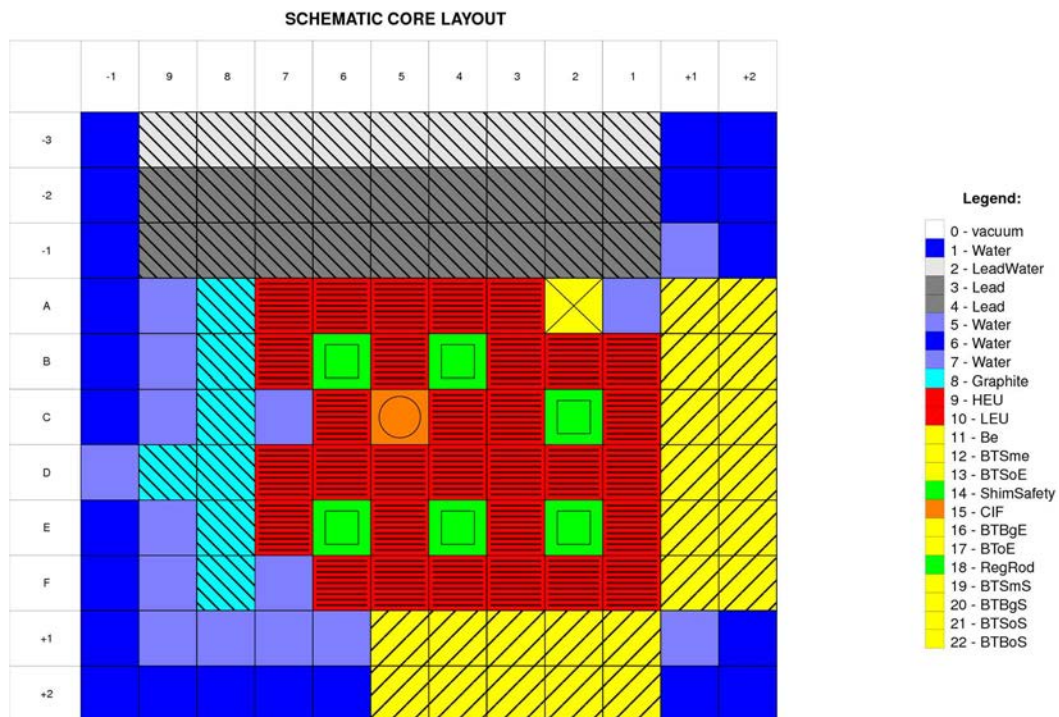


FIG. III-8. Above view of the nodalization for core 54A.

The calculational mesh consists of 11 and 12 nodes along the y- and x-directions respectively and 12 nodes in the z-direction. Using the core model described above, the selected core change experiments were modeled and compared to the experimental data.

III-4. DESCRIPTION OF EXPERIMENT

The MNR benchmark analysis consists of the following parts, each one addressing different aspects of the MNR core:

- Regulating Rod Calibration via Doubling Time Method;
- Shim-Safety Rod Calibration via Cross Calibration Method;
- Miscellaneous Reactivity Tests;
- Radial Flux Mapping;
- Axial Flux Wire Activation;
- Void Substitution Experiment;
- Pool Temperature Experiment.

The first part is comprised of what can be classified as typical core change measurements and includes (i) absorber rod worth measurements, (ii) miscellaneous reactivity change measurements, and (iii) radial flux wire mapping.

The second part of the benchmark is concerned with a set of full-axial-length flux wire irradiations, performed using copper wire at low power in a variety of sample irradiation positions. These measurements were conducted on the same core as used for the first part of the benchmark analysis.

The third part of the benchmark analysis is a series of simulated void experiments which involved inserting aluminium plates into the coolant channels of a variety of fuel assemblies. The associated reactivity changes were measured in terms of changes in critical rod positions. The final part of the benchmark analysis is a pool temperature experiment which involved the slow heating of the MNR primary system and the monitoring of the absorber rod positions to provide the associated change in reactivity data, again expressed in terms of changes in critical rod positions.

These different parts of the benchmark analysis are described in more detail in the following sections. For each part of the benchmark analysis a brief description of the experiment is provided along with a summary and comparison of the analysis results as well as conclusions and recommendations.

III-4.1. Experiment 1: Regulating Rod Calibration

III-4.1.1. Short description of experiment

The regulating rod calibration is the first step in what can be classified as typical core change measurements at MNR. This calibration is performed using the Doubling Time method, which involves establishing a critical state, withdrawing the Regulating Rod by a certain amount, thus providing a relatively small positive reactivity change to the core, and initiating a slow power increase. Once a stable period has been established the doubling time of this power increase is recorded. The reactor is then brought back to critical by adjusting the compensating shim-safety rod bank position. This is performed at low power involving a series of steps over the entire length of the Regulating Rod from 0% withdrawn to 100% withdrawn. The relationship between the stable reactor period and the step-change in reactivity is given by the Inhour Equation, also referred to as the ‘reactivity equation’ (see for example [III-1]):

$$\rho = \omega\Lambda + \sum_{i=1}^6 \frac{(\omega\gamma_i\beta_i)}{(\omega + \lambda_i)} \quad (\text{III-1})$$

Where ρ is the reactivity $\equiv (k-1)/k$, k is the effective multiplication factor, ω = the roots of this equation; the largest of these roots is $1/T$, the stable period, $\Lambda = l/k$ which is the prompt neutron generation time, where l is the prompt neutron lifetime, β_i is the absolute abundance of delayed neutrons for the i -th precursor group, where $\beta = \sum(\beta_i)$, γ_i = a scaling factor for the effectiveness (in producing fission) of i -th group delayed neutrons compared with prompt neutrons, and λ_i is the decay constant for the ' i -th' precursor group.

The product $\gamma_i\beta_i$ can be considered the 'effective' absolute abundance of delayed neutrons for the i -th precursor group. The effectiveness factors are often not explicitly included in the literature but are important to recognise as part of the above formulation. A simplifying approximation is to assume that the delayed neutron effectiveness is the same for each delayed precursor group, i.e.:

$$\gamma_i\beta_i \cong \left(\frac{\beta_{eff}}{\beta}\right)\beta_i = \left(\frac{\beta_i}{\beta}\right)\beta_{eff} \quad (\text{III-2})$$

Two sets of Doubling Time measurements are recorded for each Regulating Rod change in position. The experimental data is presented in Table III-5.

TABLE III-5. REGULATING ROD CALIBRATION - MEASURED DATA

Calibration Step No.	Regulating rod Position (%)		Measured DT (1) (s)	Measured DT (2) (s)	Measured DT (avg) (s)
	(start)	(end)			
1	0	18.72	144	170	157
2	18.72	28.46	133	152	142.5
3	28.46	38.43	93	106	99.5
4	38.43	47.01	121	133	127
5	47.01	55.95	136	154	145
6	55.95	65.43	162	179	170.5
7	65.43	76.46	207	236	221.5
8	76.46	100	204	244	224

For this section of the benchmark analysis the participant is asked to:

- Predict the doubling times corresponding to each change in Regulating Rod position;
- Convert the measured Doubling Times to associated reactivity worth;
- Calculate the Integral and Differential rod worth of the Regulating Rod.

As part of the prediction of doubling times and the conversion of doubling times to reactivity values, the participant will need to obtain the relevant set of kinetics parameters and group-wise constants for use in the Inhour Equation. More information on this part of the MNR benchmark analysis can be found in Reference [III-2].

The calculation of doubling times represents the only direct comparison point to measured values for this section of the benchmark analysis, while the remainder of the calculations offers a calculation comparison between participating groups and a consistency check on the calculations of each group.

III-4.1.2. Summary and comparison of benchmark results

The ARG and SAF groups participated in this section of the MNR benchmark analysis. The direct comparison of calculated to measured values is to the doubling time measurements. This approach requires the derivation of kinetics parameters. Kinetics parameters used by the participating analysis groups are summarized in Table III-6.

TABLE III-6. CALCULATED KINETICS PARAMETERS FOR MNR

Participant	ARG	SAF
Parameter	Value	Value
ℓ (μsec)	63.0	51.0
β_{eff}	0.00738	0.00727
$\beta, i/\beta$		
1	0.0325	0.0384
2	0.2180	0.2090
3	0.1957	0.1884
4	0.3947	0.4071
5	0.1167	0.1300
6	0.0424	0.0271
λ_i (/sec)		
1	0.0124	0.0127
2	0.0305	0.0317
3	0.1110	0.1167
4	0.3010	0.3121
5	1.1400	1.3985
6	3.0100	3.8521

The ARG group obtained kinetics parameter estimates directly from their MNR models, as standard output from the CONDOR/CITVAP codes. The SAF group did not calculate kinetics parameters so values were adopted from [III-1] which are specific to the LEU IAEA 10 MW MTR benchmark analysis, with the exception of the prompt neutron lifetime estimate which was adopted from the MNR Operations documentation.

Both participating groups calculated reactivity change for each calibration step of the measurements via successive k_{eff} calculations from the respective core models and then used the Inhour Equation to convert these reactivity estimates to doubling times. The resulting doubling times corresponding to the measured change in rod positions are summarized in Table III-7 and shown in comparison to the measured data in Fig. III-9.

In general, the calculated doubling times are on the order of the measured values but not consistently within the range of the experimental measurements. Please note that the vertical error bars in Fig. III-9 are associated with the range of the measured values as noted in Table III-7. Worth remarking is the large deviation of the ARG group data point for calibration step 8 compared to measurement. Calculated to Experimental (C:E) ratios ranged from 0.87 to 1.57 for the results from the ARG group and 0.91 to 1.35 for the SAF group. There is also some concern on the trend of the predicted data from the ARG group compared to the measured values over steps 1 to 6.

TABLE III-7. MEASURED AND CALCULATED DOUBLING TIMES

CALI- BRATION STEP NO.	MEASURED			ARG		SAF		
	DT(avg)	+/-	$\Delta\rho$	DT	DT	$\Delta\rho$	DT	DT
	(SEC)	(SEC)	CALC	CALC	C:E	CALC	CALC	C:E
	(SEC)	(SEC)	(PCM/ STEP)	(SEC)	RATIO	(PCM/ STEP)	(SEC)	RATIO
1	157	13.0	47.60	168	1.07	43.26	147	0.94
2	142.5	9.5	45.10	179	1.25	40.13	159	1.11
3	99.5	6.5	50.10	158	1.59	47.30	135	1.35
4	127	6.0	50.70	156	1.22	41.09	155	1.22
5	145	9.0	49.90	159	1.09	42.08	151	1.04
6	170.5	8.5	53.50	146	0.86	36.92	173	1.01
7	221.5	14.5	40.50	203	0.91	31.77	200	0.91
8	224	20.0	26.30	330	1.47	27.66	230	1.03

Note: the \pm associated with the measured value of DT(avg) is the absolute value of $(DT(1)-DT(2))/2$

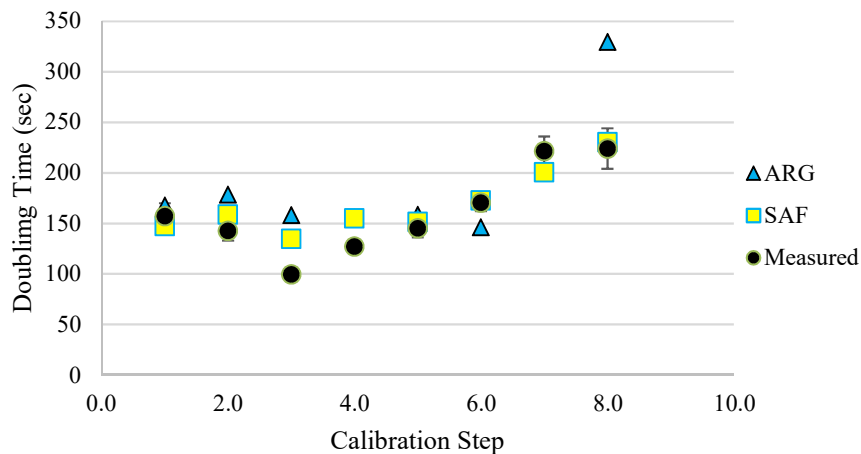


FIG. III-9. Measured and calculated doubling times.

The remainder of this section of the MNR benchmark analysis provides only a comparison of calculated results. Reactivity estimates were calculated in two ways by each participating analysis group: (i) by conversion of measured doubling times (DTs), and (ii) by a series of criticality (k_{eff}) cases for the recorded rod positions. These are labelled in the figures as (i) ‘from DTs’, and (ii) ‘from k_{eff} ’, respectively.

The reactivity estimates derived from the doubling times by each participant group are shown in Fig. III-10. Both participating groups calculated reactivity estimates for the two sets of measured doubling times, DT(1) and DT(2), and the average of the two sets, DT(avg) from Table III-5. As such the data points in Fig. III-10 represent the reactivity estimates for the DT(avg) data and the vertical error bars give the range for the estimates from the DT(1) and DT(2) sets.

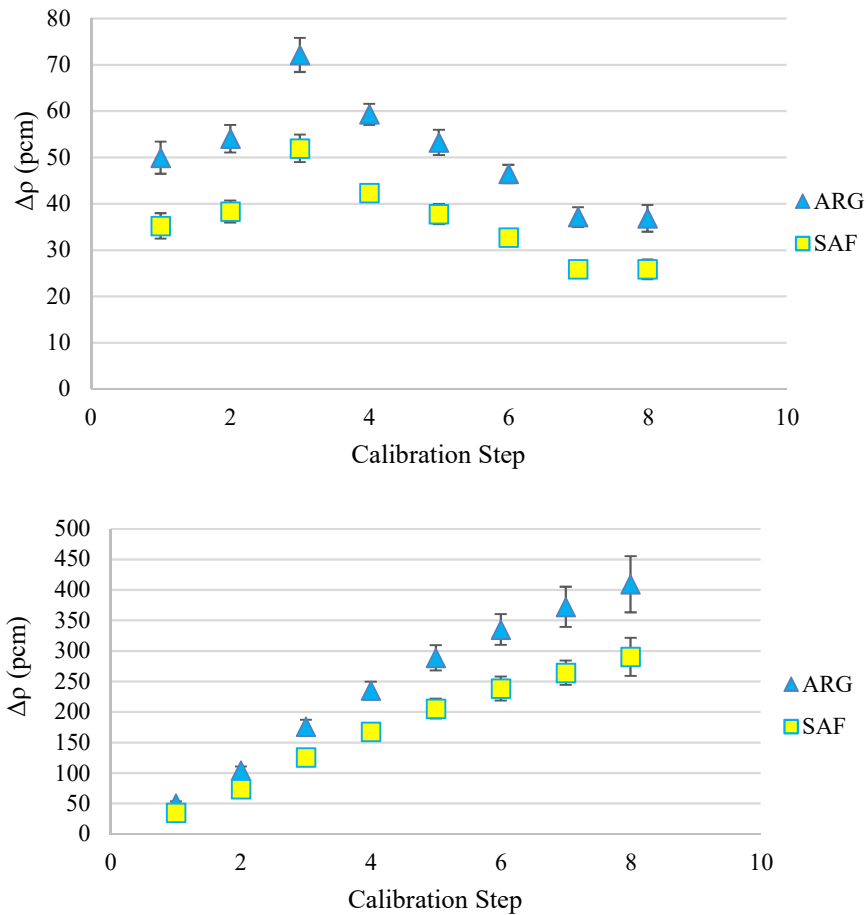


FIG. III-10. Reactivity estimates from doubling time measurements.

For the estimation of reactivity from the doubling times, the ARG and SAF results show similar profiles (i.e., shape) but a difference on the order of 40% in magnitude. This difference in magnitude of the estimates is beyond that associated with the range of measured doubling time data and suggests a significant sensitivity and a difference in kinetic parameter estimates.

The reactivity estimates derived from k_{eff} calculations by each participant group are shown in Fig. III-11. These estimates are found from successive criticality calculations for the reported rod positions (see Table III-5).

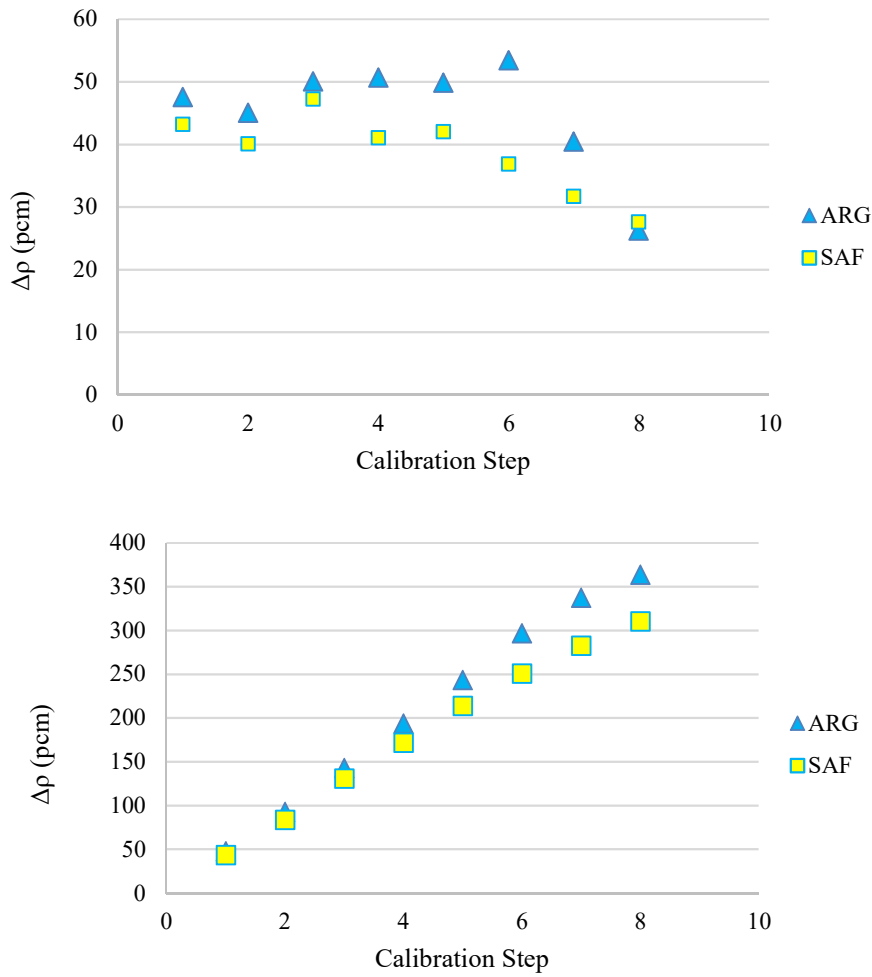


FIG. III-11. Reactivity estimates from k_{eff} calculations.

Unlike the estimates derived from the doubling time data the estimates of reactivity from k_{eff} calculations produced by the two participating groups show a variation in profile and a difference in magnitude, especially for calibration steps 4 to 7. As found for the estimates from doubling time conversion (Fig. III-10), the k_{eff} based estimates from the ARG group are larger in magnitude (~17%) than those from the SAF group. It is possible that the variation in both profile and magnitude of estimates in Fig. III-11 could be attributed, at least in part, to the uncertainty/convergence of the k_{eff} calculations and the relatively small reactivity changes being considered. Uncertainties associated with the calculations were not supplied by either participant, so this is left for future investigation.

The differences in the estimates obtained from the two different methods are highlighted in Fig. III-12 and Fig. III-13, for the SAF and ARG groups, respectively.

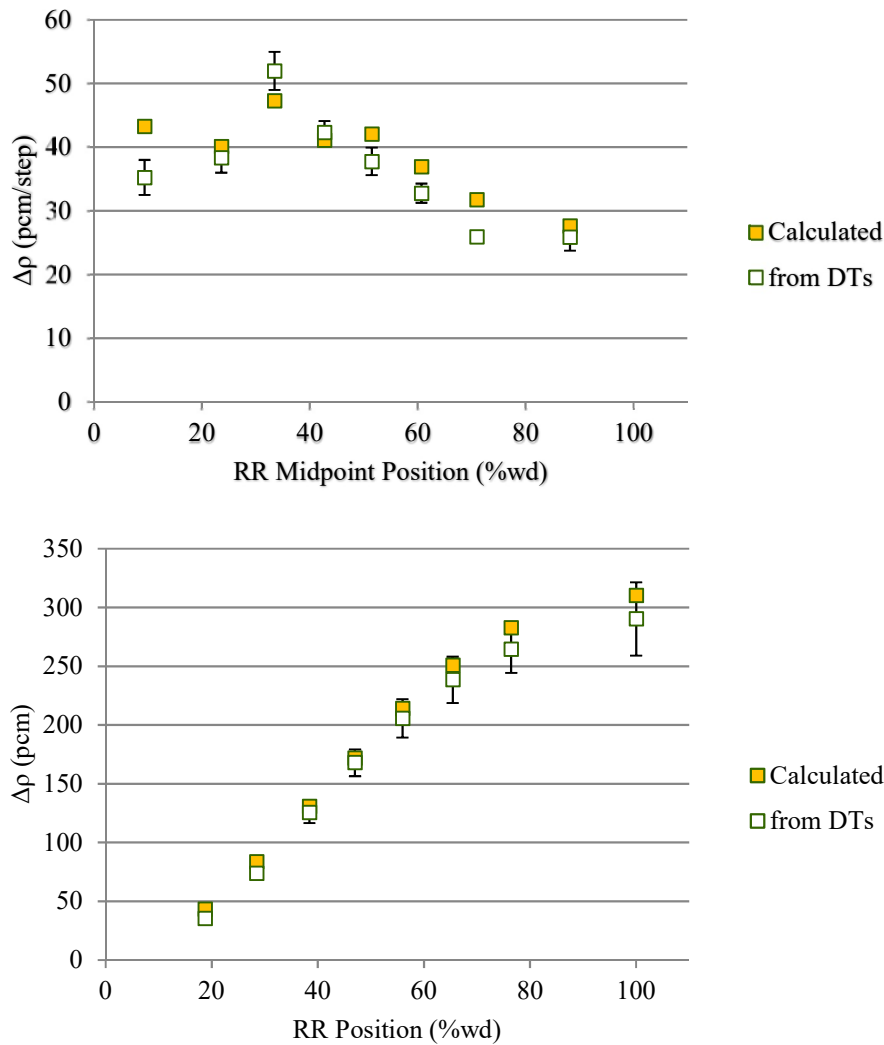


FIG. III-12. Calculation method comparison SAF.

The calculated reactivity worth estimates from SAF (Fig. III-12) appear self-consistent. Although some differences exist in the reactivity per calibration step estimates between results from the two calculation methods, the estimates for the integral rod worth curve based on k_{eff} calculations agree within the range associated with the experimental data for estimates based on the measured doubling times.

The ARG results (Fig. III-13) show a notable difference in the shapes of the differential worth curves produced by the two calculation methods. The DT-based integral-worth estimates also appear slightly higher than those based on the k_{eff} calculations. The sources of these discrepancies have not been identified at the time of report writing and are left for future investigation.

The total rod worth estimates for the MNR regulating rod are summarized in Table III-8. Of note are that the estimates calculated from criticality models show closer agreement between the participating groups than those derived by converting the measured doubling times. Also of note are that the ARG group C:E value for the total worth is < 1 while that from the SAF group is > 1 . The overall range of total worth estimates for the Regulating Rod is large relative to the magnitude of the effect being calculated, ranging from 290 pcm from the SAF group (from DTs) up to 409 pcm as calculated by the ARG group (from DTs).

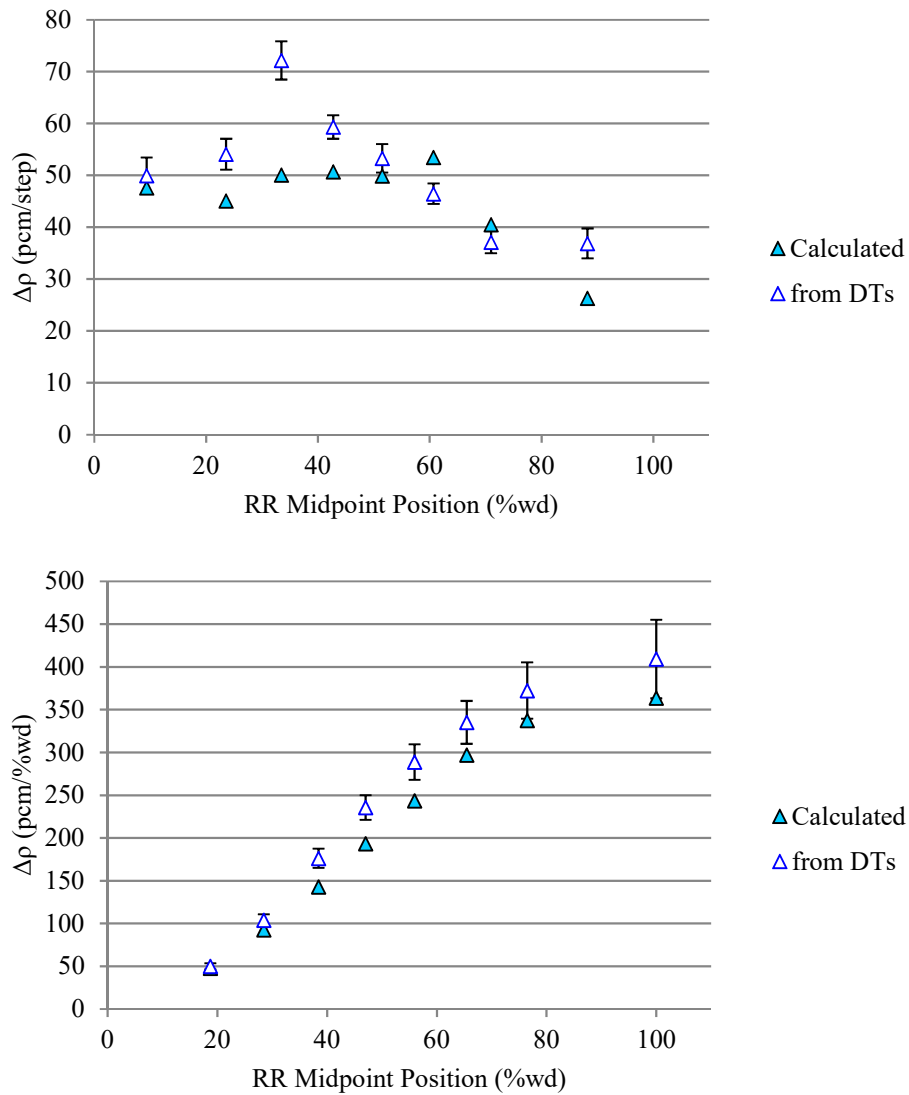


FIG. III-13. Calculation method comparison ARG.

TABLE III-8. TOTAL REACTIVITY WORTH OF MNR REGULATING ROD (PCM)

Participant	ARG	SAF	ARG:SAF
from k_{eff}	364	310	1.17
from DTs	409	290	1.41
k_{eff}/DTs	0.89	1.07	-

* k_{eff}/DTs is the ratio of the reactivity estimates from these methods

III-4.1.3. Conclusions and recommendations

The main observations noted from this data consolidation are as follows:

- There were differences found in the calculated kinetics parameters made by the ARG group compared to the values adopted from literature by the SAF group;
- The doubling time estimates made by the SAF group were in general agreement with the measured data but were still beyond the range of measured values for many of the

calibration steps. The doubling time estimates made by the ARG group showed greater discrepancy to the measured values;

- The ARG group found notable differences between the reactivity estimates derived from the doubling time measurements compared to those derived from criticality calculations indicating a lack of consistency in the calculations despite using the same codes and input cases;
- The SAF group found better self-consistency in their doubling-time-based and criticality-calculation based estimates despite adopting non-MNR-specific kinetics parameters from literature;
- The reactivity worth estimates made by the SAF group were significantly lower than those made by the ARG group for both doubling-time-based and criticality-calculation-based estimates.

The results of this benchmark analysis indicate that notable variability can be found in low-worth absorber rod reactivity estimates based on similar simulation models and approaches. The root cause of this is not clear but appears related to differences in estimated kinetics parameters as well as the calculation of reactivity changes from criticality calculations. No conclusions have been drawn at this time as to the effect of using nodal-diffusion theory compared to finite-difference diffusion theory approaches. Similarly, the contribution of using different fuel material composition input has not been evaluated at this time but could be considered a future activity.

Assessment of the simulation results suggests that there is some need to standardize a set of methodologies for calculating and provide validation for the calculation of point kinetics parameters: β_{eff} , ℓ , Λ , and group-wise precursor data. An experimental method for validating these calculations on equilibrium core of research reactors would be valuable for the research reactor community.

III-4.2. Experiment 2: Shim-Safety Rod Calibration

III-4.2.1. Short description of experiment

Calibration of the five MNR shim-safety rods follows immediately after the calibration of the regulating rod. The procedure is to cross calibrate each rod in turn, against the previous rod as shown in Table III-9. This is achieved by positioning the rod to be calibrated in a fully withdrawn position and the rod to be calibrated against in a fully inserted position with the remainder of the rods positioned such that the reactor is critical at low power. The rod to be calibrated is then inserted stepwise while the rod being calibrated against is withdrawn to compensate for the change in reactivity. This is repeated for every 5% travel distance of the rod to be calibrated until the entire length of the rod has been measured. Depending on the relative worth of the two rods being moved the reactor may need to be ‘shimmed’, i.e., move the remainder of the shim-safety rods, during the calibration.

The lowest worth shim-safety rod is first cross-calibrated against the regulating rod. Once this first shim-safety rod has been calibrated, it is then used to cross calibrate the next lowest worth rod. The procedure is repeated for the remainder of the rods. The rod calibration order is shown in Table III-9.

TABLE III-9. MNR ABSORBER ROD CALIBRATION STAGES

Rod being calibrated		Rod being calibrated against	
Rod number	Core position	Rod number	Core position
5	6E	Regulating Rod	2E
1	2C	5	6E
4	6B	1	2C
2	4E	4	6B
3	4B	2	4E

For this section of the benchmark analysis the participant is given the sequential rod positions in terms of percentage withdrawn and asked to:

- Supply k_{eff} values for all critical rod positions;
- Translate the previously converted Regulating Rod doubling time measurement reactivity estimates to produce differential and integral reactivity worth estimates for each of the five shim-safety rods using the recorded rod positions. These will be referred to as estimates calculated ‘from RR DTs’ herein;
- Estimate the differential and integral reactivity worth for the five shim-safety rods, independent of the Regulating Rod doubling time measurements. Both participating analysis groups performed this stage of the benchmark analysis via a series of criticality calculations for the recorded rod positions used during the calibration procedure. As a result, the associated reactivity estimates are referred to as calculated ‘from k_{eff} ’ herein.

More information on this part of the MNR benchmark analysis can be found in [III-2]. For this section of the benchmark analysis the criticality estimates for critical rod positions represents the only direct comparison point to measured values. The previous section on calibration of the regulating rod, the remainder of the calculations offers a calculation comparison between participating groups and a consistency check on the calculations of each group.

III-4.2.2. Summary and comparison of benchmark results

The shim-safety rod calibration measurements represent an extensive set of critical rod position measurements. Both the ARG and SAF groups calculated rod worth estimates from a series of k_{eff} calculations. The compilation of the critical rod position k_{eff} estimates provides a comparison point between calculation and measurement. These results are summarized in Table III-10 and shown in Fig. III-14.

TABLE III-10. CRITICAL ROD POSITION K_{EFF} ESTIMATES

Group	$\langle k_{eff} \rangle$	Offset (pcm)	Std. Dev. (pcm)
ARG	0.9967	333	39
SAF	0.9852	1484	94

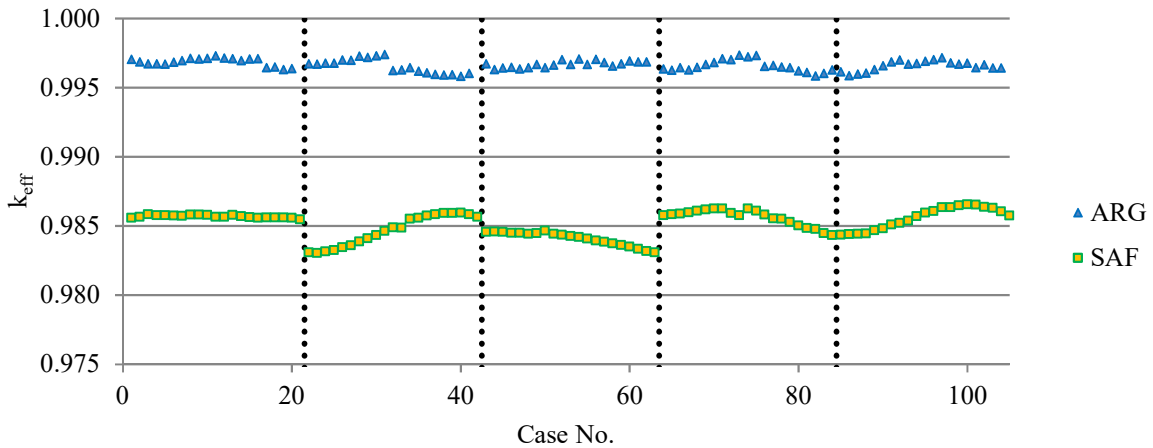


FIG. III-14. Shim-safety rod calibration critical rod position k_{eff} estimates.

It is evident from the critical rod position k_{eff} results that the model consistency for the two participants is comparable, i.e., that the movement of one rod is properly compensated for by the movement of a second rod, with similar variation in the results over the calibration steps. However, there does appear to be trends in the k_{eff} values calculated by the SAF group (e.g., see cases for Rod 1 in Fig. III-14) which warrant further investigation with respect to modelling details. In addition, the SAF results were found to be associated with a larger systematic offset compared to the ARG results. Preliminary investigation by the ARG group suggests that much of this difference may be attributable to differences in the fuel material compositions used by the two participating groups. Given the approximate nature of the modelling adopted by both groups with respect to regions outside of the active fuel zone it would also be beneficial to determine what sort of k_{eff} offsets are associated with typical approximations.

The remainder of the estimates in this section of the benchmark analysis represent a comparison of calculation methods. Reactivity estimates are derived by (i) translating the measured Regulating Rod doubling times to worth estimates for the shim-safety rods based on compensating rod movements, and (ii) by calculating reactivity from the associated k_{eff} estimates for each set of rod movements. These results are referred to as ‘from RR Dts’ and ‘from k_{eff} ’, respectively, in the figures and tables herein. Total reactivity worth estimates are summarized in Table III-11.

TABLE III-11. CALCULATED MNR SHIM-SAFETY ROD REACTIVITY WORTH SUMMARY

Rod Number	From k_{eff} (pcm)	ARG		k_{eff} : Dts Ratio	SAF		ARG:SAF	
		From RR Dts (pcm)	k_{eff} : Dts Ratio		From RR Dts (pcm)	k_{eff} : Dts Ratio	From k_{eff} Ratio	From RR Dts Ratio
5	1084	1189	0.91	928	845	1.10	1.17	1.41
1	1991	2062	0.97	1960	1461	1.34	1.02	1.41
4	992	978	1.01	898	692	1.30	1.10	1.41
2	2183	2505	0.87	1888	1766	1.07	1.16	1.42
3	1776	2138	0.83	1856	1506	1.23	0.96	1.42
Total	8026	8873	0.90	7529	6270	1.20	1.07	1.42

Figure III-15 to Fig. III-19 show the integral and differential rod worth curves calculated by the ARG group by these two methods. The figures are ordered by the calibration sequence of the rods.

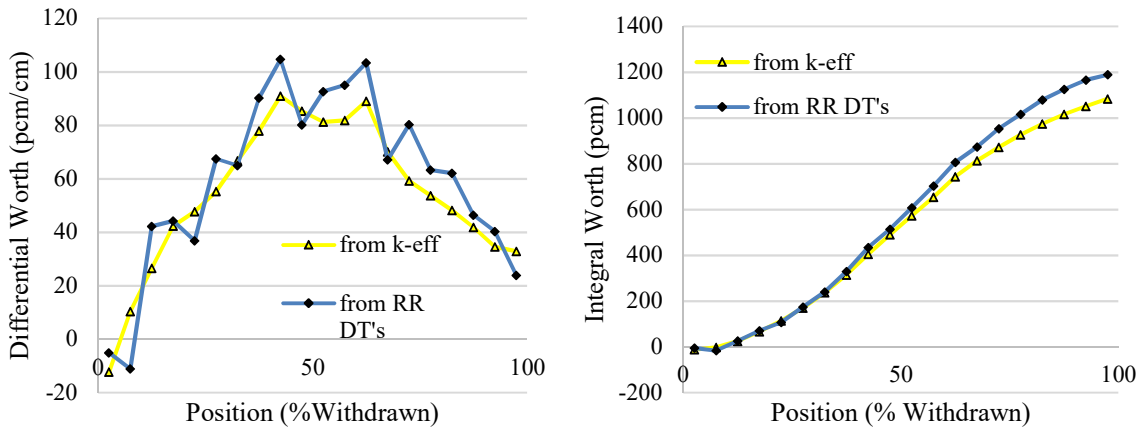


FIG. III-15. Calculated Shim-Safety Rod 5 reactivity curves for ARG.

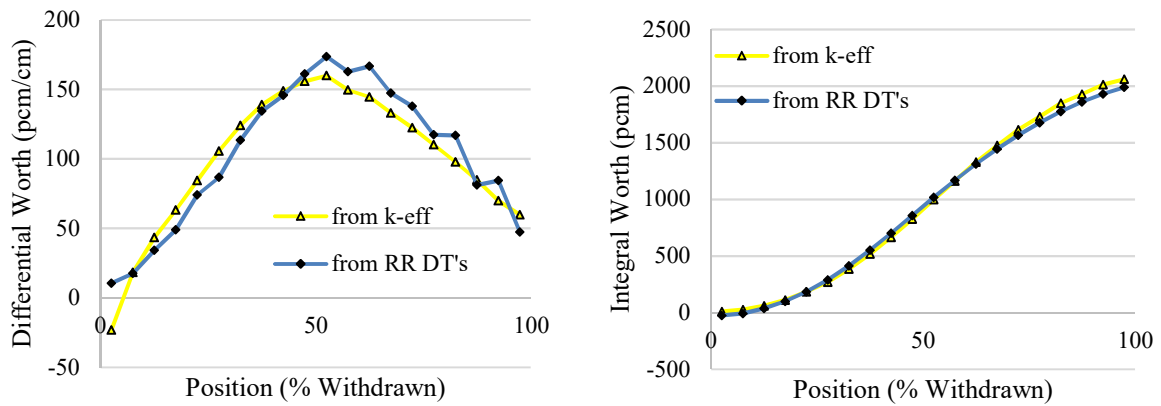


FIG. III-16. Calculated Shim-Safety Rod 1 reactivity curves for ARG.

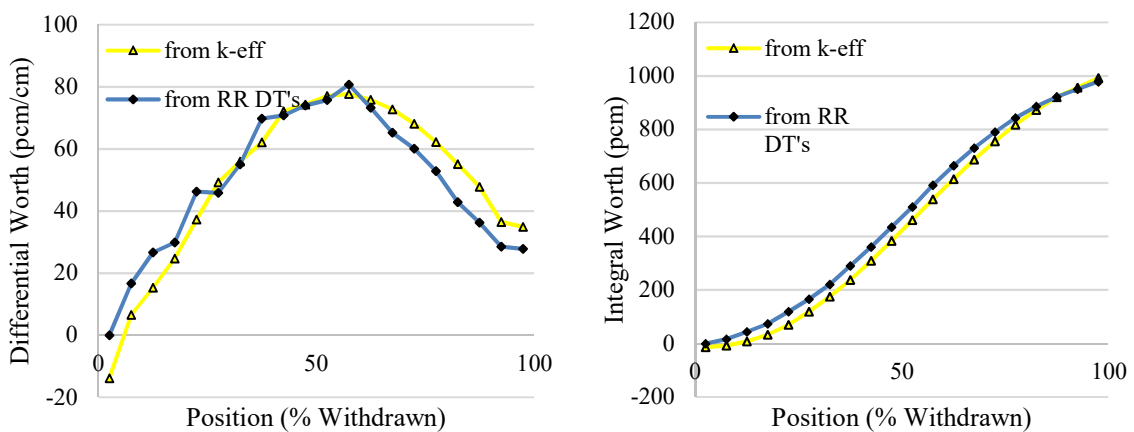


FIG. III-17. Calculated Shim-Safety Rod 4 reactivity curves for ARG.

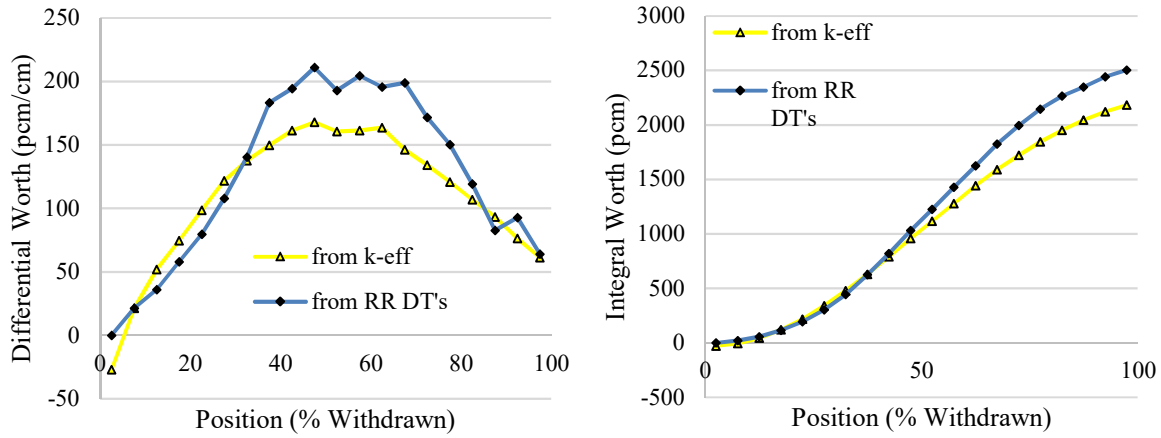


FIG. III-18. Calculated Shim-Safety Rod 2 reactivity curves for ARG.

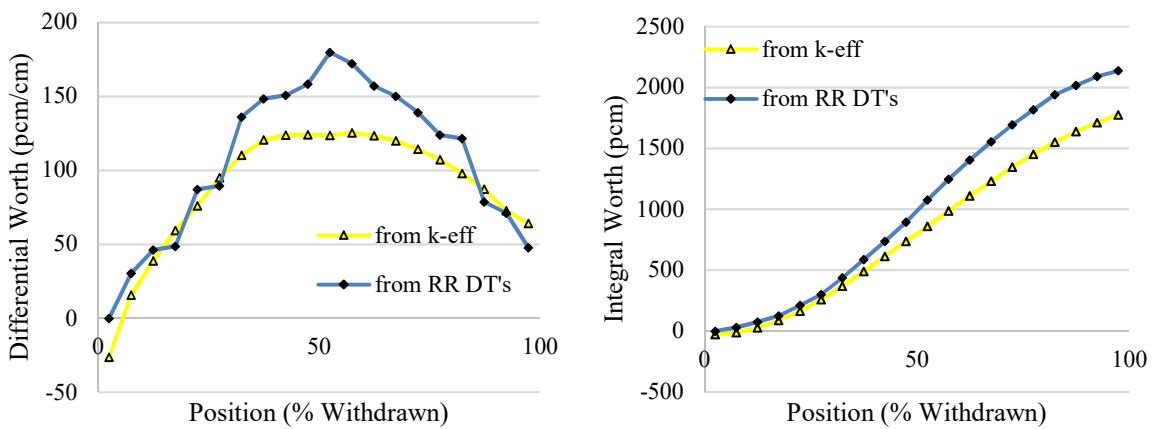


FIG. III-19. Calculated Shim-Safety Rod 3 reactivity curves for ARG.

In general, the ARG group found agreement between reactivity worth estimates from criticality calculations (i.e., based on k_{eff} calculations) for the highly absorbing shim-safety rods compared to estimates made by sequentially translating measured doubling time values from the low worth regulating rod calibration (i.e., doubling time based calculations). The ARG group predicted generally lower reactivity worth from k_{eff} estimates compared to their estimates from the translation of the regulating rod doubling times, with ratios of the total worth for the five rods ranging from 0.83 to 1.01, and the ratio of the total shim-safety bank worth for the two methods of 0.90. This indicates a reasonable consistency between the two calculation methods and is consistent with the comparison of ARG group results for the lower-worth regulating rod.

Figure III-20 to Fig. III-24 present the SAF group calculated results. As per the ARG results, these figures are ordered by the calibration sequence of the rods.

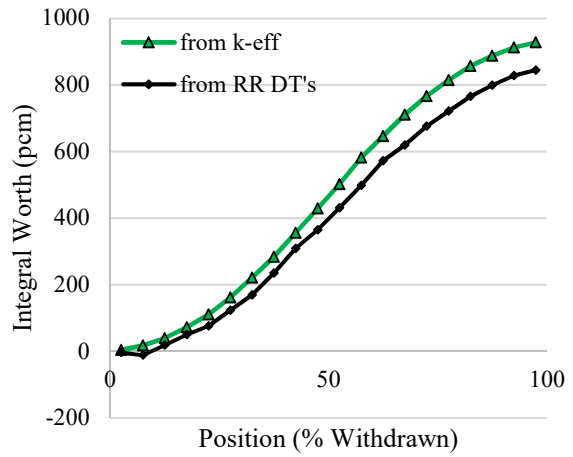
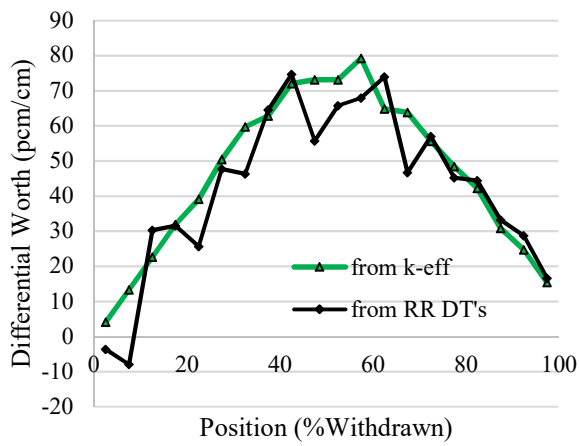


FIG. III-20. Calculated Shim-Safety Rod 5 reactivity curves for SAF.

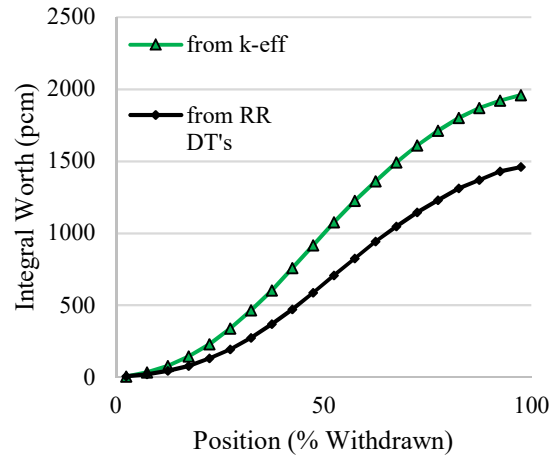
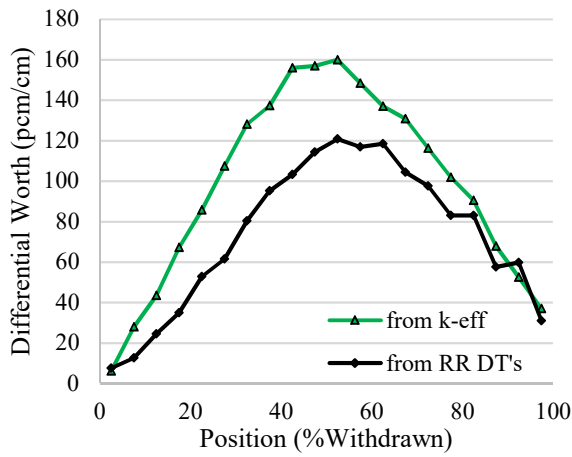


FIG. III-21. Calculated Shim-Safety Rod 1 reactivity curves for SAF.

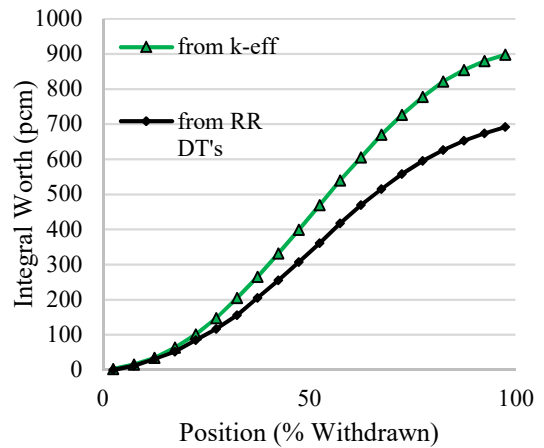
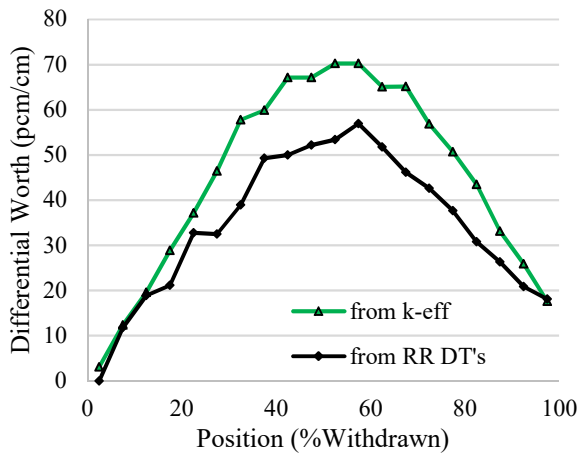


FIG. III-22. Calculated Shim-Safety Rod 4 reactivity curves for SAF.

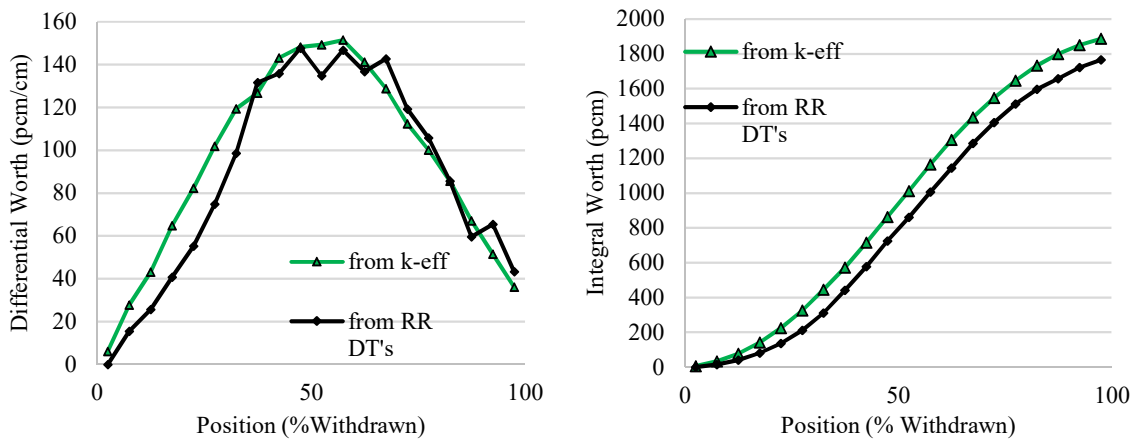


FIG. III-23. Calculated Shim-Safety Rod 2 reactivity curves for SAF.

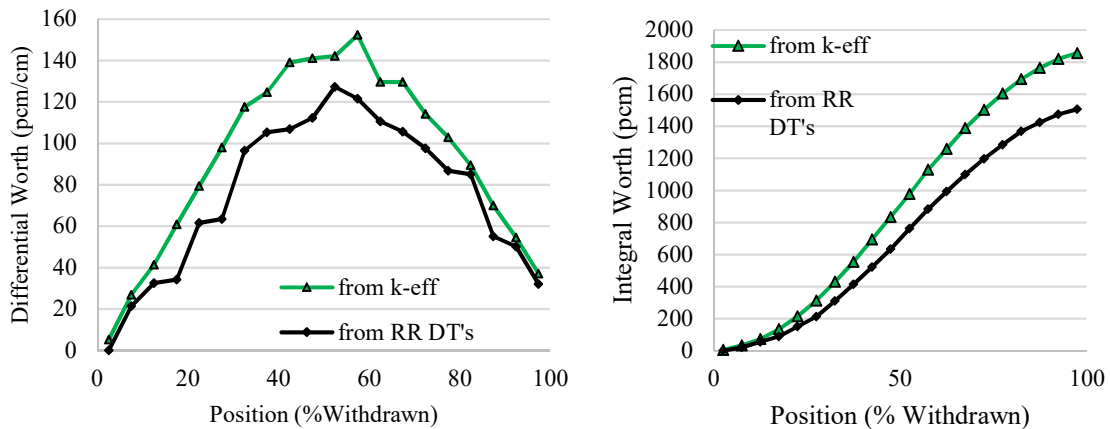


FIG. III-24. Calculated Shim-Safety Rod 3 reactivity curves.

In contrast to the ARG results, the SAF group predicted larger reactivity worth from k_{eff} estimates compared to their estimates from the translation of the regulating rod doubling times, with ratios of the total worth for the five rods ranging from 1.07 to 1.34, and the ratio of the total shim-safety bank worth for the two methods of 1.20. This degree of discrepancy is beyond that which was found by the SAF group for the regulating rod reactivity estimates from these calculation methods.

Both participating groups found noticeable variation in the rod worth estimates for shim-safety rod #5 based on the Regulating Rod doubling time reactivity estimates (see Fig. III-5 and Fig. III-20). This illustrates the challenges experienced when estimating the small-worth changes associated with the regulating rod.

In the same manner as done for the Regulating Rod results, it is useful to compare the results from the two participating groups. This is done in the last two columns of Table III-11 and in Fig. III-25 to Fig. III-28. For three of the five rods as well as the sum of the all the rods, the ARG group predicts higher reactivity worth than the SAF group from k_{eff} calculations.

The rod-worth profiles calculated by the ARG and SAF groups based on the doubling times are consistent in shape for each rod but differ significantly in magnitude as shown for example in Fig. III-25 and Fig. III-26. These result comparisons are illustrative of the entire set of rod calibrations. For the Regulating Rod Doubling Time based calculations, the ARG estimates are consistently a factor of 1.4 larger than the SAF estimates. This latter point is related to the

different kinetics parameter values adopted by the two participating groups as used in the Inhour equation.

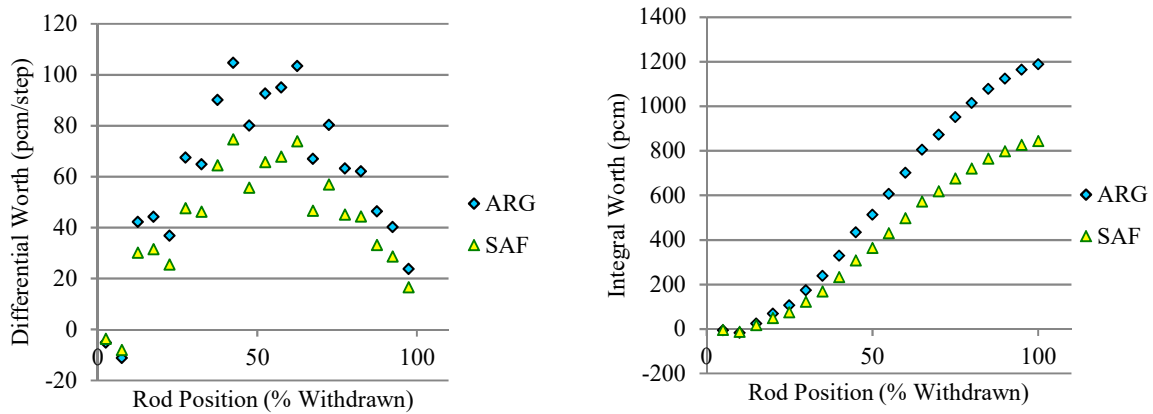


FIG. III-25. Comparison of DT-based reactivity estimates for Shim-Safety Rod 5.

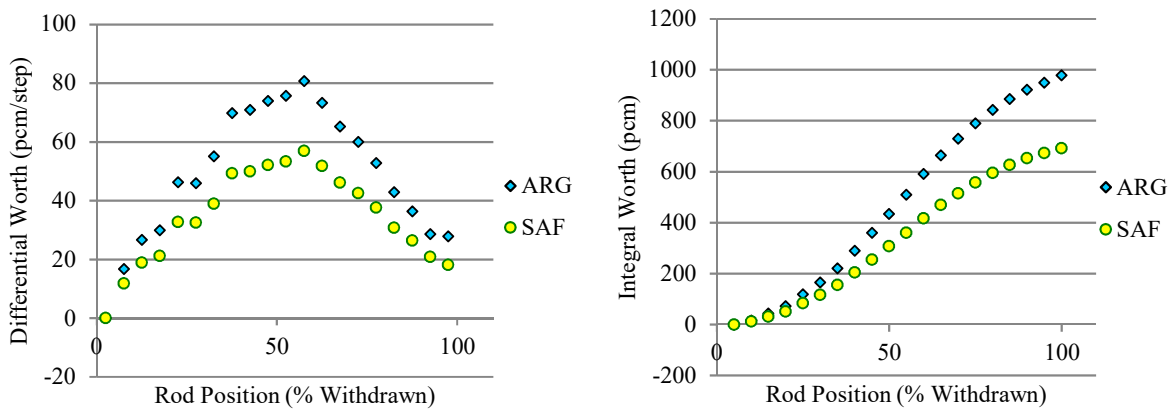


FIG. III-26. Comparison of DT-based reactivity estimates for Shim-Safety Rod 4.

The calculated rod worth profiles based on k_{eff} estimates from the ARG and SAF participants show minor differences in shape, as shown for example in Fig. III-27 and Fig. III-28. Of note are that the ARG and SAF groups estimate reactivity worth of opposite sign near the bottom of the core (from 0-5% withdrawn position) and present worth profiles which are slightly shifted with respect to rod position (seen clearly in the differential worth curve) towards the top of the core (100% withdrawn position). The former effect is evident in the experimental data for Shim-Safety Rod #5 but was not picked up by the SAF group. This may be due to numerical uncertainty in the calculated results given the uncertainty in the critical rod position k_{eff} estimates shown in Fig. III-14 and the magnitude of the differential worth in these positions, or due to details of the modelling geometry.

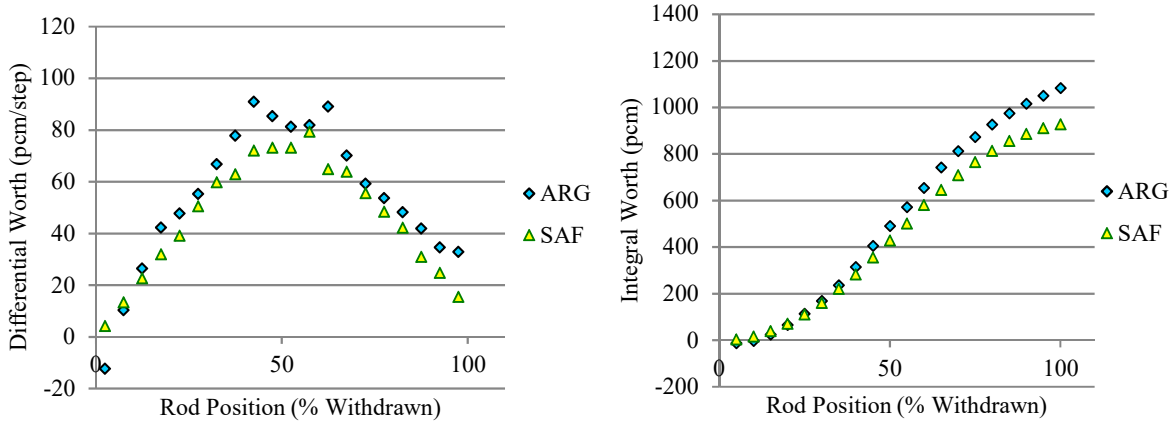


FIG. III-27. Comparison of k_{eff} -Based Reactivity Estimates for Shim-Safety Rod 5.

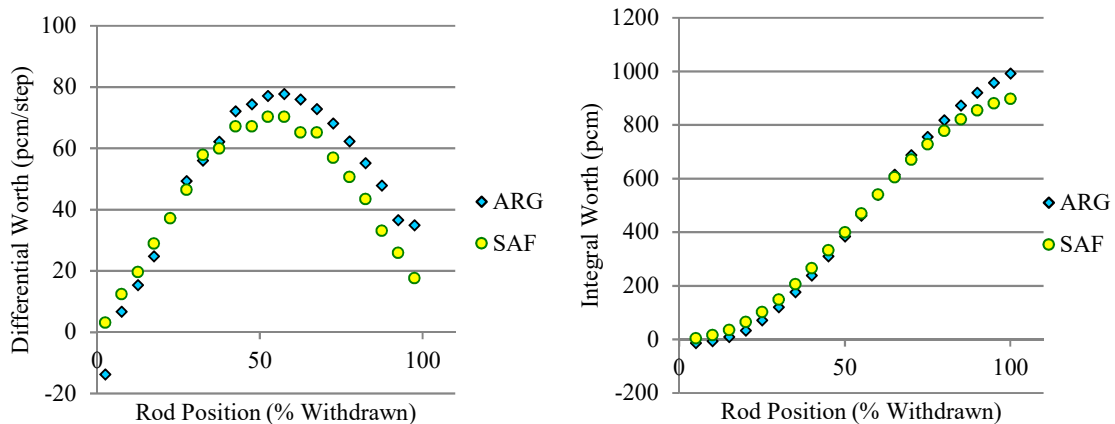


FIG. III-28. Comparison of k_{eff} -Based Reactivity Estimates for Shim-Safety Rod 4.

III-4.2.3. Conclusions and recommendations

This section of the benchmark is based upon what can be considered standard operational rod worth calibration measurements for a research reactor.

Critical rod position criticality estimates appeared comparable for both participating groups (ARG and SAF) with some trending left unexplained in the SAF results. The associated estimates from the two participating groups for the shim-safety rod worth based on criticality calculations for recorded rod positions were consistent, with some minor variations noted. It appears that the level of detail included in the model, while perhaps not grossly affecting the integrated rod worth of an absorber rod in an MTR-type reactor, may be important to second order details in reactivity profile estimates.

Relatively large systematic differences were found in the estimates made by the two participating groups based on the translated regulating rod doubling times, with the SAF group reporting lower worth estimates by a factor of 1.4. This suggests that differences are due to input data (kinetics parameters) used for the translation of doubling time to reactivity, and a relatively high sensitivity of the results to these parameters.

Given that methods seem less standardized for the estimation of kinetics parameters compared to criticality calculations it is recommended that further benchmarking activities be investigated

to explore the comparison of calculations to measurements of kinetics parameters for an operating research reactor facility and the consistency between these kinetics parameters and typical criticality estimates.

It is difficult to make any conclusive remarks on the success of the participants calculations compared to experiment given the single comparison point to measured doubling times of the single low-worth regulating rod. Limitations in the measured data are that the uncertainties on the measurements are not well defined and will be propagated through the sequential calibration procedure. No calculation was produced to directly compare calculated shim-safety rod worth to measured values but rather this comparison relied on translation of the measured doubling times to reactivity values.

It is recommended that to use a benchmark analysis of this type a direct calibration, rather than, or in addition to, a cross-calibration of each rod be included. It would also be beneficial to have a supplementary experimental measurement approach, such as the rod drop method to provide a consistency check on the measured values.

III-4.3. Experiment 4: Radial Flux Wire Mapping

III-4.3.1. Short description of experiment

Following each core change flux wires are inserted into each standard fuel assembly in the core and irradiated at low power. The counting of these wires provides a relative flux distribution in the core. These results, coupled with the fuel assembly inventory records for the end of the previous core, provide a power distribution for the new core, allowing calculations of burn-up to be performed, based on the operating power and operating time.

Short-length 0.0762 cm diameter, 78.4% manganese-copper wires are attached to a set of wire holders which are then inserted one per assembly, into a central coolant channel. Wire/holder positioning is performed by operations staff from the operations bridge, directly above the core. Each wire holder is lowered into the core on a string into the desired assembly, attempting to insert this between fuel plates as near the centre of the assembly as possible. The location of the handle on the standard fuel assemblies prevents the wires from being inserted into the centremost coolant channels. The holder design is such that the wire is positioned close to the fuel axial centreline with the collar of the wire holder resting on the top of the fuel plates.

Once all wires have been positioned the reactor is started up to low power (typically 200 W). Irradiation is for approximately 10 minutes at which point the reactor is shut down and the wires are removed. After the appropriate decay time the wires are removed from their holders. Activities are measured on a sodium iodide detector system. Wire position, clock time, activation and background are measured. Relative activities of the wires are used to create an estimate of relative assembly power.

III-4.3.2. Summary and comparison of benchmark results

The Canadian and South African groups participated in this section of the benchmark analysis. Different calculation approaches were used by CAN and SAF respectively.

Results calculated by CAN were done using infinite dilution reaction rates from an MCNP5 core model over the entire energy range. The flux wires were not included explicitly in the core model, but scores were tallied over a cell of dimensions 0.3cm x 1.0 cm x 2.32cm centred at a nominal position in coolant channel 7 of each standard fuel assembly. Using this model for

the flux wires, the saturation activity values for the ^{55}Mn (n,γ) reaction were calculated and normalized to the average across the calculated results.

For the SAF calculated results, the built-in OSCAR-4 system detector model was used to calculate the activation of the wires inserted into the various positions. The saturation activity was calculated for the full energy range by using the detector constants generated during the cross-section homogenization procedure and the reconstructed heterogeneous flux at the detector positions in the diffusion calculation. Wire geometry, such as volume and length, were taken into account when the activation was calculated.

The measured ^{55}Mn activity (normalized) and the calculated results, for both SAF and CAN, are summarized in Table III-12. The calculated to experimental ratios are also shown in Table III-13 and Table III-14 in the form of the grid positions and are plotted in Fig. III-29.

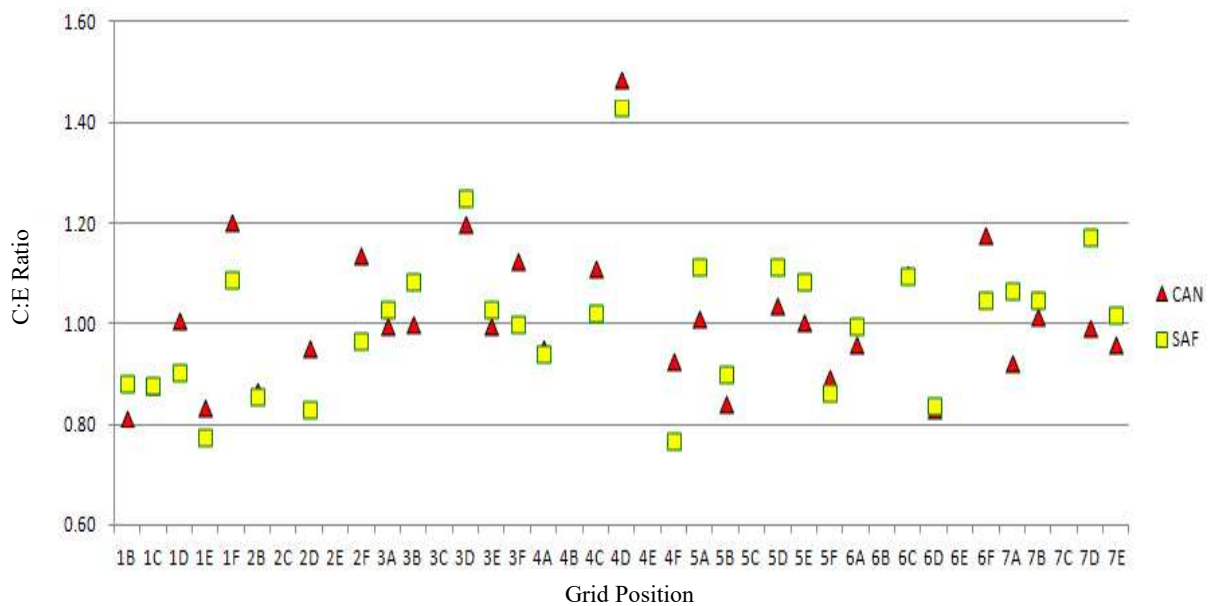


FIG. III-29. Radial flux wires - calculated to experimental ratios for each grid position.

TABLE III-12. RADIAL FLUX WIRE RESULT SUMMARY

Grid Site	Assembly ID	Burn-up (%)	Measured (E)	CAN		SAF	
				(C)	C:E	(C)	C:E
1B	MNR-310	46.2	0.99	0.81	0.81	0.88	0.88
1C	MNR-323	29.6	0.97	0.85	0.88	0.86	0.88
1D	MNR-317	34.1	0.93	0.94	1.01	0.84	0.91
1E	MNR-315	33.4	0.96	0.80	0.83	0.74	0.78
1F	MNR-304	48.0	0.51	0.61	1.20	0.56	1.09
2B	MNR-313	37.1	1.42	1.24	0.87	1.22	0.86
2C	MNR-C64	10.0				1.63	
2D	MNR-333	0.5	1.23	1.17	0.95	1.03	0.83
2E	MNR-361	24.7				1.65	
2F	MNR-330	7.0	0.60	0.68	1.14	0.58	0.97
3A	MNR-319	28.3	0.96	0.96	1.00	0.99	1.03
3B	MNR-321	33.1	1.32	1.32	1.00	1.44	1.09
3C	MNR-322	27.9		1.52		1.57	
3D	MNR-306	46.9	1.49	1.79	1.20	1.86	1.25
3E	MNR-328	14.2	1.24	1.24	1.00	1.28	1.03
3F	MNR-307	47.6	0.99	1.11	1.12	0.99	1.00
4A	MNR-326	20.2	0.94	0.89	0.95	0.89	0.94
4B	MNR-C63	26.0				1.60	
4C	MNR-324	30.5	1.43	1.59	1.11	1.46	1.02
4D	MNR-327	15.6	0.99	1.47	1.48	1.42	1.43
4E	MNR-C65	10.2				1.52	
4F	MNR-314	38.0	1.16	1.08	0.93	0.89	0.77
5A	MNR-303	48.5	0.94	0.95	1.01	1.05	1.12
5B	MNR-312	40.7	1.41	1.18	0.84	1.27	0.90
5C							
5D	MNR-309	39.1	1.45	1.50	1.04	1.62	1.12
5E	MNR-329	12.8	1.07	1.07	1.00	1.16	1.09
5F	MNR-305	41.6	1.06	0.94	0.89	0.91	0.86
6A	MNR-311	29.9	0.71	0.68	0.96	0.71	1.00
6B	MNR-C66	0.5				0.88	
6C	MNR-308	4.0.9	1.01	1.11	1.10	1.11	1.10
6D	MNR-325	21.6	1.23	1.02	0.83	1.03	0.84
6E	MNR-C62	24.4				1.09	
6F	MNR-320	21.3	0.55	0.65	1.18	0.58	1.05
7A	MNR-189	53.1	0.70	0.65	0.92	0.75	1.07
7B	MNR-331	1.9	0.49	0.49	1.01	0.51	1.05
7C							
7D	MNR-318	26.1	0.69	0.69	0.99	0.82	1.18
7E	MNR-332	1.5	0.55	0.52	0.96	0.56	1.02

TABLE III-13. RADIAL WIRE C:E RATIOS (CAN)

Grid Position	7	6	5	4	3	2	1
A	0.92	0.96	1.01	0.95	1.00		
B	1.01		0.84		1.00	0.87	0.81
C		1.10		1.11			0.88
D	0.99	0.83	1.04	1.48	1.20	0.95	1.01
E	0.96		1.00		1.00		0.83
F		1.18	0.89	0.93	1.12	1.14	1.20

TABLE III-14. RADIAL WIRE C:E RATIOS (SAF)

Grid Position	7	6	5	4	3	2	1
A	1.07	1.00	1.12	0.94	1.03		
B	1.05		0.90		1.09	0.86	0.88
C		1.10		1.02			0.88
D	1.18	0.84	1.12	1.43	1.25	0.83	0.91
E	1.02		1.09		1.03		0.78
F		1.05	0.86	0.77	1.00	0.97	1.09

The calculated results from the two participating groups show comparable differences with respect to the experimental data. Calculated to Experimental ratios are associated with standard deviations of approximately 0.14 for both the CAN and SAF groups.

There is a suggestion that there is some sensitivity to results related to proximity of the grid site to the radial beam tubes. Specifically, the C:E ratios of the SAF results are consistently lower than those of the CAN group for the Column F and Row 1 sites (exceptions being sites 1B and 1C adjacent to more removed beam tube #1). Differences may be related to details of the modelling approaches used by the two participating groups. Apart from these calculation-to-calculation comparisons, no trends in the calculated values compared to the experimental measurements have been identified with respect to (i) grid position, or (ii) assembly depletion. The largest discrepancy between the measured and calculated values is associated with core grid site 4D with C:E ratios of 1.48 from CAN and 1.43 from SAF. A comparison of the measured value in site 4D with a selection of values for other core grid positions is shown in Table III-15.

TABLE III-15. COMPARISON OF MEASURED VALUES FOR SELECTED GRID POSITIONS

Site	Assembly	Burn-up (%)	(E)
3D	MNR-306	46.9	1.49
3F	MNR-307	47.6	0.99
4D	MNR-327	15.6	0.99
4F	MNR-314	38.0	1.16
5D	MNR-309	39.1	1.45

It is surprising that the measured value for Site 4D (0.99) is the same as that for Site 3F which contains the same type of fuel assembly but with a higher depletion in a more peripheral core position. Similar comparisons can be made to the other selected sites in Table III-15. Any uncertainty in the 4D measured value would contribute to the large C:E values found by the two participants

To help quantify expected experimental uncertainty the CAN analysis included a sensitivity study on wire placement within a given fuel assembly, considering both lateral and axial variation of the wire position. With regards to the experiment, while the axial position of the wire when installed in the core is quite well defined by geometric fit of the holder collar and the top of the fuel plates, the installation is performed by manually lowering the wire, on string, from the operations bridge, some 10 meters above the core and through 8 meters of pool water.

The target area is only the width of a coolant channel. In reality it is hard to identify which coolant channel ends up housing each individual wire. Acceptable positions are anywhere

within the half of the assembly from the top handle to the outermost fuel plate, side to side variation in position is common. This variation was assessed by adding tally cells were added in coolant channels 3, 5, 7, 11, 13, and 15 as shown in Fig. III-30. Additional tally cells were also added in $\pm \Delta Z$ locations offset 2.54 cm from the nominal axial position of the central tally cells in each fuel channel. This is shown in Fig. III-31.

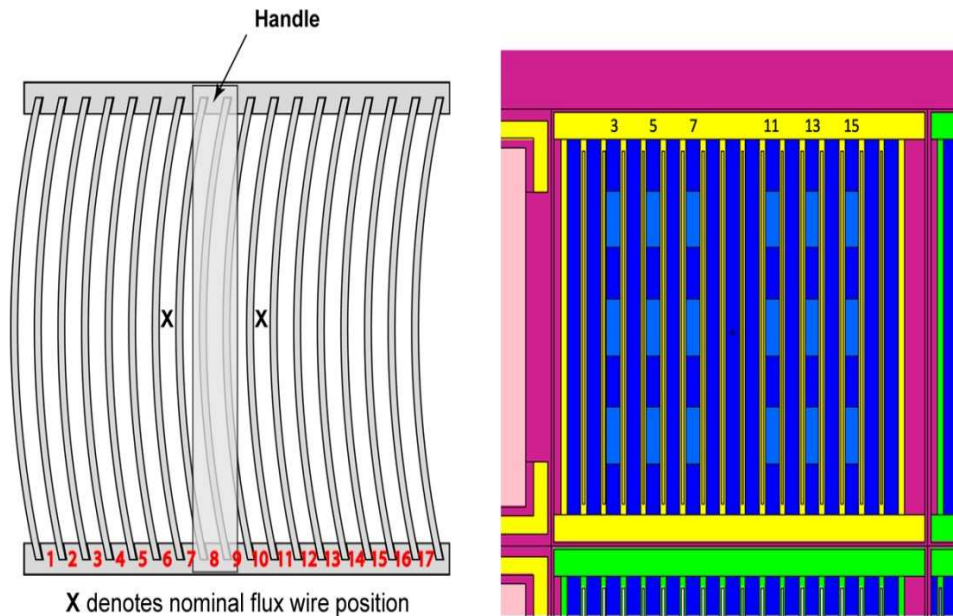


FIG. III-20. MNR radial flux wire nominal position & CAN sensitivity analysis geometry.

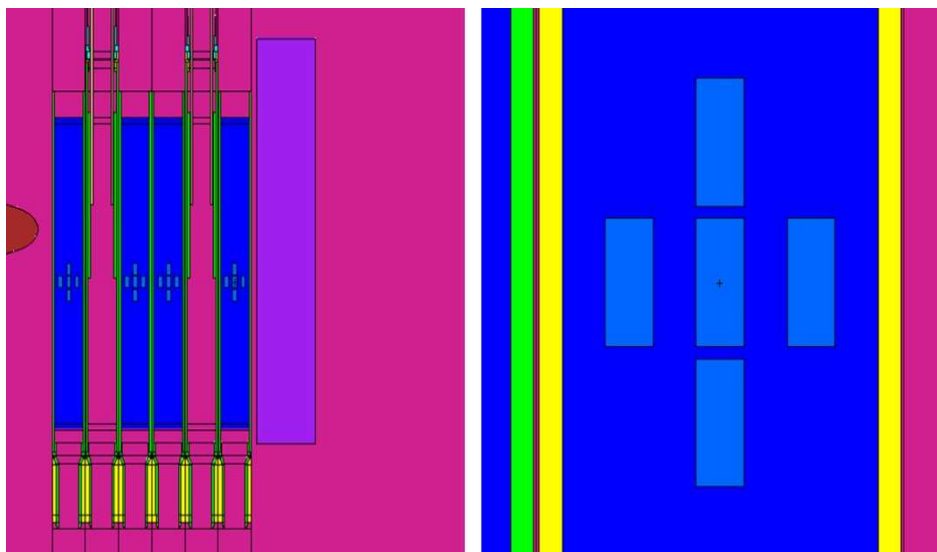


FIG. III-31. Vertical MNR radial flux wire CAN sensitivity analysis geometry.

Results from the CAN sensitivity analysis suggest that measured values may be over-predicted by up to 30% and under-predicted by as much as 10% as a result of variation of irradiation position. This magnitude of variation is on the order of the standard deviation of the calculated-to-measured results. The CAN modelling represents an average plate burn-up composition within the assembly axial zone rather than a plate-to-plate or side-to-side plate burn-up so some variation due to the burn-up distribution may not be captured in the sensitivity analysis estimates.

III-4.3.3. Conclusions and recommendations

This section of the benchmark is based upon what can be considered typical flux wire irradiation measurements for a research reactor. One conclusion from this section of the benchmark analysis is that for such ^{55}Mn activation measurements the approximation of flux, from SAF, to activation, from CAN, is a suitable approach.

The calculated results for both CAN and SAF show similar errors, as compared to the experimental measurements, across all positions with the exception of a few. The range of calculated-to-experimental values found by both groups is consistent with estimates of the uncertainty in the experimental data as found from some scoping sensitivity analysis related to experimental wire position.

Some of the larger differences between the CAN results and the SAF results occur on the core periphery. In these areas the difference between the diffusion approximation, used in the SAF approach, and the transport model used in the CAN approach become more pronounced.

As a result of this analysis and comparison it may be concluded that an experiment of this type is valuable for static neutronic benchmarking, but that the design of the experiment and the collection of the experimental data is of paramount importance in order to produce experimental data of the quality needed to make the exercise valuable.

III-4.4. Experiment 5: Axial Flux Wire Activation

III-4.4.1. Short description of experiment

Full-length copper wires were placed in a series of MNR in-core irradiation sites in Core 54A at the core beginning-of-life directly following the rod calibration measurements. Irradiations were performed at low power. Wires were threaded through wire holders which in turn were placed in MNR sample holders. These holders were then manually placed, with the aid of MNR sample handling tools, into the desired core positions. Experiment positions are shown in Fig. III-32.

The flux wires were irradiated in two sets. The first set included all positions except 9D. For the second set a wire was placed in the 9D position only. For the irradiations a 0.10 cm diameter copper wire was threaded by hand into an aluminium wire holder, which in turn was placed inside a standard MNR sample holder (also aluminium). The collar of the sample holder determines the axial position of the sample in the specific irradiation site as it sits with the bottom of the collar on top of the irradiation position assembly.

All samples were loaded into the core before start-up. The reactor was then brought to low power. This start-up from zero power to 200 W took approximately 3 1/3 minutes on a 35 second period. Following irradiation, the reactor was shut down. Samples were then removed from the core and allowed to decay before removal and counting of the wires.

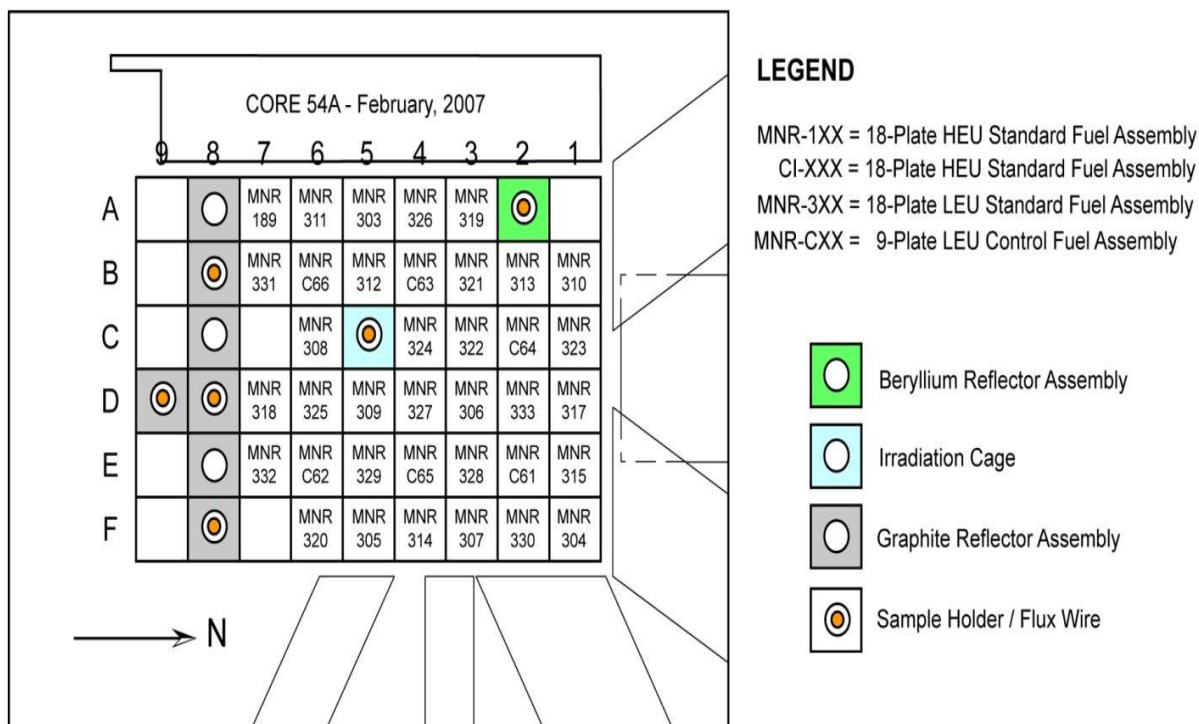


FIG. III-32. MNR core 54A flux wire locations.

Post irradiation, the copper wires were manually cut into pieces on the order of 2 cm in length. These pieces were then individually weighed, and their activation was measured in the MNR Centre for Neutron Activation labs. The 511 keV peak for ^{63}Cu activation was measured. Count times were adjusted so that statistical uncertainty on the peak counts was less than 2%.

The irradiation experiments were performed on Thursday, February 21st and Friday, February 22nd, 2007. The reactor had been shut down for a core change and testing since the previous Friday evening, February 16th (the last full power operation at 3 MWth) and only operated for periods at low power (up to 200 W) up to and including these irradiations. As such, the core can be considered practically free of Xenon.

III-4.4.2. Summary and comparison of benchmark results

The ARG, CAN and SAF groups participated in this section of the MNR benchmark analysis. In the modelling of this experiment two different simulation methods were adopted. For the ARG and SAF submissions diffusion methods were used to calculate axial flux profiles in the experimental positions, while an explicit device model in the MCNP transport code was used by CAN to calculate the ^{63}Cu activation in each of the positions.

Throughout all submissions the control rods were placed at the positions as specified in the benchmark description [III-2]. That is, for the first measurement that occurred on 21 February (measurement of grid positions 5C, 2A, 8B, 8D, 8F) the regulating rod was positioned at 50% withdrawn and the shim safety rods were all positioned at 67% withdrawn. For the measurement on 22 February (measurement of position 9D) the regulating rod was again positioned at 50% withdrawn while the shim safety rods were positioned at 68% withdrawn. For the ARG results, a thermal flux calculation was performed using the CITVAP code, only considering energies below 0.625 eV. The axial flux values were calculated only over the active height of the core for each channel and normalized to the peak in each of the individual channels.

Similar to the ARG group, the SAF group also used a diffusion method to perform a flux calculation with the MGRAC code, but the entire energy range (0–10 MeV) was considered. Currently the functionality to carry detector constants through from the lattice calculation to the core simulator for non-fuel components is not implemented. The detector constants produced in the lattice code for these components, were manually multiplied with the node average flux in each of the axial nodes. The calculated flux values were then normalized to the peak in each of the respective channels for the comparison with the measured ^{63}Cu activation.

The CAN group used an explicit device model for the copper wire as well as its housing assembly in the MCNP transport code. Using this model the ^{63}Cu activation throughout the entire axial height of each wire was calculated. Once again, the calculated activation was normalized to the peak in the individual channels for comparison purposes. Figure III-33 to Fig. III-38 show summary comparisons between all the calculated results and the experimentally measured results for each flux wire grid position.

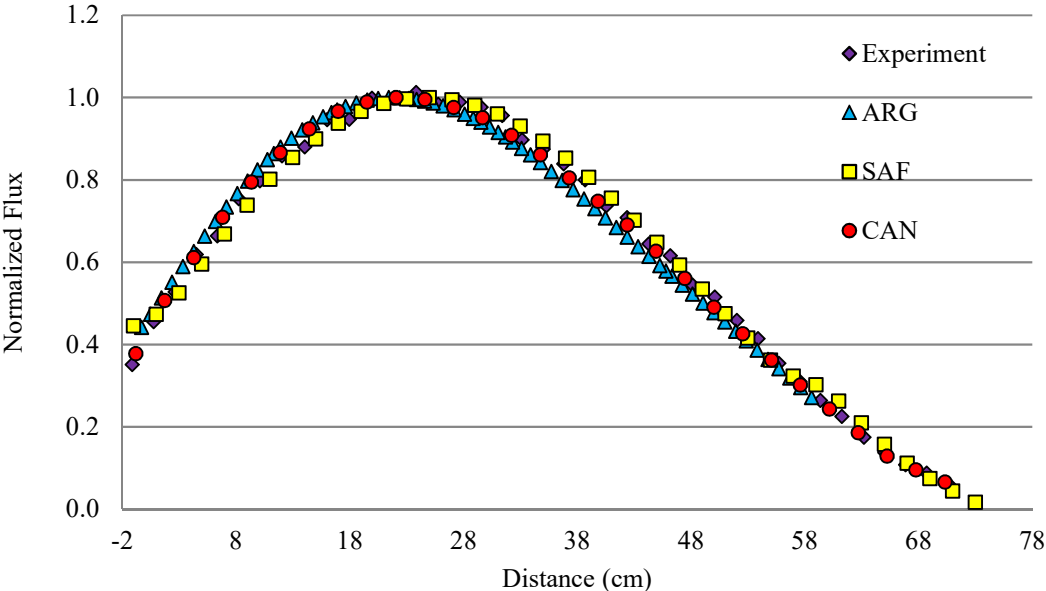


FIG. III-33. Axial flux wire results for site 5C.

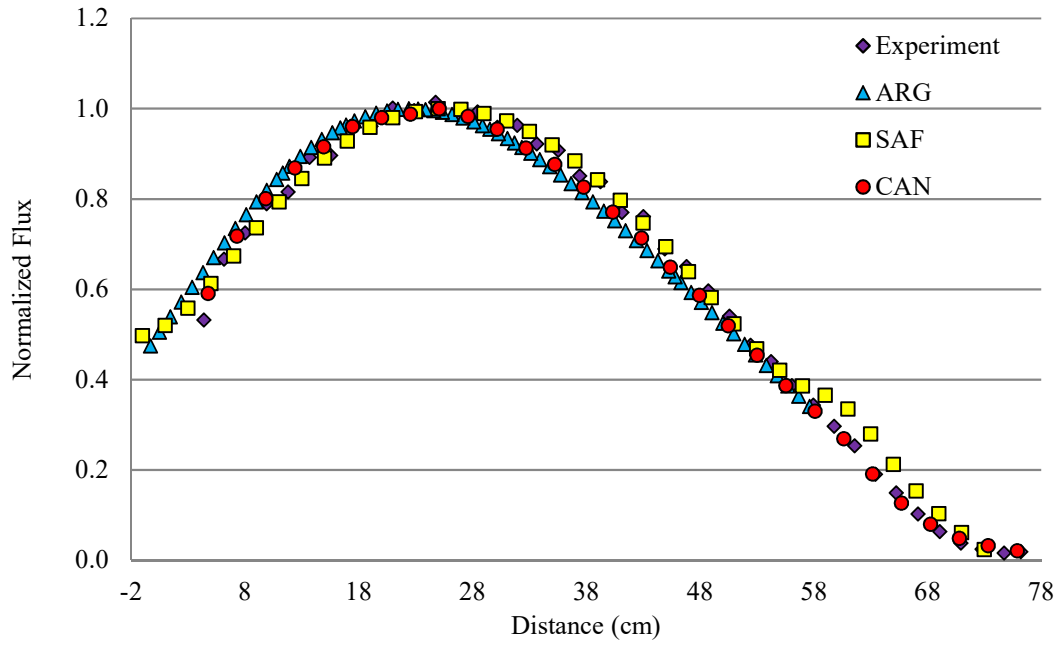


FIG. III-34. Axial flux wire results for site 2A.

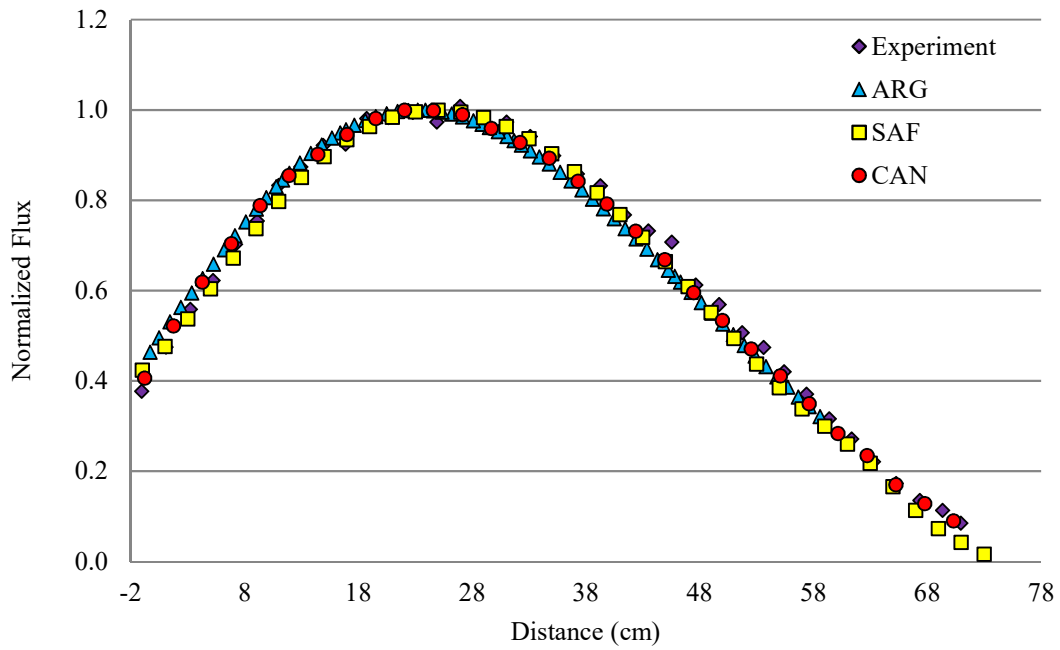


FIG. III-35. Axial flux wire results for site 8B.

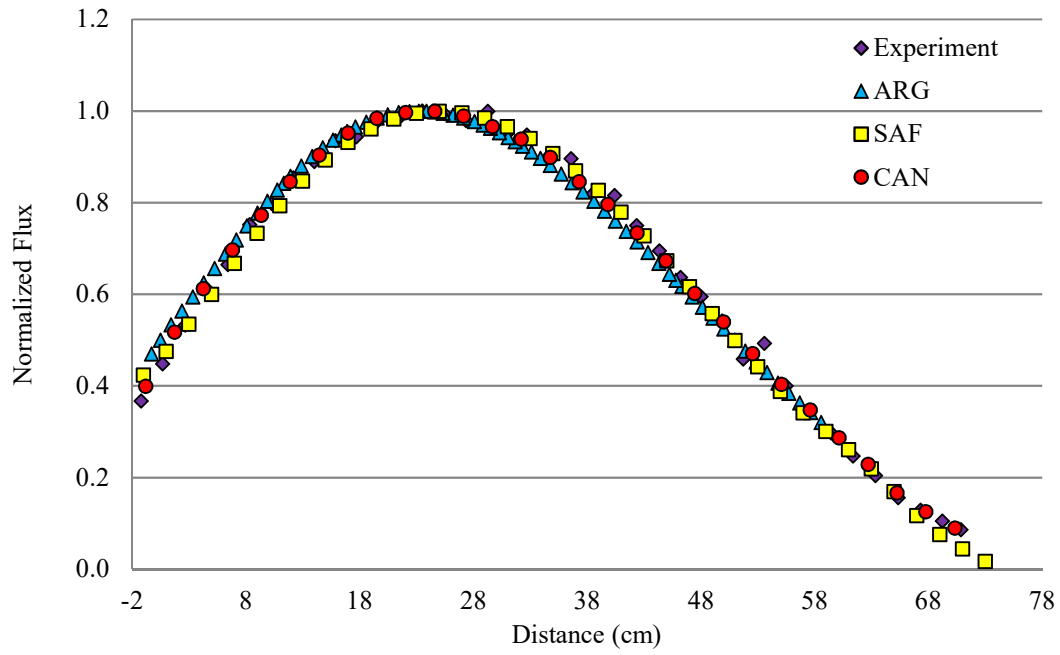


FIG. III-36. Axial flux wire results for site 8D.

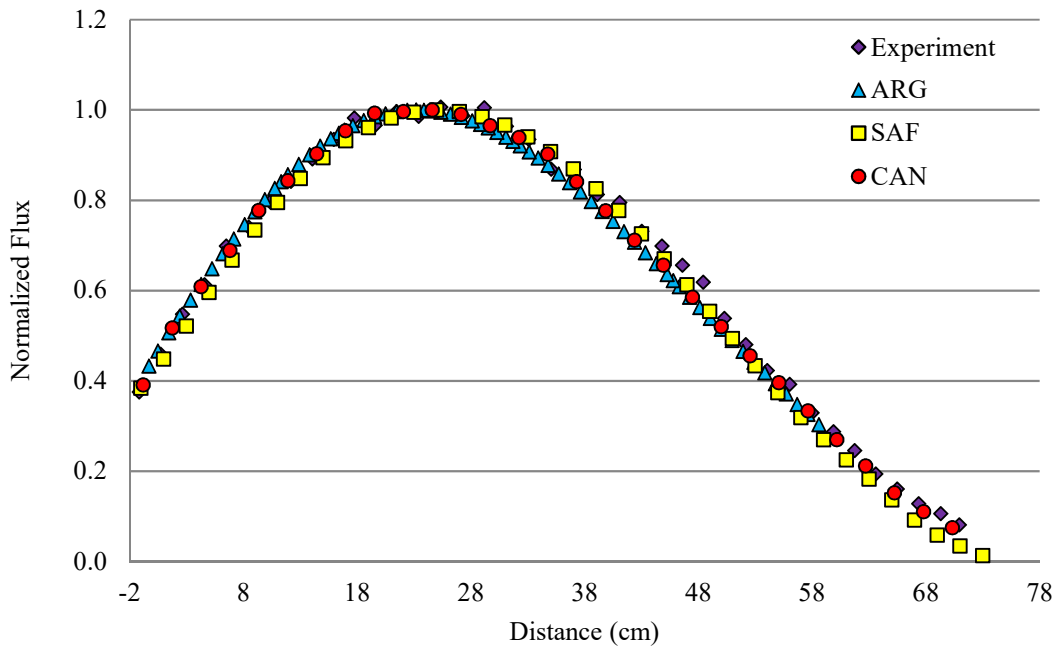


FIG. III-37. Axial flux wire results for site 8F.

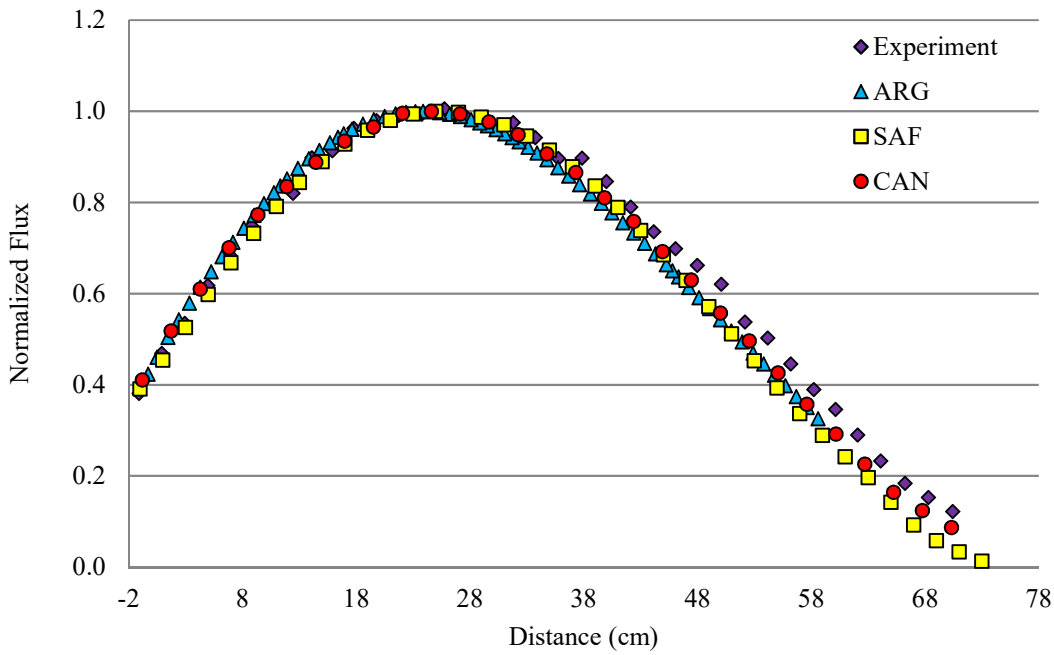


FIG. III-38. Axial flux wire results for site 9D.

All groups showed reasonable agreement with measured values with the largest differences found for the wire irradiation in core position 9D where all participating groups under-predicted the activity/flux in the upper half of the core. At present no reason has been identified for this discrepancy.

Upon closer examination there are some minor differences of note between the calculated and experimental results. The ARG group results are slightly offset relative to the measured data towards the bottom of the core. This offset is on the order of 1 to 1.5 cm and is shown in Fig. III-39. The two profiles shown are representative of all six wire positions indicating a common factor in the modelling.

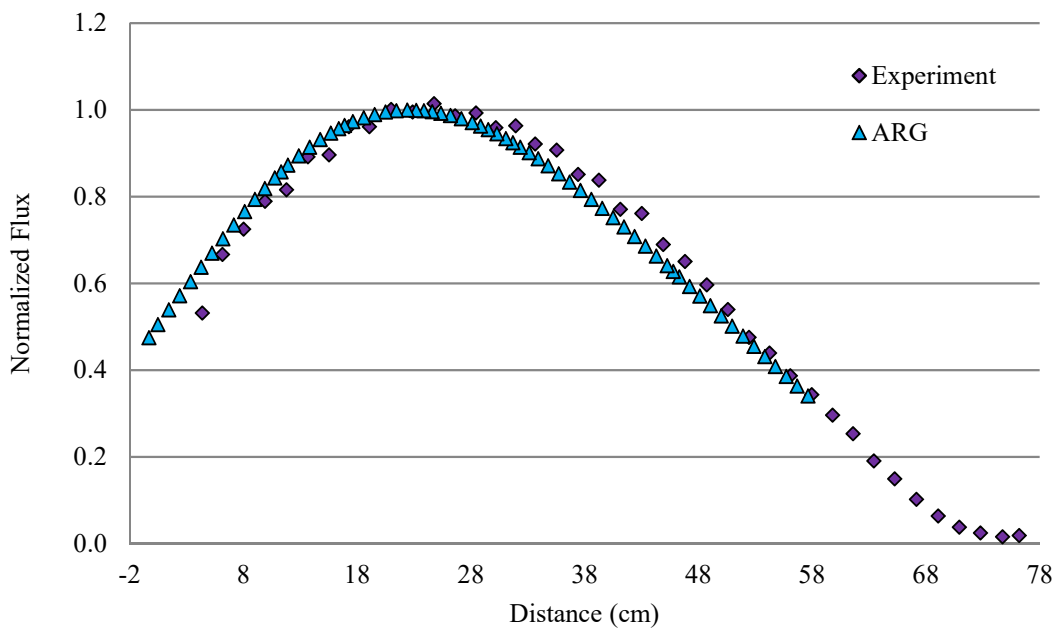
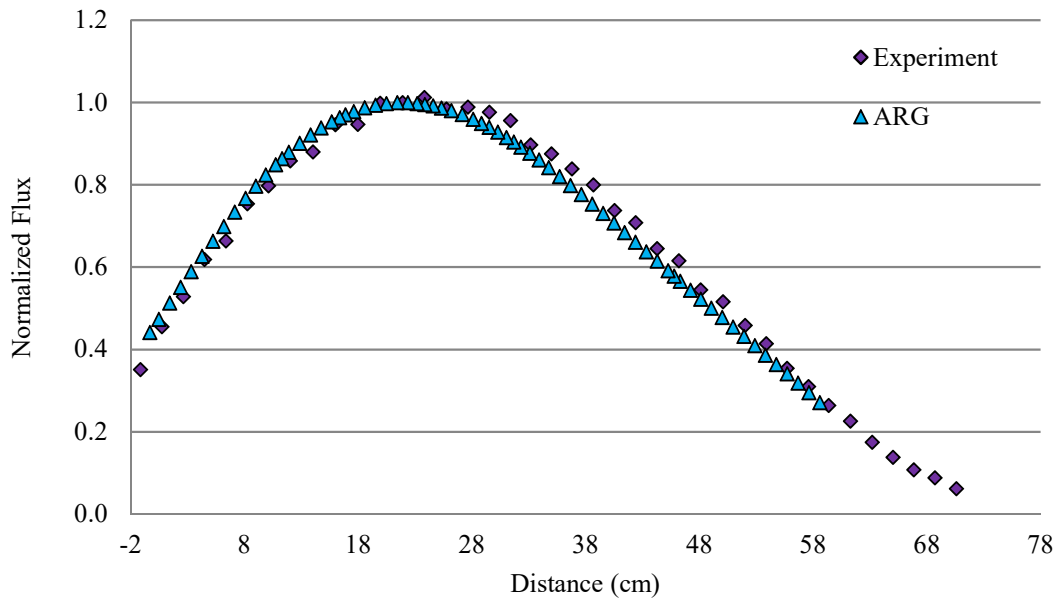


FIG. III-39. Argentina axial flux wire results for site 5C (top) and 2A (bottom)

The SAF group results match well to the peak wire flux/activity position but do show a departure from measured values both at the bottom (0 cm) and the top (60 cm) of the active fuel zone for the wires in positions 5C and 2A, as shown in Fig. III-40. The reason for this deviation from measured results is thought to be due to the fact that the SAF model did not include any structural material above or below the active zone of the core for these positions. For the graphite reflector positions the assembly material model extended further axially and this effect was not observed.

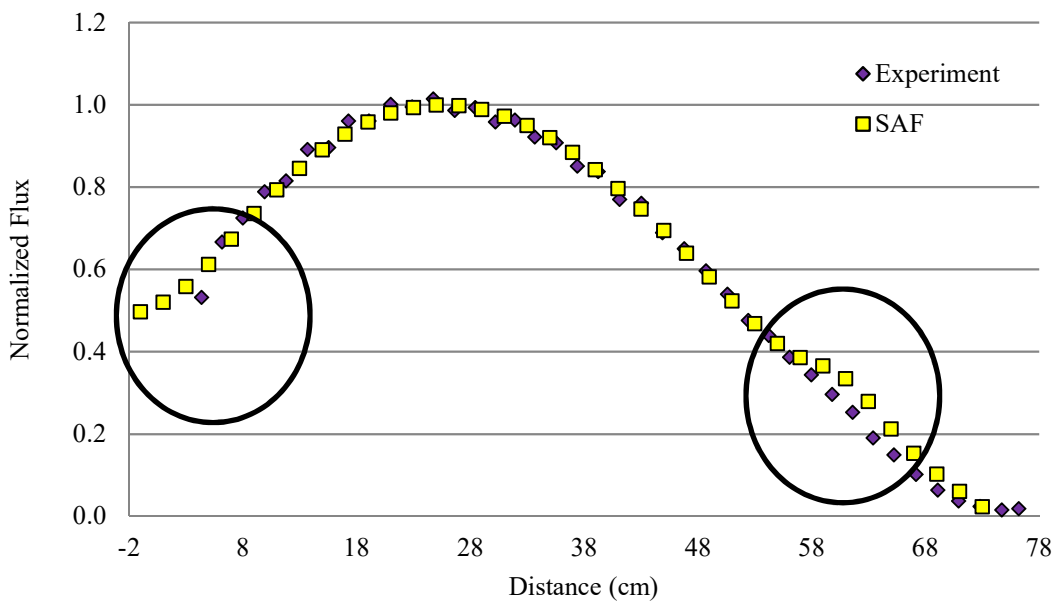
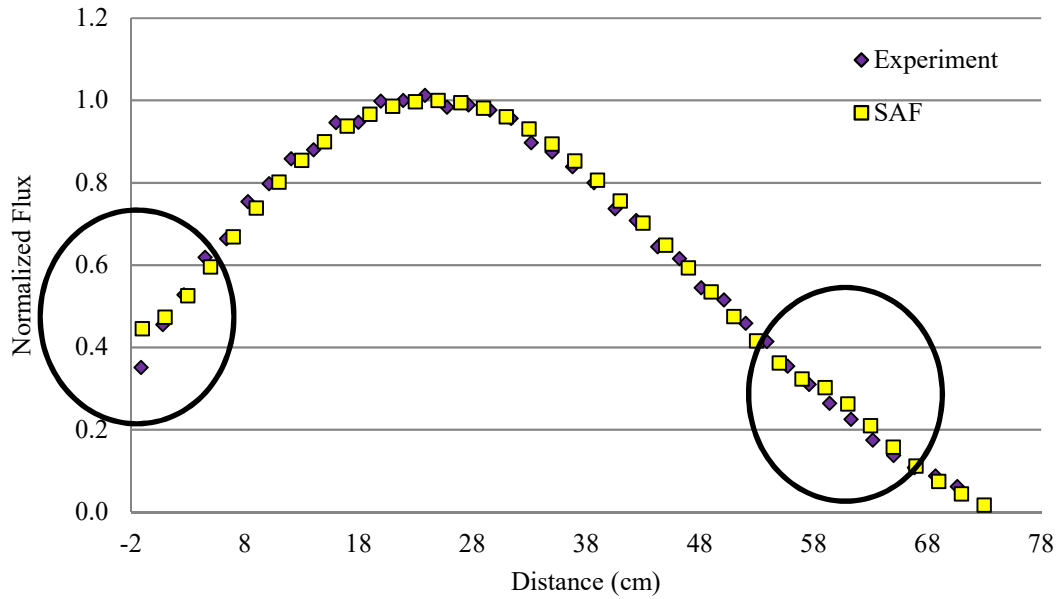


FIG. III-40. South Africa axial flux wire results for 5C (top) and 2A (bottom)

The more detailed MCNP model used by the CAN group included the explicit geometry for the different assemblies and core structure and matched the shape of the experimental measurements over the entire height of the flux wires, as shown in Fig. III-41. Apart from the differences common to all groups for the wire in position 9D, the CAN simulation results match well to the axial distribution for each wire.

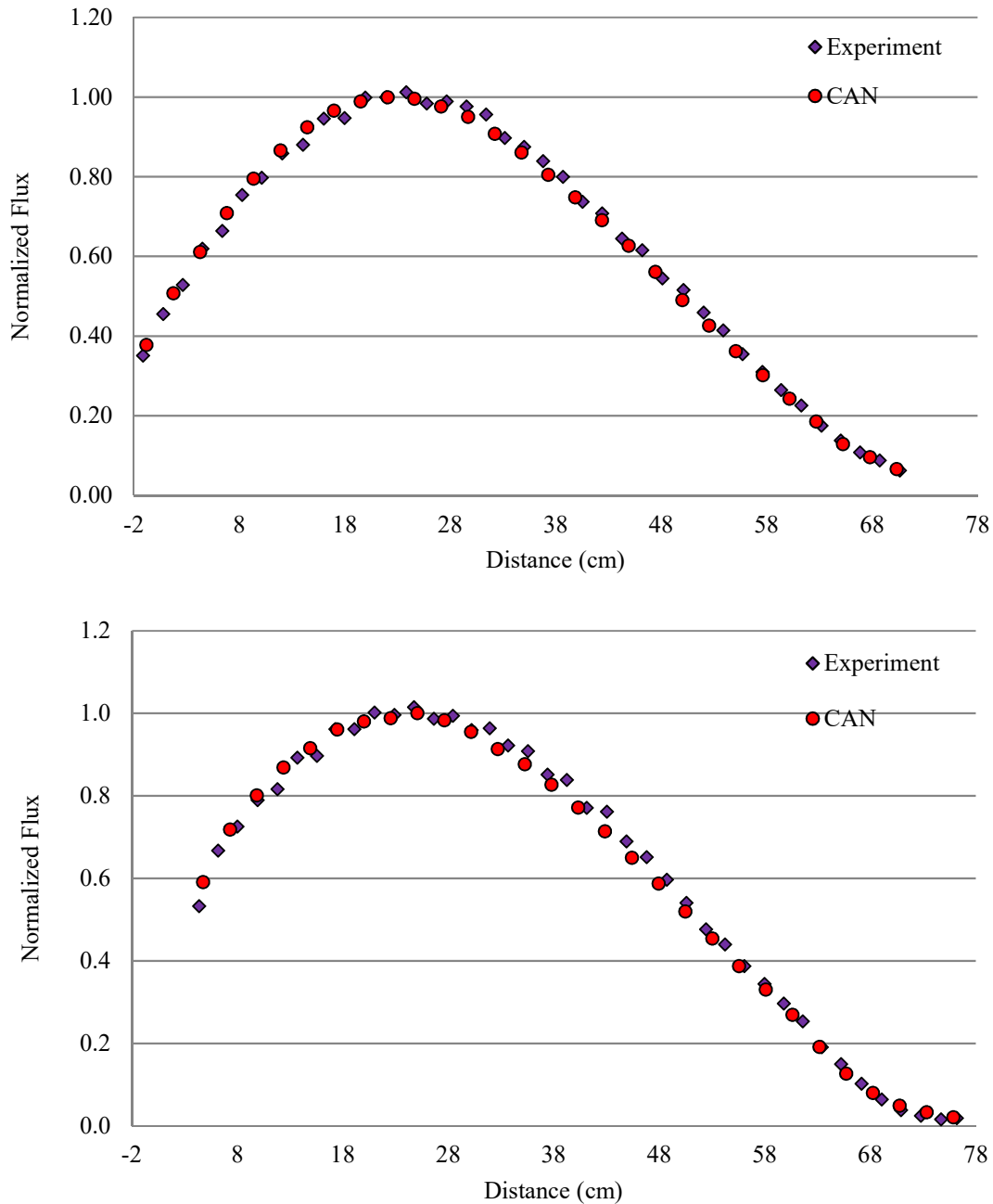


FIG. III-41. Canada axial flux wire results for 5C (top) and 2A (bottom)

Peak-to-average and peak-to-peak comparisons from each of the participating analysis groups are presented in Table III-16 to Table III-18. The peak-to-average values for each wire provide a second comparison of the calculated to experimental axial distribution for each wire position to expand on the axial plots shown in the figures. In general, the agreement between calculated and experimental results are quite good with C:E ratios ranging from 0.93 to 1.03, which is considered reasonable for flux wire measurements. The peak-to-average values presented for the ARG group are associated with only the axial height of the core as calculated results were only generated for this range. The CAN and SAF results are for the entire height of the wire as specified in the benchmark documentation.

To assess the agreement between calculation and measurement across the core the peak-to-peak values are compared for each site relative to the wire in site 5C (highest flux site). The ARG and CAN groups found good agreement, within 10% of the experimental peak-to-average comparison to Site 5C, with the exception of that ARG result for the lowest flux site, 9D. Of note also is the C:E peak-to-average value for Site 5C which influences the peak-to-peak results. The SAF group found noticeable differences in their site-to-5C comparisons, beyond the 10% range. The source of this variation has yet to be determined.

TABLE III-16. AXIAL FLUX WIRE RELATIVE RESULTS FOR ARG

Irradiation Position	Peak-to-average ratio*			Peak-to-peak (5C) ratio		
	Measured	Calculated	C:E	Measured	Calculated	C:E
5C	1.41	1.35	0.96	1.00	1.00	1.00
2A	1.33	1.32	0.99	0.42	0.42	0.99
8D	1.36	1.32	0.97	0.25	0.25	1.01
8B	1.42	1.32	0.93	0.21	0.21	1.02
8F	1.37	1.34	0.98	0.16	0.16	0.99
9D	1.36	1.32	0.97	0.12	0.10	0.81

C:E is Calculated to Measured Ratio

** Note: ARG results were only provided over axial height of the core (0-60cm)*

TABLE III-17. AXIAL FLUX WIRE RELATIVE RESULTS FOR CAN

Irradiation Position	Peak-to-average ratio			Peak-to-peak (5C) ratio		
	Measured	Calculated	C:E	Measured	Calculated	C:E
5C	1.59	1.62	1.02	1.00	1.00	1.00
2A	1.62	1.60	0.99	0.42	0.45	1.09
8D	1.54	1.57	1.01	0.25	0.26	1.04
8B	1.53	1.57	1.03	0.21	0.23	1.05
8F	1.54	1.59	1.03	0.16	0.17	1.10
9D	1.51	1.55	1.03	0.12	0.13	1.07

TABLE III-18. AXIAL FLUX WIRE RELATIVE RESULTS FOR SAF

Irradiation Position	Peak-to-average ratio			Peak-to-peak (5C) ratio		
	Measured	Calculated	C:E	Measured	Calculated	C:E
5C	1.59	1.55	0.97	1.00	1.00	1.00
2A	1.62	1.48	0.92	0.42	0.47	1.12
8D	1.54	1.53	0.99	0.25	0.30	1.22
8B	1.53	1.54	1.00	0.21	0.27	1.28
8F	1.54	1.55	1.01	0.16	0.21	1.30
9D	1.51	1.54	1.02	0.12	0.12	1.01

III-4.4.3. Conclusions and recommendations

In general, the calculated results by the problem participants, agreed quite well with the experimental measurements. Some variation was noted, likely as a result of degree of modelling detail on the axial flux distributions, and some variation, up to 30% was found on distribution

between different experimental positions in the core grid. The reason for this latter effect has yet to be determined and may be relevant to differences found in the radial flux wire section of the benchmark analysis.

This section of the benchmark is based upon what can be considered typical flux wire irradiation measurements for a research reactor. One conclusion from this section of the benchmark analysis is that for such ^{63}Cu activation measurements the approximation of infinite dilution total or thermal flux estimates is suitable and equivalent to a more explicit activation calculation including the explicit wire material.

An additional conclusion is that nodal diffusion theory, finite-difference diffusion theory, and explicit-geometry continuous-energy MCNP models can all be deployed to accurately model such irradiation experiments. A qualifying remark to this is that while it is standard practice when using diffusion theory approaches to simplify structural, end fitting, and reflector zones outside of the active zone of the core, such approximations may impact the accuracy of flux wire simulations depending upon the specifics of the experiment.

III-5. CONCLUSIONS

The experiments that comprise the MNR benchmark analysis are based on standard operational measurements for an open-pool MTR-type research reactor and represent what are considered typical or routine neutronic simulation problems.

It was found that both diffusion-theory-based simulation and Monte-Carlo-transport theory-based calculations, resulted in a similar level of accuracy compared to experiment. No proper comparison of the methods is available at this time, with respect to absorber reactivity calculations, and is left as future work. The quality and extent of the experimental data and the limited participation in this benchmark analysis, are not sufficient to evaluate the different modelling approaches apart from having identified a user effect due to modelling details of structural and reflector zones, and in the geometrical details of experimental equipment. These effects were noted in the shim-safety rod calibration and the axial flux wire sections of the problem.

Despite the routine nature of the calculations a valuable aspect of this problem appears to be the requirement to compare reactivity estimates made from a series of criticality calculations to estimates based upon kinetics parameters and doubling time measurements. Future effort in this area appears warranted. The participants found limited success in this section of the benchmark. Limitations in the benchmark analysis itself were also identified as shim-safety rods are cross-calibrated so the single point of comparison is to the low-worth regulating rod calibration. As such, this appears to be an area in which the research reactor community could benefit from increased knowledge sharing in order to evaluate and develop methods and understanding.

It is therefore recommended to further investigate absorber reactivity calculations in the context of kinetics-based (e.g., doubling time) calibrations and to extend the problem to include a second point of reference to measurement, such as total reactivity worth via rod drop measurement. A further improvement in the design of a benchmark analysis revision would be to perform independent calibration measurements on each absorber rod so as to reduce propagation of error by providing multiple points of comparison to measurement. A valuable aspect of the MNR benchmark analysis is that the absorber calibration involves two different absorber materials and a difference in magnitude of reactivity worth for these absorbers. A further limitation of the current benchmark specification is that detailed specifications for the

low-worth regulating rod had to be assumed as original engineering documentation was not available. This may have affected calculations.

The MNR benchmark analysis, overall, would also benefit from an improvement in the experimental measurements in this area, with more strict control on the measurements and documentation of related uncertainties. This is common to all sections of this benchmark analysis apart from the axial flux wire measurements which were performed as a dedicated experiment rather than simply operational measurements. The question of quality of the measured data is especially evident in the Regulating Rod doubling time and radial flux wire sections of the problem.

One of the major aspects of the MNR benchmark analysis which distinguishes it from other similar collections of experimental data is that the measurements were performed on an equilibrium core. Significant variation in critical rod position k_{eff} values were found between participants using different fuel material composition estimates. This represents an area for future improvement as fuel depletion estimates were based on operational estimates only which lacked verification. These supplied assembly-averaged ^{235}U depletion estimates were then left for the user to develop into more detailed fuel compositions without the benefit of a full operation history. The quality of this type of benchmark analysis would be significantly enhanced with improvements in this area.

In addition, it may be of interest to study the impact of the added complication of fuel material depletion with respect to kinetics parameter calculation. As a result, this area is recommended for future study in order to standardize methodology and investigate tools and user effect. Similarly, to the area of kinetics parameter estimation, it appears that the calculation of fuel depletion composition is an area in which the research reactor community could benefit from knowledge sharing in order to develop and standardize tools and techniques.

As such, this benchmark analysis is a valuable contribution despite the limitations in terms of uncertainty on experimental data. This limitation highlights the potential difference between what a considered operational data and research and development-oriented experiments. An additional future recommendation is to develop a revised set of experimental data subject to more stringent controlled conditions and practices.

REFERENCES TO ANNEX III

- [III-1] DAY, S.E., McMaster Nuclear Reactor – Reactor Specification, Technical Report Series 480, IAEA, Vienna, (2011).
- [III-2] DAY, S.E., McMaster Nuclear Reactor – Benchmark Specification, Technical Report Series 480, IAEA, Vienna, (2012).
- [III-3] PRINSLOO, R., ERASMUS, B., VAN HEERDEN, F., BELAL, M., ELSEKHAWY, K., NECSA Contribution to the Proceedings of the IAEA CRP 1496, NECSA, Pelindaba, Church Street extension west, Pretoria-West, Pretoria, South Africa, 0001, (2013).

ANNEX IV

BENCHMARK CONSOLIDATED RESULTS AGAINST EXPERIMENTAL DATA FROM OPAL

G. BRAOUDAKIS*, E. VILLARINO**, A. BUSTELO**, E. CUELLO**, M. BELAL***, D. BOTES***, F. VAN HEERDEN***, R. PRINSLOO***, C. PARK+, H. KIM+, B. LEE+

* Australia's Nuclear Science and Technology Organization (ANSTO), New Illawarra Road, Lucas Heights NSW, Australia

** INVAP, Nuclear Engineering Department, S.C de Bariloche - Rio Negro - Argentina

*** South African Nuclear Energy Corporation (Necsa), Pelindaba, Pretoria, South Africa

+ Korea Atomic Energy Research Institute (KAERI), Daedeok-daero, Yuseong-gu, Daejeon, Republic of Korea

Annex Consolidator: G. Braoudakis

Abstract

The IAEA CRP No. 1496 on 'Benchmarking, against Experimental Data, of the Neutronic and Thermal-hydraulic Computational Methods and Tools for Operation and Safety Analysis for Research Reactors' provides a novel opportunity to benchmark and compare the accuracy and efficiency of both off-the-shelf and locally developed computational tools to a wide set of experimental research reactor benchmark analysis. In the scope of this project, various analysis groups have evaluated the OPAL benchmark analysis, consisting of steady state flux, critical control rod configurations, control rod worth, burnup and kinetic parameter measurements. This report summarizes and compares the analysis methodologies adopted, the code systems employed, and the simulation results generated by the different analysis groups. A comparison of the computational results to supplied experimental results is also provided in this report.

IV-1. FOREWORD

The OPAL reactor is a compact core reactor with a heavy water reflector similar to many modern designs and provides a unique opportunity to benchmark many safety and operational related parameters. The OPAL benchmark data was used by four institutes from four countries to benchmark five different neutronics codes. The codes range from multi-group nodal diffusion to direct Monte Carlo and coarse particle Monte Carlo on a mesh. Table IV-1 provides a summary of the codes, methodologies and participants in this benchmark analysis.

TABLE IV-1. PARTICIPANTS AND CODES

Country Group (Institute)	Code	Solution method
ARG (INVAP)	MTR-PC	Diffusion theory
AUS (ANSTO)	MTR-PC	Diffusion theory
ROK (KAERI)	McCARD	Monte Carlo
SAF (Necsa)	MCNP	Monte Carlo
	OSCAR	Nodal diffusion
	CUCGP	Coarse particle Monte Carlo

IV-2. DESCRIPTION OF TOOLDS, CODES AND METHODS

A short description is provided of the most relevant features of the codes used during the benchmarking studies. For further details the reader is referred to the references provided.

IV-2.1. MCNP5

The results presented in this report were obtained using MCNP5 version 1.40. A detailed model was developed for the OPAL reactor. The model included the reflector vessel and reactor pool regions with the cold neutron source, beams (extended from the core face to the reflector vessel), bulk production facilities, pneumatic facilities, except for the Surveillance probe and FFX facilities that were not modelled. The geometry and material composition of each facility was used as in the specifications given in [IV-1].

Inside the chimney the core is modelled exactly as specified. Below the core region only water moderator is present and the grid plate was not modelled, and above the core there are only control rod portions and the guide box extension.

Moreover, the flux experiment was used to validate the model, and during this exercise certain adopted approximations were adjusted depending on interpretations of the engineering drawings and component locations.

IV-2.2. McCARD

The OPAL reactor was described by McCARD as detailed as possible. In the geometric model, the whole heavy water reflector and all facilities described in [IV-1] were included. In the radial and axial directions, the boundary was ± 100 cm from the active core centre.

The McCARD model was confirmed by comparing the calculated k_{eff} to an MCNP model. The differences in the calculated k_{eff} for a representative 6 critical states between the MCNP and McCARD were 28~91 pcm. The fractional standard deviations of the calculated k_{eff} by MCNP and McCARD were about 0.00013.

IV-2.3. MTR-PC

MTR-PC [IV-2] is a system of computer codes based on deterministic methods developed to perform neutronic, thermal-hydraulic and shielding calculations of MTR-type reactors.

The results presented in this report were obtained with two versions of the codes CONDOR 2.55/CITVAP 3.5 and CONDOR 2.62/CITVAP 3.8. Cell calculations were performed using CONDOR for the fuel assemblies, control rods other core components and irradiation facilities. A 3-group (thermal, epithermal and fast) and a 10-group (more fast groups) cross section library was developed using the various cell models. The former was used for all reactivity and flux calculations and the latter was used with microscopic cross sections for calculation of kinetic parameters using the CITVAP core code. The core model was 3-dimensional.

Some important and noteworthy features of the reactor model include:

1. Separate representation of fuel plate-coolant region and side plate region in fuel assemblies. This allows accurate calculation of the respective fluxes and spectrum for each region which can vary significantly across a fuel assembly.
2. Explicit representation of all irradiation facilities close to the core. This allows accurate calculation of the overall core reactivity and any asymmetric power tilt on the core.
3. Explicit representation of beam facilities including the cold neutron source. These large regions of effective void have a significant effect on the core reactivity and core power distribution. The helium inside the beam tubes was represented by 10% density heavy

water to facilitate convergence of the diffusion solution and account for the reactivity and power tilt effects. It will not provide reliable fluxes within the beam tubes as they will be highly directional and require discrete ordinates or other methods but will reproduce the global effects.

4. The use of different heavy water cross-sections depending on distance from core. Three sets of cross-sections were obtained by condensing over the relevant neutron spectrum in the appropriate region. This is important for the slowing down of neutrons within the reflector region and contribution to core reactivity.
5. The detailed structure above and below the core, specifically the core grid and the upper fuel assembly zone were not modelled. Instead these regions were modelled as simply light water. This will produce local artefacts but have only a slight impact on the global parameters.

IV-2.4. OSCAR-4

The OSCAR-4 model for the OPAL reactor benchmark specifications was set up, with the following design selections considered pertinent to the modelling:

1. A 7-group structure (3 fast, 1 epithermal and 3 thermal) was selected for the global diffusion solution in OSCAR-4. All the lattice calculations were performed utilizing the 172 group WIMS-E fine-group cross-section library, based on JEFF 2.2.
2. A semi-heterogeneous burnable absorber (BA) treatment to improve the accuracy of the BA reactivity contribution and depletion rate prediction. A BA side-flux model was employed, which homogenizes the cross-section for the BA material with the heterogeneous assembly side flux.
3. Colourset environments for the generation of appropriate equivalence parameters were utilized. The following summarizes the most relevant:
 - a. Fuel elements (212 g, 383 g and 484 g) homogenized in infinite lattices.
 - b. Control elements homogenized within their nearest neighbour environments.
 - c. Heavy water reflector homogenized in an inner and outer region, utilizing the 484 grams fuel element as a driver zone.
 - d. The beams and cold neutron sources are modelled approximately, with He used as a gas to fill these facilities.
4. Nodes close to the core all include the generation of discontinuity factors, hence establishing local equivalence between the heterogeneous transport and homogeneous diffusion calculations.
5. A total of 40 cm of heavy water was modelled around the active core. This amount of heavy water was not sufficient to capture the full reflection effect of the heavy water tank but it was selected for stability in the nodal diffusion solution.

IV-2.5. CUCGP Code System

A detailed full core model was developed for the OPAL reactor. The model included the full reflector region with all the specified external facilities. The geometry and material composition of each component was kept as close as possible to the specifications given in [IV-1], with the exception of the internal structures of certain ex-core facilities (cold neutron source, the pneumatic facilities and the fast flux facility), which were replaced with volume weighted homogenized material mixtures. The geometric model produced a tetrahedral mesh of ≈ 1.5 million elements. Control rod channels were meshed separately, which allows rod movement without re-meshing the entire problem.

All the simulations were performed using the 172 group WIMS-D format library of the WIMS update project [IV-3]. The existing libraries were modified to include P1 scattering cross sections for all the isotopes. Since similar libraries are also used in the homogenization procedure of the OSCAR-4 code system, this allows for a more direct comparison between the two codes.

IV-3. DESCRIPTION OF FACILITY AND EXPERIMENT

The OPAL reactor is a 20 MW open pool type research reactor. It is composed of a compact core of sixteen fuel assemblies and five control rods surrounded by a heavy water reflector. Each fuel assembly contains 21 flat fuel plates supported by two aluminium side plates. The fuel is 19.8 wt% enriched U_3Si_2-Al and the uranium density for standard fuel is 4.8 g-U/cm^3 . The startup core utilized fuel at three different uranium densities to approximate an equilibrium core. To assist reactivity control cadmium wires within the side plates are used as burnable poison.

Inside the reflector are located a number of irradiation facilities, beam facilities and a cold neutron source. The irradiation facilities are utilized for the production of radioisotopes, neutron activation analysis, delayed neutron activation analysis and silicon transmutation doping. There are also five beam facilities, two for thermal neutron studies, two for cold neutron studies and one for future hot neutron source studies that is currently a thermal neutron beam. The layout of the reflector is presented in Fig. IV-1 and further details can be found in Ref. [IV-1].

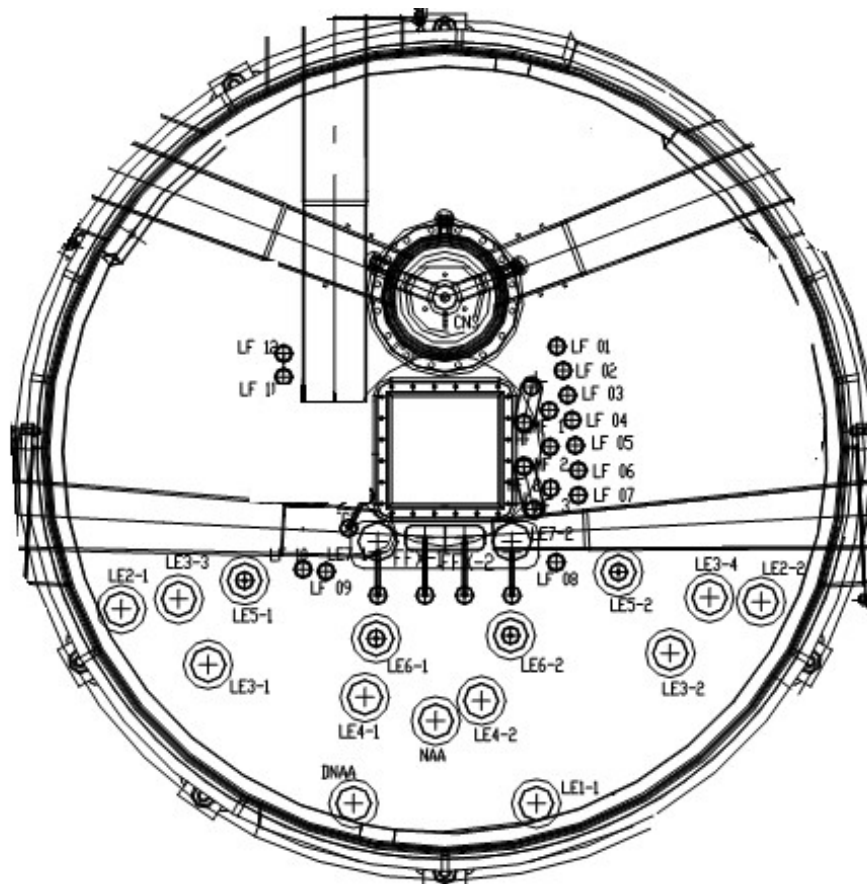


FIG. IV-1. Plan view of the reflector vessel showing the neutron beam and irradiation facilities.

The experimental results presented in this report are from commissioning activities performed during the start-up of the OPAL reactor and normal operational data collected over the initial operation. A summary of the results available is provided in Table IV-2.

TABLE IV-2. EXPERIMENTAL RESULTS AND CALCULATIONAL CONTRIBUTIONS AVAILABLE

	ARG	AUS	ROK	SAF (OSCAR-4)	SAF (CUCGP)	SAF (MCNP)
Steady state flux	✓	✓	✓	✓	✓	✓
Critical configurations	✓	✓	✓	✓	✓	
Control rod worth	✓	✓	✓	✓	✓	
Fuel burnup	✓	✓		partial		
Kinetic parameters		✓	✓			✓

IV-3.1. Steady State Flux Distribution

The thermal neutron flux distribution within the core was determined experimentally using Au-Al wires. They were irradiated both with and without cadmium covers mounted on an aluminium plate within a coolant channel at low power. The diluted gold wires were activated and the activity of ^{198}Au measured to determine the thermal neutron flux at various locations within the core. The measurements were made, and the results analysed following the ASTM standard [IV-4]. Both the activation values for the wires and the integrated thermal neutron flux (energy less than 0.625 eV) were provided to the research groups. The measurements were performed during the initial stages of OPAL commissioning.

As the reactor power was increased through the commissioning stages the fission detectors used for reactor power monitoring were moved to optimize their response over the reactor power operating range. The reactor power instrumentation was calibrated during the high-power commissioning stages by performing a thermal balance. These results had to be extrapolated back to the low power conditions and this introduces some uncertainty in the power level during the flux measurements. Taking into account this uncertainty the estimated reactor power during the irradiations was 36 ± 6 kW. Further details concerning the procedure can be found in [IV- 5].

IV-3.1.1. Summary and comparison of benchmark results

A total of six sets of results were submitted for this experiment utilizing several different techniques for modelling and calculating the thermal neutron flux distribution. Two of the axial flux distributions are presented in Fig. IV-2 and IV-3 that are typical of the results obtained. Position 1 as at the top of the fuelled region and position 21 at the bottom. They indicate that the overall features of the distributions are well reproduced by all the codes, but some are better at the finer details than others. In particular the Monte Carlo based codes (McCARD and MCNP) tend to reproduce the local changes better and show less extreme differences compared to the measured values. The ratio between calculated and measured flux for all the data available is presented in Fig. IV-4. It indicates that for some points all the codes display significant discrepancies but the MCNP results tend to be better than the others.

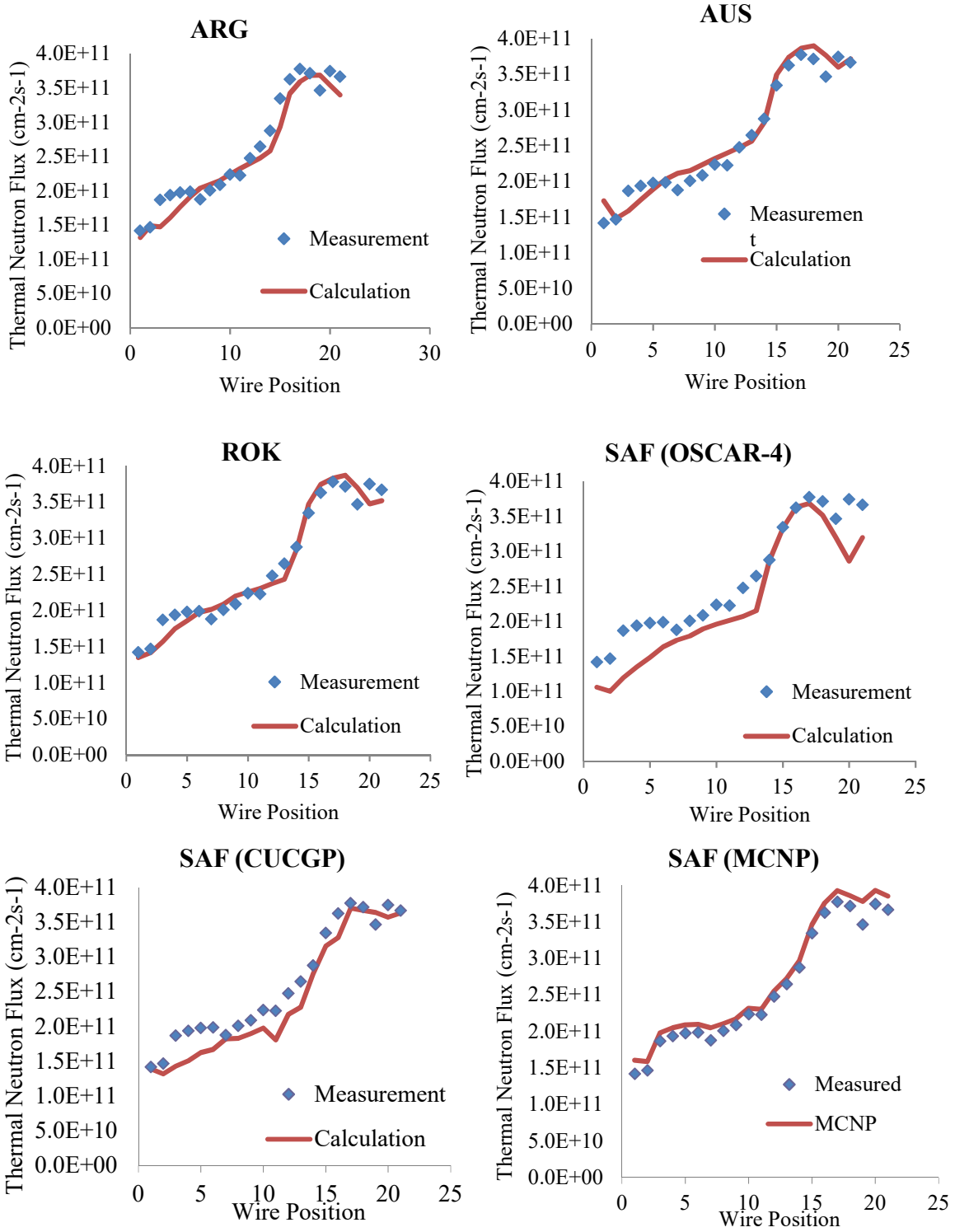


FIG. IV-2. Thermal neutron flux axial profile for position A2.

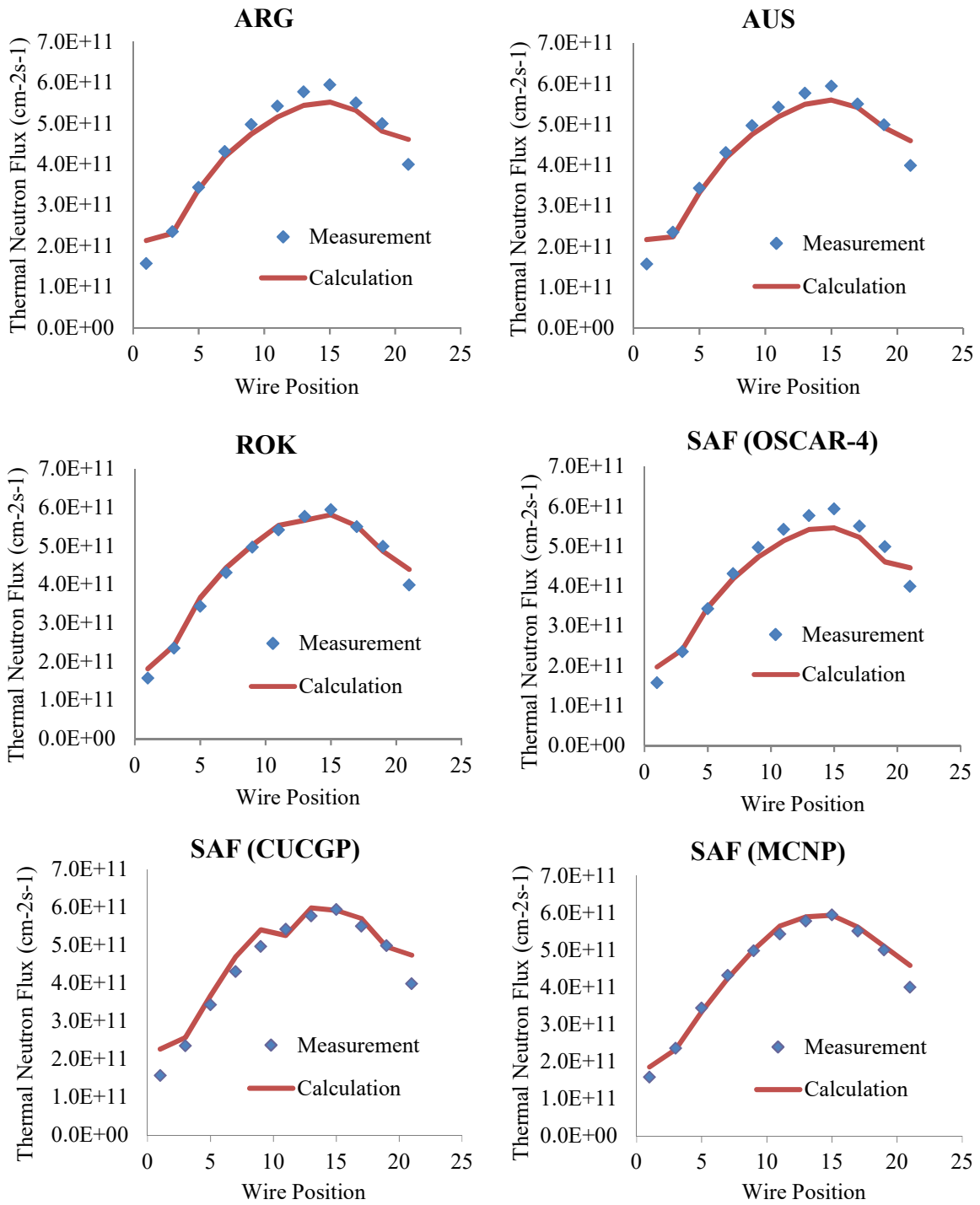


FIG. IV-3. Thermal neutron flux axial profile for position B1.

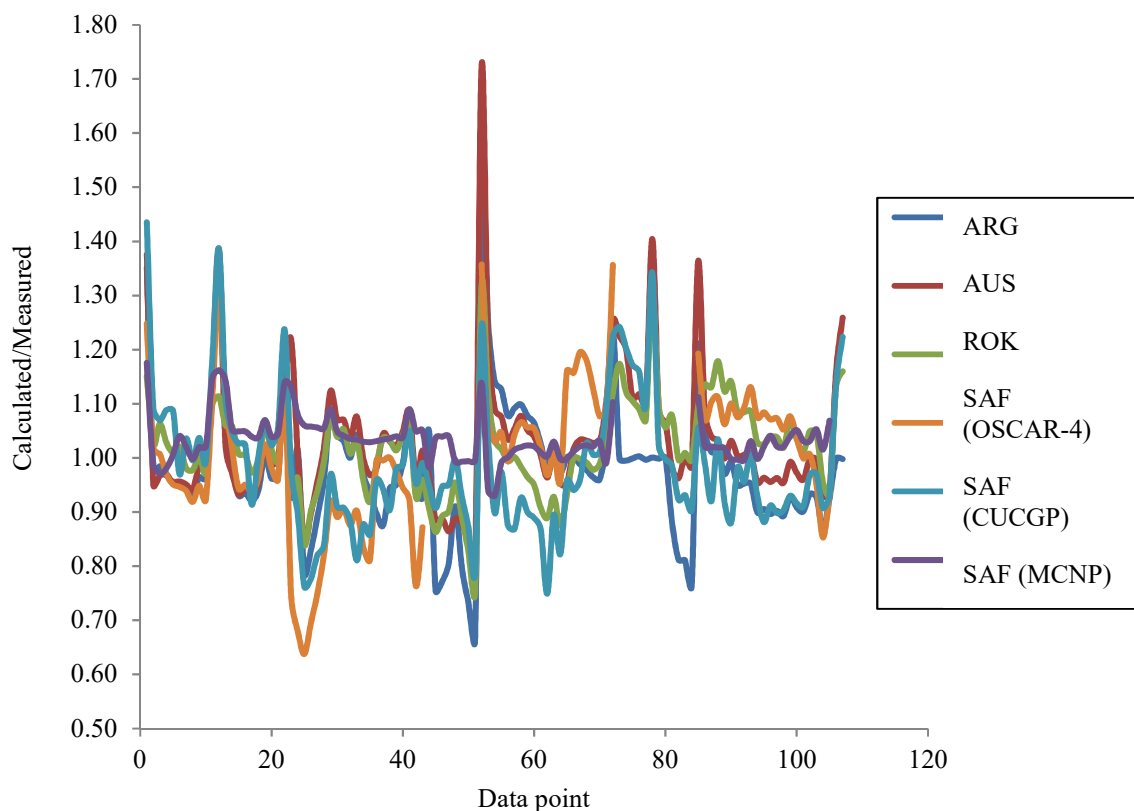


FIG. IV-4. Comparison of calculated/measured fluxes for all codes and data points.

IV-3.1.2. Discussion

A key aspect to the calculated flux values was adopting a power level for the reactor to normalize the calculated flux values. The experimental determination of the reactor power during the measurements contained a significant uncertainty. This was managed by most of the analysts by optimising the adopted reactor power level to minimize the difference between the calculated and measured fluxes. This was accomplished by either normalising the average (or total) flux either globally (over all measurements) or locally (for each individual fuel assembly) or minimising the unweighted chi-square statistic. The relevant details for each calculation are presented in Table IV-3.

TABLE IV-3. FLUX NORMALISATION METHODOLOGY

Calculation	Adopted Power [kW]	Method
ARG	36	Experiment specifications
AUS	41.65	Chi-square
ROK	42	Not specified
SAF (OSCAR-4)		Global flux
SAF (CUCGP)		Global flux
SAF (MCNP)		Local flux

The thermal flux distributions depend on the local conditions at the point of measurement and so it is important to capture all the local effects (materials, geometry and temperature) to accurately determine the distributions. One feature of the results, evident in Fig. IV-4, are peaks where calculated fluxes are significantly higher than the measured fluxes. These points are

almost always at the top or bottom of the core and indicate a systematic overestimation of the thermal neutron flux in this region.

Most of the calculations are based on models with a simplified representation of these regions (usually just water and no fuel assembly component) and this is consistent with the results obtained. In addition, the experimental data provided is based on interpolation of the limited cadmium ratio measurements available. For the end points (top and bottom) if these were not measured they were set to be the same as the nearest measured cadmium ratio. This could introduce an underestimate in the cadmium ratio and hence the measured thermal neutron flux. One of the points that is overestimated is not at the extreme axial locations. It is possible that this measurement is in error.

The MCNP calculated results agree with the measurements. This could be due, in part, to the method used to normalize the power and local flux that minimizes the difference for each fuel assembly. For all calculations the ratio of calculated and measured is within 10% for at least 80% of the data points and although this is based on normalized fits, it indicates reliable estimates of the flux distributions within the core.

IV-3.1.3. Conclusions and recommendations

The compact core of the OPAL reactor along with the effects of the cadmium burnable wires and perturbations of the reflector facilities provide challenges for some of the widely used numerical modelling techniques (such as diffusion and nodal). The results reproduce well the shapes of the various axial profiles. The results from the flux normalisations carried out by several of the groups indicate that the reactor power during the measurements may have been slightly higher than the best estimate provided.

Better estimates for the cadmium ratio for the end points need to be made.

IV-3.2. Critical Configurations

All control rods (CR) were calibrated using the asymptotic period method at low power for a clean core (negligible burnup and fission product poisons). During each step of this procedure the core is placed initially in a critical condition and this provides many critical CR configurations. The critical CR configurations are detailed in the experimental data [IV-5] and will not be presented here.

IV-3.2.1. Summary and comparison of benchmark results

The calculated core reactivity of the 74 critical configurations for five sets of calculations is presented in Fig. IV-5. The results are separated into three groups representing the three sets of measurements performed (CR4/CR1, CR5 and CR2/CR3). All codes provided reliable results with the McCARD providing the best average, 17 pcm, but the CITVAP (ANSTO) results the least standard deviation with an offset of -346 pcm. The average and standard deviations are provided in Table IV-4.

Both CITVAP models from ARG and AUS are almost identical, they have a common starting point and only minor changes introduced by each group. These small modelling differences and slight differences in the code version produce a difference of 100- 50 pcm in the CITVAP results.

TABLE IV-4. REACTIVITY FOR CRITICAL CORE CONFIGURATIONS

Calculation	Average reactivity [pcm]	Standard deviation [pcm]
ARG	-222	86
AUS	-346	39
ROK	17	81
SAF (OSCAR-4)	368	177
SAF (CUCGP)	-241	72

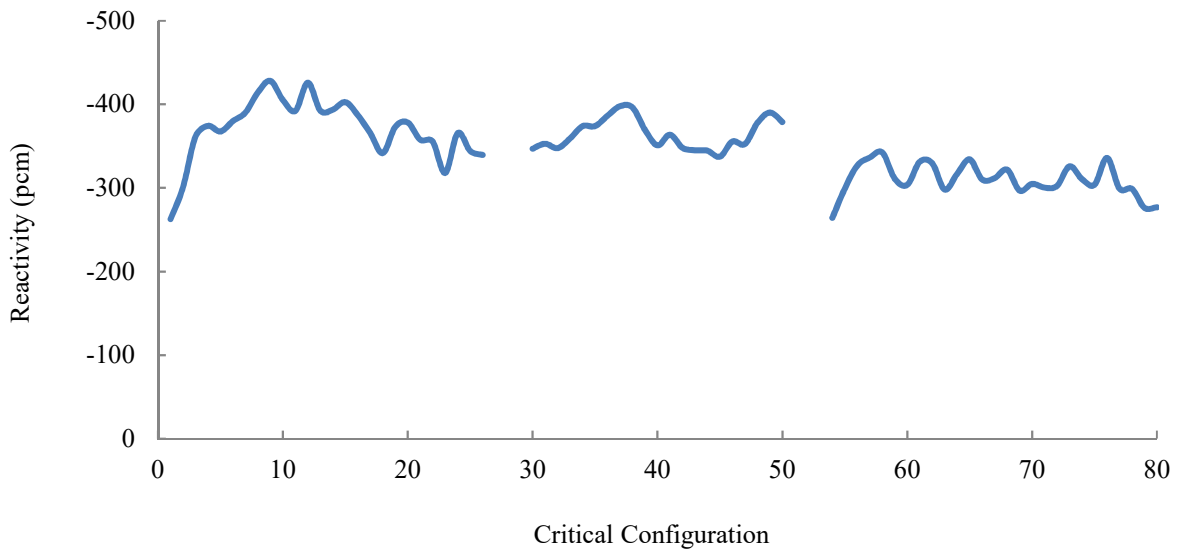
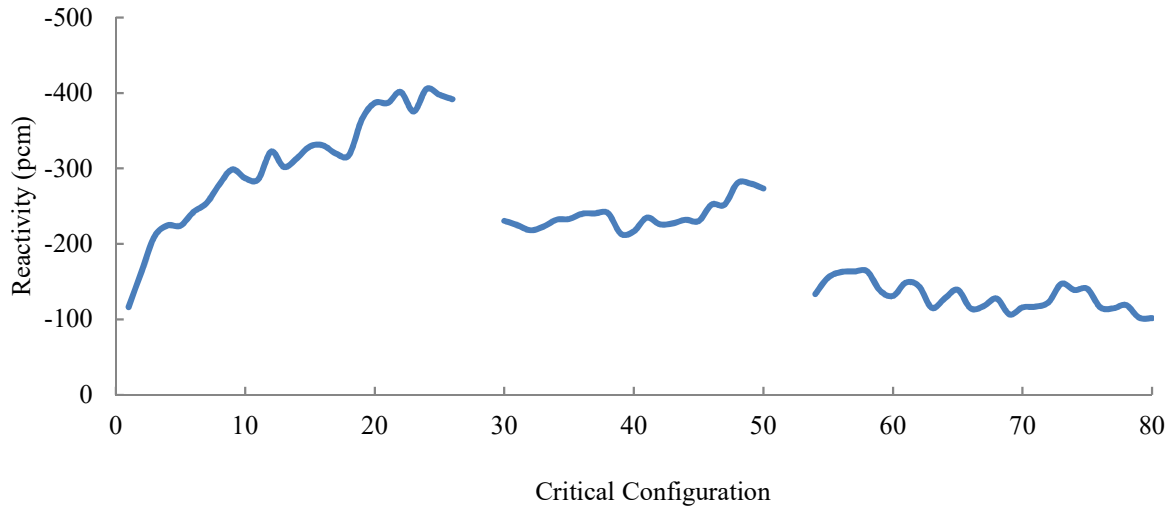


FIG. IV-5a. ARG (top) and AUS (bottom) calculated reactivity for critical core configurations with CITVAP

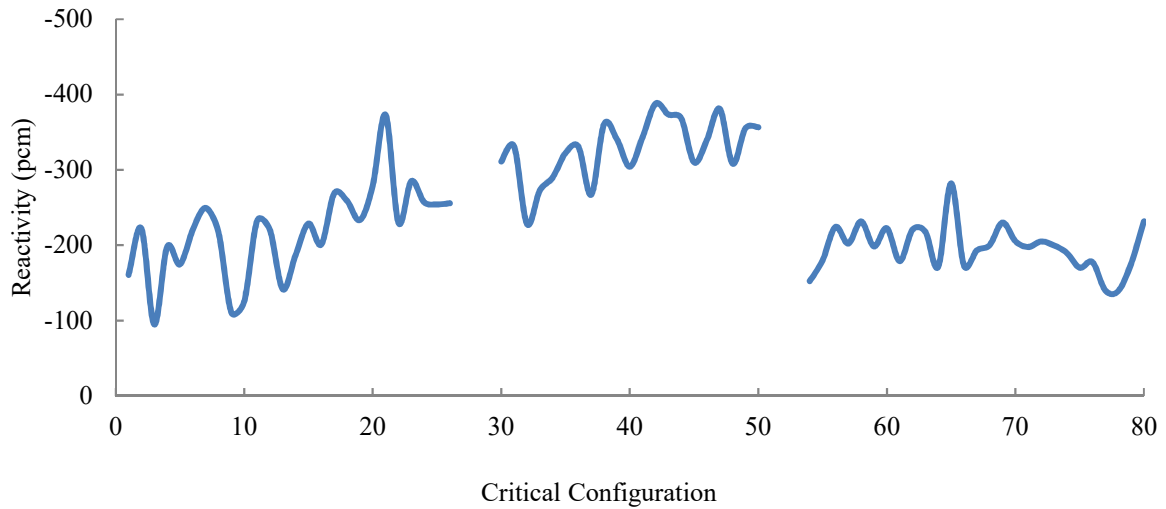
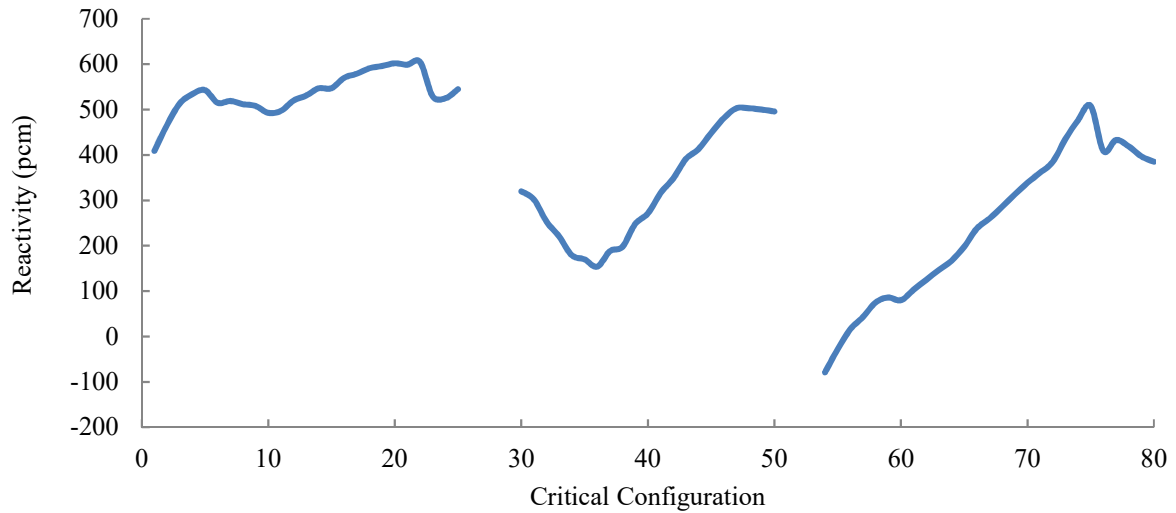


FIG. IV-5b. SAF calculated reactivity for critical core configurations with OSCAR-4 (top) and CUCGP (bottom).

IV-3.2.2. Discussion

The core reactivity is a global parameter that depends on many variables but seems to be insensitive to finer details. All the codes have demonstrated the capability to estimate core reactivity well within 1000 pcm. The predictability can be further improved by implementing a bias adjustment. Given the significant effect on reactivity of the control rods, burnable poison, the reflector and reflector facilities the results agree with the experiment.

IV-3.2.3. Conclusions and recommendations

All the codes predicted the core reactivity, to allow their use in operational and safety analyses. The set of data is of valuable addition to other criticality benchmarks.

IV-3.3. Control Rod Worth

Control rod calibration was conducted using the asymptotic period method on a critical reactor at low power (negligible feedback effects), no external neutron sources and negligible build-up of neutron poisons during the measurements. The point kinetics equation that relates the stable period measured and the reactivity in dollar units (\$) was used to obtain the experimentally determined value for the reactivity of the portion of control rod extracted. Further details on the experimental method and calculations performed are in Ref. [IV-5].

IV-3.3.1. Summary and comparison of benchmark results

The comparison of the calculated and measured reactivity worth of the five control rods is indicated in Table IV-5 for five sets of calculations. In addition, the effective delayed neutron fraction adopted to convert the reactivity into \$ is also provided. It is interesting to note the two calculations using CITVAP produce different results that correspond to variations of 2% for one group and 5% for the other. The variations for the OSCAR-4 and CUCGP results are much greater.

TABLE IV-5. CALCULATED/MEASURED CONTROL ROD WORTH

Control rod	Reactivity (\$)		Calculated/Measured			
	Measured	ARG	AUS	ROK	SAF (OSCAR-4)	SAF (CUCGP)
1	5.689	1.04	0.98	1.05	0.89	1.14
2	5.697	1.05	0.98	1.01	1.00	1.06
3	4.850	1.02	0.98	1.01	1.03	1.08
4	5.330	1.01	0.98	1.06	0.89	1.15
5	4.335	0.95	0.99	1.06	0.85	1.03
β_{eff} (pcm)		768	768	720	716	718

IV-3.3.2. Discussion

The compact core of the OPAL reactor along with the presence of burnable poison in the form of cadmium wires presents a challenge for the calculation of control rod worth as these cause significant fluctuations in flux over small changes in distance. These calculations are also very sensitive to the representation of the geometric and material details of the control rods and surrounding regions. Depending on the calculation scheme employed and approximations adopted the accuracy of the results can vary. The different behaviour of results evident in Table IV-5 is most likely due to these details.

As an interesting aside the β_{eff} value adopted for the conversion from pcm to \$ has been provided for comparison. It is interesting to note that the CITVAP results are significantly different to all the others. This will no doubt affect the control rod worth values and other results. Calculation of β_{eff} requires data for the delayed neutron groups in terms of energy spectrum and absolute fraction. There are several standard sources of such data and this can result in differences in values of β_{eff} . This is a possible origin of this difference.

IV-3.3.3. Conclusions and recommendations

Consistent and reliable results for the control rod worth were provided by two of the codes, CITVAP and McCARD, benchmarked. The other two codes, OSCAR-4 and CUCGP, showed a much greater variability. It is recommended that modelling sensitivity studies be performed for the latter two codes to quantify any effect on the results.

In addition, the difference in β_{eff} between the CITVAP code and the other three codes needs to be investigated and resolved.

IV-3.4. Fuel Burnup

Operational data was provided for OPAL during operation cycles 007 through to 012. This information is a simplification of the detailed data but allows the reactor power and control rod configuration to be specified at various time intervals. This data is useful in benchmarking fuel burnup and in the case of OPAL the depletion of burnable poisons within the fuel. The data also captures transients (scrams) encountered during operation and can be used to benchmark the evolution of xenon, iodine and samarium fission products.

IV-3.4.1. Summary and comparison of benchmark results

Two sets of complete results and one set of partial results were submitted. In all cases the data provided in the benchmark was processed to provide input closer to the standard format and methodology of the three groups. In the case of AUS the results are in terms of full power days (the reactor operating at a steady power of 20 MW). The final results are presented in Fig. IV-6. The results for ARG were analysed in the same manner as the AUS but also by using the actual reactor power and following the transients during operation. Both sets of results are presented in Fig. IV-6 clearly demonstrating the effects of the transients on the calculated reactivity. The results for SAF using OSCAR-4 represent operation of Cycle 007, this is represented in the AUS results as the first 26 full power days. All sets of results appear to provide sub-critical values for reactivity and in particular for the transients resulting in shutdowns. The results for SAF using OSCAR-4 and ARG transients appear more consistent over Cycle 007.

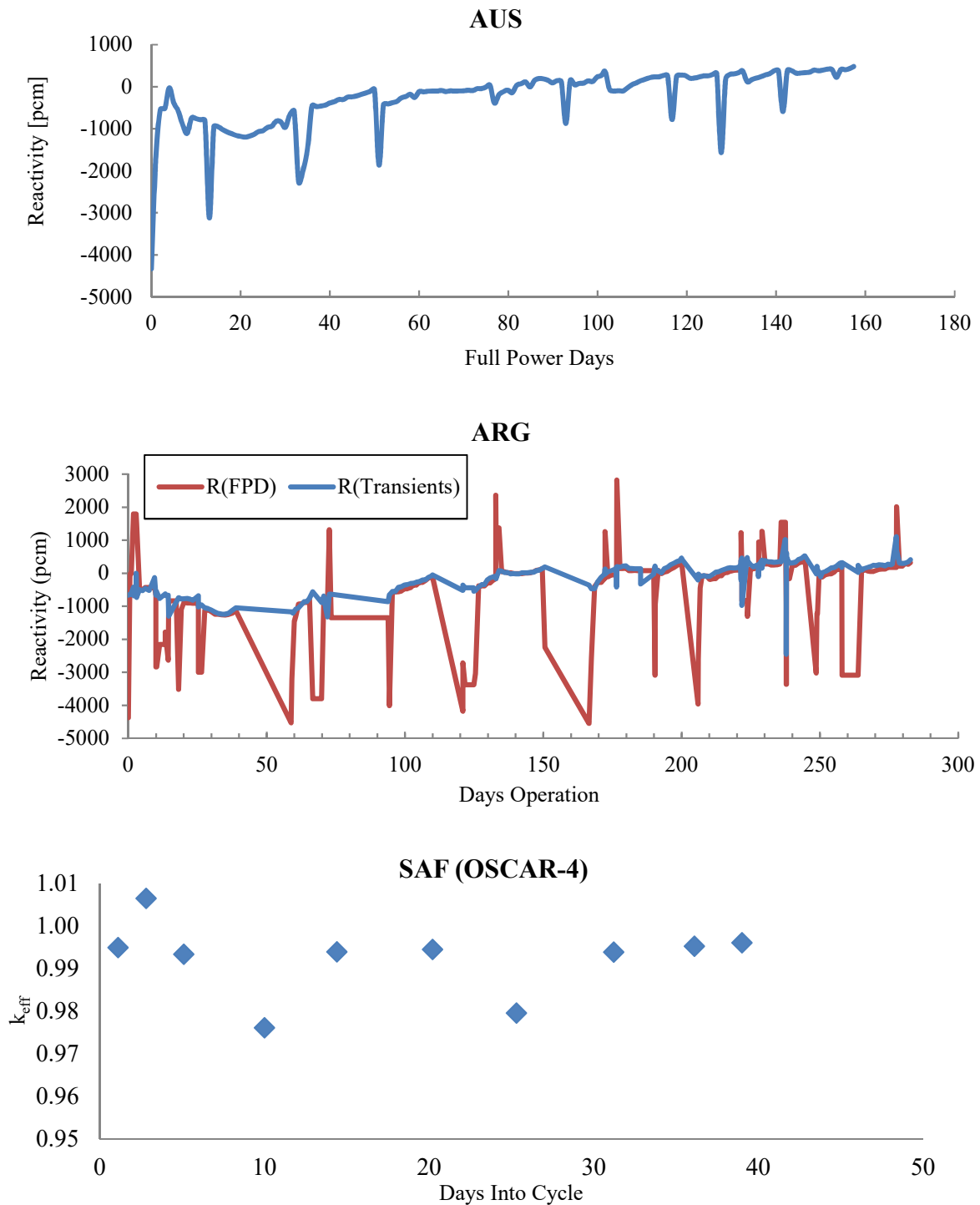


FIG. IV-6. Calculated reactor state during operation.

IV-3.4.2. Discussion

There are several interesting features in the results presented in Fig. IV-6. The first 26 full power days in the CITVAP results correspond to Cycle 007. Operation of Cycle 007 was particularly irregular with many shutdowns during the early part of the cycle and operation at lower powers. The standard CITVAP models do not account for transients or the lower power operation and this results in significant variations in reactivity. The SAF results show less variation accounting for the transients somewhat better. Following this cycle there is a general trend for the CITVAP calculated reactivity to increase up to cycle 012 with an apparent tapering off. This could be related to the changing number of fuel assemblies with cadmium wires and

the effect of this on the calculated core reactivity. During Cycle 007 there are nine fuel assemblies with fresh burnable poison, but this number reduces to three by Cycle 012 and almost all of the original nine fuel assemblies with burnable poison are discharged. The representation of a strong absorber such as cadmium in diffusion models and the burnup throughout operation is challenging for current numerical techniques.

At the beginning of each cycle there appears to be a step change down in calculated reactivity from the end of the previous cycle. During the cycle the reactivity then increases with a further steep increase in the final stages of the cycle. The reason for this behaviour is not clear. Despite these trends and characteristics calculated reactivity are generally within ± 500 pcm from Cycle 009 onwards.

IV-3.4.3. Conclusions and recommendations

The two codes benchmarked indicate similar behaviour with good agreement for steady operating conditions but significant deviations for transients. In the case of CITVAP this is to be expected as fission product poisons are assumed to be constant. The CITVAP results suggest a trend of calculated reactivity with full power days that needs to be verified with further data.

IV-3.5. Kinetic Parameters

The kinetic parameters of a core determine the characteristics of the transient behaviour of the core and as such are important for safety analyses. The kinetic parameters of interest are the effective delayed neutron fraction, β_{eff} , and the prompt neutron lifetime, l_p . During OPAL commissioning, the ratio of these parameters and the prompt neutron decay constant were determined using the Feynman- α method [IV-5]. The measurements were performed on a core with 15 fuel assemblies as the method requires an in-core measuring location.

IV-3.5.1. Summary and comparison of benchmark results

Three sets of results for the prompt neutron decay constant were submitted. The results are presented in Table IV-6. Agreement amongst the calculated values is good and also with the measured value. As noted previously the calculated values for β_{eff} indicate significant discrepancies but the prompt neutron lifetime less so.

TABLE IV-6. CALCULATED AND MEASURED KINETIC PARAMETERS

Parameter	ARG	AUS	ROK	Measured
β_{eff}	-	0.00770	0.0072	-
l_p (μs)	-	194	184	-
α (s^{-1})	37.2	39.7	38.96	38.1

IV-3.5.2. Discussion

Calculation of β_{eff} requires data for the delayed neutron groups in terms of energy spectrum and absolute fraction. There are several standard sources of such data and this can result in differences in values of β_{eff} and the prompt neutron decay constant. This comparison also provides an indication of the sensitivity of the calculated value to the delayed neutron data. Regardless of this the calculated prompt neutron decay constant values are all within 5% of the

measured value which provides confidence in the benchmarked codes capability to determine this parameter.

IV-3.5.3. Conclusions and recommendations

The calculated and measured prompt neutron decay constants agree well.

IV-4. CONCLUSIONS

The OPAL experimental results benchmarked were steady state flux distributions, critical control rod configurations, control rod worths, fuel burnup and kinetic parameters. These reactor parameters are important for safety analyses and normal operating conditions to optimize reactor performance and utilization. The computer codes employed ranged from Monte Carlo based (MCNP and McCARD), to diffusion (CITVAP), to nodal (OSCAR-4) and to coarse particle Monte Carlo (CUCGP). This allowed a comparison of different calculation methodologies over a range of parameters.

All the codes were able to reproduce the general shapes of the various flux profiles. The MCNP and McCARD codes were also able to reproduce some of the finer details and generally provide better absolute agreement. For all calculations at least 80% of the results are within 10% of the measured value. Considering the compact core of the OPAL reactor along with the effects of the cadmium burnable wires and perturbations of the reflector facilities this is an excellent result.

Five sets of results were received for the 74 critical control rod configurations. All were within 600 pcm of critical with most results significantly better. The McCARD results were the best providing an average reactivity of just 17 pcm for all configurations. This provides a high degree of confidence in terms of calculating core reactivity.

Control rod worth estimates were within 6% for the CITVAP and McCARD results. This level of agreement is acceptable for use in safety analyses without imposing additional demands on the shutdown systems. The OSCAR-4 and CUCGP results were not as good indicating discrepancies of up to 15%.

A limited set of results was available for the fuel burnup benchmark. Although no direct measurements were provided for fuel burnup the core evolution during operation depends on the ability to predict fuel burnup and in the case of OPAL also cadmium wire burnup. The calculation results indicate that the burnup can be predicted well but there is clearly a trend evident for the CITVAP results. The source of this trend, an increase in reactivity with accumulated burnup, is not clear. The partial results from OSCAR-4 do not show any evidence of such a trend. The level of agreement for all results is good and certainly adequate for fuel management purposes.

Three codes were used to provide results for the prompt neutron decay constant. All these were within 5% of the measured value and this is very good. It provides confidence that these codes can estimate this important kinetic parameter used for accident analyses.

In summary the MCNP, McCARD and CITVAP codes had no difficulties to provide estimates for all results submitted. Results from OSCAR-4 and CUCGP were for some parameters not as accurate but these codes and models were optimized for speed rather than accuracy. Additionally, the benchmark data itself and facility specification are adequate for benchmarking of neutron transport codes.

REFERENCES TO ANNEX IV

- [IV-1] BRAOUDAKIS, G., OPAL Nuclear Reactor Specification, Technical Report Series 480, IAEA, Vienna, (2012).
- [IV-2] MANTOS, J.E., PENNINGTON, K. E., Safety-related benchmark calculations for MTR-type reactors with HEU, MEU and LEU fuels, IAEA-TECDOC-643, Appendix G-1, Argonne National Laboratory, (1992).
- [IV-3] DEEN, J.R., WOODRUFF, W.L., COSTESCU, C.I., LEOPANDO L.S., WIMS-ANL User Manual, Rev 6, Argonne National Laboratory, ANL/TD/TM99-07, (2004).
- [IV-4] AMERICAN SOCIETY FOR TESTING AND MATERIALS, Standard test method for determining thermal neutron reaction and fluence rates by radioactivation techniques ASTM standard, United States (1998).
- [IV-5] BRAOUDAKIS, G., OPAL Nuclear Reactor Experimental Data, Technical Report Series 480, IAEA, Vienna, (2012).

ANNEX V

BENCHMARK CONSOLIDATED RESULTS AGAINST EXPERIMENTAL DATA FROM RSG-GAS

S. CHATZIDAKIS*

*Email: schatzid@purdue.edu (Currently with Purdue University, School of Nuclear Engineering, West Lafayette, IN 47907)

Annex Consolidator: S. Chatzidakis

Abstract

The IAEA CRP No. 1496 on ‘Benchmarking, against Experimental Data, of the Neutronic and Thermal-hydraulic Computational Methods and Tools for Operation and Safety Analysis for Research Reactors’ provides a novel opportunity to benchmark and compare the accuracy and efficiency of both off-the-shelf and locally developed computational tools to a wide set of experimental research reactor benchmark analysis. In the scope of this project, various analysis groups have evaluated the RSG-GAS benchmark analysis – consisting of steady state and loss of flow transient measurements. This report summarizes and compares the analysis methodologies adopted, the code systems employed, and the simulation results generated by the different analysis groups. A comparison of the computational results to supplied experimental results is also provided in this report.

V-1. FOREWORD

The RSG-GAS benchmark analysis is documented in Ref. [V-1] and is divided into two sections: (i) steady state measurements, and (ii) transient measurements (loss of flow). The participation for this problem is summarized in the following table.

TABLE V-1. RSG-GAS BENCHMARK PARTICIPANTS

Group	Steady state	Transient
ARG	Yes	Yes
EGY	Yes	Yes
GRE	Yes	Yes
SYR	Yes	Yes

The consolidation report includes results related to the benchmark analysis associated with more than one submission. Details on the individual results for the RSG-GAS benchmark analysis can be found in the individual country reports.

V-2. DESCRIPTION OF TOOLS, CODES AND METHODS

A short description of the code combinations and tools used by each group is given in Table V-2 and in the following sections.

TABLE V-2. CODES USED BY PARTICIPATING GROUPS

Group	Steady State	Transient
ARG	RELAP5/MOD3.2	RELAP5/MOD3.2
EGY	RELAP5/MOD3.4	RELAP5/MOD3.4
GRE	PARET-ANL RELAP5/MOD3.3	PARET-ANL RELAP5/MOD3.3
SYR	MERSAT RELAP5/MOD3.3	MERSAT RELAP5/MOD3.3

V-2.1. Argentina: Codes, Tools and Methods

Argentina employed the RELAP5/MOD3.2 code [V-2] to model the RSG-GAS reactor and provide modelling results for both steady state and transient measurements. The thermal–hydraulic model of RSG-GAS is a one-dimensional nodalization of the reactor consisting of 62 control volumes and 10 heat structures. Only the primary cooling system is considered while the secondary cooling system is defined as a boundary condition. The primary cooling system includes the core, the reactor pool, the decay tank, the pumps, the heat exchangers and the piping connecting the mentioned components. Figure V-1 shows the nodalization scheme.

The pool is modelled with three stack vertical control volumes with junctions in both directions to provide a good mixing in the pool. The core is modelled by means of 5 channels: hot and average channels for each kind of fuel element, standard and control fuel element, and a bypass channel. The hot channel has two heat structures associated with the maximum heat flux of the core. The flow area of this channel corresponds to the area of a single channel of the fuel element. The rest of the fuel elements are lumped in the average channel as a separate pipe component considering the rest of the coolant channels. Figure V-2 shows the thermocouples positions, based on the reactor specification, and according to the interpretation of the supplied information.

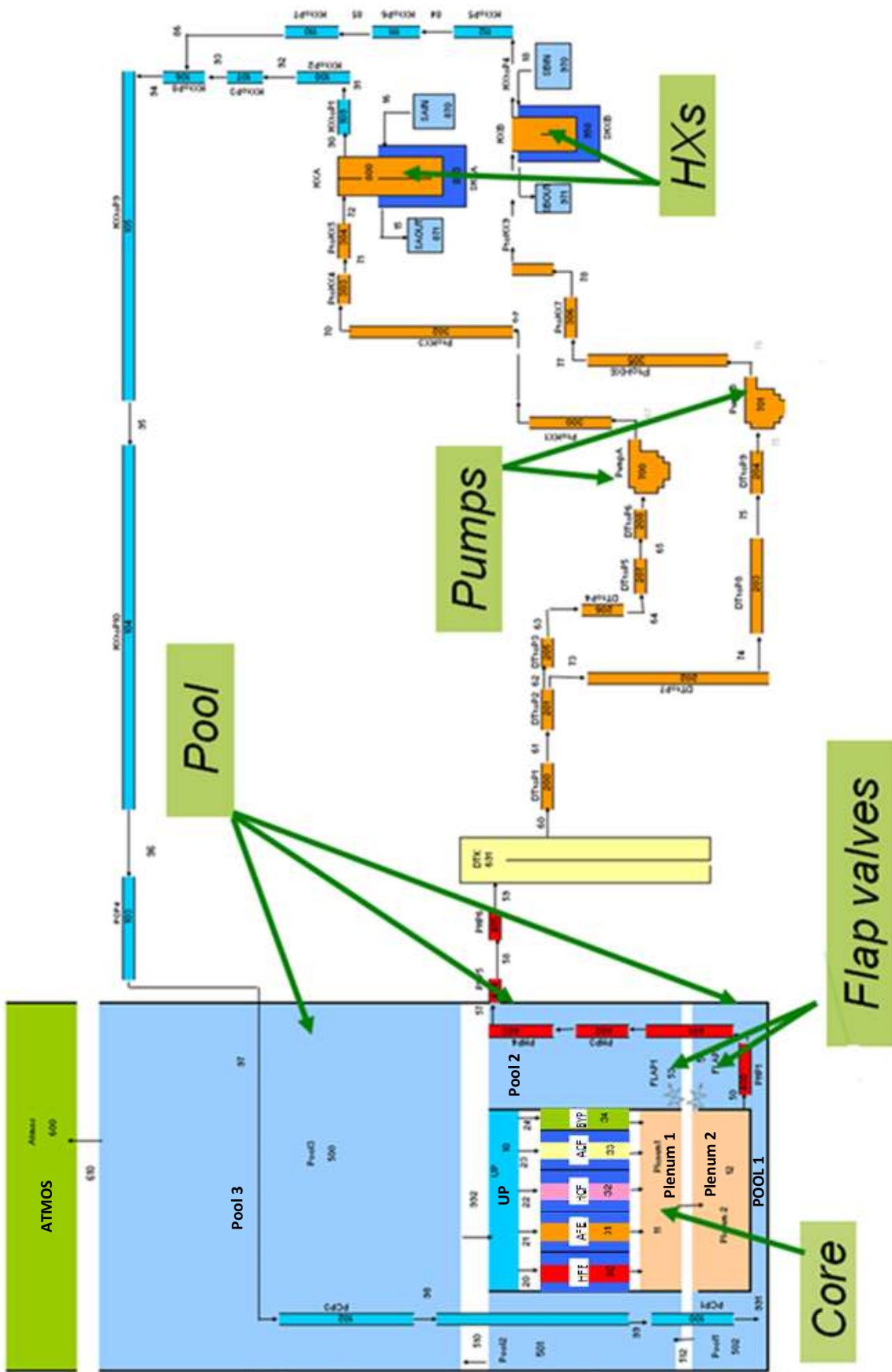


FIG. V-1. RSG-GAS nodalization for RELAP5 model for ARG.

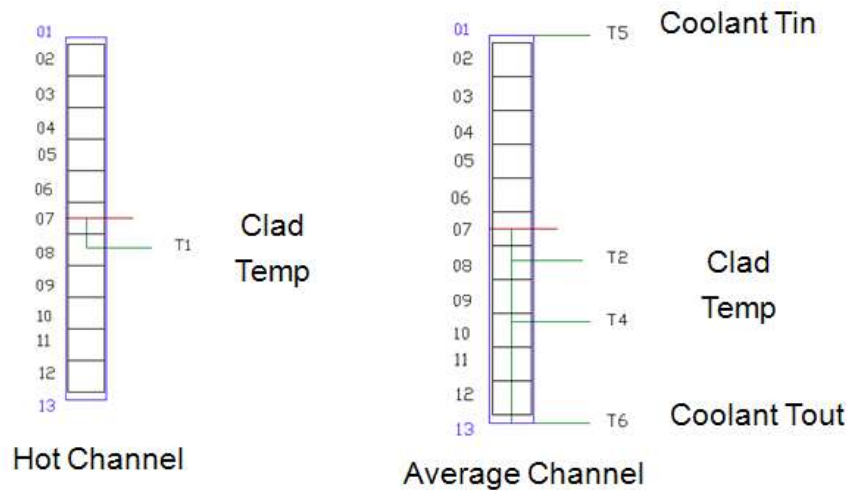


FIG. V-2. Adopted position of thermocouples in RELAP5 model.

The boundary and initial conditions (prior to transient initiation) are listed below:

- Reactor Power: 30 MW, constant operation for 24 h;
- Pool coolant temperature: 30 °C;
- Core configuration: 48 fuel elements (8 Control fuel elements + 40 Standard fuel elements);
- SCRAM set point: 90 % of nominal Primary System volumetric flow rate;
- SCRAM Delay: 2.2 seconds according to the data provided.

The general hypotheses adopted considered best-estimate calculations with conservative assumptions to simulate the event including no heat loss to the environment and constant power prior to SCRAM. A summary of the model input data can be found in Tables V-3a to V-3c.

V-2.2. Egypt: Codes, Tools and Methods

Egypt employed the RELAP5/MOD3.4 code [V-2] to simulate the steady state and transient experiments of the RSG-GAS reactor. The core was modeled as two different components, one representing the hot channel and geometrically equal to a single fuel element, and the other one, representative of the rest of the core, has the characteristics of an average fuel assembly. The coolant system nodalization is shown in Fig. V-3.

The component 090 represents the main pump. Two vertical shell and tube U-shape heat exchangers are represented as an annulus and a pipe. Annulus (094 and 194) is the primary side (shell part) and the pipe is the secondary side. Component 400 is a single volume and it represents the upper plenum of the core. At this volume the flow divided into 2 parts, one part of flow goes to average channels and the other part of flow goes to hot channel. Pipes 301 and 201 represent the hot channel and core average channels respectively. The pool is simulated as a time dependent volume (component 611). The natural convection is simulated by using pipe 603 which carries the coolant from pool to the bottom of the core and valve 604. The flapper valve remains closed as long as the primary flow is driven by the core cooling pumps (during normal operation) and opens by gravity after shutdown or after scram then the natural convection is established and the cooling flow in the core reverses its direction. The other components are used to complete the model loop and its geometry and were adjusted depending on flow and pressure drop. A summary of the model input data can be found in Tables V-3a to V-3c.

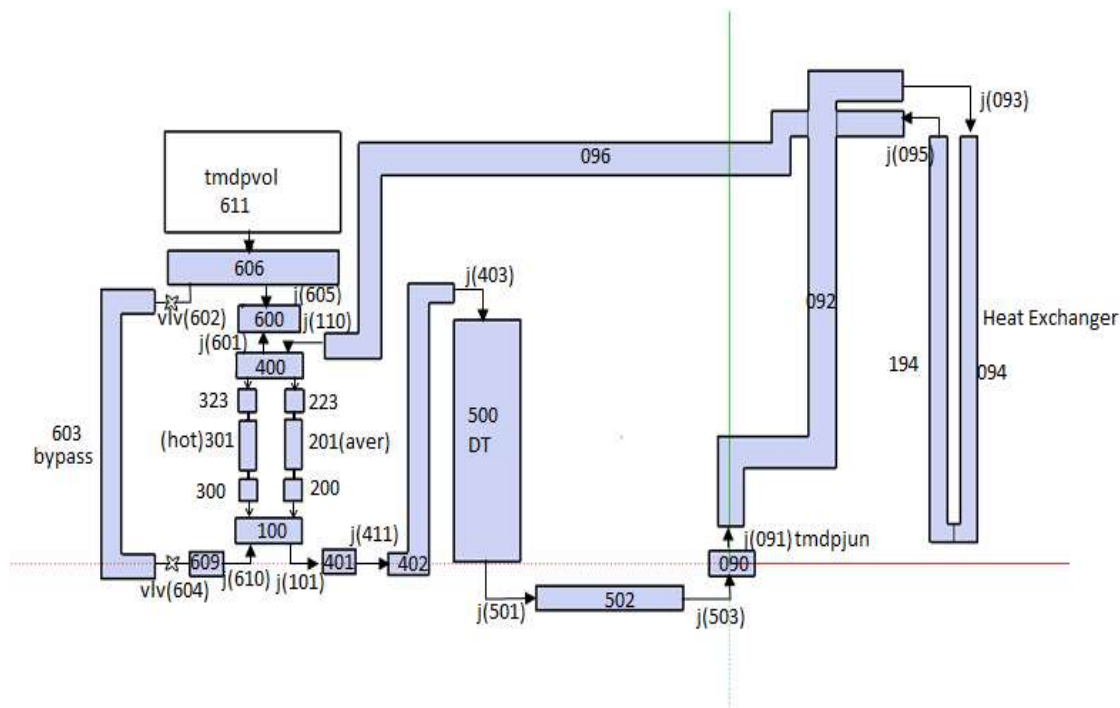


FIG. V-3. RELAP5/MOD3.4 nodalization scheme for EGY.

V-2.3. Greece: Codes, Tools and Methods

Greece employed the PARET-ANL [V-3, V-4] and RELAP5/MOD3.3 [V-2] codes for simulation of the RSG-GAS reactor. The RELAP5/MOD3.3 nodalization scheme devised for RSG-GAS is shown in Fig. V-4. The reactor pool, core and cooling systems in conjunction with the safety systems (i.e., flapper) have been modelled in detail. The reactor core is represented with three channels. Two channels are used to simulate the instrumented fuel elements. The remaining core is represented with an average channel. The radial discretization of the fuel and clad regions was five and two nodes, respectively.

The numbers of axial node points (set to ten equally spaced nodes over the active core region) model kinetic parameters (neutron lifetime and delayed neutron fraction) as well as the axial and radial peaking factors were set in accordance to the reactor specifics.

Steady-state and transient (loss of flow) simulations were performed to estimate the cladding temperatures. The reactor shutdown and natural circulation flapper were activated when the coolant flow-rate reached 85% and 15% of its nominal value, respectively. Neutronic analysis [V-1] estimated the axial peaking factor for the RSG-GAS reactor as 1.603 and the radial peaking factor as 1.48. The pressure drop across the coolant channel includes the entrance effects and the handle effect to the fuel channel, the friction loss in the fuel channel and the pressure loss at the exit of the fuel channel. A conservative value for the entrance and exit loss coefficient is $K=0.6$. For turbulent flow in smooth channels, the friction factor is expressed with the Blasius equation. Since there was a lack of available information, such as flapper dimensions or water column below the core, nominal values were adopted obtained from similar MTR reactors. A parametric study showed that the selected values did not affect significantly the temperature estimations.

Five temperature estimations were obtained from the numerical results, thermocouples T1, T2, T4, T5 and T6 (see also Fig. V-2). Both the hot and average channels were simulated because

the T1 thermocouple is located in the hot channel, whereas thermocouples T2 and T4 are located in the average channel. Thermocouples T5 and T6 represent core inlet and outlet temperatures. A summary of the model input data can be found in Tables V-3a to V-3c while additional details can be found in Refs. [V-5] and [V-6].

V-2.4. Syrian Arab Republic: Codes, Tools and Methods

Syrian Arab Republic employed the MERSAT [V-7] and RELAP5/MOD3.3 [V-2] codes for simulation of the RSG-GAS reactor. The primary loop has been modelled as an open loop without pumps and heat exchanger. Fill and Leak are used to simulate inlet and outlet of coolant. The nodalization of the primary loop is presented in Fig. V-5. The 48 fuel elements are distributed to five fuel element groups in addition to the bypass channel. The hot channel incorporates 10 fuel elements with the highest radial power factor of 1.48. Fourth and fifth groups represent the 8 control rods. Every fuel element is discretized axially in 10 adequate control volumes.

In a similar way like the MERSAT benchmark analysis, the code RELAP5/MOD3.3 has been also employed to perform benchmark analysis for the Indonesian reactor RSG-GAS. Fig. V-6 represents the RELAP5 nodalization scheme of the primary loop of RSG-GAS reactor.

The following boundary conditions were used:

- Coolant pressure (at core outlet): 199.7 kPa;
- Nominal Power: 30 MW;
- Total Flow Rate (core and Bypass): 860 m³/hr;
- Initial coolant inlet temperature: 40 °C.

A summary of the model input data can be found in Tables V-3a to V-3c.

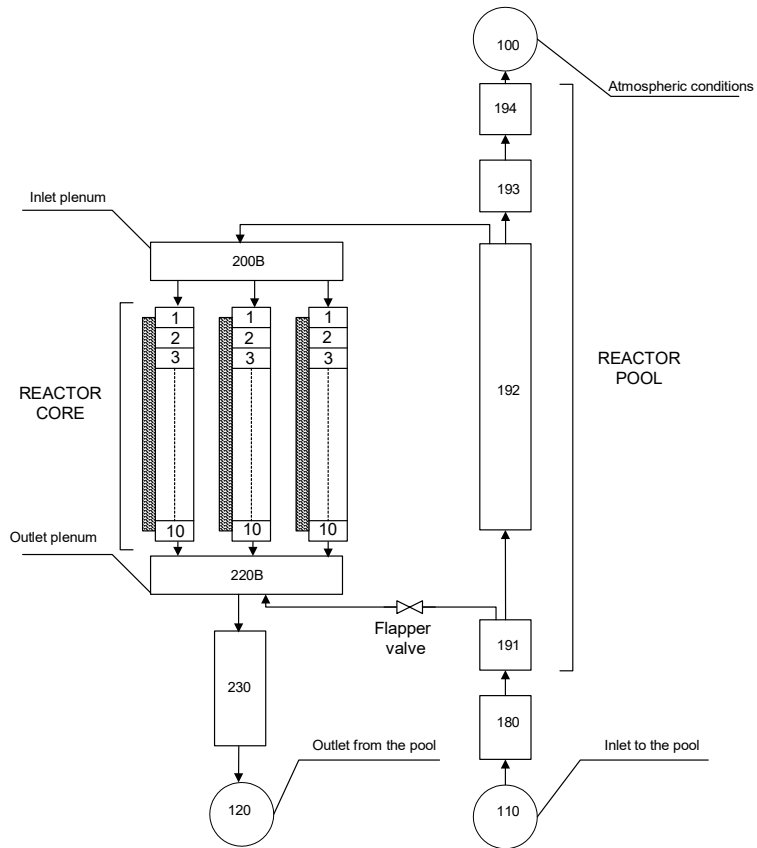


FIG. V-4. RSG-GAS nodalization in RELAP5/MOD3.3 for GRE.

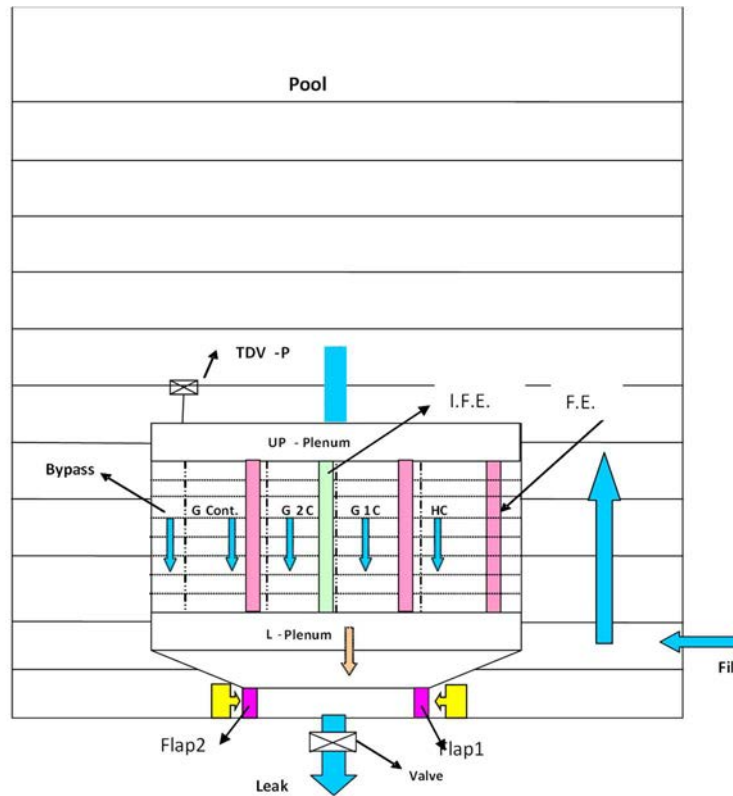


FIG. V-5. MERSAT Model for the Core of RSG-GAS reactor for SYR.

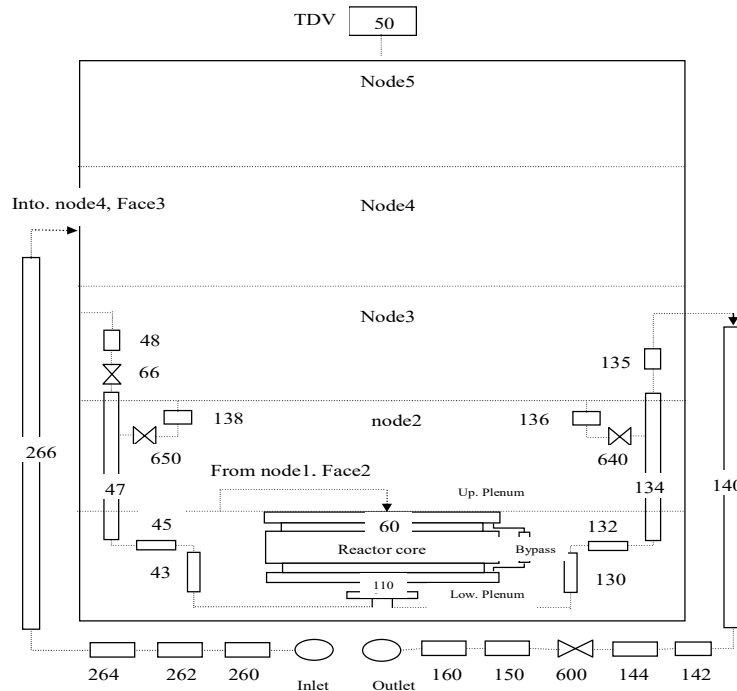


FIG. V-6. RELAP5 Model for the Core of RSG-GAS reactor for SYR.

V-3. DESCRIPTION OF FACILITY AND EXPERIMENT

The RSG-GAS (Reactor Serba Guna GA Siwabessy), located at Serpong Atomic Energy Research Center in Indonesia, is a 30 MW light water moderated and cooled multipurpose research reactor. The reactor's average thermal neutron flux is 2.5×10^{14} n/ (cm² sec¹). The reactor operates with 40 standard fuel elements and 8 control fuel elements on a 10×10 core grid. The heat generated in the fuel elements is transferred to the coolant flowing in channel. The water flows downward because of forced convection induced by the primary cooling pumps. Coolant water from different core sections is mixed in the lower plenum located at the bottom of the reactor core. Two natural circulation flaps are installed in the plenum and are gravity driven.

The experiment to be simulated is a Loss of Flow and it consists on the measurement of fuel element temperatures including steady state and transient conditions considering the coast down flow calculation. The experimental measurements consist of fuel cladding temperatures and also coolant temperatures in several positions of the reactor core, using Instrumented Fuel Elements (IFE) which were installed for this experiment at several positions.

Two IFE were used during this experiment, namely in RI-10 and RI-11 core grid positions. Each IFE contained three thermocouples installed in different radial/axial positions of those fuel elements. Fuel RI-11 contains three thermocouples (T1, T2 and T3) to measure cladding temperatures at the outer and middle plates.

The other IFE, RI-10, was equipped with three thermocouples to measure cladding temperature and coolant temperatures. The positions of the thermocouples are:

- T1 is on the hot channel, 50 mm below fuel plate mid-height;
- T2 is on the average channel, 50 mm below fuel plate mid-height;
- T3 is not operational during experiment;
- T4 is on the average channel, 150 mm below fuel plate mid-height;
- T5 is on the average channel, 331 mm above fuel plate mid-height;
- T6 is on the average channel, 331 mm below fuel plate mid-height.

V-3.1. Benchmark Experiment

V-3.1.1. Short description of benchmark experiment

The main steps of the experiment were:

- The reactor was operated in steady state condition for 24 hours, before the loss of flow transient experiment;
- The primary pumps were manually switched off;
- The reactor scram system actuated to shut down the reactor;
- Natural circulation flaps opened when the coolant flow-rate reached 15% of its nominal value.

The experimental measurements consist of fuel cladding temperatures and coolant temperatures at several positions of the reactor core, using Instrumented (thermocouple) Fuel Elements which were installed for this experiment at two positions.

V-3.1.2. Summary and comparison of benchmark results

The independent model estimations of the cladding temperatures T1, T2, T4, T5 and T6 during steady state operation are summarized in Table V-4 and Fig. V-7. Sufficient agreement appears among the group estimations with the computed difference between measurements and predictions to be lower than 10°C.

The cladding temperature estimations during a loss of flow transient are shown in Figs. V-8 to 11. As expected the results are representative of loss of flow transients in typical MTRs with downward flow. The cladding temperatures initially increase as a result of the pump coast down and following the reactor scram they sharply decrease until decay heat conditions are achieved. As the flow rate continues to decrease a moderate increase in cladding temperatures is observed up to the point where the flapper opens, and flow reversal phenomena are established. At this point, the flow direction is inverted from downwards to upwards attaining a temperature value slightly below 100°C. The recorded differences among different model estimates can be attributed to the discrepancies among the fuel and cladding thermal parameter values selected and to the adopted values for the maximum heat flux (Tables V-3a to V-3c).

In general, all available models capture the transient trend and properly depict the relative cladding temperature behavior. The RELAP5/MOD3 models exhibit good agreement with the experimental values differing only by 4 to 8 °C up to the flapper opening point. As soon as flow reversal and natural circulation phenomena take place the discrepancies increase and become in the order of 15 to 20 °C. The RELAP5/MOD3.3 natural circulation correlation over-estimates the clad temperature rise during the entire natural convection time span. On the other hand, PARET-ANL slightly underestimates the cladding temperatures during natural convection whereas MERSAT is in better agreement with the experimental measurements.

For the coast-down flow rates differences arise from the different approaches considered by the teams, as shown in Fig. V-12. The natural convection flow rate estimates (Fig. V-13) show substantial difference among the modelling groups. RELAP5/MOD3 estimations follow the same trend but attain different maxima by approximately 20 kg/s. PARET-ANL predicts a different behavior with a sharp spike reaching 80 kg/s following the flapper opening which suddenly drops at about 35 kg/s. MERSAT predicts significantly lower natural convection flow rate in the order of 20 kg/s.

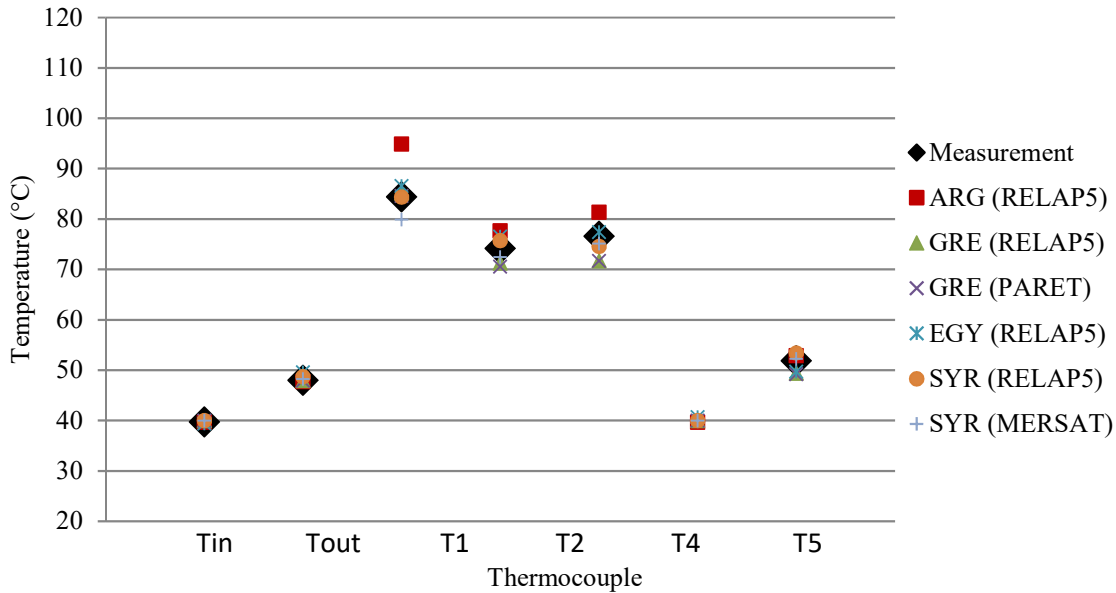


FIG. V-7. Steady state model estimates vs. thermocouple measurements.

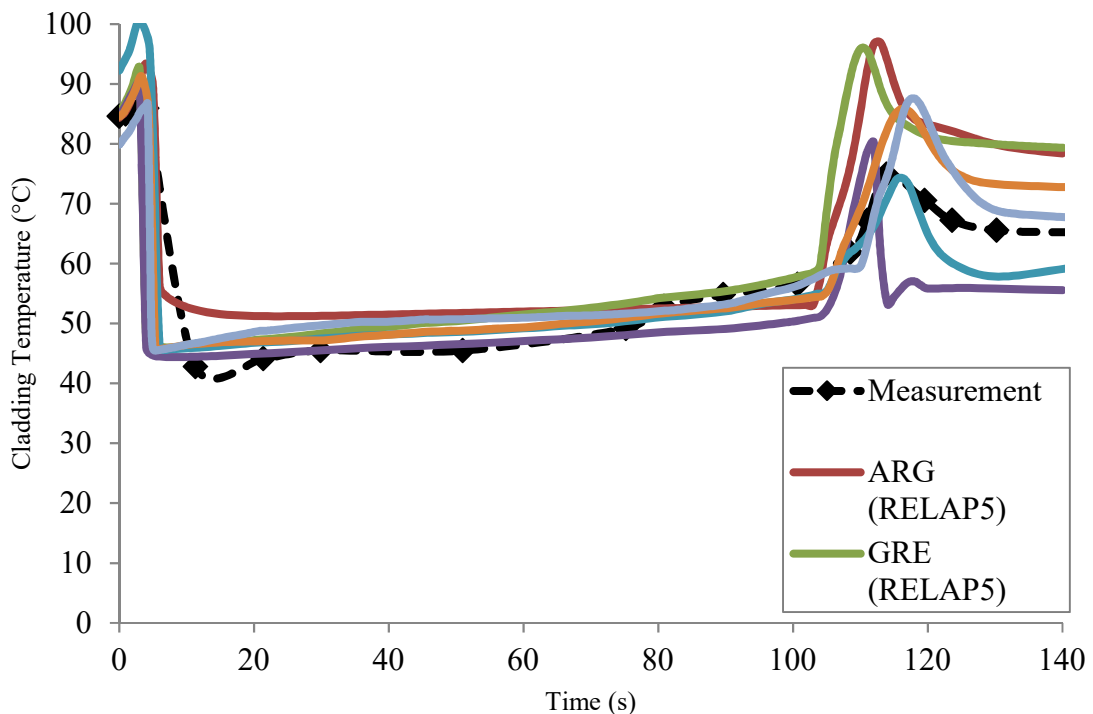


FIG. V-8. Predicted vs. measured cladding temperature of T1 thermocouple.

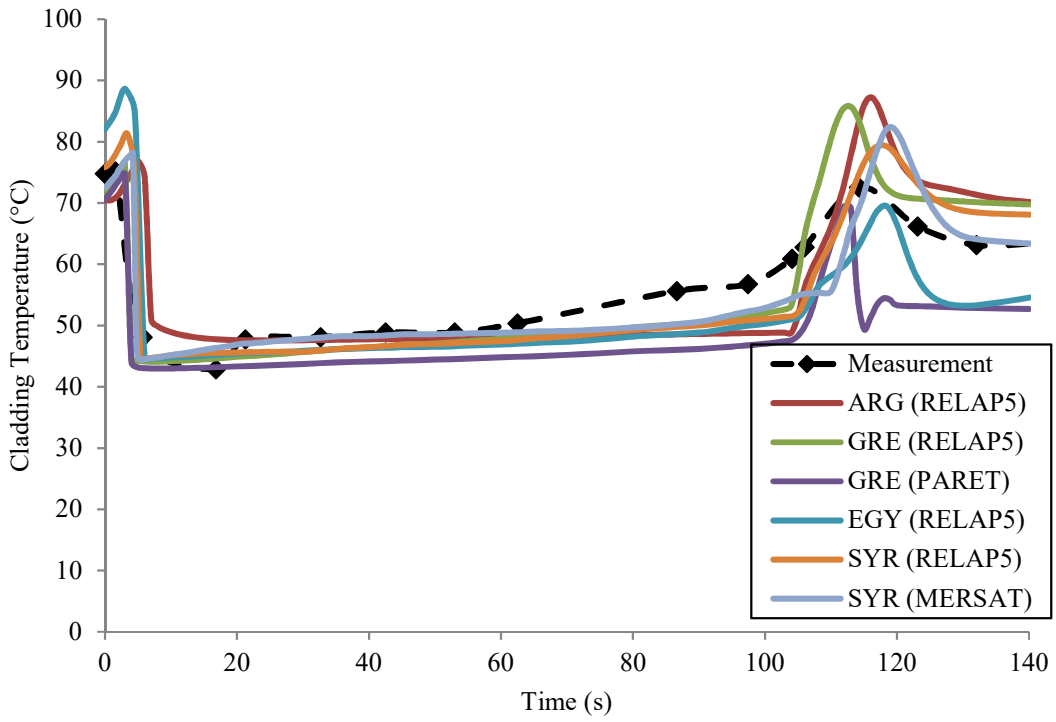


FIG. V-9. Predicted vs. measured cladding temperature of T2 thermocouple.

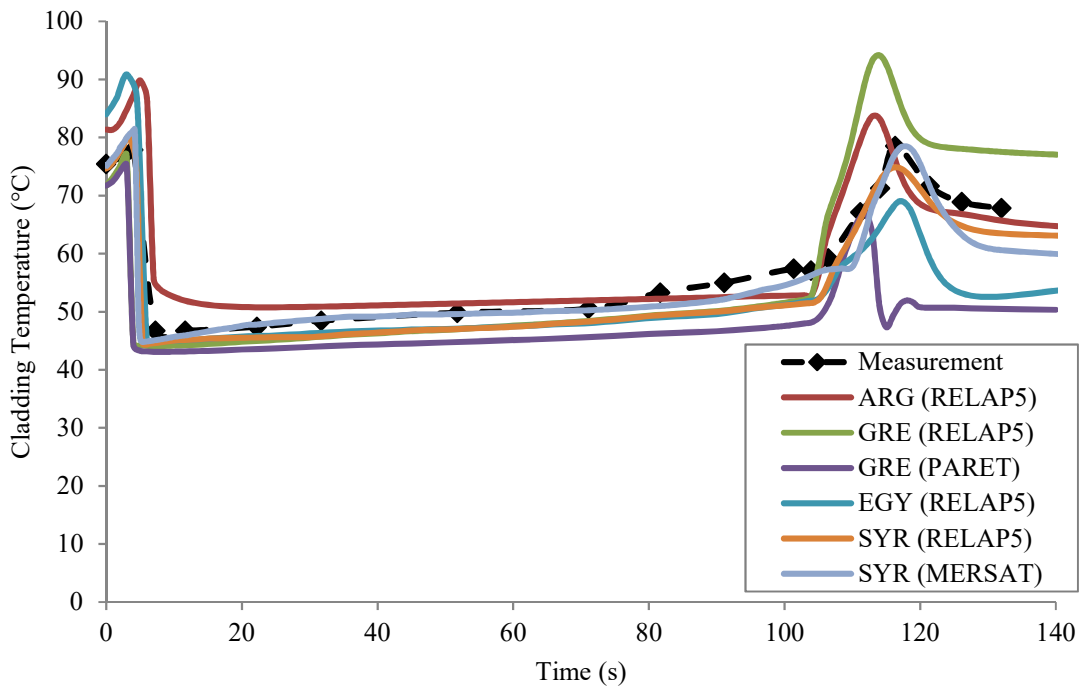


FIG. V-10. Predicted vs. measured cladding temperature of T4 thermocouple.

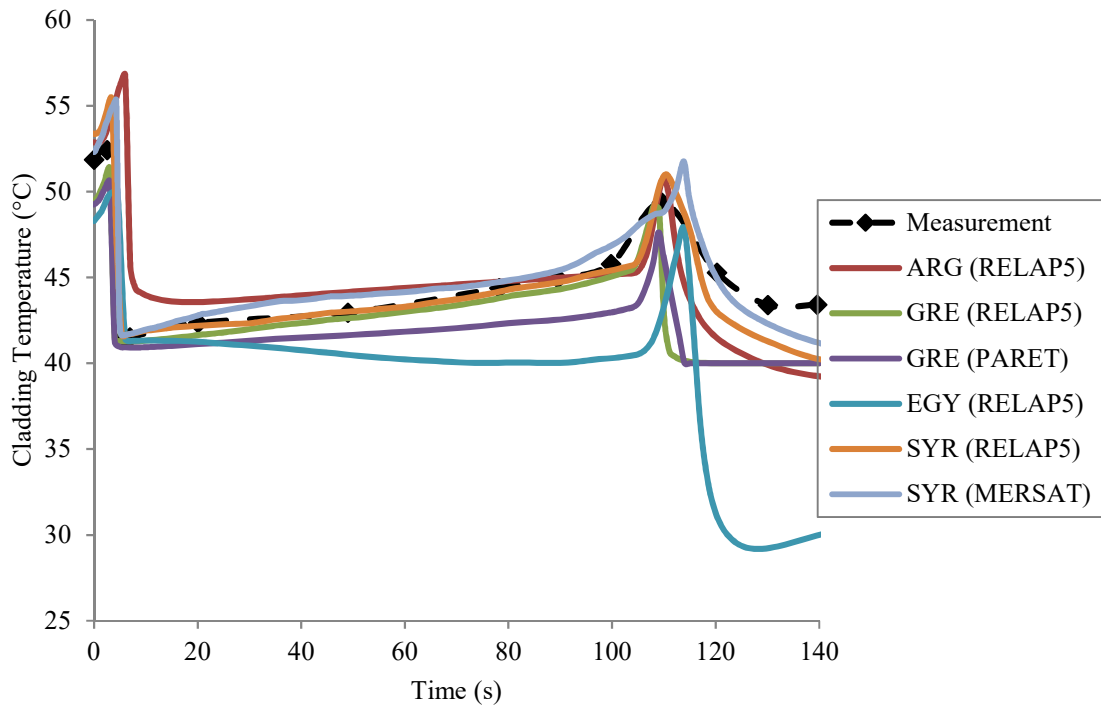


FIG. V-11. Predicted vs. measured outlet temperature of T6 thermocouple.

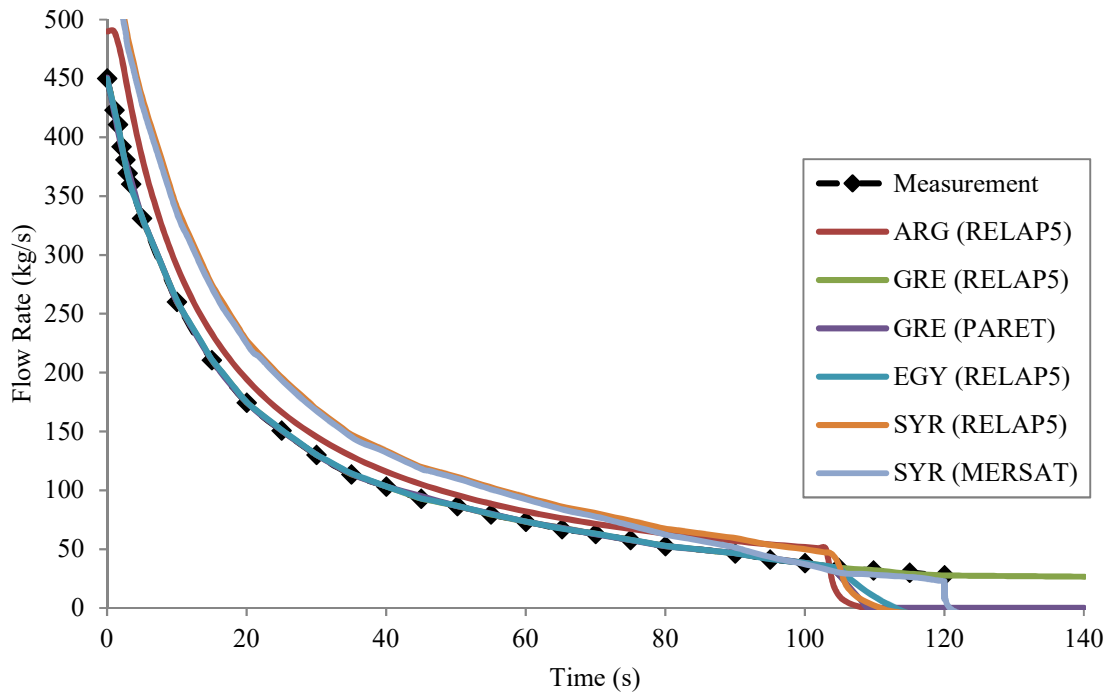


FIG. V-12. Predicted forced flow rate.

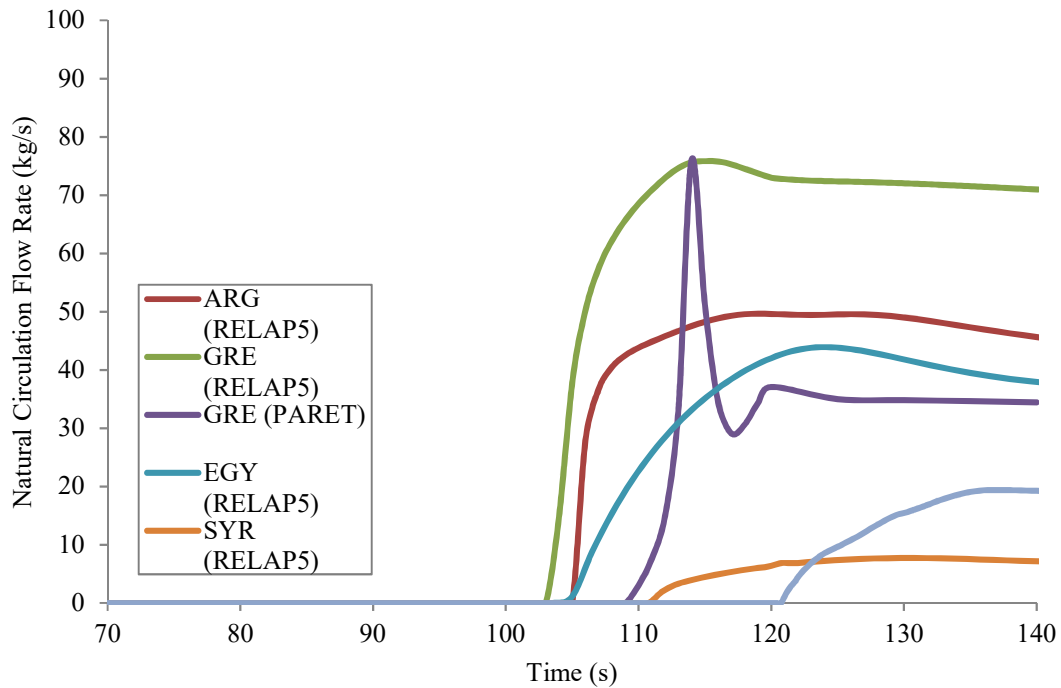


FIG. V-13. Predicted natural convection flow rate.

RELAP5/MOD3 was used by all analysis teams as one of the computational tools. EGY used the RELAP5/MOD3 release 3.4, GRE and SYR used the RELAP5/MOD3 release 3.3 and ARG the RELAP5/MOD3 release 3.2. The differences appear, mainly in the modelling approaches, specifically in the number of control volumes and the way the primary cooling system was modeled. Regarding nodalization, different numbers of channels were specified for the core. ARG and SYR adopted five channels while GRE considered three channels and EGY two channels. Concerning the modelling of the cooling system, ARG adopted the built-in pump model while SYR and GRE preferred to supply the provided flow-rate as was measured during the experiment. These differences influence the temperature evolution and maximum values attained. However, this cannot be directly inferred from the results in Figs. V-8 to 11. Those figures show the temperature behavior for four thermocouples and, surprisingly, the GRE and ARG results come close despite the modelling differences. Temperature spikes reach similar values at almost the same time while SYR values present a similar evolution but with lower peak values.

The flow coast down rate (Fig. V-12), SYR and ARG correctly modeled the opening of the flapper. This flow evolution is due to the transition from forced flow to establishment of natural circulation, shown in the same figure. Although the four groups predict the same evolution there is a difference of around 20 kg/s in the natural circulation flow rate amongst them.

TABLE V-3a. MODEL INPUT SUMMARY

Parameter	ARG	EGY	GRE	SYR
Power (MW)	30.045	30	30	30
Overpower (MW)	-	-	34.2	-
Total No of plates	960	960	960	960
Plates per standard assembly	21	21	21	21
Plates per control assembly	15	15	15	15
Standard assemblies in core	40	40	40	40
Control assemblies in core	8	8	8	8
Average power per plate (kW)	31.25	31.25	31.25	31.25
Maximum plate power	46.25	46.25	46.25	46.25
Flow rate (m ³ /h)	3200	3246.5	3270	3200
Flow rate (kg/sec)	860	900	900	860
Flow rate per plate (kg/sec)	0.517	0.9375	0.936	0.613
Coolant channel velocity (m/s)	3.23	5.19	5.58	3.61
Velocity mass flow rate (kg/sm ²)	3202.4	3552.7	5524.2	3583
Inlet pressure (bar)	1.997	2	1.997	1.997
Inlet temperature (°C)	40.5	41.2	40	40.5
Reference density(kg/m ³)	992	998	990	993
Axial peaking factor	1.63	1.26	1.603	1.603
Radial peaking factor	1.48	1.48	1.48	1.48
Fb	N/A	N/A	1.215	N/A
Fq	N/A	N/A	1.2	N/A
Uranium density (gr/cm ³)	2.96	2.96	2.96	2.96
Effective delayed neutron fraction	0.00765	0.00769	0.00765	0.00765

TABLE V-3b. MODEL INPUT SUMMARY (cont'd)

Parameter	ARG	EGY	GRE	SYR
Fuel conductivity (U3Si2-Al) (W/cm°C)	48	107	150	107
Clad conductivity (AlMg) (W/cm°C)	167	216	200	216
Fuel volumetric heat capacity (J/m ³ K)				
at 15 °C	2.24×10 ⁶	1.4326×10 ⁶	1.4×10 ⁶	0.46×10 ⁶
at 400 °C	2.68×10 ⁶	1.4326×10 ⁶	1.74×10 ⁶	0.485×10 ⁶
Clad volumetric heat capacity (J/m ³ K)				
at 15 °C	2.43×10 ⁶	2.585×10 ⁶	2.1×10 ⁶	2.6×10 ⁶
at 400 °C	2.91×10 ⁶	2.585×10 ⁶	2.5×10 ⁶	2.6×10 ⁶
Moderator temp. coeff. (Δp/K)	-1.1×10 ⁻⁴	-	-0.0149	-
Void coeff. (Δp/s)	-1.2×10 ⁻³	-	-0.1751	-
Doppler coeff. (\$/°C)	-1.6×10 ⁻⁵	-	0.9368-0.0032×T+10 ⁻⁶ ×T ²	-
Control rod drop velocity (m/sec)	0.42	-	0.42	0.42
Delay time (sec)	0.5	-	0.5	0.5
Control rod negative reactivity (\$)	-24.56	-	-24.56	-24.56
Resistance coeff (inlet)	1.5	-	0.6	0.49
Resistance coeff (outlet)	1.5	-	0.6	0.98
Heat transfer correlation	Dittus-Boelter	Dittus-Boelter	Dittus-Boelter	Dittus-Boelter

TABLE V-3c. MODEL INPUT SUMMARY (cont'd)

Parameter	ARG	EGY	GRE	SYR
Fueled length (m)	0.6	0.6	0.6	0.6
Fueled width (m)	0.06275	0.06275	0.06275	0.06275
Fuel thickness (m)	0.00054	0.00054	0.00054	0.00054
Unfueled length (inlet)	0.0125	0.0125	0.0125	0.012
Unfueled length (outlet)	0.0125	0.0125	0.0125	0.013
Total length (m)	0.625	0.625	0.625	0.625
Total thickness (m)	0.0013	0.0013	0.0013	0.0013
Clad thickness (m)	0.00038	0.00038	0.00038	0.00038
Coolant channel thickness (m)	0.00255	0.00255	0.0024	0.00255
Coolant channel width (m)	0.06331	0.07075	0.07075	0.0671
Flow area (m ²) (inner channel)	0.0001614	0.00018054	0.0001698	0.000171
Hydraulic diameter (m) (inner channel)	0.0049025	0.0051	0.0046425	-
Heated area (m ²) (per plate)	0.0753	0.0658875	0.0753	0.08
Average heat flux (MW/m ²)	0.415	0.474	0.415	0.385
Maximum heat flux (MW/m ²)	1.0	0.6	0.614	0.6
Fuel volume (m ³)	0.0195	0.00002	0.000020331	-
Core fuel volume (m ³)	0.1786	0.0711	0.01951776	-
Moderator volume (m ³)	-	-	0.000106125	-
Core moderator volume (m ³)	-	-	0.10188	-
Height above core (m)	12	7	12.45	12.9
Height below core (m)	1.2	0.01	0.2	1.245
Inlet plenum (m)	0.4	0.4	0.072	1.05
Outlet plenum (m)	0.8	0.8	0.171	0.195
Hydraulic diameter inlet plenum	0.78	0.47	0.0782	0.61
Hydraulic diameter outlet plenum	0.78	0.677	0.0478	0.61

TABLE V-4. RSG-GAS STEADY STATE RESULTS

Reactor System Parameter	Measured Data	ARG ¹	Diff.	EGY ¹	Diff.	GRE ¹	Diff.	GRE ²	Diff.	SYR ¹	Diff.	SYR ³	Diff.
Primary Coolant Flow, m ³ /hr	3269 ± 48	3200	(-)	3246.5	(-)	3270	(-)	3270	(-)	3200	(-)	3200	(-)
Reactor Inlet Temp, °C	39.75	39.7	0.05	39.45	0.3	40	0.25	40.00	0.25	40.00	0.25	40.00	0.25
Reactor Outlet Temp, °C	48.03	47.8	0.2	49.62	1.59	47.99	0.04	47.99	0.04	48.70	0.67	48.30	0.27
Reactor Power, MW	30.045	30	(-)	30.0	(-)	30	(-)	30	(-)	30	(-)	30	(-)
Primary Cooling System Clad Temp T1, °C	84.44	94.9	10.5	86.61	2.71	85.22	0.78	84.60	0.16	84.39	0.05	79.91	4.53
Clad Temp T2, °C	74.21	77.7	3.5	76.56	2.35	71.26	2.95	70.57	3.64	75.72	1.51	72.50	1.71
Clad Temp T4, °C	76.61	81.4	5.8	77.45	0.84	71.74	4.87	71.70	4.91	74.57	2.04	75.15	1.46
Coolant Inlet Temp T5, °C	Not Recorded	39.7	(-)	40.74	(-)	40	0.25	40.00	(-)	40.00	(-)	40.00	(-)
Coolant Outlet Temp T6, °C	51.88	52.9	1	49.72	2.16	49.41	2.47	49.25	2.63	53.42	1.54	52.23	0.35
Heat Exch. Inlet Temp, °C	42.6	41.8	0.8	-	-	-	-	-	-	-	-	-	-
Heat Exch. Outlet Temp, °C	35.4	35.6	0.2	-	-	-	-	-	-	-	-	-	-
Flow Rate, m ³ /hr	2050	2049	(-)	-	-	-	-	-	-	-	-	-	-

1: RELAP5, 2: PARET-ANL, 3: MERSAT

Diff.: Difference with respect to measured data

V-4. CONCLUSIONS

During the IAEA CRP, a great volume of the experimental data was obtained from different participants, covering a wide range of research reactor types, neutronics and thermal-hydraulic parameters, power levels and experimental configurations. This database is now compiled into the facility specifications, experiment descriptions and corresponding experiment data for 9 research reactors. Each data set is prepared in a way to serve as a stand-alone resource to perform independent benchmark exercises by interested institutions world-wide. In this report, the results provided by four research groups for the RSG-GAS benchmark analysis were presented.

The conducted benchmark analysis of MERSAT, RELAP5 and PARET-ANL codes against the measurements of IFE of RSG-GAS reactor show that all codes are able to simulate the evolution of coolant and clad temperatures during steady and transient conditions. For the steady state MERSAT and RELAP overestimate coolant and cladding temperature. The relative maximum deviation of prediction to experiment reaches 7% and 10% for MERSAT and RELAP respectively. For the loss of flow transient both codes predict correctly the flow reversal from downward forced to upward natural circulation.

For the first phase of the transient all codes show very good agreement with the measurement whereas for the 2nd phase MERSAT and RELAP5 overestimate the measurements regarding coolant and fuel temperature and the time at which flow reversal occurs. The qualitative evolution of the clad and coolant temperatures is properly predicted despite the uncertainty on the thermocouples position. The calculated values overestimate the experimental data but, from the safety analysis point of view, these results are conservative and provide an adequate approach. An important aspect related to nodalization is that it can be considered appropriate when it has a geometric fidelity with the system, it reproduces the measured steady-state condition of the system, and it follows the evolution of the transient.

In general, the RSG-GAS transient model predictions exhibit similar behavior despite the differences among the computational platforms, input decks and modelling approaches. The discrepancies observed between the various model predictions themselves and the experimental measurements can be attributed to different interpretations and assumptions made by the modelling groups (e.g., thermocouple positions, transient sequence, flapper opening time etc.). However, as long as the 1-D phenomena prevail, as in the forced convection region, the model estimates have good agreement with the experimental results.

When natural convection phenomena take place all model estimates start to deviate from the measurements. The temperature estimates during natural convection are more conservative with the exception of PARET-ANL which underestimates the cladding temperatures throughout the natural convection region. Finally, the different nodalization schemes and methodologies adopted (built-in models vs. custom models) as well as the different input parameters due to specifications, data interpretation, assumptions, or unknown values all represent important sources of discrepancies.

REFERENCES TO ANNEX V

- [V-1] INTERNATIONAL ATOMIC ENERGY AGENCY, Research Reactor Benchmarking Database: facility specification and experimental data, Proceedings Series, IAEA, Vienna (2013).
- [V-2] NUCLEAR REGULATORY COMMISSION, RELAP5/MOD3.3 Code Manuals, Idaho National Engineering Laboratory, NUREG/CR-5535 (1995).
- [V-3] OBENCHAIN, C. F, PARET-A Program for the Analysis of Reactor Transients, US AEC Technical Report IDO-17282, Phillips Petroleum Company (1969).
- [V-4] WOODRUFF, W. L., and SMITH, R. S, A users guide for the ANL version of the PARET Code, PARET/ANL, ANL/RERTR/TM-16, (2001).
- [V-5] CHATZIDAKIS, S., IKONOMOPOULOS, A., RIDIKAS, D., Evaluation of RELAP5/MOD3 behavior against loss of flow experimental results from two research reactor facilities, Nuclear Engineering Desisng **255** (2013) 321-329.
- [V-6] CHATZIDAKIS, S., HAINOUN, A., DOVAL, A., ALHABET, F., FRANCIONI, F., IKONOMOPOULOS, A., RIDIKAS, D., A comparative assessment of independent thermal-hydraulic models for research reactors: the RSG-GAS case, Nuc. Eng. Des., Under review
- [V-7] HAINOUN, A., GHAZI, N., ALHABIT, F., Simulation of LOFA and RIA for the IEA-R1 Research Reactor using the code MERSAT, Ann. of Nucl. Energy **35** (2008) 2093–2104.

ANNEX VI

BENCHMARK CONSOLIDATED RESULTS AGAINST EXPERIMENTAL DATA FROM SPERT III

A. P. OLSON*, M. MLADIN**, D. MLADIN**, S. DULUGEAC**, G. BUDRIMAN**

*GTRI/RERTR Programme, Argonne National Lab, 9700 S. Cass Avenue, 208-E219, Argonne, IL 60439, USA

** Reactor Physics and Nuclear Safety Division, Institute for Nuclear Research, P.O. Box 78 Pitesti, Arges, Romania

Annex Consolidator: A. P. Olson

Abstract

The SPERT III research reactor was used as a benchmark for the IAEA's 'benchmark against experimental data on neutronics and thermal-hydraulic computational methods' Coordinated Research Project. Data from SPERT III was provided in the form of reactor description with technical information, static neutronics and transient reactor power to two groups. The U.S. group used MNCP5 and PARET code for neutronics and thermal-hydraulics simulations respectively. Romania's group used MCNP5 and WIMSD5B for the neutronics simulation and CATHARE-2 for the thermal-hydraulic analysis. The Annex summarizes the codes used by each group, the simulation results and a comparison between the experimental and computational results.

VI-1. FOREWORD

The SPERT III reactor facility historical documentation was assembled into a benchmark specification. Recommendations were made in that specification as to which tests would be of interest for the benchmark analysis. This benchmark specification was used by analysts from Romania and the USA to construct computational models of the experiments. The work required 3- dimensional neutronics, to generate point reactor kinetics parameters, power shapes, and reactivity feedback coefficients. It then required coupled space-time kinetics in the point-kinetics mode, using reactivity feedback from the Doppler Effect caused by heat-up of the fuel, reactivity feedback from coolant heat-up, and feedback from void production.

Selected SPERT III Experiments were analysed by two organizations:

1. M. Mladin, D. Mladin, S. Dulugeac, G. Budriman – INR, Romania, Final Report, Contract no. 15350, February 8, 2013
2. Arne P. Olson, NEUTRONICS CALCULATIONS for SPERT III, E-CORE, Argonne, IL 60439 USA, April 15, 2013

The purpose of this report is to compare the work of these two organizations and to summarize overall findings and recommendations for future work.

VI-1.1. Remarks Concerning Analysis of the Experimental Programme

The E-core experimental programme was divided into low-initial-power and high-initial-power test phases. Low-initial-power (≈ 50 W) excursions were performed for cold- and hot-startup conditions. High-initial-power excursions were performed for hot-standby and operating-power conditions. Reactor physics and thermal-hydraulic analyses were performed for three different reactor conditions of temperature, pressure, coolant flow rate, and initial power. Table VI-1 lists the estimated standard deviation for key measured parameters.

TABLE VI-1. ESTIMATED STANDARD DEVIATION FOR MEASURED PARAMETERS

Reactor period	2 %
Reduced prompt neutron generation time	2.5 %
Delayed neutron parameters	7-15 %
Derived reactivity insertion	4 %
Reactivity compensation at peak power	11 %

It is suspected that the reactivity insertion was known more accurately than the quoted standard deviation of 4% because of the large effect of this apparently small range. It is also noted that the reactor period is known with half the uncertainty of the reactivity insertion. Analysis codes such as PARET cannot search for a desired period. It is recommended that future analysts first calculate reactor period vs. reactivity for a class of experiments. Second, they could interpolate on period to find the reactivity to match the particular experimental reactivity insertion. Finally, they could run the case and refine it to match the expected period. This is a rather complex and multi-step process.

The analysis by Romania for case T-86 was carried out using a reactivity input of 1.17 \$, as the base. ROM also performed analyses using uncertainty limits on the low side of ± 0.03 and showed that their results compared very well with experiment when they included direct heating to the moderator. These results showed the value of not using the upper limits on the reactivity uncertainty when performing bounding calculations for these tests.

VI-2. DESCRIPTION OF TOOLS, CODES AND METHODS

A short description of the code combinations used by each group is given in the following table:

TABLE VI-2. CODES USED BY PARTICIPATING GROUPS

Group	Static Neutronics Codes	Transient Coupled Neutronics/Thermal-hydraulics Codes
USA	MCNP5	PARET/ANL v7.5
ROM	MCNP5, WIMSD5B	CATHARE-2

VI-2.1. Comments on The MCNP5 Neutronics Models

The MCNP5 code used for the analysis by USA was version 1.60, with standard libraries (ENDF-B/VII). It is documented in Ref. [VI-1].

The entire reactor including radial shielding was modelled except for the core support plate and upper end fittings. The fuel rods were modelled individually as oxide cylinders surrounded by a gap and then an annulus of clad. Control and transient rods were explicitly modeled. Axial power shapes were computed over 20 uniform length axial nodes. Results of kinetics parameters, feedback coefficients, and power profiles were obtained for the three temperature and pressure conditions of the test series, for conditions with about 1 \$ of excess reactivity, the transient rod fully out, and the control rods banked to achieve that reactivity.

Romania also used MCNP but did not identify the version. They obtained delayed neutron kinetics parameters in 6 groups with β_{eff} of 0.00783 obtained vs. the design value of 0.008. They obtained a prompt neutron generation time by a $1/v$ absorber method of 20.636 micro-seconds

for cold conditions which was used for all temperatures. The axial power profile was calculated for 12 nodes. The USA obtained β_{eff} of 0.00778 and a prompt neutron generation time of 17.72 micro-seconds at 294 K.

Neither USA nor ROM calculated the direct heating to the moderator. Instead, the USA used a value of 2.6%, which was assumed as typical of a PWR UO₂ fuel rod [VI-2]. Subsequent PARET calculations for experiment T-86 confirmed that direct heating was significant. As a result, experiments T-79 through T-86 were recomputed using direct heating. The other cases assumed no direct heating, because the coolant temperature rise in those tests was so small as to make negligible the effect of direct heating.

One important modelling difference between the USA and Romania, concerns the 4 control rods of 8 special assemblies. They have fueled followers which are in the core over a greater axial length than are the absorber sections. The Romanian MCNP model did not include the fueled followers, while the USA model did include them. As a result, the Romanian model may have a less accurate prediction of the axial power profile since the control rod position is incorrect.

VI-2.2. Comments on the PARET Model Created by USA

Analysts at ANL are divided as to what is the best procedure to follow when creating a PARET model. Some believe that a two-channel model is best when one only has reactor-averaged feedback coefficients. In that case, one would use one channel to represent the hottest fuel rod or plate, and the 2nd channel to represent the remainder of the core. USA created a 5-channel core representation in order to attempt to follow the consequences of heat up of smaller groups of channels, rather than one representing the core average. The 5-channel model would theoretically be even better if channel-dependant feedback coefficients were available, this requires much more analysis. Future studies of the effect of multi-channel analysis, to account for spatial effects on reactivity feedback, are recommended. There were 20 axial nodes in each channel. Although in principle the reactivity feedback from Doppler, void, and coolant temperature effects are spatially-dependent, the USA model used no spatial weighting. One would expect that the USA results would be conservative as a result of this choice since the worth of feedback effects near core centre are much larger than near the axial ends, or the radial periphery.

VI-2.3. Comments on the CATHARE-2 Model Created by Romania

The CATHARE-2 code is defined as a ‘best estimate’ code which was created for PWR applications. It uses a 2-fluid, 6-equation model of all flow regimes and all heat transfer regimes. Reactivity feedback coefficients derived by MCNP5 were smaller than those obtained from WIMSD5B. The WIMSD5B values apparently gave better results. The supplied results used the WIMSD5B feedback coefficients.

VI-3. DISCUSSION OF RESULTS CONCERNING REACTIVITY FEEDBACK, AND CLAD SURFACE TEMPERATURE RISE

There is some uncertainty as to the initial power of each test. One can see that typical calculations of power show about the same slope, indicating that the period is correct, but that there may be a time offset caused by this uncertainty in initial power. If the calculated initial power is assumed to be 5 W, but it actually was 50 W, then there will be a time lapse between calculation and experiment.

It is noted that the PARET results are always conservative: they predict too high a peak power, and too high an energy release. This leads to predicting too high a temperature rise in the clad. This comparison is somewhat imprecise because the axial locations of the measurement may not be quite the same as computed (for example, PARET reports the absolute maximum found), and because the axial power shape in the calculations is sensitive to the position of the control rods. As modeled, the control rods are quite close to the correct initial condition locations for each experiment but are not precise. It is concluded that the Cold-Startup tests, which had no flow at the start of each transient, significantly over-predicts temperature rise in the clad. This may be due to insufficient induced natural convection flow, which in turn is a consequence of inadequate modelling of the flow circuit by a 1-dimensional model without recirculation (PARET). The other test conditions with flow also over-predict but appear to be quite reasonable.

One can also observe the similar trends in power vs. reactivity. This is fine for reactor safety and licensing because then the reactor performance can conservatively be predicted for similar designs with similar conditions covered by the test envelope. Clearly, the Doppler Effect from heat-up of the UO₂ dominates the shape of each test's power vs. time curve. There is little temperature rise in the low-power tests that there is no void production, and the temperature coefficient for the water is quite small.

Both the USA and Romania reported that their calculated Doppler feedback coefficients were too small compared to the evolution of the experiments. This is an analysis area needing further study. One consideration to investigate is the reactivity feedback effect from swelling of the fuel rod cladding as they heat up. This reduces the water volume in the coolant because the lattice pitch does not change during a short transient. The pitch is constrained by spacers that do not heat up very much relative to the clad.

VI-3.1. Comparison of Analysis by USA and by Romania for Test T-86

Figures VI-1 and VI-2 are representative of the results obtained for each experiment, by the USA and ROM. Test T-86 is the most extreme test of them all. It is noteworthy that ROM evaluated the test using plus or minus one standard deviation on the reactivity inserted. This procedure used by ROM bounds the test results, not only for this test, but for all tests that they analysed.

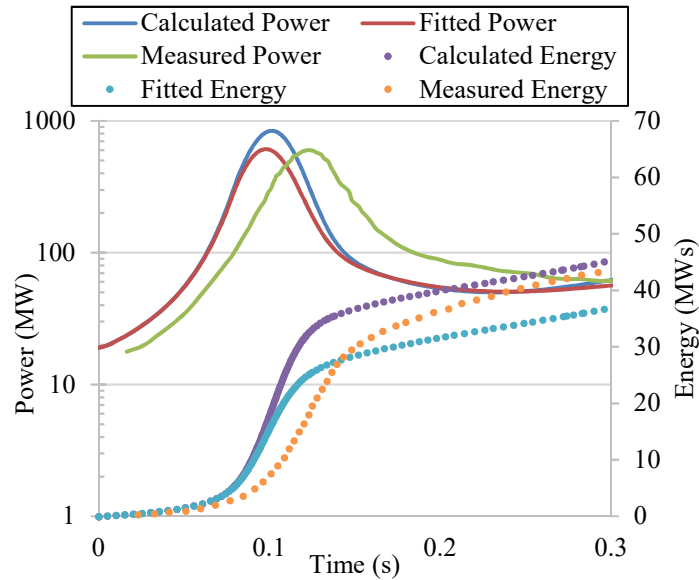


FIG. VI-1. USA test T-86 vs. experiment.

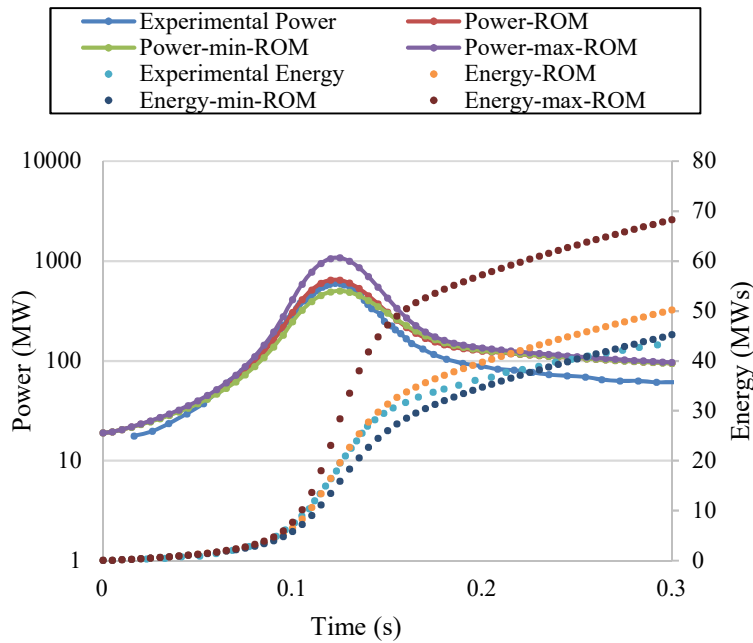


FIG. VI-2. ROM test T-86 vs. experiment.

VI-3.2. Discussion of Transient Rod Ejection (USA)

Figure VI-3 shows an approximate set of transient rod worth curves as functions of time after initiating transient rod ejection, from low power at 533 K. The curves are not smooth due in part to statistical uncertainties in the derived reactivities for small changes in the rod position, and because more axial locations are needed to better define the curves. One can see that using a fixed insertion rate of 15 \$/s is about right for a desired insertion of 1 \$, but it is too slow for insertions > 1\$, and too fast for insertions < 1\$. As a result, one can expect a shift in time for the power peak, between measurements and calculations. The report by USA observed that curves similar to Fig. VI-3 could be obtained for the other temperature conditions of interest at 294 K and at 400 K. Time shift is not important, but changes in predicted peak power and peak clad surface temperature are important.

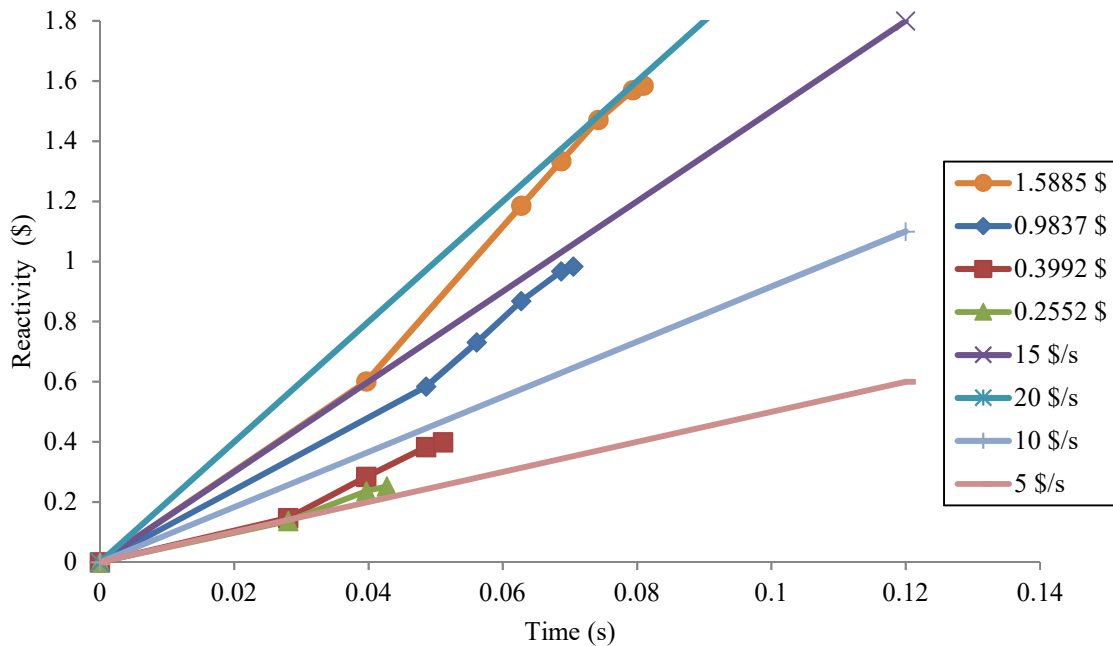


FIG. VI-3. MCNP Calculations by USA of reactivity insertion rate as transient rod is ejected for low power at 533 K.

VI-4. CONCLUSIONS

All results obtained by the USA and ROM used the nominal 15\$/s reactivity insertion rate recommended by the original analysts. As a check on this assumption, the USA performed a sensitivity study of the transient rod worth vs. time, during its ejection from the core. This was accomplished by computing the reactivity for the control rod located at many positions in the core. Knowing the design acceleration of the transient rod, it was possible to convert change in position to change in time. This was based on the assumption that the transient rod was ejected with the design acceleration of 787.4 cm/s².

It was shown, for the cases investigated, that the effects of deviation from a linear ramp rate were quite small.

Key conclusions are:

- a. ROM results using reactivity upper and lower bounds bracket the measured results in all tests;
- b. ROM results for calculated peak clad temperature are always high but are very good vs. experiment. USA results were similar but deviated more;
- c. ROM results for nominal reactivity match very well to all tests;
 - i. It is unknown if they shifted their results in time, or not;
 - ii. Example shows direct heating is important for operating-power tests;
- d. USA results using fitted Doppler Feedback coefficient predict test trends well;
- e. USA nominal results (not using a fitted Doppler coef.) are very conservative. Some investigation of why the MCNP models produces too low feedback is recommended;

- f. The results typically show that the PARET/ANL v7.5 code is conservative in its predictions of peak power, energy release, and peak clad surface temperature. PARET is known as a conservative, rather than a best-estimate, code;
- g. Trends in peak power vs. reactivity insertion are very good;
- h. Reactivity compensation at peak power compares well with values deduced by the experimentalists (it is inferred, not explicitly measured). USA updated their draft report by improving their MCNP model for the control rods, and by calculating axial power shapes for the transient rod out, with about 1\$ of excess reactivity, for temperatures of 294, 400, and 533 K. ROM made the approximation that the power shape change between 294 and 400K was not expected to be very large, so they used a single shape at 294 K;
- i. There is enough design information in text, photographs, and diagrams to enable a reasonably complete reconstruction of this 1965 SPERT III E-Core test series. Details of transient rod and control rod configuration at the junction between absorber and follower are not clear. This uncertainty affects predicted axial power shapes and reactivity. The user community is asked to provide any additional documentation that they may have regarding fuel assembly and control assembly design drawings and specifications. Dimensional details of the junction between the boron-steel absorber box and the fueled follower at this time are ill-defined. With more information about that junction, it will be possible to locate the control and transient rods more precisely for initial criticality and for each class of test;
- j. Space-dependent feedback coefficients were not used in this work. They are recommended;
- k. There are significant uncertainties on measured reactivity insertion that have a very large effect on computed results. It is recommended that future analysts fit reactivity to measured period, rather than use quoted inferred reactivity in dollars. This will reduce uncertainties;
- l. The problem of determining reactivity insertion vs. time needs further study;
- m. The reactivity feedback effect of clad heat-up (expansion) on change in coolant water volume, and the effect of fuel heat-up (Doppler), requires further study.

REFERENCES TO ANNEX VI

- [VI-1] LA-UR003-1987, MCNP— A General Monte Carlo N-Particle Transport Code, Version 5, Volume I: Overview and Theory, X-5 Monte Carlo Team, (2003).
- [VI-2] AOKI, S., SUEMURA, T., OGAWA, J., TAKEDA, T., Analysis of the SPERT III E- Core Using ANCK Code with the Chord Weighting Method, Journal of NUCLEAR SCIENCE and TECHNOLOGY **46**, (2009) 239-251.

ANNEX VII

BENCHMARK CONSOLIDATED RESULTS AGAINST EXPERIMENTAL DATA FROM SPERT IV TRANSIENTS

A. HAINOUN*, N. GHAZI*, F. ALHABIT*, S. BOURDON**, P. FERRO***, E. IVANOV+, G. BRAOUDAKIS++, L. WONG++, W. LU++, J. OSBORN++, T. ERSEZ++, H. WU++, M. J. H. KHAN+++, B. N. HAMID+++, M. S. MAHMOOD+++, M. A. MOTALAB+++, M. A. HOSSEN+++, Z. I. LYRIC+++, M. SARKER+++, M. RAHMAN+++, I. H. BOKHARI§, S. CHATZIDAKIS§§

*Atomic Energy Commission of Syria, Nuclear Engineering Department, P.O. Box 6091, Damascus, Syrian Arab Republic

**CEA, DEN, DER, Cadarache, F-13108 Saint Paul lez Durance, France

***CEA, INSTN-GA, Cadarache, F-13108 Saint Paul lez Durance, France

+Institute de radioprotection et de surete nucleaire, DSR/SEGRE/BESTARE, BP. 17, 92262 Fontenay-aux-roses Cedex

++Australian Nuclear Science and Technology Organization, New Illawarra Road, Lucas Heights NSW 2234 Sydney, Australia

+++Reactor Physics and Engineering Division, Institute of Nuclear Science and Technology, Atomic Energy Research Establishment, Savar, Dhaka-1349, Bangladesh

§Pakistan Atomic Energy Commission, Pakistan Institute of Nuclear Science and Technology, Division of Nuclear Engineering, P.O. Nilore, Islamabad

§§ Institute of Nuclear Technology and Radiation Protection, National Center for Scientific Research ‘Demokritos’, 15130, Athens, Greece

Annex Consolidator: S. Chatzidakis

Abstract

The IAEA CRP No. 1496 on ‘Benchmarking, against Experimental Data, of the Neutronic and Thermal-hydraulic Computational Methods and Tools for Operation and Safety Analysis for Research Reactors’ provides a novel opportunity to benchmark and compare the accuracy and efficiency of both off-the-shelf and locally developed computational tools to a wide set of experimental research reactor benchmark analysis. In the scope of this project, various analysis groups have evaluated the SPERT IV benchmark analysis – consisting of a variety of commissioning and Reactivity Insertion Accident (RIA) measurements. This report summarizes and compares the analysis methodologies adopted, the code systems employed, and the simulation results generated by the different analysis groups. A comparison of the computational results to supplied experimental results is also provided in this report.

VII-1. FOREWORD

The SPERT IV benchmark analysis is documented in [VII-1] and is divided into two sections: (i) statics (neutronics) and (ii) transient (Reactivity Insertion Accident (RIA) - coupled neutronics/thermal-hydraulics). The participation for this problem is summarized in the following table.

TABLE VII-1. SPERT IV BENCHMARK ANALYSIS PARTICIPANTS

Group	Statics (Neutronics)	Transient (RIA)
AUS	Yes	Yes
BGD	Yes	Yes
GRE	-	Yes
FRA*	Yes	Yes
FRA2*	Yes	Yes
PAK	Yes	Yes
SYR	Yes	Yes

*FRA is referring to CEA France and FRA2 is referring to IRSN France

The static part is described in Annex VIII. Only the transient (RIA) section is summarized herein. The consolidation report includes the results related to the benchmark analysis associated with more than one submission. Details on the individual results for the SPERT IV benchmark analysis can be found in the individual country reports.

VII-2. DESCRIPTION OF TOOLS, CODES AND METHODS

A short description of the codes and tools used by each group is given in Table VII-2 and in the following sections.

TABLE VII-2. CODES USED BY PARTICIPATING GROUPS

Group	Transient (RIA) Codes
AUS	PARET-ANL
BGD	EUREKA-2/RR
GRE	PARET-ANL
FRA	CATHARE-2
FRA2	ASTEC
PAK	PARET-ANL
SYR	MERSAT/RELAP5

VII-2.1. Australia: Codes, Tools and Methods

For the transient portion of this problem the Australian (AUS) group used the PARET-ANL v7.4 code [VII-2, VII-3] to model SPERT IV. The SPERT IV reactor core was modelled using two channels, each with 21 axial nodes, 5 radial nodes representing the fuel and 2 radial nodes representing the fuel cladding. The ‘hot channel’ axial power profile, obtained from MCNP calculations, is representative of the coolant channel where the fuel plate temperature is measured in the experiment while the ‘average channel’ is representative of the remainder of the core. The reference pressure of the system is specified as the outlet pressure of the core of 5.486 m hydrostatic head, and thus inlet and outlet pressure losses are not considered in this calculation. The dimensions of the inlet and outlet plenum lengths were set to 0.0 m. Natural convection was modelled by specifying an inlet flow rate equivalent to 0.3 cm/s.

The thermal properties of the fuel and cladding were obtained from data obtained from the SPERT I D-12/25 fuel plates. The heat transfer at the clad-coolant interface is governed by user specified heat transfer correlations. The Dittus-Boelter correlation was selected for the single-phase heat transfer coefficient under forced convection, and the Rosenthal-Miller correlation was used for single phase heat transfer under natural convection. The Rosenthal-Miller heat transfer coefficient was also used for forced convection ($Re > 2000$) if the heat transfer coefficient value computed is larger than that computed using the Dittus-Boelter correlation. The transition between the single phase and two-phase regimes was modelled using PARET’s transition model. The two-phase correlation selected, since PARET-ANL allows user specified selection, was Bergles-Rohsenow for all natural convection transients and for the forced convection transients with reactivity inserted less than or equal to 1.14 \$. The McAdams two-phase correlation was used for larger reactivity insertions in the forced flow tests. For departure from nucleate boiling heat flux calculation, the Tong correlation was chosen, following findings of previous sensitivity studies [VII-4, VII-5].

The kinetic parameters were obtained from MCNP calculations of the static experiments. The void feedback coefficient is the value obtained from both the experiment and MCNP calculation. The coolant temperature feedback coefficient is a value calculated for the SPERT I D-12/25 core. In all transients, the reactivity was ramp inserted in 1 ms. The time step used in these calculations ranged from 1 to 10 μ s.

A summary of the input parameters of the PARET model is presented in Tables VII-7a, VII-7b and VII-7c. In this benchmark study, only tests with 5.486 m hydrostatic head were simulated using the PARET-ANL code. Calculations of transients B-15 to B-16 failed to complete and so no results will be presented. Transients B17 – B19 (0.6096 m hydrostatic head) were not studied.

VII-2.2. Bangladesh: Codes, Tools and Methods

For the transient portion of the SPERT IV benchmark analysis, the Bangladesh (BGD) group used the EUREKA-2/RR code [VII-6]. This is a coupled neutronics, thermal-hydraulics and point kinetics code. EUREKA-2/RR is a revised version of EUREKA-2 which was originally developed by JAEA for reactivity accident analysis for nuclear power plants. A heat transfer package is added to EUREKA-2 to modify it to EUREKA-2/RR where the heat transfer correlations considered in the heat transfer package were obtained or estimated from heat transfer experiments in which thermal-hydraulic features of the upgraded JRR-3 core were properly reflected.

Neutronics input for the EUREKA-2/RR analysis was obtained from the MVP models created for the Static portion of the benchmark analysis. Three utility codes were also employed to provide input data for the EUREKA-2/RR model: DISSUE, ICETEA and PREDISCO. DISSUE calculates power fraction of each heat slab based on the calculation of total peaking factors obtained from the associated MVP model, ICETEA calculates the coolant temperature distribution and PREDISCO calculates the pressure distributions in the coolant.

The Dittus-Boelter correlation is used for single phase forced convection turbulent regime, the Bergles-Rohsenow correlation is used for onset of nucleate boiling and the modified Chen correlation is used to predict the nucleate boiling in the EUREKA-2/RR code. For DNB heat flux calculation, the Sudo-Kaminaga correlation is used. The heat conduction model is based on the method of one-dimensional time dependent heat conduction equations. The thermal-hydraulic solution assumed to contain one-dimensional homogeneous fluid with the vapor and liquid phases in thermodynamic equilibrium. The whole core was divided into several regions called channels in the code as shown in Figs. VII-1 and VII-2. These channels differ from each other by power generation, coolant mass flow rate and hydraulic diameters. The core contains 20 standard fuel assemblies and 5 control fuel assemblies. Each standard fuel assembly contains 12 fuel plates and each control fuel assembly contains 6 fuel plates. All these fuel assemblies are distributed into 5 distinct channels. The radial peaking factors are calculated using the MVP code. In the present model, each channel consists of 10 heat slabs along with 10 nodes. The model in total then consists of 52 nodes, 50 heat slabs and 56 junctions.

A summary of the input parameters of the EUREKA-2/RR model is presented in Tables VII-7a, 7b and 7c. In this benchmark study, only tests with 5.486 m hydrostatic head were simulated using the PARET/ANL code. Transients B-1 to B-16 (tests with natural circulation) and B17- B19 (0.6096 m hydrostatic head) were not studied.

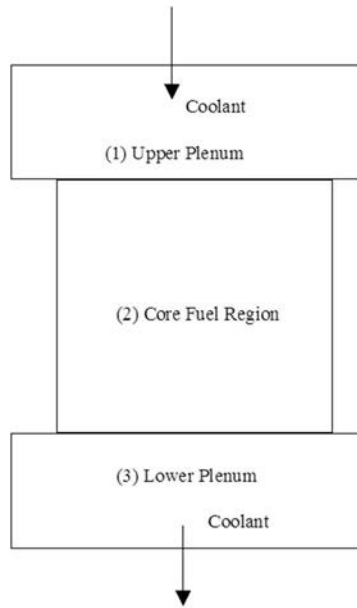


FIG. VII-1. EUREKA-2/RR block diagram.

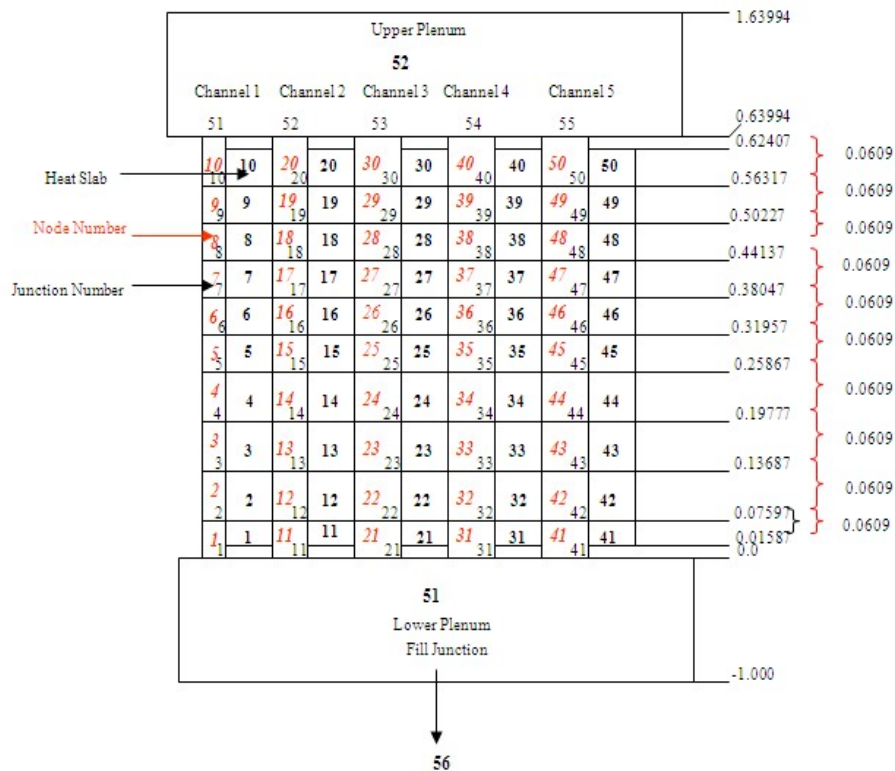


FIG. VII-2. EUREKA-2/RR model nodalization.

VII-2.3. Greece: Codes, Tools and Methods

Greece (GRE) employed the code PARET-ANL v7.0 [VII-2, VII-3] to model the transient part of the SPERT IV reactor. The code PARET-ANL has been originally developed at Idaho

National Laboratory and subsequently improved at Argonne National Laboratory. It is a widely used calculational tool for carrying out coupled neutronic, thermal-hydraulic simulations in research reactors. The code employs one-dimensional hydrodynamics, one-dimensional heat transfer, and point kinetics with continuous reactivity feedback, Ref. [VII-3]. A simplified void fraction model is included. The Dittus-Boelter correlation was chosen to provide the Nusselt number in the single-phase forced coolant convection turbulent regime. The Bergles-Rohsenow correlation is used to predict the onset of nucleate boiling and since the single-phase, heat transfer coefficient is no longer valid in two-phase flow regimes PARET-ANL includes the Bergles-Rohsenow transition boiling model for prediction of the wall temperature. The Bergles-Rohsenow correlation was also chosen to provide the wall temperature for fully developed nucleate boiling regime.

A two-channel PARET-ANL model was used comprised of a ‘hot channel’ and an ‘average channel’ (Fig. VI-3). The ‘hot channel’ is representative of the limiting fuel plate/coolant channel at the peak power density position while the ‘average channel’ represents the remainder of the core. Power densities were taken from the reported experimental commissioning data [VII-1]. Each channel represents a 1-D slab geometry of a half fuel plate, extending from the plate centerline to the coolant channel centerline. Radially the model was discretized into 10 nodes. The number of axial node points is set to 12. The input of the model kinetic parameters has been set in accordance to the results obtained from the initial critical experiments conducted in the SPERT IV facility preceding the power excursion tests. Channel velocity was taken as the average channel velocity by dividing reported the total core flow with the number of the core channels

A summary of the input parameters of the PARET model is presented in Tables VII-7a, 7b and 7c. In this benchmark study, only tests with 5.486 m hydrostatic head were simulated using the PARET/ANL code. Transients B-17 to B-19 (0.6096 m hydrostatic head) were not studied.

VII-2.4. France-CEA: Codes, Tools and Methods

France CEA (FRA) employed the CATHARE2 code [VII-7] for the transient section of the analysis (Fig. VII-4). The code is a ‘best-estimate’ one dimensional code, based on a 2 fluid-6 equation model. Non-condensable gases (nitrogen, hydrogen, air) or radio-chemical components can also be modelled. The code integrates a point kinetics module for modelling the reactivity feedback effect and the control rods displacement. In the single-phase forced coolant convection turbulent regime, the Sieder-Tate correlation provides the Nusselt number and the heat transfer coefficient. CATHARE2 includes the Thom correlation for nucleate boiling, the Saha-Zuber correlation for steam generation prediction and the critical heat flux is estimated with the use of the Groeneveld look-up tables.

The axial and radial power profiles were derived from the TRIPOLI4 calculations. The axial power profile introduced in the CATHARE2 code is representative of a mean insertion of reactivity of ~ 1.27 \$. The radial power distribution in the fuel assembly considered in CATHARE2 was calculated using TRIPOLI4 code without the central transient control rod. The total nuclear power generated in the SPERT IV D-12/25 core was calculated by CATHARE2 code using a point kinetics model. The reactivity insertion and the feedback effect of the moderator were introduced by means of a coded function in the CATHARE2 input-deck. A summary of the input parameters of the CATHARE2 model is presented in Tables VII-7a, 7b and 7c.

VII-2.5. France-IRSN: Codes, Tools and Methods

The France-IRSN (FRA2) employed the ASTEC code [VII-8] to model the transient (RIA) section of SPERT IV.

Only hand-made thermal-hydraulic ASTEC modules were used for the model of SPERT IV. In this ASTEC version, heat transfer coefficients were adjusted and directly used instead of correlations that were relevant to pin cooling. The adjusted heat transfer coefficients are parameterized as function of pressure, temperature, flow rate and heat flux. Additionally, it was assumed that heat was generated only in fuel plates. An assembly was represented in the model via 12 plates for fuel assemblies and 6 plates for control assemblies. 15 axial and 10 radial nodes used for fuel whereas 10 radial nodes for cladding. Inlet boundary conditions were selected as constant temperature and mass flow rate. The reactor power was taken from experimental measurements. The axial and radial power distributions were calculated using the code MORET. A summary of the input parameters of the ASTEC model is presented in Tables VII-7a, VII-7b and VII-7c.

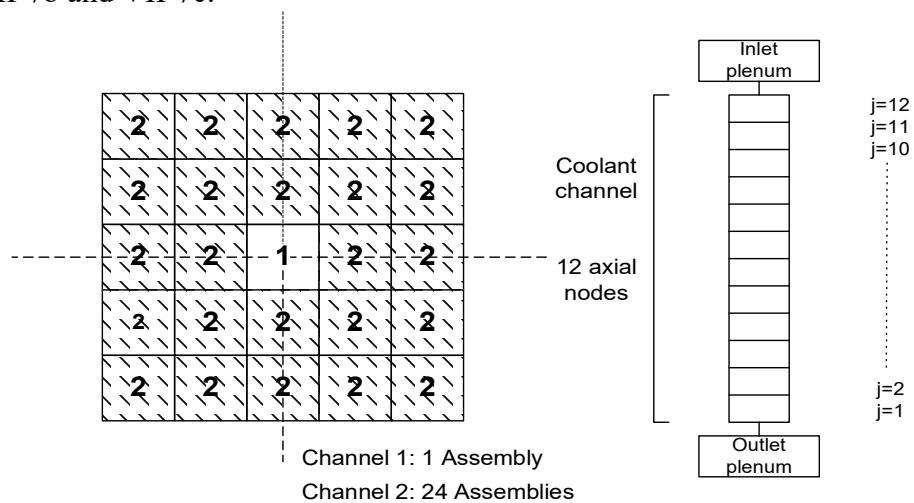


FIG. VII-3. PARET-ANL model nodalization.

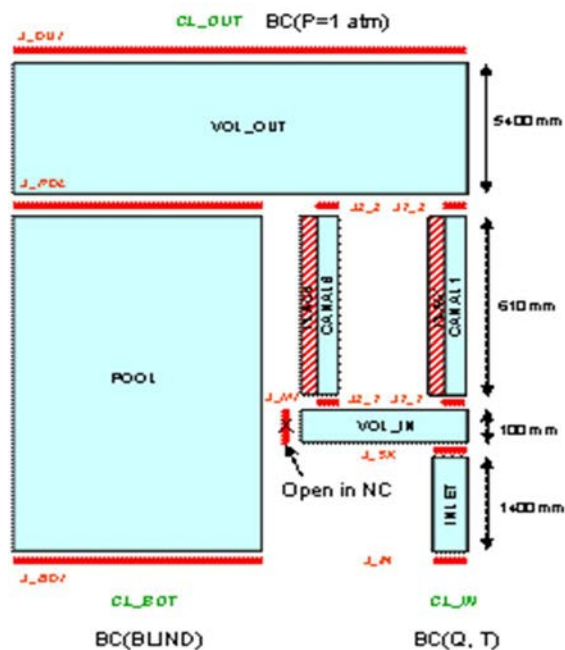


FIG. VII-4. CATHARE2 model nodalization.

VII-2.6. Pakistan: Codes, Tools and Methods

The computer code PARET-ANL 1992 version [VII-2, VII-3] was employed to carry out the analysis of the transient section of the SPERT IV benchmark analysis. A two-channel model was adopted in the code. One channel represents the hottest plate and associated flow channel with the second channel in the model representing an average plate and flow channel. A summary of the input parameters of the PARET model is presented in Tables VII-7a, VII-7b and VII-7c.

VII-2.7. Syrian Arab Republic: Codes, Tools and Methods

Syrian Arab Republic (SYR) employed MERSAT [VII-9] and RELAP5/MOD3.3 [VII-10] codes to model the transient section of SPERT IV. The primary loop has been modelled as an open loop without pumps and heat exchanger. 'Fill and Leak' components connected to inlet and outlet plenum are used to simulate inlet and outlet flow of coolant. The nodalization of the primary loop is presented in Fig. VII-5. The 25 fuel elements were modelled with 3 different radial zones for fuel and clad material (without gap). One flow channel has been used for every fuel element. In the axial direction every fuel element is divided into 10 equal nodes. The employed axial power profile is adopted from the measurements [VII-1]. For the hot channel the radial peaking factor is calculated to be 1.23. The RELAP5/MOD3.3 model is similar to the MERSAT model.

A summary of the input parameters of the MERSAT and RELAP5/MOD3.3 models is presented in Tables VII-7a, VII-7b and VII-7c. In this benchmark study, only tests with 5.486 m hydrostatic head were simulated using the PARET/ANL code. Transients B-1 to B-19 were not studied. The benchmark analysis focused on the selection of 2 experiments for every flow rate making a total of 10 cases.

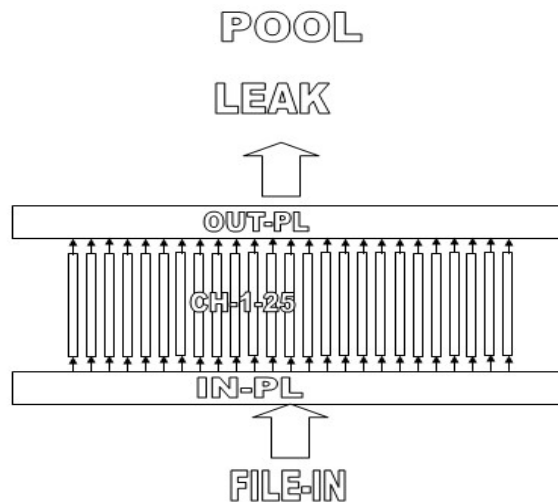


FIG. VII-5. MERSAT model nodalization.

VII-3. DESCRIPTION OF FACILITY AND EXPERIMENT

SPERT IV was a light water cooled and moderated, pool type reactor with provisions for both upward forced and natural convection cooling. The reactor core was suspended from a moveable bridge and positioned near the bottom of the reactor pool.

The SPERT IV D-12/25 core was the final aluminium plate-type core studied as part of the SPERT Project. The reactor core was composed of 25 fuel assemblies (20 standard, 4 control

fuel assemblies and 1 transient rod assembly) in a square five-by-five section of the nine-by-nine supporting grid (Fig. VII-6). Apart from the positions of the four control fuel assemblies (which were moved to move central grid positions), the D-core was identical to the D-12/25 core used in the destructive test series in the SPERT I Facility.

The Type-D fuel plates were HEU UAl_x-Al alloy fuel clad in aluminum. Each Type-D standard fuel assembly contained 12 removable flat fuel plates, housed in an aluminium assembly can. Four gang-operated boron-alloy double-blade control rods and one central transient rod of the same style were accommodated in modified six-plate fuel assemblies. General reactor data and fuel assembly specifications can be seen in Tables VII-3 and 4. A full description of the Spert IV D-12/25 core is available in Reference [VII-1].

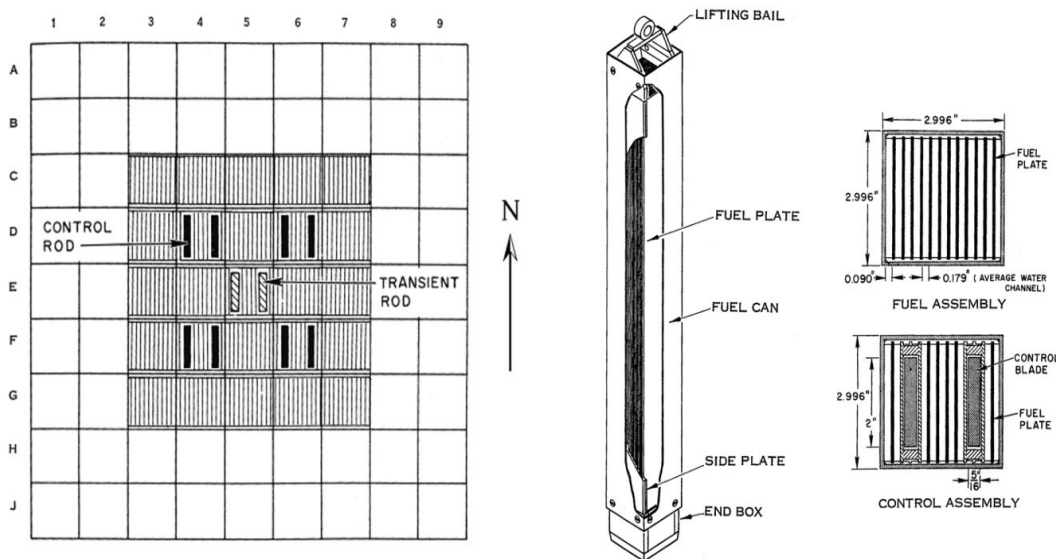


FIG. VII-6. Reactor core configuration and fuel assembly details.

TABLE VII-3. SPERT IV GENERAL REACTOR DATA

Parameter	Value
Type of Reactor	Open Pool MTR-type
Core shape	25 assemblies in 5 x 5 array
Fuel type	UAl Alloy, Al-clad flat plate fuel
Enrichment	HEU (93%)
Site Elevation	Approximately 1500 m above sea level
Pool height	7.62 m
Pool diameter	6.096 m
Hydrostatic Head	5.4846 m
Reference Pressure of the Facility	Pool open to atmosphere
Nominal Reference Temperature	Room Temperature (20°C)
Coolant (type and flow direction)	Light water, natural circulation or forced upward flow
Moderator	Light water
Reflector	Light water
Nominal Flow Rate	Varied with Test

TABLE VII-4. SPERT IV FUEL ASSEMBLY SPECIFICATIONS

Fuel Assembly	
Assembly geometry	Rectangular
No of std assemblies	20
No of control assemblies	5
No of plates per std assembly	12
No of plates per control assembly	6
Total No of fuel plates	270
Fuel Plate	
Plate material	Al 6061
Plate geometry	Flat
Plate width	0.06659 m
Plate half-thickness	0.000762 m
Clad-fuel gap	None
Fuel	
Fuel material	UAl alloy
Fuel half-thickness	0.000254 m
Fuel width	0.06223 m
Active fuel length	0.6069 m
Unfueled inlet section	0.0142875 m
Unfueled outlet section	0.0142875 m
Coolant channel	
Thickness	0.0045466 m
Width	0.06659 m
Cross-section	0.000302798 m ²
Perimeter	0.1422908 m

VII-3.1. Transient (RIA) Experiments

VII-3.1.1. Short description of transient experiments

The SPERT IV experiments included a series of self-limiting, non-destructive reactivity insertion tests for a variety of coolant flow conditions. The series of tests were performed by stepwise addition of positive reactivity.

The test sequence is graphically depicted in Fig. VII-7 identifying the five transient phases. Initially, the reactor was brought to criticality at a power level of a few watts. Tests were initiated by the sudden ejection of the central transient control rod rendering the reactor supercritical. For all tests the transients were initiated with the reactor critical at a power of approximately one watt, except for those for periods of less than 15 milliseconds for which the reactor was initially subcritical at a power in the milli-watt range to accommodate complete reactivity insertion prior to a notable power rise.

Total reactor power was measured via a series of out-of-core ion chambers while fuel plate temperatures were recorded from a set of fast-response thermocouples spot-welded to the surface of the fuel plate cladding at various locations.

Reactivity insertion values for the tests were varied in the range between 0.8 \$ and 2.14 \$ generating transients with initial periods of between 980 and 7 msec. The initial bulk moderator temperature was at ambient room temperature (approximately 20 °C – specific initial temperatures are reported for each transient) while the total core coolant flow rate was

controlled at the 0, 500, 1000, 2500, and 5000 gpm levels. Peak power (P_{max}), maximum fuel plate surface temperature at the time of peak power (T_{tm}), maximum energy at time of peak power (E_{tm}) and maximum fuel plate surface temperature (T_{max}) experimental results are summarized in Tables VII-5 and VII-6. The results can be thought of loosely in terms of long-period (> 200 msec) and short-period transients (< 50 msec) with a transition region (between 200 msec and 50 msec), where each range is associated with different transient characteristics. A more complete description of the Spert IV D-12/25 transient tests is available in Ref. [VII-1].

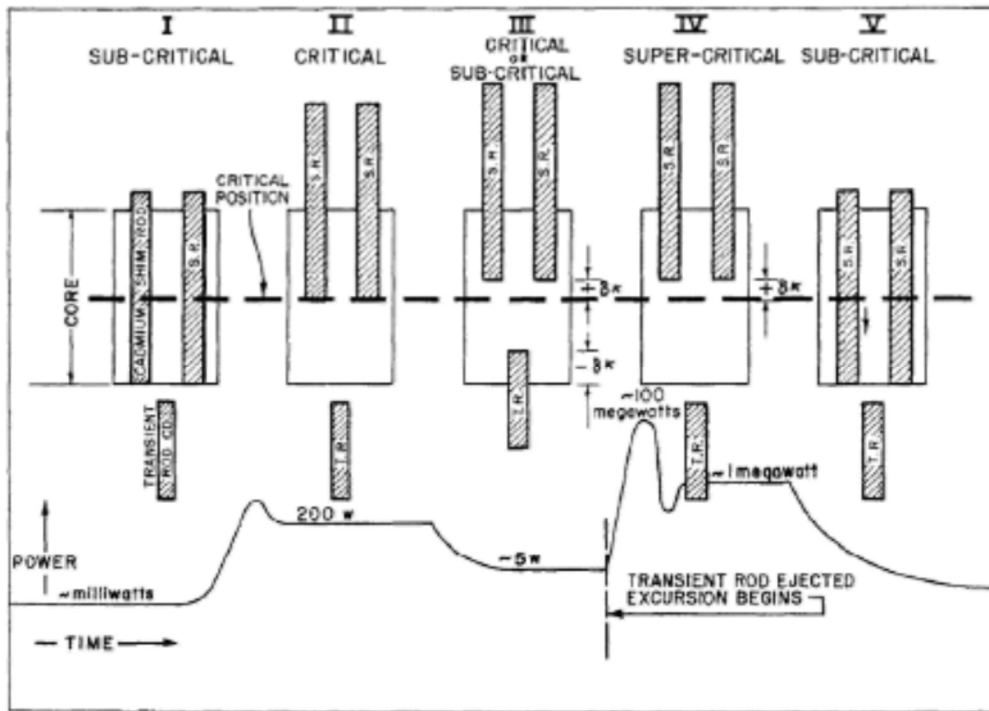


FIG. VII-7. SPERT IV reactivity insertion test sequence.

TABLE VII-5. SUMMARY DATA FOR TESTS WITH NATURAL CIRCULATION

Test number	Reactivity (\$)	Period (msec)	Initial cool. temp. (°C)	Pmax (MW)	Etm (MWs)	Ttm (°C)	Tmax (°C)
Natural circulation (No forced flow)							
B1	0.80	980	19.0	0.77	2.18	71	93
B2	0.88	598	20.0	1.12	1.56	68	103
B3	0.92	374	21.8	1.55	1.27	68	113
B4	0.98	190	20.9	3.32	1.08	63	121
B5	1.04	107	22.2	6.9	1.18	73	122
B6	1.11	62.4	22.4	17.5	1.64	99	128
B7	1.15	49.8	22.2	25.1	1.83	113	124
B8	1.26	29.6	22.4	68.5	3.00	136	141
B9	1.40	19.6	22.4	147	3.23	148	162
B10	1.53	15.8	20.5	220	4.40	160	165
B11	1.54	14.5	22.2	247	4.40	165	178
B12	1.68	11.7	22.3	350	4.84	175	179
B13	1.82	10.1	22.2	467	4.94	183	191
B14	1.91	8.48	22.0	615	5.66	170	212
B15	2.00	7.8	19.9	705	6.35	167	270
B16	2.14	7.0	19.8	875	8.50	170	338
B17	1.40	21.3	22.0	145	3.49	131	138
B18	1.68	12.0	21.8	340	4.43	155	156
B19	1.91	8.8	21.7	570	5.18	165	184

Note: Test number refers to the Figure number of the test as per [VII-1].

Note: all tests were performed with a 5.486 m hydrostatic head above the core except for B17-B19 for which the hydrostatic head was 0.6096 mt above the core

TABLE VII-6. SUMMARY DATA FOR TESTS WITH FORCED FLOW

Test number	Reactivity (\$)	Period (msec)	Initial cool. temp. (°C)	Pmax (MW)	Etm (MWs)	Ttm (°C)	Tmax (°C)
500 gpm forced flow							
B20	0.88	560	21.9	(a)	(a)	(a)	97
B21	1.14	54.2	22.8	21.5	2.32	103	125
B22	1.66	11.9	23.3	322	5.26	163	169
B23	1.80	10.1	23.2	435	5.97	165	173
1000 gpm forced flow							
B24	0.88	529	22.0	(a)	(a)	(a)	99
B25	1.04	103	22.5	7.5	1.30	64	110
B26	1.14	54.5	22.8	22.5	2.35	124	136
B27	1.39	20.0	23.0	130	4.94	138	144
B28	1.66	12.3	22.9	292	5.49	160	168
B29	1.80	10.4	22.9	425	6.05	167	184
2500 gpm forced flow							
B30	0.88	531	22.5	(a)	(a)	(a)	105
B31	1.14	52.1	22.7	22.5	2.51	91	110
B32	1.66	12.2	22.6	320	5.41	169	176
B33	1.80	10.0	23.2	435	6.13	182	182
5000 gpm forced flow							
B34	0.88	516	21.9	(a)	(a)	(a)	93
B35	1.05	104	22.0	9.8	1.79	58	102
B36	1.14	49.3	22.4	30.2	2.71	90	108
B37	1.39	20.7	22.8	169	4.78	149	152
B38	1.66	12.2	23.4	370	5.26	167	173
B39	1.80	10.1	23.7	505	6.08	185	192

(a) power exhibited no peak

Note: Test number refers to the Figure number of the test as per [VII-1].

VII-3.1.2. Summary and comparison of benchmark results

The independent model estimations of the power, energy and cladding temperatures included the test series for the entire range of reactivity insertions under both forced and natural circulation conditions. The main parameters simulated were power, energy, and cladding temperature in full accordance to the published results of the original benchmark tests. This benchmark is very extensive, covering a broad range of flow conditions and reactivity insertions. The results comprised of more than 100 graphs each including 3 to 8 curves adding up on average more than 500 independent model estimates. It is noted that, contrary to earlier benchmarking efforts, Ref. [VII-11], where the intention was to evaluate the code performance during separate and integral effect tests, the present study is focused on independent modelling efforts of an actual reactor utilizing available experimental data.

A thermal-hydraulic input deck is comprised of a large number of input parameters that cover geometrical, thermal and hydraulic characteristics. A number of these parameters are well defined where others are easily measured. It appears that generally geometrical parameters such as fuel and cladding dimensions are identical in all models. However, additional parameters that are difficult to measure or not properly defined are frequently required. The modelling teams adopted a common practice of approximating parameters that are not readily available (e.g., resistance coefficients, fuel and cladding thermal properties, plenum characteristics) with either values from similar reactor types or from related calculations. Typical examples are fuel thermal properties, resistance coefficients as well as plenum geometry and reactivity insertion times. Tables VII-7a, 7b and 7c dictate that the most significant differences among the modelling groups appear in these parameters. It was noted that not all of these differences lead to a considerably different calculation result. For example, sensitivity studies performed by the participants on fuel thermal properties and reactivity insertion times showed that these do not have a large impact on the final result.

The evolution of the power and cladding temperature rise for some representative transients are shown in Figs. VII-8 through VII-21. Tables VII-8 through VII-11 provide the peak power and peak temperatures estimates and experimental measurements for all transients as provided by all modelling teams. A range of discrepancies are observed with some modelling teams presenting sufficient agreement with the experimental measurements while others having considerable differences. A graphical representation of the peak power and temperature estimates is shown in Figs. VII-22 to VII-31 and the range of discrepancies is depicted in Figs. VII-32 to VII-43. The peak temperature calculation over measurement ratio is shown in Figs. VII-44 for tests with natural circulation and in Figs. VII-45 to VII-48 for tests with forced flow.

For the tests with natural circulation, three regions can be identified:

1. Region 1: Inverse period lower than 20 s^{-1} . This region includes transients B1 to B6 or transients in the period range of 980 to 50 msec (corresponding to step reactivity insertions up to 1.14\$ in magnitude). Transients in this range can be considered 'long period'. It can be stated that for inverse periods $<20 \text{ s}^{-1}$ the power and temperature estimates are in adequate agreement with the experimental measurements. As shown in Fig. VII-32 the peak power estimates are very small, below 30 MW, up to transient B7. With regard to peak temperature estimates, Fig. VII-38 suggests that the differences are adequately small for all modelling teams. Overall, FRA slightly underestimates both peak power and peak temperature while GRE underestimates peak power but overestimates peak temperature.

2. Region 2: Inverse period between 20 and 80 s⁻¹. This region includes transients B7 to B10 or transients in the period range of 50 to 15.8 msec (corresponding to step reactivity insertions from 1.14\$ to 1.53\$). Transients in this range can be considered relatively fast but precluding fuel damage. In this region, the parameter estimates start to deviate more. PAK overestimates peak power by as much as 100 MW whereas CEA tend to underestimate with the degree of underestimation increasing gradually with the severity of the transient. With regard to peak temperatures, there is a considerable overestimation of the peak temperature ranging from 50-100 °C for GRE and AUS up to 400°C for PAK. CEA and IRSN provide good estimates with the differences lower than 20°C.
3. Region 3: Inverse period larger than 80 s⁻¹. This region includes transients B11 to B16 or transients with period < 15 msec (corresponding to step reactivity insertions from 1.54\$ up to 2.14\$). Transients in this range can be considered fast and approaching fuel damage limits. In this region, including the more severe transients B13 to B16 (1.82 – 2.14 \$) large discrepancies are observed in the peak power estimates, in the order of 200 MW or higher. It is worth noting that the peak power is underestimated by all modelling teams, AUS, GRE, CEA and PAK. On the contrary, peak temperature is largely overestimated by AUS and PAK (~100-200°C difference) and underestimated by FRA, IRSN and GRE. It is noted that GRE, AUS and PAK use the same code, PARET-ANL. Larger discrepancies occur for inverse periods >20 s⁻¹. AUS, FRA and GRE underestimate the peak power, in some cases the difference is in the order of 300 MW. Despite the power underestimation the peak temperature is overestimated. PAK results show a different behavior with overestimation of power for the middle transients and then an underestimation for the faster ones (shorter period).

A similar classification can be proposed for tests with forced flow. In that case the regions of interest are two:

1. Region 1: Inverse period lower than 20 s⁻¹. Small deviations are observed for peak power and temperature for all modelling teams independently of the different flow rates.
2. Region 2: Inverse period larger than 80 s⁻¹. The power differences between code estimates and experimental measurements are in the order of 50 to 100 MW for the more severe transients with the exceptions of PAK and BGD where differences in the order of 300 MW are observed. This trend is followed despite the difference flow rates. SYR constantly overestimates peak power and temperature. AUS and GRE provide reasonable estimates for peak power, but peak temperatures are generally overestimated. For larger inverse periods, peak temperature differences may reach 200°C with AUS to predict generally higher temperature estimates than GRE despite the use of the same code (PARET-ANL). Discrepancies tend to reduce at higher flowrates. PAK peak temperature estimates are even higher than AUS and GRE.

Overall, for the tests with forced flow the differences are less exaggerated. With regard to temperatures, the differences are below 50 °C for mild transients and are then increased up to 200 °C for the more severe transients. In some cases, unreasonably high temperature estimates (in the order of 800 °C or higher) are observed. In most cases, the achieved calculation results reproduce adequately the trend and the expected transient behaviour of the reactor power and fuel clad temperature. Yet, considerable discrepancy between calculation and measurement is identified for large reactivity insertions.

In general, it is observed that for the more severe the RIA tests are (especially tests with reactivity insertion greater than ~1.40\$) the calculated clad temperatures are significantly

higher than the experimental measurements. This effect is augmented in cases of low flow rate such as during natural circulation.

It appears that FRA and IRSN have the best agreement with experimental measurements. However, they have somehow modified the heat transfer models of the code. For example, preliminary analyses performed by FRA using the CATHARE2 code showed large discrepancies between the calculations and the measurements. As such, a specific methodology was employed to estimate corrective factors associated to the heat exchange and the critical heat flux correlations. In addition, FRA2 employed modified heat transfer coefficients instead of the ASTEC built-in correlations.

Discrepancies for peak power for BGD are in the order of 30% to 50%. In the case of SYR (MERSAT and RELAP5/MOD3.3) the calculations overestimate largely the measurements although RELAP5/MOD3.3 results seem to be better than those of MERSAT. For the case of B-27 the MERSAT peak power prediction appears to be delayed and is higher by a factor two whereas the cladding temperature rise is 7 times higher than the experimental measurements. For very high reactivity insertions (e.g. B39, 1.8\$) RELAP5/MOD3.3 produces an adequate prediction of the peak power, yet there is a clear overestimation of peak clad temperature (401°C compared to 192°C in the experiment).

PARET-ANL (used by AUS, GRE and PAK) is generally shown to provide conservative estimates of peak power and temperatures, with the degree of conservatism to depend highly on the modelling team. A user effect can easily be identified in that case. In many cases the code results were found not to accurately capture the details of the transient response. Of note are the non-conservative results in the low reactivity range during natural convection. Also, worth noting that results are not very accurate for reactivity insertions > 1.9 again in the natural convection regime. On the contrary, when forced convection comes into play, the results are in fair agreement with the experiments and on what is called the 'safe-side' (i.e., conservative).

Sensitivity studies performed by AUS showed that PARET calculations for larger reactivity insertions are very sensitive to the time step chosen. For the case of the test B-39 (1.80 \$), using a time step of 1 μ s adequately reproduced the frequency of the power and clad temperature oscillations in the transient, while a time step of 5 μ s resulted in largely dampened oscillations and a slightly larger oscillation frequency. This suggests that time step convergence tests are extremely important to produce accurate results. In addition, it was found that the selection of the Bergles-Rohsenow or McAdams ONB correlation may also be of critical importance. In the short period transients, such as B-39, the calculated results are found to be very sensitive to the choice of void and coolant temperature feedback coefficients. Using a slightly larger void coefficient dampens the oscillation of the clad temperature and power. A B-39 simulation using the experimental coolant temperature feedback coefficient of $-1.2\phi/^\circ\text{C}$ results in a calculation which failed to complete due to an excessively high calculated clad temperature. These results demonstrate that feedback coefficients need to be chosen with care, particularly the coolant temperature feedback coefficient which is treated as a constant but is actually a function of temperature. PARET also provides the user with the ability to weight the void reactivity feedback coefficient along the vertical axis to consider the vertical void feedback coefficient profile. Comparison of the temperature evolutions resulting from a uniform void feedback coefficient at each axial mesh and applying the vertical void worth profile shows a reduction in the maximum calculated cladding temperature by around 50 °C, due to a larger void feedback coefficient at the power hotspot. Adopting a void coefficient profile reduces the overshoot in the calculated clad temperature compared to the experimental measurement.

PARET-ANL was used by three modelling teams (AUS, GRE and PAK) as one of the computational tools. The differences appear, mainly, in the way that each channel was modeled (axial/radial profile and nodes). Concerning the modelling of the core channels, AUS and PAK adopted the power profiles provided by the respective neutronic calculations while GRE preferred to use the experimental measurements. These differences may have an effect the temperature evolution and maximum values attained. Surprisingly, the GRE and AUS results come close despite the modelling differences. Temperature spikes reach similar values at almost the same time while PAK values present a similar evolution but with higher peak values.

TABLE VII-7a. INPUT SUMMARY DATA

Parameter	SPERT IV	AUS	GRE	SYR	FRA	FRA2	PAK	BGD
General reactor characteristics								
Total number of plates	270	270	270	270	270	270	270	270
Plates per standard assembly	12	12	12	12	12	12	12	12
Plates per control assembly	6	6	6	6	6	6	6	6
Standard in-core assemblies	20	20	20	20	20	20	20	20
Control in-core assemblies	5	5	5	5	5	5	5	5
Power (MW)	T/D	T/D	T/D	T/D	T/D	T/D	T/D	T/D
Flow rate (m ³ /h)	T/D	T/D	T/D	T/D	T/D	T/D	T/D	T/D
Flow direction	Upward	Upward	Upward	Upward	Upward	Upward	Upward	Upward
Inlet pressure (bar)	1.4	1.4	1.4	1.4	**	1.4	1.4	1.4
Inlet temperature (°C)	~20	~20	~20	~20	~20	~20	~20	~20
Neutronic related parameters								
Eff. delayed neutron fraction (-)	-	0.00765	0.00666	0.0079749	0.00768	0.007828	0.007832	0.0069
Prompt neutron lifetime (μs)	53.4	63.5	53.4	79.4	64	63.9	62.2	64
Reactivity insertion time (ms)	~100	1	100	~100	100	100	10	-
Coolant feedback coeff. (\$/°C)		-0.02801	-0.012	Function	Function	Function	-0.016	-0.012
Void feedback coeff. (\$/% void)		-0.415	-0.415	Function	Function	Function	-0.357	-0.415
Axial peaking factor (-)	-	1.47	1.49	1.47	1.45	1.43	1.39	1.47
Radial peaking factor (-)	-	1.57	1.57	1.51	1.275***	Step-wise	1.46	1.0

*T/D: Transient Dependent

**Depends on flow rate, outlet pressure = 1 bar

***For an insertion of 0.88\$ with insertion of the transient rod.

TABLE VII-7b. INPUT SUMMARY DATA (cont'd)

Parameter	SPERT IV	AUS	GRE	SYR	FRA	FRA2	PAK	BGD
Geometrical parameters								
Fueled length (m)	0.6069	0.6069	0.600	0.6069	0.61	0.6096	0.06069	0.6096
Fueled width (m)	0.06223	0.06223	0.06223	0.06223	0.066	0.06223	0.6223	0.06223
Fuel thickness (m)	0.000508	0.000508	0.000508	0.000508	0.066	0.000508	0.000508	0.000508
Total length (m)	0.625	0.6382	0.625	0.625	0.61	0.625	0.6355	0.63818
Total thickness (m)	0.001524	0.001524	0.001524	0.001524	0.00152	0.001524	0.001524	0.001524
Clad thickness (m)	0.000508	0.000508	-	0.000508	0.005	-	0.000508	0.000508
Coolant channel thickness (m)	0.0024	0.0045466	0.0024	0.0024	0.00455	0.0024	0.0045466	0.00455
Coolant channel width (m)	0.07075	0.0665988	0.07075	0.07075	0.0666	0.07075	0.06868	0.06223
Unfueled length (inlet) (m)	0.0142875	0.0142875	0.0142875	0.0142875	-	0.0142875	0.0142875	0.0041275
Unfueled length (outlet) (m)	0.0142875	0.0142875	0.0142875	0.0142875	-	0.0142875	0.0142875	0.0041275
Coolant channel velocity (m/s)	-	-	0.387-3.859	T/D	0-3.67	-	0.377-3.77	0.365-3.657
Velocity mass flow rate (kg/sm ²)	-	371.9 - 3719	386.55-3852	T/D	0-3670	-	374.1-3741	458-2292.07
Reference density(kg/m ³)	-	1000	998	997.5	Function**	998	992	-
Flow area (inner channel) (m ²)	-	0.0848	0.08175546	0.003711	-	-	0.0843	-
Resistance coeff. (inlet)	-	-	0.55	-	0.5	-	0.55	1.81
Resistance coeff. (outlet)	-	-	0.65	-	1.0	-	0.65	2.12
Hydraulic diameter (m) (inner channel)	-	-	0.008512	0.008522	~0.0076	-	0.06069	0.008557
Heated area (per plate) (m ²)	-	-	-	-	0.066x0.61	-	-	-
Height above core (m)	5.4864	-	5.4864	5.4864	5.4	5.4864	-	1
Height below core (m)	1.524	-	1.524	1.524	1.4	1.524	-	1

*T/D: Transient Dependent

**Density=-0.2163×T+ 3227.7 (kg/m³)

TABLE VII-7c. INPUT SUMMARY DATA (cont'd)

Parameter	SPERT IV	AUS	GRE	SYR	FRA	FRA2	PAK	BGD
Thermal properties								
Fuel conductivity (W/mK)	-	$-0.042 \times T + 173.64$ $-1.57 \times 10^{-4} \times T^2 +$	150	158	Function*		142	150
Clad conductivity (W/mK)	-	$0.093 \times T + 163.18$ $-0.586 \times T^2 +$ $1414 \times T + 2.2343 \times 10^6$	180	180	Function**		180	180
Fuel heat capacity (J/m ³ K)		$1146 \times T + 2.4058 \times 10^6$		2.1×10^6	Function*		2.3608×10^6	-
Cladding heat capacity (J/m ³ K)				2.086×10^6	Function**		2.5078×10^6	-
Modelling parameters								
Axial nodes	-	21	12	10	61	15	21	10
Radial nodes	-	7	7	-	5	10	7	-
No. channels	-	2	2	25	5	6	2	5
Time step (μ s)	-	1-10	1-10	1-10	10^{-4}	1-10	1-10	-
Single phase heat transfer correlation	-	D-B	D-B	D-B	S-T***	D-B	D-B	D-B
ONB correlation	-	B-R/McAdams	B-R	B-R	Thom***	Thom	McAdams	B-R
DNB correlation	-	Tong	Tong	Tong	Groeneveld***	hand-made	Mirshak	Sudo-Kamin.

D-B: Dittus-Boelter, S-T: Sieder-Tate, B-R: Bergles-Rohsenow

*Fuel conductivity= $-0.0414 \times T + 173.60$ (W/m²C), Heat capacity= $0.3783 \times T + 703.38$ (J/kg²C),

Cladding conductivity= $4.18 \times (0.390 + 2.22d - 4 \times T - 3.76d - 7 \times T^{2} + 2.42d - 10 \times T^{**3}) \times 100$ (W/m²C), Heat capacity= $0.4242 \times T + 890.19$ (kg/m³C), density= 2700 (kg/m³)

*** modified

TABLE VII- 8. PEAK POWER RESULTS FOR TESTS WITH NATURAL CIRCULATION

Test number	Inverse period (s ⁻¹)	Peak power (MW)				
		Measurement	AUS	FRA	GRE	PAK
Natural Circulation (No forced flow)						
B-1	1.0	0.8	0.7	0.8	3.7	0.7
B-2	1.7	1.1	1.6	1.2	5.7	1.5
B-3	2.7	1.6	2.0	1.5	1.9	2.5
B-4	5.3	3.3	4.2	3.2	3.9	6.8
B-5	9.3	6.9	10.4	7.1	10.8	20.5
B-6	16.0	17.5	27.6	14.7	32.1	44.9
B-7	20.1	25.1	43.5	22.4	45.7	59.9
B-8	33.8	68.5	103.7	53.5	89.3	118.7
B-9	51.0	147.0	169.5	111.9	151.9	232.9
B-10	63.3	220.0	240.2	166.2	216.0	365.6
B-11	69.0	247.0	233.1	168.3	170.4	388.1
B-12	85.5	350.0	323.1	239.5	275.8	477.1
B-13	99.0	467.0	390.2	309.3	315.8	496.7
B-14	117.9	615.0	446.4	551.0	376.4	612.0
B-15	128.2	705.0	-	430.0	441.7	611.0
B-16	142.9	875.0	-	540.5	560.5	744.2
B-17	46.9	145.0	-	87.7	-	192.9
B-18	83.3	340.0	-	208.8	-	358.0
B-19	113.6	570.0	-	360.8	-	510.7

TABLE VII-9. PEAK POWER RESULTS FOR TESTS WITH FORCED FLOW

Test number	Inverse period (s ⁻¹)	Measurement	Peak power (MW)						
			AUS	FRA	GRE	BGD	SYR ¹	SYR ²	PAK
500 gpm									
B-20	1.8	-	-	4.9	3.9	0.9	4.2	3.5	3.8
B-21	18.5	21.5	31.1	22.0	43.2	7.1	22.1	45.4	58.2
B-22	84.0	322.0	333.3	230.1	276.2	77.5	-	-	390.2
B-23	99.0	435.0	423.1	312.7	339.1	150.7	1361.0	3163.5	442.9
1000 gpm									
B-24	1.9	-	-	0.3	1.6	0.9	7.7	6.5	3.0
B-25	9.7	7.5	6.5	8.0	11.8	1.7	19.3	8.5	7.4
B-26	18.3	22.5	31.6	25.3	43.5	6.3	-	-	33.4
B-27	50.0	130.0	159.5	114.5	126.3	37.2	177.1	276.1	176.0
B-28	81.3	292.0	299.0	250.7	247.4	101.7	-	-	374.7
B-29	96.2	425.0	436.1	341.2	349.9	150.7	-	-	446.3
2500 gpm									
B-30	1.9	-	-	22.9	12.9	0.9	6.4	13.5	10.3
B-31	19.2	22.5	34.1	29.3	42.3	6.3	45.6	32.7	34.4
B-32	82.0	320.0	322.2	330.2	279.2	99.4	-	-	369.0
B-33	100.0	435.0	368.2	445.7	347.3	153.1	568.7	2258.5	784.7
5000 gpm									
B-34	1.9	-	-	36.5	22.3	0.9	34.3	16.8	13.8
B-35	9.6	9.8	11.5	52.3	22.3	2.4	-	-	16.7
B-36	20.3	30.2	31.8	34.8	35.5	6.4	40.7	33.7	30.2
B-37	48.3	169.0	148.3	170.5	151.2	37.5	-	-	172.4
B-38	82.0	370.0	333.1	426.7	194.5	102.3	-	-	348.7
B-39	99.0	505.0	459.2	589.4	355.2	148.5	377.8	1911.8	453.4

1: RELAP5/MOD3, 2: MERSAT

TABLE VII-10. PEAK TEMPERATURE RESULTS FOR TESTS WITH NATURAL CIRCULATION

Test number	Inverse period (s ⁻¹)	Peak temperature (°C)					
		Measurement	AUS	FRA	GRE	FRA2	PAK
Natural Convection (No forced flow)							
B-1	1.0	93.0	94.4	96.6	94.3	-	111.6
B-2	1.7	103.0	116.6	109.9	108.0	-	127.6
B-3	2.7	113.0	117.8	112.9	75.6	-	131.6
B-4	5.3	121.0	118.1	117.2	90.8	-	137.1
B-5	9.3	122.0	123.9	120.7	122.8	-	118.8
B-6	16.0	128.0	130.2	125.8	129.7	-	117.8
B-7	20.1	124.0	134.8	130.2	136.0	-	117.3
B-8	33.8	141.0	229.9	140.8	176.0	129.1	654.7
B-9	51.0	162.0	265.5	147.7	219.4	152.1	282.8
B-10	63.3	165.0	319.4	154.0	204.6	161.8	409.0
B-11	69.0	178.0	269.2	154.4	223.5	168.4	573.0
B-12	85.5	179.0	326.0	162.8	178.9	172.0	227.4
B-13	99.0	191.0	338.1	168.2	161.4	181.7	350.0
B-14	117.9	212.0	364.0	185.8	185.2	187.5	418.0
B-15	128.2	270.0	-	179.5	230.4	323.8	381.0
B-16	142.9	338.0	-	187.0	357.2	392.6	683.0
B-17	46.9	138.0	-	133.9	-	141.5	375.0
B-18	83.3	156.0	-	150.5	-	171.6	248.0
B-19	113.6	184.0	-	165.8	-	177.7	469.0

TABLE VII-11. PEAK TEMPERATURE RESULTS FOR TESTS WITH FORCED FLOW

Test number	Inverse period (s ⁻¹)	Measurement	Peak temperature (°C)							
			AUS	FRA	GRE	FRA2	BGD	SYR ¹	SYR ²	PAK
500 gpm										
B-20	1.8	97.0	119.9	112.9	94.4	85.6	64.0	94.0	117.3	133.7
B-21	18.5	125.0	132.5	126.2	133.0	129.0	116.4	88.2	195.2	191.4
B-22	84.0	169.0	327.6	172.4	259.8	172.3	150.1	-	-	357.2
B-23	99.0	173.0	361.2	176.4	287.2	182.3	166.4	425.1	4475.6	321.3
1000 gpm										
B-24	1.9	99.0	122.8	112.8	53.0	95.7	44.4	86.7	105.8	92.2
B-25	9.7	110.0	124.8	113.2	123.7	98.3	59.2	117.0	105.8	135.5
B-26	18.3	136.0	132.6	124.6	132.3	-	107.4	-	-	145.3
B-27	50.0	144.0	238.8	149.1	190.8	149.7	134.2	184.4	782.8	490.8
B-28	81.3	168.0	297.9	168.7	240.1	166.3	155.0	-	-	361.0
B-29	96.2	184.0	382.6	179.0	276.9	182.5	166.1	-	-	427.2
2500 gpm										
B-30	1.9	105.0	127.1	120.1	124.8	93.2	64.5	55.7	123.8	140.8
B-31	19.2	110.0	133.6	114.3	132.0	99.4	108.0	105.5	127.9	146.2
B-32	82.0	176.0	282.3	180.5	240.5	163.5	156.9	-	-	352.8
B-33	100.0	182.0	295.2	192.0	240.1	175.5	167.7	323.0	4333.1	360.9
5000 gpm										
B-34	1.9	93.0	131.1	116.3	128.7	135.5	64.5	116.0	102.3	101.1
B-35	9.6	102.0	131.3	125.1	128.6	146.5	91.6	-	-	143.9
B-36	20.3	108.0	133.1	116.6	133.4	140.0	109.6	82.3	119.2	147.1
B-37	48.3	152.0	186.0	156.1	163.3	161.2	142.8	-	-	156.3
B-38	82.0	173.0	257.8	261.4	188.1	183.1	160.0	-	-	323.4
B-39	99.0	192.0	300.1	207.8	243.8	207.1	168.2	401.1	3827.9	289.6

1: RELAP5/MOD3, 2: MERSAT

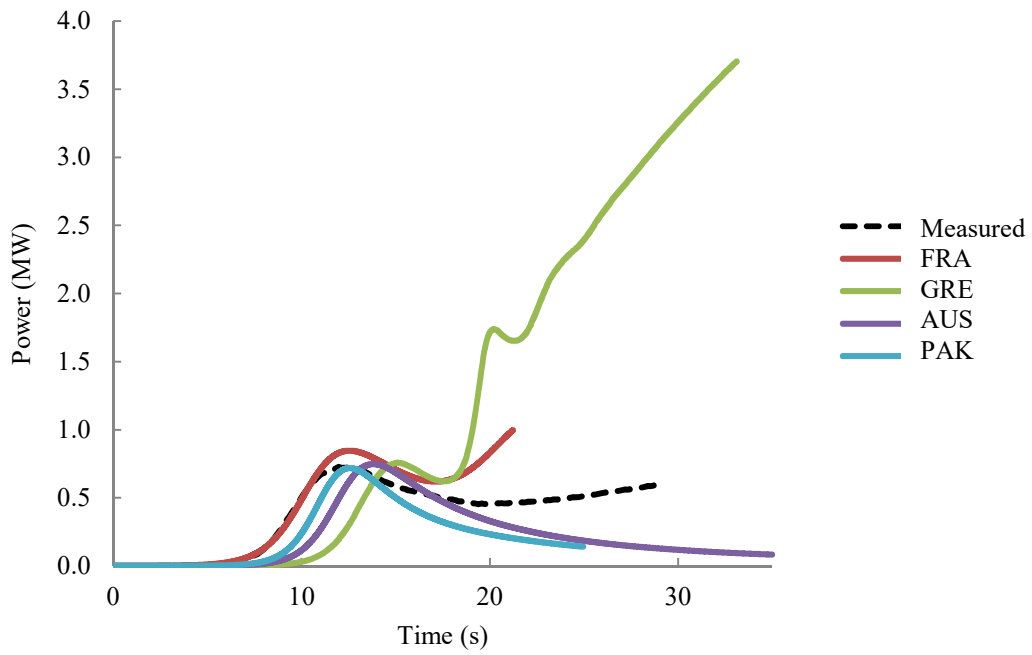


FIG. VII-8. Power estimates vs. experimental measurements for transient B-1.

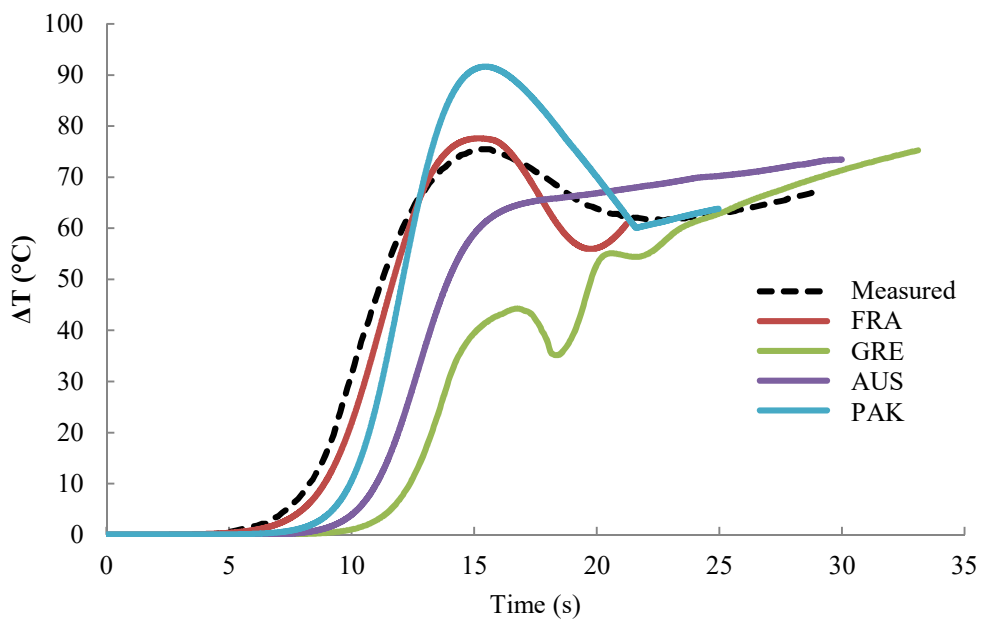


FIG. VII-9. Temperature estimates vs. experimental measurements for transient B-1.

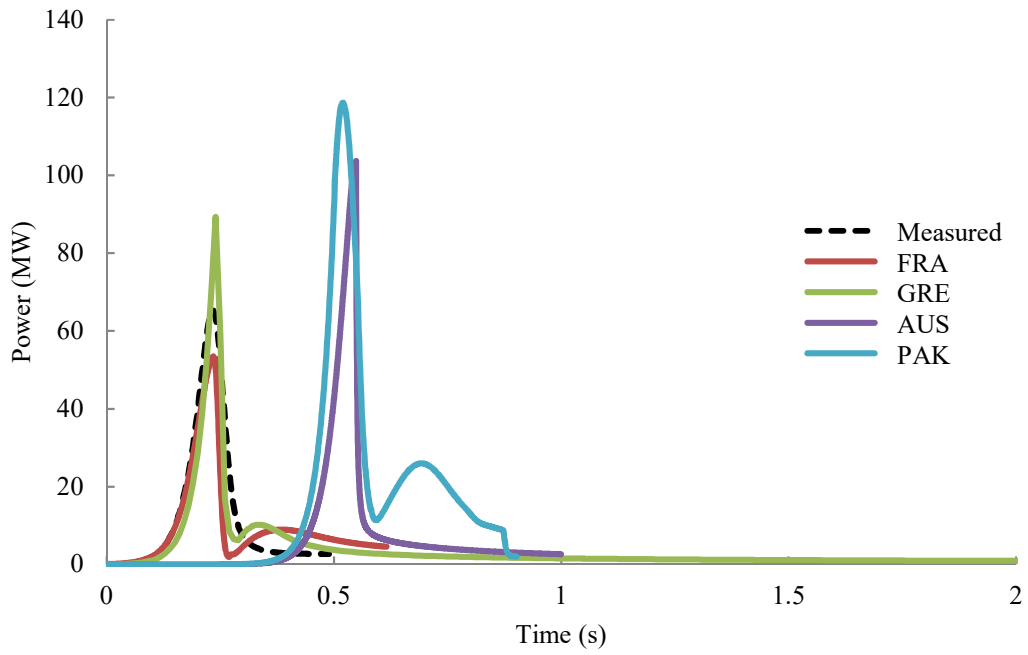


FIG. VII-10. Power estimates vs. experimental measurements for transient B-8.

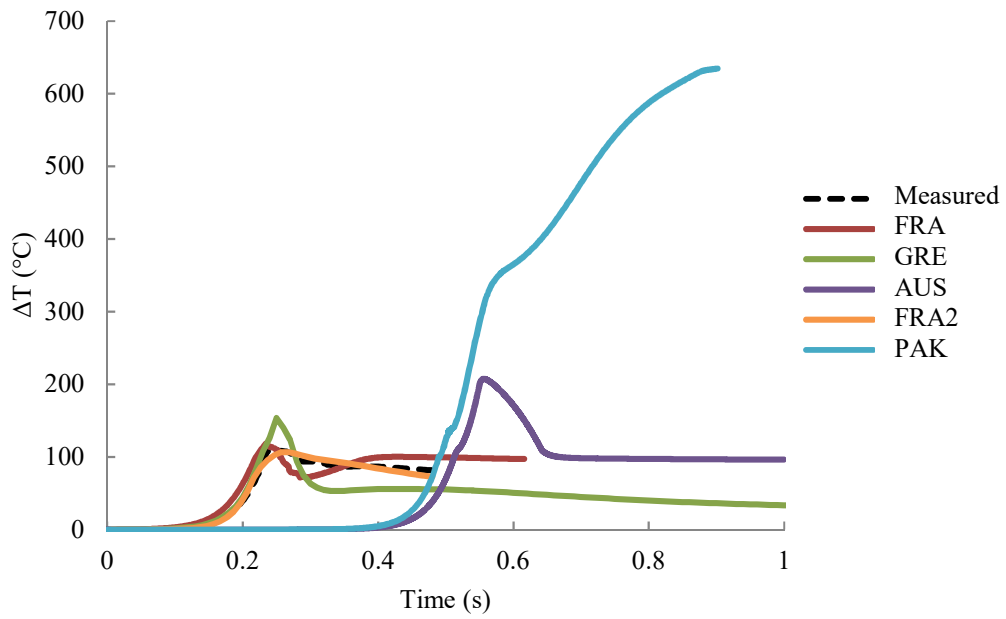


FIG. VII-11. Temperature estimates vs. experimental measurements for transient B-8.

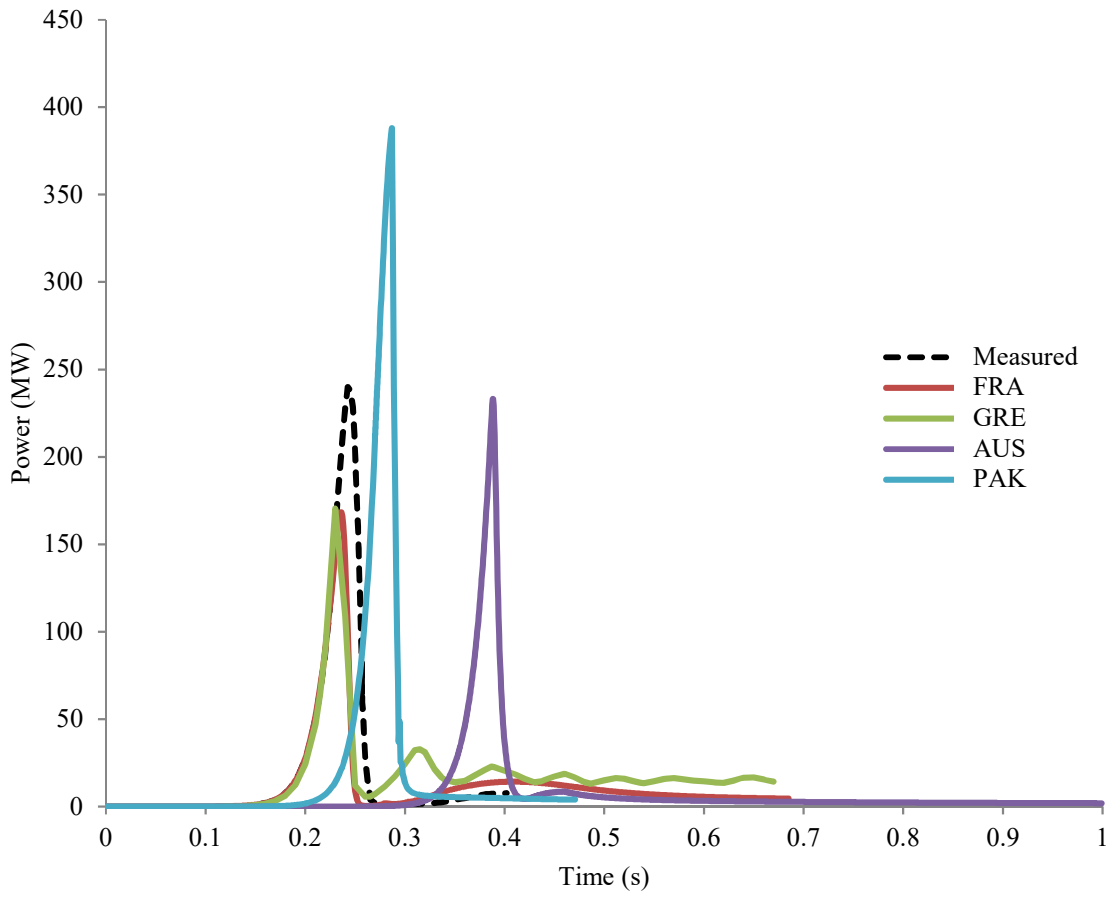


FIG. VII-12. Power estimates vs. experimental measurements for transient B-11.

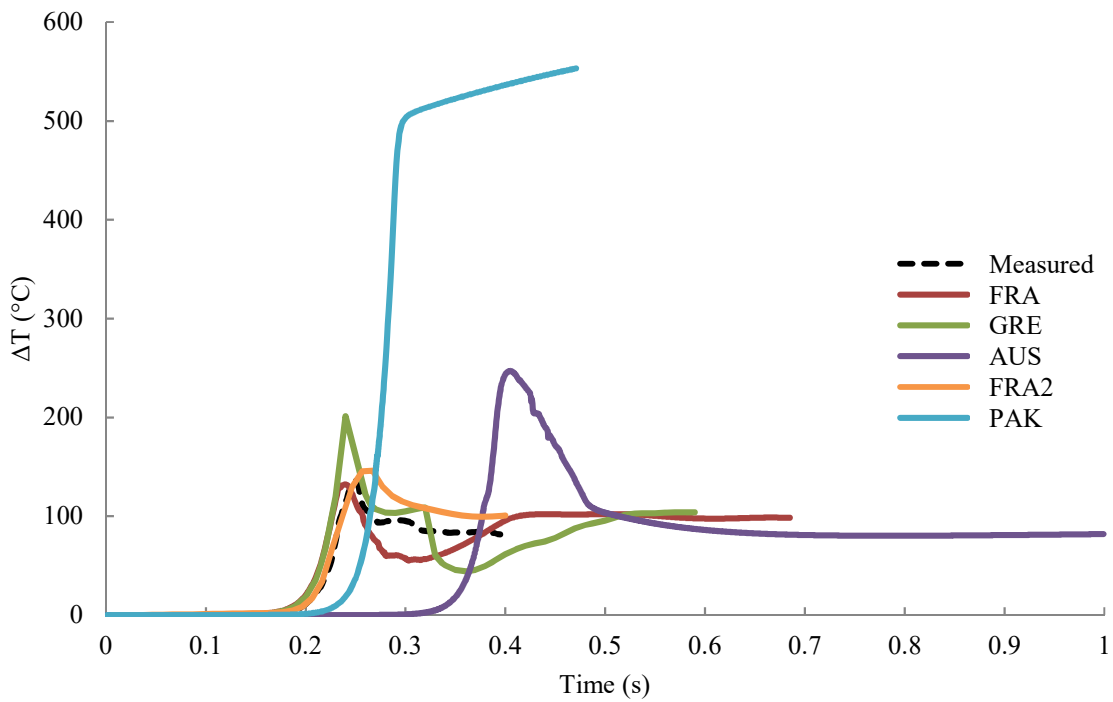


FIG. VII-13. Temperature estimates vs. experimental measurements for transient B-11.

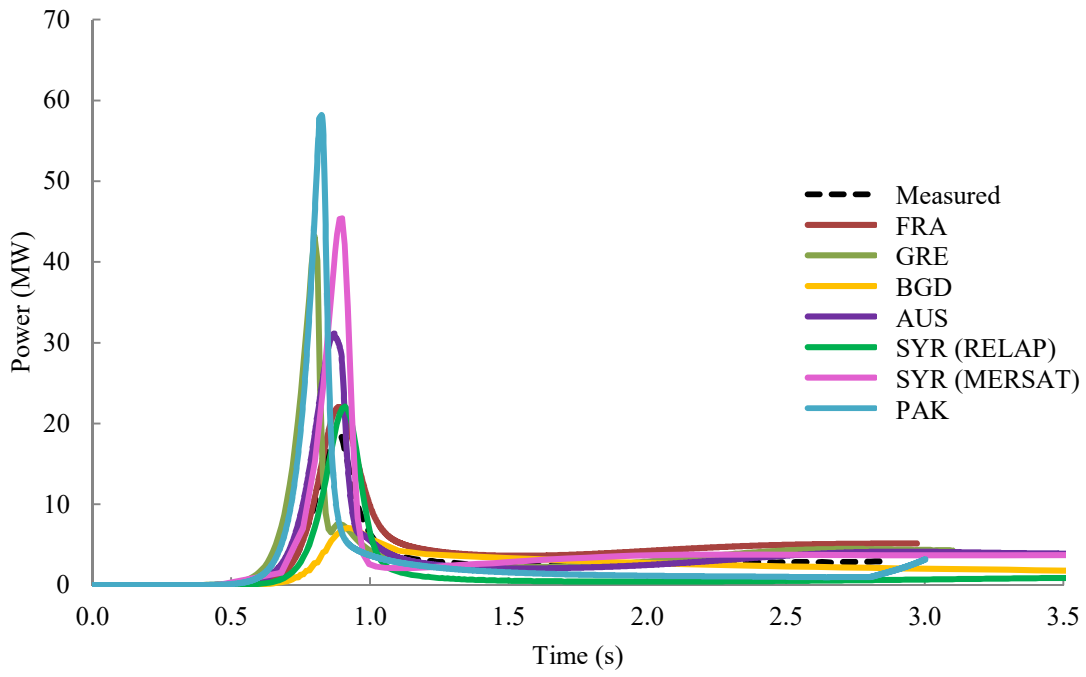


FIG. VII-14. Power estimates vs. experimental measurements for transient B-21.

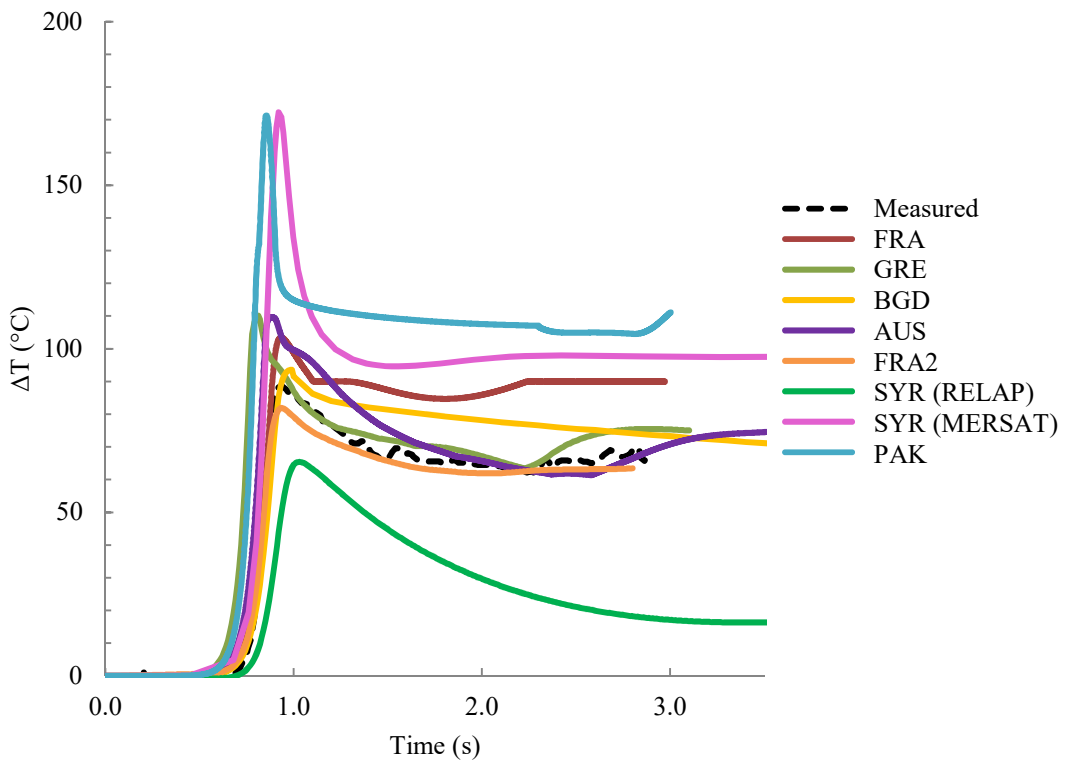


FIG. VII-15. Temperature estimates vs. experimental measurements for transient B-21.

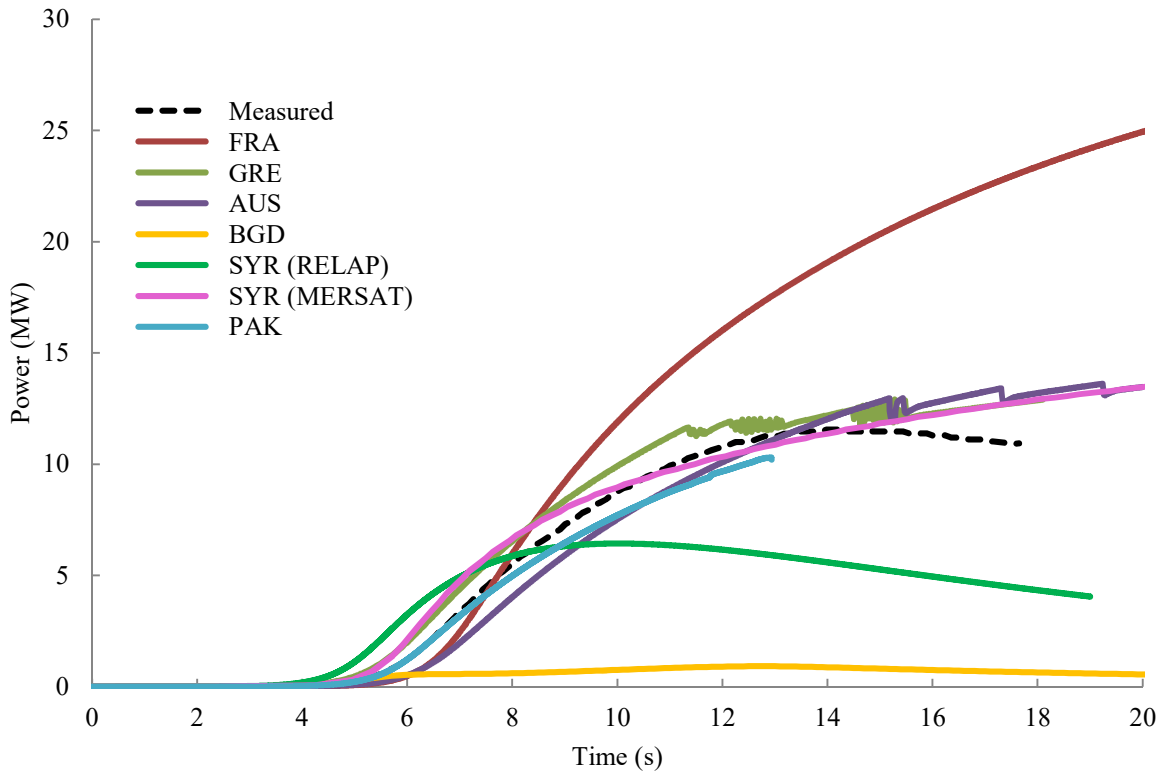


FIG. VII-16. Power estimates vs. experimental measurements for transient B-30.

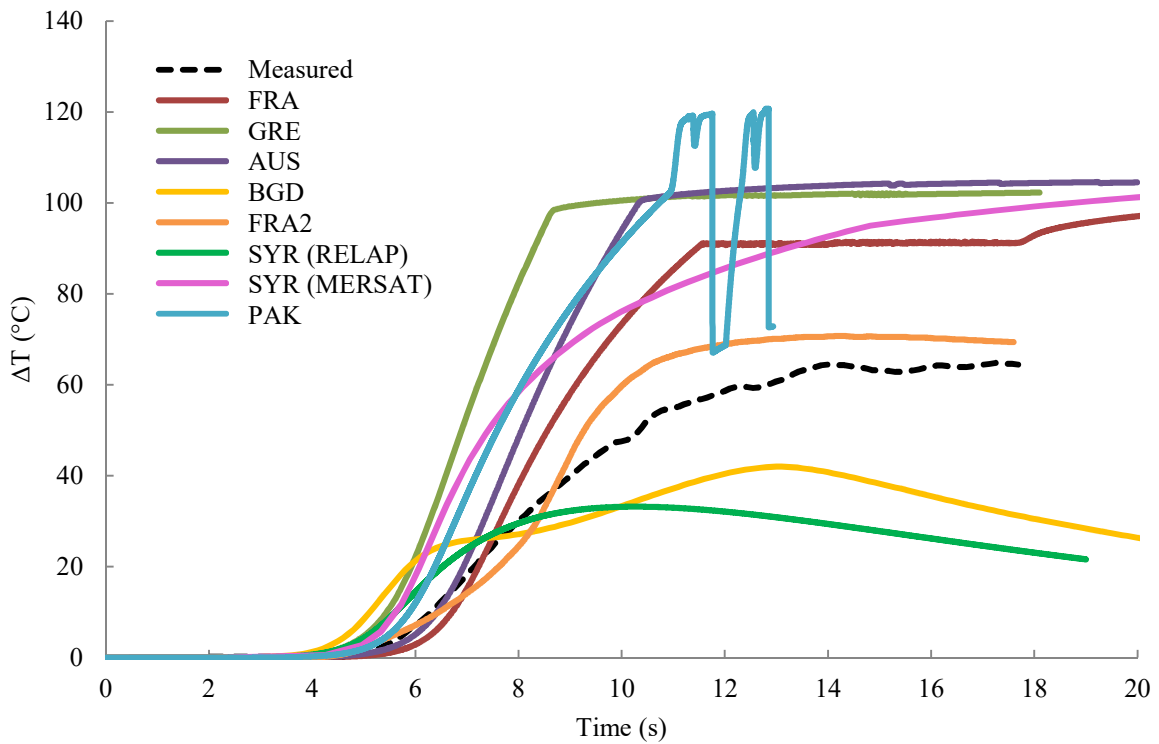


FIG. VII-17. Temperature estimates vs. experimental measurements for transient B-30.

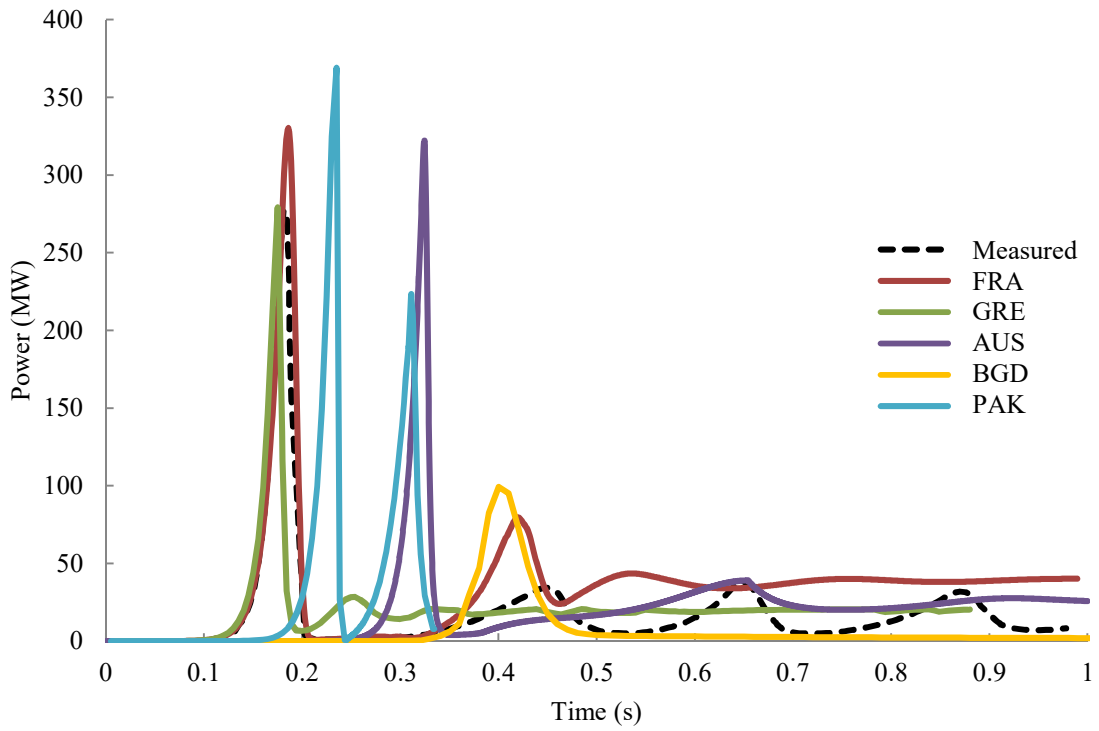


FIG. VII-18. Power estimates vs. experimental measurements for transient B-32.

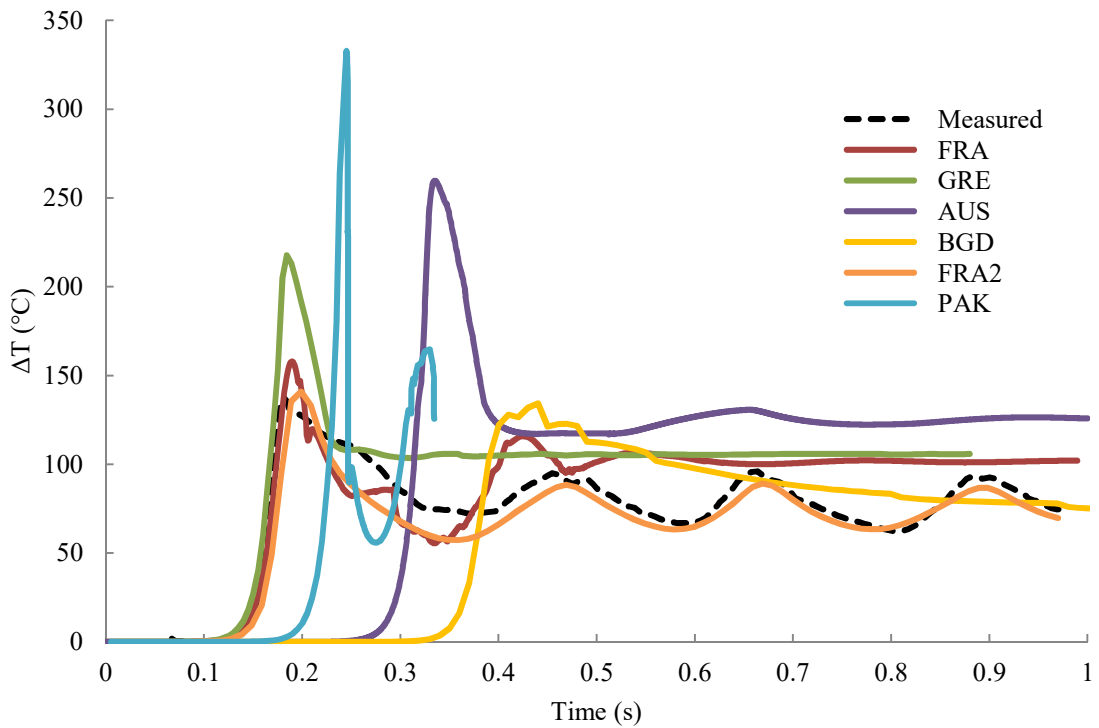


FIG. VII-19. Temperature estimates vs. experimental measurements for transient B-32.

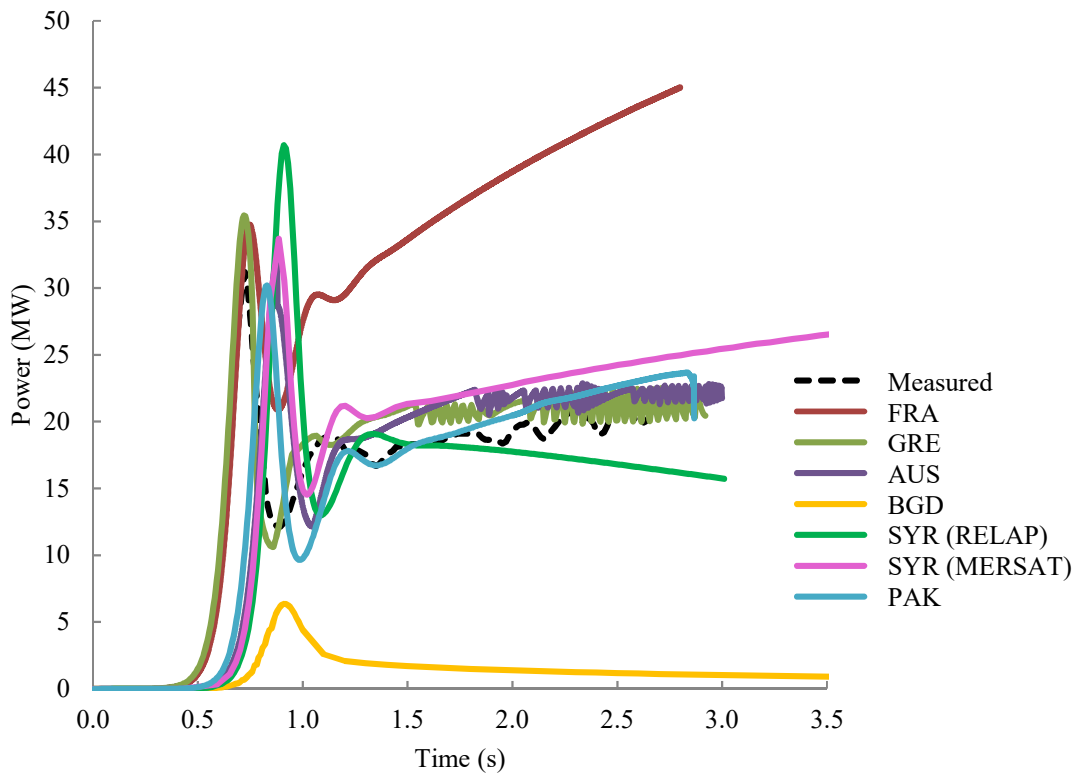


FIG. VII-20. Power estimates vs. experimental measurements for transient B-36.

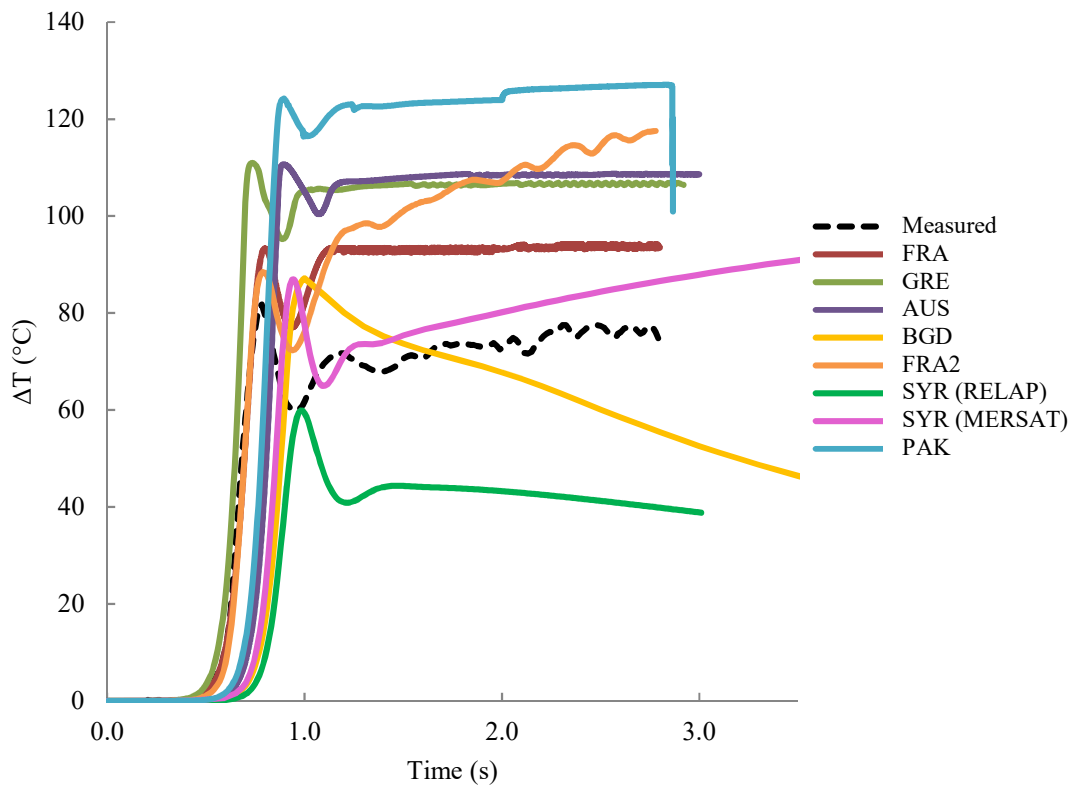


FIG. VII-21. Temperature estimates vs. experimental measurements for transient B-36.

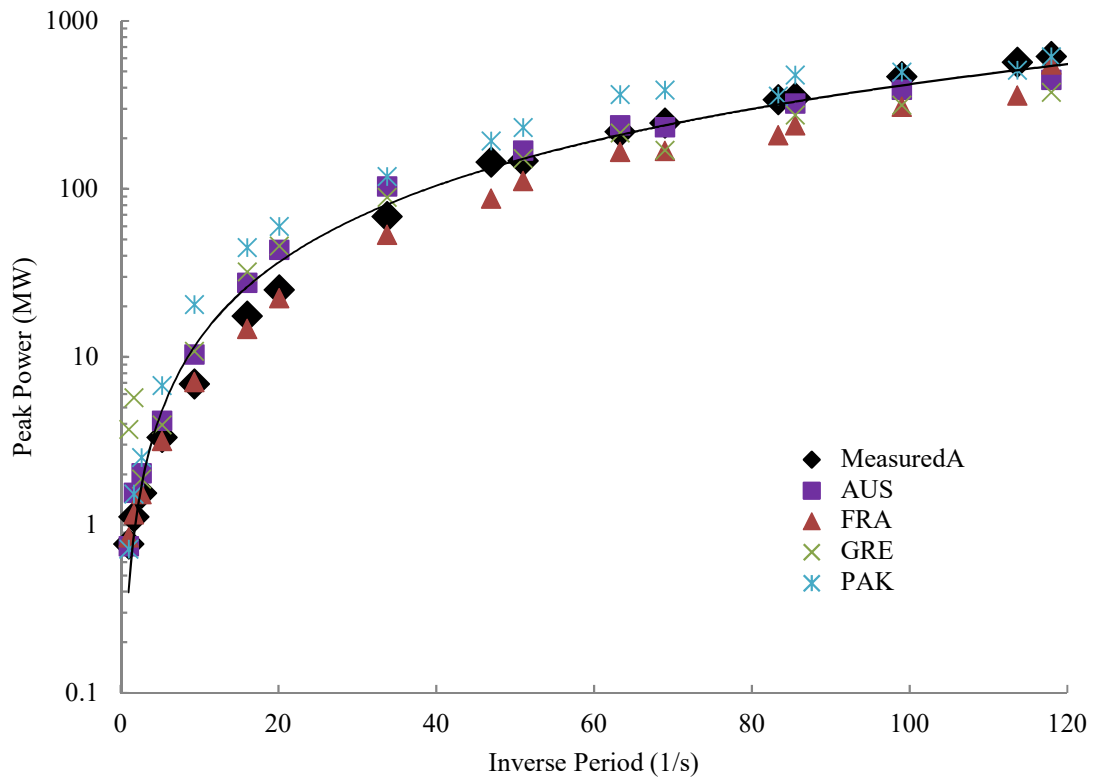


FIG. VII-22. Peak power vs. inverse period for Transients B1-B19 with natural circulation

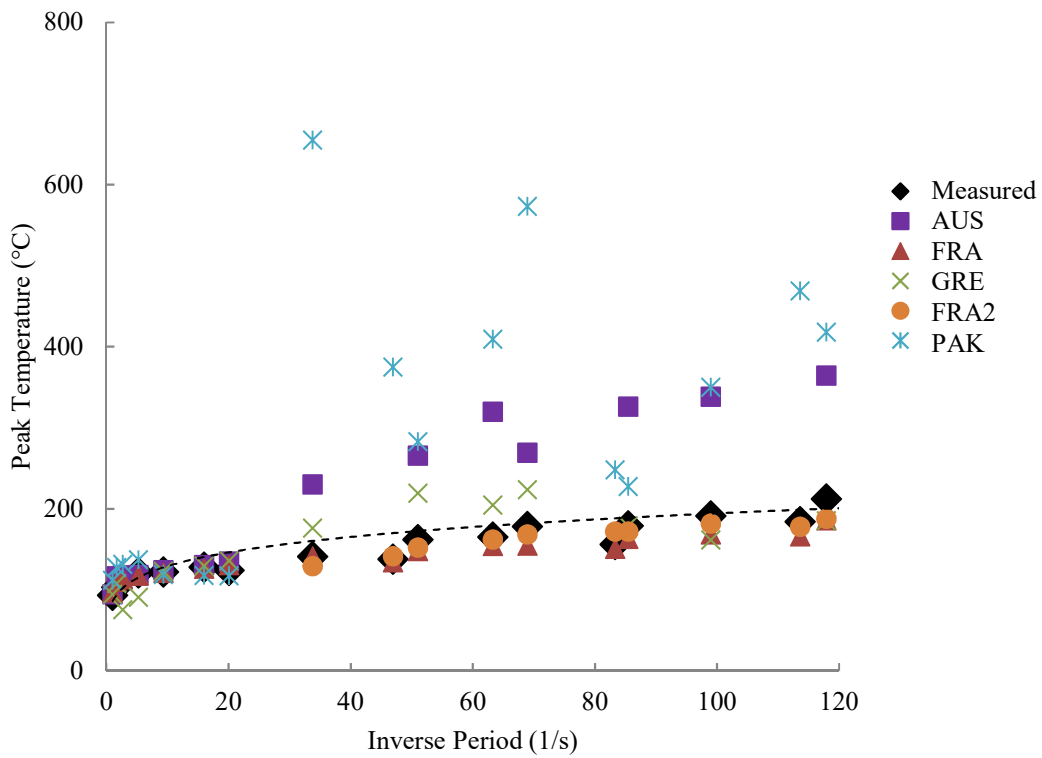


FIG. VII-23. Peak temperature vs. inverse period for Transients B1-B19 with natural circulation

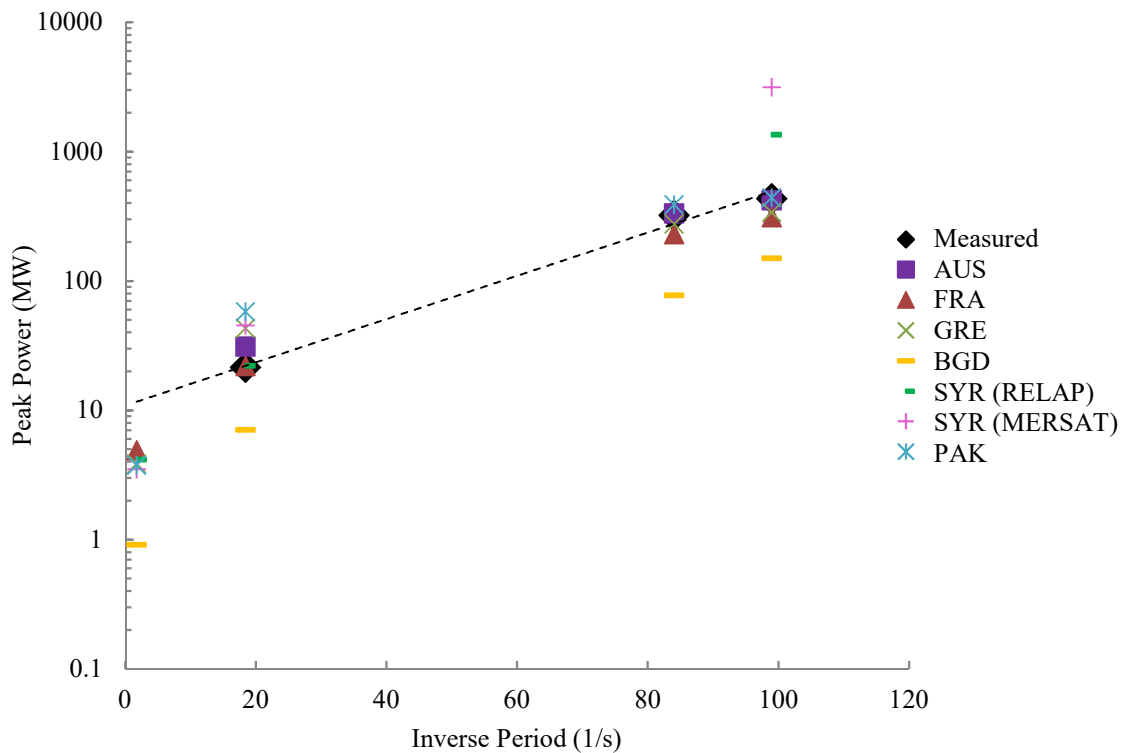


FIG. VII-24. Peak power vs. inverse period for Transients B20-23 with forced flow (500 gpm)

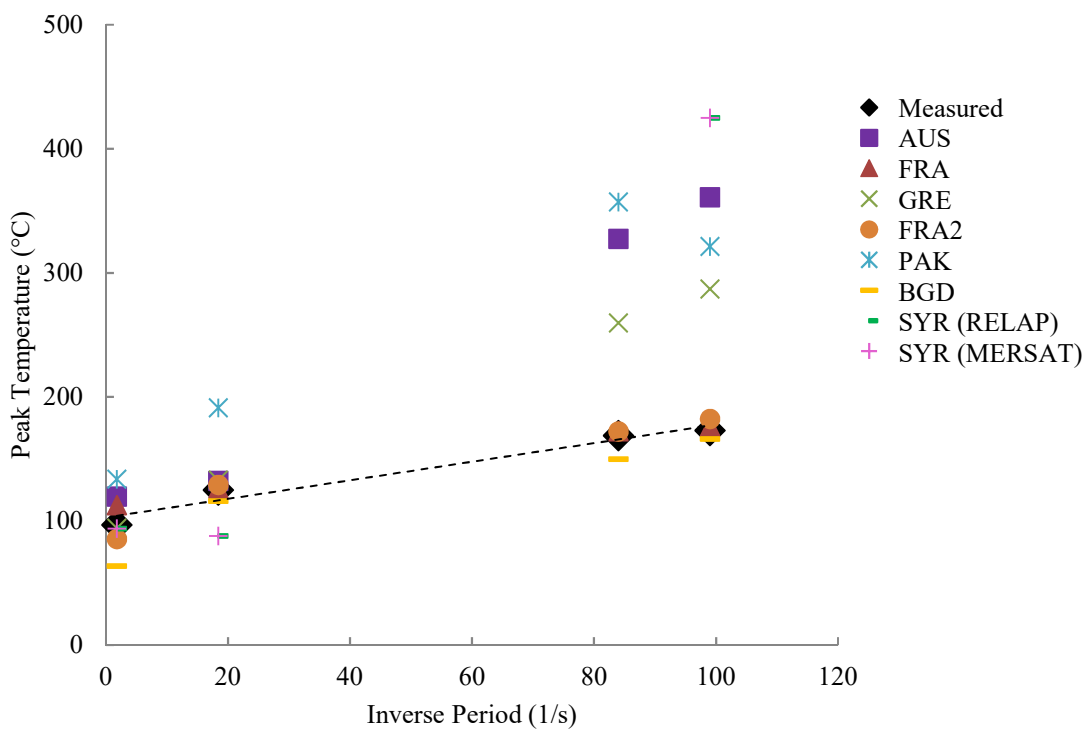


FIG. VII-25. Peak temperature vs. inverse period for Transients B20-23 with forced flow (500 gpm)

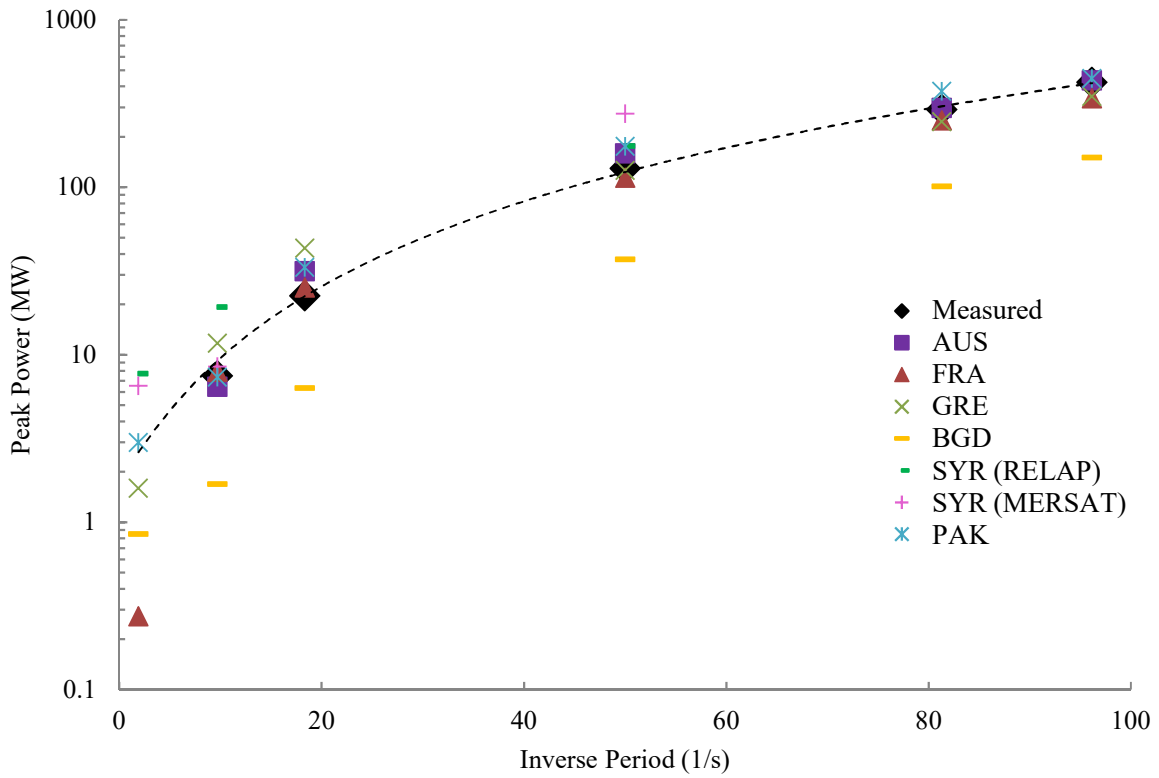


FIG. VII-26. Peak power vs. inverse period for Transients B24-B29 with forced flow (1000 gpm)

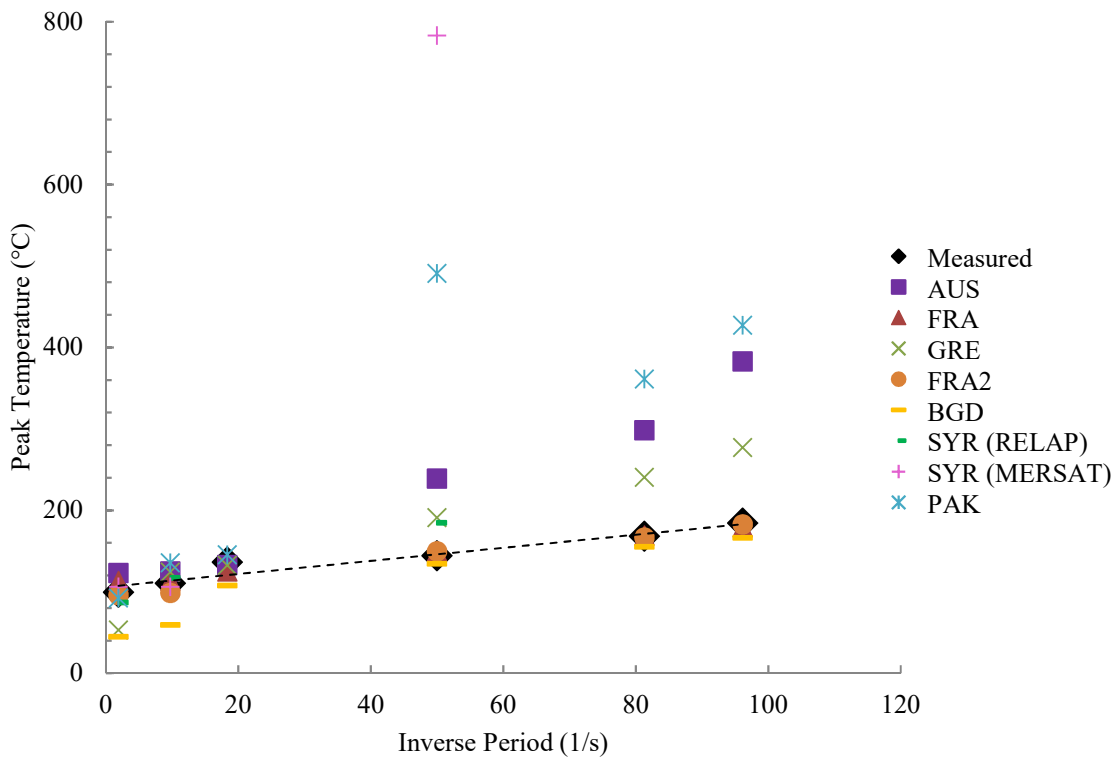


FIG. VII-27. Peak temperature vs. inverse period for Transients B24-B29 with forced flow (1000 gpm)

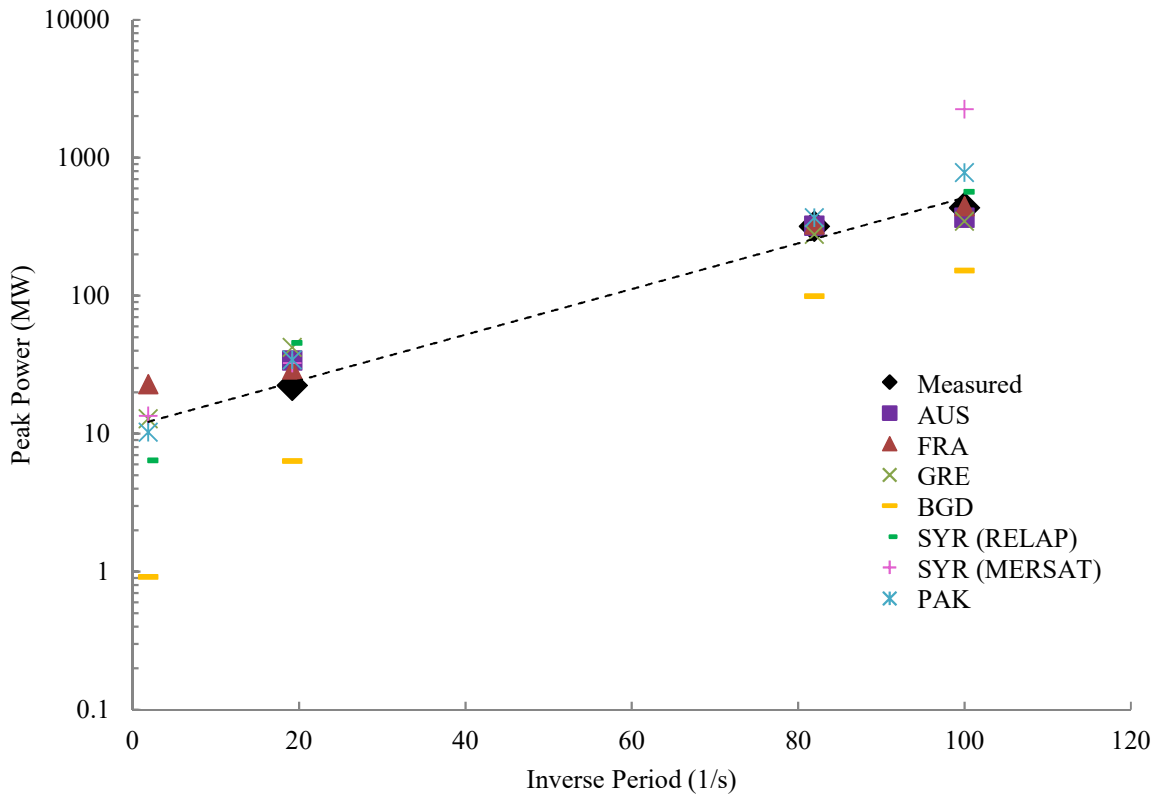


FIG. VII-28. Peak power vs. inverse period for Transients B30-B33 with forced flow (2500 gpm)

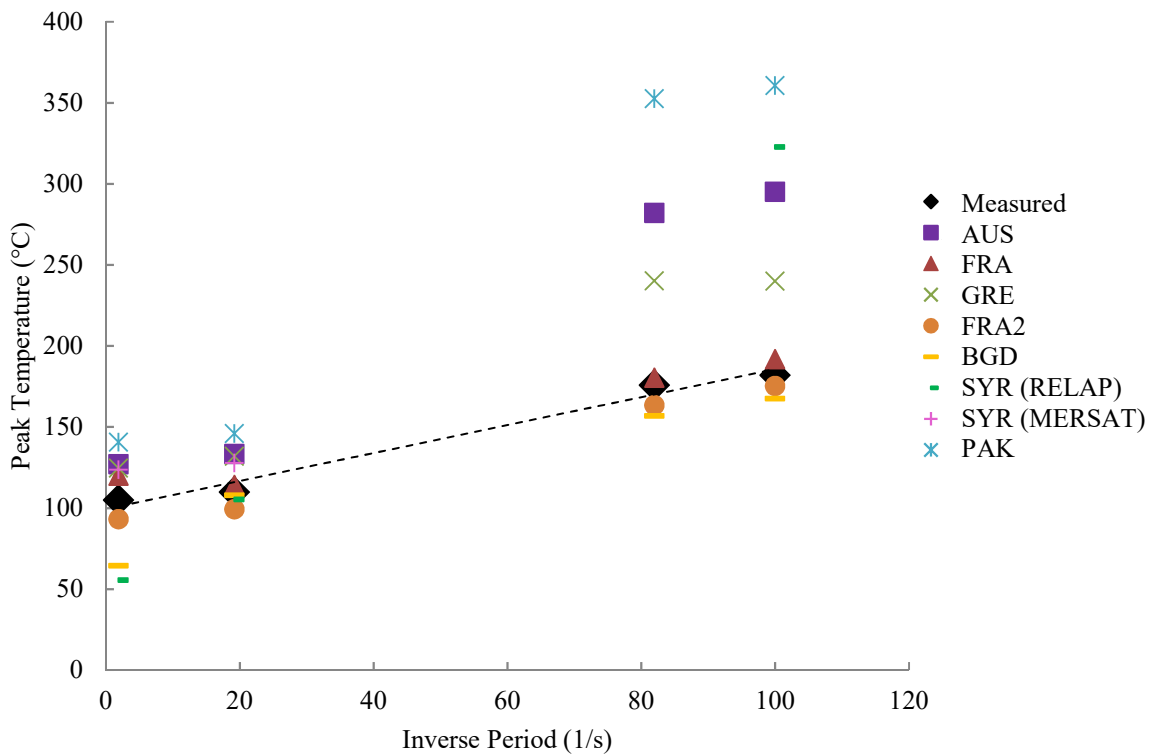


FIG. VII-29. Peak temperature vs. inverse period for Transients B30-B33 with forced flow (2500 gpm)

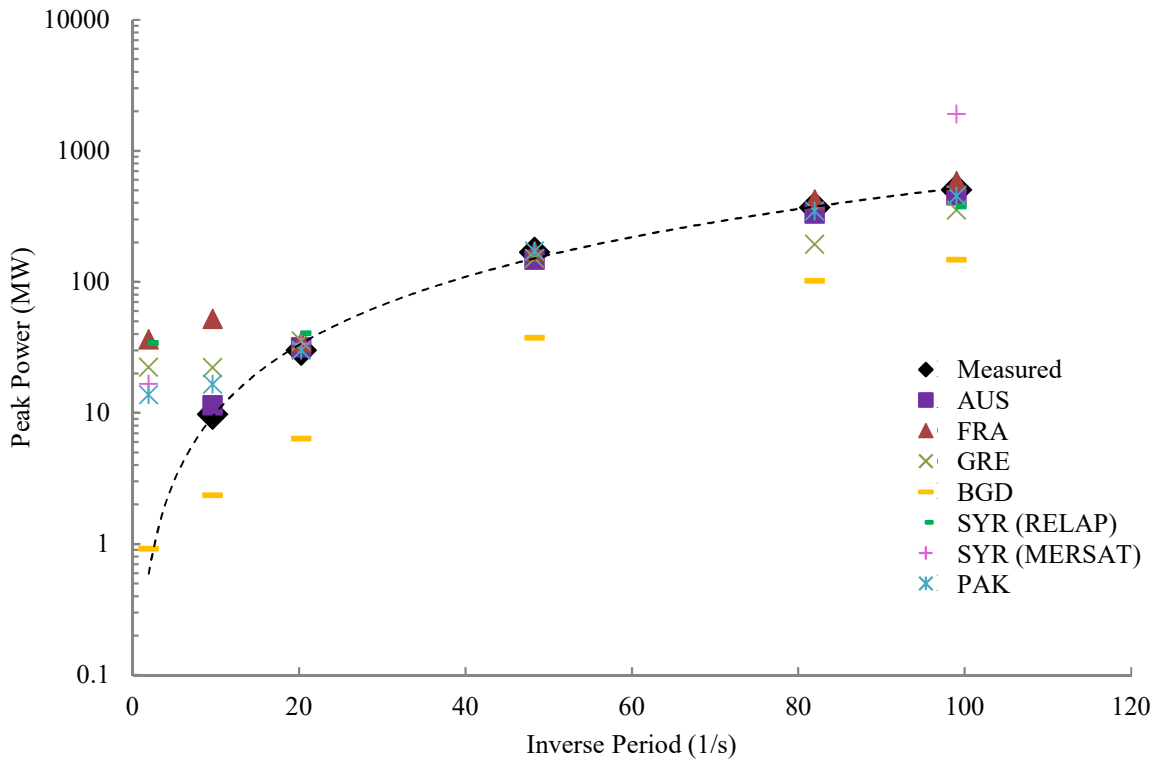


FIG. VII-30. Peak power vs. inverse period for Transients B34-B39 with forced flow (5000 gpm)

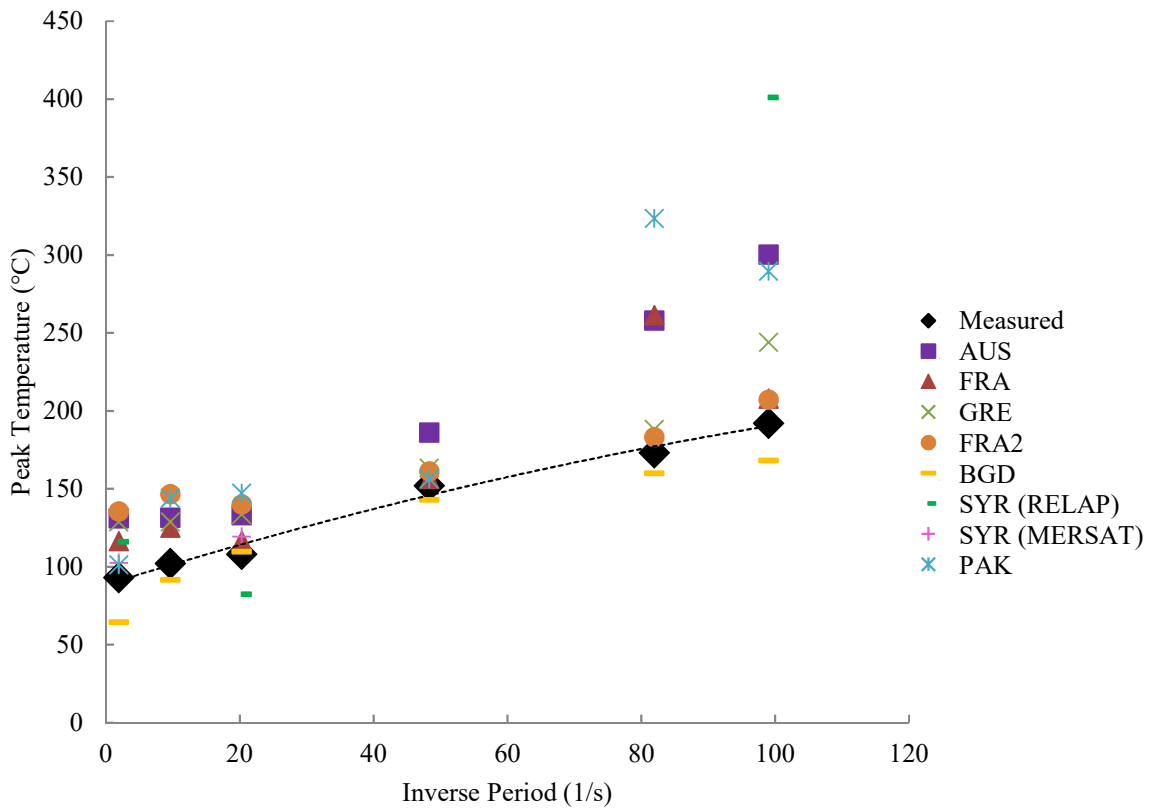


FIG. VII-31. Peak temperature vs. inverse period for Transients B34-B39 with forced flow (5000 gpm)

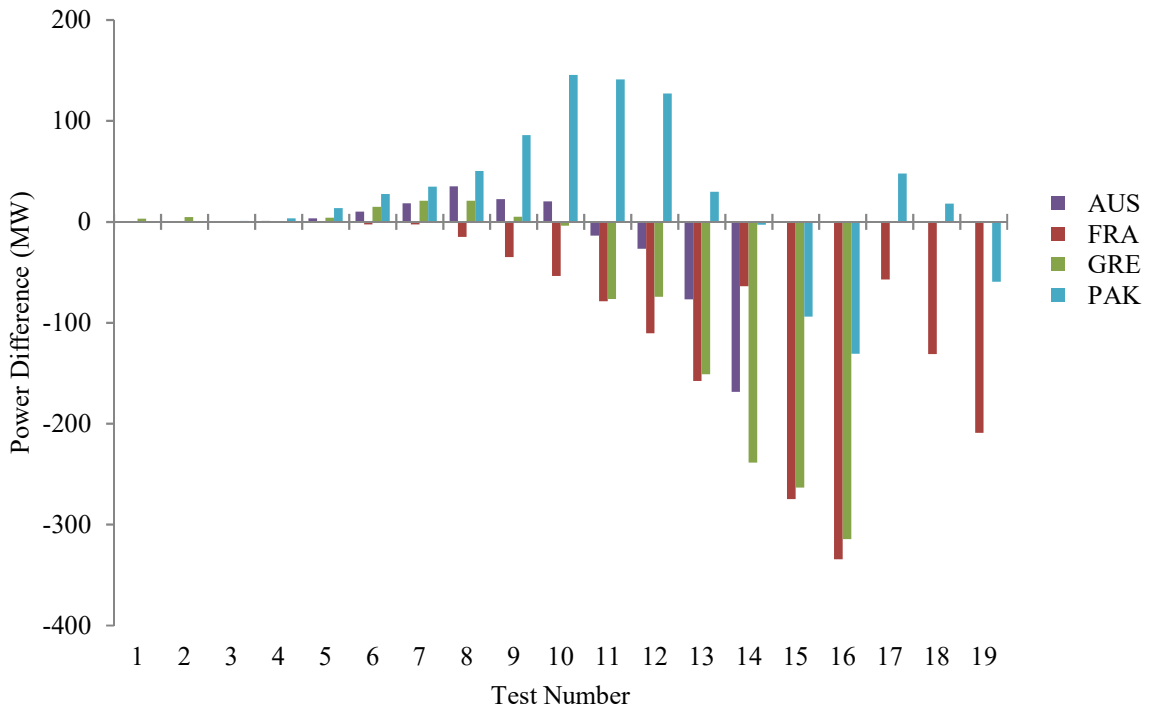


FIG. VII-32. Peak power difference ($P_{calc}-P_{exp}$) for Transients B1-B19 with natural circulation

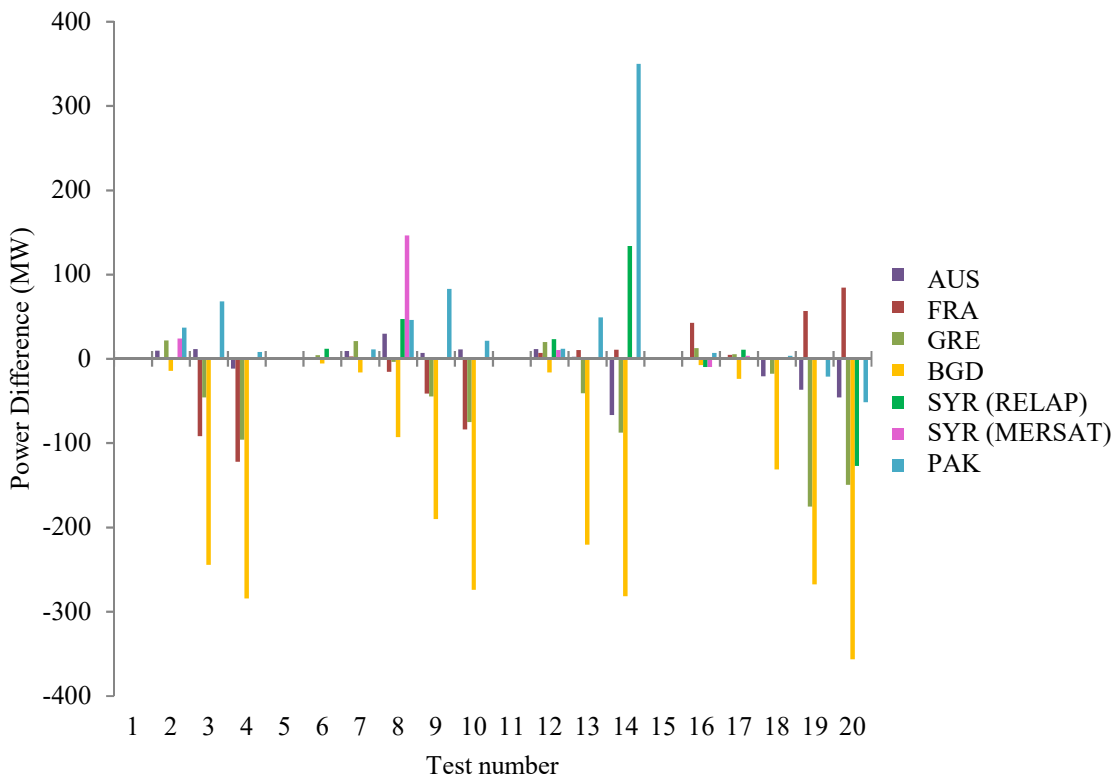


FIG. VII-33. Peak power difference ($P_{calc}-P_{exp}$) for Transients B20-B39 with forced flow (500–5000 gpm)

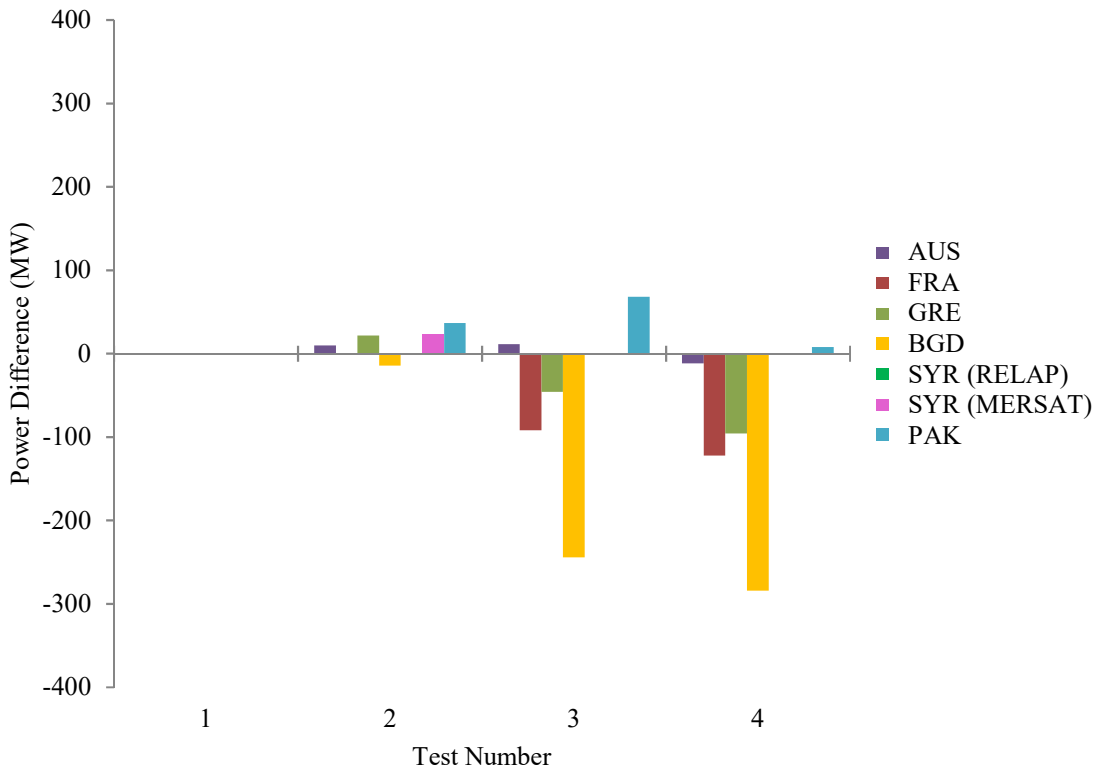


FIG. VII-34. Peak power difference ($P_{calc}-P_{exp}$) for Transients B20-B23 with forced flow (500 gpm)

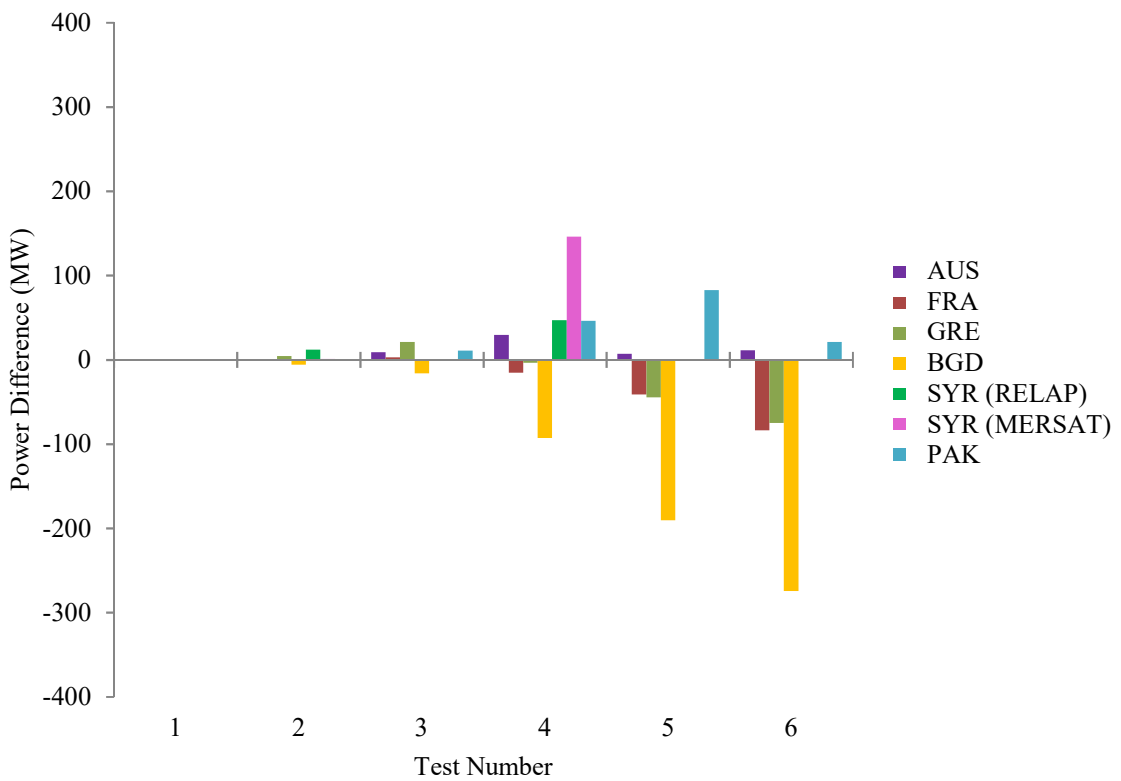


FIG. VII-35. Peak power difference ($P_{calc}-P_{exp}$) for Transients B24-B29 with forced flow (1000 gpm)

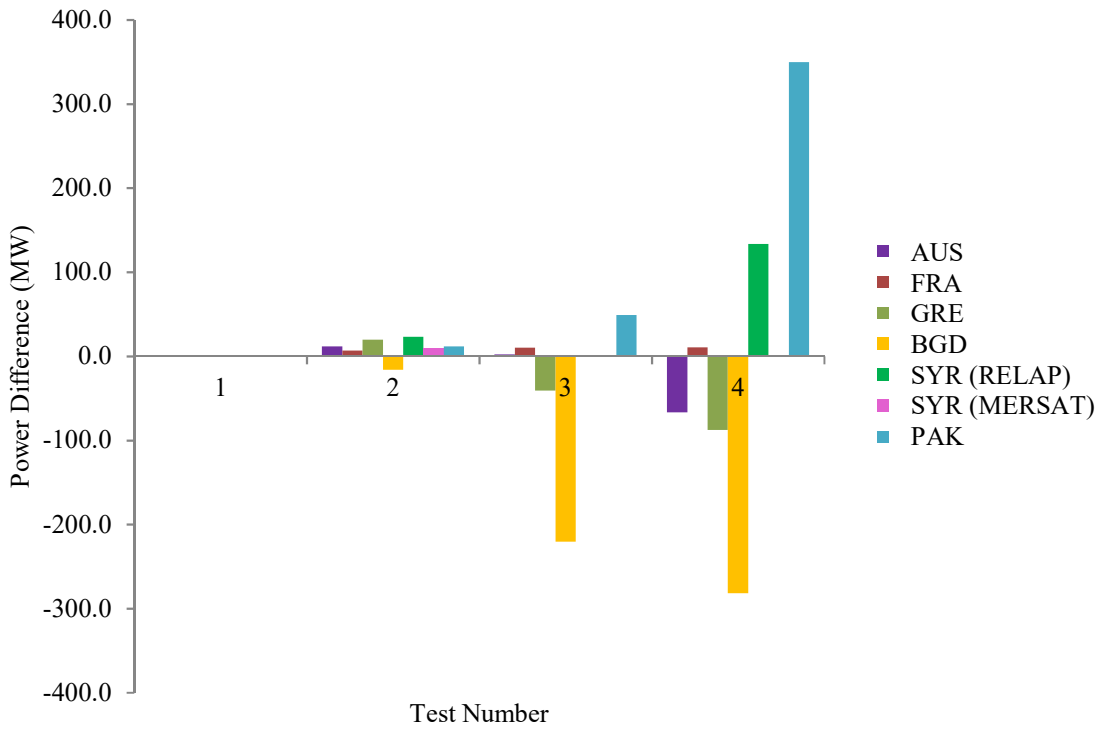


FIG. VII-36. Peak power difference ($P_{calc} - P_{exp}$) for Transients B30-B33 with forced flow (2500 gpm)

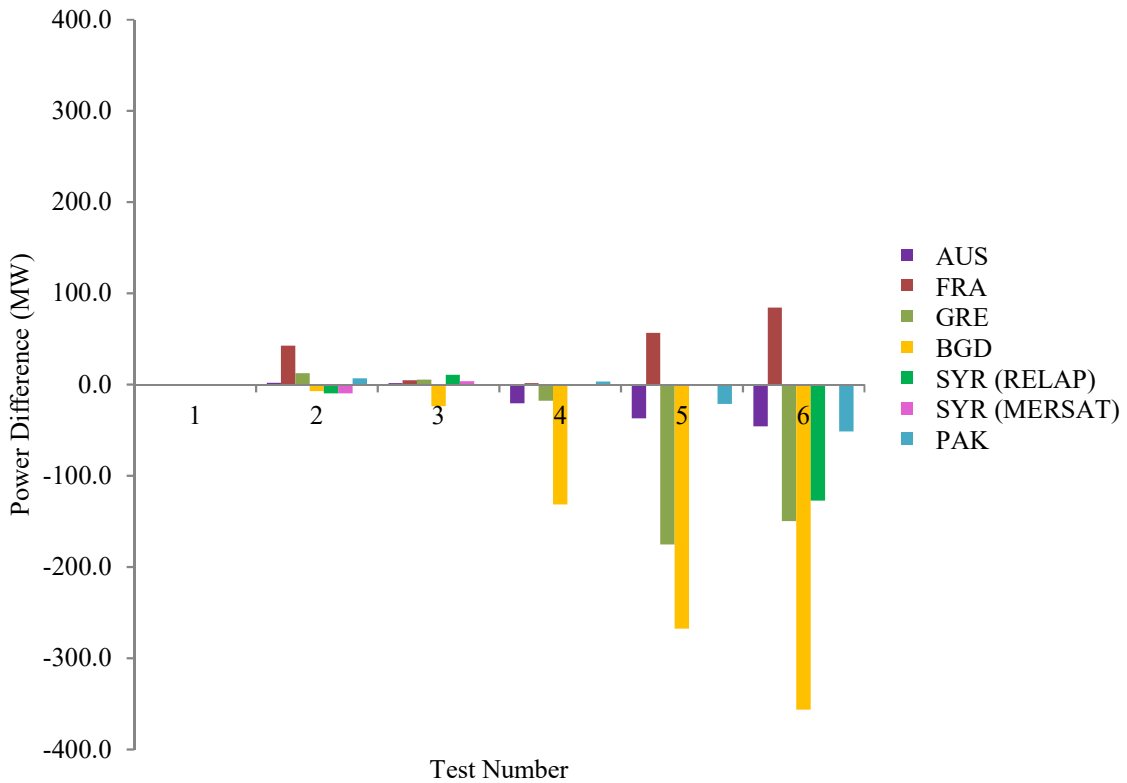


FIG. VII-37. Peak power difference ($P_{calc} - P_{exp}$) for Transients B34-B39 with forced flow (5000 gpm)

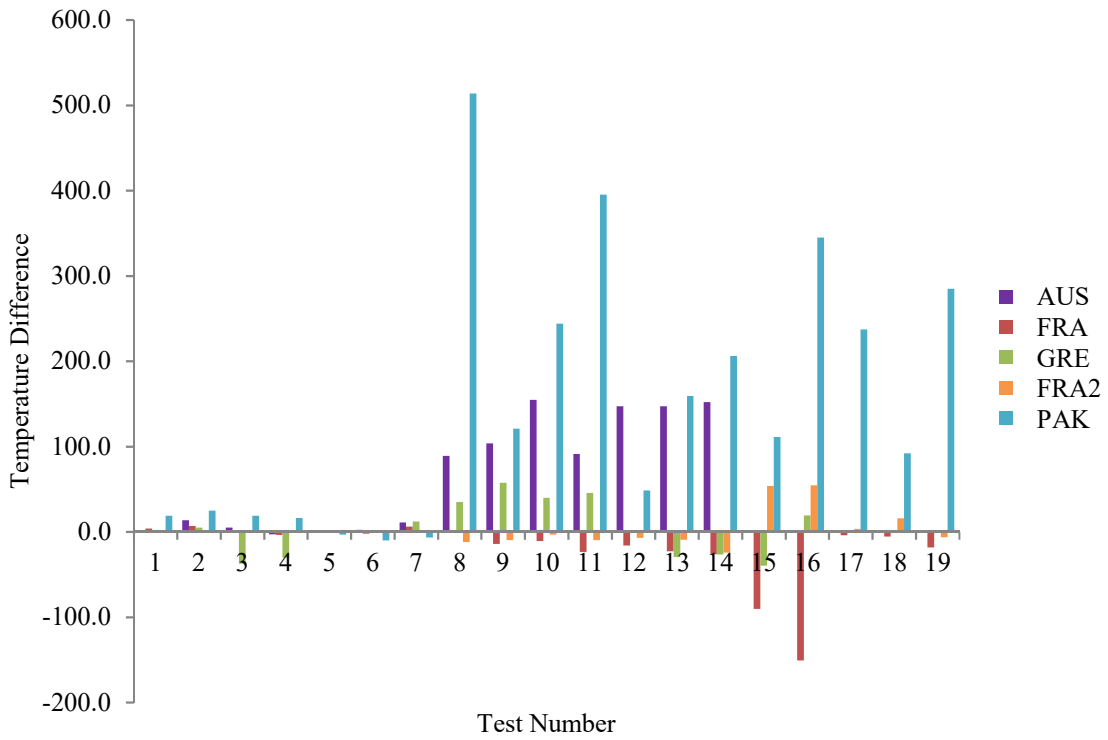


FIG. VII-38. Peak temperature difference ($T_{calc} - T_{exp}$) for B1-B19 with natural circulation

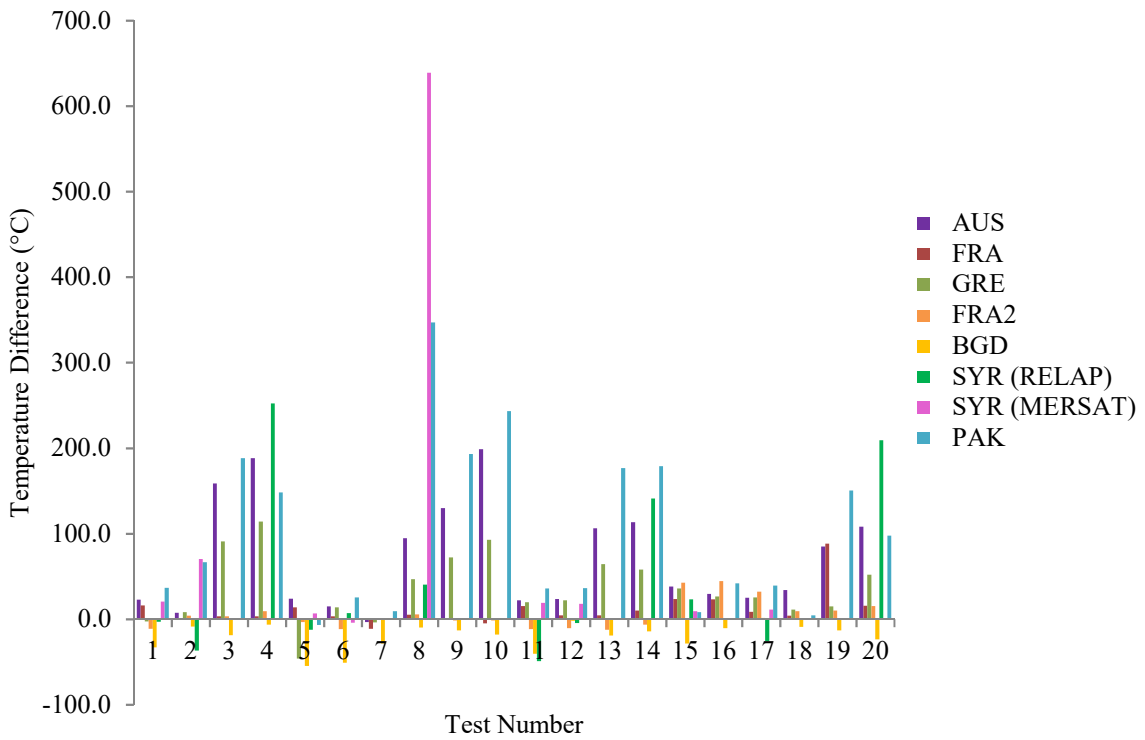


FIG. VII-39. Peak temperature difference ($T_{calc} - T_{exp}$) for B20-B39 with forced flow (500–5000 gpm)

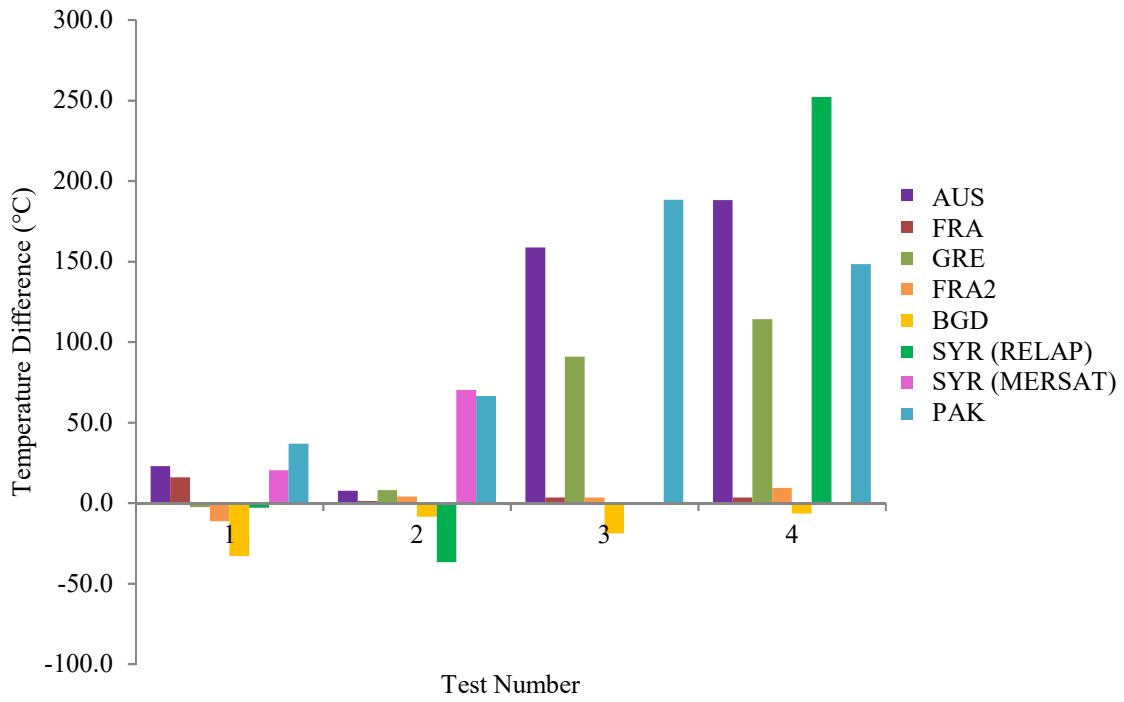


FIG. VII-40. Peak temperature difference ($T_{calc} - T_{exp}$) for Transients B20-B23 with forced flow (500 gpm)

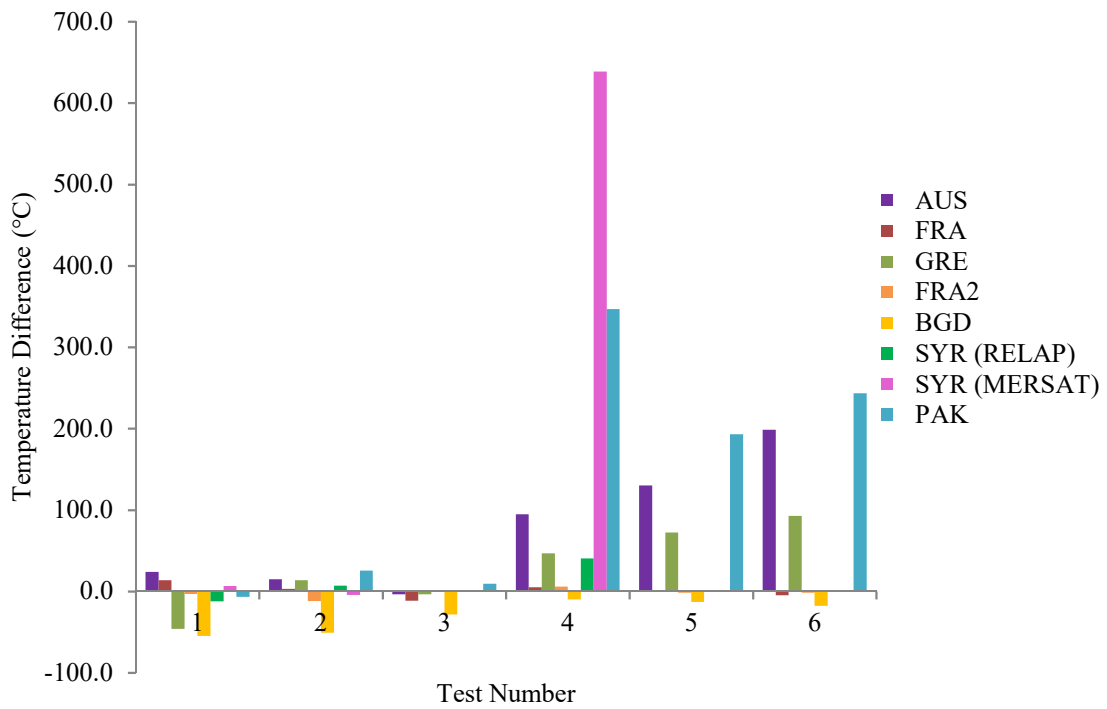


FIG. VII-41. Peak temperature difference ($T_{calc} - T_{exp}$) for Transients B24-B29 with forced flow (1000 gpm)

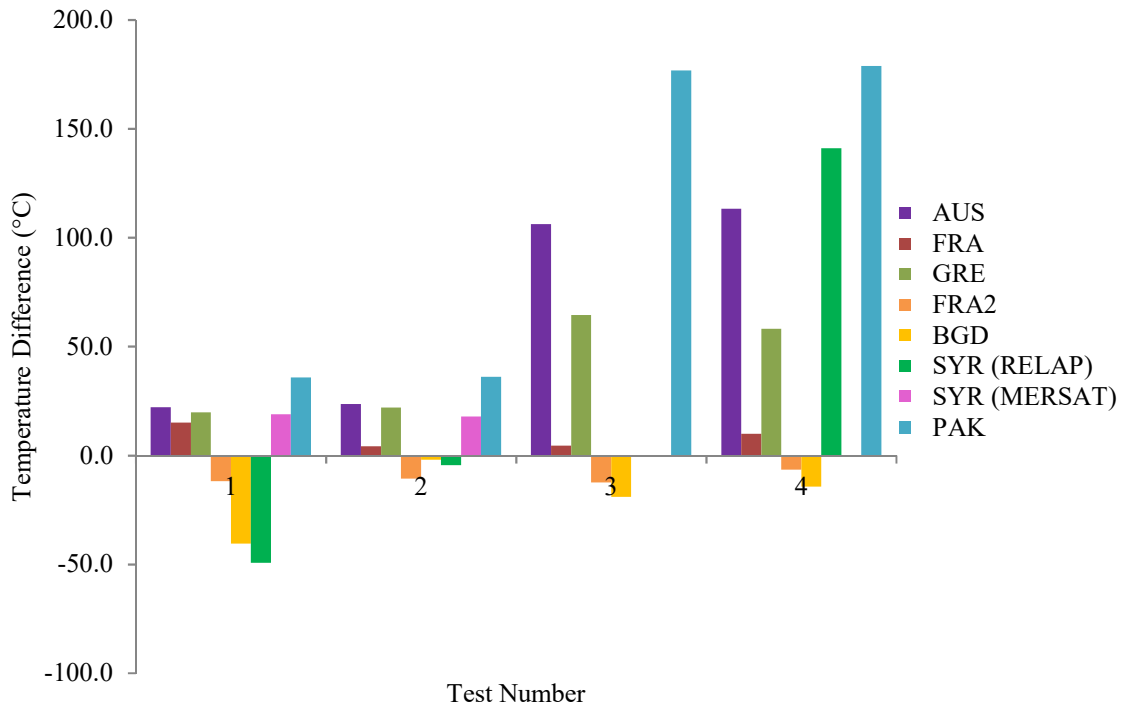


FIG. VII-42. Peak temperature difference ($T_{calc} - T_{exp}$) for Transients B30-B33 with forced flow (2500 gpm)

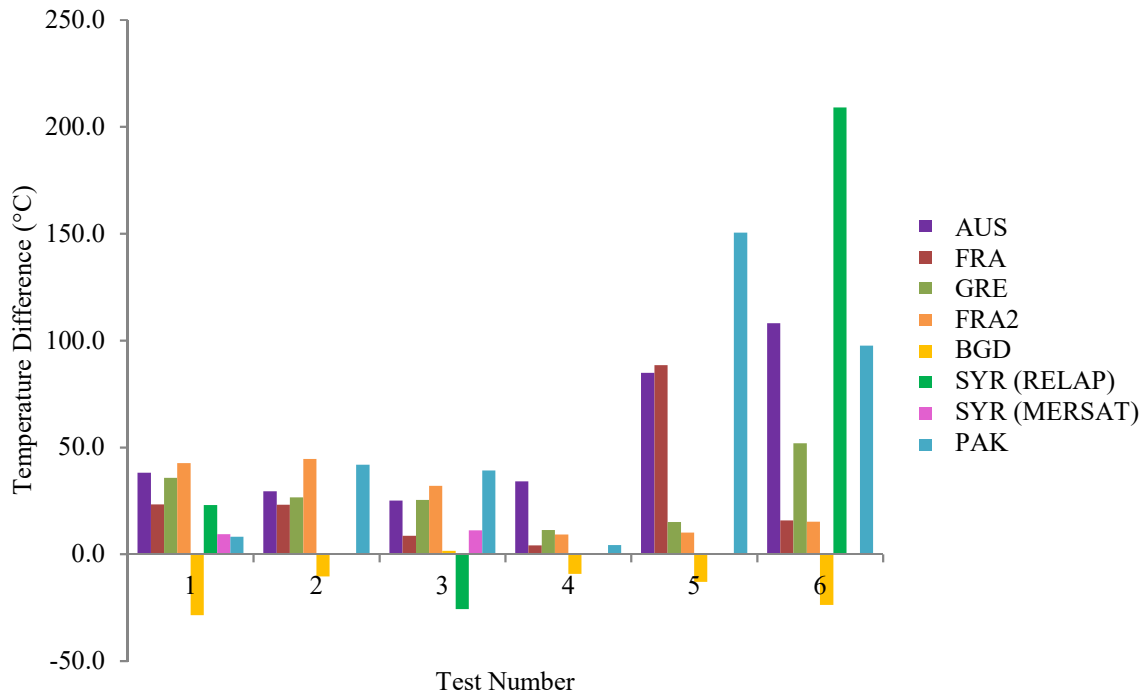


FIG. VII-43. Peak temperature difference ($T_{calc} - T_{exp}$) for Transients B34-B39 with forced flow (5000 gpm)

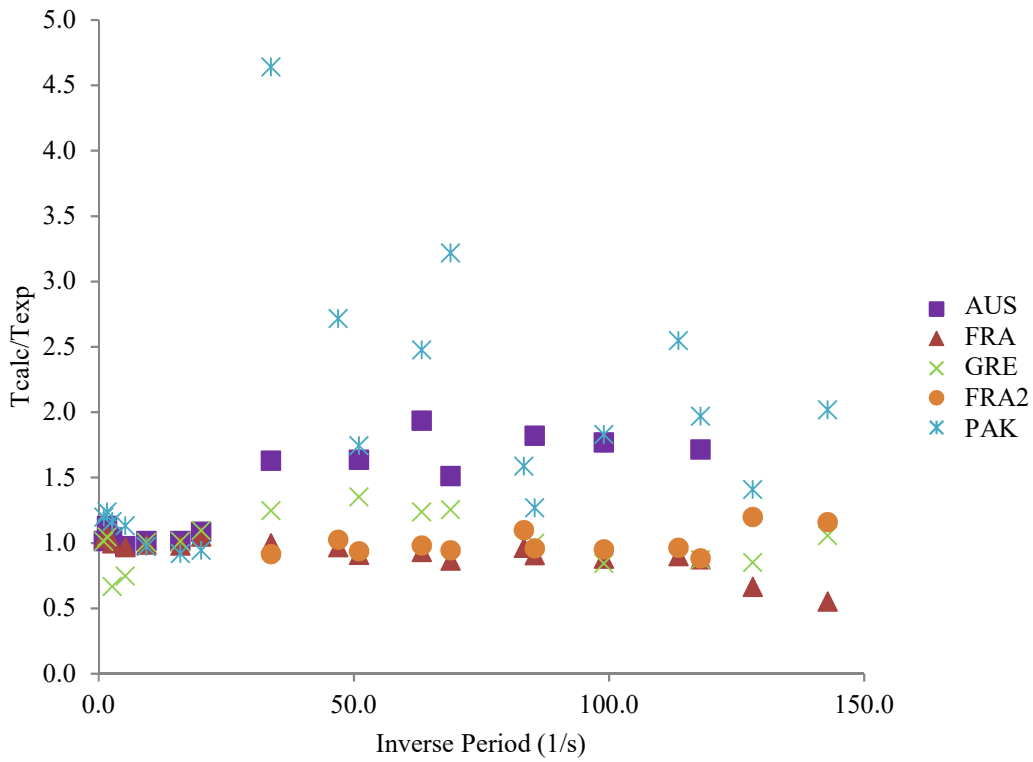


FIG. VII-44. Temperature ratio (T_{calc}/T_{exp}) for Transients B1-B19 with natural circulation

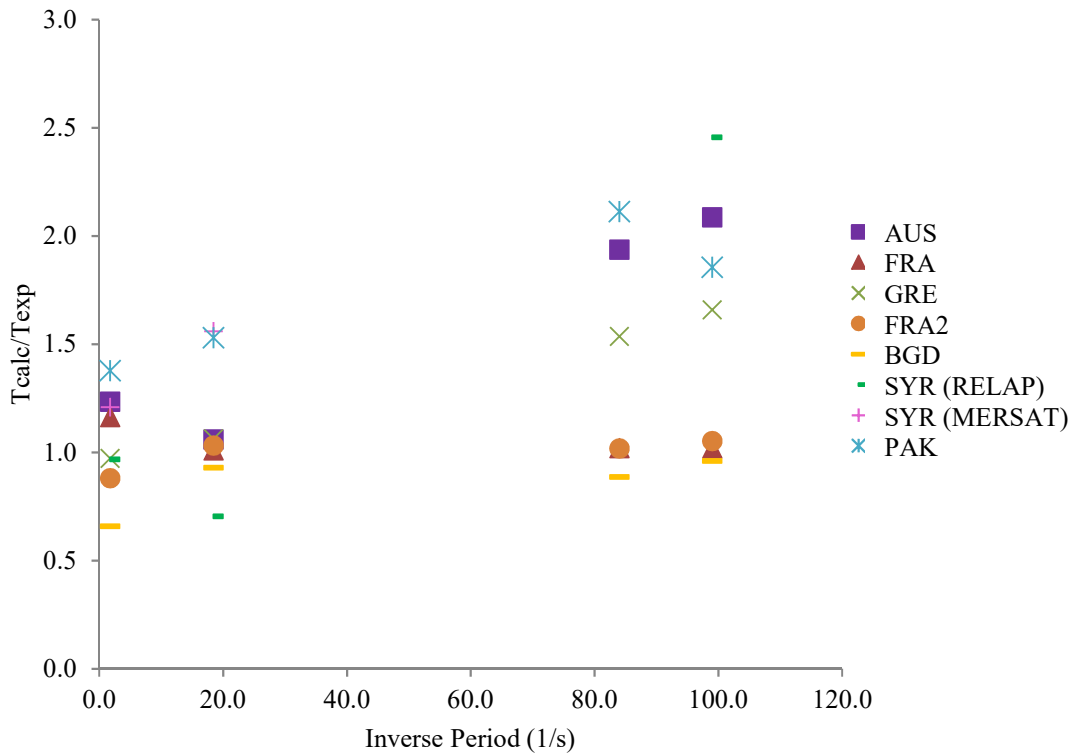


FIG. VII-45. Temperature ratio (T_{calc}/T_{exp}) for Transients B20-B23 with forced flow (500 gpm).

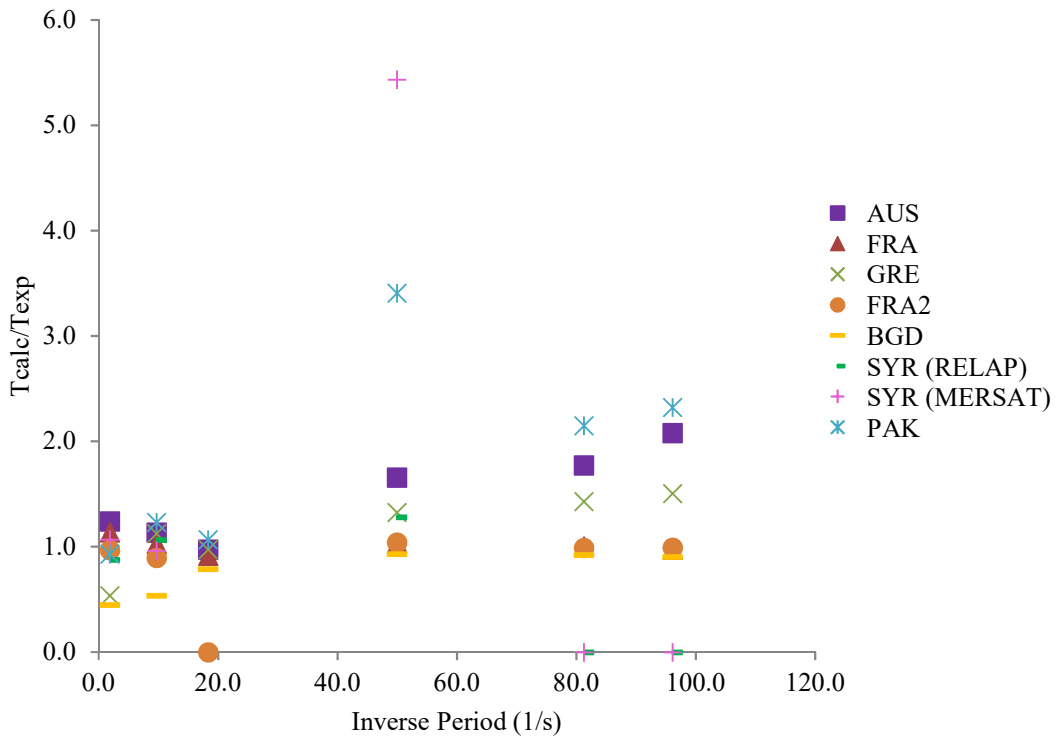


FIG. VII-46. Temperature ratio (T_{calc}/T_{exp}) for Transients B24-B29 with forced flow (1000 gpm)

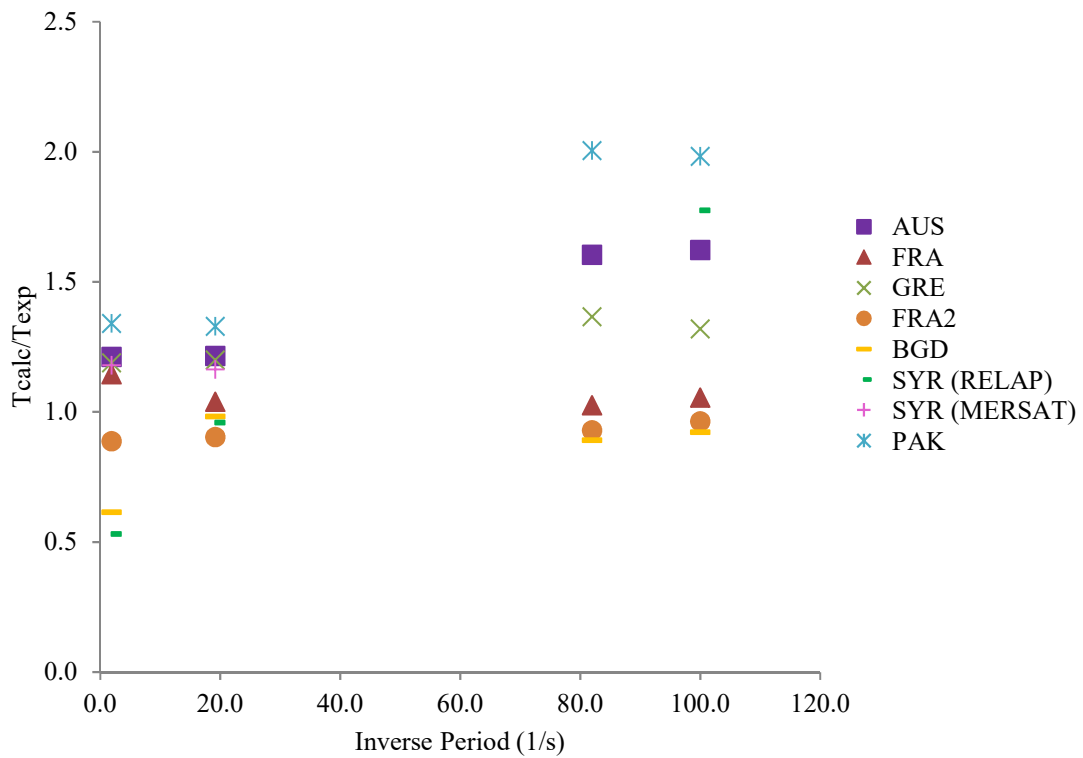


FIG. VII-47. Temperature ratio (T_{calc}/T_{exp}) for Transients B30-B33 with forced flow (2500 gpm)

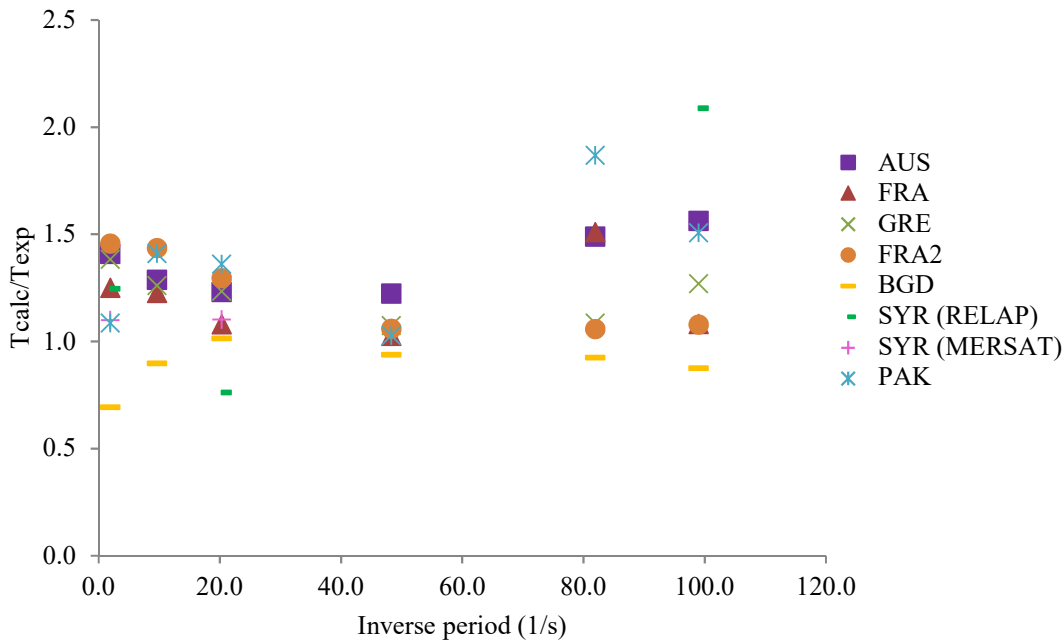


FIG. VII-48. Temperature ratio (T_{calc}/T_{exp}) for Transients B34-B39 with forced flow (5000 gpm)

VII-4. CONCLUSIONS

The work herein has illustrated the capability of a number of codes and methods to consistently predict reactivity insertion transients with a variable degree of accuracy and has identified a notable dependency of simulation results on the reactivity insertion severity (slow vs. fast transients) and flow rate conditions (natural vs. forced flow). Sensitivity studies were performed to determine the influence of several parameters on the calculated results. These studies demonstrated that the choice of a sufficiently small-time step is necessary to capture the oscillatory nature of the power and clad temperature evolutions of the fast-transient B-39. In addition, the choice of ONB correlation is also important, with the Bergles-Rohsenow correlation more suitable for longer reactor periods, and the McAdams correlation for larger reactivity insertions. Finally, this study also examined the sensitivity of the PARET calculations to the coolant temperature and void feedback coefficients. The calculated results of short period transients depend heavily on both feedback methods: a slightly larger void coefficient causes the power and temperature oscillations to be damped, while a smaller coolant temperature coefficient provides insufficient feedback and results in calculation failure due to high clad temperature. Also, the inclusion of a void feedback coefficient vertical profile compared to using a uniform profile, reduces the maximum cladding temperature significantly in transient cases where boiling occurs. As such, use of the most appropriate ONB and DNB correlations and calculation time step is needed. In addition, the calculations are highly sensitive to the reactivity feedback coefficient values.

A notable user effect was identified among users of the same code. In general, the discrepancies observed among modelling teams using the same code may be attributed to the different nodalization schemes (e.g., channels and axial and radial nodes) different methodologies followed (e.g., experimental based power profile vs. calculated) and/or different input parameters (e.g., misinterpretation of specifications, assumptions, unknown values). Among others, fuel and cladding thermal properties, reactivity insertion time and hydraulic parameters, which may be important for natural convection, such as resistance coefficients. It has also been

observed that kinetic parameters and feedback coefficients significantly affect the course of the transient. For example, a simulation using uniform vs. non-uniform void profile predicted considerably different temperature estimates.

As a conclusion it may be stated that validating the code along with the available set of correlations against experimental data is a continuous effort that is worth pursuing since it has been found that results in this benchmark analysis are quite sensitive to various code options. This indicates that without proper training and code validation a user could end up with completely inaccurate results, both qualitatively and quantitatively, which would lead to incorrect interpretation of mechanisms behind transient response as well as incorrect conclusions. This in turn suggests an important finding related to safety analysis for research reactors, *i.e.*, that in order to avoid incorrect results and associated conclusions, a code has to be used with caution to predict or extrapolate certain aspects of severe accident behavior for severe reactivity insertion situations.

That can be drawn from this benchmark analysis are the following:

1. There are a lot of subtleties involved in developing computer code models and inputs. The SPERT IV benchmark analysis can not be considered purely thermal-hydraulics but rather a coupled neutronics/thermal-hydraulics problem.
2. The results represent the modelling state of analysis capability in the research reactor community, which at this time does not allow drawing conclusions on the best model or the best code.
3. There is a clear identified user effect among modelling teams using the same code.
4. Sensitivity analysis and adequate training are recommended as possible ways to reduce user effect. Emphasis on this being a coupled neutronics/thermal-hydraulics problem was identified as opposed to a purely thermal-hydraulics problem.

REFERENCES TO ANNEX VII

- [VII-1] INTERNATIONAL ATOMIC ENERGY AGENCY, Research Reactor Benchmarking Database: facility specification and experimental data, Proceedings Series, IAEA, Vienna (2013).
- [VII-2] OBENCHAIN, C. F., PARET-A Program for the Analysis of Reactor Transients, US AEC Technical Report IDO-17282, Phillips Petroleum Company (1969).
- [VII-3] WOODRUFF, W. L., SMITH, R. S, A users guide for the ANL version of the PARET Code, PARET/ANL, ANL/RERTR/TM-16, (2001).
- [VII-4] CHATZIDAKIS, S., IKONOMOPOULOS, A., DAY, S.E., PARENT-ANL modelling of a SPERT IV experiment under different departure from nucleate boiling correlations, Nuclear Technology 177 (2012) 119-131.
- [VII-5] WOODRUFF, W. L., A kinetics and thermal-hydraulics capability for the analysis of research reactors, Nuclear Technology 64 (1984) 196.
- [VII-6] MASANORI K., EUREKA-2/RR: A Computer Code for the Reactivity Accident Analyses in Research Reactors, Japan Atomic Energy Agency.
- [VII-7] EYMARD, C., CATHARE2 V2. 5 User Manual, SSTH/LDAS/EM/2004-040, CEA, Grenoble, France (2005).
- [VII-8] VAN DORSSELAERE, J., P., SERPIAN, C., CHATELARD, P., JACQ, F., FLEUROT, J., GIORDANO, P., REINKE, N., LUTHER, W., The ASTEC integral code for severe accident simulation, Nucl. Technol. 165 (2009) 293-307.
- [VII-9] HAINOUN, A., GHAZI, N., ALHABIT, F., Simulation of LOFA and RIA for the IEA-R1 Research Reactor using the code MERSAT, Ann. of Nucl. Energy **35** (2008) 2093–2104.
- [VII-10] NUCLEAR REGULATORY COMMISSION, RELAP5/MOD3.3 Code Manuals, Idaho National Engineering Laboratory, NUREG/CR-5535 (1995).
- [VII-11] ORGANISATION FOR ECONOMIC CO-OPERATION AND DEVELOPMENT/NUCLEAR ENERGY AGENCY, User effects on the transient system code calculations, NEA/CSNI/R (1995).

ANNEX VIII

BENCHMARK CONSOLIDATED RESULTS AGAINST EXPERIMENTAL DATA FROM SPERT IV STATICS

S. E. DAY*, G. BRAOUDAKIS**, L. WONG**

* McMaster Nuclear Reactor, McMaster University, 1280 Main St. W., Hamilton, Ontario, Canada, L8S 4K1

** Australia's Nuclear Science and Technology Organization (ANSTO), New Illawarra Road,
Lucas Heights NSW 2234 Australia

Annex Consolidator: S. E. Day

Abstract.

The IAEA CRP (CRP 1496) on 'Benchmarking, against Experimental Data, of the Neutronic and Thermalhydraulic Computational Methods and Tools for Operation and Safety Analysis for Research Reactors' provides a unique opportunity to benchmark and compare the accuracy and efficiency of both off-the-shelf and locally developed computational tools to a wide set of experimental research reactor benchmark analysis. In the scope of this project, various analysis groups have evaluated the SPERT IV benchmark analysis – consisting of a variety of commissioning experiments and multiple sets of Reactivity Insertion Accident (RIA) measurements. This report is focused on the commissioning experiments and associated measurements, referred to herein as the 'Statics' or neutronic section of the SPERT IV benchmark analysis. It summarizes and compares the analysis methodologies adopted, the code systems employed, and the simulation results generated by the various analysis groups. A comparison of the computational results to available experimental results is also provided in this report.

VIII-1. FOREWORD

The SPERT IV benchmark analysis is divided into two sections: (i) statics and (ii) transient. The static portion of the SPERT IV D-12/25 core benchmark analysis provides a comprehensive set of experimental results for neutronics comparison. The benchmark specifications have been documented in Ref.s [VIII-1] and [VIII-2]. The participation for the statics (neutronics) section of the benchmark analysis is summarized in the following table.

TABLE VIII-1. SPERT IV BENCHMARK ANALYSIS PARTICIPANTS

Group	Criticality k_{eff}	Rod Worth	Void Reactivity	Temperature Reactivity	Flux Wires	Kinetic Parameters
AUS	✓	✓	✓	✓	✓	✓
BGD	✓	✓	✓	-	✓	✓
FRA	✓	✓	✓	✓	✓	✓
FRA2	-	✓	Partial	-	-	✓
PAK	-	Partial	Partial	Partial	Partial	✓
SYR	✓	✓	Partial	✓	Partial	✓

VIII-2. DESCRIPTION OF FACILITY

SPERT IV was a light water cooled and moderated, pool type reactor with provisions for both upward forced and natural convection cooling. The reactor core was suspended from a moveable bridge and positioned near the bottom of the reactor pool.

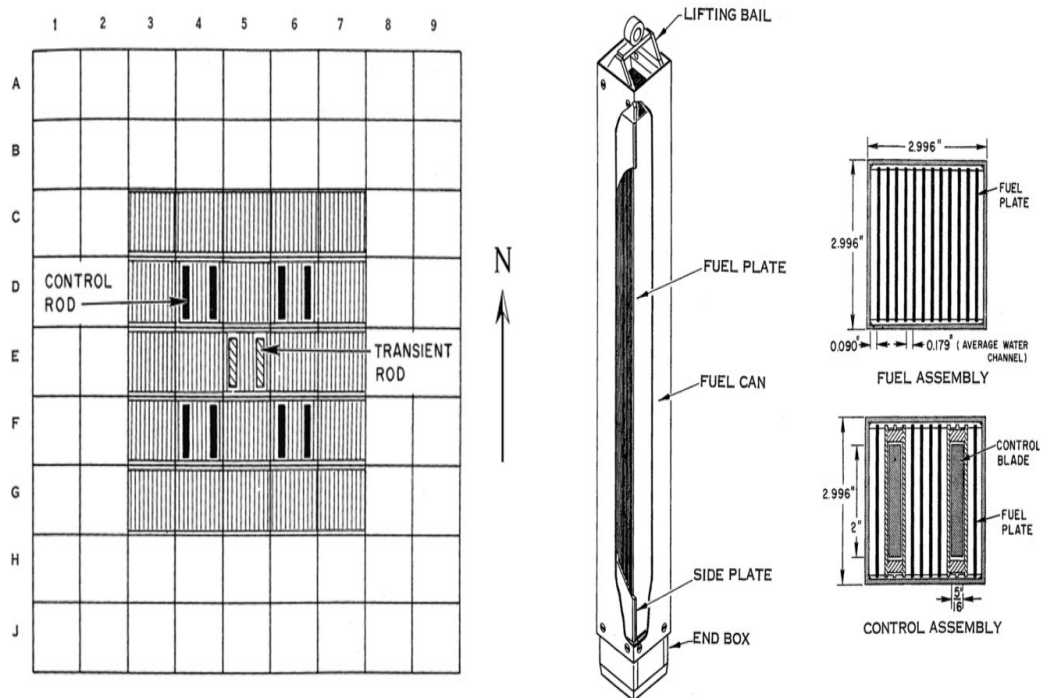


FIG. VIII-1. SPERT IV reactor core configuration and fuel assembly details.

TABLE VIII-2. SPERT IV GENERAL REACTOR DATA

Parameter	Value
Type of Reactor	Open Pool MTR-type
Core shape	25 assemblies in 5 x 5 array
Fuel Type	UAl _x -Al Alloy, Al-clad flat plate fuel
Enrichment	HEU (93%)
Site Elevation	Approximately 1500 m above sea level
Pool height	7.62 m
Pool diameter	6.096 m
Hydrostatic Head	5.4846 m
Reference Pressure of the Facility	Pool open to atmosphere
Nominal Reference Temperature	Room Temperature (20°C)
Coolant (type and flow direction)	Light water, natural circulation or forced upward flow
Moderator	Light water
Reflector	Light water
Nominal Flow Rate	Varied with Test

The SPERT IV D-12/25 core was the final aluminium plate-type core studied as part of the SPERT Project. The reactor core was composed of 25 fuel assemblies (20 standard and 5 control fuel assemblies) in a square five-by-five section of the nine-by-nine supporting grid as shown in Fig. VIII-1. Apart from the positions of the four control fuel assemblies (which were moved to more central grid positions), the D-core was identical to the D-12/25 core used in the destructive test series in the SPERT I Facility.

The Type-D fuel plates were HEU UAl_x-Al alloy fuel clad in aluminium. Each Type-D standard fuel assembly contained 12 removable flat fuel plates, housed in an aluminium assembly can. Four gang-operated boron-alloy double-blade control rods and one central transient rod of the same style were accommodated in modified six-plate fuel assemblies. General reactor data and fuel assembly specifications can be seen in Table VIII-2 and Table VIII-3. A full description of the SPERT IV D-12/25 core is available in Reference [VIII-1].

TABLE VIII-3. SPERT IV FUEL ASSEMBLY SPECIFICATIONS

Fuel Assembly	
Assembly geometry	Rectangular
No of std assemblies	20
No of control assemblies	5
No of plates per std assembly	12
No of plates per control assembly	6
Total No of fuel plates	270
Fuel Plate	
Plate material	Al 6061
Plate geometry	Straight
Plate width	0.06660 m
Plate half-thickness	0.000762 m
Clad-fuel gap	None
Fuel	
Fuel material	UAl _x -Al alloy
Fuel half-thickness	0.000254 m
Fuel width	0.06223 m
Active fuel length	0.6096 m
Unfuelled inlet section	0.0142875 m
Unfuelled outlet section	0.0142875 m
Coolant channel	
Thickness	0.0045466 m
Width	0.06660 m
Cross-section	0.000302798 m ²
Perimeter	0.1422908 m

VIII-3. DESCRIPTION OF TOOLS, CODES AND METHODS

The codes used by each group for the two main sections of the benchmark analysis are summarized in Table VIII-4. A short description of the codes, models and methods used by each group is given in the following sections.

TABLE VIII-4. CODES USED BY PARTICIPATING GROUPS

Group	Code	Nuclear data library
AUS	MCNP5	ENDF/B-VI.2
BGD	MVP	JENDL/JEFF3.0
FRA	TRIPOLI-4	JEFF3.1.1
FRA2	SCALE-6.0	ENDF/B-VII.0
PAK	MTR-PC	Not specified
SYR	MCNP-4C	ENDF/B-VI.2

VIII-3.1. Australia: Codes, Tools and Methods

The Australian (AUS) results for the static section of the SPERT benchmark analysis were obtained using MCNP5 1.40. Apart from the calculation of kinetic parameters, all calculations used the neutron cross section library ENDF/B-VI.2. Older cross section libraries were used for isotopes not included in the ENDF/B-VI.2 library. Most elements of the core were modelled explicitly in dimension and material composition. Some simplifications and assumptions to the system geometry were adopted. These include:

- Reactor pool diameter reduction to 1.5 m;
- Flow skirt, lifting bail and perforations in the lower blade guide were not incorporated in the model;
- Transient rod was positioned with the poison section situated from 20 in. below the axial centre of the fuel;
- Tapering at the junction of the poison and aluminium was not included in the model. The degree of control rod tapering was not specified in the reactor description. Thus, a taper was not adopted in the model; instead, there is a horizontal interface between the Binal and Al sections of the control rod, with a 1/2 in. offset to approximate the taper region. This offset was applied to the documented experimental control rod bank position and was incorporated in all models for the static calculation section of the benchmark analysis.

For general k_{eff} calculations the runs used 5000 source particles/cycle and 6000 active and 15 inactive cycles. For the kinetic parameters and the temperature reactivity coefficient 50000 source particles/cycle and 16000 active and 15 inactive cycles were used.

VIII-3.2. Bangladesh: Codes, Tools and Methods

For the static portion of this problem the Bangladesh (BGD) group used the MVP Monte Carlo code, version 2.0. The accompanying nuclear cross section data library is based on the JENDL-3.3 [VIII-1] and JEFF-3.0 compilations. Calculations were performed on a serial machine with processor Intel Core 2 Duo, 2.66 GHz.

A full-core MVP model was constructed to simulate the static experiments (Figs. VIII-2 to VIII-4). This model explicitly included the full geometry of the standard and control fuel assemblies, including lower end boxes and absorber blade guides as described in [VIII-1].

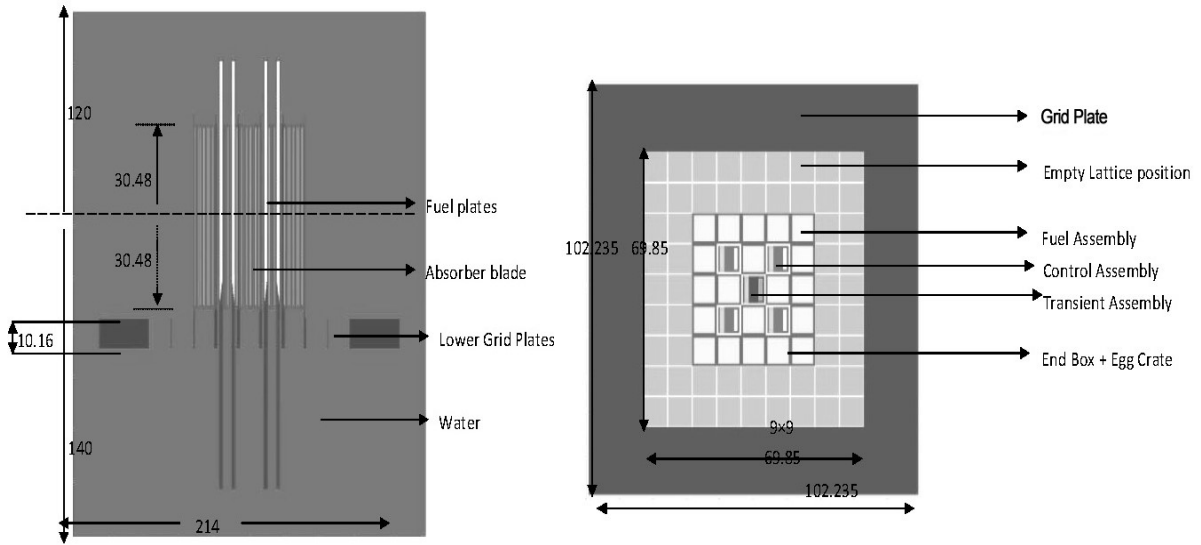


FIG. VIII-2. MVP model of SPERT IV D-Core from BGD.

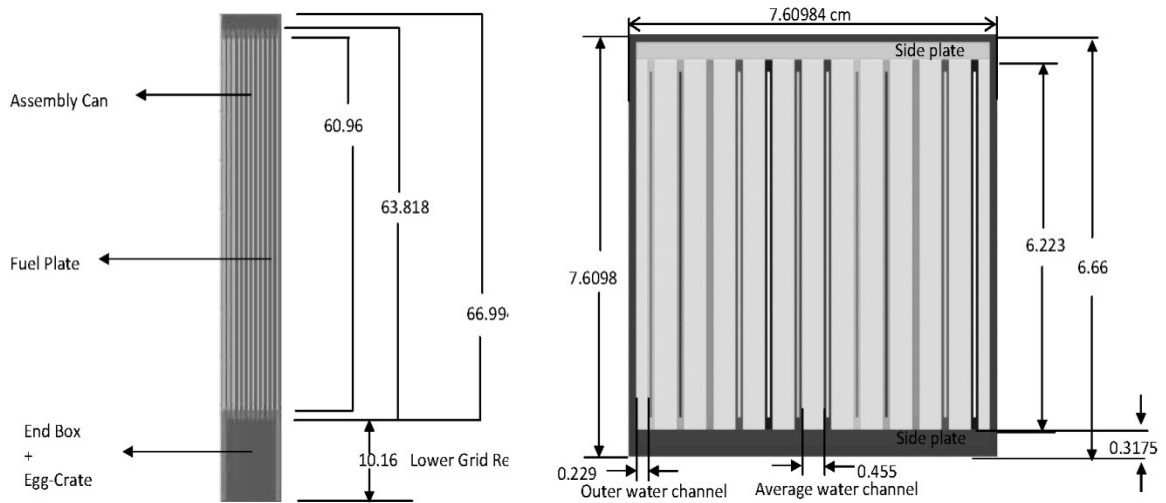


FIG. VIII-3. MVP model of SPERT IV D-Type fuel from BGD.

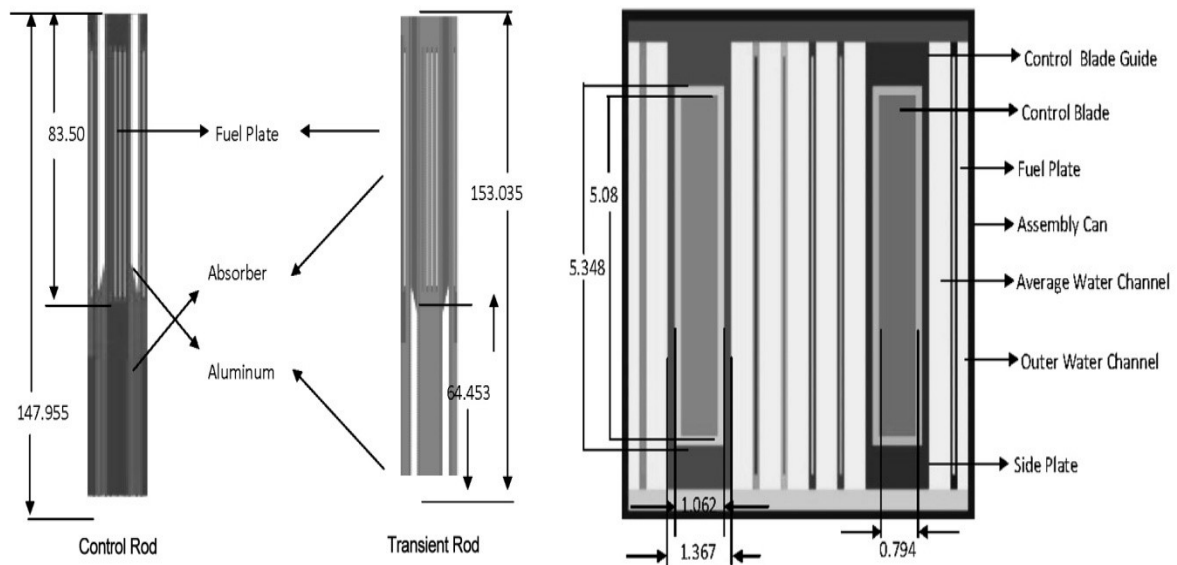


FIG. VIII-4. MVP model of SPERT IV D-Core absorber rods from BGD.

The absorber rods were modeled explicitly with only the minor approximation of ignoring the holes in the rod follower sections. A wedge-shaped tapering of length 3.28 cm was assumed for the rods and followers. In addition, an assumption was made regarding the tapering of the absorber and follower pieces, such that when the rods are fully inserted into the core the entire tapered length of the absorber is located within the fuelled height of the core. Vacuum boundary conditions were used on the periphery of the model.

Other approximations in the model were:

- The bottom end box and the lower grid assembly were modeled as a single aluminium structure in the lower reflector region of the model;
- The top end box, handles, hold down bars, and absorber drives were not included in model;
- No other top, lateral, or lower peripheral structures were included;
- All materials were modeled at a temperature of 20 °C (reflective of the cold, clean, state of the core).

For all criticality cases the MVP models were executed, in criticality mode, using 10,000 particles/batch, 1000 active batches, and 100 skipped batches. For the flux distribution cases the number of active and skipped batches were increased to 10,000 and 500 respectively.

An error in the carbon and aluminium atom densities in the absorber rod material was discovered post calculations (refer to Table VIII-5). The effect of this on the calculated benchmark results has not been determined.

TABLE VIII-5. BGD ERROR IN BINAL MATERIAL STRUCTURE COMPOSITION

Material	Modelled Atom Density (/b-cm)	Specified Atom Density (/b-cm)
C-natural	1.02×10^{-2}	2.61×10^{-3}
Aluminium	3.62×10^{-2}	5.45×10^{-2}

VIII-3.3. France-CEA: Codes, Tools and Methods

France CEA (FRA) used the TRIPOLI4 code for the static part of the analysis. The model represents the SPERT IV D-12/25 core as a 3D geometry consisting of about 1000 volumes. The standard and control fuel assembly geometry was modeled explicitly as shown in Fig. VIII-5. The upper and lower end boxes were approximated by extending the side plates and assembly cans through the upper and lower end box regions. The lower grid assembly and the associated structure (lifting bails, rod drives) were not included in the model. The model included 300 cm of light water beyond the 5 x 5 fuel array in the X, Y and Z directions. Reflective boundary conditions were used on outer model boundaries in the X, Y, and Z directions.

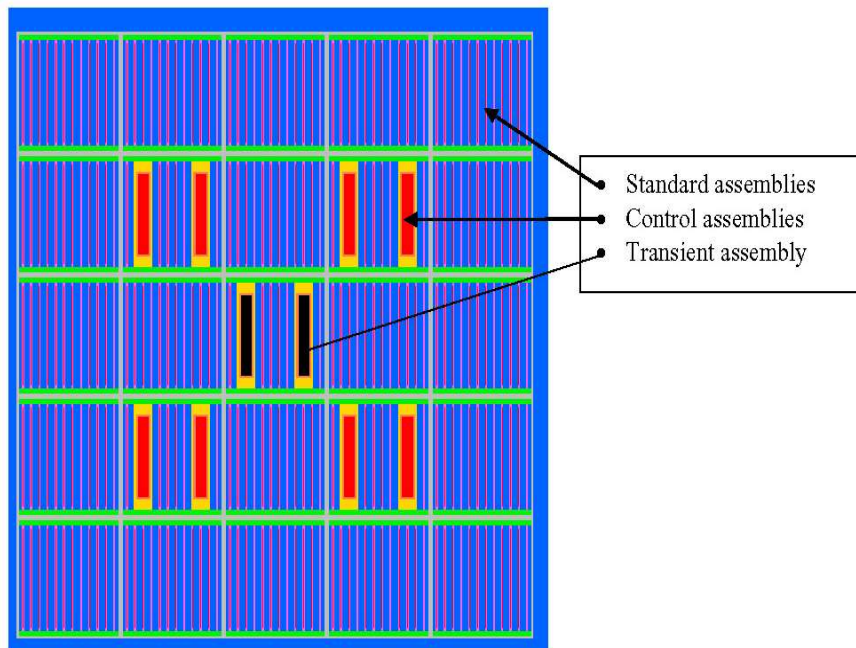


FIG. VIII-5. TRIPOLI4 geometry of SPERT IV D-Core from FRA.

The geometry of the tapering of the absorber and its aluminium follower in the control rod assemblies was optimized using the available geometrical information and the experimental measurements of the axial flux distribution. Based on this optimization, the calculated rod worth and the flux shape at the level of the junction are in good agreement with data. The rod positioning was assumed such that the axial position of the control rods corresponds to the lower extent of the tapering. The same approach was adopted for positioning of the transient rod but this is more relevant to the RIA simulations which are not reported herein. The rod tapering approximation is shown in Fig. VIII-6. Rod positioning was assumed to be with reference to the leading tip of the taper.

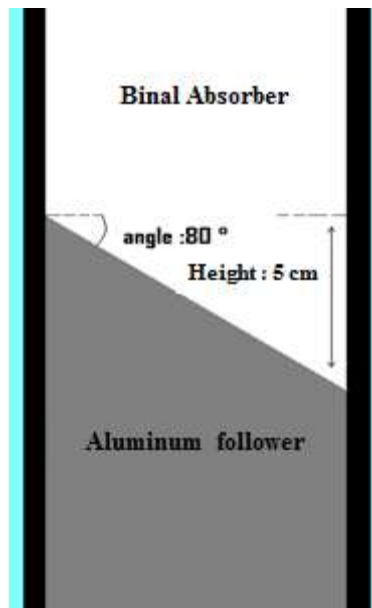


FIG. VIII-6. Optimized rod tapering adopted by FRA.

Most of the calculations were performed with the material defined at 20°C, the standard temperature available for all isotopes in the JEFF3.1.1 library. For the core moderator coefficient dedicated calculations were made over the applicable range of temperatures.

The TRIPOLI4 calculations used 10,000 batches of 10,000 particles/batch (100 million particles) for cases in which k_{eff} was the primary parameter of interest. These specifications were altered to 60,000 batches of 30,000 particles/batch (1.8 billion particles) for the flux distribution calculations.

VIII-3.4. France-IRSN: Codes, Tools and Methods

France-IRSN (FRA2) used the ORNL SCALE 6.0 package [VIII-3] for the static part of the analysis. While rod worth and power distributions were calculated directly the reactivity profile was studied with perturbation theory provided in SCALE/TSUNAMI modules. In these calculations the moderator was smeared along entire sub-assemblies contrary to experiments where void worth was simulated by placing aluminium strips between fuel plates of widths and length shorter than that of the coolant channels. Perturbation theory has been also applied for kinetic parameters β_{eff} and β_{eff} calculations.

No further details of the modelling have been provided by the FRA2 participants.

VIII-3.5. Pakistan: Codes, Tools and Methods

The Pakistan (PAK) group used a deterministic approach to model the SPERT IV D-core via the MTR-PC26 code package. The default WIMS/D4 69-group library was used in the cell calculations.

A four-region 1D slab cell model with reflective boundary conditions, representing a half-plate and associated coolant and structure material, was employed for cross-sections generation of D-12/25 SPERT IV fuel. Separate cell calculations were performed for the non-fuelled width of the fuel assemblies, control absorber region, control follower region, guide tube, grid plate, reflector and structural regions of the core. Condensation was to ten energy groups (Table VIII-6), with the last three groups considered to be of the thermal range.

TABLE VIII-6. PAK DIFFUSION THEORY MODEL ENERGY GROUPS

Energy Group No.	Upper Energy Bound (eV)
1	10×10^6
2	0.821×10^6
3	0.3025×10^6
4	0.183×10^6
5	367.262
6	1.15
7	0.972
8	0.625
9	0.14
10	0.05

VIII-3.6. Syrian Arab Republic: Codes, Tools and Methods

Syrian Arab Republic (SYR) used the Monte Carlo code MCNP-4C [VIII-4] and the associated ENDF/B-VI.2 library to model the SPERT IV D-12/25 core for the static part of the benchmark analysis. Figure VIII-7 shows the developed full MCNP model for the core of SPERT IV. Fig. VIII-8 shows horizontal cross section for the SPERT IV standard and control fuel assemblies.

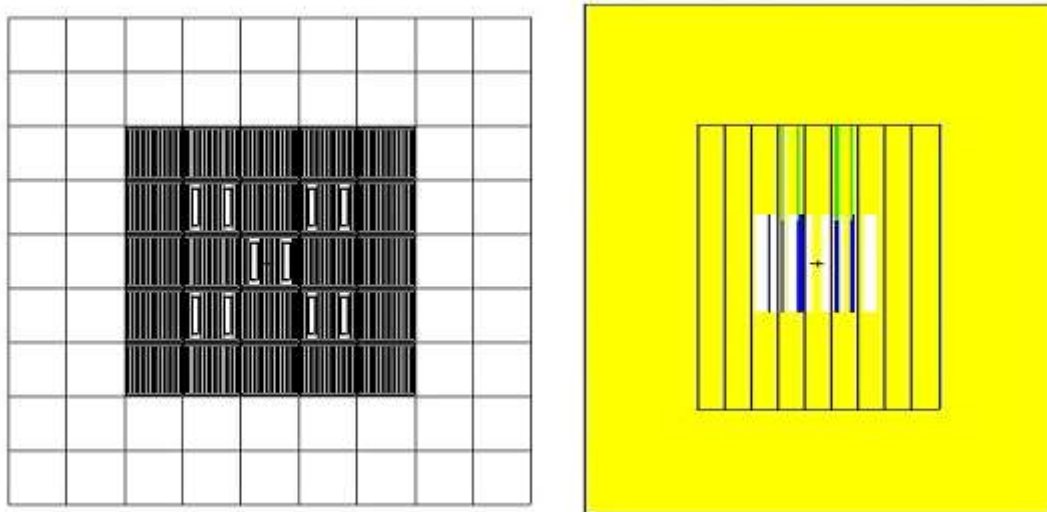


FIG. VIII-7. Group MCNP model of the SPERT IV D-12/25 core from SYR.

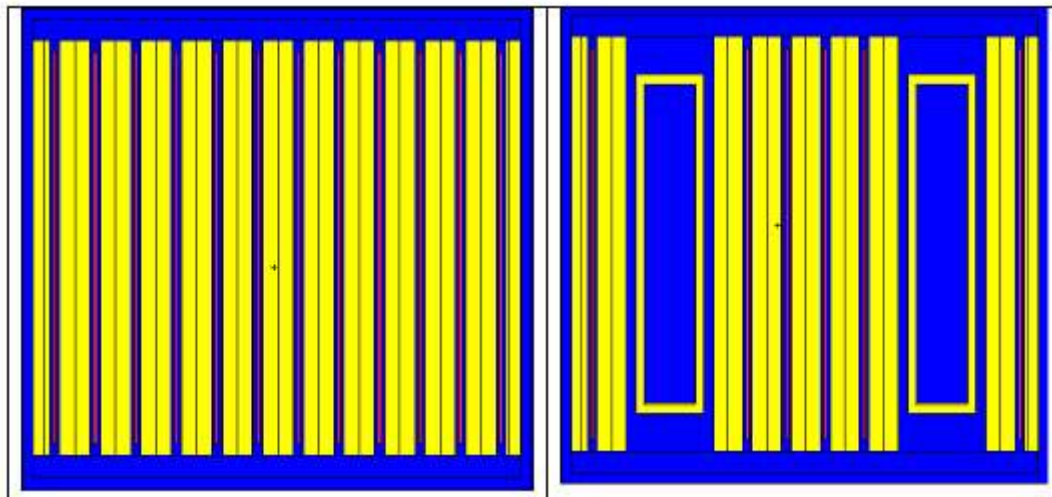


FIG. VIII-8. Group MCNP model of SPERT IV standard and control fuel from SYR.

The *kcode* parameters used in the MCNP-4C model are specified with 3000 histories per cycle, 100 skipped cycles and 3000 active cycles (9 million active particle histories).

VIII-4. DESCRIPTION OF EXPERIMENTS

The static (neutronics) section of the SPERT IV Benchmark analysis is based upon the static experiments for core characterization as conducted for commissioning of the SPERT IV D-12/25 core. The static experiment section consists of the following sub-sections:

- Initial Critical Experiment & Operational Loading;
- Control rod worth calibration (combined bank worth);
- Void substitution reactivity changes;
- System temperature reactivity changes;
- Flux distributions via Co-59 wire activation;
- Kinetics Parameters.

Each of these experiments and the associated simulation results from the participating analysis groups are summarized in the following sections. Further information on the experimental specifications and results can be found in Reference [VIII-2].

VIII-4.1. Initial Critical Experiment and Operational Loading

VIII-4.1.1. Short description of the experiment

VIII-4.1.1.1. Initial Critical Experiment

The purpose of this experiment was to determine the minimum critical loading for the SPERT IV 12-plate D-core and to provide a safe and efficient method for loading the operational core. In the approach-to-critical, the multiplication, M , of the core was determined from neutron counting data and the inverse-multiplication, $1/M$, technique was used to experimentally determine the number of assemblies or mass of Uranium-235 that would be required for criticality. Following each fuel addition, neutron counting rates were obtained with the control rods fully inserted, raised to 6, 12, and 18 in., and to the upper limit of control rod travel, 23.2 in. For each core loading and control rod position, plots were made of reciprocal multiplication vs. the number of assemblies in the core. Straight line extrapolations of these curves to $1/M = 0$

gave the predictions of the number of assemblies required for criticality. The experimental data for the approach to critical experiment is a table of loading configurations and a plot of inverse multiplication against loading configuration. This plot was digitized for use in this benchmarking exercise.

The requirements for this section of the benchmark analysis are to produce k_{eff} estimates for the approach to critical core loadings as described in the Table VIII-7.

TABLE VIII-7. APPROACH TO CRITICAL CORE LOADINGS & CRITICALITY PREDICTIONS

Load Number	Core Position(s) added	Mass Addition (kg U-235)	Total Mass (kg U-235)	No. Assemblies	Criticality Predictions	
					No. of Assemblies	Mass of U-235 (kg)
1	E-5, D-4, D-6, F-4, F-6	0.415	0.415	5	-	-
2	F-5, D-5, E-6, E-4	0.665	1.08	9	14	1.83
3	G-5, C-5	0.321	1.41	11	17	2.32
4	E-7, E-3	0.333	1.74	13	17	2.57
5	C-4, G-6	0.332	2.08	15	19	2.65
6	D-7, F-3	0.334	2.41	17	20	2.86
7	F-7	0.166	2.58	18	20	2.87
8	D-3	0.167	2.74	19	21	2.97
9	G-4	0.169	2.91	20	21	3.04
10	C-6	-	3.08	21	(a)	(a)

(a) Critical with 21 assemblies and control rods at 21.6 in. withdrawn

VIII-4.1.1.2. Operational Loading Experiment

Following the initial critical experiment, the loading of the SPERT IV 12-plate type-D fuel was continued for the purpose of assembling a core with sufficient excess reactivity to allow a thorough investigation of reactor instabilities at various initial conditions of temperature, flow, and upper-reflector height.

Following each fuel assembly addition to the initial critical core, the reactor power was allowed to rise on several relatively long ($T > 10$ sec) periods, where the prompt term of the inhour equation is small compared with the delayed (summation) term, and, therefore, the reactivity of the system can be determined from the summation term. From these data, an approximate differential control rod worth curve was produced, the integration of which allowed the determination of approximate values for the reactivity worth of that fuel addition and the total available excess reactivity. By this method a core composed of a 5 x 5 array of 12-plate, type-D control and fuel assemblies was determined to have an excess reactivity of 5.4\$. The total fuel loading in this core, the SPERT IV D-12/25 core, was 3.75 kg of U-235. More details on the experimental measurements for this section of the benchmark analysis are available in Reference [VIII-2]. The experimental data for this section of the benchmark analysis are plots of excess reactivity and critical rod position against number of fuel assemblies in the core, and a companion table summarizing the results.

The requirements for this section of the benchmark analysis are to simulate the experimental critical rod positions and provide k_{eff} estimates and excess reactivity estimates for the various operational core loadings.

VIII-4.1.2. Description and comparison of analysis approaches

The AUS, BGD, FRA and SYR groups participated in this section of the benchmark analysis. All groups used Monte Carlo transport-theory codes to complete the analysis. All groups completed this section of the benchmark by performing a series of criticality calculations to estimate the multiplication factor for each experimental core loading.

The modelling difference of most relevance to the comparison of the simulation results are the approximations/assumptions adopted by each participating group with respect to the absorber rod tapering. This specification was not available for definition of the problem and as a result represents a degree of freedom in associated simulation. The tapering detail and rod positioning definition adopted by each participating group are summarized in Table VIII-8.

Minor modelling differences were primarily in the degree of detail included in the non-active zones of the core, the amount of reflector included, the assumptions and approximations adopted for the absorber tapering and positioning, and the use of nominal rather than assembly specific loading of ^{235}U . Differences in the solution employed by the different groups involved the particle batching and total histories defined for the calculation.

TABLE VIII-8. SUMMARY OF ABSORBER ROD MODELLING APPROACHES

Participant	Tapering Detail	Positioning Detail
AUS	Horizontal interface offset 1.27 cm from reported position, equivalent to 2.54 cm tapered height	Horizontal interface positioned according to reported rod position
BGD	3.28 cm tapered height	Leading tip of taper aligned with reported rod position
FRA	5.00 cm tapered height	Leading tip of taper aligned with reported rod position
FRA2	No details provided	No details provided
PAK	Tapering ignored. Height of absorber taken to be 83.5 cm as per specification.	No details provided
SYR	No details provided	No details provided

VIII-4.1.3. Summary and comparison of benchmark results

The simulation results for the approach to critical experiment summarized in for the reported core loading stages. These k_{eff} estimates are then compared to experimental values ($1/M \equiv 1 - k_{\text{eff}}$) in Table VIII-9, Table VIII-10 and Fig. VIII-9.

TABLE VIII-9. APPROACH TO CRITICAL EXPERIMENT CALCULATED VALUES

Load	Rod	AUS		BGD		FRA		SYR	
Number	Positions	k_{eff}	$\sigma(k_{eff})$	k_{eff}	$\sigma(k_{eff})$	k_{eff}	$\sigma(k_{eff})$	k_{eff}	$\sigma(k_{eff})$
1	upper limit	0.4155	0.0001	0.4163	0.0002	0.41519	0.000059	0.4182	0.0004
2	upper limit	0.7374	0.0001	0.7375	0.0003	0.73837	0.000059	0.7410	0.0006
3	upper limit	0.7953	0.0001	0.7951	0.0003	0.79602	0.000059	0.7997	0.0005
4	upper limit	0.8444	0.0001	0.8449	0.0003	0.84544	0.000059	0.8490	0.0006
5	upper limit	0.8850	0.0001	0.8851	0.0003	0.88585	0.000059	0.8905	0.0006
6	upper limit	0.9205	0.0001	0.9213	0.0003	0.92157	0.000059	0.9246	0.0006
7	upper limit	0.9439	0.0001	0.9454	0.0003	0.94478	0.000059	0.9501	0.0006
8	upper limit	0.9637	0.0001	0.9645	0.0003	0.96443	0.000059	0.9687	0.0006
9	upper limit	0.9839	0.0001	0.9843	0.0003	0.98457	0.000059	0.9895	0.0006
10	21.6	0.9981	0.0001	0.9988	0.0003	1.00115	0.000033	1.0000	0.0006

note: rod positions are in inches withdrawn for Load Number 10

TABLE VIII-10. MEASURED AND CALCULATED 1/M RESULTS

Load		1/M				$\Delta(1/M) \times 1 \times 10^5$			
Number	Measured	AUS	BGD	FRA	SYR	AUS	BGD	FRA	SYR
1	0.627	0.5845	0.5837	0.5848	0.5818	-4212	-4285	-4178	-4482
2	0.324	0.2626	0.2625	0.2616	0.2590	-6130	-6141	-6226	-6487
3	0.243	0.2047	0.2049	0.2040	0.2004	-3882	-3861	-3950	-4312
4	0.171	0.1556	0.1551	0.1546	0.1510	-1564	-1617	-1671	-2031
5	0.111	0.1150	0.1149	0.1142	0.1095	370	357	281	-184
6	0.061	0.0795	0.0787	0.0784	0.0754	1851	1770	1746	1439
7	0.042	0.0561	0.0546	0.0552	0.0499	1418	1272	1331	803
8	0.023	0.0363	0.0355	0.0356	0.0313	1342	1268	1270	843
9	0.008	0.0161	0.0157	0.0154	0.0000	819	777	752	264
10	0.000	0.0032	0.0012	-0.0011	-0.0064	189	121	-115	-3

(1) Measured 1/M values were digitized from Figure 11 of [VIII-1],

(2) Simulation 1/M values are calculated as $1/M = 1 - k_{eff}$

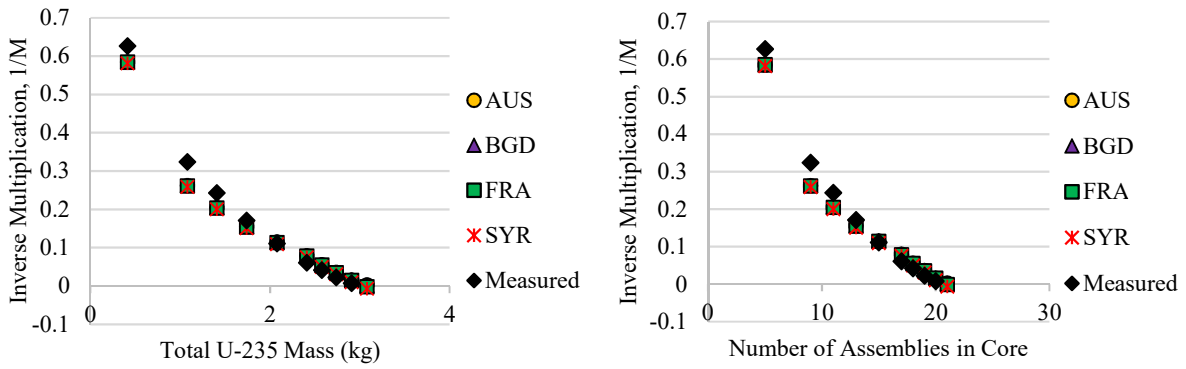


FIG. VIII-9. SPERT IV D-Core approach to critical results.

The approach to critical (1/M, inverse multiplication) experiment was simulated successfully by all groups. The results from all groups show a deviation from the experiment for deeply subcritical configurations, $1/M > 0.1$ ($k_{\text{eff}} < 0.9$). This is expected as most codes do not simulate the inherent correlated physical parameters required to provide accurate representation of these time dependent systems. The nominal ^{235}U mass (per assembly) as specified is slightly different than the actual ^{235}U loadings of the fuel assemblies used in this experiment (as per Table VIII-7). The FRA results are based on an adjusted fuel concentration required to achieve consistent ^{235}U masses across the various fuel assemblies. Although this does affect the FRA results, it does not appear to introduce any systematic differences compared to the other results.

The operational loading measurements of the SPERT IV D-core provide critical rod positions for a series of core loadings. Results of critical rod position k_{eff} results are shown in Fig. VIII-10. Results are all within 400 pcm of $k_{\text{eff}} = 1$.

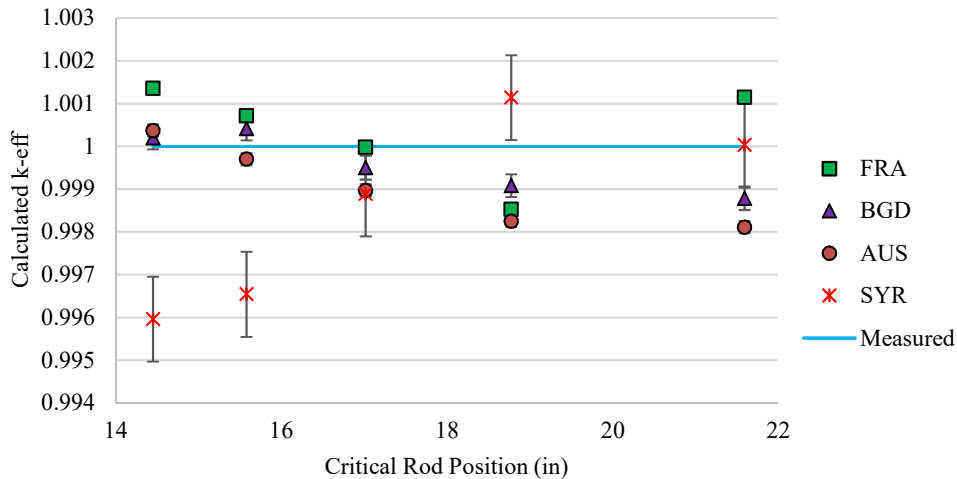


FIG. VIII-10. SPERT IV D critical rod position k_{eff} results.

The predicted vs. experimental results for excess reactivity of the SPERT IV D-12/25 core are summarized in Fig. VIII-11 and Table VIII-11.

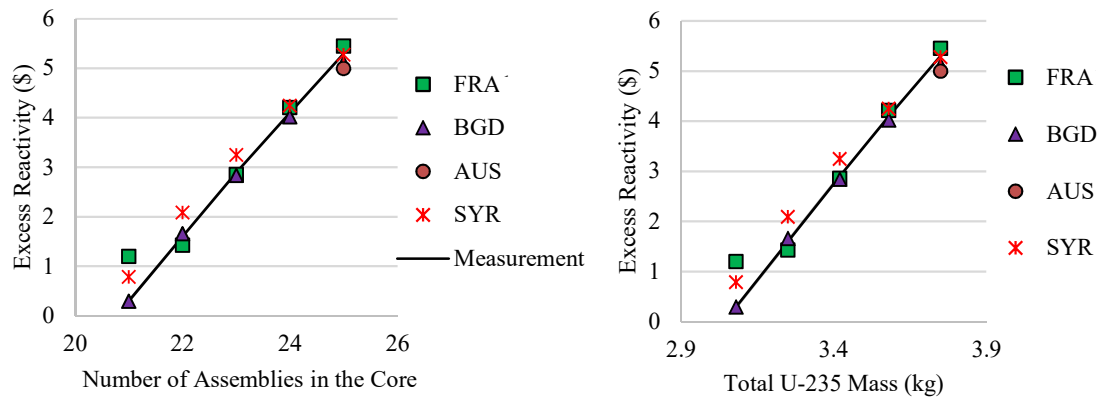


FIG. VIII-11. SPERT IV D-12/25 excess reactivity results.

TABLE VIII-11. SPERT IV D-12/25 CALCULATED AND MEASURED EXCESS REACTIVITY

Experiment	ρ excess (pcm)	β_{eff} (pcm)	ρ excess (\$)	σ (ρ excess) (\$)	C/E
	-	-	5.3	-	-
AUS	3827	765	5	-	0.94
BGD	3986	780	5.110	0.037	0.96
FRA	4186	768	5.45	0.13	1.03
SYR	4211	797	5.28	-	1.00

All groups provide reasonable estimates of excess reactivity for the final loading of the SPERT IV D-12/25 core compared to the experimental value, with C/E ratios between 0.94 and 1.03. Differences in β_{eff} , which is used to convert the calculated estimates to units of \$, have to be noted. An over-prediction of the experimental values is produced by the SYR group for 21, 22, and 23 assembly configurations.

VIII-4.1.4. Conclusions and recommendations

The Monte Carlo transport-theory calculation tool appears well suited for the prediction of approach-to-critical experiments and operational loading critical rod position and excess reactivity calculations. Minor variations are found between groups for k_{eff} estimates, with critical configurations predicted within 400 pcm. These results have in most cases been somewhat optimized via adjustment of the absorber rod tapering details.

The results from all groups show a deviation from the experiment for deeply subcritical configurations. This is expected as most codes do not simulate the inherent correlated physical parameters required to provide accurate representation of these time dependent systems.

VIII-4.2. Absorber Rod Worth Calibration

VIII-4.2.1. Short description of the experiment

The control rods of the SPERT IV D-12/25 core were calibrated as a bank from the cold, clean critical position to the upper limit of travel by the period technique using boric acid as

a reactivity shim. The purpose of this experiment was to obtain a more precise value of the available excess reactivity of the core and to obtain operational information which is necessary for accurate adjustment of the control rods during the kinetics testing programme. The differential worth of the control rods was found to vary, almost linearly, from 1.07 \$/in. at the cold, clean critical position of 14.5 in. to 0.19 \$/in. at their upper limit of travel 23.2 in. The available excess reactivity of the core was determined to be 5.3 \$ from the data taken in this experiment. Experimental results for the rod worth calibration were digitized from the figures included in Reference [VIII-2].

The requirements for this section of the benchmark analysis are to produce the following results for comparison to the experiments:

1. Differential control rod bank worth from the clean critical position of 14.5 inches withdrawn to the upper limit of travel of 23.2 inches withdrawn. Consider withdrawal steps of 1 inch for the rod bank. Present results in tabular format and graphically as per the experimental data in Fig. VIII-12. Note: the tapering on the absorber rods was not specified in the reactor description and as such represents a degree of freedom in the calculation. The user can adjust the tapering of rods (effectively the amount of absorber in the end section of the rod) to improve agreement with experiment.
2. Integral control rod bank worth for the same range of rod insertion as above to generate results as presented in Fig. VIII-13. Results need to be presented both in tabular format and graphically as in [VIII-2]. The same rod tapering as used in the differential worth curve needs to be retained for the integral worth curve. Note: as above with respect to the lack of tapering specification, this will manifest itself in the form of a systematic offset between the calculated and experimental results. The user has to compare the shape of the integral rod worth curve as well as the absolute values.

VIII-4.2.2. Description and comparison of analysis approaches

All groups calculated the rod worth as the change in reactivity associated with a change in rod position from criticality calculations. The FRA2 group fitted the raw integral rod worth results to a second order polynomial and performed further analysis using the fitted data.

Differences in absorber rod tapering details adopted by each group, as summarized in Table VIII-8, are relevant to this section of the benchmark analysis as are estimates of β_{eff} .

VIII-4.2.3. Summary and comparison of benchmark results

The AUS, BGD, FRA, FRA2, and SYR groups participated in this section of the benchmark analysis. Differential and integral rod worth results are shown in Fig. VIII-12 and Fig. VIII-13, respectively. Results are presented both in units of dollars (\$) as per the reported measurements and *pcm*. This is done in order to evaluate the dependence upon the calculated β_{eff} value. Differential rod worth results from SYR are not included as they were not submitted and depend upon method for calculation from integral results.

There appears to be some notable discrepancy between the measured values and the simulation estimates submitted by SYR. Given the lack of details available for the SYR model no further comment can be made at this time.

Apart from the results from SYR, all other results reproduced the variation of worth with position well, but there is some scatter due to the statistical fluctuations of the Monte Carlo method. There is a slight systematic shift in the calculated rod worth, most evident in the AUS

results, as the rods are withdrawn. This is not surprising as during the experiment the core reactivity is balanced by adding boric acid and this approach changes the flux profile of the core and the worth of the control rods. This effect was neglected in all the calculations.

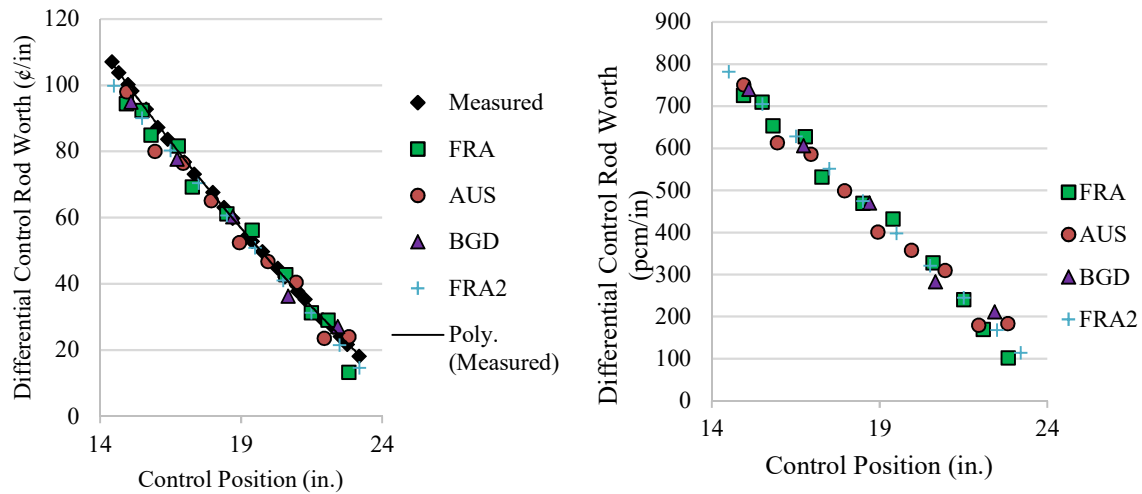


FIG. VIII-12. SPERT IV D-12/75 differential rod worth results.

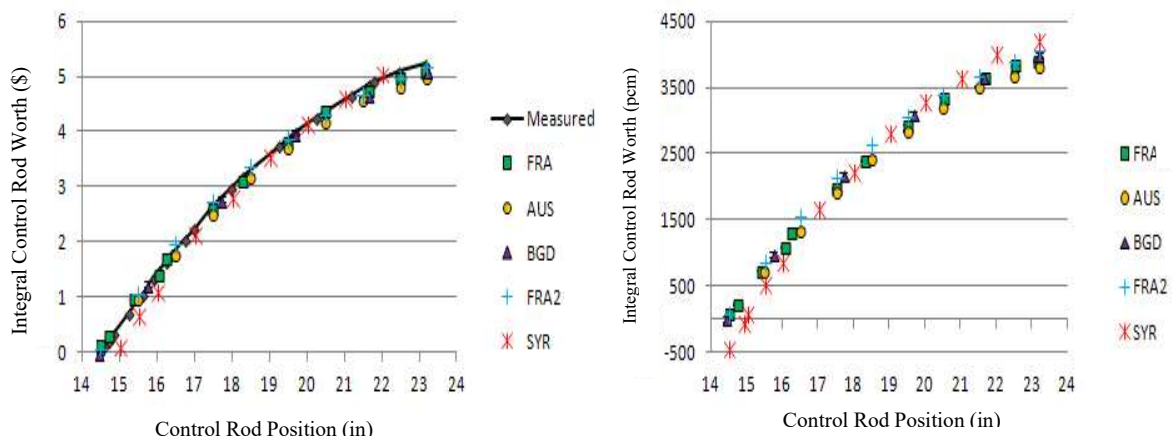


FIG. VIII-13. SPERT IV D-12/25 integral rod worth results.

VIII-4.2.4. Conclusions and recommendations

Overall, the measured control rod worth was successfully simulated by participating groups indicating that the specification for this section of the benchmark analysis is sufficient. Integral control rod worth estimates appear consistent between participating groups as directly calculated in units of pcm as well as when converted to units of dollars showing little sensitivity to the estimated value of β_{eff} . The one exception is the results from SYR which show a more pronounced worth profile. The reason for this discrepancy has not been identified. Results do not appear to be sensitive to the assumptions related to rod tapering which were adopted by the different participants (see Table VIII-8).

All other groups show good agreement for both differential and integral control rod worth with the measured data. Results from Monte Carlo calculations are limited by statistical fluctuations, but the slowly varying profile of the control rod worth allows an integral rod worth to be calculated and a fitted curve can then be used to deduce the differential worth. This reduces the effect of the statistical fluctuations without compromising the detail available. Overall the

integral control rod worth was calculated to within 5% by all groups and this is consistent with the expected accuracy of such calculations.

VIII-4.3. Void Substitution Reactivity Changes

VIII-4.3.1. Short description of the experiment

The D-12/25 core was the first core installed in SPERT IV. It was composed of 25 fuel assemblies in a square five by five section of the nine by nine supporting grid (Fig. VIII-14). Assembly locations are denoted by row/column combination, e.g., E5 is central transient rod assembly location.

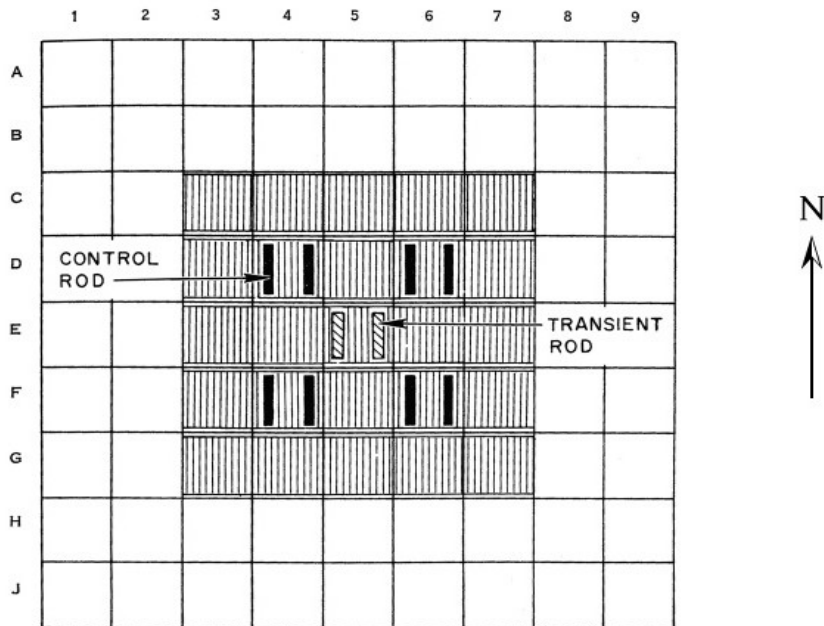


FIG. VIII-14. SPERT IV D-12/25 core configuration (Ref. A-21).

The void coefficient of reactivity was measured in the D-12/25 core using aluminium strips to simulate voids. Three kinds of measurement were made:

1. A measurement for a uniform core distribution of full-core length void strips.
2. A radial Importance measurement using full-length void strips in various fuel assembly positions.
3. A measurement of the vertical void importance.

The uniform void distribution was simulated for several void volumes by placing an equal number of full-core-length aluminium strips in each of the 20 non-rodded fuel assemblies. Assemblies were loaded with between one and eight strips. Reactivity loss was calculated from the change in critical rod position using the differential control rod worth curve. The results of the uniform void distribution measurements as a function of total volume voided are shown in Fig. VIII-15. The measured coefficient is $-41.5\phi/\%$ decrease in moderator density or $-0.080\phi/\text{cm}^3$ of water replaced. The coefficient is independent of the total void volume in the core for the range investigated (about 11% moderator displacement).

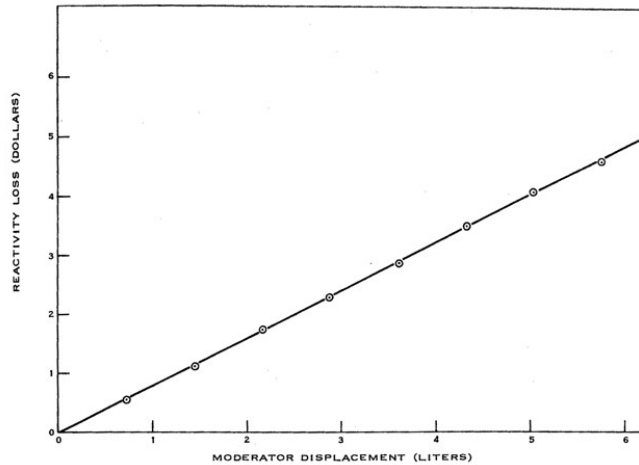


FIG. VIII-15. Measured reactivity loss vs moderator volume displaced by void strips for uniform void distribution.

For the radial importance measurement, the critical position was determined with a fuel assembly containing 24 full-core-length aluminium strips loaded at different representative lattice positions. The total volume of the aluminium strips in the voided fuel assembly was 864 cm³, which is equivalent to 1.66% of the total moderator volume in the core. For the measurement in the transient rod assembly position 18 aluminium strips were used, equivalent to 1.24% of the total moderator volume. The reactivity worth of the voided assembly was determined from the change in the critical control rod position from the unvoided critical position. Figure VIII-16 shows the void coefficient results obtained for various lattice positions.

21.1 (0.040)	32.7 (0.063)	39.9 (0.077)		
34.6 (0.066)	CR-4	60.4 (0.116)	CR-1	
41.7 (0.080)	59.4 (0.114)	TR 47.9 (0.092)	58.4 (0.112)	
	CR-3	59.1 (0.114)	CR-2	
NOTE: NUMBERS IN PARENTHESES ARE % / CM ³				

FIG. VIII-16. Local void coefficient in cents per percent moderator density change.

The reactivity worth of 2-in.-high void strips distributed throughout the core was determined as a function of vertical position in the core. The void strips were attached by nylon cord to the transient rod drive mechanism to permit control of the vertical position of the void strips. The strips were initially positioned with their centerlines 1 in. above the bottom of the active fuel region and were then raised in 2-in. increments. The reactivity worth as a function of vertical position was determined from changes in the critical position of the calibrated control rods. The position of the void strips within an assembly and the results of this experiment are shown in Fig. VIII-17. The peak of the void worth curve has a value of approximately -80¢ per percent decrease in moderator density. The peak occurs at about 8.5 in. above the bottom of the fuel.

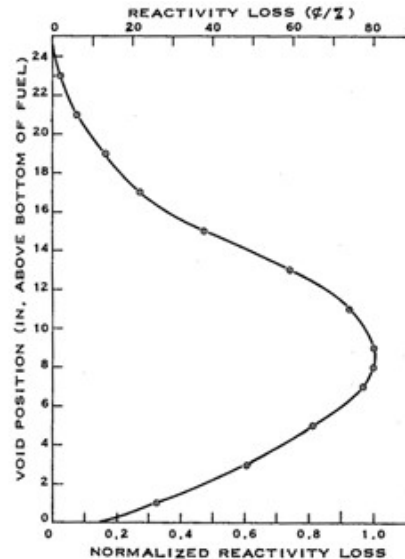
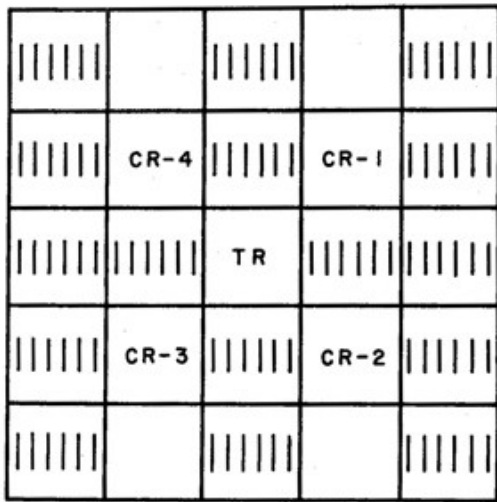


FIG. VIII-17. Vertical void experiment - location of void strips (left) and reactivity loss vs vertical position (right).

Further experimental details are found in Reference [VIII-2]. The requirement for this section of the benchmark analysis is to simulate the change in reactivity of the core for the following aluminium void plate additions related to the three experiments described above.

VIII-4.3.2. Description and comparison of analysis approaches

For the uniform void coefficient simulation all participants, except FRA2, modelled the aluminium void strips explicitly within the coolant channels rather than using void (reduced coolant density). There was no information on the actual configurations used for the uniform or radial void measurements, so all participants were left to independently determine how to place the strips within the coolant channels. Most also performed sensitivity studies on the effect of different configurations.

Figure VIII-18 shows two possible configurations for the 8 strips in the uniform void experiment, as simulated by AUS. The difference in reactivity worth of these configurations is some 13%, a very significant difference. Most participants optimised the configurations within some reason to achieve best agreement with the experiment results.

The aluminium strip configuration adopted by FRA for the radial void coefficient is presented in Fig. VIII-19(a). As part of their analysis FRA included sensitivity work to specific location of the strips and found that the void effect could vary by about 8% depending on the configuration. In contrast the configuration adopted by AUS is indicated in Fig. VIII-19(b).

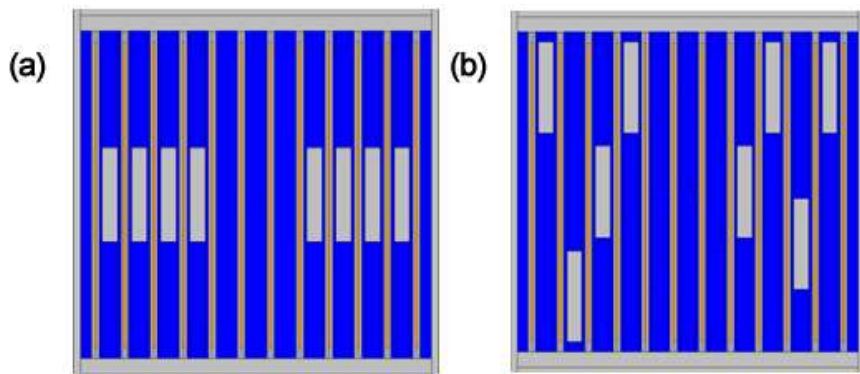


FIG. VIII-18. Void strip placement sensitivity analysis from AUS.

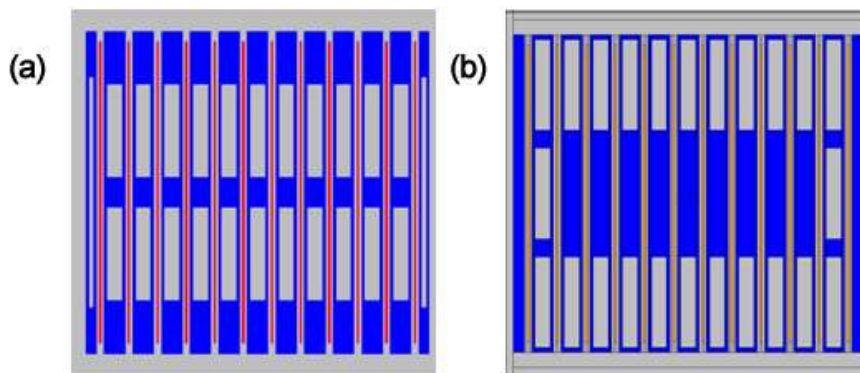


FIG. VIII-19. FRA (a) and AUS (b) radial void strip placement.

The FRA2 group approached the problem using perturbation theory via the SCALE/TSUNAMI code module. In these calculations the coolant density was adjusted inside of height limits of the experiment. No further details of the FRA2 model have been presented.

VIII-4.3.3. Summary and comparison of benchmark results

VIII-4.3.3.1. Uniform Void Reactivity

AUS, BGD, FRA, FRA2, and SYR groups provided results for this section of the benchmark experiment (Figs. VIII-20 and 21). The results from SYR did not report an estimate of the uniform coefficient of reactivity so a linear-least-squares fit to the submitted data was used to produce the value reported in Table VIII-12. PAK provided an overall reactivity coefficient but no further results or description of the analysis approach.

The AUS, FRA, and FRA2 calculated results agree well with the reported experimental values, with reactivity estimates agreeing within 10% of measurement and estimates of the uniform reactivity coefficient agreeing with measurement within 2%. These results can be considered consistent with measurement given uncertainty in experimental details of void plate placement.

TABLE VIII-12. SPERT IV D-12/25 UNIFORM VOID REACTIVITY RESULTS

	β_{eff} (pcm)	α (pcm/cm ³)	α (ϕ /cm ³)	C/E ratio
Measurement	-	-	-0.080	-
AUS	765	-0.62	-0.081	1.01
BGD	780	-0.73	-0.093	1.16
FRA	768	-0.62	-0.081	1.01
FRA2	783	-0.61	-0.078	0.98
PAK	783	-0.54	-0.069	0.86
SYR	797	-0.71	-0.089	1.12

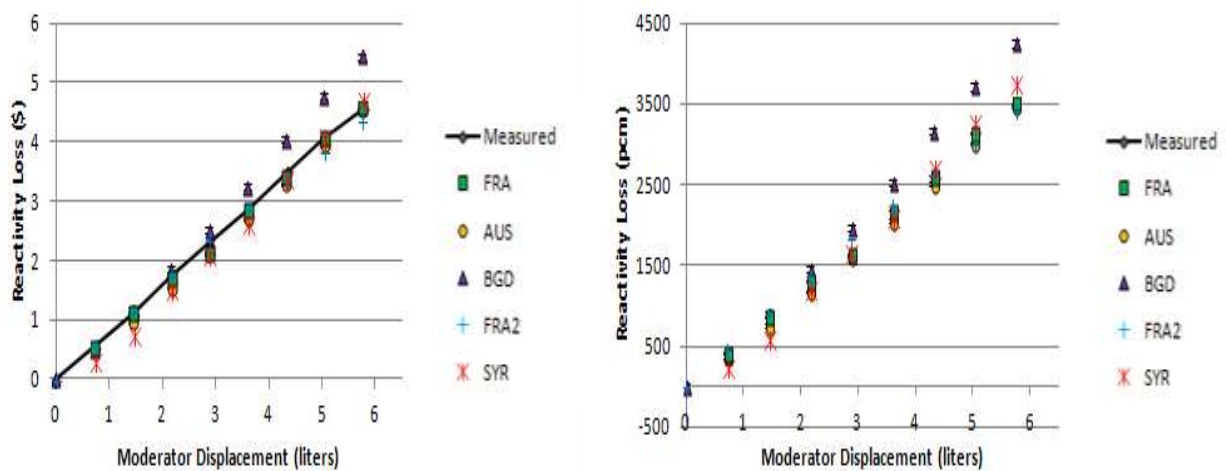


FIG. VIII-20. SPERT IV D-12/25 uniform void reactivity results.

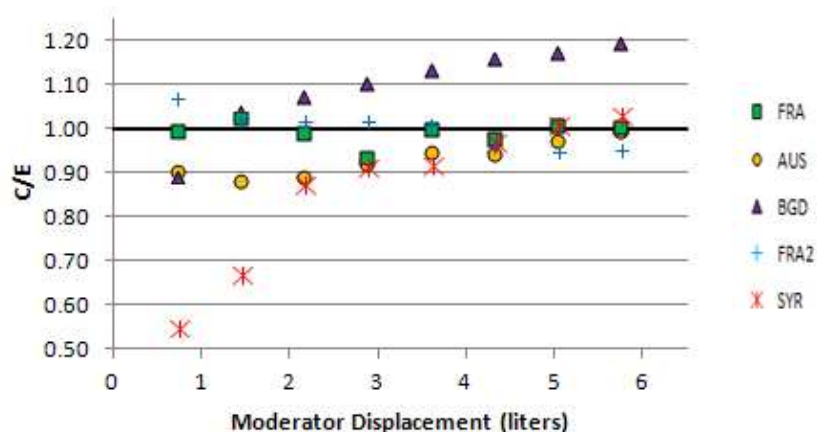


FIG. VIII-21. SPERT IV D-12/25 uniform void reactivity estimates C/E ratios.

The BGD, PAK, and SYR groups obtained void reactivity estimates beyond what was expected from sensitivity analysis work related to the positioning of the fuel plates. The PAK group underestimated the uniform reactivity coefficient while the BGD and SYR groups overestimated the same value. Since only a reactivity coefficient was reported by the PAK

group no further assessment of their analysis is possible at this time. The BGD and SYR reactivity estimates both showed trends with moderator displacement different from those reported from experiment. This may be due at least in part to void plate positioning adopted in the simulations, although for the first step of the void addition (one plate in each assembly) it is not expected that this would be overly relevant. The SYR group plate placement is shown in Fig. VIII-22 and can be compared to that used by the AUS group (Fig. VIII-23). These two groups took very different approaches in the placement of the strips, one having the strips adjacent and the other spreading them out.

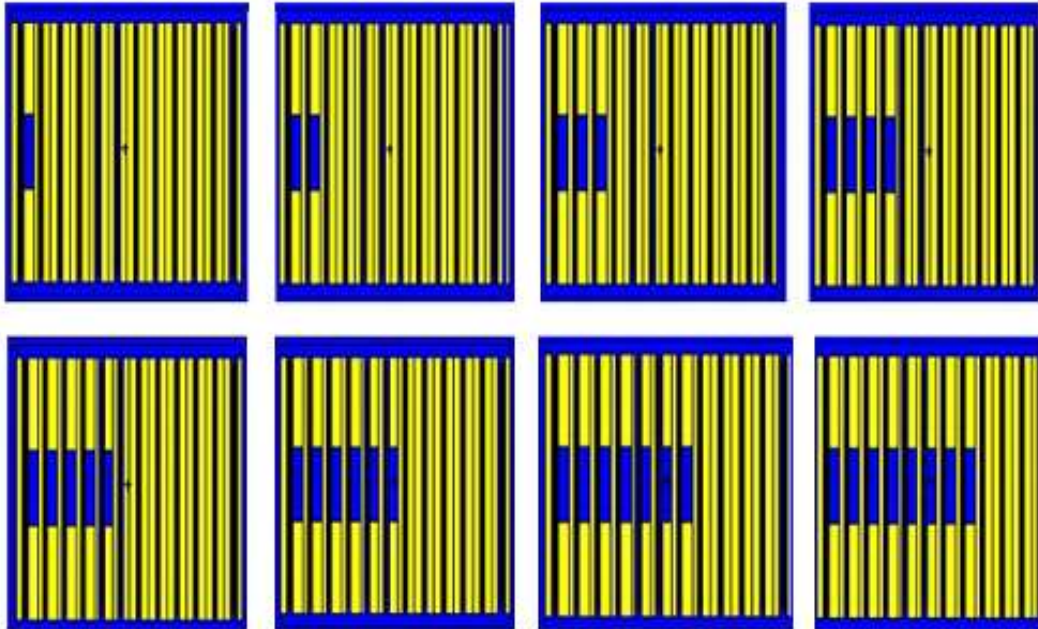


FIG. VIII-22. Uniform void calculation sequential plate placement from SYR.

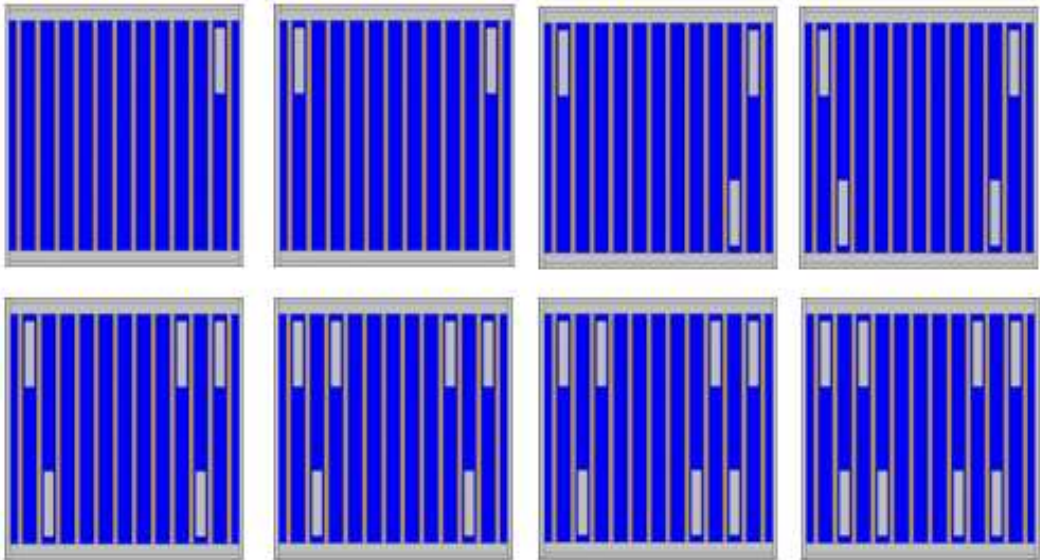


FIG. VIII-23. Uniform void calculation sequential plate placement from AUS.

VIII-4.3.3.2. Radial Void Reactivity

Only the AUS, BGD and FRA groups completed this section of the benchmark analysis. Results are summarized in Fig. VIII-24. While the C/E ratios are beyond the precision of the simulation

and experimental data, calculated results do agree with the experimental data within the uncertainty (8%) associated with the location of the void strips within the assemblies. Of note is that all groups obtained estimates of the void reactivity which over-predicted the effect in the centre of the core and under-predicted the effect on the core periphery.

The BGD group adjusted the position of the absorber rods to give $k_{eff}=1$ for the configuration with no void plates in the core. It appears that this modelling approach has only a secondary effect on estimates.

	3		4		5		6		7	
C	21.1	0.04	32.7	0.063	39.9	0.077				
	AUS	0.95	AUS	0.99	AUS	1.01				
	BGD	0.96	BGD	1.04	BGD	1.00				
	FRA	0.97	FRA	1.00	FRA	1.01				
D	34.6	0.066			60.4	0.116				
	AUS	0.99			AUS	1.02				
	BGD	0.92			BGD	1.01				
	FRA	0.98			FRA	1.02				
E	41.7	0.08	59.4	0.114	47.9	0.092	58.4	0.112		
	AUS	0.98	AUS	1.05	AUS	1.08	AUS	1.05		
	BGD	0.99	BGD	1.03	BGD	1.02	BGD	1.03		
	FRA	0.99	FRA	1.04	FRA	1.05	FRA	1.04		
F					59.1	0.114				
					AUS	1.06				
					BGD	1.03				
					FRA	1.04				
G							Measurement →	(c/mod%)	(c/cm ³)	
								AUS	C/E	
								BGD	C/E	
								FRA	C/E	

FIG. VIII-24. SPERT IV D-12/25 radial void reactivity results.

VIII-4.3.3.3. Vertical Void Reactivity

The AUS, BGD, FRA2 and FRA2 groups participated in this section of the benchmark analysis. Individual group results are compared to measured values in Fig. VIII-25 and Fig. VIII-26 and a combined plot of all results is shown in Fig. VIII-27. Error bars were not included in the combined results figure and were not supplied by the FRA2 group. The placement of the aluminium strips was again left for the participants to interpret. Although Figure 17 in [VIII-2] indicates the strips are spread out and aligned within a fuel assembly the exact details are not provided. The BGD group placed strips in every other channel, skipping the outer most channels (that are too narrow). The AUS group similarly placed strips in every other channel, skipping the outer most but adjacent strips were displaced along the width of the coolant channel to make the distribution uniform across the fuel assembly.

Both the AUS and BGD group results agree with experiment within the uncertainty of the calculated values although the uncertainties are reduced by running longer calculations to improve predictions if curve fitting is to be applied to results for any application. The FRA results agree well with experiment and have very small calculation uncertainty. Minor discrepancies are likely within experimental and digitization uncertainty of the measured data. The FRA2 results show large discrepancies with experiment as can be seen in Fig. VIII-26 where the results are normalized to the axial peak value. The FRA2 results are also shown in Fig. VIII-28 in terms of absolute value, showing that the estimated profile is significantly flatter than the measured profile. The two sets of simulation estimates are based upon slightly different values of volume of void per moderator % (0.50 and 0.53) which were used to convert the units of the estimated results. As no details of the FRA2 modelling and methodology were supplied these discrepancies cannot be assessed further.

All the results are plotted in Fig. VIII-27 showing that with the exception of FRA2 all the calculations were able to reliably reproduce the profile of the vertical void reactivity loss. The small value at the bottom and particularly the top of the fuel requires long computations with Monte Carlo codes to reduce the statistical fluctuations relative to the value itself.

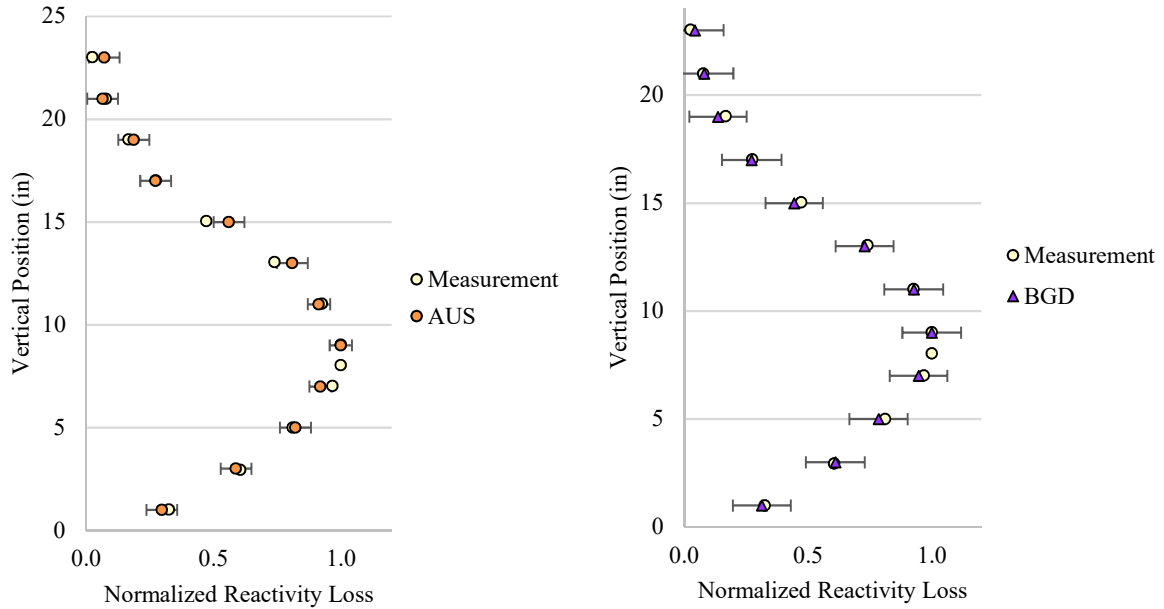


FIG. VIII-25. SPERT IV D-12/25 vertical void reactivity results.

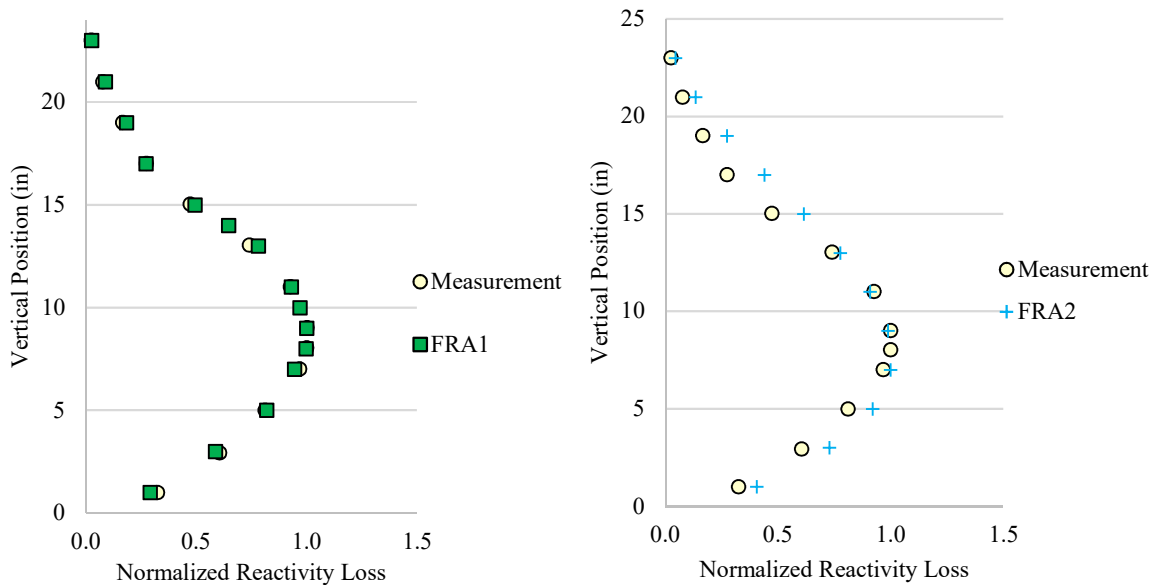


FIG. VIII-26. SPERT IV D-12/25 vertical void reactivity results.

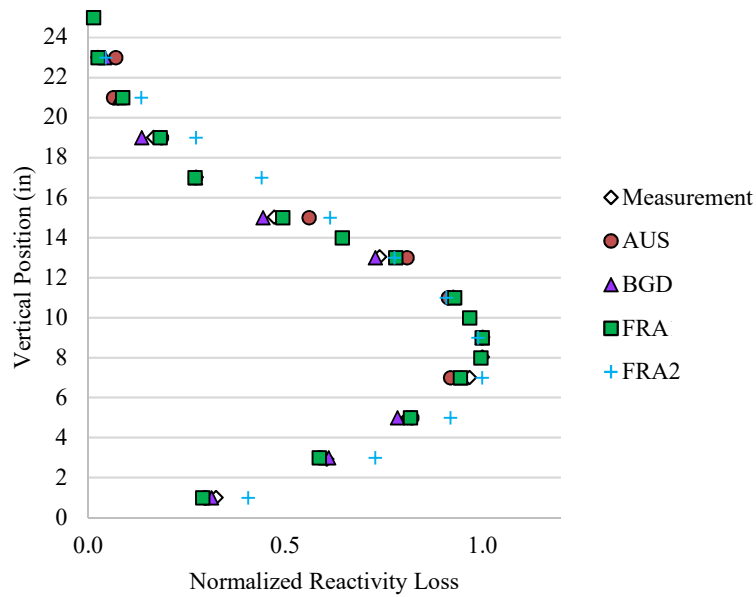


FIG. VIII-27. SPERT IV D-12/25 vertical void reactivity results.

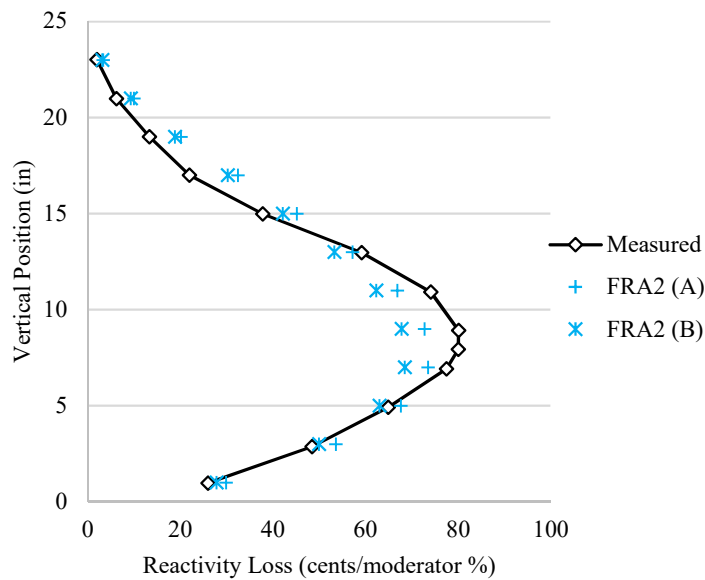


FIG. VIII-28. SPERT IV D-12/25 vertical void reactivity from FRA2.

VIII-4.3.4. Conclusions and recommendations

In general, the applied models and methods appear well-suited to the simulation of the void substitution experiment. Most calculated results were within 10% of the measured values and generally much better than this. More specifically:

- Uniform void coefficient – estimates are within 2% after optimization of experimental details regarding void plate positioning (qualified by BGD, PAK, and SYR results – see below);
- Radial void coefficient – estimates are within 8% in highest worth regions of core. Some systematic variation of C/E ratio was noted across the core positions;

- Vertical void coefficient – estimates agree with measured values within the statistical uncertainty of the calculations, except for the estimates produced by the FRA2 group. This latter set of results highlights the importance of capturing experimental detail in simulation exercises.

Despite some challenges related to achieving sufficient statistical precision compared to magnitude of the effect being estimated, it can be concluded that Monte Carlo based simulations appear well suited to this type of calculation and in particular can not only provide reliable estimates of uniform void coefficient but can also reproduce the radial and vertical profiles.

There continue to exist unresolved issues regarding the discrepancies for some of the void results and in particular uncertainty regarding placement of the void strips for several of the experimental configurations. It is not clear if the observed discrepancies are a result of adopted assumptions or the calculation and analysis methods employed but these appear to be the exceptions.

VIII-4.4. System Temperature Reactivity Changes

VIII-4.4.1. Short description of the experiment

Isothermal temperature coefficient measurements have been made for the SPERT IV D-12/25 core over the temperature range from approximately 20 to 35°C. In the measurements the bulk-water temperature in the SPERT IV calibration tank was raised from room temperature to 35°C by operating the reactor core at a steady-state power level of approximately 170 kW. The water was then cooled in steps by draining some of the hot water from the tank and refilling with cooler makeup water. After each addition of cooler water, the water was stirred continuously until the water temperature reached isothermal conditions. The instrumentation used in this experiment was the same as that used in the calorimetric power calibration, a 4-junction thermopile below the core, a 7-junction thermopile in the reflector region, and single thermocouples in a moderator channel in the core and above the core.

At each temperature the critical position of the calibrated control rods was determined and the reactivity difference between any two temperatures could then be determined by the change in the critical position of the calibrated control rods. By this technique the temperature coefficient was found to vary as the coefficient of expansion of water from approximately $-0.7\text{¢}/\text{°C}$ at 20°C to $-1.2\text{¢}/\text{°C}$ at 35°C. Experimental data is available in the form of a plot of isothermal temperature coefficient vs. temperature, reproduced in Fig. VIII-29. Data was extracted by digitizing this figure.

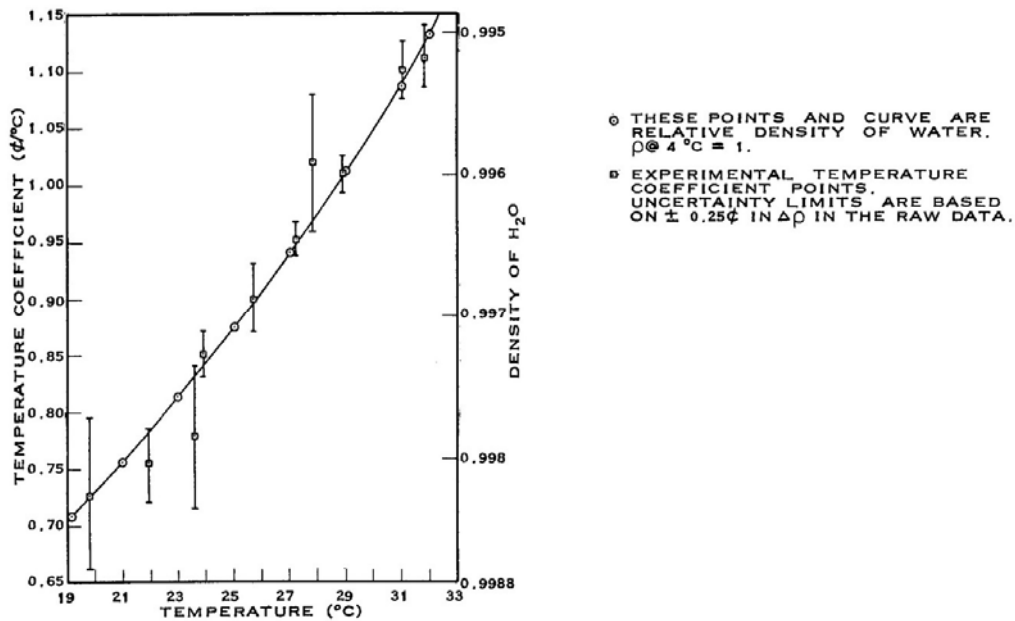


FIG. VIII-29. Isothermal temperature coefficient as a function of temperature.

VIII-4.4.2. Description and comparison of analysis approaches

The moderator temperature coefficient can be separated into two components, the density changes with temperature and the cross-section (both scattering and absorption) change. In the case of FRA, AUS and SYR the cross-section effect was ignored and only the density change with temperature was taken into account. In the case of FRA cross-section data for water was available at 294, 300, 324, 374 and 424K with the appropriate thermal scattering data. FRA performed a sensitivity study at 294 and 300K and deduced the cross-section effect is smaller than the density effect (about 10%) and was ignored in the detailed analysis. The result from PAK most likely includes the cross-section effect but the details provided do not permit confirmation of this.

AUS and FRA calculated the temperature reactivity coefficient from the raw reactivity change as a function of temperature by first fitting a quadratic to the results and then differentiating. In this way the statistical fluctuations in the small reactivity differences were averaged out and yielded a straight line fit for the temperature reactivity coefficient.

VIII-4.4.3. Summary and comparison of benchmark results

The AUS, FRA and SYR groups participated in this section of the benchmark analysis. These results are shown along with the experimental values in Fig. VIII-30. The results are re-plotted in units of pcm/°C for a more direct comparison between groups, given that the SYR group used a noticeably larger value of β_{eff} in their conversions to units of cents/°C. In addition, the PAK group supplied a single value for the temperature coefficient of reactivity for the temperature range 20-35 °C of $-1.6 \phi/^{\circ}\text{C}$ for comparison to the experimental range of $-0.7 \phi/^{\circ}\text{C}$ at 20°C to $-1.2 \phi/^{\circ}\text{C}$ at 35°C.

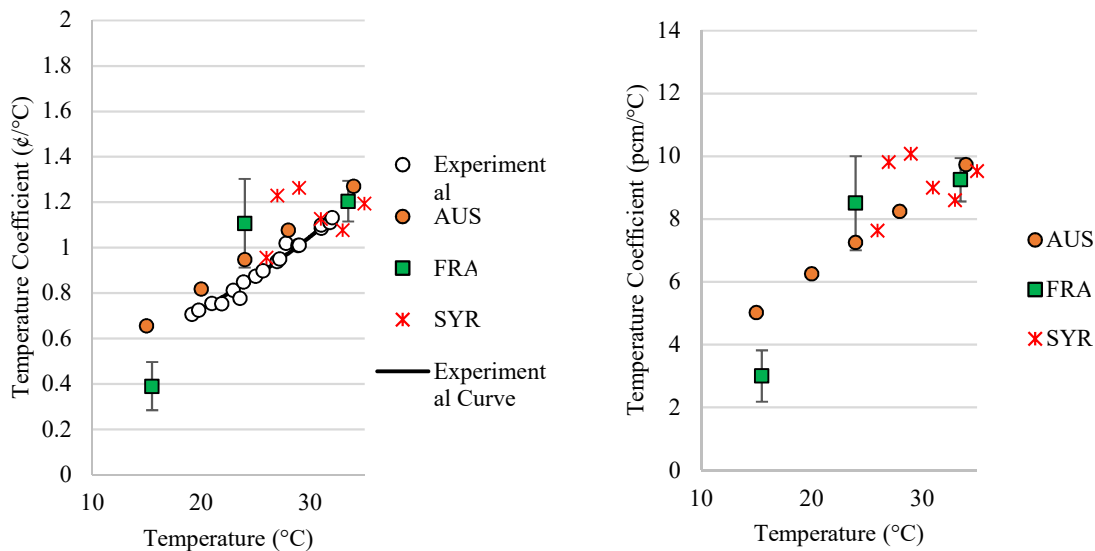


FIG. VIII-30. SPERT IV D-12/25 temperature reactivity results.

VIII-4.4.4. Conclusions and recommendations

All groups using Monte Carlo codes found that since the reactivity change associated with the change in temperature is relatively small, the statistical convergence of Monte Carlo calculations was a limiting factor in the determination. Even for a minimum number of data points and an extended temperature range the uncertainty on the calculated values is large and only limited conclusions can be drawn in comparison to the measured data. Overall the magnitude of the calculated values compares well to the measured but fitting the various results would yield a diverse set of curves with some having a similar slope but displaced while others crossed the experimental curve. Including the cross-section effect in the AUS results would mostly likely shift the values even further from the measured results.

VIII-4.5. Flux Distributions

VIII-4.5.1. Short description of the experiment

Neutron flux was measured in the SPERT IV D-12/25 core for three core variants:

1. The normal operational (clean) core.
2. The operational core with the central region partially voided with full-core-length aluminium strips worth 2\$ of reactivity. The void strip positions are displayed in Fig. VIII-31.
3. The operational core poisoned with boron-plastic strips worth 2\$ of reactivity. Six full-core-length poison strips were placed in each of the non-rodded fuel assemblies of the core. The locations of the poison strips are shown in Fig. VIII-32.

For each core condition, the flux was determined from the activation of cobalt wires located at the positions indicated in Fig. VIII-33. Some wires had cadmium sleeves covering two positions (12.5 in. and 18.5 in. from the top of the fuel plates).

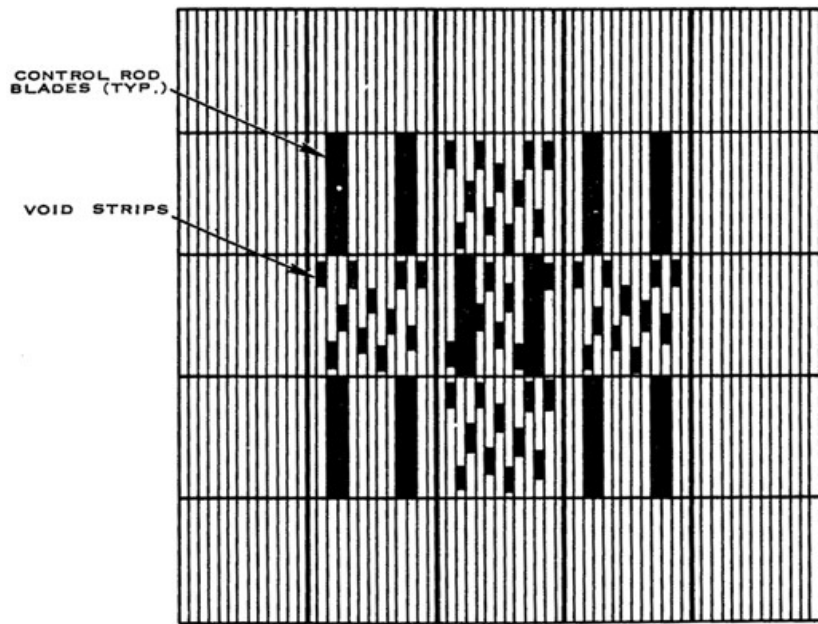


FIG. VIII-31. SPERT IV core diagram showing positions of void strips.

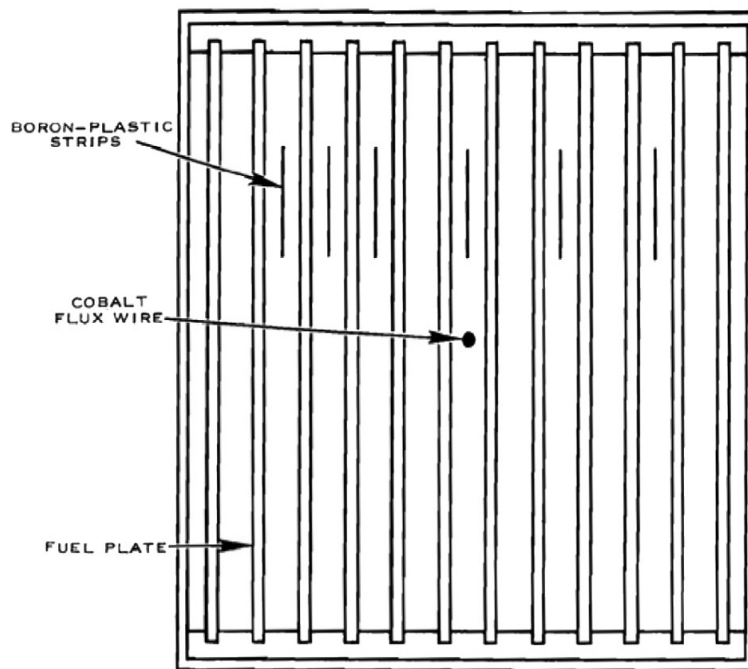


FIG. VIII-32. Location of poison strips in a SPERT IV fuel assembly.

TABLE VIII-13. SPERT IV D-12/25 EXPERIMENTAL FLUX VALUES (ORIGINALLY TABLE V FROM REF. [VIII-2]).

Poisoned core		Voided core		Clean core	
Wire	Average (nvt) $\times 10^{14}$	Wire	Average (nvt) $\times 10^{14}$	Wire	Average (nvt) $\times 10^{14}$
C-7	3.08	C-7	2.97	C-7	2.85
C-6	4.13	C-6	3.90	C-6	3.47
C-5 ₂	4.40	C-5 ₂	4.15	C-5 ₂	3.97
D-3	4.40	D-3	3.76	D-3	3.62
D-4	5.30	D-4	4.79	D-4	4.46
D-5 ₂	5.70	D-5 ₂	4.24	D-5 ₂	5.18
F-5	5.90	F-5	4.63	F-5	5.24
E-3	4.27	E-3	4.26	E-3	4.17
E-4	5.74	E-4	4.46	E-4	5.25
E-5 ₁	6.84	E-5 ₁	5.46	E-5 ₁	6.21
Core average	4.50		3.97		3.95
Maximum	10.85		7.75		9.30
Peak to average	2.41		1.95		2.35

Considerable effort was made to reconcile normalization between the vertical and horizontal flux profiles and the data presented in Table VIII-13. The vertical and horizontal flux profiles were found to be self-consistent for each core configuration, but the normalizations between the clean, voided and poisoned cores were not the same and none matched to that used in Table VIII-13. The core average data in Table VIII-13 can be verified from the Average (nvt) values in the same table using the formula:

$$\text{Core Average} = \frac{((C-7) + 4(C-6) + 2(C-5_2) + 4(D-3) + 2(D-4) + (D-5_2) + (F-5) + 2(E-3) + 2(E-4) + 0.5(E-5_1))}{22.5} \quad (\text{VIII-1})$$

Where $\langle C-7 \rangle$ is the average nvt value. Participants were asked to generate the vertical and horizontal flux profiles as per the experimental data, to normalize their calculated values using the above formula to the core average values in Table VIII-13, and to reproduce the table. In order to compare vertical and horizontal flux/activation estimates to measured data the digitized experimental profiles were also re-normalized in this manner. It is not clear from the literature what length of the vertical profile data is to be used to derive average (nvt) values for the individual wire positions. The description of the experiment notes that “The wires in the core were taped to the surfaces of the fuel plates along the centrelines and extended the full length of the assemblies” Ref. [VIII-2]. It is not clear if the ‘full length’ refers to the fuel plate height (7.94 m), the height of the assembly can (9.82 m), or some extended height. The data presented in the vertical flux profiles is relative to the top of the fuel plates and suggests that the range is from the top of the assembly can to the bottom of the lower end box.

Participants were asked to average the calculated vertical profiles over the range -2.54 cm to 77.47 cm below the top of the fuel plates as part of the normalization. Using this same approach, the digitized data was averaged and normalized to the Table VIII-13 core average values. The comparison of the tabular and digitized vertical profile data is shown in Table VIII-14. The ratios for the table values to the values derived from the vertical profiles are generally within ± 0.05 . This discrepancy can likely be attributed to the quality of the vertical profile data, uncertainty in the digitization process, and assumptions (range) and approximations (some profiles did not extend over the entire range and discrete digitized points used in the averaging were close but not exact with reference to the range considered) used in the averaging of the vertical profile data.

TABLE VIII-14. COMPARISON OF TABULATED AND VERTICAL PROFILE DATA FROM LITERATURE

Wire Location	Reported Data (Table V)			Vertical Profile Data (Renormalized)		
	Clean Average (nvt)	Voided Average (nvt)	Poisoned Average (nvt)	Clean Table:Profile Ratio	Voided Table:Profile Ratio	Poisoned Table:Profile Ratio
C - 7	2.85	2.97	3.08	1.03	0.99	0.98
C - 6	3.47	3.90	4.13	0.95	0.99	0.99
C - 5 ₂	3.97	4.15	4.40	1.01	1.01	0.98
D - 3	3.62	3.76	4.40	1.01	1.01	0.99
D - 4	4.46	4.79	5.30	1.01	1.01	1.00
D - 5 ₂	5.18	4.24	5.71	1.02	0.98	1.01
F - 5	5.24	4.63	5.90	1.00	1.02	0.99
E - 3	4.17	4.26	4.27	1.01	1.00	1.02
E - 4	5.25	4.46	5.74	1.00	0.99	1.00
E - 5 ₁	6.21	5.46	6.84	1.03	1.03	1.06
Core Avg	3.95	3.97	4.50	1.00	1.00	1.00
Maximum	9.30	7.75	10.85	0.96	0.94	1.02
Peak to Avg	2.35	1.95	2.41	0.95	0.94	1.02
Renormalization Factor				1.06	1.09	1.54

note: range for vertical profile data is -1.27 cm to 78.74 cm (where available)

VIII-4.5.2. Description and comparison of analysis approaches

The AUS, BGD and FRA groups provided complete results for the flux wire measurements section of the benchmark analysis while the PAK and SYR groups provided partial results. All groups used Monte Carlo codes for the flux analysis except for the PAK group which based their analysis on a diffusion theory code model.

Generally, only the complete flux results from AUS, BGD and FRA are discussed in detail in this report. Some of the PAK and SYR results are presented when relevant to the general discussion. All the partial flux profile results from PAK and SYR are included in the Appendices. The flux values presented in this report are normalised to the experimental core average flux for that particular core state using the results in Table V of [VIII-2] (Table VIII-13 above).

The average fluxes from the AUS and BGD groups were calculated between -2.54 cm and 77.47 cm below the top of the fuel plates. The FRA average fluxes for wires in G-7, C-6, C-5₂, D-3, D-4, D-5₂, F-5, E-3, E-4 and E-5₁ were evaluated between -5.08 cm and 81.28 cm. The average fluxes of the remaining wires were calculated between -2.54 cm and 77.47 cm. Calculated

results are evaluated against the average experimental fluxes across the entire range of available data. The average flux value varies up to approximately 10 %, depending on the range over which the average is calculated.

The AUS computed the flux across a volume of dimensions 0.45466 x 2 x 5.08 cm in the centre of the coolant channel in order to improve the statistics of the calculation. The thickness of the volume is equivalent to the size of the inner coolant gap. The (n, γ) reaction for Co-59 was applied to the volume averaged flux tally. The presented flux values are restricted to neutrons with energy less than 0.625eV. The control rod position used in the clean core calculations was the critical position of 14.45 in. withdrawn. The control rod position was adjusted to provide 2\$ of reactivity compensation for the voided and poisoned core. For the voided and poisoned core, the control rod position was 16.75 in. withdrawn.

The BGD group calculated the flux using the collision estimator option of MVP. At the tallying locations, small spherical water bubbles of radius 0.2 cm were defined in the locations of the flux measurements. Water bubbles were placed every 3cm from 2cm above from the top of the fuel plate to 78 cm below the top of the fuel plate. The flux tallies were calculated over the volume of these water bubbles. The energy bin 5×10^{-1} eV to 1×10^{-5} eV was considered as thermal flux. The calculated reactivity worth of the aluminium strips was found to be 2.22 \$. The rod bank was withdrawn up to 16.93 in. from the bottom of the fuel plate to add 2.22 \$ of the reactivity to compensate for the voids. The reactivity worth of the poison strips was calculated to be 2.05 \$. The rod bank was withdrawn from the bottom of the fuel plate up to 16.73 in. to add 2.05 \$ of reactivity to maintain a critical core.

The FRA group did not consider the Co-59 wires in the presented flux calculations. Instead, FRA used a function of TRIPOLI4 that computes the flux distributions over a user defined meshing. An axial meshing was defined at the centreline of all assemblies, and the thermal flux was calculated over this mesh. The location of 2\$ worth of aluminium void strips and 2\$ worth of borated strips for the poisoned core are presented in Fig. VIII-34. The FRA group positioned the control rods at 14.45 in. withdrawn for the clean core (reported critical position) and 16.7 in. withdrawn for the voided and poisoned cores (determined from the experimental control rod worth curve for 2\$ reactivity compensation).

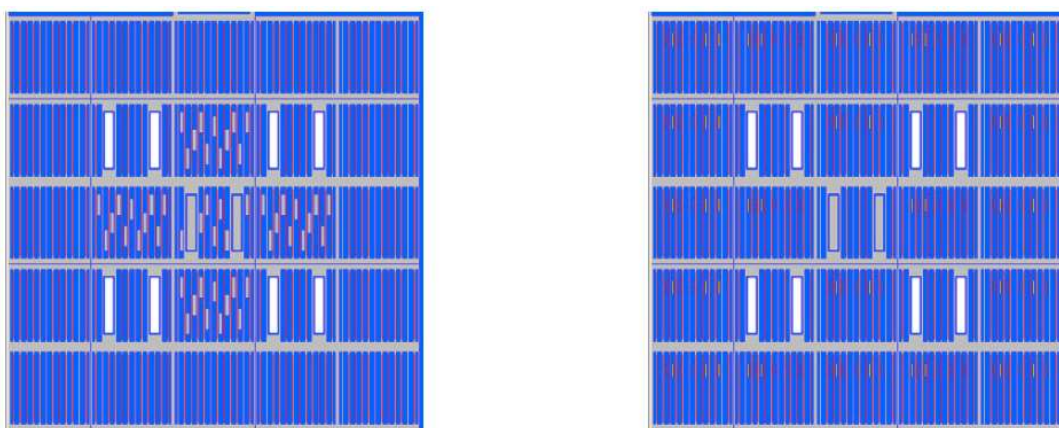


FIG. VIII-34. Locations of experimental strips in the void (left) and poisoned (right) cores for FRA.

VIII-4.5.3. Summary and comparison of benchmark results

The calculated results are presented below for each experimental core configuration: (i) clean, (ii) voided, and (iii) poisoned. Estimates from simulation are compared to the experimental values from Table VIII-13 for in-core wire positions and the digitized vertical profiles as a series of calculated to experimental (C/E) ratios for the reflector positions and for the points reported for the horizontal flux profiles. Select vertical profiles are presented while the complete sets of vertical and horizontal profiles are included in the appendices.

VIII-4.5.3.1. Clean Core

Table VIII-15 shows the calculated to experimental ratios for the clean core flux wire estimates from the AUS, BGD and FRA participants. With the exception of the core maximum values predicted by the BGD and FRA groups the results agree with measurement with C:E values ranging between 0.9 and 1.1, and generally with better agreement.

TABLE VIII-15. CLEAN CORE COMPARISON TO EXPERIMENTAL TABLE VALUES

Clean Core Wire	Average (nvt)	C:E Ratio AUS	C:E Ratio BGD	C:E Ratio FRA	D:E Ratio Profile
C - 7	2.85	0.96	0.98	0.96	0.98
C - 6	3.47	1.07	1.05	1.05	1.05
C - 5 ₂	3.97	1.01	1.01	1.01	0.99
D - 3	3.62	1.00	1.01	1.00	0.99
D - 4	4.46	0.99	0.99	1.00	0.99
D - 5 ₂	5.18	1.00	1.00	1.01	0.98
F - 5	5.24	0.99	1.00	1.00	1.00
E - 3	4.17	0.96	0.96	0.96	0.99
E - 4	5.25	0.99	0.98	0.99	1.00
E - 5 ₁	6.21	0.98	0.93	1.01	0.97
Core Avg	3.95	1.00	1.00	1.00	1.00
Maximum	9.30	1.03	1.12	1.15	1.06
Peak to Avg	2.35	1.03	1.12	1.15	1.06

note: C:E ratio is Calculated to Table Value, D:E ratio is Digitized Profile to Table ratio

Select vertical flux profiles for the in-core positions are shown in Fig. VIII-35. These are illustrative of the degree of agreement between the calculated and measured results. In general all three groups reproduced the experimental values to good agreement and to an uncertainty consistent with the values derived from the digitized vertical flux profiles. While some variation was found between the calculated and measured results in general the shape of the estimated profiles were consistent with the measured profiles including the position of the vertical flux peaks. The profile for position E-5₁ in Fig. VIII-35 as estimated by the FRA group represents the estimated maximum core value and accounts for this variation from measurement in Table VIII-15.

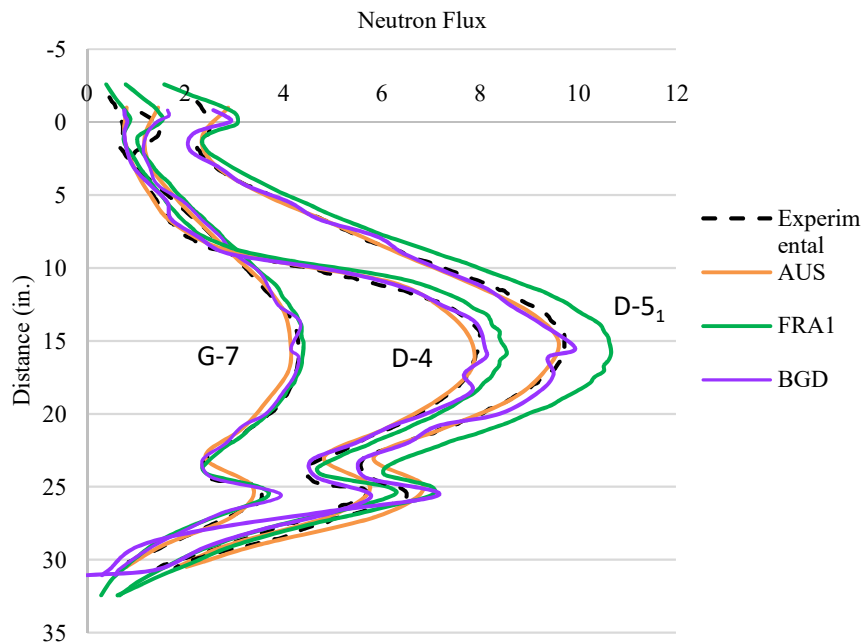


FIG. VIII-35. Clean core normalized vertical flux profiles for positions G-7, D-4, And E-5₁.

While tabular data is reported only for in-core wire positions calculated values for the ex-core wire locations (B-5 and E-2) can be compared to the data extracted from the vertical flux profiles for these positions. These comparisons are summarized in Table VIII-16. A similar degree of agreement is found between the calculated and measured values for these reflector positions as for the in-core wires. It is however of note that in general the reflector average and peak values are overestimated, with good agreement to the peak-to-average ratio for the AUS and FRA results.

Calculated results were also found to be consistent with measured values for the specified horizontal profiles through the clean core configuration. The data for the calculated horizontal flux profile estimates from each participating group was extracted from the respective vertical flux profiles. The horizontal profile through the N-S direction at the 22.86 cm elevation below the top of the fuel plates is shown in Fig. VIII-36 and is illustrative of the comparison of calculated estimates to experimental results. The FRA results in Fig. VIII-36 overestimate the measured values with C:E ratios of up to 1.17. Better agreement is observed for the FRA results for the other elevations. The complete set of horizontal flux profile comparisons is included in Appendix A.

TABLE VIII-16. CLEAN CORE COMPARISON TO DIGITIZED VERTICAL PROFILES (REFLECTOR POSITIONS)

Wire	Experimental			AUS (C:E)			BGD (C:E)			FRA (C:E)		
	Avg	Peak	Peak: Avg	Avg	Peak	Peak: Avg	Avg	Peak	Peak: Avg	Avg	Peak	Peak: Avg
B-5 ₁	5.70	9.70	1.70	0.96	0.94	0.98	1.04	0.94	0.91	1.04	1.04	1.00
B-5 ₂	5.67	9.51	1.68	1.04	1.04	1.00	1.08	1.16	1.07	1.08	1.11	1.03
B-5 ₃	5.23	8.86	1.69	1.08	1.08	1.00	1.07	1.13	1.05	1.07	1.10	1.03
B-5 ₄	4.00	7.08	1.77	1.05	1.02	0.97	0.99	0.96	0.96	0.99	0.97	0.98
E-2 ₁	5.57	9.34	1.68	0.98	0.96	0.99	1.05	1.07	1.01	1.05	1.08	1.02
E-2 ₂	5.84	10.0	1.71	1.02	1.01	0.99	1.06	1.07	1.01	1.06	1.07	1.01
E-2 ₃	5.39	9.13	1.69	1.05	1.06	1.02	1.05	1.09	1.04	1.05	1.08	1.03
E-2 ₄	3.99	6.76	1.70	1.07	1.09	1.02	1.01	1.05	1.05	1.01	1.03	1.02
min				0.96	0.94	0.97	0.99	0.94	0.91	0.99	0.97	0.98
max				1.08	1.09	1.02	1.08	1.16	1.07	1.08	1.11	1.03

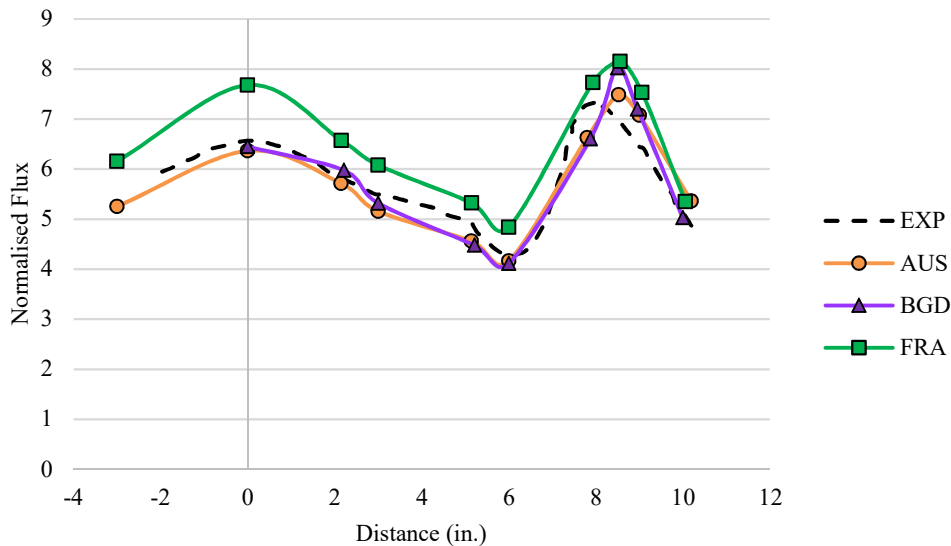


FIG. VIII-36. Clean core horizontal flux N-S profile at 22.86 cm elevation.

The PAK and SYR groups submitted partial results for the SPERT IV D-12/25 clean core flux profiles. The PAK group report vertical flux profiles for the C-6, D-3, E-4, F-5, and G-7 positions while the SYR group reports a single vertical flux profile for the E-5-2 position. These groups did not submit results for either the voided or poisoned core configurations.

Figure VIII-37 is illustrative of the PAK results. The general features of the vertical flux profile, i.e., the axial and reflector flux peaks, are captured in the PAK estimates which are consistent with the estimates from the other participants and the experimental data. There is some difference to the experimental profile shape beyond that found with the estimates from the AUS, BGD, and FRA. Without further information the source of the differences cannot be identified. Similarly, Fig. VIII-38 shows the vertical profile submitted by the SYR group overlaid on the estimates from the AUS, BGD, and FRA groups and the experimental data. As per the PAK groups, a general agreement and emulation of profile features is observed. Of note are

differences in the top reflector region of the profile and an offset of the profile compared to the experimental data in the bottom half of the curve. Again, without further information the source of these differences cannot be identified.

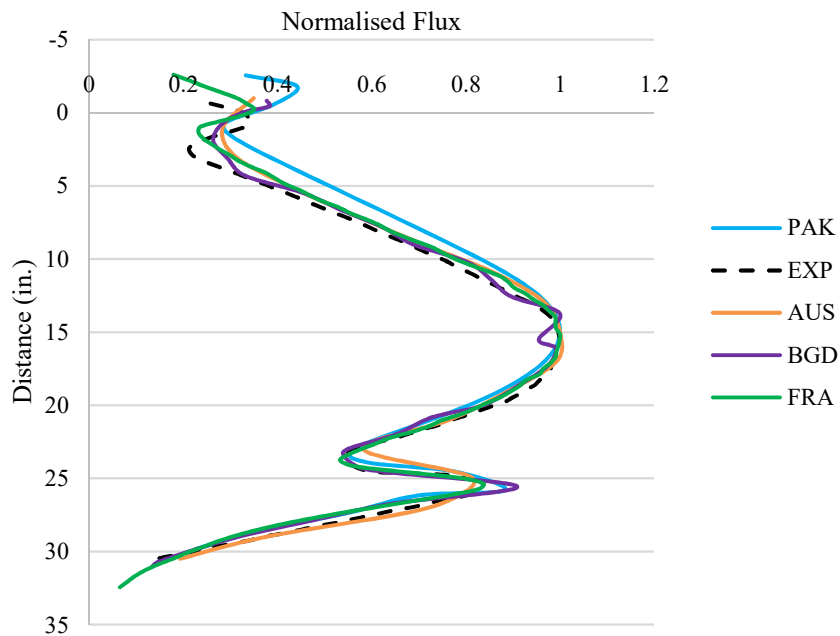


FIG. VIII-37. Clean core normalized vertical flux profile for position G-7, normalized to peak.

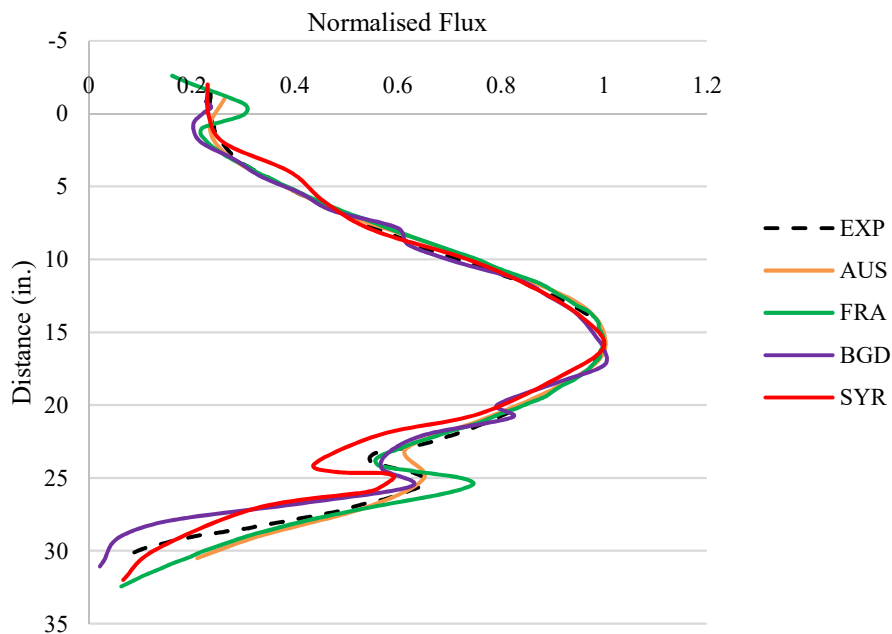


FIG. VIII-38. Clean core normalized vertical flux profile for position E-5-2, normalized to peak.

VIII-4.5.3.2. Voided Core

Table VIII-17 presents the calculated to experimental ratios for the voided core flux wire estimates from the AUS, BGD and FRA participants. C:E values are mostly between 0.9 and 1.1 with only a few exceptions and generally closer to 1.0. The same overestimation of the core *maximum* value is observed for the BGD and FRA results.

TABLE VIII-17. VOIDED CORE COMPARISON TO EXPERIMENTAL TABLE VALUES

Voided Core Wire	Average (nvt)	C:E Ratio AUS	C:E Ratio BGD	C:E Ratio FRA	D:E Ratio Profile
C - 7	2.97	0.96	0.95	0.96	1.01
C - 6	3.90	1.03	0.96	0.98	1.01
C - 5 ₂	4.15	0.99	1.01	1.00	0.99
D - 3	3.76	1.00	1.02	1.01	0.99
D - 4	4.79	0.97	0.98	0.98	0.99
D - 5 ₂	4.24	1.08	1.12	1.10	1.02
F - 5	4.63	1.00	1.03	1.01	0.98
E - 3	4.26	0.95	0.97	0.97	1.00
E - 4	4.46	1.04	1.07	1.05	1.02
E - 5 ₁	5.46	0.99	1.00	1.02	0.97
Core Avg	3.97	1.00	1.00	1.00	1.00
Maximum	7.75	1.02	1.13	1.13	1.09
Peak to Avg	1.95	1.02	1.13	1.13	1.09

Note: C:E ratio is Calculated to Table Value, D:E ratio is Digitized Profile to Table ratio

As for the clean core configuration the most significant deviations from the calculated results are observed in the reflector region for the wires in the B-5 and E-2 locations. The C:E ratios for the calculated results compared to the experimental results extracted from the vertical flux profiles are summarized in Table VIII-18 for these positions. Again, the general trend is towards an overestimation of the flux in these reflector positions.

The same select vertical profiles as presented for the clean core are shown for the voided core in Fig. VIII-39. These are illustrative of the degree of agreement between the calculated and measured results. As for the clean core, good agreement was found between the calculated estimates and the experimental results, consistent with the uncertainty in the values derived from the digitized vertical flux profiles. While some variation was found between the calculated and measured results, in general the shapes of the estimated profiles were consistent with the measured profiles including the position of the vertical flux peaks.

TABLE VIII-18. VOIDED CORE COMPARISON TO DIGITIZED VERTICAL PROFILES (REFLECTOR POSITIONS)

Wire	Experimental			AUS (C:E)			BGD (C:E)			FRA (C:E)		
	Avg	Peak	Peak:Avg	Avg	Peak	Peak:Avg	Avg	Peak	Peak:Avg	Avg	Peak	Peak:Avg
B-5 ₁	5.77	9.57	1.66	0.98	0.95	0.97	0.99	1.02	1.03	1.07	1.07	1.00
B-5 ₂	5.93	9.88	1.67	1.03	1.03	1.00	1.07	1.07	1.01	1.09	1.11	1.02
B-5 ₃	5.32	8.93	1.68	1.09	1.08	0.99	1.10	1.13	1.03	1.10	1.12	1.02
B-5 ₄	4.07	6.80	1.67	1.07	1.08	1.00	1.01	1.09	1.08	1.03	1.04	1.02
E-2 ₁	5.78	9.45	1.64	0.97	0.97	1.00	1.04	1.06	1.02	1.07	1.08	1.02
E-2 ₂	6.00	10.07	1.68	1.02	1.01	0.99	1.07	1.07	1.00	1.08	1.08	1.01
E-2 ₃	5.35	8.81	1.65	1.09	1.11	1.02	1.12	1.19	1.06	1.11	1.14	1.03
E-2 ₄	4.11	6.96	1.69	1.07	1.06	0.99	1.02	1.09	1.07	1.02	1.02	1.00
min				0.97	0.95	0.97	0.99	1.02	1.00	1.02	1.02	1.00
max				1.09	1.11	1.02	1.12	1.19	1.08	1.11	1.14	1.03

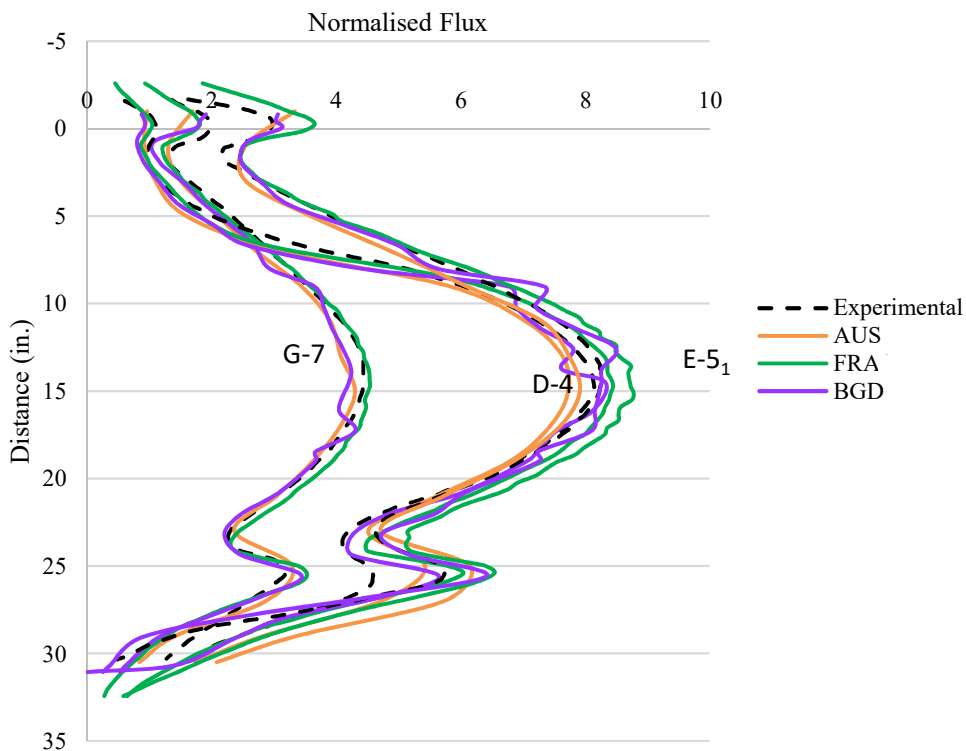


FIG. VIII-39. Voided core normalized vertical flux profiles for positions G-7, D-4, and E-5₁.

It was also found that for some wire positions there is an offset of the measured and calculated peak of the vertical profiles. This is shown in Fig. VIII-40 for position E-4 and was also observed for the reflector positions. Both Fig. VIII-39 and Fig. VIII-40 illustrate fluctuations in the BGD profiles beyond the statistical uncertainty of the calculations. This characteristic was also observed on the clean core and poisoned core BGD results. Investigation of this is left as future work.

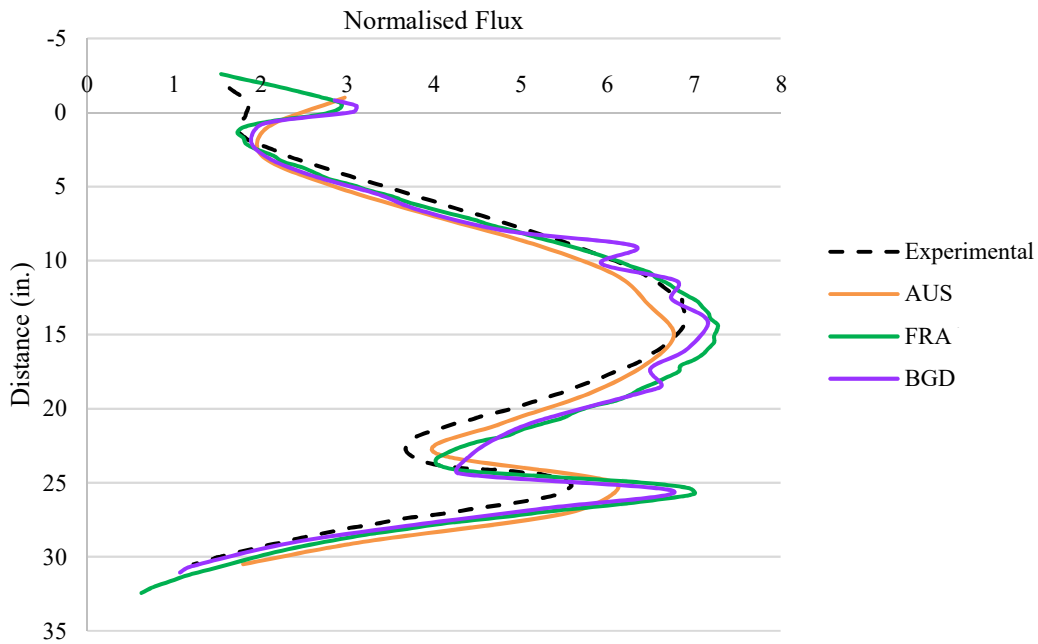


FIG. VIII-40. Voided core normalized vertical flux profile for position E-4.

Calculated results were also found to be consistent with measured values for the specified horizontal profiles through the voided core configuration. The data for the calculated horizontal flux profile estimates from each participating group was extracted from the respective vertical flux profiles. The horizontal profile through the N-S direction at the 36.83 cm elevation below the top of the fuel plates is shown in Fig. VIII-41 and is illustrative of the comparison of calculated estimates to experimental results. The FRA results in Fig. VIII-41 overestimate the measured values with C:E ratios of up to 1.13. The complete set of horizontal flux profile comparisons is included in Appendix C.

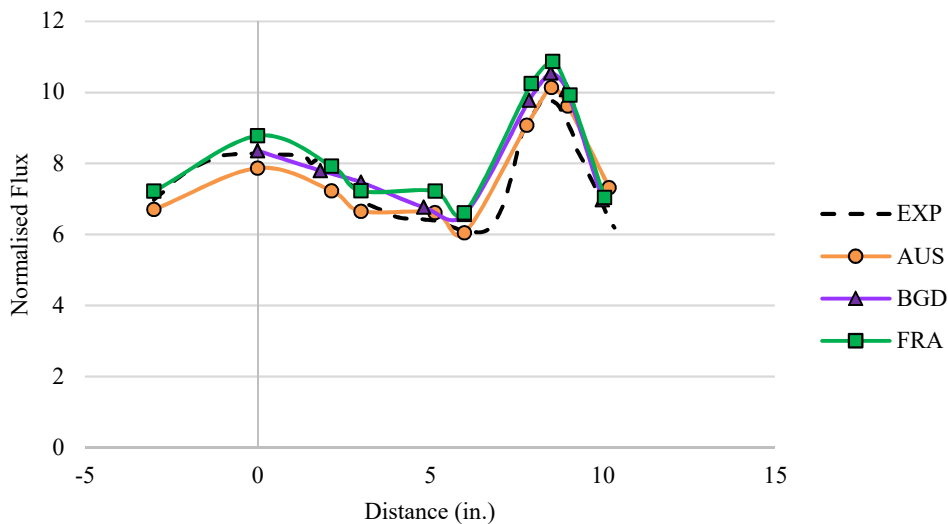


FIG. VIII-41. Voided core horizontal flux N-S profile at 36.83cm elevation.

VIII-4.5.3.3. Poisoned Core

Table VIII-19 presents the calculated to experimental ratios for the poisoned core flux wire estimates from the AUS, BGD and FRA participants. C:E values are mostly between 0.9 and 1.1 with only a few exceptions and generally much closer to 1.0.

As for the clean and voided core configurations the most significant deviations from the calculated results are observed in the reflector region for the wires in the B-5 and E-2 locations. The C:E ratios for the calculated results compared to the experimental results extracted from the vertical flux profiles are summarized in Table VIII-20 for these positions. Again the general trend is towards an overestimation of the flux in these reflector positions.

TABLE VIII-19. POISONED CORE COMPARISON TO EXPERIMENTAL TABLE VALUES

Poisoned Core Wire	Average (nvt)	C:E Ratio AUS	C:E Ratio BGD	C:E Ratio FRA	D:E Ratio Profile
C - 7	3.08	1.01	1.00	1.00	1.02
C - 6	4.13	1.00	1.00	1.00	1.01
C - 5 ₂	4.40	1.03	1.03	1.03	1.02
D - 3	4.40	0.93	0.94	0.93	1.01
D - 4	5.30	1.00	1.00	1.00	1.00
D - 5 ₂	5.71	1.04	1.04	1.04	0.99
F - 5	5.90	1.00	1.00	1.01	1.01
E - 3	4.27	1.05	1.07	1.06	0.98
E - 4	5.74	1.03	1.02	1.03	1.00
E - 5 ₁	6.84	1.03	0.99	1.07	0.95
Core Avg	4.50	1.00	1.00	1.00	1.00
Maximum	10.85	0.98	1.05	1.11	1.08
Peak to Avg	2.41	0.98	1.05	1.11	1.08

TABLE VIII-20. POISONED CORE COMPARISON TO DIGITIZED VERTICAL PROFILES (REFLECTOR POSITIONS)

Wire	Experimental			AUS (C:E)			BGD (C:E)			FRA (C:E)		
	Avg	Peak	Peak:Avg	Avg	Peak	Peak:Avg	Avg	Peak	Peak:Avg	Avg	Peak	Peak:Avg
B-5 ₁	6.27	10.5	1.70	0.99	0.94	0.96	1.11	1.14	1.03	1.07	1.04	0.98
B-5 ₂	6.50	11.26	1.73	1.04	0.99	0.96	1.09	1.11	1.02	1.08	1.05	0.98
B-5 ₃	5.82	10.19	1.75	1.09	1.05	0.96	1.10	1.07	0.97	1.10	1.06	0.97
B-5 ₄	4.45	7.66	1.72	1.08	1.06	0.98	1.01	1.03	1.03	1.02	1.01	0.99
E-2 ₁	6.52	10.63	1.63	0.95	0.96	1.01	1.05	1.11	1.05	1.03	1.05	1.02
E-2 ₂	6.50	10.47	1.61	1.05	1.09	1.04	1.10	1.17	1.07	1.09	1.14	1.05
E-2 ₃	5.91	9.91	1.68	1.10	1.11	1.01	1.11	1.12	1.02	1.10	1.11	1.01
E-2 ₄	4.37	7.24	1.66	1.12	1.14	1.02	1.04	1.15	1.11	1.06	1.09	1.03
min				0.95	0.94	0.96	1.01	1.03	0.97	1.02	1.01	0.97
max				1.12	1.14	1.04	1.11	1.17	1.11	1.10	1.14	1.05

The same select vertical profiles as presented for the clean and voided cores are shown for the poisoned core in Fig. VIII-42. These are illustrative of the degree of agreement between the

calculated and measured results. As for the clean and voided cores, good agreement was found between the calculated estimates and the experimental results, consistent with the uncertainty in the values derived from the digitized vertical flux profiles. While some variation was found between the calculated and measured results in general the shape of the estimated profiles were consistent with the measured profiles.

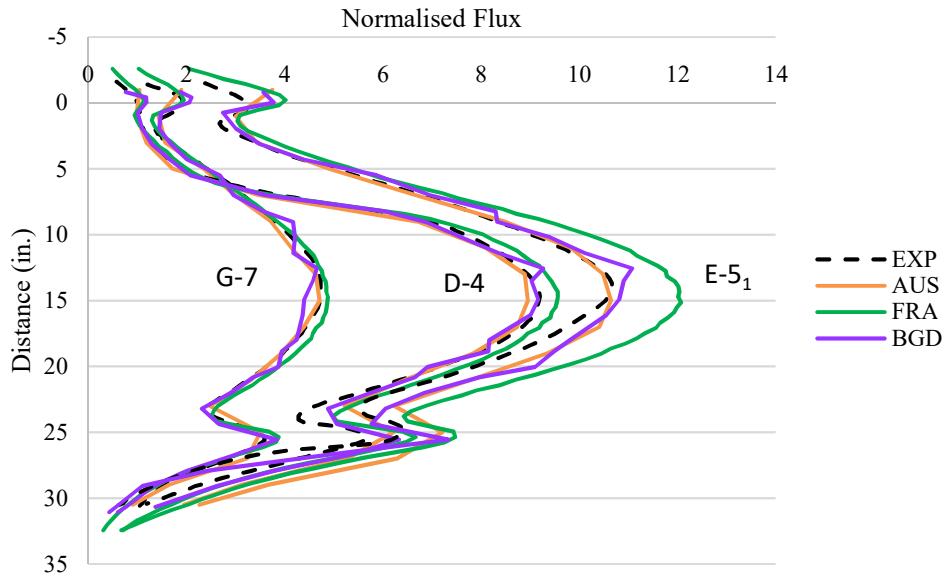


FIG. VIII-42. Poisoned core normalized vertical flux profiles for positions G-7, D-4, and E-5₁

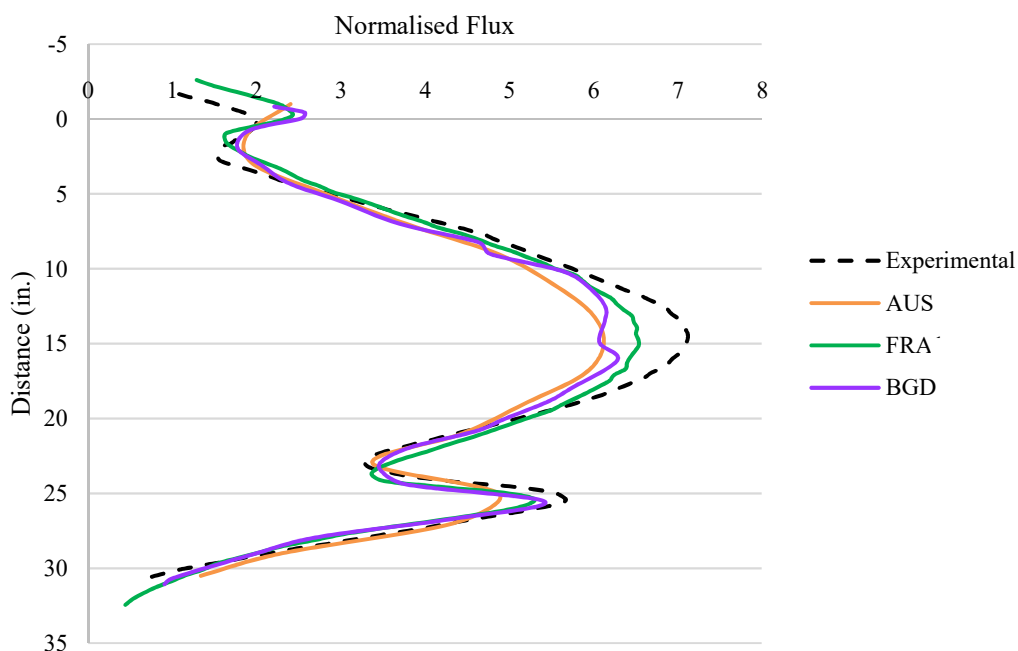


FIG. VIII-43. Poisoned core normalized flux profile of D-3.

Figure VIII-43 displays the flux profile at position D-3 of the poisoned core, showing a significant underestimation of the peak flux by all groups, ranging from 10% up to 16%. However, most of the other features of the flux profile are well estimated. This appears anomalous as the estimates for the other profiles do not exhibit this significant underestimation.

VIII-4.5.4. Conclusions and recommendations

The experimental flux profiles were well reproduced by all groups. Minor deviations of around 10% from the measured results were observed in some specific cases. In particular the results for the voided and poisoned core had the largest discrepancies and in some cases there were shifts in the position of the vertical flux peak. All complete sets of calculated results were generated from Monte Carlo codes, demonstrating that this method is well suited to this detailed analysis. The general good agreement with experimental results and common underestimation (Fig. VIII-43) and overestimation (Fig. VIII-42) of some flux profiles indicate that the user/code effect in this analysis is small and that a more likely explanation in these particular instances is the quality or interpretation of the data itself.

VIII-4.6. Cadmium Ratio

VIII-4.6.1. Short description of the experiment

The Cadmium ratio at 12 in. below the top of the fuel plates was determined by irradiating bare ^{59}Co wires and Cd covered ^{59}Co wires both within the core and just outside in the reflector to determine how the neutron spectrum varies with location and for each of the core states. Details of the wire locations are displayed in Fig. VIII-33.

VIII-4.6.2. Description and comparison of analysis approaches

The FRA group did not complete the cadmium ratio section due to convergence difficulties in TRIPOLI4. In addition, the meshing function used to compute the flux in section 4.5 is not applicable in this situation.

The AUS group completed the cadmium ratio calculations by modifying the MCNP model of the SPERT IV D-12/25 core to include ^{59}Co wires and Cd sleeves. The ^{59}Co wire and Cd sleeve were centred 12.5 in. from the top of the fuel plates and were 1.25 in. long. These were located in the coolant channel positions E-5₁, E-4, E-3, and E-2₃. A surface source file was written for the boundary surfaces of the coolant channels containing Cd sleeves and ^{59}Co wires.

Two simplified models were then created to reduce the computational time required to calculate a statistically meaningful flux averaged over the ^{59}Co wire volume. The first model consisted of four coolant channels E-5₁, E-4, E-3, and E-2₃ with ^{59}Co wires in each channel; the second model comprised of the same four coolant channels with ^{59}Co wires encased in Cd sleeves. The coolant channels were surrounded by a void region.

MCNP calculations using the surface source file as the neutron source were executed for these models, with the calculations terminated after ten times the original number of histories in the surface source file were run. The cadmium ratio was then computed by calculating the ratio of the Co-59 reaction rates between the bare wire and the Cd covered wire.

The BGD group placed a 0.2 cm diameter ^{59}Co sphere at 30.48 cm below from the top of the fuel plate at E-5₁, E-4, E-3, E-2₃ locations. The absorption reaction rate at the ^{59}Co sphere was calculated in three different energy bins: 2×10^7 to 1×10^3 and 1×10^3 to 5×10^{-1} and 5×10^{-1} to 1×10^{-5} eV. The Cd-ratio was computed by dividing the total reaction rate by the reaction rate at the high energy range (2×10^7 to 3×10^{-1}) eV.

VIII-4.6.3. Summary and comparison of benchmark results

The Cd ratio for the clean, voided and poisoned core configurations are displayed in Table VIII-21 to Table VIII-23 and Figs. VIII-44 to VIII-46.

For the clean core configuration (Table VIII-21 and Fig. VIII-44), the AUS group underestimated the Cd ratio by up to 26%, while the BGD group overestimated the Cd ratio by up to 31% within the core boundary and by 115% outside of the fueled core.

TABLE VIII-21. CD RATIO OF THE CLEAN CORE

Distance	Clean Core Cd Ratio			C/E	
	EXP	AUS	BGD	AUS	BGD
0	7.54	6.34	9.86	0.84	1.31
3	7.48	6.85	8.30	0.92	1.11
6	7.95	5.88	10.15	0.74	1.28
9	19.12	14.98	41.07	0.78	2.15

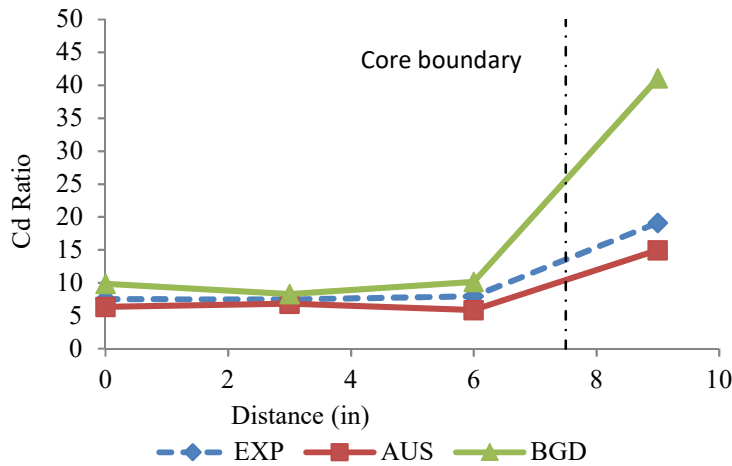


FIG. VIII-44. CD ratio of the clean core.

The Cd ratio for the voided core is displayed in Table VIII-22 and Fig. VIII-45 below. The Cd ratios in the core computed by the AUS group agree to within 11% of the experiment results; however, there is a significant discrepancy of 21% outside of the core. The BGD calculated Cd ratios are up to 48% higher than the experimental results in the core and 133% higher outside the core.

TABLE VIII-22. CD RATIO OF THE VOIDED CORE

Distance	Voided Core Cd Ratio			C/E	
	EXP	AUS	BGD	AUS	BGD
0	6.69	6.13	9.91	0.92	1.48
3	5.90	6.55	7.78	1.11	1.32
6	7.42	7.15	9.18	0.96	1.24
9	19.66	15.60	45.81	0.79	2.33

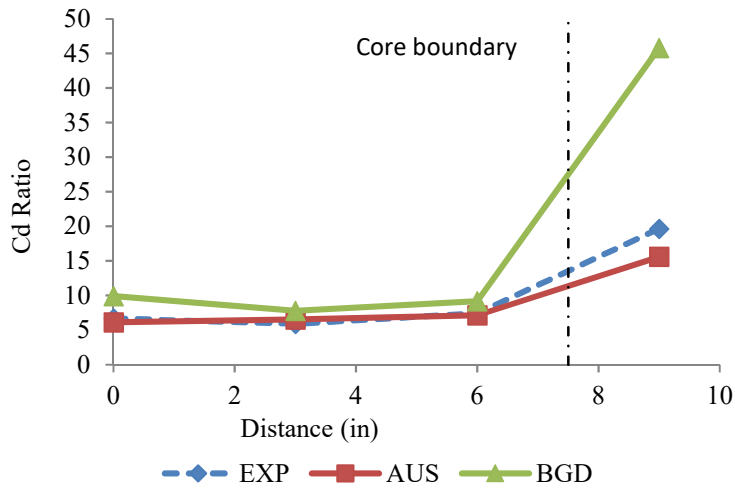


FIG. VIII-45. CD ratio of the voided core.

Table VIII-23 and Fig. VIII-46 display the Cd ratios of the poisoned core configuration. The AUS group calculated a Cd ratio up to 24% lower than the experimental value within the core, and 36% lower than the experimental value outside of the core. The BGD results overestimate the Cd ratio by 7% at the centre of the core and up to 87% outside of the core boundary.

TABLE VIII-23. CD RATIO OF THE POISONED CORE

Distance	Poisoned Core Cd Ratio			C/E	
	EXP	AUS	BGD	AUS	BGD
0	8.77	6.65	9.41	0.76	1.07
3	7.21	5.69	9.44	0.79	1.31
6	7.07	7.44	9.99	1.05	1.41
9	21.89	13.95	40.86	0.64	1.87

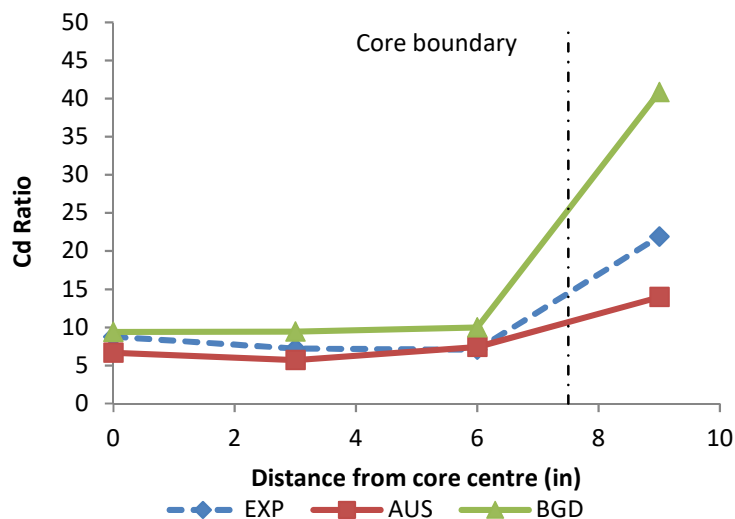


FIG. VIII-46. CD ratio of the poisoned core.

Generally, the Cd ratios were underestimated by the AUS group and overestimated by the BGD group. The largest difference between measured and calculated results occurred outside of the core boundary at position E-2.

VIII-4.6.4. Conclusions and recommendations

Both sets of results for this section of the benchmark yielded Cd ratios which were in poor agreement with the experimental results. In addition, the FRA group was unable to compute the Cd ratio. This is a reflection of the difficulty and lack of experience in this type of calculation amongst the participants. In the case of the method implemented by both participants the results are sensitive to some of the adopted parameters. In the case of the AUS calculation the choice of surface source will have some impact on the result obtained. In the case of the BGD calculation the choice of energy cut-off to represent the effect of the Cd cover will have a significant impact on the result (in particular for the well thermalized reflector region). In both cases it is not clear if these parameters were studied and optimized to yield the best result, but such an exercise needs to be performed given the numerical approximations adopted.

VIII-4.7. Kinetics Parameters

VIII-4.7.1. Short description of the experiment

The reduced prompt neutron lifetime, ℓ/β_{eff} was measured for the SPERT IV D-core via both noise analysis and transient methods. Further details can be found in [VIII-2].

VIII-4.7.2. Description and comparison of analysis approaches

AUS, SYR, FRA and FRA2 used Monte Carlo codes to compute the kinetic parameters. PAK utilized a diffusion code, while BGD calculated the reduced prompt neutron lifetime directly by the Feynman alpha method using data generated by Monte Carlo. AUS used MCNP with the library ENDF/B-VII.0 for calculation of the kinetic parameters. β_{eff} was computed by MCNP calculations of k_{eff} for the SPERT IV D-12/25 core for all neutrons (k_a) and for prompt neutrons only (k_p). The effective delayed neutron fraction was calculated using the following formula:

$$\beta_{\text{eff}} = \frac{(k_a - k_p)}{k_a} \quad (\text{VIII.2})$$

The prompt neutron lifetime was calculated using the $1/v$ insertion method. The prompt neutron lifetime was obtained by calculating k_{eff} for a uniform distribution of different concentrations (N) of a $1/v$ neutron absorber in the MCNP model. The prompt neutron lifetime is obtained from the equation below as the absorber concentration approaches zero.

$$l_p = \lim_{N \rightarrow 0} \frac{\delta k}{k_p N \sigma_{a0} V_0} \quad (\text{VIII.3})$$

B-10 was used as the absorber, with $\sigma_{a0} = 3837$ barns and $v_0 = 2200 \text{ m}\cdot\text{s}^{-1}$. BGD calculated the reduced prompt neutron lifetime by using MVP to generate time correlated data to analyse with the Feynman alpha formula. Data was analysed for gate widths less than 0.2s. MVP was also used to calculate β_{eff} as the ratio of the fission rates for delayed neutrons to total (prompt and delayed). The fission rates were calculated for ^{234}U , ^{235}U , ^{236}U and ^{238}U nuclides. Data was taken from JENDL 3.3 library. The prompt neutron lifetime was calculated using the reduced prompt neutron lifetime and β_{eff} .

FRA utilized a new function of the Monte Carlo code, TRIPOLI4 to calculate β_{eff} using the prompt method. The new function also provided the prompt neutron lifetime.

FRA2 utilized the sensitivity coefficients computed with TRIPOLI-3D module in SCALE 6.0 to apply them to the variation of fission spectra perturbation as follows:

$$\beta_{eff} = \sum_g S_{\chi,g} \frac{\chi_{d,g}}{\chi_g} \quad (\text{VIII.4})$$

Where $S_{\chi,g}$ is group-wise sensitivity coefficient which has been calculated for the entire core, χ_g is the group-wise fission spectrum and $\chi_{d,g}$ are the group-wise delayed neutron spectra. Neutron generation lifetime has been estimated using the $1/v$ absorber method that is the strict formalism of boron poisoning used by AUS.

PAK used the diffusion code CITATION with the in-built standard flux and adjoint flux solutions for effective delayed neutron fraction and prompt neutron lifetime. The SYR group used the Monte Carlo code MCNP to calculate the kinetic parameters in this benchmark. No further details were provided from this group.

VIII-4.7.3. Summary and comparison of benchmark results

A summary of the measured and calculated kinetic parameters of the SPERT IV D-12/25 core is presented in Table VIII-24. There is good agreement between most groups for β_{eff} , with the calculated range between 765 and 797 pcm. BGD reports a value of 650 pcm, which is significantly lower than the value obtained by the other participants. The prompt neutron lifetime was calculated to be in the narrow range of 62.2 to 64 μsec for the PAK, AUS and FRA groups. However, the SYR and BGD values were significantly higher at 79.4 and 89.5 μsec , respectively. The reduced prompt neutron lifetime, ℓ/β_{eff} , computed by the AUS, FRA and PAK groups agreed well with the measured value, with a discrepancy of less than 3%. In contrast, the BGD and SYR groups overestimate the measured value by 70% and 23%, respectively.

TABLE VIII-24. KINETIC PARAMETERS

Source	β_{eff} (pcm)	$\sigma(\beta_{eff})$ (pcm)	ℓ (μsec)	$\sigma(\ell)$ (μsec)	ℓ/β_{eff} (sec)	$\sigma(\ell/\beta_{eff})$ (sec)	ℓ/β_{eff} C/E
Measured 1 ¹	-	-	-	-	8.10×10^{-3}	9.00×10^{-5}	-
Measured 2 ¹	-	-	-	-	8.10×10^{-3}	1.70×10^{-4}	-
AUS	765	4	63.5	5.1	8.30×10^{-3}	6.65×10^{-4}	1.02
BGD ²	780	-	89.5	-	1.38×10^{-2}	-	1.70
FRA	768	9	64.0	0.2	8.33×10^{-3}	1.30×10^{-4}	1.03
FRA2	783	-*	63.9	-	8.17×10^{-3}	-	1.01
PAK	783	-	62.2	-	7.94×10^{-3}	-	0.98
SYR	797	-	79.4	-	9.95×10^{-3}	-	1.23

¹ Measured 1 is from transient data, Measured 2 is from subcritical noise analysis

² BGD reports a value of 650 pcm for β_{eff} but uses a value of 780 pcm for converting units

(*) The uncertainty was not shown because Monte-Carlo statistical fluctuations are negligible compared to systematic uncertainties

VIII-4.7.4. Conclusions and recommendations

All groups except BGD calculated β_{eff} within a narrow range that can be classed as good agreement. These results indicate that the inbuilt functions of the Monte Carlo codes, MCNP and TRIPOLI4, produce reliable delayed neutron fraction results. Large discrepancies in the

BGD and SYR groups' calculations of the prompt neutron lifetime resulted in large C/E ratios of 1.23 and 1.70, respectively, for the reduced prompt neutron lifetime. The use of the inbuilt TRIPOLI4 function to compute the prompt neutron lifetime generated a reduced prompt neutron lifetime which is in excellent agreement with the measured value. Similarly, the good agreement of AUS reduced prompt neutron lifetime to the measured value validates the $1/v$ perturbation method to compute the prompt neutron lifetime. The CITATION diffusion code utilized by the PAK group also produces results which are in good agreement with the measured value.

VIII-5. CONCLUSIONS

FRA Monte Carlo transport-theory based TRIPOLI 4.7 calculations were found to be overall reasonably accurate in comparison to experimental values. Some limitations were noted for situations of simulation of small reactivity changes, such as the temperature coefficient of the system over small temperature ranges, where the statistical uncertainty and convergence of the Monte Carlo calculations requires many histories. In this case alternative methods need to be considered. Good agreement was observed for core flux distribution with most values within 10%. Relative values and features such as peaks and troughs were generally well predicted. Good agreement with experiment was also demonstrated for the reduced prompt neutron lifetime ℓ/β_{eff} ratio of the kinetics parameters.

AUS Monte Carlo based MCNP calculations provided reliable results and good agreement for most of the experimental data. Statistical fluctuations in some of the results were managed by fitting the calculated results to smooth functions. This method of analysis proved adequate for some cases. Good agreement was observed for core flux distribution with most values within 10%. Relative values and features such as peaks and troughs were generally well predicted. Good agreement with experiment was also demonstrated for the reduced prompt neutron lifetime ℓ/β_{eff} ratio of the kinetics parameters.

BGD Monte Carlo based code MVP provided reliable results for most experiments but unreliable estimates for others. The basic reactor reactivity, excess reactivity and control rod worths were well estimated. Reliable estimates were also provided for reactivity void coefficients and flux profiles. Unreliable estimates were obtained for the kinetic parameters and Cd ratios although this is more likely to be a result of the method adopted to calculate these values rather than the direct results from the code and model themselves. Some further work in these areas may eventually yield improved results as obtained by some of the other Monte Carlo codes.

Some of the observed discrepancies are attributed to uncertainties regarding particular experimental details and it is recommended that more precise data be provided, for example, the location of aluminium strips used in the void experiments.

The process of compiling and assessing the various analysis submissions served to help identify and highlight areas in which the quality of the SPERT IV D-12/25 Core benchmark analysis could be improved. Suggested revisions to the benchmark specification include adding:

1. Detailed specifications associated with the tapering of the poison and follower sections of the control rods. This degree of freedom allowed participating groups to optimize their results to such an extent that modelling and methodology effects related to criticality predictions could not be fully assessed.

2. The explicit definition of absorber rod positioning, i.e., the tip of the taper of the poison section of the absorber rods relative to the top or bottom of the fuel zone, would further aid in assessing criticality estimates.
3. Specific fuel assembly fissile loading and assembly location in the core configurations used in the experiments. This would help refine the assessment of calculated estimates compared to measurement.
4. Experimental details of the location of the aluminium void strips within the associated fuel assemblies for the uniform, radial, and vertical void reactivity experiments. This degree of freedom was again used to optimize participant estimates.
5. While assessed to be a minor effect, explicit specifications for the top and bottom end boxes of the fuel assemblies, lifting bails, lower grid structure, and flow skirt would remove some secondary uncertainty related to the calculations.
6. Clarification of the flux and fluence results presented and in particular the definition of flux adopted.
7. Clarification of the averaging procedure adopted for the Table V fluence values.

REFERENCES TO ANNEX VIII

- [VIII-1] DAY, S. E., SPERT IV D-12/25 Reactor Specification, Technical Report Series 480, IAEA, Vienna, (2012).
- [VIII-2] DAY, S. E., SPERT IV D-12/25 Benchmark Specification, Technical Report Series 480, IAEA, Vienna, (2012).
- [VIII-3] SCALE: A Modular Code System for Performing Standardized Computer Analyses for Licensing Evaluation, ORNL/TM-2005/39, Version 6, Vols. I–III, Oak Ridge National Laboratory, Oak Ridge, Tennessee, (2009).
- [VIII-4] BRIESMEISTER, J.F., MCNP–A General Monte Carlo N-Particle Transport Code 276 (Version C). Oak Ridge National Lab, Tennessee, (1997).

ANNEX IX

REPORTS FROM THE PARTICIPANTS OF THE COORDINATED RESEARCH PROJECT

CD-ROM for individual participant reports (prepared and published as working document).

LIST OF ABBREVIATIONS

Abbreviation	Full Name
ALG	Algeria
ANS	American Nuclear Society
ANSTO	Australia's Nuclear Science and Technology Organization
ARG	Argentina
ASTEC	Accident Source Term Evaluation Code
AUS	Australia
BATAN	National Nuclear Energy Agency of Indonesia
BGD	Bangladesh
BRA	Brazil
CAN	Canada
CATHARE	Code for Analysis of Thermal-hydraulics during Accident of Reactor and Safety Evaluation
CEA	Commissariat à L'Energie Atomique et Aux Energies Alternatives
CIF	Central Irradiation Facility
CRP	Coordinated Research Project
CUCGP	CUDA Course Grained Particles
DCH	Direct Containment Heating
DNB	Departure from Nucleate Boiling
DT	Doubling Times
EAEA	Egyptian Atomic Energy Authority
EGY	Egypt
ETR-2	Experimental Training Research Reactor - 2
FRA	France-CEA
FRA2	France-IRSN
GHA	Ghana
GRE	Greece
HEU	High Enriched Uranium
IAEA	International Atomic Energy Agency
IEA	Instituto de Energia Atômica
IFA	Instrument Fuel Assembly
IFE	Instrumented Fuel Elements
INVAP	Investigaciones Aplicadas
IPEN	Instituto de Pesquisas Energéticas e Nucleares
IRSN	Institut de Radioprotection et de Sûreté Nucléaire
ITER	International Thermonuclear Experimental Reactor
JAEA	Japan Atomic Energy Agency
LANL	Los Alamos National Laboratory
LEU	Low Enriched Uranium
LOCA	Loss of Coolant Accident

LOFA	Loss of Flow Accident
LOFT	Loss of Flow Transient
McCARD	Monte Carlo Code for Advanced Reactor Design Analysis
MCNP	Monte Carlo N-Particle Transport Code
MERSAT	Model for Evaluation of Reactor Safety Analysis of Thermal-hydraulics
MNR	McMaster Nuclear Reactor
MNSR	Miniature Neutron Source Reactor
MTR	Material Testing Reactor
NC	Natural Circulation
NEA	Nuclear Energy Agency
OECD	Organization for Economics Cooperation and Development
ONB	Onset Nucleate Boiling
OPAL	Open Pool Australian Lightwater reactor
ORNL	Oak Ridge National Lab
OSCAR-4	Overall System for Calculation of Reactors-4
PAK	Pakistan
PARET-ANL	Program for the Analysis of Reactor Transients
PWR	Pressurized Water Reactor
RCM	Research Coordination Meeting
RELAP	Reactor Excursion and Leak Analysis Program
RERTR	Reduced Enrichment for Research and Test Reactor
RIA	Reactivity Initiated Accident
ROK	Republic of Korea
ROM	Romania
RSG-GAS	Reactor Serba Guna GA Siwabessy
SAF	South Africa
SPERT	Special Power Excursion Reactor Test
SS	Steady State
SYR	Syrian Arab Republic
USA	United States of America
WB	With Box
WIMS	Winfrith Improved Multigroup Scheme
WOB	Without Box

CONTRIBUTERS TO DRAFTING AND REVIEW

Abdelrazek, I. D.	Egyptian Atomic Energy Authority
Bokhari, I. H.	Pakistan Atomic Energy Commission, Pakistan
Borio Di Tigliole, A.	International Atomic Energy Agency
Braoudakis, G.	Australia's Nuclear Science and Technology Organization, Australia
Cabral, A.	International Atomic Energy Agency
Chatzidakis, S.	Center for Scientific Research, Demokritos, Greece
Day, S. E.	McMaster University, Canada
Doval, A. S.	Investigaciones Aplicadas (INVAP S.E.), Argentina
Ghoneim, A. M.	International Atomic Energy Agency
Goh, B.	International Atomic Energy Agency
Hainoun, A.	Atomic Energy Commission of Syria, Syrian Arab Republic
Ivanov, E.	Institute de Radioprotection et de Surete Nucleaire (IRSN), France
Kennedy, W.	International Atomic Energy Agency
Marshall, F.M.	International Atomic Energy Agency
Mladin, M.	Institute for Nuclear Research, Romania
Morris, C. R.	International Atomic Energy Agency
Naseer, F.	International Atomic Energy Agency
Olson, A. P.	Arrgonne National Laboratory (ANL), United States of America
Park, S.	Korea Atomic Energy Research Institute, Republic of Korea
Pessoa Barradas, N.	International Atomic Energy Agency
Prinsloo, R.	Nuclear Energy Corporation of South Africa, South Africa
Rao, D. V.	International Atomic Energy Agency
Ridikas, D.	International Atomic Energy Agency
Sembiring, T. M.	National Nuclear Energy Agency (BATAN), Indonesia

Shokr, A. M. International Atomic Energy Agency

Sireta, P. Commissariat à L'Energie Atomique et Aux Energies Alternatives
(CEA CADARACHE), France

Soares, A. International Atomic Energy Agency

Springfels, D. International Atomic Energy Agency

Umbehaun, P. E. Instituto de Pesquisas Energéticas e Nucleares (IPEN-CNEN), Brazil



IAEA

International Atomic Energy Agency

No. 26

ORDERING LOCALLY

IAEA priced publications may be purchased from the sources listed below or from major local booksellers.

Orders for unpriced publications should be made directly to the IAEA. The contact details are given at the end of this list.

NORTH AMERICA

Bernan / Rowman & Littlefield

15250 NBN Way, Blue Ridge Summit, PA 17214, USA

Telephone: +1 800 462 6420 • Fax: +1 800 338 4550

Email: orders@rowman.com • Web site: www.rowman.com/bernan

Renouf Publishing Co. Ltd

22-1010 Polytek Street, Ottawa, ON K1J 9J1, CANADA

Telephone: +1 613 745 2665 • Fax: +1 613 745 7660

Email: orders@renoufbooks.com • Web site: www.renoufbooks.com

REST OF WORLD

Please contact your preferred local supplier, or our lead distributor:

Eurospan Group

Gray's Inn House

127 Clerkenwell Road

London EC1R 5DB

United Kingdom

Trade orders and enquiries:

Telephone: +44 (0)176 760 4972 • Fax: +44 (0)176 760 1640

Email: eurospan@turpin-distribution.com

Individual orders:

www.eurospanbookstore.com/iaea

For further information:

Telephone: +44 (0)207 240 0856 • Fax: +44 (0)207 379 0609

Email: info@eurospangroup.com • Web site: www.eurospangroup.com

Orders for both priced and unpriced publications may be addressed directly to:

Marketing and Sales Unit

International Atomic Energy Agency

Vienna International Centre, PO Box 100, 1400 Vienna, Austria

Telephone: +43 1 2600 22529 or 22530 • Fax: +43 1 26007 22529

Email: sales.publications@iaea.org • Web site: www.iaea.org/books

International Atomic Energy Agency
Vienna
ISBN 978-92-0-109619-7
ISSN 1011-4289